



**HAL**  
open science

# Structural and dynamic studies of TCTP protein : deciphering a complex interaction network involved in tumor reversion

Florian Malard

► **To cite this version:**

Florian Malard. Structural and dynamic studies of TCTP protein : deciphering a complex interaction network involved in tumor reversion. Cancer. Université Paris Saclay (COMUE), 2019. English. NNT : 2019SACLS540 . tel-03091992

**HAL Id: tel-03091992**

**<https://theses.hal.science/tel-03091992v1>**

Submitted on 1 Jan 2021

**HAL** is a multi-disciplinary open access archive for the deposit and dissemination of scientific research documents, whether they are published or not. The documents may come from teaching and research institutions in France or abroad, or from public or private research centers.

L'archive ouverte pluridisciplinaire **HAL**, est destinée au dépôt et à la diffusion de documents scientifiques de niveau recherche, publiés ou non, émanant des établissements d'enseignement et de recherche français ou étrangers, des laboratoires publics ou privés.

# Structural and dynamic studies of TCTP protein: deciphering a complex interaction network involved in tumor reversion

Thèse de doctorat de l'Université Paris-Saclay  
préparée à l'Université Paris-Sud

Ecole doctorale n°569 Innovation thérapeutique du fondamental à l'appliqué (ITFA)  
Spécialité de doctorat : Biochimie et Biologie Structurale

Thèse présentée et soutenue à Gif-sur-Yvette, le 03/12/2019, par

**FLORIAN MALARD**

Composition du Jury :

**Tâp Ha-Duong**

Professeur des Universités - BioCIS, Université Paris-Saclay

Président

**Virginie Gervais**

CR CNRS (HDR) - IPBS, Université Paul-Sabatier

Rapportrice

**Guy Lippens**

DR CNRS - LISBP, INSA Toulouse

Rapporteur

**Samir Messaoudi**

DR CNRS - BioCIS, Université Paris-Saclay

Examineur

**Xavier Morelli**

DR CNRS - CRCM, Université Aix-Marseille

Examineur

**Palma Rocchi**

CR INSERM (HDR) - CRCM, Université Aix-Marseille

Examinatrice

**Ewen Lescop**

CR CNRS (HDR) - ICSN, Université Paris-Saclay

Directeur de thèse



*Le cadre, cette idée qui nous empêche,*

*je dédie cette thèse à Pétronille.*



# Table of Contents

<b>1</b>	<b>Introduction</b>	<b>1</b>
1.1	Introduction to cancer biology . . . . .	1
1.1.1	The cell cycle . . . . .	2
1.1.2	Apoptosis pathway . . . . .	3
1.1.3	Tumorigenesis . . . . .	11
1.2	TCTP protein is a switch of tumor reversion . . . . .	13
1.2.1	The tumor reversion at a glance . . . . .	13
1.2.2	TCTP protein: structure, interactome and functions . . . . .	15
1.2.3	TCTP-regulated pathways in apoptosis and tumor reversion . . . . .	22
1.3	Structural insights into TCTP and its interactions with ligands and proteins . . . . .	29
1.4	Biophysical investigation of TCTP interactome in apoptosis and tumor reversion . . . . .	68
<b>2</b>	<b>Materials and Methods</b>	<b>75</b>
2.1	Wetlab routines . . . . .	75
2.1.1	Bacterial transformation, storage and culture . . . . .	76
2.1.2	Protein analysis . . . . .	77
2.1.3	Cristallogenesis . . . . .	79
2.2	Protein design, production and purification . . . . .	79
2.2.1	Design and engineering of relevant proteins . . . . .	79
2.2.2	Large-scale protein production protocols . . . . .	85
2.2.3	General procedure for protein purification . . . . .	85
2.3	Biophysical and computational methods . . . . .	89
2.3.1	Nuclear Magnetic Resonance (NMR) . . . . .	89
2.3.2	Biophysical methods for investigation of proteins structure . . . . .	98
2.3.3	Informatics, software routines and modelling tools . . . . .	101
<b>3</b>	<b>Research for alternative TCTP states</b>	<b>105</b>
3.1	Diversity of TCTP structures . . . . .	106

3.1.1	NMR assignment and dynamics along TCTP backbone . . . . .	106
3.1.2	TCTP forms salt- and IDR- dependent dimers . . . . .	109
3.1.3	Phosphorylation in TCTP IDR by Polo-like kinase 1 (Plk-1) . . . . .	113
3.2	<i>Research paper</i> TCTP IDR upon phosphorylation and calcium binding . . . . .	119
3.3	The molten-globule state TCTP* . . . . .	140
3.3.1	Evaluation of protein stability in diverse conditions . . . . .	140
3.3.2	Identification of TCTP* and structural characterization . . . . .	145
3.3.3	Evidences for the pre-existing character of TCTP* . . . . .	159
3.4	Discussion . . . . .	161
<b>4</b>	<b>TCTP &amp; Bcl-2 family proteins Bcl-xL and Mcl-1</b>	<b>165</b>
4.1	Structure and dynamics of TCTP upon complex formation . . . . .	166
4.1.1	Stoichiometry and quaternary structure of TCTP complexes . . . . .	166
4.1.2	Structure of TCTP upon binding to Bcl-2 family partners . . . . .	171
4.1.3	Molten-globule TCTP* readily interacts with Mcl-1 . . . . .	182
4.2	Study of Bcl-xL and Mcl-1 in complex with TCTP and BH3 peptides . . . . .	185
4.2.1	Complex between Mcl-1 and the native BH3-like peptide from TCTP . . . . .	185
4.2.2	Binding studies of Mcl-1 and Bcl-xL with full length TCTP . . . . .	197
4.2.3	Transient association of TCTP with Bcl-2 partners . . . . .	205
4.3	Canonical and BH3-like motifs at Mcl-1 protein . . . . .	209
4.3.1	Complex of Mcl-1 with BH3 peptides from TCTP and Mule . . . . .	210
4.3.2	Canonical and BH3-like sequences at Mcl-1 protein . . . . .	215
4.3.3	Relative affinity of BH3 peptides and TCTP protein for Mcl-1 . . . . .	220
4.4	Discussion . . . . .	227
<b>5</b>	<b>Exploration and frontiers in TCTP interactome</b>	<b>229</b>
5.1	TCTP complex with proteins and RNA . . . . .	230
5.1.1	The E3 ubiquitin ligase MDM2 . . . . .	230
5.1.2	Interaction studies between TCTP and RNAs . . . . .	232
5.1.3	TCTP and the RNA binding YB-1 protein . . . . .	234
5.2	Inhibitors of TCTP for anti-cancer therapy . . . . .	241
5.2.1	Sertraline and other ligands at TCTP protein . . . . .	242
5.2.2	Binding of sertraline on phosphorylated TCTP . . . . .	246
5.2.3	Impact of sertraline on the melting temperature of TCTP . . . . .	246
5.3	Selective Mcl-1 inhibitors . . . . .	248
5.3.1	Solubility of Na-1-115-7 and FD-24-3 . . . . .	249
5.3.2	Binding study with Mcl-1 selective FD-24-3 . . . . .	250

---

5.3.3	Binding study with Mcl-1 selective Na-1-115-7 . . . . .	252
5.4	Discussion . . . . .	258
<b>6</b>	<b>General discussion</b>	<b>261</b>
6.1	Molten-globule states . . . . .	262
6.2	TCTP in complex with Bcl-xL and Mcl-1: functional hypothesis . . . . .	264
6.3	Toward a representative definition for all natural BH3 motifs . . . . .	266
	<b>References</b>	<b>271</b>
	<b>List of Figures</b>	<b>295</b>
	<b>List of Tables</b>	<b>299</b>
	<b>List of Listings</b>	<b>299</b>
	<b>Appendix</b>	<b>303</b>



# Acronyms

**AML** Acute Myeloid Leukemia.

**ANS** 8-Anilinonaphthalene-1-sulfonic acid.

**APL** Acute Promyelocytic Leukemia.

**ASO** antisense oligonucleotide.

**Bad** Bcl-2-associated death promoter.

**Bak** Bcl-2 homologous antagonist killer.

**BALF** Broncho-Alveolar Lavage Fluids.

**Bax** Bcl-2 associated X protein.

**Bcl-2** B-cell-lymphoma 2 protein.

**Bcl-xL** B-cell-lymphoma-extra large protein.

**BH** Bcl-2 Homology.

**BH3** Bcl-2 Homology motif 3.

**Bid** BH3 interacting-domain death agonist.

**Bim** Bcl-2-like protein 11.

**BSA** Bovine Serum Albumin.

**CAD** Caspase-Activated Dnase.

**CD** Circular Dichroism.

**CDKs** Cyclin-Dependent Kinases.

**CEST** Chemical Exchange Saturation Transfer.

**CNS** Central Nervous System.

**co-IP** co-immunoprecipitation.

**CPMG** Carr-Purcell-Meiboom-Gill.

**CRPC** Castration-Resistant Prostate Cancer.

**CSD** Cold Shock Domain.

**CV** Column Volume.

**DISC** Death-Inducing Signaling Complex.

**DLS** Dynamic Light Scattering.

**DOSY** Diffusion-Ordered Spectroscopy.

**EC** extracellular.

**ER** Endoplasmic Reticulum.

**FADD** Fas-Associated protein with Death Domain.

**FID** Free Induced Decay.

**FT** Fourier Transform.

**GEF** Guanine nucleotide Exchange Factor.

**GNU** Gnu's Not Unix.

**HDD** Hard Disk Drive.

**HDX** Hydrogen/Deuterium-eXchange.

**HMQC** Heteronuclear Multiple-Quantum Correlation.

**HP-NMR** High-Pressure NMR.

**HRF** Histamine Releasing Factor.

**Hsp27** Heat shock protein 27.

**HSQC** Heteronuclear Simple-Quantum Correlation.

**IC** intracellular.

**IDR** Intrinsically Disordered Region.

**IPTG** isopropyl  $\beta$ -D-1-thiogalactopyranoside.

**MALDI** Matrix-assisted laser desorption/ionization.

**MALS** Multi-Angle Light Scattering.

**MBP** Maltose Binding Protein.

**Mcl-1** Induced myeloid leukemia cell differentiation protein 1.

**MD** Molecular Dynamics.

**MDM2** Mouse Double Minute 2 homolog.

**MG** Molten-Globule.

**MOM** Mitochondrial Outer Membrane.

**MOMP** Mitochondrial Outer Membrane Permeabilization.

**MS** Mass Spectrometry.

**MST** Microscale Thermophoresis.

**mTOR** mammalian Target Of Rapamycin.

**MW** Molecular Weight.

**MWCO** Molecular Weight Cutoff.

**NMR** Nuclear Magnetic Resonance.

**NOESY** NOE Spectroscopy.

**NPS** Network Protein Server.

**OD** Optical Density.

**ORF** Open Reading Frame.

**p53** Tumor protein p53.

**PAGE** Polyacrylamide Gel Electrophoresis.

**PCR** Polymerase Chain Reaction.

**PEST** Proline, glutamic acid, serine and threonine rich domain.

**PF** Protection Factor.

**PIC** Protease Inhibitor Cocktail.

**Plk-1** Polo-like kinase 1.

**PMID** Pubmed Central ID.

**ppm** parts per million.

**PTM** Post-Translational Modifications.

**RIPs** Receptor Interacting Protein kinases.

**RMSD** Root Mean Square Deviation.

**SAXS** Small-Angle X-ray Scattering.

**SCID** Severe Combined Immune Deficiency.

**SEC** Size Exclusion Chromatography.

**SERT** serotonin transporter.

**SPR** Surface Plasmon Resonance.

**SSD** Solid State Drive.

**SSRI** Selective Serotonin Reuptake Inhibitor.

**TCTP** Translationally Controlled Tumor Protein.

**TCTP FL** full length TCTP.

**TEV** Tobacco Etch Virus protease.

**TM** Transmembrane.

**TNF** Tumoral Necrosis Factor.

**TOF** Time Of Flight.

**TRADD** Tumor necrosis factor Receptor type 1-Associated DEATH Domain.

**TROSY** Transverse Relaxation-Optimized Spectroscopy.

**TSA** Thermal Shift Assay.

**U2OS** Human Bone Osteosarcoma Epithelial Cells.

**USPX9** Ubiquitin Specific Peptidase 9 X-Linked.

**YB-1** Y-Box associated protein 1.



# Chapter 1

## Introduction

In this manuscript, we report our work at studying Translationally Controlled Tumor Protein (TCTP) and its interaction network in the context of apoptosis and tumor reversion. We gained insights into the molecular basis of TCTP-based interactions, including changes in the structure and dynamics of the protein and partners.

In this introduction, we will first present cancer biology with the description of the cell cycle, apoptosis and tumorigenesis pathways (Sec. 1.1). Then, we will describe the role of TCTP protein in tumor reversion, a rare and spontaneously occurring biological event in which a cancer cell can lose its malignant phenotype, to recover characteristics of benign cells, including sensitivity toward apoptosis (Sec. 1.2). Third, we will report our review of TCTP interactome and associated functions in which we propose hypothesis to explain how TCTP can adapt to its myriad of partners (Sec. 1.3). Finally, we will summarize our three objectives in the current study as well as methods we used to fulfill our goals (Sec. 1.4).

### 1.1 Introduction to cancer biology

Cancer can result from unconstrained cell proliferation. This involves progression through the cell cycle and defects in associated control checkpoints as well as evasion of apoptosis [1]. Cancer initiation and progression are promoted through deregulated molecular pathways and can be seen as a cell de-differentiation process, leading to invasion and metastasis [2]. Here, we briefly introduce cancer biology by presenting the cell cycle and its controls (Sec. 1.1.1), the apoptosis pathway (Sec. 1.1.2) and the tumorigenesis process (Sec. 1.1.3).

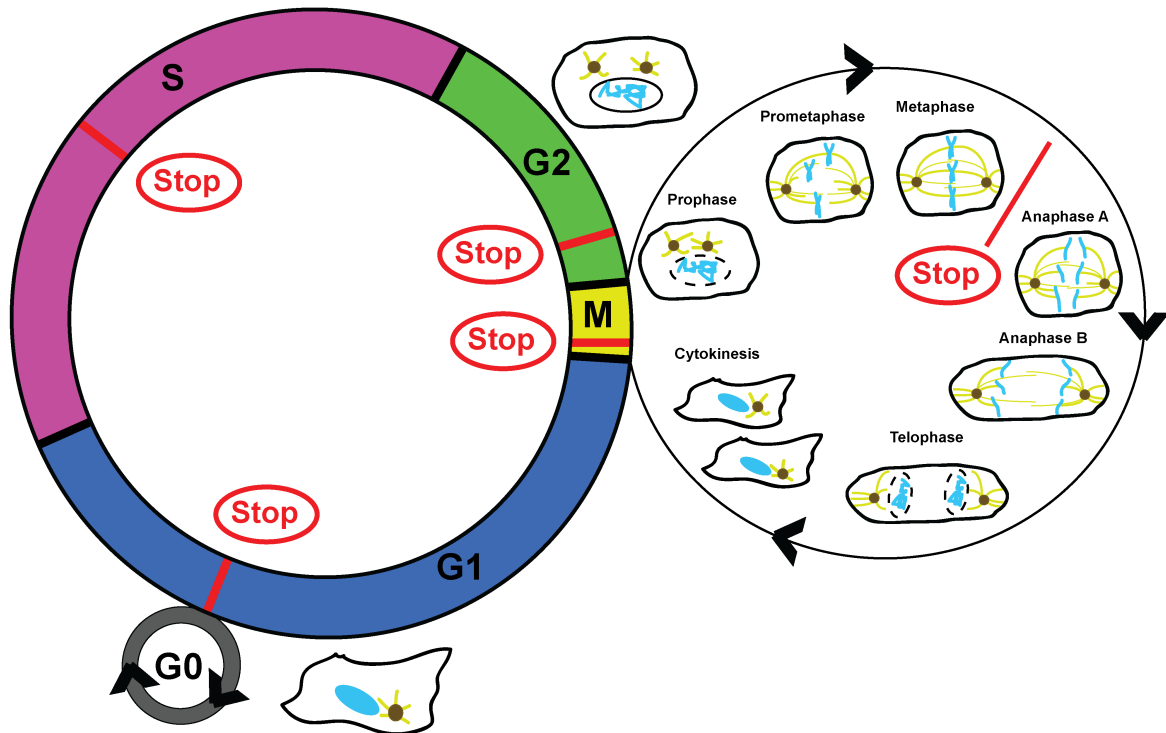


Fig. 1.1 **Cell cycle and mitosis.** The different phases of the cell cycle and mitosis are presented (left). G0 is the quiescent phase and the passive state of the cell cycle. G1, S and G2 are included in the interphase and they represent the pre-replicative, replicative and pre-mitosis phases, respectively. The mitosis (M) phase is shown and detailed (right). In mitosis, all successive steps are namely prophase, prometaphase, metaphase, anaphase, telophase and cytokinesis. "Stop" labels indicates cell cycle control checkpoints under control of Cyclin-Dependent Kinases (CDKs) and cyclin protein regulators.

### 1.1.1 The cell cycle

In general, the cell cycle describes all possible states for a single cell at different moments (Fig. 1.1). It was described through an extensive number of papers over the past thirty years and conclusions were compiled in numerous reviews and books [3–5]. Regulation pathways and control checkpoints [6–10] were identified and extensively described with the emergence of Tumor protein p53 (p53) as a guardian of genomic integrity and a major cancer-related protein which is inactivated in about half of all human cancers [11]. Of particular interest, the cell cycle was often linked with apoptosis in reviews within the last quarter century [12–22]. Mitosis [23] and meiosis [24] are the two known mechanisms for an eukaryotic cell to divide at the end of a regular cell cycle. The cell cycle includes a passive state (G0) and four different active states (G1, S, G2, M) (Fig. 1.1).

In normal conditions, cells are sensitive to environmental factors such as presence of nutrients or growth factors to pass from the quiescent G0 state into the active cell cycle in G1 phase. A

first checkpoint G0/G1 ensures that appropriate signaling inputs are present prior to engage G1 phase upon induction of a specific set of genes [25]. The interphase starts in G1 phase and continues in S and G2 phases, the whole interphase accounting for 95 % of the active cell cycle time [26]. In phase G1, cells grow, develop more organelles and proteins, and present generally high biosynthetic activities to further replicate DNA in S phase. Prior to DNA replication, an intra S cell cycle checkpoint controls parameters relative to genomic integrity to allow the transition in phase S. In the replicative phase histones modifications permit genome decompaction [27] and replication through DNA polymerases to yield bi-chromatid chromosomes. In the next G2 phase, a period of protein synthesis and rapid cell growth develops to prepare mitosis. Another G2/M cell cycle checkpoint ensures that DNA lesions are repaired prior engaging mitosis. Microtubules start to reorganize at two centrosomes upon entry in mitosis (Fig. 1.1).

This highly dynamic and complicated process leads to genetic material sharing and membrane splitting. First, the nuclear membrane decomposes under lamine dissociation via specific signaling. In the following prometaphase microtubules anchor to cell poles from centrosomes and other microtubules project toward chromosomal DNA in the center on the cell. In metaphase, chromosomes are all attached to the mitotic spindle [28–30] via the kinetochore complex. Chromosomes are aligned and equidistant from both centrosomes. Then, a last cell cycle checkpoint allows for proceeding in anaphase by separating chromatids (anaphase A) and by expanding the cell size (anaphase B). In metaphase, the TCTP protein, which is the central protein of this manuscript, associates with the mitotic spindle and is dissociated upon Polo-like kinase 1 (Plk-1) mediated phosphorylation, allowing metaphase completion and termination of both mitosis [31] and meiosis [32]. Indeed, TCTP was demonstrated to be phosphorylated at residues S46/S64 by the Plk-1 [33] in both *in vitro* and *in vivo* context, with positive effect on cell proliferation. In the telophase, nuclear lamine reorganizes to reconstitute a nuclear envelope and the plasmic membrane shrinks until the two cells are almost separated by a specific actin-related ring. The proper cell-cell separation happens during cytokinesis [34], thus terminating mitosis and the whole cell cycle (Fig. 1.1).

## 1.1.2 Apoptosis pathway

### 1.1.2.1 Activation routes and execution of apoptosis

The term apoptosis was first used in 1972 [35] to name an organized mechanism for cell deletion, with complementary but opposite role compared to mitosis. It is one of the three types of cellular death with necrosis [36] and autophagy [37]. Apoptosis is often named *The programmed cell death* [38] since the process is highly organized, sequential

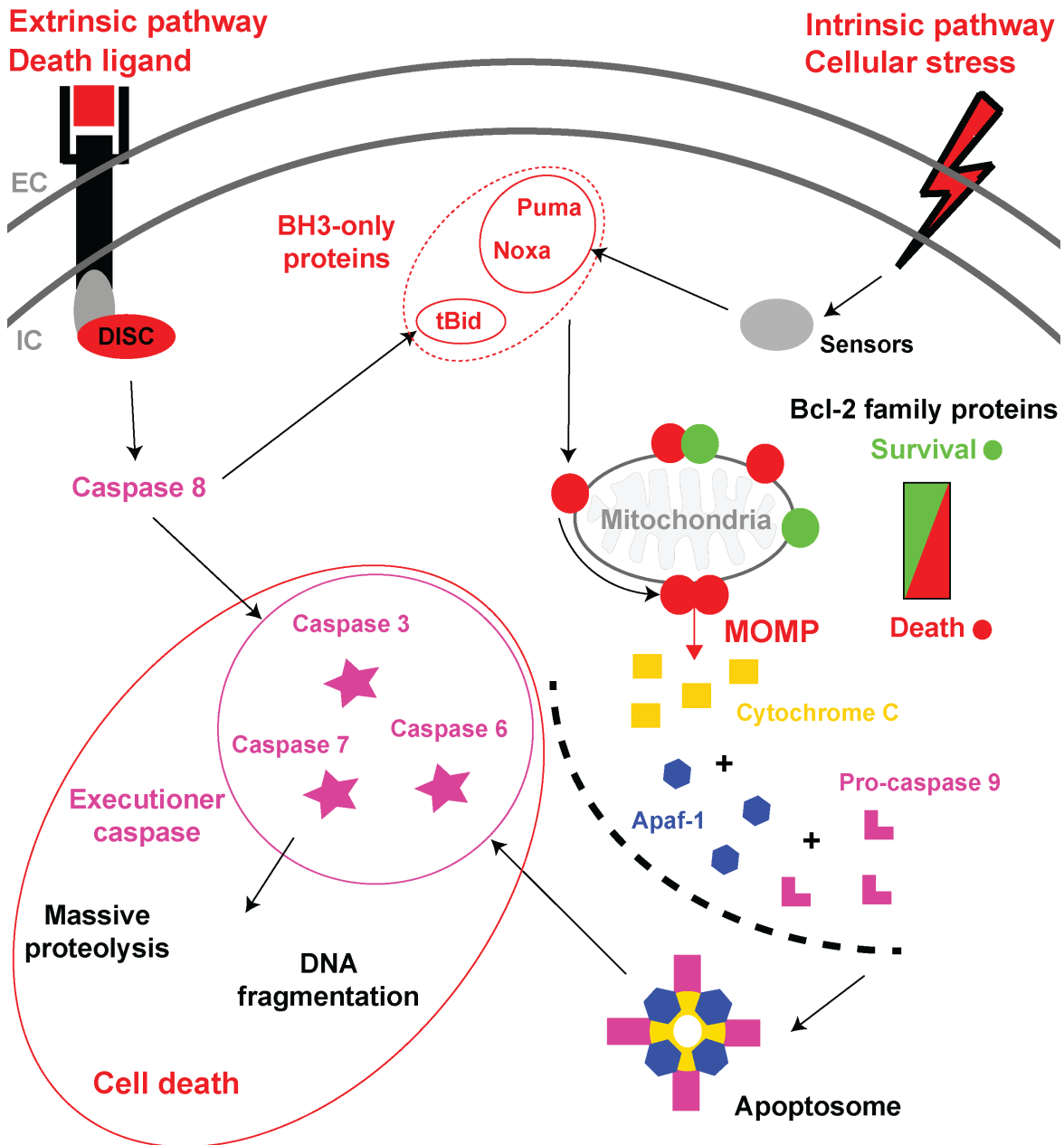


**Fig. 1.2 Overview of apoptosis pathway.** Principal aspects of apoptosis pathway are presented including both extrinsic and intrinsic activation modes and execution phase. Pro-death actors (red) and specifically caspases (magenta) are highlighted. The Death-Inducing Signaling Complex (DISC) and the Mitochondrial Outer Membrane Permeabilization (MOMP) are labeled. The extracellular (EC) and intracellular (IC) regions are noted. Arrows indicate positive influence from line origin to arrowhead.

and genetically encoded (Fig. 1.2). Various stress sensors [39] and molecular balances [40] permit to tightly tune the pathway in function of diverse environmental parameters. It is a vital component of diverse and important physiological processes such as cell turnover [41],

embryonic development [42] or functioning of the immune [43] and nervous [44] systems. Several papers reviewed the apoptosis in the context of cancer [45] and associated efforts to develop therapy [46] which aim at promoting apoptosis in cancer cells. Indeed, apoptosis rederegulation and unconstrained proliferation are key elements to initiate tumorigenesis [47] and to promote tumor progression and maintenance. In mammals, both intrinsic [48] and extrinsic [49] activation modes of apoptosis pathway were reported and they differ in the way they initiate apoptosis by communicating with specific molecular actors (Fig. 1.2). Execution phase of apoptosis is then mediated by the caspase family of proteases.

In the extrinsic pathway, the activation of apoptosis is mediated through activation of death receptors at the molecular membrane of the cell upon death ligand binding. These receptors include the Tumoral Necrosis Factor (TNF) receptor gene superfamily [50]. Upon activation, the intracellular death domain recruits adapter proteins [51–53] such as Tumor necrosis factor Receptor type 1-Associated DEATH Domain (TRADD), Fas-Associated protein with Death Domain (FADD) and Receptor Interacting Protein kinases (RIPs). They mediate the interaction between the death receptor and procaspase-8 to form the DISC which results in the auto-catalytic activation of pro-caspase 8 [54]. In the intrinsic pathway, the activation of apoptosis is regulated by a wide range of non-receptor mediated stimuli (Fig. 1.2). These stimuli induce changes in the Mitochondrial Outer Membrane (MOM) via the B-cell-lymphoma 2 protein (Bcl-2) family [55] and BH3-only proteins. These can ultimately lead to MOMP and release of pro-apoptotic proteins [56] such as cytochrome c [57] (Fig. 1.2). Other pro-death factors then associate in a macromolecular assembly called apoptosome [58, 59] which activates the intrinsic apoptosis pathway and triggers the execution phase of apoptosis [60] by activating executioner caspases. Even though crosstalks in early steps were reported, extrinsic and intrinsic activation pathways usually converge upon activation of executioner caspases in the execution phase (Fig. 1.2).

The latter phase consists in the degradation of nucleic acids and proteins by endonucleases and caspases. Caspase-3, -6 and -7 are known as the executioner caspases [61] and they ultimately transform cell morphology and metabolism upon activation. Caspase-3 is widely presented as the principal of the three since it is activated by any of the initiator caspases and is responsible for triggering DNA fragmentation through activation of Caspase-Activated Dnase (CAD) endonuclease [62]. Caspase-3 is also reported to be important for anti-apoptotic body formation through cytoskeleton destabilization. In the end of apoptosis, the immune system takes the apoptotic bodies in charge through phagocytosis events.

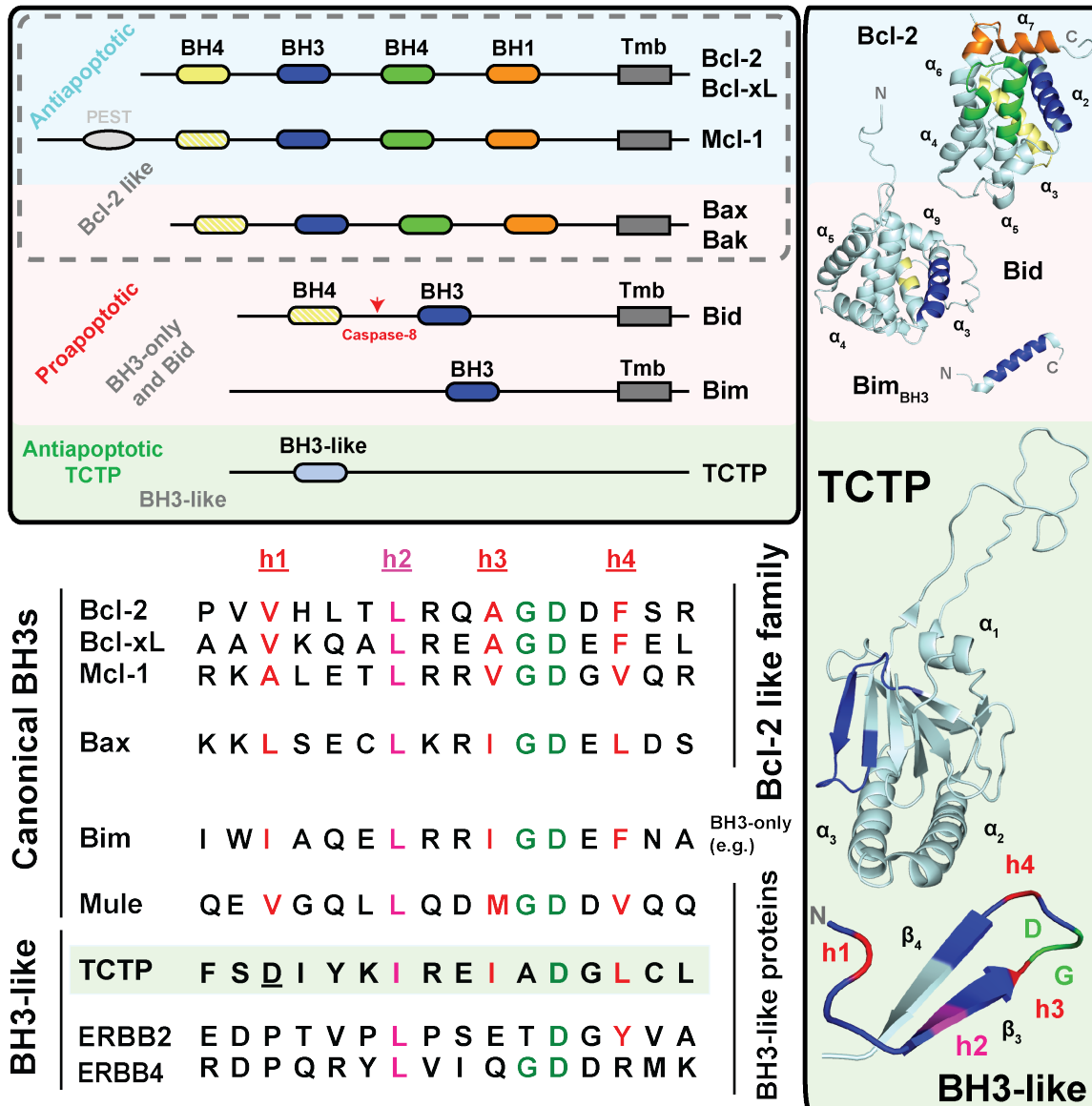
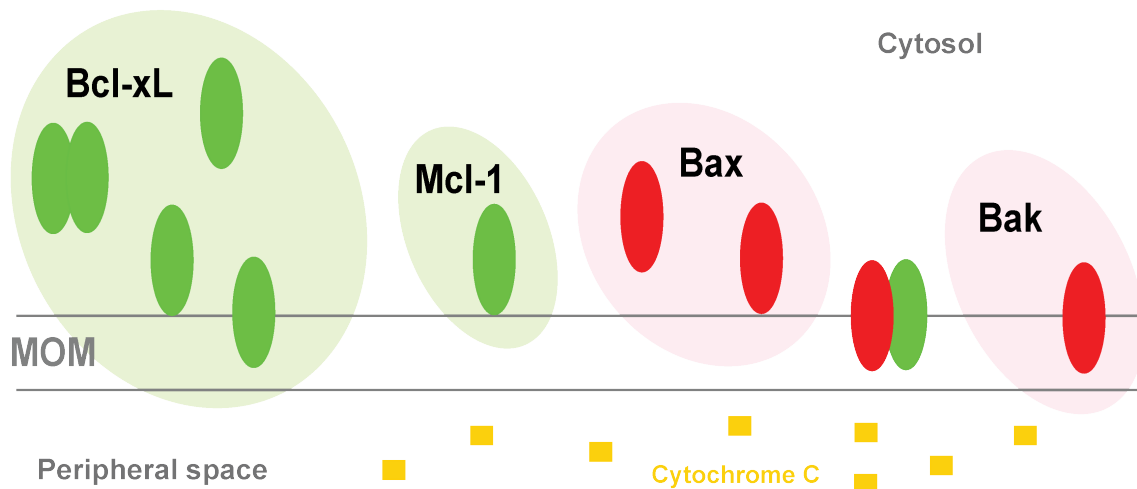


Fig. 1.3 **Bcl-2 family and BH3-only proteins: structure, topology and sequences.** Topology of Bcl-2 family, BH3-only and TCTP proteins (top-left frame). Antiapoptotic (blue background), proapoptotic (pink) Bcl-2 family proteins and antiapoptotic TCTP (green) are shown. Bcl-2 family is grouped (dashed) and all members have Bcl-2 Homology (BH) motifs 1-4 (orange, green, blue, yellow). The caspase-8 cleavage site activating BH3 interacting-domain death agonist (Bid) protein is highlighted. Transmembrane parts to anchor in the MOM are shown (grey). The structure of TCTP (pdb code: 2HR9) with unusual BH3-like motif in  $\beta$ -sheet embedded in core domain is shown (bottom-right). Bcl-2 (pdb code: 1GJH), Bid (pdb code: 2BID) and Bim<sub>BH3</sub> in complex with B-cell-lymphoma-extra large protein (Bcl-xL) (pdb code: 1PQ1) are shown. An alignment of Bcl-2 Homology motif 3 (BH3) and BH3-like sequences is also shown (bottom-left).

### Normal situation



**Fig. 1.4 Bcl-2 family proteins at the MOM.** In differentiated tissues, Bcl-xL is constitutively expressed as cytosolic monomers and dimers, loosely attached and anchored into the MOM. Induced myeloid leukemia cell differentiation protein 1 (Mcl-1) is only transiently expressed and is predominantly found loosely attached to the MOM in its free state. Both Bcl-xL and Mcl-1 can still heterodimerize in the MOM with proapoptotic Bcl-2 family members such as Bcl-2 associated X protein (Bax) and Bcl-2 homologous antagonist killer (Bak), respectively. This prevents Bax-related proteins from oligomerization and pore formation that leads to membrane permeabilization and cytochrome c release in case of pro-death signaling. In this case, cytochrome c is retained in the mitochondria peripheral space between the outer and inner mitochondrial membranes.

#### 1.1.2.2 Bcl-2 family and BH3-only proteins

Key players of the intrinsic apoptosis pathway are the evolutionary unrelated [63] BH3-only and Bcl-2 family (Bcl-2 like) proteins (Fig. 1.3). In particular, the Bcl-2 family proteins balance pro-death and pro-survival signaling [64, 65] to tightly regulate MOMP under influence of the BH3-only proteins. In the database of Bcl-2 family members and BH3-only proteins BCL2DB [66], we count 10 Bcl-2 like proteins (6 anti-, 4 pro-), 9 BH3-only and 44 additional non canonical BH3-containing proteins [66]. Despite sharing core mechanisms [67] in regulating the MOMP and thus cytochrome c release, Bcl-2 family proteins still present disparities and are regulated by specific BH3-only proteins partners. Moreover, the Bcl-2 family proteins can also be regulated by proteins harboring a BH3-like motif, expanding the panel of intrinsic apoptosis regulators. Here, we present the molecular players of apoptosis with focus on the Bcl-2 family, BH3-only and BH3-like proteins. We discuss the interplay between them all with a particular focus on Bcl-xL and Mcl-1 proteins whose interactions with TCTP will be studied in this work.

### **Bcl-2 family proteins**

Bcl-2 family proteins have multiple functions in cells including regulation of autophagy [68], calcium handling [69] and energetics [70] but are mostly known for their critical role as arbiters of apoptosis with growing importance as cancer targets [71, 72]. Bcl-2 family proteins are usually distinguished in two classes according to the specific antiapoptotic or proapoptotic activity of the protein (Fig. 1.3). Over the last 30 years, antiapoptotic Bcl-2 family proteins Bcl-2 [73, 74], Bcl-xL [75] and Mcl-1 [76] were identified whereas proapoptotic Bax [77] and Bak [78] were also discovered (Fig. 1.3). All Bcl-2 family proteins are evolutionary related [63] and share both C-terminal membrane anchor and strong structural homology between each others. Four conserved BH motifs are generally present in the primary sequence of Bcl-2 family proteins [79]. Antiapoptotic Bcl-2 family proteins all sequester at least one proapoptotic Bcl-2 family protein. This heterodimerization process prevents from oligomerization of Bax-related proteins, pore formation in the MOM and thus membrane permeabilization and cytochrome c release. Although being strongly related, Bcl-2 family members have specific localization, behavior and structure in cells.

Bcl-xL is constitutively expressed in the vast majority of tissues and exists as cytosolic monomer, dimer and loosely bound to the MOM [80–83] prior to apoptosis induction or ligand binding (Fig. 1.4). By contrast, Mcl-1 is predominantly present at significant levels during development and cancer in a tissue-specific manner and is loosely attached to the MOM [84] prior to apoptosis. Functionally, Mcl-1 has more rapid turnover compared to Bcl-xL due to fast proteasome-mediated degradation and its overexpression was frequently reported in drug-resistant cancer cells. Poly-ubiquitinylation of Mcl-1 necessitates the E3 ubiquitin ligase Mule [85]. In particular circumstances, Mcl-1 can be deubiquitinated by the Ubiquitin Specific Peptidase 9 X-Linked (USPX9) in a phosphorylation-dependent manner mediated by the Proline, glutamic acid, serine and threonine rich domain (PEST) domain [86]. In term of interactions, Bax has high affinity for Bcl-xL and Bcl-2 and Bak for Mcl-1 and Bcl-xL [87, 88].

In term of structure, Mcl-1 does not contain an internal IDR region as observed for Bcl-xL (Fig. 1.5 A) but the protein has a 200 amino-acid N-terminal flexible PEST domain with numerous phosphorylations sites documented to regulate ubiquitinylation and proteasome-mediated degradation. The PEST domain was suggested to weaken the binding affinity of BH3 ligands at Mcl-1 protein but without altering the selectivity [89]. The Mcl-1 protein is generally studied as a soluble truncate for the PEST and C-terminal transmembrane domain. The electrostatic surface map of human Bcl-xL shows a predominantly acidic environment in the BH3-binding groove of the protein whereas a basic situation is observed in human Mcl-1 (Fig. 1.5 B). Mcl-1 has a deeper hydrophobic pocket compared to Bcl-xL and is more

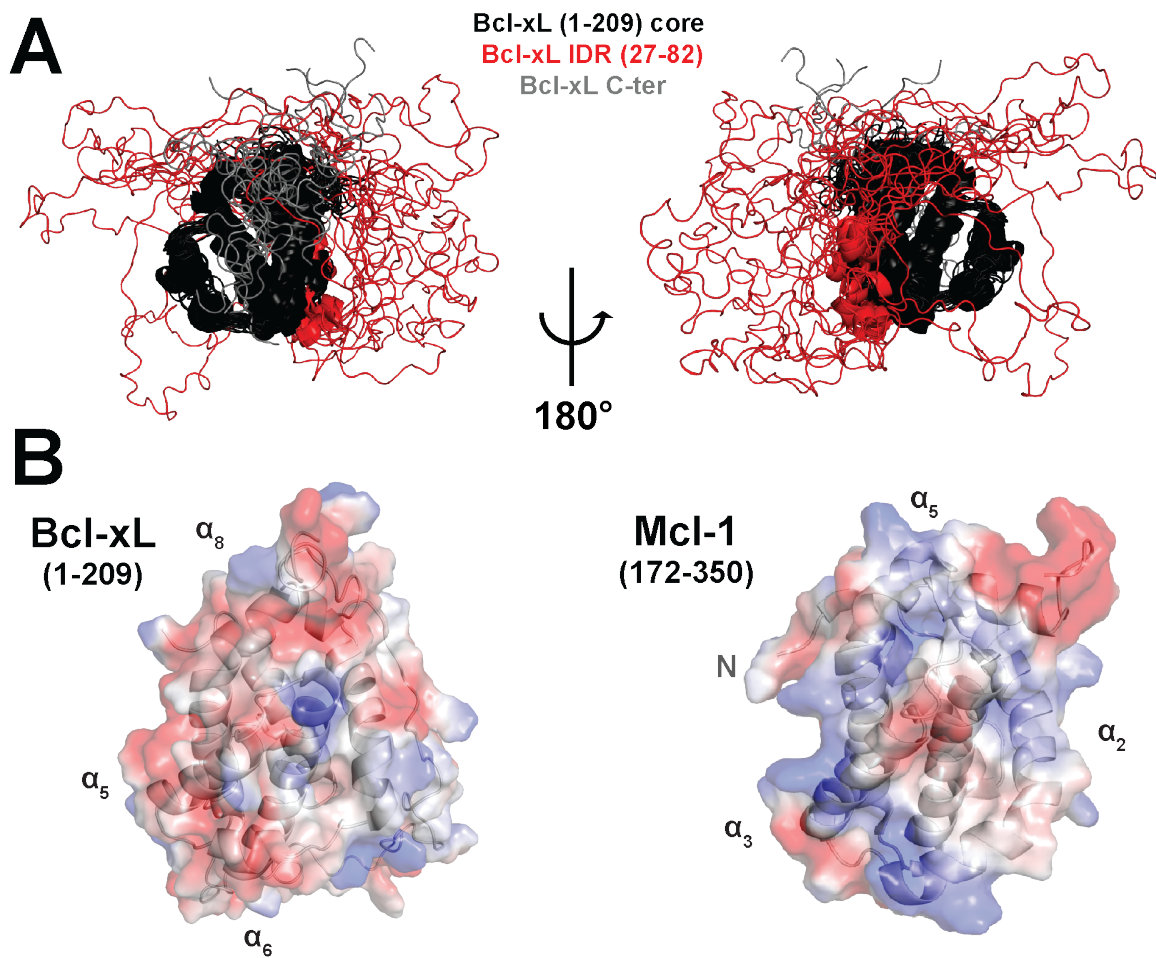


**Fig. 1.5 Bcl-xL Intrinsically Disordered Region (IDR) and electrostatic surface map of Bcl-xL and Mcl-1.** (A) Structural alignment of all twenty models in the NMR ensemble of Bcl-xL  $\Delta$ TM (pdb code: 2ME9). The Bcl-xL IDR (red), the C-terminal tail (grey) and the globular core of the protein (black) are highlighted. (B) Electrostatic surface map of Bcl-xL  $\Delta$ Transmembrane (TM) (pdb code: 2ME9) and Mcl-1  $\Delta$ PEST $\Delta$ TM (pdb code: 2MHS).

rigid, opening the door to the development of Mcl-1 specific inhibitors [72, 90] (Fig. 1.12 B) which is important for the treatment of Acute Myeloid Leukemia (AML) for example, where people want to preserve constitutive Bcl-xL and healthy immune cells to selectively target the overexpressed Mcl-1 protein in malignant cells.

### BH3-only and BH3-like proteins

In this manuscript, we often refer to canonical "BH3" or "BH3-like" motifs and associated "BH3-only" or "BH3-like" proteins. First, the canonical BH3 motif was originally found in BH3-only proteins which refer to promoters of apoptosis that interact with Bcl-2 family proteins through their BH3 motif and were discovered for most in the 1990's [91, 92]

(Fig. 1.3). They have no evolutionary link with the proteins from the Bcl-2 family [63] but still converged to include the BH3 motif [93, 94] in their primary sequence. The canonical BH3 motif was first defined as a short amino-acids stretch (7-15 residues) with four conserved hydrophobic residues spanning in the short sequence from position h1 to h4 with critical importance for anchoring into the BH3 binding groove of Bcl-2 proteins [95, 96]. These residues are spaced by less conserved amino-acids between sequences. About ten different BH3-only proteins such as Bcl-2-like protein 11 (Bim), Bcl-2-associated death promoter (Bad) (Fig. 1.3) were reported and all act as sensors which permit to transduce death signaling upon a wide variety of stress [92]. In BH3-only proteins, the BH3 motif is unstructured [97, 98] prior to bind Bcl-2 family members and the proteins have no stable tertiary structure. They can anchor into the MOM through their C-terminal tail and upon interaction with Bcl-2 family partners, thus achieving their proapoptotic functions by regulating Bcl-2 family proteins [99–102]. The local MOM organization [103] and specific receptors [104] can influence the recruitment of the BH3-only proteins.

Interestingly, the regulation of BH3-only proteins by post-translational modifications [105] can switch the protein from inactive to active state, as exemplified by the proteolytic cleavage of the contested BH3-only protein Bid prior to Bcl-2 family members binding which exposes the BH3 motif (Fig. 1.3). Indeed, the solution structure of the Bid protein [106, 107] did surprisingly show a similar fold compared to Bcl-2 family proteins. Bid had tertiary structure organization with the BH3 motif preformed as an  $\alpha$ -helix, which contradicts observations for all others BH3-only proteins. Later after the discovery of Bid it was proposed that the BH4 motif [108] could be finally present in the protein. Similarities and differences between Bid and both BH3-only and Bcl-2 family proteins were reviewed and led to propose that Bid could be more related to the Bcl-2 family than BH3-only proteins [109, 91].

Beyond BH3-only proteins, several unrelated proteins were found to encompass a canonical BH3 sequence in their primary sequence. Due to structure/function divergence compared to the classical BH3-only proteins or just no sufficient data to establish similarities, these were classified as BH3-like proteins. For example, the E3 ubiquitine ligase Mule that targets Mcl-1 to promote proteasome-mediated degradation of the protein owns a canonical BH3 motif but is ranked with the BH3-like proteins according to BCL2DB (Fig. 1.3). But BH3-like proteins can also contain non-canonical BH3 motif, the BH3-like motif, and still interact with Bcl-2 family members. The BH3-like motif does not include all hydrophobic residues at position h1, h3 and h4 and one or more can be missed, still allowing the motif to bind Bcl-2 family proteins and regulate them. In the database of Bcl-2 family members and BH3-only proteins BCL2DB [66], we count 44 BH3-like proteins whereas only 10 Bcl-2 like proteins

(6 anti-, 4 pro-) and 9 BH3-only proteins [66] are reported. The vast majority of BH3-like proteins were reported to have proapoptotic properties and to function as sensitizer BH3s. A rare example of antiapoptotic BH3-like protein is the telomerase reverse transcriptase binds to Bcl-xL and Mcl-1 and inhibits apoptosis in cancer cells [110]. Importantly, TCTP was also identified among the few BH3-like proteins that inhibit apoptosis rather than promoting it [111] (Fig. 1.3).

### 1.1.3 Tumorigenesis

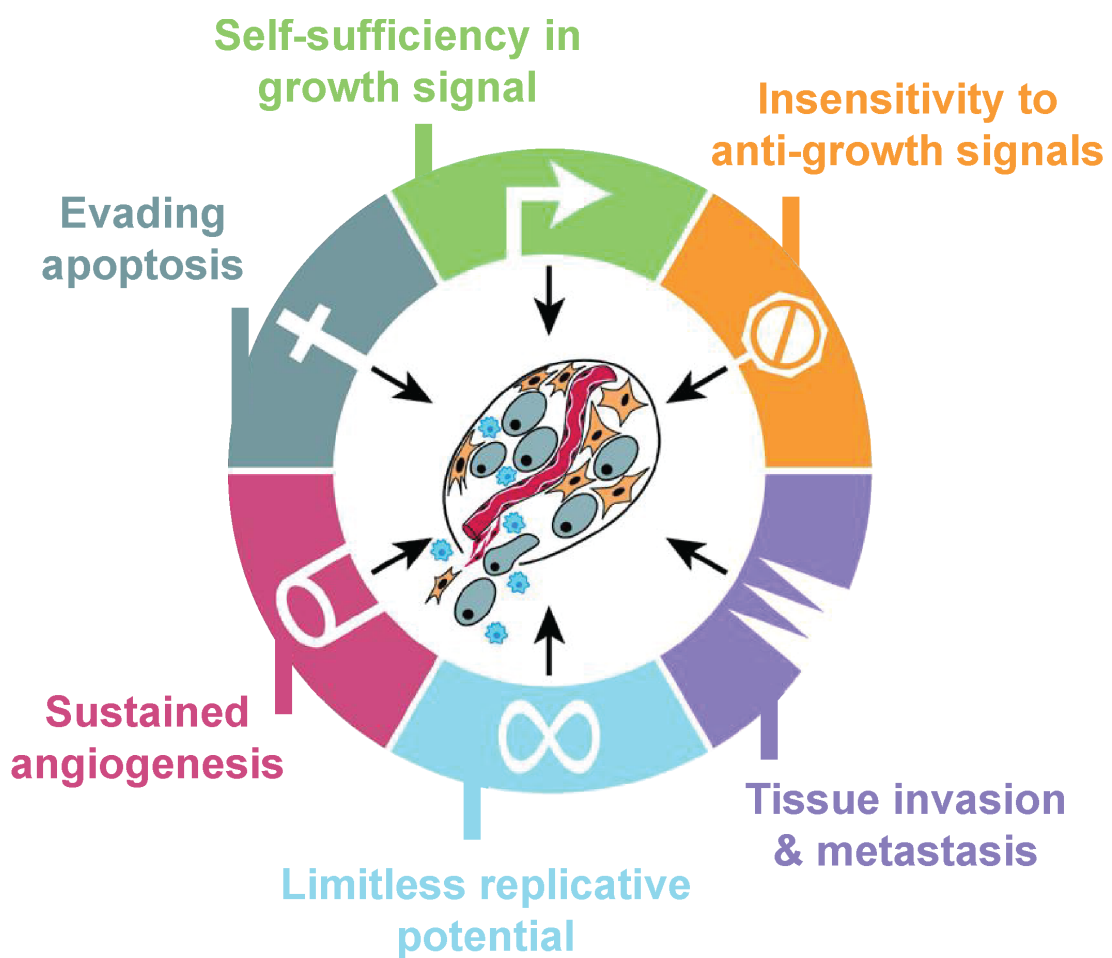


Fig. 1.6 **The hallmarks of cancer.** Acquired capabilities of cancer cells and tumor upon tumorigenesis. Figure taken from "*The Hallmarks of Cancer*" [1] original paper. Cancer cells acquire capabilities such as self-sufficiency in growth signal, insensitivity to anti-growth signals, evading apoptosis and limitless replicative potential. Sustained angiogenesis plus tissue invasion and metastasis are acquired capabilities in the context of the tumor.

The scientific community in cancer biology and beyond has embraced a model for tumorigenesis in article "*The Hallmarks of Cancer*" [1] (2000) which received more than 30 000 citations reported in peer-reviewed academic journals. Published ten years later, the article "*The Hallmarks of Cancer: the next generation*" [112] (2011) received exceptional attention with more than 36 000 citations. In the initial paper, the authors have introduced cancer as a disease involving dynamic changes in the genome. They present tumor development as a process formally analogous to Darwinian evolution in which accumulation of genetic changes leads to the apparition of new characteristics conferring an advantage for tumor cells compared to normal cells. Considering the almost beyond measure corpus of data regarding cancer research, the authors of "*The Hallmarks of Cancer*" [1] established and discussed a limited number of characteristics shared by all cancer cell lines and tumors to propose a simple model of the tumorigenesis process (Fig. 1.6). These shared characteristics depend on genes promoting or inhibiting the transition from normal to tumor-associated phenotype. The corresponding proteins were historically classified as oncogene or tumor suppressor, respectively [113]. Six different capabilities were introduced to describe all different types of cancer cells, regardless the particular genetic profile of the cell. Self-sufficiency in growth signal was historically the first capability to be clearly established in cancer cell phenotypes [114, 115]. Reciprocally, cancer cells can turn insensitive toward anti-growth signals such as tumor suppressors that normally maintain the cellular quiescence and their inactivation can promote entry in the G1 phase of the cell cycle [116]. Intimately linked with proliferative capabilities, evasion of apoptosis is the third trait represented in all cancer cell types [117]. Inhibition of apoptosis can be achieved by different ways including survival factors production [118] and direct inhibition at the mitochondria [119]. The simultaneous acquisition of the proliferative potential and apoptosis resistance is rare in a normal pool of cells because proliferation constitutively promotes apoptosis and is repressed upon proapoptotic signaling [18] in differentiated cells of any tissue. The concept of cancer cell platform was proposed to describe a cell which acquired both proliferating capability and apoptosis resistance [47] and this can promote neoplasia upon proliferation, which is the early step of tumor manifestation at the tissue scale [120, 121]. The limitless replicative potential, often through telomerase activation [122], is the fourth trait of cancer cells. In solid tumors, sustained angiogenesis capabilities can be developed [123]. Finally, tissue invasion and metastasis is the ultimate capability of cells completing tumorigenesis. In the update of "*The Hallmarks of Cancer: the next generation*" [112], two major traits were added to the current description. Reprogramming of energy metabolism [124] and evading immune system [125] completed the criteria set, thus unifying all cancer cell types under a same phenotypical description.

## 1.2 TCTP protein is a switch of tumor reversion

In a rare but spontaneous and naturally occurring manner, cancer cells can lose characteristics of the associated phenotype to recover some characteristics associated with healthy cells, such as susceptibility toward apoptosis and proliferation arrest [126]. Such process was described as the tumor reversion program and represents the step beyond malignant transformation [127]. The TCTP protein was largely described in this context and is considered as a molecular switch of the signalization pathway. But TCTP protein has also many other roles and functions in cells unrelated to apoptosis and cancer. In the current section, we introduce the concept of tumor reversion and establish its relevance in cancer treatment regarding the literature and the work of our collaborators A. Telerman and R. Amson (IGR, CNRS/Université Paris-Saclay) (Sec. 1.2.1). Then, we discuss other partners and roles reported for TCTP in both cellular and physiological contexts (Sec. 1.2.2.2). We finally detail the role of TCTP in apoptosis pathway in the context of cancer cells (Sec. 1.2.3) as we extensively worked at unveiling the molecular basis that could explain the impact of TCTP protein on apoptosis inhibition and tumor reversion.

### 1.2.1 The tumor reversion at a glance

Tumorigenesis can represent a dedifferentiation process [2] in which highly specialized cells develop characteristics of undifferentiated cells with associated apoptosis resistance and proliferation capabilities. Reciprocally, tumor reversion can be described as a re-differentiation process by which highly tumorigenic cells lose a great extent of their malignant phenotype and can recover sensitivity toward apoptosis [126]. It should not be considered as an antagonist mechanism compared to tumorigenesis, but more as the step beyond malignant transformation [127], with accumulation of more genetic abnormalities from cancer to revertant cells (Fig. 1.7 B). First experimental evidences of tumor reversion were reported in 1907 upon re-differentiation of teratoma cells in normal somatic tissues [128]. Since then, tumor reversion was demonstrated in plants [129], upon viral infection and transformation of hamster cells [130], all-trans-retinoic acid administration for Acute Promyelocytic Leukemia (APL) treatment [131] and integrin blockers in both *in vitro* and *in vivo* [132] conditions, among others [127].

Ten years ago a comprehensive model was proposed after extensive review of available data in biological models of tumor reversion [127] (Fig. 1.7 B, C). Using erythroleukaemia (K562), myelomonocytic leukaemia (U937) and other human cell lines the authors have taken advantage of the H1 parvovirus capacity to preferentially kill cancer cells compared to

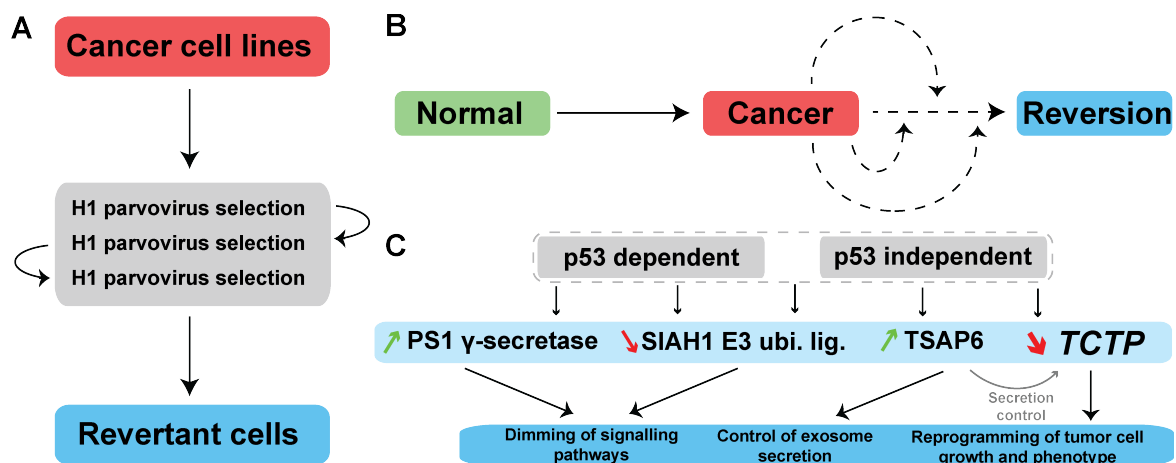


**Fig. 1.7 The tumor reversion at a glance** (A) Biological models of tumor reversion. To study tumor reversion in relevant cell models the H1 parvovirus (grey) is used to negatively select cancer cells (red) leading to the relative increase of revertant cell population (blue). Three rounds of selection are applied with specific regeneration periods to yield a pool of revertant cells. Upon selection, the resulting cell line is stable even in absence in selection pressure, suggesting that this cell has undergone specific reprogramming. (B) Theoretical model of tumor reversion. In normal cells (green) genomic instability can lead to cancer transformation (red). The tumor reversion results from further impairments in genomic integrity leading to recovery of characteristics of healthy cells (blue). From a single cancer cell, genomic events leading to tumor reversion can be multiple (dashed lines). (C) Overview of molecular pathways of tumor reversion. Initiation of tumor reversion can originate from p53-dependent or independent events. Major molecular hubs in regulating tumor reversion are presented: the E3 ubiquitin ligase SIAH1, the presenilin-1  $\gamma$ -secretase, the metalloredutase TSAP6 and the TCTP protein. All schemes are adapted from *"The molecular program of tumor reversion: the steps beyond malignant transformation"* [127].

normal cells [133]. Revertant cells were obtained after three rounds of negative selection using H1 parvovirus on cancer cell lines (Fig. 1.7 A). Historically, this experiment was done on erythroleukaemia cell line K562 and took more than three years to obtain K562 suppressed (KS) cells. These cells did not undergo re-differentiation upon selection, but the tumorigenicity was essentially lost after parvovirus H1 selection. The experiment was repeated with U937 cells from myelomonocytic leukaemia solid tumors. The U937 suppressed (US) revertant cells failed to grow in soft agar and very little tumorigenicity was observed upon injection of US cells in Severe Combined Immune Deficiency (SCID) mice. This highlights the potential of tumor reversion for cancer treatment since the natural process is very rare (one in  $10^6$ - $10^7$ ) upon application of H1 parvovirus and is unlikely to occur with clinical significance in human tumors. Next, proteomic studies and mRNA sequencing from revertant and cancer cells were done to identify both genetic determinants and molecular pathways of tumor reversion [134–137]. More than 300 different genes were recapitulated

and are implicated in the tumor reversion program [127] since their expression levels were modified from tumor cells U937 compared to revertant US cells.

Within the large gene ensemble, four were more extensively described by the historical authors and encode for hub proteins at the crossroad of various signaling pathways (Fig. 1.7 C). The E3 ubiquitin ligase SIAH1 and the transmembrane ferrireductase TSAP6 were upregulated in revertants whereas the protease PS1  $\gamma$ -secretase and the TCTP were downregulated in revertant cells [138, 137]. Upstream signaling relevant to tumor reversion at the four proteins are multiple and either p53-dependent or p53-independent. Moreover, cross-talks between the four proteins were reported as exemplified for TSAP6 which promotes exosome-mediated secretion of TCTP [138], reinforcing the highly intricate nature of the molecular routes in tumor reversion. The molecular pathway of tumor reversion was further developed [137, 139] and evidence has made TCTP the essential molecular switch to enable or disable tumor reversion. In cancer cells, high TCTP levels can inhibit apoptosis mainly in the context of both p53/Mouse Double Minute 2 homolog (MDM2) axis and Bcl-2 family proteins in the intrinsic apoptosis pathway. Lower TCTP levels promote tumor reversion, highlighting the protein as a key actor of phenotypic reprogramming from malignant to healthy-like phenotypes [140].

## 1.2.2 TCTP protein: structure, interactome and functions

### 1.2.2.1 Structure and conservation of TCTP protein

#### TPT1 gene encodes for the TCTP protein

The human TCTP gene (TPT1) includes six exons and five introns spanning on 3819 nucleotides and gives two different transcripts with variable 3'UTR length and no functional role established so far [141, 142]. TCTP messenger RNAs are highly structured and were shown to activate the dsRNA-activated protein kinase PKR [143]. Translationally Controlled Tumor Protein name originates from initial findings where the protein mRNAs were found abundantly in untranslated cytosolic particles [144].

#### Description of the human TCTP structure

At the protein level, alignment of TCTP primary sequences from diverse organisms showed strong conservation across phylogeny [145]. Several high-resolution structures of TCTP in different organisms were published from the first solution structure in *Schizosaccharomyces pombe* [146] to the recent in the microalga *Nannochloropsis oceanica* [147]. In all TCTP structures variations of position and length for secondary structure elements can be observed

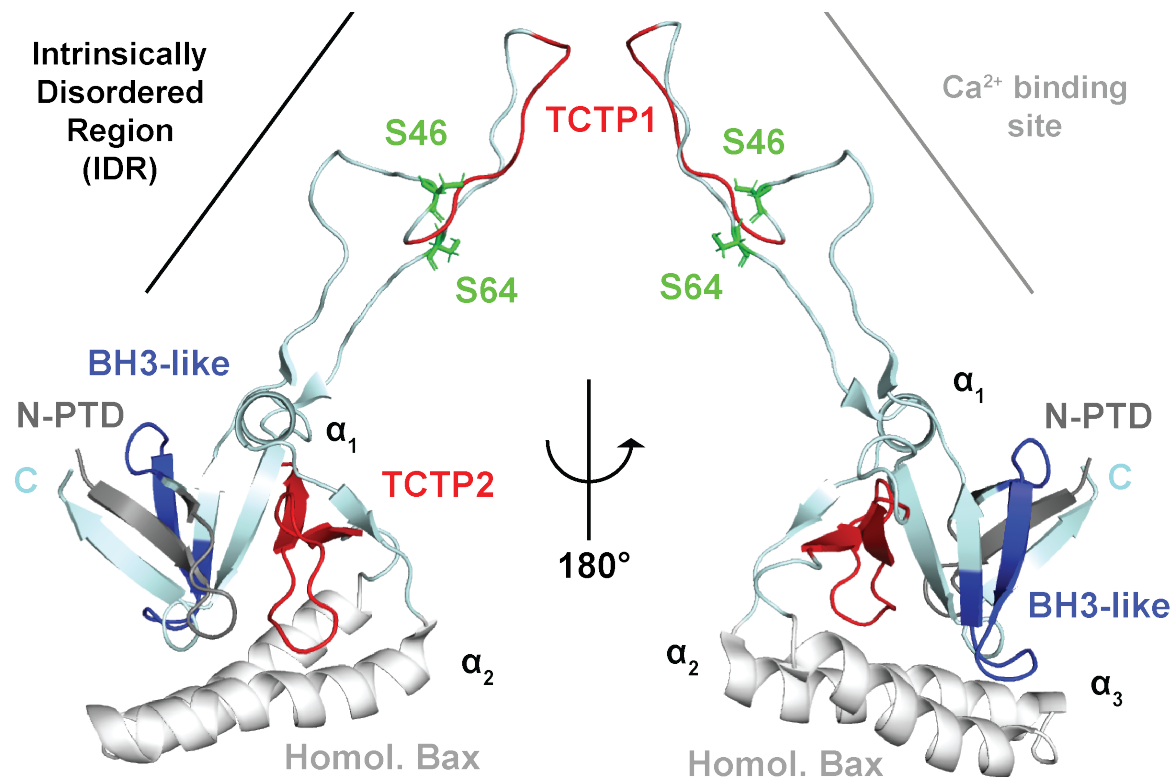


**Fig. 1.8 Structure of TCTP and particular elements.** The lowest energy structure from TCTP Nuclear Magnetic Resonance (NMR) ensemble (pdb code: 2HR9) is presented. Colors indicate the Protein Transduction Domain (1-13) (grey), the BH3-like region (15-29) (blue), the TCTP signature TCTP1 (48-56), TCTP2 (133-151) (red) and the Bax-homology domain H2-H3 (white). Phosphorylation sites S46 and S64 are also shown (green). The IDR (38-66) and seat of calcium binding is highlighted.

with no important differences in term of structure elements and tertiary organization. Here, we report the solution structure of human TCTP (Fig. 1.8).

TCTP is usually described as a monomeric protein and is a small (20 kDa), single-domain entity which includes a globular core and an internal IDR which projects far away from the globular domain of the protein. The TCTP fold contains three  $\alpha$ -helices ( $\alpha_1$ ,  $\alpha_2$  and  $\alpha_3$ ) and eleven  $\beta$ -strands. These are arranged in a small  $\beta$ -sheet  $\beta_5, \beta_6$  and two larger  $\beta$ -sheets  $\beta_7, \beta_8, \beta_9$  and  $\beta_{10}, \beta_4 - \beta_3$ . The two latter  $\beta$ -sheets arrange together to adopt  $\beta$ -tent organization [148].

Despite no evolutionary link established so far between TCTP and other proteins, a structural homology between  $\alpha$ -helices H2-H3 of TCTP and H5-H6 of Bax was suggested [149] with possible implications for TCTP insertion into the MOM. Finally, the N-terminal contains an elevated number of residues for which no variation was observed across phyla. TCTP

protein has conserved signatures TCTP1 (48-56) and TCTP2 (133-151) in the IDR with no functional role documented at the beginning of this PhD thesis. Also in the IDR, residues S46 and S64 are targets of the Plk-1 and are highly conserved in all aligned mammalians sequences (Fig. 1.8).

### The BH3-like motif in TCTP protein

Most importantly in the frame of the current work, TCTP contains a N-terminal BH3-like motif [111] embedded in the globular domain of the protein (Fig. 1.8) with strong conservation. The BH3-like motif in TCTP is between residues D16 (h1) and L27 (h4) and is a short amino-acid sequence involved in the regulation of the intrinsic apoptosis pathway via interactions with Bcl-2 family proteins. Compared to canonical BH3 motifs, the BH3-like motif of TCTP (TCTP<sub>BH3</sub>) contains I20, I23 and L27 at conserved positions h2, h3 and h4 but lacks an hydrophobic residue in position h1 were D16 is strictly conserved across the phylogeny.

#### 1.2.2.2 TCTP interactome and functional consequences

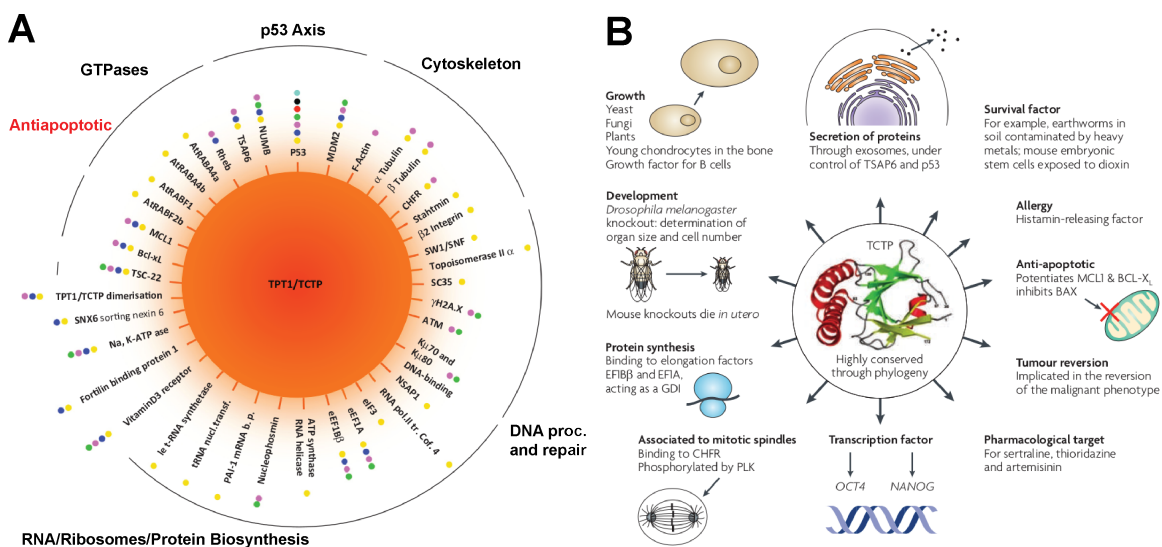


**Fig. 1.9 Interactome and functions of TCTP protein.** (A) Schematic representation of the proteins interacting with TCTP [140]. Identification or partners by yeast two-hybrid screening (yellow), co-immunoprecipitation of overexpressed proteins (blue), subcellular colocalization, Surface Plasmon Resonance (SPR) and pull-down assays (pink), immunoprecipitation of endogenous proteins (green), genetic interactions in murine models (red), use of pharmacological agents (black), or clinical relevance in a cohort of breast cancer patients (turquoise). These TCTP interactions with other proteins are represented according to seven functionally different categories [140]. Partners are grouped by type of underlying function. The list is not exhaustive and was updated recently [145]. (B) TCTP is a multifunctional protein [127].

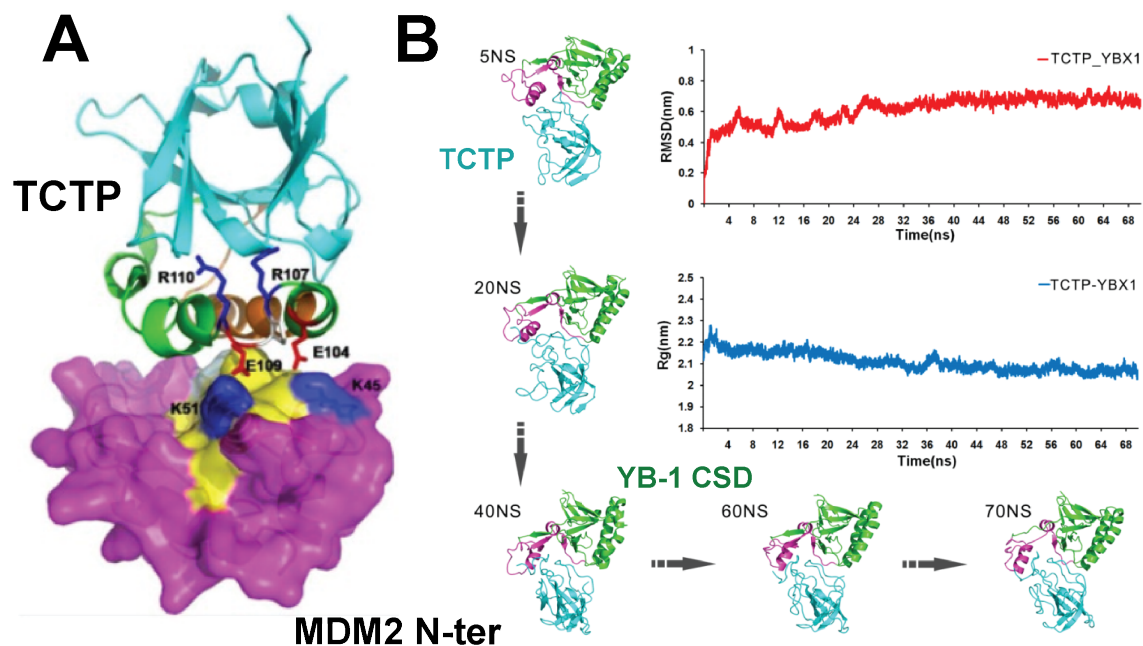


Fig. 1.10 **Structural model of TCTP/Y-Box associated protein 1 (YB-1) and TCTP/MDM2 complexes [150, 151].** (A) Model of the putative interactions between TCTP and the MDM2 N-terminal domain [150] (B) Molecular Dynamics (MD) simulation of TCTP and YB-1 [151]. Representative conformation snapshots of the TCTP/YB-1 (1–129) complex structure in the period 70 ns. Root Mean Square Deviation (RMSD) and radius of gyration (Rg) of the TCTP/YB-1 (1–129) complex.

The variety of TCTP partners led to a myriad of cellular and physiological functions for TCTP protein. These include development and cancer, immune system, gene expression, mitosis and more [127] (Fig. 1.9 B). Experimentally validated protein partners for TCTP were extensively reported a few years ago [140] (Fig. 1.9 A). These partners were classified according to their functions and range from anti-apoptotic proteins to cytoskeleton, DNA processing and repair, GTPases, p53 axis, cytoskeleton and mitotic machinery and RNA/ribosome/protein biogenesis. The list was recently updated [145] since several other TCTP partners were reported within the past six years including YB-1 [151] or IgE/IgG [152] proteins. Moreover, TCTP has many different localization and can be found in the cytosol, mitochondria, nucleus or even in the extracellular space. In this section, we report several interactions and associated functions of TCTP protein, including TCTP self-association and cytokine-like activity. We also discuss the importance of post-translational modifications in regulating the protein interaction and function. In the next section, we will more extensively focus on apoptosis-related interactions since it represents the core of the current study.

**TCTP in development**

TCTP is required for embryonic development in mice and is a transcription factor for genes Oct4 and nanog that repress genes associated with differentiated cells [31]. In this context, TCTP can prevent cells from undergoing differentiation and this can be one reason why it is important in development, since embryonic cells must have proliferative and pluripotency potentials which is a definition of non-differentiated cells.

**TCTP in protein synthesis**

Interestingly, TCTP interacts with the elongation factor eEF1B [153]. Using a structural approach, it was shown that TCTP interacts with eEF1B using predominantly its highly basic helical domain ( $\alpha_2$ ,  $\alpha_3$ ) by conserved hydrophobic and electrostatic interactions. Herein, this interaction is related to protein synthesis. Indeed, TCTP is found in all eukaria and p53 is not found in plants, for example. It is tempting to think that divergence in protein conservation across species is an indication that p53 might not be the first interest of TCTP in cells and the authors of the paper we mentioned proposed that the more largely conserved TCTP/eEF1B interaction might represent a primary role for TCTP in normal and deregulated cells.

**TCTP and the mammalian Target Of Rapamycin (mTOR) pathway**

TCTP/TPT1 has no evolutionary link reported with other proteins/genes, even though the protein was found structurally related to the Mss4/Dss4 chaperone family. Although challenged since the first study, TCTP was shown, as for Mss4, to be a weak Guanine nucleotide Exchange Factor (GEF). The suggested role of TCTP as a GEF at the GTPase Rheb in *Drosophila melanogaster* [154] led to also describe TCTP in the context of the mTOR pathway, since Rheb regulate mTOR proteins complex. The mTOR pathway regulates many processes in cells, such as cell size and number, and is described as a sensing system for the integration of environmental and intracellular signals.

**TCTP, Heat shock protein 27 (Hsp27) and chaperone activity**

Interestingly, TCTP was also identified as a chaperone protein with role in stress response. Reciprocally, chaperone protein that target TCTP were reported with, for example, Hsp27 protein [155]. The TCTP/Hsp27 interaction has a pro-survival impact in Castration-Resistant Prostate Cancer (CRPC) cells since Hsp27 inhibits stress-induced ubiquitination and proteosomal degradation of TCTP. In the context of the castration-resistant prostate cancers, TCTP emerges as an apoptosis inhibitor and a pharmacological target of choice since it is usually not expressed at high levels in healthy, differentiated cells. The antisense oligonucleotide (ASO) approach was used to target TCTP mRNA in a CRPC context and did restore p53 expression and function. Interestingly, the sensitivity of cells for docetaxel, an anti-tumor agent, was raised upon targeting of TCTP using the ASO drug. This emphasizes on the opportunity to

develop TCTP-based bi-therapy for cancer treatment, as we will discuss latter of ongoing clinical trial with sertraline and Ara-C drugs in a bi-therapy context (Sec. 1.2.3.3).

### **Self-association of TCTP protein**

Before its identification as a molecular switch of tumor reversion, TCTP was first described as Histamine Releasing Factor (HRF) with cytokine-like activity in allergy response. The cytokine-like activity was linked with the presence of covalent TCTP dimers forming upon short (1-11) or long (1-35) truncation of the N-terminal region [156]. In the same study, the covalent dimerization involved predominantly the C-terminal, solvent-exposed C172 residue but covalent dimers could still be detected upon C172S mutation, which demonstrated that TCTP can still form covalent dimers via C28 residue. This is surprising considering that residue C28 is included in the BH3-like motif of TCTP which is buried in the hydrophobic core of the protein, not readily accessible for disulfide bond formation. As mentioned, TCTP covalent dimers form upon short (1-11) or long (1-35) truncation of the N-terminal in TCTP and this first truncation (1-11) could free the BH3-like region (15-29) from the anchoring to TCTP core, thus allowing for covalent dimers formation. Notably, the presence of the same covalent TCTP dimer was confirmed *in vivo* in the sera of atopic and asthmatic patients and in Broncho-Alveolar Lavage Fluids (BALF) from mice with airway inflammation but could not be detected in cells which suggests that this covalent dimer has existence and functions outside of cells, in a more physiological perspective. Interestingly, the anti-malarial drug artemisinin was shown to bind TCTP and to also induce the formation of covalent dimers [157] in presence of heme. The authors suggested that the drug could bind to preformed TCTP dimers related to its cytokine-like activity in allergy-related pathways. They propose the mechanism to be part of the anti-malarial effect of artemisinin and also relate the importance of C172 residue for disulfide bond formation.

Even though TCTP protein is most often described to be monomeric in solution as shown by the solution structures of the native protein from various species, covalent and non-covalent dimers of TCTP were reported in the literature under particular circumstances. Non-covalent dimers and oligomers were found by yeast two-hybrid screen with cDNA library from rats [158] and upon heme addition [159]. Interestingly, hemin-induced TCTP dimer was found more resistant to urea denaturation than the monomeric form promoted upon calcium addition. Non-covalent interactions between TCTP units in crystals from the protein were conserved through species, giving indications about possible interfaces for non-covalent dimers in solution.

### 1.2.2.3 The pleiotropic YB-1 protein associates with TCTP

Among the recently identified TCTP-binding protein, YB-1 is a pleiotropic protein originally described for its role in DNA transcription but has recently emerged as a potential biomarker and novel therapeutic target [160]. TCTP was recently found to interact with YB-1 protein [151]. Using co-immunoprecipitation (co-IP) and Mass Spectrometry (MS) in HeLa cells the authors found 98 different TCTP partners and the interaction with YB-1 was confirmed through *in vitro* and *in vivo* experiments. The authors have demonstrated the dependence of the interaction toward segments of YB-1 (1-129) and TCTP (42-83). Additionally, they have calculated a structural model of the complex in direct interaction through MD experiments (Fig. 1.10 B). However, no information regarding the interplay of YB-1/TCTP and RNAs was unveiled yet. Indeed, unpublished data suggest that TCTP and YB-1 could be involved in RNA sorting and more specifically the subcellular and extracellular distribution of RNA.

### 1.2.2.4 Post-translational modifications in TCTP protein

TCTP is predicted to undergo Post-Translational Modifications (PTM) [145] after estimation with the ELM server [161]. Among these, phosphorylation at residues S46 and S64 by Plk-1 was confirmed *in vivo* and was required for correct mitosis [33] and meiosis [32] termination. Indeed, the phosphorylation events in TCTP IDR permits to detach TCTP from the mitotic spindle [31], thus allowing to proceed in anaphase and further to achieve cell division. This example of PTM in TCTP IDR influences the localization of TCTP [33, 162, 163] and S46 phosphorylation is also a biomarker of Plk-1 activity in cancer cells as well as a prognosis factor [164] with potential interest in anti-cancer strategy. In another study, only phosphorylated TCTP at residue S46 was reported in mitotic cells [165]. Others *In vitro* experiments [166] suggest that TCTP could be phosphorylated at position S64 in specific conditions. In general, a hierarchical mechanism is proposed for Plk-1 mediated phosphorylation of protein targets. Moreover, S46 residue is conserved across all eukarya whereas S64 is only conserved in mammals. Thus, the impact of the couple might then be limited to higher eukarya. Other sites were experimentally reported to be phosphorylated upon particular events. Residues S9 and S15 in an insulin-dependent manner [167] and T39, S53 in mitotic cells [165]. Different other PTM events were experimentally validated such as N-glycosylation [168] and sumoylation. The latter contributes to regulate TCTP localization in cells [169]. Notable predicted PTMs include cleavage sites for caspases 3 and 7 in solvent-exposed regions of the protein.

### 1.2.3 TCTP-regulated pathways in apoptosis and tumor reversion

#### 1.2.3.1 Apoptosis inhibition routes

TCTP directly interacts and regulates several proteins involved in cell cycle and apoptosis regulation including the E3 ubiquitin ligase MDM2 [170] and the antiapoptotic Bcl-2 family proteins Bcl-xL [171] and Mcl-1 [172]. The pro-survival properties of TCTP in cancer cells is likely to originate at least in part from these interactions since TCTP diminishes p53 levels via inhibition of MDM2 autoubiquitylation [173] and stimulates the antiapoptotic properties of Bcl-2 family members Bcl-xL and Mcl-1 [171, 172].

On the p53 axis, TCTP was reported to directly interact with p53-MDM2 containing complexes in a competitive manner with NUMB [173]. The direct nature of TCTP and MDM2 interaction was validated *in vitro* by SPR experiments [173] and TCTP was shown to inhibit MDM2 auto-ubiquitylation in functional assays, thus promoting p53 proteasome-dependent degradation. TCTP was proposed to bind MDM2 C-terminal domain through its N-terminal segment (1-68). In another study a small molecule known to promote apoptosis and cell cycle arrest by blocking binding between MDM2 and p53 had inhibitory effect on TCTP and MDM2 interaction, suggesting a common binding site for p53 and TCTP on MDM2 protein [150]. This suggests that TCTP may have multiple binding sites on MDM2 to regulate its activity and p53 cellular fate. In the same study, the interaction site was in MDM2 N-terminal domain and the Bax-homology domain ( $\alpha$ -helices  $\alpha_2$ ,  $\alpha_3$ ) in TCTP (Fig. 1.10 A). To add complexity in the interplay, the direct binding of TCTP to p53 and its functional impact was also reported a few years ago [174]. The authors developed an overexpression system of TCTP and p53 in lung carcinoma cancer cells and found that TCTP overexpression reversed p53 mediated apoptosis. Consistently, RNA silencing of TCTP did restore apoptosis in the corresponding cells. Overexpression of TCTP was accompanied by degradation of p53, consistently with the suggested inhibition of MDM2 degradation upon interaction with TCTP.

Although controversial, TCTP could also inhibit apoptosis by scavenging calcium ions upon efflux from the Endoplasmic Reticulum (ER) [175, 176]. To summarize, TCTP prevents cancer cells from undergoing tumor reversion at least in part by inhibiting apoptosis and thus favoring tumor cells maintenance and progression.

### 1.2.3.2 TCTP and Bcl-2 family members Bcl-xL and Mcl-1 at the MOM

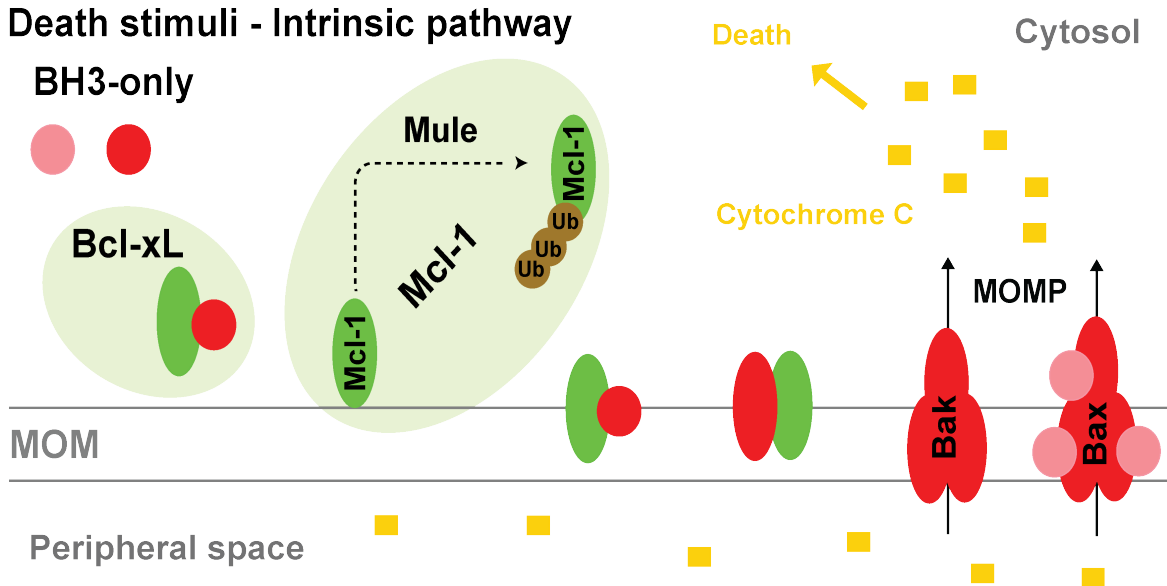
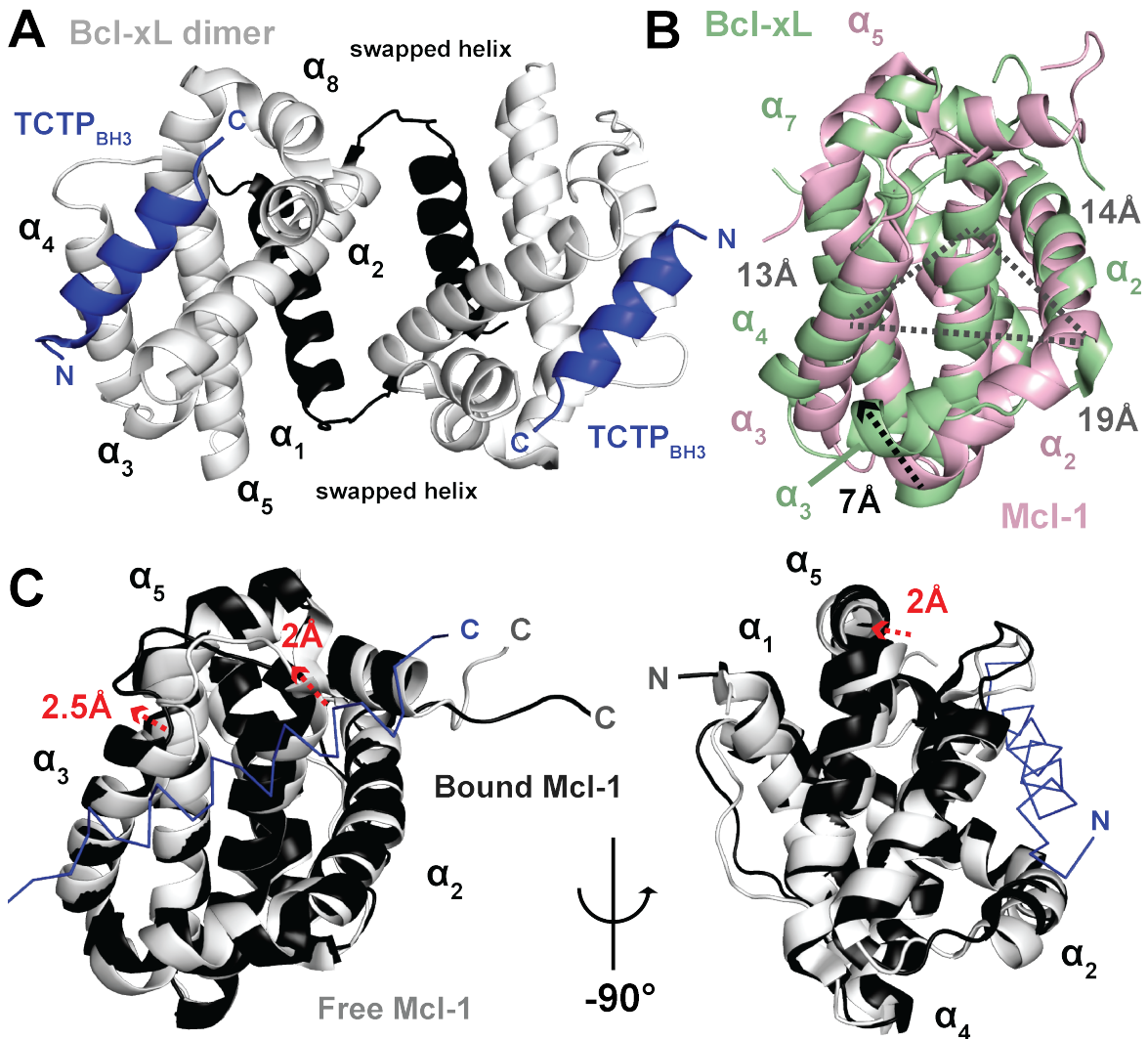


Fig. 1.11 **Intrinsic pathway activation via BH3-only proteins.** In presence of cellular stress such as DNA damage BH3-only proteins are induced by tumor suppressors such as p53. These can be activators BH3s and bind Bax-related proteins (pink circle) or they can be sensitizer BH3s (red circle) and inhibit antiapoptotic Bcl-2 family proteins to prevent heterodimerization with proapoptotic Bcl-2 proteins. The latter can oligomerize to form pores in the MOM, leading to membrane permeabilization, cytochrome c release and death induction. For Bcl-xL, the cytosolic dimer is reported to dissociate upon ligand binding, but cytosolic heterodimers can still be observed. Additionally, Mcl-1 undergoes a fast degradation through the proteasome pathway, possibly under the dependence of the E3 ligase, such as Mule.

#### Regulation of the Bcl-2 family by BH3-only proteins

Bcl-2 family members can be regulated by BH3-only (Fig. 1.11) and non canonical BH3 containing proteins, referred to as BH3-like proteins. In general, BH3-only and BH3-like proteins are proapoptotic in the context of the intrinsic apoptosis pathway and thus they inhibit antiapoptotic Bcl-2 family members or activate proapoptotic proteins from the same family. Even though Bcl-2 family proteins share common structural properties, they have specific BH3-only protein partners [177] and mode of action. This was theorized by the "embedded together" model [178, 179, 99, 180] and simplified "unified" model [88] which describe the interplay between Bcl-2 family and BH3-only proteins at the MOM in the context of pro-death stimuli. BH3-only proteins that inhibit antiapoptotic Bcl-2 family members such as Bcl-xL and Mcl-1 are said sensitizer BH3s. BH3-only proteins that activate proapoptotic Bcl-2 family members such as Bax are activator BH3s. Inhibited Bcl-xL and Mcl-1 could not heterodimerize anymore with Bax and Bak, respectively. Bax is activated



**Fig. 1.12 Structures of free Bcl-xL and Mcl-1 and complex with BH3 peptides.** (A) Crystal structure of Bcl-xL/TCTP<sub>BH3</sub> [111]. Bcl-xL (white) and swapped helix  $\alpha_1$  (black) as well as TCTP<sub>BH3</sub> (blue) are differentiated. (B) Structural alignment of free Bcl-xL (pdb code: 2ME9) (green) and Mcl-1 (pdb code: 2MHS) (pink). (C) Structural alignment of free Mcl-1 (pdb code: 2MHS) (white) and upon complex formation with Mule<sub>BH3</sub> (pdb code: 5C6H) (black). Mule<sub>BH3</sub> (blue ribbon) is shown.

by the direct binding of activator BH3 and can then oligomerize in the MOM, as Bak also does from its free state directly, leading to pore formation and membrane permeabilization, cytochrome c release and subsequent activation of the intrinsic apoptosis pathway. In term of cellular localization in presence of death stimuli, Bcl-xL and Mcl-1 exist as MOM-anchored heterodimer with sensitizer BH3 or proapoptotic Bax and Bak, respectively. Mcl-1 can be readily degraded via the proteasome pathway upon binding and ubiquitinylation by Mule, an E3 ubiquitine ligase with canonical BH3 sequence that targets Mcl-1 (Fig. 1.11).

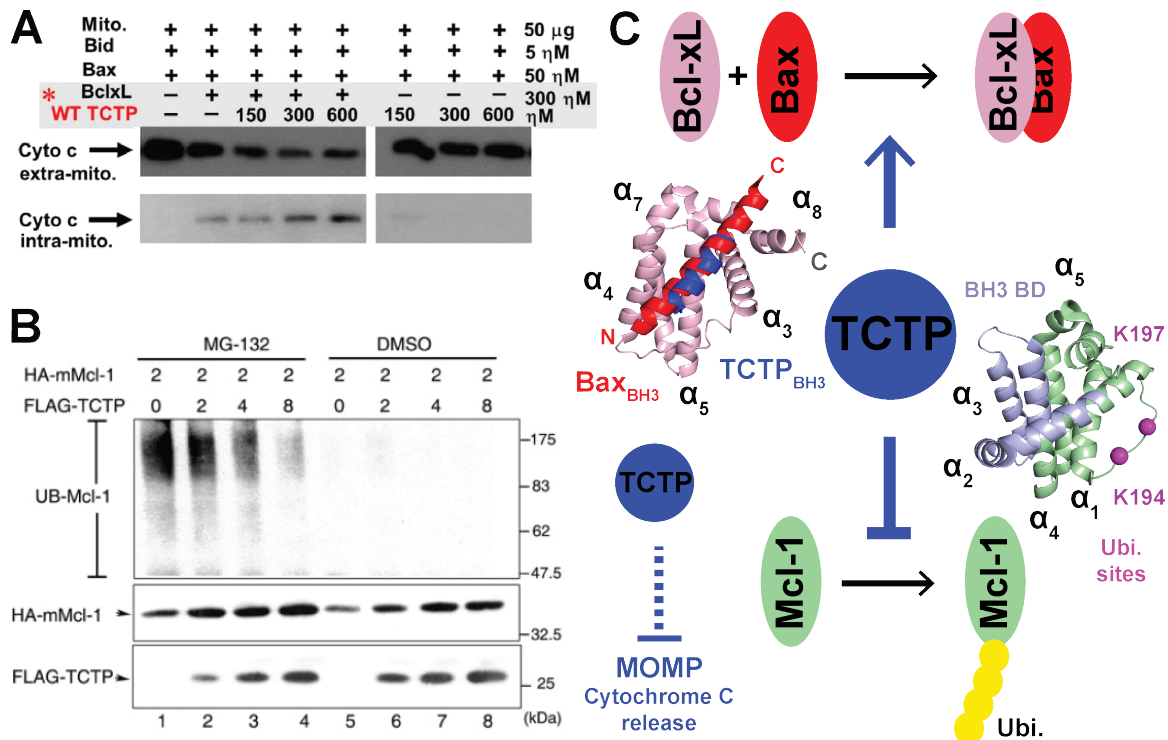


**Fig. 1.13 State of the art in TCTP complex with Bcl-xL and Mcl-1.** (A) Mitochondrial membrane permeabilization assay with TCTP at increasing concentrations on a Bcl-xL/Bax *in vitro* mitochondrial membrane permeabilization assay [111]. (B) Detection of ubiquitinated Mcl-1 at increasing concentration of TCTP [172]. (C) Graphical overview of the TCTP effect on Bcl-xL/Bax association and Mcl-1 ubiquitinylation. Crystal structure of Bcl-xL/TCTP<sub>BH3</sub> [111] and Bcl-xL/Bax<sub>BH3</sub> are shown with the structure of isolated Mcl-1 (pdb code: 2MHS) with highlight on K194, K197 ubiquitinylation sites (magenta) and BH3 binding groove (mauve).

### TCTP stimulates the antiapoptotic Bcl-xL to promote Bcl-xL/Bax interaction

TCTP and Bcl-xL interaction was reported to be dependent of the N-terminal region of TCTP [171] and to be abolished upon R21A and Y101K mutation at TCTP or Bcl-xL [111], respectively. In this context, the anti-apoptotic activity of TCTP was linked to its capacity to bind Bcl-xL. The N-terminal region of TCTP was shown to contain a BH3-like motif [111] with residue D16 in position h1 where canonical BH3 motifs have conserved hydrophobic type of residue. Despite being anchored in a globular domain and structured, the BH3-like motif still interacts with Bcl-xL but efficiently form complexes only in alkaline (pH 9) conditions, low salt concentration (50 mM NaCl) and high temperature (35 °C). This suggests a high energetic cost for the TCTP and Bcl-xL complex to assemble. In the crystal structure of Bcl-xL/TCTP<sub>BH3</sub> published in 2016, the BH3-like peptide adopted an helical conformation in the BH3 binding groove of Bcl-xL, forming a heterotetrameric complex with 3D swapped Bcl-xL dimer (Fig. 1.12). Interestingly, the main difference in the binding of TCTP to the

BH3 binding groove of Bcl-xL compared to canonical BH3 of higher affinity is the absence of the first helix turn just before canonical h1 position, which is non-conserved in TCTP since D16 residue is present [111]. This also presumes that full length TCTP should undergo a dramatic structure and dynamics change to accommodate in the crystal structure of the Bcl-xL/TCTP<sub>BH3</sub> complex since the BH3-like motif is  $\alpha$ -helical as a bound peptide whereas it is a  $\beta$ -sheet in free full length TCTP (TCTP FL).

In a functional frame, it was reported from mitochondrial membrane permeabilization assay that TCTP inhibits Bax dependent cytochrome c release by interacting with Bcl-xL, since it was also shown to not interact with Bax. This means that TCTP potentiates Bcl-xL ability to interact with Bax protein, reducing Bax oligomers and pores formation, finally preventing cytochrome c release (Fig. 1.13 A). It is unknown how full length TCTP could promote Bcl-xL/Bax interaction, especially when considering that BH3 peptides from Bax and TCTP do share the same binding pocket in Bcl-xL protein (Fig. 1.13 C). This could be possibly mediated by Bcl-xL 3D swapped dimer, since this form crystallized with TCTP<sub>BH3</sub> (Fig. 1.12 A) whereas it was reported that Bcl-xL self-oligomerization could compete with binding of BH3 ligands [83].

### **TCTP/Mcl-1 interaction has pro-survival impact**

TCTP was also proposed to stabilize Mcl-1 against proteasome-dependent degradation [172] by reducing its ubiquitinylation, thus reinforcing its anti-apoptotic signaling (Fig. 1.13 B). In another study, it was proposed that Mcl-1 itself did stabilize TCTP [181]. Despite unclear mechanism, the functional interaction between TCTP and the Bcl-2 family protein Mcl-1 could also be mediated by the BH3-like motif in TCTP, as shown with Bcl-xL. To explain how TCTP could inhibit Mcl-1 ubiquitinylation, the protein could either mask the ubiquitinylation sites K194 and K197 in Mcl-1 or compete with the E3 ligase Mule to bind the BH3 binding groove of Mcl-1 if we consider the  $\Delta$ PEST  $\Delta$ TM protein truncate generally used for structural studies (Fig. 1.13 C). Interestingly, it was reported that TCTP and Mcl-1 achieve their antiapoptotic functions independently, since siRNA strategies in Human Bone Osteosarcoma Epithelial Cells (U2OS) showed that upon silencing of TCTP or Mcl-1, the remaining partner was still able to protect cell from 5-FU induced apoptosis in a dose-dependent manner [182]. Thus, the biological relevance of this interaction between TCTP and Mcl-1 could be linked to the mutual stabilization of TCTP and Mcl-1, thus allowing both proteins to exert their antiapoptotic functions.

### **Binding profiles of BH3 ligands at Mcl-1 protein**

Since we more extensively worked on Mcl-1 protein compared to Bcl-xL, we report a NMR study with a human Mcl-1 construct. In this work, the binding of Bid<sub>BH3</sub> induced spectral

perturbations from residues at the BH3 binding groove ( $\alpha_{2-4}$ ) but also in helix  $\alpha_5$  [89], with respect to the nomenclature of the manuscript (Fig. 1.12 B). In the same study [89], the authors claim these perturbations are consistent with published structures of Mcl-1 complex. The helix  $\alpha_5$  in Mcl-1 is seen to displace upon binding of BH3 ligands, which explains why it is affected whereas it does not define the BH3-binding groove of the protein. We give an example with the Mcl-1/Mule<sub>BH3</sub> complex (Fig. 1.12 C) (pdb code: 5C6H) where  $\alpha_5$  moves from 2 Å backwards in the bound Mcl-1 state compared to free state. Between the free and bound Mcl-1 structure, helix  $\alpha_5$  is pushed by helix  $\alpha_3$  which moves from 2.5 Å.

### 1.2.3.3 TCTP-inhibitors for cancer treatment

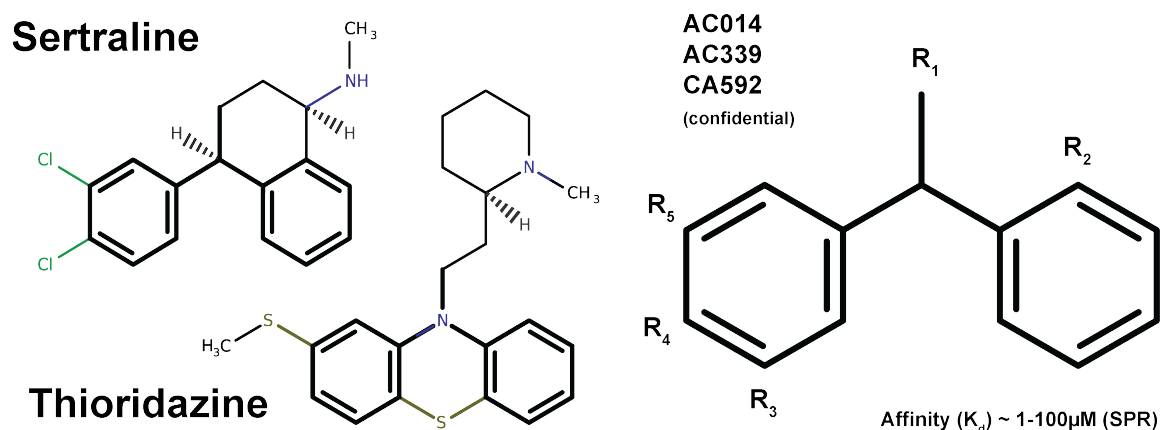


Fig. 1.14 **Ligands targeting TCTP available for studies.** The conserved molecular scaffold is highlighted (thick black bars). Molecules name are indicated and atoms are colored according to their type.

TCTP is a pharmacological target of interest in cancer treatment [183], especially when considering that its overexpression is often associated with malignancy and chemoresistance, consistently with its major role as a blocker of tumor reversion and apoptosis recovery. Historically, antihistamine drugs were thought to be putative inhibitors of TCTP since the protein was first identified through its activity in histamine release. Based on this idea, the antihistamine drug hydroxyzine was shown to bind TCTP and to decrease its levels in cell, and to present anti-tumoral activity [139]. Hydroxyzine is a substituted piperazine which has antagonist activity at histamine H<sub>1</sub> receptors in smooth muscles, vascular endothelial cells, heart and Central Nervous System (CNS). On-label use of hydroxyzine includes itchiness, anxiety, nausea and other histamine-related allergies. In the hydroxyzine molecule, the piperazine scaffold is substituted by a substituted diphenylmethyl- motif. Research for structurally close molecules led to discover more efficient drugs at targeting TCTP in both

*in vitro* binding assays and *ex vivo* or *in vivo* contexts. These were other antihistamine drugs [184] or the antipsychotic thioridazine [139, 185, 173, 186] and the antidepressant sertraline [139, 173, 186]. Thioridazine has a phenothiazine scaffold where the diphenylmethyl is conserved through the analogous diphenylamine- motif. It has an antagonist activity at dopamine D<sub>1</sub> receptors and is used as antipsychotic in psychiatry. Sertraline contains the diphenylmethyl- scaffold and is a famous antidepressant, number two in the USA under the brand name Zoloft. It is a Selective Serotonin Reuptake Inhibitor (SSRI) and binds to the serotonin transporter (SERT) in the CNS, principally. Interestingly, both drugs were shown to have anti-tumor activity in lung cancer thus permitting longer survival in patients when administrated for depression-related purpose, originally [187]. Targeting TCTP to induce tumor reversion with sertraline was tested through clinical studies phase I and II about fifteen years ago which were stopped due to unfavorable benefit/risk balance [188]. Nowadays, sertraline is tested in bi-therapy with cytosine arabinoside in adults with relapsed and refractory AML [189].

Sertraline and thioridazine were shown to directly bind TCTP by SPR [173] experiments with 34  $\mu$ M and 47  $\mu$ M dissociation constant ( $K_d$ ), respectively. The interaction between TCTP and sertraline was also observed by Thermal Shift Assay (TSA) where, surprisingly, the molecule did destabilize TCTP and decrease its melting temperature by five degrees [155], while intermolecular molecular interaction usually stabilizes complexes. The impact of thioridazine and sertraline in elevating p53 levels in cells was proposed to be mediated by TCTP since the interaction between TCTP and MDM2 is inhibited upon ligands addition *in vitro*, thus recovering higher p53 levels *in vivo* [173]. However, the binding interaction between TCTP and the molecules was not confirmed by other techniques and data describing the binding site of the molecules on TCTP are still unavailable. We know that phosphorylation mimetics with mutations S46E and S64E did abolish ligand binding, suggesting that the TCTP IDR where the two phosphorylation sites are located might be involved in the association process. Moreover, a study confirmed the *in vitro* interaction of TCTP with phenothiazine-derived ligands by Microscale Thermophoresis (MST) with similar affinities in the micromolar range. Further docking experiments have shown that all molecules docked at the same site on the TCTP IDR. The binding pocket included path T39-I48 and E60-T65, both containing the phosphorylation sites S46 and S64. However, this study was done on a single conformation of TCTP whereas the IDR is described to sample conformations highly divergent between each other considering the highly flexible nature of the protein segment. Besides the well known inhibitors such as sertraline and thioridazine, our collaborators A. Telerman and S. Messaoudi's group are currently developing new molecules based on a novel scaffold to improve TCTP inhibition (Fig. 1.14) with micromolar affinity in SPR experiments and are

of interest to study by NMR in order to further improve drug development targeting TCTP protein.

### **1.3 Structural insights into TCTP and its interactions with ligands and proteins**

We published a chapter in the book [145] in TCTP/TPT1 - Remodeling signaling from stem cell to disease [190] after invitation from our collaborators A. Telerman and R. Amson (IGR, CNRS/Université Paris-Saclay). We reported data from the literature regarding TCTP interactions with partners of diverse nature such as proteins, peptides, nucleic acids, carbohydrates or small molecules in both structural and functional perspectives. We also extensively described TCTP structure, post-translational modifications, conservation and structural resemblances to evolutionary unrelated proteins. Even though high-resolution data are still poor concerning TCTP and its interactions, we reported that most TCTP surface patches are potential binding sites as compared with structurally related proteins from the  $\beta$ -tent family [148]. Interestingly, the essential of the published experimental work regarding binding sites in the protein were obtained by peptidic approaches of questionable relevance since the protein is a single-domain entity, thus likely loosing its tertiary organization upon production of separated segments. This raises the need for interaction studies with full length TCTP to confirm and complement the work with peptides but also encourages to think that TCTP has a labile structure. Indeed, if unfolded peptides from TCTP are functional at partners, we can expect them not to be active in the context of the well folded protein. We develop the case example of the BH3-like motif at Bcl-xL and Mcl-1 that is buried and not accessible for interaction in the native protein. As the main conclusion of the book chapter, we predicted that TCTP could undergo major structural rearrangements upon binding to partners

### **Structural Insights into TCTP and Its Interactions with Ligands and Proteins**

Nadine Assrir, Florian Malard, and Ewen Lescop

# Structural Insights into TCTP and Its Interactions with Ligands and Proteins

Nadine Assrir, Florian Malard, and Ewen Lescop

**Abstract** The 19–24 kDa Translationally Controlled Tumor Protein (TCTP) is involved in a wide range of molecular interactions with biological and nonbiological partners of various chemical compositions such as proteins, peptides, nucleic acids, carbohydrates, or small molecules. TCTP is therefore an important and versatile binding platform. Many of these protein–protein interactions have been validated, albeit only few received an in-depth structural characterization. In this chapter, we will focus on the structural analysis of TCTP and we will review the available literature regarding its interaction network from a structural perspective.

## 2.1 Introduction

This chapter will focus on the structural aspects of TCTP in the context of its wide interaction network, with the aim of being as comprehensive as possible. First we will describe the available structures of TCTP and compare them with other structurally related proteins. Then in a second part, we will discuss the properties of some amino acid regions of TCTP that are important due to their conservation and/or specific functions. Then the last two parts will describe the large interactome of TCTP involving non-proteic or proteic molecules. Two recent reviews (Kawakami et al. 2012; Amson et al. 2013) also covered part of the topics of this chapter. However, the last 4 years have witnessed astonishing progress in TCTP field, and we felt that an updated description of TCTP interactome was necessary. We believe this chapter will be useful not only for the general reader but also for TCTP experts, to overcome the difficulties associated with the multiple names of TCTP found in literature. Indeed, depending on its intra- or extracellular localization, or on the species, TCTP is also called Histamine-Releasing factor (HRF), p23, p21, Q23, fortilin, Mmi1p (yeast), or Tpt1. This confusing nomenclature

---

N. Assrir • F. Malard • E. Lescop (✉)

Institut de Chimie des Substances Naturelles, CNRS UPR2301, Université Paris-Sud,  
Université Paris-Saclay, 1 avenue de la Terrasse, 91190 Gif-sur-Yvette, France  
e-mail: [Ewen.LESCOP@cnrs.fr](mailto:Ewen.LESCOP@cnrs.fr)

© Springer International Publishing AG 2017

A. Teلمان, R. Amson (eds.), *TCTP/tpt1 - Remodeling Signaling from Stem Cell to Disease*, Results and Problems in Cell Differentiation 64,  
DOI 10.1007/978-3-319-67591-6\_2

9

undoubtedly hinders the diffusion of knowledge on this protein within the community and hence slows down the progress of its characterization.

## 2.2 Sequence and Structure of TCTP

### 2.2.1 Description of the Structure of TCTP

The high-resolution structures of TCTP from different organisms have been determined by NMR or X-ray crystallography (see Fig. 2.1). These include the malaria parasites *Plasmodium falciparum* (Eichhorn et al. 2013) and *knowlesi* (Vedadi et al. 2007), the yeast *Schizosaccharomyces pombe* (Thaw et al. 2001), the worm *Caenorhabditis elegans* (Lange et al. 2012), and wild type (Feng et al. 2007; Susini et al. 2008) or E12V mutant (Dong et al. 2009) human TCTP. The structures of TCTP are highly conserved between different organisms. TCTP is a monomeric protein, although covalent and non-covalent TCTP dimers have been observed, as discussed in Sect. 2.4.3. The TCTP fold contains three  $\alpha$ -helices ( $\alpha_1$ ,  $\alpha_2$ ,  $\alpha_3$ ) and eleven  $\beta$ -strands arranged in two small  $\beta$ -sheets  $\beta_2$ - $\beta_1$ - $\beta_{11}$  and  $\beta_5$ - $\beta_6$  and a larger  $\beta$ -sheet  $\beta_7$ - $\beta_8$ - $\beta_9$ - $\beta_{10}$ - $\beta_4$ - $\beta_3$  (Fig. 2.1a). The two  $\beta$ -sheets  $\beta_2$ - $\beta_1$ - $\beta_{11}$  and  $\beta_7$ - $\beta_8$ - $\beta_9$ - $\beta_{10}$ - $\beta_4$ - $\beta_3$  are twisted and their relative arrangement forms a  $\beta$ -tent (Lupas et al. 2015). The helices  $\alpha_2$  and  $\alpha_3$  are connected by a short loop that creates a kink to form a helical hairpin. This hairpin sits on one side of the large surface defined by the six-stranded  $\beta$ -sheet. The different TCTP structures differ by the secondary structure elements that slightly vary in length and relative positioning. For example, the  $\beta$ -sheet  $\beta_2$ - $\beta_1$ - $\beta_{11}$  is severely distorted in *C. elegans* TCTP compared to the other structures. One conserved feature of TCTP structures is the long  $\sim 30$ – $33$ -amino acid loop connecting strands  $\beta_5$  and  $\beta_6$  (between residues T39 and V66 in human TCTP sequence, see sequence alignment in Fig. 2.2). This loop is highly flexible as judged from missing electron density in crystal structures (Eichhorn et al. 2013; Vedadi et al. 2007; Susini et al. 2008; Dong et al. 2009) and from the scarcity of long-range NOE restraints in this region leading to poor structural convergence in NMR structures (Thaw et al. 2001; Lange et al. 2012; Feng et al. 2007). The  $^{15}\text{N}$  relaxation NMR study revealed that, in human TCTP, the loop explores a wide conformation range at the pico- to nano-second timescale (Feng et al. 2007). The N- and C-extremities of the loop are more or less rigid and tend to form a short  $\beta$ -sheet  $\beta_5$ - $\beta_6$  that projects the loop towards the bulk solution and away from the core structure. This is clearly visible in the NMR structures of human and *S. pombe* TCTP (Fig. 2.1b). The NMR structure ensemble of *C. elegans* TCTP (Fig. 2.1b) is more compact and the loop explores a more restricted conformational space, suggesting that a few long-range NOE-derived distances bring the loop in relative close proximity to the core TCTP structure. It is therefore possible that this loop may have distinct dynamic properties in the different species.

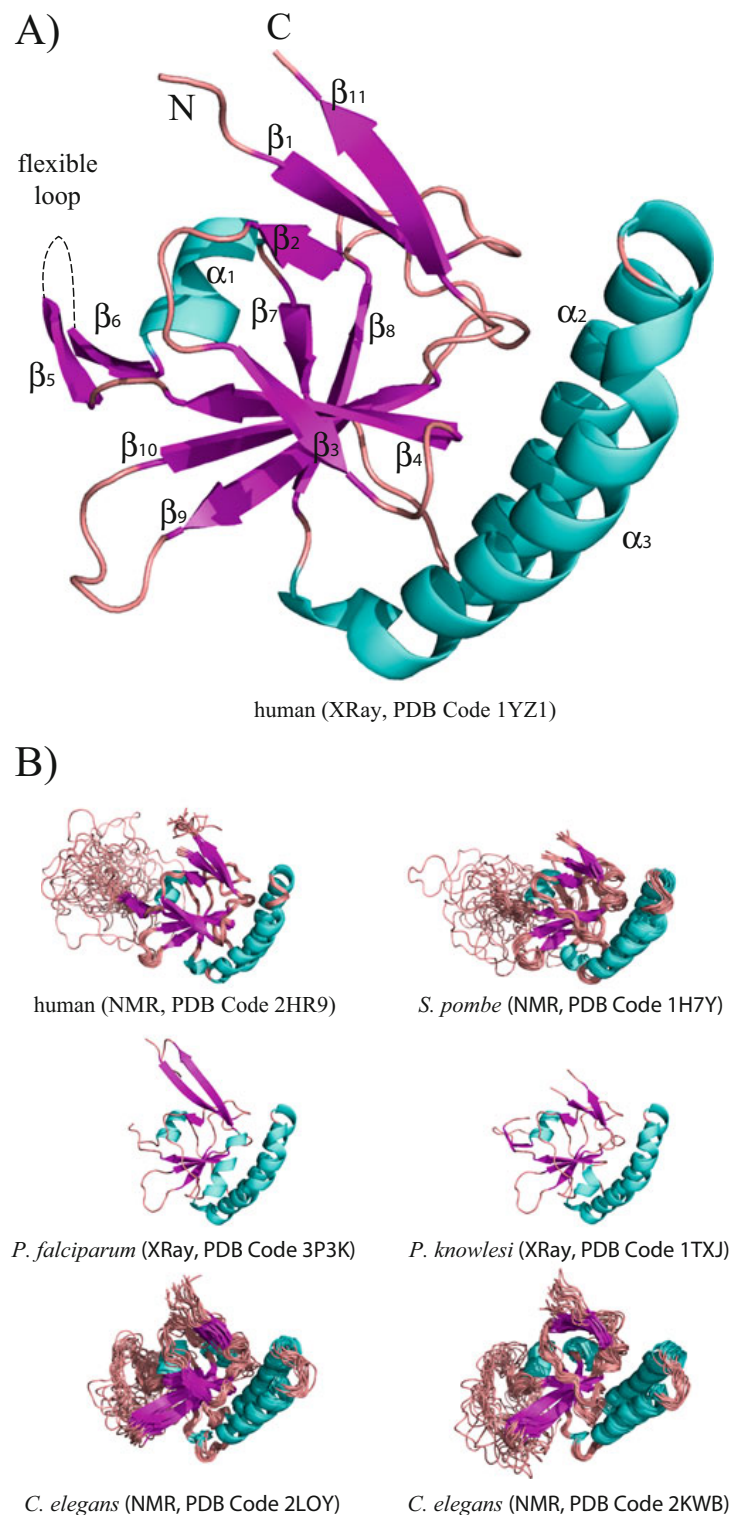


**Fig. 2.1** Ribbon representation of the structures of TCTP from different organisms. (a) Crystal structure of the human TCTP [PDB Code 1YZ1 (Susini et al. 2008)]. The secondary structure elements are shown using the nomenclature from Fig. 2.2 and the  $\alpha$ -helical,  $\beta$ -strand, and coil

TCTP is a highly charged acidic protein with an isoelectric point around 4.5. Accordingly, the 172 amino acid human TCTP contains up to 31 Asp/Glu and 20 Lys/Arg amino acid residues. The vast majority of these charged residues are solvent-exposed at the surface of the protein, making TCTP a highly water-soluble molecule. TCTP is amongst the most abundant proteins in many eukaryotic cells, and the high solubility of TCTP is therefore an important feature. Several charged residues form salt bridges that are partially buried at the surface of the protein. In all TCTP structures, one aspartate residue (D6 in human TCTP sequence) located at the C-terminus of strand  $\beta_1$  is significantly buried in a hydrophobic environment where it makes hydrogen bond with the main chain amides of I8 and S9 forming an Asx-turn motif on the loop  $\beta_1$ - $\beta_2$ . D6 forms an additional H-bond with the amide group of M145 at the N-terminus of strand  $\beta_9$  and, hence, creates contact between the  $\beta_2$ - $\beta_1$ - $\beta_{11}$  and  $\beta_7$ - $\beta_8$ - $\beta_9$ - $\beta_{10}$ - $\beta_4$ - $\beta_3$   $\beta$ -sheets that define the  $\beta$ -tent. Another aspartate (D11), located at the beginning of strand  $\beta_2$ , is also partially buried and form H-bond with the backbone of N139 in the loop  $\beta_8$ - $\beta_9$ . Both D6 and D11 are strictly conserved, thus revealing their potential roles in the stabilization of the  $\beta$ -tent conformation and consequently of the TCTP fold.

### 2.2.2 Structural Homologues of TCTP

The long helical hairpin represents a hallmark of TCTP and shares strong structural similarity with other proteins (Susini et al. 2008). These include transmembrane domains of diphtheria toxin and bacterial colicins as well as the helices H5–H6 found in Bcl-2 family proteins, such as Bax (Susini et al. 2008). However, the similarity is restricted to structural features since there is poor amino acid homology between these proteins. The helical hairpin, and in particular residue K102, plays a role in the anti-apoptotic function of TCTP (Susini et al. 2008). Bax has a strong pro-apoptotic property, and remarkably, replacing the essential helices H5–H6 of Bax by helices  $\alpha_2$  and  $\alpha_3$  from TCTP does not change much Bax pro-apoptotic functions suggesting that TCTP helical hairpin can structurally and functionally replace Bax helical hairpin (Susini et al. 2008).

With the determination of the structure of TCTP, it was also realized that TCTP shares strong structural similarities with the MsrB and Mss4/Dss4 families (Thaw

---

**Fig. 2.1** (continued) regions are colored *cyan*, *magenta*, and *rose*, respectively. The 30–33 amino acid long loop between strands  $\beta_5$  and  $\beta_6$  is not visible in the crystal structure and is indicated as a *dotted line*. Of note, the length of the *dotted line* does not represent the effective length of the loop. (b) TCTP structures from human (Feng et al. 2007), fission yeast *Schizosaccharomyces pombe* (Thaw et al. 2001), the parasites *Plasmodium falciparum* (Eichhorn et al. 2013) and *knowlesi* (Vedadi et al. 2007), and the worm *Caenorhabditis elegans* (Lange et al. 2012). For NMR structures, the ensemble of conformations is shown to illustrate the flexibility of the long loop due to the absence or scarcity of experimentally determined long-range distance constraints in this region

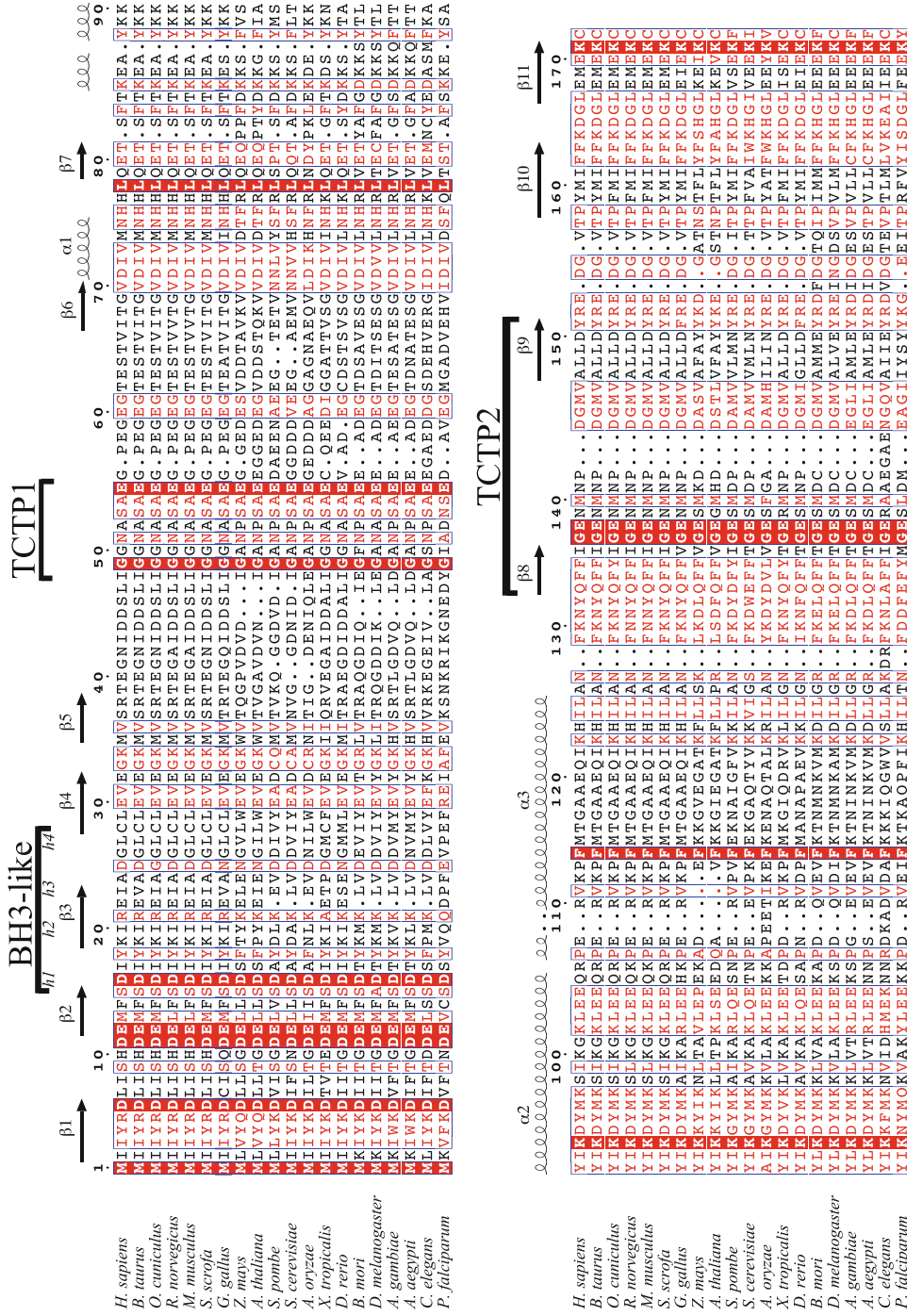


**Fig. 2.2** Amino acid alignment of selected TCTP sequences from mammals, parasites, plants and insects. The amino acid numbering and the secondary structures are from the human sequences (PDB 2HR9) and are shown on the top of the alignment. The picture was prepared using the ESPrInt webserver (Robert and Guet 2014) with the Blossum62 color scheme. Specific sequences such as TCTP1 and TCTP2 signatures and the BH3-like domain together with the h1, h2, h3, h4 positions conserved in conventional BH3 domains are highlighted

et al. 2001; Lowther et al. 2002) (see Fig. 2.3f,g). The methionine-R-sulfoxide reductase B (MsrB) is an enzyme involved in the protection of cell against oxidation damages by reducing methionine sulfoxide back to methionine. The Mss4/Dss4 proteins bind the GDP/GTP free form of Rab GTPase proteins and act as a poorly efficient guanine nucleotide exchange factor or guanine nucleotide-free chaperon (Itzen et al. 2006). Despite their different functions, the three protein families share a similar topology. Although the length of the  $\beta$ -strands differs in the different families, they all have in common the two  $\beta$ -sheets forming the  $\beta$ -tent. Nevertheless, some clear variations occur. Firstly, the long flexible loop is absent in MsrB and Mss4/Dss4 proteins and is specific to TCTP. Secondly, the MsrB and Mss4/Dss4 families do not possess the long helical hairpin present in TCTP. In the case of Mss4/Dss4 proteins, an additional two-stranded  $\beta$ -sheet occupies roughly the position where the helical hairpin is located in TCTP structure (see Fig. 2.3d,f,g). In MsrB, a short helical hairpin is present roughly at the same spatial position as the long helical hairpin of TCTP with respect to the  $\beta$ -tent; however, in MsrB the two helices represent insertions at the N-terminus instead of being inserted between strands  $\beta_7$ – $\beta_8$  as in TCTP. The size and the position of the helical hairpin in MsrB allows the positioning of the substrate on the solvent accessible surface of the larger  $\beta$ -sheet as seen in Fig. 2.3g. The similarity of TCTP and Mss4 folds has prompted studies to explore the role of TCTP in guanine nucleotide exchange. TCTP was found to be a GDP exchange inhibitor in the elongation step of protein synthesis (Cans et al. 2003). In contrast, it has been proposed to stimulate the GTP/GDP exchange on the Rheb GTP-binding protein to control mTORC1-dependent cell growth and proliferation (Dong et al. 2009; Hsu et al. 2007), although this function has been challenged (Rehmann et al. 2008; Wang et al. 2008).

The Protein DataBank was recently interrogated for structural similarities (Amson et al. 2013; Lupas et al. 2015) and several new TCTP structural homologues were identified, although the proteins shared very little sequence homology: Cereblon, Mis18, RIG-I, and DUF427 (Fig. 2.3). Because structural similarities could reveal hints about yet unknown TCTP function, we will describe those proteins from a structural but also interactome perspective.

Cereblon (CRBN) is a multidomain protein that interacts with the damaged DNA-binding protein 1 (DDB1) and forms one component of the CUL4–RBX1–DDB1–CRBN E3 ubiquitin ligase complex to regulate the selective proteolysis of key proteins in DNA repair, replication, and transcription (Iovine et al. 2011). The N-terminal extremity of Cereblon contains the LON protease domain and the DDB1-binding region whereas the C-terminal extremity contains the CULT domain [Cereblon domain of Unknown activity, binding cellular Ligands and Thalidomide (Lupas et al. 2015)] that shows structural homology to TCTP. Cereblon has been identified as the primary teratogenic target of the well-known thalidomide drug (Ito et al. 2010), and the thalidomide-binding region is located in the CULT domain (Fischer et al. 2014) (see Fig. 2.3a). The binding of the immunomodulatory (IMiD) agents such as thalidomide to Cereblon inhibits ubiquitination of the CUL4–RBX1–DDB1–CRBN E3 ubiquitin ligase substrates and redirects the enzyme towards new protein targets such as the ikaros family of transcription

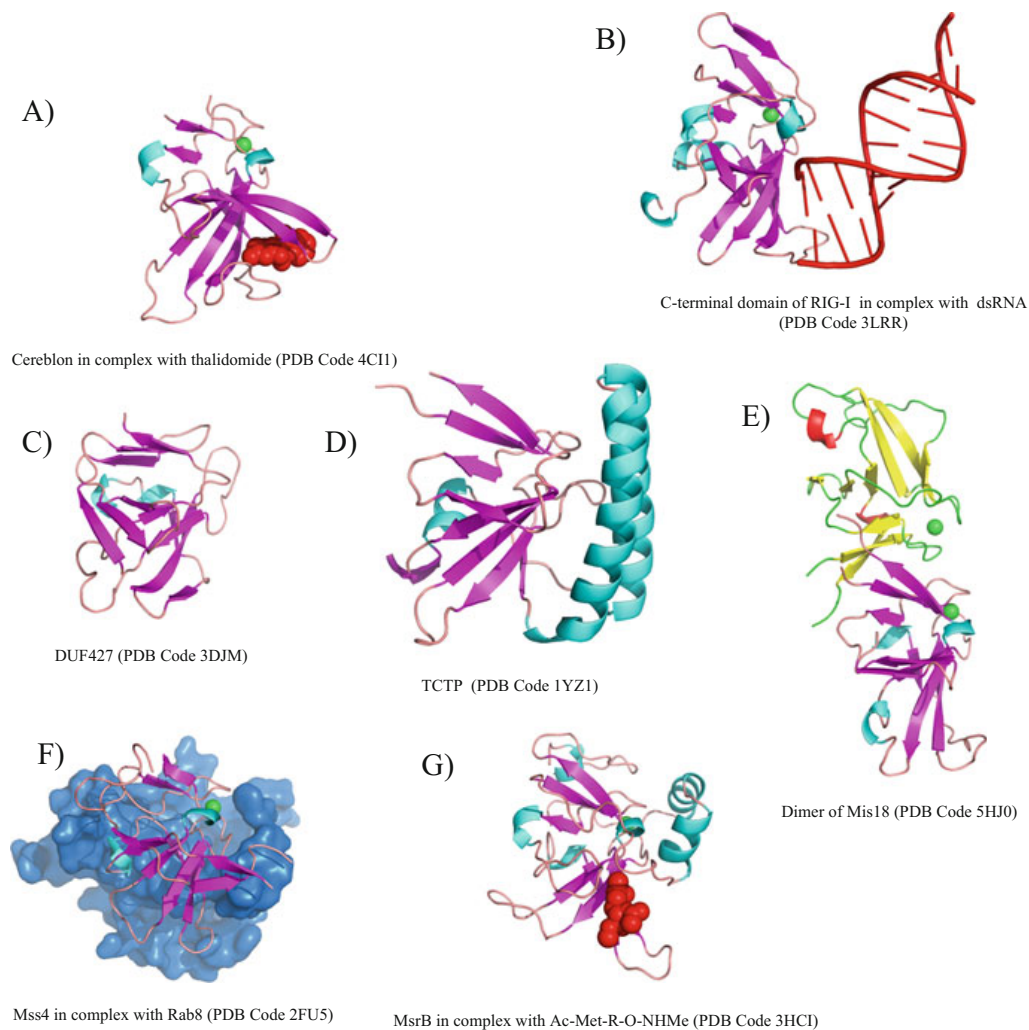


**Fig. 2.3** Comparison of structures showing homology to TCTP: TCTP [PDB code 1YZ1 (Susini et al. 2008)], Cereblon in complex with thalidomide [PDB Code 4CI1 (Fischer et al. 2014)], C-terminal domain of RIG-I in complex with dsRNA [PDB 3LRR (Lu et al. 2010)], DUF427 (PDB Code 3DJM, unpublished), the dimer of Mis18 [PDB Code 5HJ0 (Subramanian et al. 2016)], Mss4 in complex with Rab8 [PDB Code 2FU5, Rab8 protein is shown as a *light blue* surface (Itzen et al. 2006)], and MsrB in complex with the substrate Ac-Met-R-O-NHMe [PDB Code 3HCI (Ranaivoson et al. 2009)]. The structures were superimposed on their common  $\beta$ -tent fold. The protein ribbons are colored according to the secondary structure elements with the  $\alpha$ -helical,  $\beta$ -strand, and coil regions colored *cyan*, *magenta*, and *rose*, respectively. For the dimeric Mis18, the two monomers are colored with different schemes. When available, zinc ions are represented as *green spheres*, and ligands are shown in *red*

factors IKZF1 and IKZF3 (Fischer et al. 2014) or casein kinase 1 $\alpha$  (CK1 $\alpha$ ) (Kronke et al. 2015). This IMiD-induced reprogramming of CUL4–RBX1–DDB1–CRBN E3 ubiquitin ligase relies on novel interactions at the surface of the IMiD–CULT domain complex (Petzold et al. 2016) that allows new substrate recognition such as CK1 $\alpha$ . Cereblon is involved in several protein–protein interactions including

BKCa, CIC-2, AMPK, PSMB4, ikaros and aiolos (IKZF3), and MEIS2 as well as with Ago2 (Xu et al. 2016).

The protein Mis18 is a component of the kinetochore, an essential actor in centromere localization. In *S. pombe*, Mis18 acts as an obligatory homodimeric form mediated by the N-terminal Yippee-like domain that adopts a  $\beta$ -tent conformation (Subramanian et al. 2016) (see Fig. 2.3e). The interface of the dimer is stabilized by strong interactions between the three-stranded  $\beta$ -sheets of the two protomers. An additional  $\alpha$ -helix at the C-terminus is involved in tetramerization (not visible in fig 2.3e). In human Mis18, oligomerization is conserved but involves a heterodimer formed between two Mis18 isoforms, Mis18 $\alpha$  and Mis18 $\beta$  that share 29% identity (Subramanian et al. 2016). Within the Mis18 complex, the Mis18 $\alpha$  and Mis18 $\beta$  have evolved to different functions. Mis18 $\alpha$  interacts with the Mis18-Binding Protein 1 (Mis18BP1) through its Yippee-like domain whereas Mis18 $\beta$  interacts with the C terminus of CENP-C also through its Yippee-like domain (Stellfox et al. 2016). The conserved substrate-binding pocket in Mis18 is required for its function although the partners are not known exactly (Subramanian et al. 2016).

The retinoic acid-inducible gene I (RIG-I) and its homologs MDA5 and LGP2 of the RIG-I like receptors (RLR) family recognize replicating viral RNA for the innate antiviral immune response. They possess a helicase domain followed by a C-terminal conserved Yippee-like domain responsible for the binding specificity to double stranded and 5'-triphosphated single stranded RNA. RNA binding induces a major conformational change that releases RLR autoinhibition and results in the activation of type I interferon for the control of viral infection (Leung and Amarasinghe 2012, 2016). The C-terminal region that shows homology to TCTP contributes to RNA recognition through a positively charged groove formed by the large  $\beta$ -sheet and involves interactions essentially with strands  $\beta_7$ - $\beta_8$ - $\beta_9$ - $\beta_{10}$ - $\beta_4$ - $\beta_3$  (Lu et al. 2010; Cui et al. 2008) (see Fig. 2.3b).

The DUF427 protein also belongs to the same structural family as judged from its 3D structure (see Fig. 2.3c). The function of this protein is currently unknown. As proposed before (Lupas et al. 2015), the glutathione-dependent formaldehyde-activating enzyme (GFA) that catalyzes the formation of S-hydroxymethylglutathione from formaldehyde and glutathione also shares some structural similarities with the abovementioned proteins. We did not include this enzyme in the analysis because the similarities are restricted to a structural subdomain.

One common feature of a subset of proteins from the  $\beta$ -tent family is to bind a zinc ( $Zn^{2+}$ ) ion at the apex of the  $\beta$ -tent. This zinc ion is present in Mis18, Cereblon, RIG-I, and MSS4 and is coordinated by two conserved CXXC motifs. It has been demonstrated that zinc binding is essential for RIG-I in vivo (Cui et al. 2008), and the zinc-binding site may contribute to stabilize the two  $\beta$ -sheets forming the  $\beta$ -tent. In contrast, the cysteines required for zinc binding are largely absent in TCTP and DUF427 and most often are lacking in MsrB. Accordingly, zinc binding has not been reported for these proteins. Consequently, zinc likely does not play any substantial role for these proteins. Alternative processes therefore stabilize the  $\beta$ -tent fold in proteins lacking the zinc-binding site. We proposed that the conserved aspartates D6/D11 could contribute to the TCTP fold (*vide supra*).

Proteins from the  $\beta$ -tent fold family share no detectable sequence homology and have very distinct biological activities and functions. They bind a wide spectrum of compounds ranging from small molecules to nucleic acids and proteins. As noted in a recent survey (Lupas et al. 2015), Cereblon, RIG-I, and MsrB bind partners (small molecules or RNA) through the solvent-exposed large C-terminal  $\beta$ -sheet. This is clearly illustrated in Fig. 2.3 that shows the similar positioning of the ligands (shown in red) sitting on the same face of the large  $\beta$ -sheet. It is likely that the  $\beta$ -tent conformation has converged to expose this binding surface. In TCTP, the binding position is occupied by the helix hairpin, which reinforces the versatility of the C-terminal  $\beta$ -sheet to bind various molecular types, including internal peptide resulting from gene evolution. The presence of the helical hairpin in TCTP clearly hampers binding of TCTP ligands on the C-terminal  $\beta$ -sheet but, at the same time, provides a novel surface formed by the helix hairpin. As shown in Fig. 2.3, other proteins adopting the  $\beta$ -tent fold expose other interfaces for interaction. In Mis18, homo- or heterodimerization occur through the smaller  $\beta$ -sheet. Another example of the versatility of the  $\beta$ -tent to expose binding surface is provided by the structure of the Mss4/Rab8 complex. In this structure, the stretch encompassing helix  $\alpha_1$  and the following strand  $\beta_7$  from Mss4 is largely involved in the interaction with Rab8. Taken together, these proteins most likely result from a convergent process to adopt the  $\beta$ -tent fold that can accommodate various binding modes and binding partners. Not surprisingly, structural elements that represent extensions when compared to the minimal fold also occupy known binding interface. This is for example illustrated by the helical hairpin of TCTP and the long insertion between strands  $\beta_3$  and  $\beta_4$  in Mss4 that both interact with the C-terminal  $\beta$ -sheet. Taken together, TCTP belongs to a large structural family that exposes different binding surfaces and has the ability to interact with molecules of various types. Due to this diversity, it is difficult to predict the interactome and the function for members from this family on the sole basis of the fold.

### 2.2.3 *Functional Elements Within TCTP Sequence*

#### 2.2.3.1 *Conserved Signatures*

TCTP amino acid sequences are highly conserved across eukaryotic cells, including in animal and plant kingdom, as well as in yeast (Hinojosa-Moya et al. 2008) (Fig. 2.2). TCTP homologues have also been detected in spider venom, *C. elegans* or various parasites. Two primary regions of high sequence homology were identified and termed TCTP1 and TCTP2 signatures (Thaw et al. 2001). TCTP1 is an eight amino acid sequence (consensus sequence IG[A-G]N[A-P]SAE) located between residues 48 and 55 in the flexible loop (we use here by default human TCTP numbering, see Fig. 2.2) and is largely hydrophilic. Because this region is not involved in the stabilization of the overall fold of the protein, its conservation is most likely related to functional constraints, such as protein–protein interaction or

posttranslational modifications. The residue S53 is a predicted phosphorylation site for PI3K kinase and its phosphorylation was observed in human cell line during mitosis (Déphoure et al. 2008), but not confirmed in two other studies (Maeng et al. 2015; Zhang et al. 2012). The conservation of S53 in TCTP1 signature might therefore be related to TCTP regulation. The TCTP2 signature is located between residues 133 and 151 and largely conserved residues are: F134-F135 in strand  $\beta_8$ , G137-E138-M140-D143 in the following  $\beta_7$ - $\beta_8$  loop, and Y151 at the C-terminal extremity of strand  $\beta_9$ . Many of these residues are solvent-exposed and do not contribute significantly to the 3D TCTP fold, suggesting that their conservation reveals nonstructural evolutionary pressure. Beyond TCTP1 and TCTP2, other residues are extremely well conserved in TCTP, including D6, D11, E12, D16, L78, K93, F114, V156, and K171. D6 and D11 have already been discussed. E12 has been shown to be essential for protein-protein interaction (Dong et al. 2009; Hsu et al. 2007; Hong and Choi 2016) and for TCTP guanine nucleotide exchange (GEF) activity (Dong et al. 2009; Hsu et al. 2007). The conserved solvent exposed residue K93 in helix  $\alpha_2$  is involved in protein-protein interaction (Wu et al. 2015).

### 2.2.3.2 Functional Motifs in TCTP

#### TCTP Contains a Noncanonical Cell-Penetrating Peptide

TCTP is able to spontaneously penetrate cells of various types but also multiple organs (Kim et al. 2011a). This property is associated to a protein transduction domain (PTD) corresponding to the first ten residues of human TCTP (MIIYRDLISH) (Kim et al. 2011a). The internalization seems to involve lipid raft-mediated endocytosis and macropinocytosis (Kim et al. 2011a, 2015). The mechanism is not yet understood and seemingly differs from other known protein transduction domain, in the sense that it does not involve recognition by the cell surface heparin sulfate (Kim et al. 2011a). TCTP-PTD has been advantageously used as a cargo for the internalization of fused peptides or proteins with potential in drug delivery (Bae and Lee 2013; Kim et al. 2011b; Lee et al. 2011). Nevertheless, the biological meaning of the cell-penetrating property of TCTP is not yet clarified. A recent study pointed out that extracellular TCTP is sufficient to reprogram intracellular signaling pathways to promote migration and invasiveness in colorectal cancer cells (Xiao et al. 2016), which strongly supports the idea that TCTP cell penetration may play (patho)physiological roles. In these processes, TCTP import may mirror the exosome-mediated TCTP export process for cell-to-cell communication (Amzallag et al. 2004). From a structural perspective, the PTD domain encompasses the first strand  $\beta_1$  and the following loop  $\beta_1$ - $\beta_2$  that form the central part of the smaller  $\beta$ -sheet. In TCTP structure, most of the side chains of the PTD are accessible for interaction at the surface. However, the 3D conformation of the peptide seems not to be required for cell penetration since the 10-mer TCTP-PTD peptide can efficiently transport various molecules, although it probably lacks

stable 3D conformation. Hence, it is not clear whether TCTP remains folded or undergoes severe unfolding during cell internalization.

### TCTP Contains a Noncanonical BH3-like Domain

The anti-apoptotic Bcl-xL protein is a partner of TCTP, and the N-terminal fifty residues of TCTP were identified to contribute to TCTP/Bcl-xL interaction (Yang et al. 2005). An in-depth sequence comparison with classical BH3 domains, that are known as Bcl-xL ligands, revealed that TCTP contains a BH3-like domain between residues 16 and 27 (Thebault et al. 2016). BH3 domains usually fold as an  $\alpha$ -helix in protein–protein complexes and are characterized by highly conserved residues at positions h1, h2, h3, and h4 that line on one face of the  $\alpha$ -helix and that contribute to stabilize the helix in the BH3-binding groove of the partners, such as Bcl-xL. Compared to classical BH3 domains, the TCTP BH3-like domain contains the conserved residues I20, I23, and L27 at h2, h3, and h4 positions, respectively, but lacks the hydrophobic residue commonly found at h1 position in canonical BH3 domains (see Fig. 2.2). In TCTP, the h1 position is occupied by the strictly conserved D16. Accordingly, the structure of Bcl-xL in complex with a peptide derived from TCTP<sub>11–31</sub> sequence showed that residues 16–27 of TCTP folds into a  $\alpha$ -helix that occupies the classical BH3-binding groove of Bcl-xL (Thebault et al. 2016). Surprisingly, instead of decreasing the anti-apoptotic activity of Bcl-xL, as would be expected from competition of TCTP BH3-like domains with canonical BH3 domains at the same binding groove on Bcl-xL, TCTP appears to potentiate the anti-apoptotic activity of Bcl-xL through a yet unknown mechanism (Thebault et al. 2016). Whether TCTP BH3-like domain acts also on other BH3-binding proteins, such as Mcl-1, remains to be investigated.

### TCTP Contains an ADP/Cofilin Motif

TCTP interacts with the actin cytoskeleton (Bazile et al. 2009). The comparison of the primary sequences of TCTP and of ADF/cofilin, a family of actin-binding proteins that destabilize actin filaments, unveiled a region of high sequence homology (Tsarova et al. 2010). Indeed, the stretch of residues G69 to E105 that encompasses the helices  $\alpha_1$  and  $\alpha_2$  and the intervening strand  $\beta_7$  shows significant conservation with the G-actin-binding site of cofilin (Tsarova et al. 2010). Accordingly, TCTP preferentially binds to the globular actin (G-actin) than to filamentous actin (F-actin), but TCTP binding does not alter actin dynamics (Tsarova et al. 2010).

### 2.2.3.3 Posttranslational Modifications of TCTP

Several posttranslational modifications are predicted on mammalian TCTP. The ELM server (Dinkel et al. 2016) (<http://elm.eu.org>) predicts for TCTP solvent-exposed regions the following modifications: cleavage sites for caspases 3 and 7, glycosaminoglycan or N-glycosylation attachment site (S53), CK2 phosphorylation sites (residues S9, S37), or Polo-like kinase-1 (Plk1) phosphorylation sites (S46, S64, T65 and S82). Experimentally, only a few posttranslational modifications have been observed.

Biologically important phosphorylations occur at residues S46 and S64. In vivo, the polo-like kinase Plk1 phosphorylates these two serines to detach TCTP from the mitotic spindle for proper mitosis (Yarm 2002). The Plk1-dependent phosphorylation of TCTP contributes to the subcellular localization of TCTP (Yarm 2002; Cucchi et al. 2010; Lucibello et al. 2015). S46 phosphorylation has been proposed to be a biomarker of Plk1 level and kinase activity, with potential interest in antitumor drug design strategy targeting Plk1 (Cucchi et al. 2010) and is observed in mitotic cells (Dephoure et al. 2008). In vitro, the activated Plk1 can phosphorylate TCTP at position S46 but not at position S64 (Johnson et al. 2008). A hierarchical mechanism by which S64 phosphorylation occurs only when S46 is already phosphorylated has also been proposed (Yarm 2002). The serine S46 is conserved in higher eukaryotes whereas S64 is only partially conserved (conserved in mammalian but not in chicken sequences for example, see Fig. 2.2a). Therefore, the impact of S46/S64 phosphorylations is limited to higher eukaryotes (Johnson et al. 2008). Mutations of serines 46 or 64 to glutamate residues abrogate TCTP binding to MDM2 and to the drugs sertraline and thioridazine (Amson et al. 2012). Considering that these mutations mimic phosphoserines, it might indicate that TCTP phosphorylation could also perturb TCTP interactome. Furthermore, it has been proposed that phosphorylated TCTP could be a target of dihydroartemisinin in cancer cells (Lucibello et al. 2015). More recently, the insulin-dependent phosphorylation of S9 and S15 has been reported (Maeng et al. 2015), albeit with yet unknown functional consequences. T39 and S53 phosphorylation have also been observed in mitotic human cell (Dephoure et al. 2008). Phosphorylation of TCTP at definite sites is therefore prone to play important roles in TCTP function.

Beyond phosphorylation, the N-glycosylation of TCTP has been reported (Teshima et al. 1998). The attachment site is not known but S53 is a serious candidate, as judged from ELM predictions. The BioGrid server (<http://thebiogrid.org>) reports several proteomics studies indicating that TCTP can be ubiquitinated or sumoylated. The Ubc9-mediated sumoylation of TCTP controls its subcellular localization, and the residue K164 was identified as a SUMO-1 substrate (Munirathinam and Ramaswamy 2012). The ubiquitination sites are not precisely known, although K19 and K112 could be potentially ubiquitinated (Kim et al. 2011c).

TCTP is known as IgE-dependent histamine-releasing factor (HRF) when it acts in the extracellular space during the human allergic response. The cytokine-like activity of TCTP seems to correlate with extensive posttranslational modifications

that may include proteolytic cleavage, dimerization, or oxidation (Kim et al. 2013). According to the group of Lee (Kim et al. 2013), dimerization is the dominant process that activates TCTP for its extracellular cytokine-like function. TCTP contains two cysteine residues C28/C172, of which C172 seems more important for dimerization (Kim et al. 2009). This can be rationalized by the fact that residue C28 is located at the beginning of strand  $\beta_4$  and its side chain is completely buried, and in contrast the C-terminal C172 is largely solvent accessible and available for self-association (Kim et al. 2009). Dimers were also observed in the C172S mutant suggesting that intermolecular C28-mediated disulfide bridge also exists (Kim et al. 2009). Dimerization as a posttranslational modification might be required for TCTP recognition by its receptor during allergy (Kim et al. 2009). To date, there is no report of the intracellular existence of such covalent dimer, suggesting that the formation of covalent dimer would be specific of the extracellular function of TCTP. Obviously, the different redox potentials in the intra- and extracellular environments might control the formation of such dimers.

### **2.3 Binding Properties and Structural Aspects of TCTP in Complex with Ions, Small Molecules, Carbohydrates, Peptides, and Nucleic Acids**

Since its discovery, the number of TCTP ligands has continuously increased. TCTP has the ability to interact with ions, small molecules, carbohydrates, nucleic acids, and proteins for its biological functions, and several small molecules or peptides have been designed to interfere with TCTP-based cellular processes. In this part, we will introduce the different TCTP non-proteic ligands (see Table 2.1).

#### **2.3.1 Calcium Binding**

Calcium ( $\text{Ca}^{2+}$ ) is one of the first molecules shown to interact with TCTP. The first evidence of calcium binding came in 1992 on the TCTP from *Trypanosoma brucei* parasite (Haghighat and Ruben 1992) and was further extended to other species such as in *Wuchereria bancrofti* (Gnanasekar et al. 2002), *Brugia malayi* (Gnanasekar et al. 2002), *Schistosoma mansoni* (Rao et al. 2002), rat (Kim et al. 2000), and human (Sanchez et al. 1997; Arcuri et al. 2004). Nevertheless,  $\text{Ca}^{2+}$ -binding is not conserved across the phyla since TCTP from ixodid ticks (Mulenga and Azad 2005) and shrimp (Bangrak et al. 2004) does not bind calcium. The functional relevance of calcium binding to TCTP is not well understood. It has been proposed that TCTP may act as a calcium scavenger in the cytosol to protect cells against  $\text{Ca}^{2+}$ -dependent apoptosis (Graidist et al. 2007). Accordingly, cells expressing TCTP mutant lacking the ability to bind calcium become more sensitive to thapsigargin-triggered apoptosis (Graidist

**Table 2.1** The list of non-proteic molecules interacting with TCTP is shown in this table. The species in which the interactions have been observed and some functional insights into the interaction are also reported

Binding partner	Species	Function and distribution	References
Calcium (Ca <sup>2+</sup> )	<i>Trypanosoma brucei</i> , <i>Schistosoma mansoni</i> , rat, human	Regulation of Ca <sup>2+</sup> homeostasis and Ca <sup>2+</sup> -induced apoptosis	Feng et al. (2007), Haghghat and Ruben (1992), Rao et al. (2002), Kim et al. (2000), Sanchez et al. (1997), Arcuri et al. (2004), Mulenga and Azad (2005), Bangrak et al. (2004), Graidist et al. (2007), Lucas et al. (2014), Xu et al. (1999)
Sertraline/thioridazine/levomepromazine/buclicizine	Human	Antihistaminic and antihistaminic-related small molecules.	Amson et al. (2012), Tuynder et al. (2004), Zhang (2014), Seo and Efferth (2016)
Peptides	Human	WGQWPYHC with specific cytotoxicity against tumor cells.	Kadioglu and Efferth (2016)
	Human	WYVYPSM and WEFPGWM against the covalent dimeric TCTP.	Kim et al. (2011d)
Artemisinin and analogues	<i>Plasmodium falciparum</i> , human	TCTP is targeted and covalently modified by artemisinin and analogues, possibly at multiple sites from F12 to Y22 in PfTCTP.	Eichhorn et al. (2013), Krishna et al. (2004), Bhisutthibhan and Meshnick (2001), Bhisutthibhan et al. (1999), Bhisutthibhan et al. (1998), Zhou et al. (2016), Li et al. (2016a)
Heme	Human	Heme binds TCTP and promotes its dimerization.	Lucas et al. (2014)
DNA (Sf1 promoter of <i>oct4</i> ) <sup>a</sup>	<i>Xenopus</i> oocyte, human	Activates transcription of <i>oct4</i> and <i>nanog</i> .	Koziol et al. (2007). See also Cheng et al. (2012)
mRNA <sup>a</sup>	HeLa cells	TCTP belongs to mRNA interactome	Castello et al. (2012)
Chitin, lipopolysaccharide, peptidoglycans, Bb ( <i>Bacillus bombyseptieus</i> ), Sm ( <i>Serratia marcescens</i> )	<i>Bombyx mori</i>	TCTP as a novel opsonic molecule. Induces the production of antimicrobial peptide.	Wang et al. (2013)

<sup>a</sup>The interactions of TCTP with DNA and RNA were observed in oocyte extracts and in HeLa cells, respectively, and have not been confirmed yet in vitro

et al. 2007). Following this idea, the anti-apoptotic role of TCTP could be due to multiple mechanisms including the direct interaction with anti-apoptotic proteins (including Bcl-xL and Mcl-1) to control their activity but also by preventing the  $\text{Ca}^{2+}$ -induced permeabilization of the mitochondrial membrane and the resulting release of pro-apoptotic molecules. The sequestering effect for calcium led recently to the hypothesis of a “buffer-like” role for TCTP to regulate cellular homeostasis by avoiding the unwanted excess of soluble ligands (Lucas et al. 2014). The interplay between TCTP and calcium is reinforced by the observation that calcium regulates TCTP at the transcriptional and posttranscriptional levels (Xu et al. 1999).

The binding of calcium was studied by different techniques that gave somehow inconsistent conclusions. In one study (Graidist et al. 2007), two rather high-affinity ( $\sim 10 \mu\text{M}$  range) and one lower-affinity binding modes were detected. In contrast, recent NMR (Feng et al. 2007) and fluorescence (Lucas et al. 2014) studies detected low-affinity binding modes (mM range) but not the high-affinity binding modes, although both techniques are sensitive over an extreme wide range of affinity. The apparent discrepancy could be due to different purification protocols or binding conditions. From a structural perspective, the double mutant (E58A/E60A) loses the ability to bind calcium with high affinity (Graidist et al. 2007), indicating that these residues that are located in the long loop are crucial for the interaction. The same study revealed that calcium binding was accompanied by a change in the secondary structure of the protein, as judged from circular dichroism (CD) (Graidist et al. 2007). In the NMR study (Feng et al. 2007), the calcium-binding site was mapped to a region of the protein involving the C-terminal extremities of helix  $\alpha_3$  and of strand  $\beta_9$  and the loop between strand  $\beta_9$  and helix  $\alpha_2$ . The oxygens from the side chains of residues N131, Q133, and D150 were proposed to coordinate  $\text{Ca}^{2+}$ . The chemical shift and intensity changes upon calcium binding were rather limited in amplitude and localized to a few amino acid residues. This suggests that TCTP conformation and oligomeric state is well conserved upon  $\text{Ca}^{2+}$  interaction, thus corroborating another CD study (Lucas et al. 2014) in which no secondary structure nor oligomeric change was observed up to 50 mM calcium concentration. Calcium triggers monomerization of hemin-induced dimerization (Lucas et al. 2014), possibly through direct competition against hemin binding. Indeed, hemin and calcium seem to share a similar binding area on TCTP (Lucas et al. 2014). In their study, Lucas et al. also observed that the presence of calcium contributes to destabilize TCTP by reducing the urea concentration required for denaturation (Lucas et al. 2014).

### **2.3.2 *Antihistaminic Drugs and the Related Sertraline/ Thioridazine***

Any compound leading to reduced TCTP levels in vivo may have potential anti-tumor activity. Accordingly, because TCTP is a histamine-releasing factor, the

group of R. Amson and A. Telerman hypothesized that antihistaminic drugs inhibiting the histaminic pathway were interesting candidates in anticancer strategies (Tuynder et al. 2004). This approach was successful, and a few antihistaminic compounds such as hydroxyzine and promethazine (see Fig. 2.4) proved efficient to kill tumor cells and to decrease the level of TCTP either directly or indirectly (Tuynder et al. 2004). Even greater antitumor activity was reported for the structurally related thioridazine and sertraline (see Fig. 2.4), although they do not display antihistaminic properties (Amson et al. 2012; Tuynder et al. 2004). The drugs thioridazine and sertraline are used for their antipsychotic and antidepressive activities, respectively. The direct interactions of sertraline and thioridazine with TCTP have been confirmed by surface plasmon resonance (SPR) (Amson et al. 2012), and dissociation constant ( $K_d$ ) of 47  $\mu\text{M}$  and 34  $\mu\text{M}$  was estimated for sertraline and thioridazine, respectively. The interaction was later confirmed for sertraline by thermal shift assays (Zhang 2014). Surprisingly, whereas ligand binding usually stabilizes proteins, sertraline has a destabilizing effect on TCTP by reducing its melting temperature. Both thioridazine and sertraline disrupt the TCTP/MDM2 interaction in vitro which provides a rationale for the restored levels of p53 in cells treated with these pharmacological compounds (Amson et al. 2012).

To date, the structural information on TCTP/ligands complexes is very limited. Two TCTP mutants (S46E and S64E) lose their ability to bind sertraline and thioridazine (Amson et al. 2012), suggesting that the residues S46 and S64 are involved in the interaction with the drugs. Accordingly, the drugs do not interfere with the interactions between MDM2 and TCTP mutants (Amson et al. 2012). As already discussed, residues S46 and S64 are located in the long inserted flexible loop. However whether these residues are directly or indirectly involved in the interaction surface with ligands remains an open question. Additional high-resolution structural information is still awaited to better characterize TCTP/ligand complexes. Interestingly, because these S $\rightarrow$ E mutants can be seen as phosphoserine mimics, it is possible that Plk1-mediated phosphorylation perturbs TCTP/ligands interaction. Drug design programs targeting TCTP should therefore take into account the potential distinct binding properties of the molecules to phosphorylated and unphosphorylated TCTP in order to inhibit the proper TCTP forms in vivo.

A recent in silico docking study (Seo and Efferth 2016) provided new insights into the molecular interaction of TCTP with 12 antihistaminic compounds. The binding of levomepromazine or buclizine (see Fig. 2.4) was confirmed in vitro by microscale thermophoresis giving dissociation constants of 57  $\mu\text{M}$  and 430  $\mu\text{M}$ , respectively (Seo and Efferth 2016). All tested ligands (except cetirizine) were found to dock onto TCTP at the same position, in an area of the loop encompassing the stretches T39-I48 and E60-T65 that contains both S46 and S64, thus confirming that these two serines could be binding hotspots in TCTP (Seo and Efferth 2016). However, the simulation was carried out on a single conformation of TCTP, and loop flexibility and the potential conformation change of the loop upon binding were not taken into account. Therefore, the binding site derived from this study remains to be confirmed.

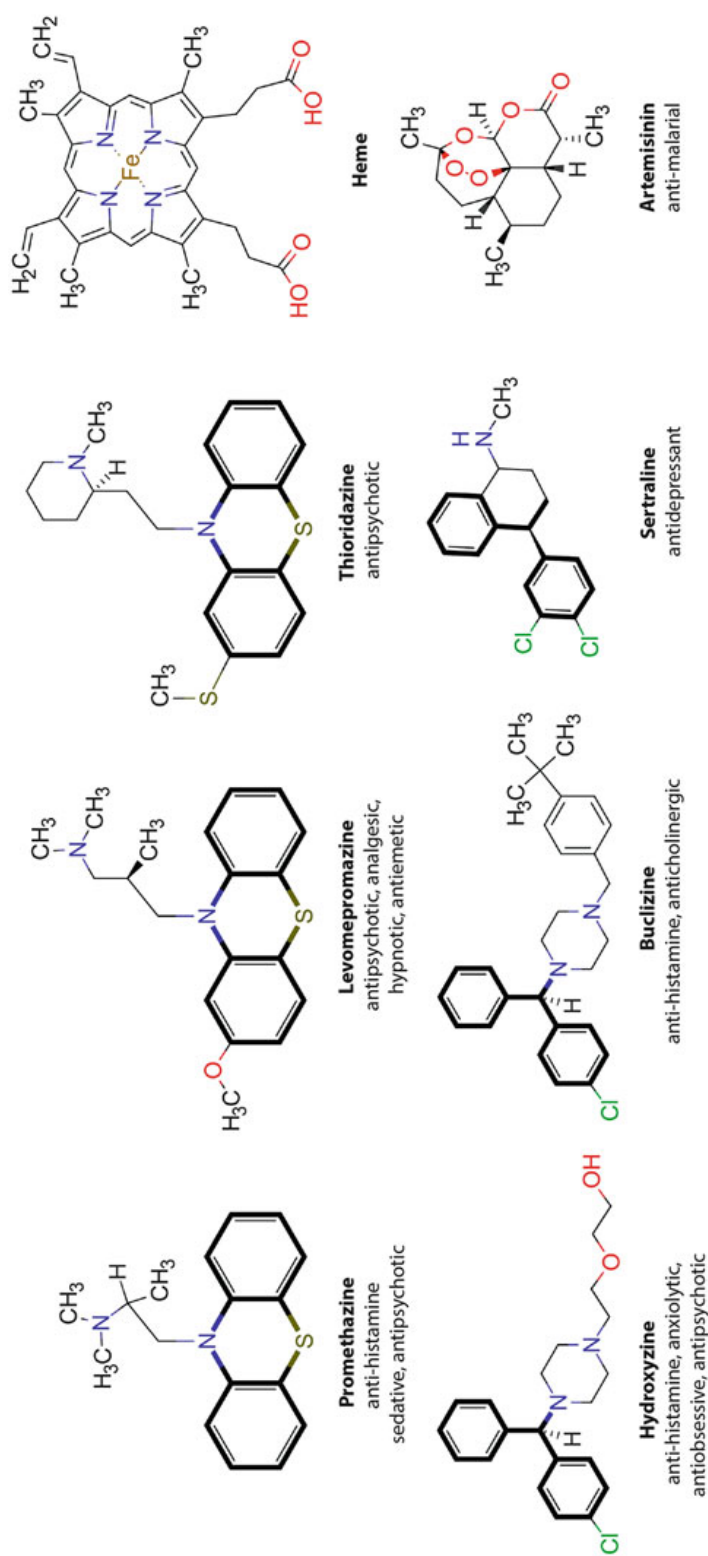


**Fig. 2.4** Structures of small molecules discussed in the manuscript. When available, the biological effects of the molecules are reported. We note that several of these molecules are chiral and often found commercially as racemic mixtures

### 2.3.3 Peptides

TCTP is now an established pharmacological target in cancer- or allergy-related diseases and hence different groups are making efforts to develop peptide-based TCTP inhibitors to interfere with the protein–protein interactions network of TCTP (Kim et al. 2011d; Kadioglu and Efferth 2016).

In their study (Kadioglu and Efferth 2016), Kadioglu and Efferth carried out an *in silico* screening of peptide libraries and selected octamer peptides with predicted high affinity. The peptide sequences were rather similar with a consensus sequence WGQWPYHX, where the last residue X is the only difference between the different peptides. In spite of the small sequence difference, the docking poses of the different peptides segregated into two families differing by the binding groove. One groove is defined by the bottom of the long flexible loop and strands  $\beta_7$ ,  $\beta_8$ , and  $\beta_9$  on one side of the larger  $\beta$ -sheet whereas the other groove is located on the other side of large  $\beta$ -sheet and includes the C-terminus of helix  $\alpha_3$ . Although the binding with TCTP was not confirmed *in vitro*, one peptide WGQWPYHC induced specific cytotoxicity against tumor cells in a TCTP-dependent manner without affecting normal cells (Kadioglu and Efferth 2016).

In another study (Kim et al. 2011d), the dimeric TCTP was targeted. The covalent dimer is thought to be the active TCTP state in inflammatory processes. With the aim to inhibit TCTP in chronic allergic diseases, three peptides dTBP1/dTBP2/dTBP3 were isolated by screening a phage-displayed 7-mer peptide library. Peptides dTBP2 (WYVYPSM) and dTBP3 (WEFPGWM) were shown to interact with TCTP and with the TCTP<sub>84–108</sub> peptide corresponding to the helix  $\alpha_2$  in TCTP. The interaction with dTBP2 was demonstrated to be specific to the dimeric versus the monomeric TCTP, and dTBP2 inhibited the cytokine-like effect of TCTP (Kim et al. 2011d). Although they have been designed for different applications and obtained by unrelated approaches, the peptides dTBP1/dTBP2 (Kim et al. 2011d) and WGQWPYHC (Kadioglu and Efferth 2016) show striking similarities: they start by a tryptophan residue and tend to contain an aromatic residue at positions 3 or 4 and a proline residue at positions 4 or 5. However, whether all these peptides share the same binding modes remain to be investigated.

### 2.3.4 Heme, Artemisinin, and Analogs

*P. falciparum* TCTP (*Pf*TCTP) is found to be one target of the antimalarial drug artemisinin (Krishna et al. 2004; Bhisutthibhan and Meshnick 2001) and forms complexes with artemisinin and its metabolites. Covalent but also non-covalent and reversible complexes have been reported (Eichhorn et al. 2013; Bhisutthibhan et al. 1998, 1999). The artemisinin-mediated alkylation of TCTP is facilitated by the presence of hemin in particular in a reducing environment (Bhisutthibhan et al. 1998, 1999; Zhou et al. 2016). To date, the exact residues of *Pf*TCTP involved in

alkylation are not identified but could be mapped within three peptidic fragments of *Pf*TCTP (Eichhorn et al. 2013). A more recent study showed that multiple amino acid at the N-terminus can be modified by a reactive artemisinin analog and that F12 and C19 are key residues for the interaction (Li et al. 2016a). The reaction is thought to occur through the naturally rare endoperoxide bridge (1,2,4-trioxane structure) that becomes activated by ferrous iron, such as heme, to generate free radicals. The direct binding of heme with human TCTP has been also demonstrated (Lucas et al. 2014) and involves the dyad H76–H77. It was proposed that heme and calcium shares a common binding pattern on TCTP (Lucas et al. 2014) and, accordingly, competes with each other. Upon complex formation with heme, TCTP forms dimers, which can be easily disrupted by calcium (Lucas et al. 2014). Therefore, ligand binding is prone to conduct to oligomers of TCTP. In *P. falciparum*, heme/TCTP interaction could be important for the fate of artemisinin in the parasite. Indeed, TCTP is associated with the parasite food vacuoles that are rich in heme, as a product of degradation of hemoglobin by the intra-erythrocytic parasite (Slomianny 1990; Abu Bakar et al. 2010; Klonis et al. 2011). However, it is yet not fully demonstrated if such mechanism can explain the anti-malarial mode of action of artemisinin.

The heme-assisted artemisinin-alkylation of TCTP could potentially affect the various TCTP-related functions. Artemisinin can be effective in cancer (Crespo-Ortiz and Wei 2012; Krishna et al. 2008), and it has been proposed that artemisinin could adopt a similar mode of action in human cells as in parasites. Interestingly, dihydroartemisinin, a metabolite of artemisinin, binds human TCTP in vitro ( $K_d$  of 38  $\mu$ M) and reduces TCTP half-life in a proteasome-dependent manner by increasing its ubiquitination (Fujita et al. 2008). Furthermore, an artemisinin analog targets human TCTP in HeLa cancer cells (Zhou et al. 2016), suggesting that artemisinin might covalently interact with TCTP from different organisms. *Pf*TCTP shares 35% sequence identity with human TCTP, and the structures of the two proteins are very similar (Eichhorn et al. 2013). Therefore, a deeper characterization of the interaction of artemisinin with TCTP and its derivatives would be helpful for a better understanding of its antimalarial activity, which is still largely unknown (O'Neill et al. 2010), but also of the role of TCTP in cancer biology.

### 2.3.5 Nucleic Acids

TCTP has been isolated from a search for proteins binding to the mouse *oct4* promoter region using radioactively labeled DNA incubated in *Xenopus* oocyte extract. The direct interaction between TCTP and the steroidogenic factor-1 (Sf1) site of *oct4* promoter was demonstrated in vivo from two independent studies carried out in *Xenopus* (Koziol et al. 2007) and in mouse pluripotent cells (Cheng et al. 2012). The first 60 amino acids of TCTP appear to be sufficient for Sf1 binding (Cheng et al. 2012). Three studies assessed the function of TCTP as a transcription factor with diverse outputs (Koziol et al. 2007; Cheng et al. 2012; Johansson and

Simonsson 2010). In one study carried out in *Xenopus* (Koziol et al. 2007), the transcription of a subset of genes including *oct4* was activated by TCTP. In their study, Johansson et al. (Johansson and Simonsson 2010) did not observe a change in *oct4* transcription upon shRNA knockdown of TCTP but observed that TCTP interacts with Oct4 protein in vivo. They proposed a mechanism in which TCTP controls *oct4* transcription by perturbing the self-regulatory transcriptional properties of the Oct4 transcription factor. The third study (Cheng et al. 2012) confirmed the binding of TCTP to the Sf1 site of *oct4* promoter in vivo, but demonstrated that DNA binding of TCTP negatively regulated the expression of Oct4 in mouse pluripotent cells. They proposed that different epigenetic modifications in amphibian oocytes and mammalian cells could explain the conflicting results. We retain from these works that TCTP has also the ability to act as a transcription factor, although the direct interaction between TCTP and DNA has to be confirmed in vitro.

TCTP has been captured in a systematic approach targeting RNA-binding proteins in HeLa cells (Castello et al. 2012). In this study, a “zero-distance” strategy was used to select direct contacts between proteins and RNA and to avoid protein–protein crosslinks. This work therefore suggests that TCTP has also the ability to directly bind RNA *in cellulo* (Castello et al. 2012).

### 2.3.6 *Bombyx mori* TCTP as a Binding Platform for Saccharides

In the silkworm *Bombyx mori*, *BmTCTP* is produced in intestinal epithelial cells and is released into the hemolymph and gut lumen in response to oral microbial infection (Wang et al. 2013). A study exploring the interaction of *BmTCTP* with a range of pathogen-associated molecular patterns (PAMP) revealed the broad binding spectrum of *BmTCTP* (Wang et al. 2013). *BmTCTP* interacts with chitin, a polymer formed of *N*-acetylglucosamine, and mixtures of *E. coli* lipopolysaccharides (LPS) or of *B. subtilis* peptidoglycans (PG). The binding of TCTP with highly negatively charged bacterial wall molecules was proposed to involve the lysine residues at the surface of TCTP (Wang et al. 2013). *BmTCTP* also tends to bind bacteria such as *Bacillus bombyseptieus* or *Serratia marcescens*. In response to PAMP, *BmTCTP* induces the production of antimicrobial peptides through the ERK pathway (Wang et al. 2013). Therefore, *BmTCTP* contributes to the insect intestinal immunity by acting as opsonin to enhance phagocytosis. To the best of our knowledge, no mammalian TCTP has been reported to date to bind saccharides (other than nucleic acids). Considering that peptide cell-penetration often involves recognition of cell-surface carbohydrates, this study on *BmTCTP* could inspire future research for a better characterization of the mechanism of TCTP cell penetration.

## 2.4 Structural Aspects of TCTP in Complex with Proteins

### 2.4.1 *TCTP Directly Interacts with Dozens of Proteins*

Over the years, the number of proteins that interact *in vivo* with TCTP has progressively increased and several dozens of TCTP partners have been identified and further confirmed *in vitro*, by pull-down assays for example. One review by Amson et al. (2013) reported the extensive list of partners known in 2013. These partners were classified according to their functions as anti-apoptotic, GTPases, p53 axis, cytoskeleton/mitotic machinery, DNA processing and repair, and RNA/ribosome/protein biogenesis. This protein repertoire has continuously expanded to include, for example, proteins such as 14-3-3 (Le et al. 2016), Apaf-1 (Jung et al. 2014), HSPA9 (Li et al. 2016b), YBX1 (Li et al. 2016b), HSP27 (Katsogiannou et al. 2014), peroxiredoxin-1 (Chattopadhyay et al. 2016), ATG16 complex (Chen et al. 2014), nucleolin (Johansson et al. 2010a), or IgE/IgG (Kashiwakura et al. 2012).

Despite the ever-accumulating evidence of the functional importance of TCTP and of its interaction with partners, the amount of structural information regarding protein–protein interaction (PPI) is yet rather limited. Each discovery of novel TCTP-related PPI is often associated to attempts to decipher the molecular basis of the PPI through peptide fragments approaches. In such strategies, peptides derived from the native proteins are designed, and the analysis of the preservation of peptide–peptide contacts leads to the identification of the protein region(s) important for the interaction under scrutiny. The TCTP-related PPI analyzed using peptide fragments were summed up in a review in 2012 (Kawakami et al. 2012). Because several novel interactions have been identified and characterized meanwhile, we propose an updated table of interactions in Table 2.2. Partners identified by coimmunoprecipitation or two-hybrid techniques may be indirect by the implication of a third partner. It is, therefore, crucial to confirm the direct interaction *in vitro* between recombinant proteins. In this table, two types of interaction were selected amongst the long list of known TCTP partners. On the one hand, we listed interactions confirmed *in vitro*, whether the biological impact is known or not. On the other hand, we chose interactions with clear biological impacts although the involvement of a third partner is not ruled out yet. The second type was included to foster future *in vitro* study to confirm biologically relevant interactions.

Table 2.2 clearly illustrates the versatility of TCTP to bind proteins of distinct cellular functions but also biochemical functions (enzymes, DNA/RNA/protein-binding proteins, scaffold proteins, . . .). The consequences of TCTP binding range from direct enzyme activation or inhibition, protein stabilization by promoting or preventing ubiquitination, protein stabilization in response to heat shock, facilitating or hindering the recruitment of other partners, and the control of phosphorylation of the partner. To play all these functions, TCTP evolved to interact with a large interactome and despite its relatively small size, it proposes different binding

**Table 2.2** The list of proteic partners identified for TCTP is shown in this table. We have reported here partners for which the interaction has been confirmed in vitro using recombinant proteins. Other interactions waiting for in vitro confirmation have also been included (proteins indicated by a star) when functional information of particular interest has been reported. When available, the amino acids and domains of TCTP and partners involved in the interaction are indicated. nd means “not determined”. When point mutants were shown to disrupt the intermolecular interaction, the single amino acid is reported. In the case of eEF1B $\delta$ , we listed the amino acids that are present at interface of the complex.

	Binding partner	Species	TCTP	Partner	Function and distribution	References
Cell cycle mitosis	$\alpha$ -tubulin	Mouse	70–130	nd	Stabilizes microtubule.	Gachet et al. (1999)
	$\beta$ -tubulin	Mouse	70–130	nd	Colocalizes with microtubules in the G1, S, G2, and early M phases of cell cycle. Regulates spindle microtubule dynamics and cell shape.	Gachet et al. (1999)
	Centrosome and Microtubules*	<i>Xenopus laevis</i> , mammalian cells	nd	nd		Bazile et al. (2009), Jaglarz et al. (2012); Jeon et al. (2016). See also Li et al. (2016b)
	Actin	Rabbit	75–97	nd	TCTP binds preferentially to G-actin than to F-actin.	Tsarova et al. (2010). See also Li et al. (2016b)
	CHFR (Checkpoint protein with FHA and RING finger domain)*	Human	nd	nd	CHFR interacts and colocalizes with TCTP to the mitotic spindle.	Burgess et al. (2008)
	Plk1 (polo-like kinase 1)	Mouse/human	107–172	Polo box	Plk1 phosphorylates TCTP on S46 and S64, which is required for proper mitosis.	Yam (2002). See also Johnson et al. (2008)
	Nucleophosmine* (Mpm1)	Mouse	nd	nd	The Mpm1/TCTP complex is a potential biomarker for mitotic ES cells.	Johansson et al. (2010b)
	Nucleolin*	Mouse	nd	nd	Interaction with phosphorylated nucleolin observed during mitosis.	Johansson et al. (2010a)
	Rheb (Ras homolog enriched in brain)	Human/drosophila	E12, K90, E138	Y35, K45	Preferential binds to nucleotide-free Rheb. Stimulates the GTP/GDP exchange on Rheb to control mTORC1-dependent cell growth and proliferation.	Dong et al. (2009), Hsu et al. (2007). See also Choi and Hsu (2007). Two other studies (Rehmann et al. 2008; Wang et al. 2008) seriously questioned this interaction and function.

	14-3-3 (14-3-3ε or 14-3-3ζ isoforms)	Drosophila	nd	nd	nd	Required for TCTP–Rheb interaction.	Le et al. (2016)	
Survival/apoptosis	p53	Human	70–119		101–300 (DNA-binding domain)	Destabilizes p53 and blocks p53-induced transcriptional activation of Bax.	Rho et al. (2011)	
		Human	1–70 + 121–172 + Y4 + E168		103–292 (DNA-binding domain)		Chen et al. (2011)	
		Human	nd		99–293 + 294–393		Amson et al. (2012)	
		NUMB	Human	1–68		20–259	Competes with NUMB for binding to MDM2.	Amson et al. (2012)
		MDM2 (murine double minute 2)	Human	1–68		134–333 + 302–435	TCTP inhibits MDM2 auto-ubiquitination and promotes MDM2-mediated ubiquitination.	Amson et al. (2012)
	Human		80–133		44–65 + M62	Funston et al. (2012)		
		Bcl-xL (B-cell lymphoma-extra large)	Mouse	1–40, I20, R21, E22, D25		1–188, L90, D95	Potentiates the anti-apoptotic activity of Bcl-xL.	Yang et al. (2005)
	Human		14–29, R21		BH3-binding domain	Thebault et al. (2016)		
		Mcl-1 (Induced Myeloid Leukemia Cell Differentiation Protein)	Human	5–172, R21		nd	Mcl-1 stabilizes TCTP and TCTP inhibits ubiquitination of Mcl-1.	Zhang et al. (2002)
	Mouse/human		14–94		K257	Liu et al. (2005)		
		Apaf-1 (Apoptotic peptidase activating factor 1)	Human	nd		1–97 (CARD domain)	Inhibits the etoposide-induced cell death.	Jung et al. (2014)
		TSC-22 (Transforming growth factor-beta stimulated clone-22)	Human	1–69		53–110	Prevents TSC-22-mediated apoptosis via the destabilization of TSC-22.	Lee et al. (2008)

(continued)

Table 2.2 (continued)

	Binding partner	Species	TCTP	Partner	Function and distribution	References
Protein synthesis	eEF1A (eukaryotic translation elongation factor I alpha)	Human	nd	nd	Preferentially binds GDP form of eEF1A and specifically antagonizes the eEF1B $\delta$ -mediated guanine nucleotide exchange reaction. Partially colocalize around the nucleus.	Cans et al. (2003). See also Leclercq et al. (2011)
	eEF1B $\delta$	Human	nd	153–281		Cans et al. (2003). See also Langdon et al. (2004)
		Human	F83, K90, I92, K93, D94, M96, K97, K100, M115, T116, A118, A119, I122, M140, P142, D143	155–189 (CAR domain)		Wu et al. (2015) high resolution structural model
DNA damage repair	40S ribosomal subunit	Yeast	nd	nd	Copurified with ribosomal complex. Required for efficient translation.	Fleischer et al. (2006)
	ATM (ataxia telangiectasia mutated)	Drosophila	61–120 + 121–172 + E12	1006–1215	Enhances the binding affinity of dATM to its substrate to promote efficient DNA repair.	Hong and Choi (2013) and related (Zhang et al. 2012)
	Ku70* (aka XRCC6), Ku80*, $\gamma$ H2A.X*	Human	nd	nd	DNA double-strand break sensing and repair.	Zhang et al. (2012), Li et al. (2016b)



Table 2.2 (continued)

Binding partner	Species	TCTP	Partner	Function and distribution	References
SWI/SNF (SWI1ch/ Sucrose Non-Fermentable) and its homologue in drosophila Brahma	Drosophila	E12	304–747 (HSA and BRK domains)	Negatively modulates Brahma activity in transcription.	Hong and Choi (2016), Telerman et al. (2006)
YBX1 (Y-box-binding protein 1)	Human	42–83	1–129	nd	Li et al. (2016b)
Marek's disease virus (MDV)-specific protein R-LORF12	Chicken	nd	nd	nd	Niikura et al. (2004)
Oct4 (octamer-binding transcription factor 4)	Mouse	nd	nd	Controls genes involved in embryonic development.	Johansson and Simonsson (2010)
ATG16 (Autophagy protein 16)*	Human, pig, mouse	nd	nd	Regulation of autophagy	Chen et al. (2014)
TCF-4 (Transcription factor 4)*	Human	nd	nd	Enhances $\beta$ -catenin/TCF-4 transcription activity.	Gu et al. (2014)
HSP27 (Heat-Shock Protein 27)*	Human	nd	nd	Protects TCTP from the ubiquitin-proteasome degradation.	Baylot et al. (2012) and the related (Zhang 2014)

modes. Table 2.2 suggests that almost all TCTP regions are potentially involved in the direct interaction with partners. For example, when mutated, residues Y4, E12, I20, R21, E22, D25, E138, or E168 abrogate binding to a range of partners. All these residues cover a wide surface on TCTP, reinforcing the idea that TCTP does not expose a unique interface for interaction. This parallels the many binding modes observed for the proteins from the  $\beta$ -tent family (see Fig. 2.3).

#### 2.4.2 Structural Information on Native Complexes

The strategy consisting in deleting large portions of protein is extremely efficient when it comes to isolate interacting domains from multidomain proteins. This approach is also useful to identify short peptide fragments from independent folding units such as protein globular domains, in particular when these fragments folds as helices at the interface of protein–protein complex. Nevertheless, short fragments might not properly fold or keep the same 3D conformation as in the native protein. In such situation, the peptide fragment approach is prone to give false negative results. Oppositely, the disruption of the 3D native fold in short fragments is prone to facilitate nonnative interaction, leading to potential false positive results. These limitations may explain some discrepancies observed in the dissection of TCTP interactions as reported in Table 2.2, such as with the p53 or MDM2 partners. For these reasons, proper interaction analysis are better carried out with native proteins, preferentially with full length proteins or at least by preserving folding units, followed by point mutations. To date, our understanding of TCTP interactions using native proteins is limited to the TCTP/eEF1B $\delta$  complex, for which a high-resolution structure have been obtained from a mixed approach based on classical NMR-based structure determination followed by molecular docking driven by experimental NMR data (Wu et al. 2015) (see Fig. 2.5a). This structure was validated by extensive site-directed mutagenesis and highlighted the role of the helical hairpin (Site I) and of a surface patch (Site II) formed by the stretch connecting helices  $\alpha_1$  and  $\alpha_2$  and including strand  $\beta_7$  (around F83) and the loop  $\beta_8$ – $\beta_9$  (containing M140 and P142) in the interaction with the CAR domain from eEF1B $\delta$  (Fig. 2.5a). In the complex, the negatively charged N-terminus of CAR adopts an extended conformation that wraps around the positively charged helical hairpin, including residues K90, I92, K93, M96, K97, K100, M115, T116, A118, A119, and I122. At its C-terminus, CAR adopts an  $\alpha$ -helical conformation that docks on a surface overlapping sites I and II through hydrophobic contacts with F83, M140, P142 and electrostatic contacts with D143 and D94. Electrostatic and hydrophobic interactions both contribute to stabilize the complex.

This work provides the most convincing study of the key role of the helical hairpin in TCTP PPI. It is most likely that this structure element is also involved in other PPIs as suggested from other studies (Amson et al. 2012; Kashiwakura et al. 2012; Rid et al. 2010; Gachet et al. 1999; Rho et al. 2011; Funston et al. 2012), with strong functional impacts such as in apoptosis (Susini et al. 2008). Another hint

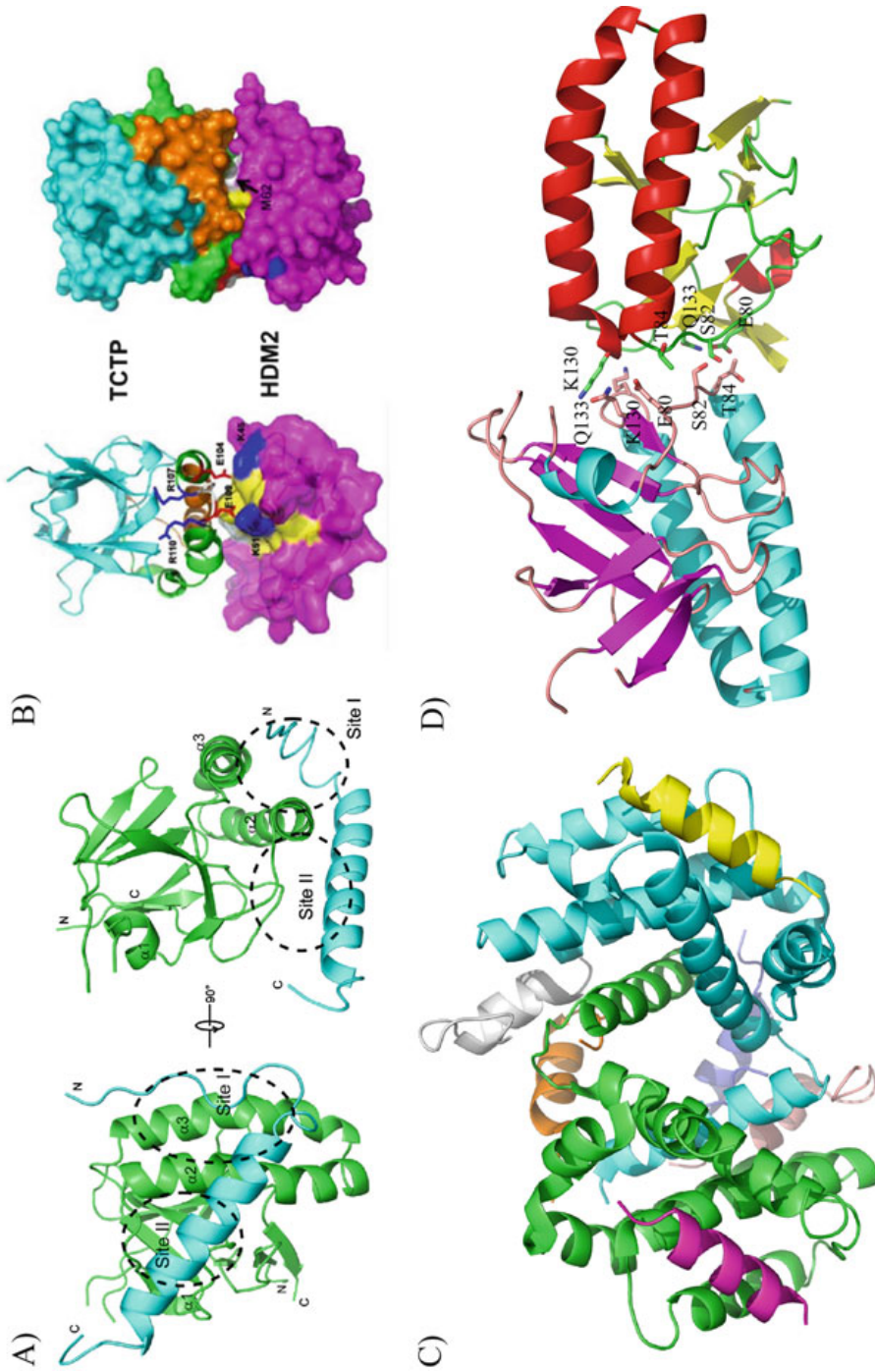


**Fig. 2.5** High-resolution structures or structural models of TCTP in interaction with protein partners. (a) NMR-based structure of TCTP in interaction with the CAR domain of eEF1Bδ (Wu et al. 2015). The two proteins are shown as *ribbons* with TCTP and eEF1Bδ in *green* and *cyan*, respectively. Two orthogonal views are

about the key role of the helical hairpin is provided by a structural model of the complex formed by TCTP and the N-terminal domain of MDM2 (Fig. 2.5b). The molecular interface of this complex has been well characterized on MDM2 side by competition with a well-known MDM2 binder (nutlin-3) or by using MDM2 mutants (M62A). However, the interface on TCTP still awaits validation with high resolution structural data from native protein and/or from point mutations. This could also resolve the somehow inconsistent results obtained from independent studies on TCTP/MDM2 interaction (Amson et al. 2012; Funston et al. 2012).

The TCTP/Bcl-xL complex is the only TCTP complex for which a crystal structure has been obtained (Fig. 2.5c). The TCTP/Bcl-xL complex with full-length proteins could be purified but only a complex of Bcl-xL with a peptide derived from the TCTP BH3-like domain was crystallized. This structure illustrates how the TCTP BH3-like peptide binds to the BH3-binding groove of Bcl-xL (Thebault et al. 2016). The crystal contained a swapped dimeric Bcl-xL, which appears to be an hallmark of this protein. Six TCTP peptides were observed, although only two of them were considered as significant. This work (Thebault et al. 2016) provided sound basis to demonstrate the existence of a functional BH3-like element in TCTP, but at the same time, raises novel questions. The BH3-like domain (residues 16 to 27) folds as strand  $\beta_3$  in the native TCTP structure and undergoes a severe conformational rearrangement in the complex with Bcl-xL. Because residues 16 to 27 play a key role in stabilizing TCTP larger  $\beta$ -sheet, it is difficult to predict the impact of the global conformation change of TCTP in the complex: is strand  $\beta_3$  the only element being affected? does TCTP completely unfold and remain unfolded at the exception of the helical BH3 region? does TCTP remold into another stable conformation unrelated to the fold of the unbound protein? does other region than the BH3 region of TCTP interact with Bcl-xL? Because TCTP binds at the Bax-binding groove of Bcl-xL, one would expect that TCTP competes with Bax to inhibit the Bax-mediated anti-apoptotic activity of Bcl-xL. Paradoxically, TCTP appears to potentiate the anti-apoptotic activity of Bcl-xL (Thebault et al. 2016). The apparently counter-intuitive structural mechanism by which TCTP activates Bcl-xL remains largely unknown. Clearly, additional structural, thermodynamic, and kinetic studies on full-length proteins are required to assess the plasticity of TCTP and to understand its role to control apoptosis.



**Fig. 2.5** (continued) shown. Picture taken with permission from Wu et al. (2015). **(b)** Energy-minimized structural model of the complex between TCTP and the N-terminal domain of human MDM2 obtained from molecular docking based on peptide deletion analysis and MDM2 M62A mutant (Funston et al. 2012). Picture taken with permission from Funston et al. (2012). **(c)** Structure of the full-length Bcl-xL in complex with the BH3-like domain of TCTP (residues 16–27) [PDB code 4Z9V (Thebault et al. 2016)]. The proteins are shown as *ribbons*. Bcl-xL (*cyan* and *green*) crystallized as a swap dimer and six BH3-like peptides were observed (*magenta*, *yellow*, *orange*, *grey*, *salmon*, *marine*). Only the *magenta* and *yellow* peptides were considered meaningful, while the others were considered as crystallization artifacts (Thebault et al. 2016). **(d)** Potential TCTP dimer structure. The chains A and D from the 1YZ1 crystal structure of TCTP are represented as *ribbons*. The two monomers have different color codes for their secondary structures. The amino acid residues at the dimer interface are labeled

### 2.4.3 TCTP Tends to Self-associate

TCTP tends to self-associate. For example, non-covalent dimers/oligomers of rat TCTP have been detected from yeast two-hybrid system (Yoon et al. 2000). The deletion of the region 126–172 resulted in loss of self-interaction of TCTP in vivo (Yoon et al. 2000). The authors concluded that this region was involved in oligomer formation. The amino acids 126–172 encompass the last four  $\beta$ -strands of TCTP that largely contribute to create the large  $\beta$ -sheet at the core of TCTP structure. Hence, its deletion is prone to severely impact the proper folding of TCTP and its oligomerization properties. It is therefore highly possible that the peptide missing residues 126–172 is not able to oligomerize because of the global unfolding of the protein, which questions the involvement of these residues in oligomerization of the native TCTP. As noted before, heme tends to favor TCTP dimer in vitro with potential role in cellular homeostasis (Lucas et al. 2014). The details of the dimer interface have not been investigated yet. In the analysis of TCTP structures so far available, we have noticed that human wild-type and E12V mutant TCTP crystallize with four molecules in the unit cell although they were obtained in different space groups. Interestingly, in the two crystals, an intermolecular interface and a relative protein orientation were clearly conserved within a pair of molecules. This is illustrated by the contacts between chains A and D from the human wild-type structure (Fig. 2.5d). Because this self-association mode is observed in different crystal packings, it is possible that the interactions at this interface of these two molecules are strong enough to exist in solution. We propose that the complex observed between chains A and D could represent the structure of TCTP dimer in solution. The proposed interface is formed by the hydrophilic and charged residues such as E80, S82, T84, Q130, and K133 as highlighted in Fig. 2.5d.

## 2.5 Conclusions

In this chapter, we have presented the structural features of TCTP with a focus on its posttranslational modifications and interaction network. Despite its relative small size and globular nature, the TCTP structure is extremely versatile and is able to interact with ions, small molecules, carbohydrates, nucleic acids, and proteins. Although high-resolution structures and more precise delineation of complex interfaces are still required, it seems that most TCTP surface patches are potential binding hotspots, which might be the hallmark of proteins from the  $\beta$ -tent family.

To date, our knowledge of the structural property of TCTP in interaction is still very limited. Although the structure of TCTP is apparently highly stable, there are some lines of evidence that TCTP is prone to major rearrangement upon interaction. On the one hand, TCTP interacts with Bcl-xL by the BH3-like domain that is partially buried in the unbound TCTP, suggesting that TCTP undergoes a severe conformational change in the complex. This could explain the difficulty to form the

TCTP/Bcl-xL complex (Thebault et al. 2016). In this regard, TCTP also interacts with the Bcl-xL-related Mcl-1, although it is not clear yet if the interaction is also mediated by the BH3-like domain. The formation of TCTP/Mcl-1 complex is also rather difficult and is greatly facilitated by the truncation of the first ten residues (Liu et al. 2005). It is likely that the removal of the N-terminal residues prevents the proper folding of TCTP. Thus, by alleviating the kinetically unfavorable unfolding barrier, this truncated TCTP form probably already exposes interacting residues, possibly in the BH3-like region, thus making the formation of the complex easier. Such a truncated form was also proved to be more active to trigger the IgE response (Kim et al. 2009). Shortened TCTP has not yet been observed *in vivo* but a TCTP isoform lacking the first 34 amino acids is reported by UniProt (P13693-2), which could have variable binding properties compared to the canonical TCTP isoform. On the other hand, TCTP penetrates cells by using a protein transduction domain that folds as a  $\beta$ -strand. It is possible that TCTP also undergoes a significant fold rearrangement during cell entry to facilitate recognition and internalization. Future researches are necessary to confirm these hypotheses. Importantly, it will be crucial to identify the molecular triggers, to assess the extent of the conformational change, and to assess the functional consequences of the rearrangement on the partners. We speculate that TCTP plasticity greatly contributes to the versatility of its effects on partners and to its multifunctional nature.

One intriguing feature of TCTP is the 30–33 amino acid long flexible loop. This region is very well conserved throughout the phylum, both in length and amino acid composition and contains the TCTP1 signature at its center. Compared to structured regions, flexible regions are in general less under evolution constraints of keeping structurally important amino acids and are therefore prone to vary in length and composition. The conservation of the loop in TCTP therefore suggests that other forces drive its conservation during evolution. In particular, one may wonder if the loop directly interacts with partners, if it controls the access to other binding hotspots on TCTP, or if it contributes to the proposed conformational rearrangement. For this, it is crucial to characterize complexes between native proteins, with a focus on the dynamics of this loop. The loop might be involved in other regulatory events such as the phosphorylation of serines S46, S53, or S64. Being part of TCTP1 signature, S53 is strictly conserved and its phosphorylation could regulate biological functions shared throughout the phylum. In contrast, S46 and S64 are found only in mammalian TCTP and most likely regulate mammalian-specific functions. The impact of phosphorylation on the dynamics of the loop and, beyond, on the structure of the protein will also provide insights into the role of the loop.

Although our knowledge of TCTP functions has greatly expanded over the last years, much remains to be done to characterize the biochemical and structural features of TCTP. No doubt that such gain in knowledge will contribute to decipher the multiple functions of TCTP in physiological and pathophysiological processes.

## References

- Abu Bakar N, Klonis N, Hanssen E, Chan C, Tilley L (2010) Digestive-vacuole genesis and endocytic processes in the early intraerythrocytic stages of *Plasmodium falciparum*. *J Cell Sci* 123(Pt 3):441–450
- Amson R, Pece S, Lespagnol A, Vyas R, Mazzarol G, Tosoni D, Colaluca I, Viale G, Rodrigues-Ferreira S, Wynendaele J, Chaloin O, Hoebeke J, Marine JC, Di Fiore PP, Telerman A (2012) Reciprocal repression between P53 and TCTP. *Nat Med* 18(1):91–99
- Amson R, Pece S, Marine JC, Di Fiore PP, Telerman A (2013) TPT1/TCTP-regulated pathways in phenotypic reprogramming. *Trends Cell Biol* 23(1):37–46
- Amzallag N, Passer BJ, Allanic D, Segura E, Thery C, Goud B, Amson R, Telerman A (2004) TSAP6 facilitates the secretion of translationally controlled tumor protein/histamine-releasing factor via a nonclassical pathway. *J Biol Chem* 279(44):46104–46112
- Arcuri F, Papa S, Carducci A, Romagnoli R, Liberatori S, Riparbelli MG, Sanchez JC, Tosi P, del Vecchio MT (2004) Translationally controlled tumor protein (TCTP) in the human prostate and prostate cancer cells: expression, distribution, and calcium binding activity. *Prostate* 60(2):130–140
- Bae HD, Lee K (2013) On employing a translationally controlled tumor protein-derived protein transduction domain analog for transmucosal delivery of drugs. *J Control Release* 170(3):358–364
- Bangrak P, Graidist P, Chotigeat W, Phongdara A (2004) Molecular cloning and expression of a mammalian homologue of a translationally controlled tumor protein (TCTP) gene from *Penaeus monodon* shrimp. *J Biotechnol* 108(3):219–226
- Baylot V, Katsogiannou M, Andrieu C, Taieb D, Acunzo J, Giusiano S, Fazli L, Gleave M, Garrido C, Rocchi P (2012) Targeting TCTP as a new therapeutic strategy in castration-resistant prostate cancer. *Mol Ther* 20(12):2244–2256
- Bazile F, Pascal A, Arnal I, Le Clainche C, Chesnel F, Kubiak JZ (2009) Complex relationship between TCTP, microtubules and actin microfilaments regulates cell shape in normal and cancer cells. *Carcinogenesis* 30(4):555–565
- Bhisutthibhan J, Meshnick SR (2001) Immunoprecipitation of [(3)H]dihydroartemisinin translationally controlled tumor protein (TCTP) adducts from *Plasmodium falciparum*-infected erythrocytes by using anti-TCTP antibodies. *Antimicrob Agents Chemother* 45(8):2397–2399
- Bhisutthibhan J, Pan XQ, Hossler PA, Walker DJ, Yowell CA, Carlton J, Dame JB, Meshnick SR (1998) The *Plasmodium falciparum* translationally controlled tumor protein homolog and its reaction with the antimalarial drug artemisinin. *J Biol Chem* 273(26):16192–16198
- Bhisutthibhan J, Philbert MA, Fujioka H, Aikawa M, Meshnick SR (1999) The *Plasmodium falciparum* translationally controlled tumor protein: subcellular localization and calcium binding. *Eur J Cell Biol* 78(9):665–670
- Burgess A, Labbe JC, Vigneron S, Bonneaud N, Strub JM, Van Dorsselaer A, Lorca T, Castro A (2008) Chfr interacts and colocalizes with TCTP to the mitotic spindle. *Oncogene* 27(42):5554–5566
- Cans C, Passer BJ, Shalak V, Nancy-Portebois V, Crible V, Amzallag N, Allanic D, Tufino R, Argentini M, Moras D, Fiucci G, Goud B, Mirande M, Amson R, Telerman A (2003) Translationally controlled tumor protein acts as a guanine nucleotide dissociation inhibitor on the translation elongation factor eEF1A. *Proc Natl Acad Sci USA* 100(24):13892–13897
- Castello A, Fischer B, Eichelbaum K, Horos R, Beckmann BM, Strein C, Davey NE, Humphreys DT, Preiss T, Steinmetz LM, Krijgsveld J, Hentze MW (2012) Insights into RNA biology from an atlas of mammalian mRNA-binding proteins. *Cell* 149(6):1393–1406
- Chattopadhyay A, Pinkaew D, Doan HQ, Jacob RB, Verma SK, Friedman H, Peterson AC, Kuyumcu-Martinez MN, McDougal OM, Fujise K (2016) Fortilin potentiates the peroxidase activity of Peroxiredoxin-1 and protects against alcohol-induced liver damage in mice. *Sci Rep* 6:18701

- Chen Y, Fujita T, Zhang D, Doan H, Pinkaew D, Liu Z, Wu J, Koide Y, Chiu A, Lin CC, Chang JY, Ruan KH, Fujise K (2011) Physical and functional antagonism between tumor suppressor protein p53 and fortilin, an anti-apoptotic protein. *J Biol Chem* 286(37):32575–32585
- Chen K, Chen S, Huang C, Cheng H, Zhou R (2013) TCTP increases stability of hypoxia-inducible factor 1alpha by interaction with and degradation of the tumour suppressor VHL. *Biol Cell* 105(5):208–218
- Chen K, Huang C, Yuan J, Cheng H, Zhou R (2014) Long-term artificial selection reveals a role of TCTP in autophagy in mammalian cells. *Mol Biol Evol* 31(8):2194–2211
- Cheng X, Li J, Deng J, Li Z, Meng S, Wang H (2012) Translationally controlled tumor protein (TCTP) downregulates Oct4 expression in mouse pluripotent cells. *BMB Rep* 45(1):20–25
- Choi KW, Hsu YC (2007) To cease or to proliferate: new insights into TCTP function from a *Drosophila* study. *Cell Adhes Migr* 1(3):129–130
- Crespo-Ortiz MP, Wei MQ (2012) Antitumor activity of artemisinin and its derivatives: from a well-known antimalarial agent to a potential anticancer drug. *J Biomed Biotechnol* 2012: 247597
- Cucchi U, Gianellini LM, De Ponti A, Sola F, Alzani R, Patton V, Pezzoni A, Troiani S, Saccardo MB, Rizzi S, Giorgini ML, Cappella P, Beria I, Valsasina B (2010) Phosphorylation of TCTP as a marker for polo-like kinase-1 activity in vivo. *Anticancer Res* 30(12):4973–4985
- Cui S, Eisenacher K, Kirchhofer A, Brzozka K, Lammens A, Lammens K, Fujita T, Conzelmann KK, Krug A, Hopfner KP (2008) The C-terminal regulatory domain is the RNA 5'-triphosphate sensor of RIG-I. *Mol Cell* 29(2):169–179
- Dephoure N, Zhou C, Villen J, Beausoleil SA, Bakalarski CE, Elledge SJ, Gygi SP (2008) A quantitative atlas of mitotic phosphorylation. *Proc Natl Acad Sci USA* 105(31):10762–10767
- Dinkel H, Van Roey K, Michael S, Kumar M, Uyar B, Altenberg B, Milchevskaya V, Schneider M, Kuhn H, Behrendt A, Dahl SL, Damerell V, Diebel S, Kalman S, Klein S, Knudsen AC, Mader C, Merrill S, Staudt A, Thiel V, Welti L, Davey NE, Diella F, Gibson TJ (2016) ELM 2016—data update and new functionality of the eukaryotic linear motif resource. *Nucleic Acids Res* 44(D1):D294–D300
- Dong X, Yang B, Li Y, Zhong C, Ding J (2009) Molecular basis of the acceleration of the GDP-GTP exchange of human ras homolog enriched in brain by human translationally controlled tumor protein. *J Biol Chem* 284(35):23754–23764
- Eichhorn T, Winter D, Buchele B, Dirdjaja N, Frank M, Lehmann WD, Mertens R, Krauth-Siegel RL, Simmet T, Granzin J, Efferth T (2013) Molecular interaction of artemisinin with translationally controlled tumor protein (TCTP) of *Plasmodium falciparum*. *Biochem Pharmacol* 85(1):38–45
- Feng Y, Liu D, Yao H, Wang J (2007) Solution structure and mapping of a very weak calcium-binding site of human translationally controlled tumor protein by NMR. *Arch Biochem Biophys* 467(1):48–57
- Fischer ES, Bohm K, Lydeard JR, Yang H, Stadler MB, Cavadini S, Nagel J, Serluca F, Acker V, Lingaraju GM, Tichkule RB, Schebesta M, Forrester WC, Schirle M, Hassiepen U, Ottl J, Hild M, Beckwith RE, Harper JW, Jenkins JL, Thoma NH (2014) Structure of the DDB1-CRBN E3 ubiquitin ligase in complex with thalidomide. *Nature* 512(7512):49–53
- Fleischer TC, Weaver CM, McAfee KJ, Jennings JL, Link AJ (2006) Systematic identification and functional screens of uncharacterized proteins associated with eukaryotic ribosomal complexes. *Genes Dev* 20(10):1294–1307
- Fujita T, Felix K, Pinkaew D, Hutadilok-Towatana N, Liu Z, Fujise K (2008) Human fortilin is a molecular target of dihydroartemisinin. *FEBS Lett* 582(7):1055–1060
- Funston G, Goh W, Wei SJ, Tng QS, Brown C, Jiah Tong L, Verma C, Lane D, Ghadessy F (2012) Binding of translationally controlled tumour protein to the N-terminal domain of HDM2 is inhibited by nutlin-3. *PLoS One* 7(8):e42642
- Gachet Y, Tournier S, Lee M, Lazaris-Karatzas A, Poulton T, Bommer UA (1999) The growth-related, translationally controlled protein P23 has properties of a tubulin binding protein and associates transiently with microtubules during the cell cycle. *J Cell Sci* 112(Pt 8):1257–1271

- Gnanasekar M, Rao KV, Chen L, Narayanan RB, Geetha M, Scott AL, Ramaswamy K, Kaliraj P (2002) Molecular characterization of a calcium binding translationally controlled tumor protein homologue from the filarial parasites *Brugia malayi* and *Wuchereria bancrofti*. *Mol Biochem Parasitol* 121(1):107–118
- Graidist P, Yazawa M, Tonganunt M, Nakatomi A, Lin CC, Chang JY, Phongdara A, Fujise K (2007) Fortilin binds Ca<sup>2+</sup> and blocks Ca<sup>2+</sup>-dependent apoptosis in vivo. *Biochem J* 408(2): 181–191
- Gu X, Yao L, Ma G, Cui L, Li Y, Liang W, Zhao B, Li K (2014) TCTP promotes glioma cell proliferation in vitro and in vivo via enhanced beta-catenin/TCF-4 transcription. *Neuro-oncology* 16(2):217–227
- Haghighat NG, Ruben L (1992) Purification of novel calcium binding proteins from *Trypanosoma brucei*: properties of 22-, 24- and 38-kilodalton proteins. *Mol Biochem Parasitol* 51(1):99–110
- Hinojosa-Moya J, Xoconostle-Cazares B, Piedra-Ibarra E, Mendez-Tenorio A, Lucas WJ, Ruiz-Medrano R (2008) Phylogenetic and structural analysis of translationally controlled tumor proteins. *J Mol Evol* 66(5):472–483
- Hong ST, Choi KW (2013) TCTP directly regulates ATM activity to control genome stability and organ development in *Drosophila melanogaster*. *Nat Commun* 4:2986
- Hong ST, Choi KW (2016) Antagonistic roles of *Drosophila* Tctp and Brahma in chromatin remodelling and stabilizing repeated sequences. *Nat Commun* 7:12988
- Hsu YC, Chern JJ, Cai Y, Liu M, Choi KW (2007) *Drosophila* TCTP is essential for growth and proliferation through regulation of dRheb GTPase. *Nature* 445(7129):785–788
- Iovine B, Iannella ML, Bevilacqua MA (2011) Damage-specific DNA binding protein 1 (DDB1): a protein with a wide range of functions. *Int J Biochem Cell Biol* 43(12):1664–1667
- Ito T, Ando H, Suzuki T, Ogura T, Hotta K, Imamura Y, Yamaguchi Y, Handa H (2010) Identification of a primary target of thalidomide teratogenicity. *Science* 327(5971):1345–1350
- Itzen A, Pylypenko O, Goody RS, Alexandrov K, Rak A (2006) Nucleotide exchange via local protein unfolding--structure of Rab8 in complex with MSS4. *EMBO J* 25(7):1445–1455
- Jaglarz MK, Bazile F, Laskowska K, Polanski Z, Chesnel F, Borsuk E, Kloc M, Kubiak JZ (2012) Association of TCTP with centrosome and microtubules. *Biochem Res Int* 2012:541906
- Jeon HJ, You SY, Park YS, Chang JW, Kim JS, Oh JS (2016) TCTP regulates spindle microtubule dynamics by stabilizing polar microtubules during mouse oocyte meiosis. *Biochim Biophys Acta* 1863(4):630–637
- Johansson H, Simonsson S (2010) Core transcription factors, Oct4, Sox2 and Nanog, individually form complexes with nucleophosmin (Npm1) to control embryonic stem (ES) cell fate determination. *Aging* 2(11):815–822
- Johansson H, Svensson F, Runnberg R, Simonsson T, Simonsson S (2010a) Phosphorylated nucleolin interacts with translationally controlled tumor protein during mitosis and with Oct4 during interphase in ES cells. *PLoS One* 5(10):e13678
- Johansson H, Vizlin-Hodzic D, Simonsson T, Simonsson S (2010b) Translationally controlled tumor protein interacts with nucleophosmin during mitosis in ES cells. *Cell Cycle* 9(11): 2160–2169
- Johnson TM, Antrobus R, Johnson LN (2008) Plk1 activation by Ste20-like kinase (Slk) phosphorylation and polo-box phosphopeptide binding assayed with the substrate translationally controlled tumor protein (TCTP). *Biochemistry* 47(12):3688–3696
- Jung J, Kim M, Kim MJ, Kim J, Moon J, Lim JS, Kim M, Lee K (2004) Translationally controlled tumor protein interacts with the third cytoplasmic domain of Na,K-ATPase alpha subunit and inhibits the pump activity in HeLa cells. *J Biol Chem* 279(48):49868–49875
- Jung J, Kim HY, Maeng J, Kim M, Shin DH, Lee K (2014) Interaction of translationally controlled tumor protein with Apaf-1 is involved in the development of chemoresistance in HeLa cells. *BMC Cancer* 14:165
- Kadioglu O, Efferth T (2016) Peptide aptamer identified by molecular docking targeting translationally controlled tumor protein in leukemia cells. *Invest New Drugs* 34(4):515–521

- Kashiwakura JC, Ando T, Matsumoto K, Kimura M, Kitaura J, Matho MH, Zajonc DM, Ozeki T, Ra C, MacDonald SM, Siraganian RP, Broide DH, Kawakami Y, Kawakami T (2012) Histamine-releasing factor has a proinflammatory role in mouse models of asthma and allergy. *J Clin Invest* 122(1):218–228
- Katsogiannou M, Andrieu C, Baylot V, Baudot A, Dusetti NJ, Gayet O, Finetti P, Garrido C, Birnbaum D, Bertucci F, Brun C, Rocchi P (2014) The functional landscape of Hsp27 reveals new cellular processes such as DNA repair and alternative splicing and proposes novel anti-cancer targets. *Mol Cell Proteomics* 13(12):3585–3601
- Kawakami T, Ando T, Kawakami Y (2012) HRF-interacting molecules. *Open Allergy J* 5(41–46)
- Kawakami T, Kashiwakura J, Kawakami Y (2014) Histamine-releasing factor and immunoglobulins in asthma and allergy. *Allergy Asthma Immunol Res* 6(1):6–12
- Kim M, Jung Y, Lee K, Kim C (2000) Identification of the calcium binding sites in translationally controlled tumor protein. *Arch Pharm Res* 23(6):633–636
- Kim M, Min HJ, Won HY, Park H, Lee JC, Park HW, Chung J, Hwang ES, Lee K (2009) Dimerization of translationally controlled tumor protein is essential for its cytokine-like activity. *PLoS One* 4(7):e6464
- Kim M, Kim M, Kim HY, Kim S, Jung J, Maeng J, Chang J, Lee K (2011a) A protein transduction domain located at the NH<sub>2</sub>-terminus of human translationally controlled tumor protein for delivery of active molecules to cells. *Biomaterials* 32(1):222–230
- Kim HY, Kim S, Youn H, Chung JK, Shin DH, Lee K (2011b) The cell penetrating ability of the proapoptotic peptide, KLAKLAKKLAKLAK fused to the N-terminal protein transduction domain of translationally controlled tumor protein, MIIYRDLISH. *Biomaterials* 32(22):5262–5268
- Kim W, Bennett EJ, Huttlin EL, Guo A, Li J, Possemato A, Sowa ME, Rad R, Rush J, Comb MJ, Harper JW, Gygi SP (2011c) Systematic and quantitative assessment of the ubiquitin-modified proteome. *Mol Cell* 44(2):325–340
- Kim M, Chung J, Lee C, Jung J, Kwon Y, Lee K (2011d) A peptide binding to dimerized translationally controlled tumor protein modulates allergic reactions. *J Mol Med* 89(6):603–610
- Kim M, Maeng J, Lee K (2013) Dimerization of TCTP and its clinical implications for allergy. *Biochimie* 95(4):659–666
- Kim HY, Kim S, Pyun HJ, Maeng J, Lee K (2015) Cellular uptake mechanism of TCTP-PTD in human lung carcinoma cells. *Mol Pharm* 12(1):194–203
- Klonis N, Crespo-Ortiz MP, Bottova I, Abu-Bakar N, Kenny S, Rosenthal PJ, Tilley L (2011) Artemisinin activity against *Plasmodium falciparum* requires hemoglobin uptake and digestion. *Proc Natl Acad Sci U S A* 108(28):11405–11410
- Koziol MJ, Garrett N, Gurdon JB (2007) Tpt1 activates transcription of oct4 and nanog in transplanted somatic nuclei. *Curr Biol* 17(9):801–807
- Krishna S, Uhlemann AC, Haynes RK (2004) Artemisinins: mechanisms of action and potential for resistance. *Drug Resist Updates* 7(4–5):233–244
- Krishna S, Bustamante L, Haynes R, Staines H (2008) Artemisinins: their growing importance in medicine. *Trends Pharmacol Sci* 29(10):520–527
- Kronke J, Fink EC, Hollenbach PW, MacBeth KJ, Hurst SN, Udeshi ND, Chamberlain PP, Mani DR, Man HW, Gandhi AK, Svinkina T, Schneider RK, McConkey M, Jaras M, Griffiths E, Wetzler M, Bullinger L, Cathers BE, Carr SA, Chopra R, Ebert BL (2015) Lenalidomide induces ubiquitination and degradation of CK1 $\alpha$  in del(5q) MDS. *Nature* 523(7559):183–188
- Langdon JM, Vonakis BM, MacDonald SM (2004) Identification of the interaction between the human recombinant histamine releasing factor/translationally controlled tumor protein and elongation factor-1 delta (also known as elongation factor-1B beta). *Biochim Biophys Acta* 1688(3):232–236
- Lange OF, Rossi P, Sgourakis NG, Song Y, Lee HW, Aramini JM, Ertekin A, Xiao R, Acton TB, Montelione GT, Baker D (2012) Determination of solution structures of proteins up to 40 kDa using CS-Rosetta with sparse NMR data from deuterated samples. *Proc Natl Acad Sci U S A* 109(27):10873–10878

- Le TP, Vuong LT, Kim AR, Hsu YC, Choi KW (2016) 14-3-3 proteins regulate Tctp-Rheb interaction for organ growth in *Drosophila*. *Nat Commun* 7:11501
- Leclercq TM, Moretti PA, Pitson SM (2011) Guanine nucleotides regulate sphingosine kinase 1 activation by eukaryotic elongation factor 1A and provide a mechanism for eEF1A-associated oncogenesis. *Oncogene* 30(3):372–378
- Lee JH, Rho SB, Park SY, Chun T (2008) Interaction between fortilin and transforming growth factor-beta stimulated clone-22 (TSC-22) prevents apoptosis via the destabilization of TSC-22. *FEBS Lett* 582(8):1210–1218
- Lee J, Kim S, Shin DH, Kim HJ, Lee K (2011) Neuroprotective effect of Cu,Zn-superoxide dismutase fused to a TCTP-derived protein transduction domain. *Eur J Pharmacol* 666(1–3): 87–92
- Leung DW, Amarasinghe GK (2012) Structural insights into RNA recognition and activation of RIG-I-like receptors. *Curr Opin Struct Biol* 22(3):297–303
- Leung DW, Amarasinghe GK (2016) When your cap matters: structural insights into self vs non-self recognition of 5' RNA by immunomodulatory host proteins. *Curr Opin Struct Biol* 36:133–141
- Li W, Zhou Y, Tang G, Xiao Y (2016a) Characterization of the artemisinin binding site for translationally controlled tumor protein (TCTP) by bioorthogonal click chemistry. *Bioconjug Chem* 27(12):2828–2833
- Li S, Chen M, Xiong Q, Zhang J, Cui Z, Ge F (2016b) Characterization of the translationally controlled tumor protein (TCTP) interactome reveals novel binding partners in human cancer cells. *J Proteome Res* 15:3741–3751
- Liu H, Peng HW, Cheng YS, Yuan HS, Yang-Yen HF (2005) Stabilization and enhancement of the antiapoptotic activity of mcl-1 by TCTP. *Mol Cell Biol* 25(8):3117–3126
- Lowther WT, Weissbach H, Etienne F, Brot N, Matthews BW (2002) The mirrored methionine sulfoxide reductases of *Neisseria gonorrhoeae* pilB. *Nat Struct Biol* 9(5):348–352
- Lu C, Xu H, Ranjith-Kumar CT, Brooks MT, Hou TY, Hu F, Herr AB, Strong RK, Kao CC, Li P (2010) The structural basis of 5' triphosphate double-stranded RNA recognition by RIG-I C-terminal domain. *Structure* 18(8):1032–1043
- Lucas AT, Fu X, Liu J, Brannon MK, Yang J, Capelluto DG, Finkielstein CV (2014) Ligand binding reveals a role for heme in translationally-controlled tumor protein dimerization. *PLoS One* 9(11):e112823
- Lucibello M, Adanti S, Antelmi E, Dezi D, Ciafre S, Carcangiu ML, Zonfrillo M, Nicotera G, Sica L, De Braud F, Pierimarchi P (2015) Phospho-TCTP as a therapeutic target of Dihydroartemisinin for aggressive breast cancer cells. *Oncotarget* 6(7):5275–5291
- Lupas AN, Zhu H, Korycinski M (2015) The thalidomide-binding domain of cereblon defines the CULT domain family and is a new member of the beta-tent fold. *PLoS Comput Biol* 11(1): e1004023
- Maeng J, Kim M, Lee H, Lee K (2015) Insulin induces phosphorylation of serine residues of translationally controlled tumor protein in 293T cells. *Int J Mol Sci* 16(4):7565–7576
- Mulenga A, Azad AF (2005) The molecular and biological analysis of ixodid ticks histamine release factors. *Exp Appl Acarol* 37(3–4):215–229
- Munirathinam G, Ramaswamy K (2012) Sumoylation of human translationally controlled tumor protein is important for its nuclear transport. *Biochem Res Int* 2012:831940
- Niikura M, Liu HC, Dodgson JB, Cheng HH (2004) A comprehensive screen for chicken proteins that interact with proteins unique to virulent strains of Marek's disease virus. *Poult Sci* 83(7): 1117–1123
- O'Neill PM, Barton VE, Ward SA (2010) The molecular mechanism of action of artemisinin—the debate continues. *Molecules* 15(3):1705–1721
- Panrat T, Sinthujaroen P, Nupan B, Wanna W, Tammi MT, Phongdara A (2012) Characterization of a novel binding protein for Fortilin/TCTP—component of a defense mechanism against viral infection in *Penaeus monodon*. *PLoS One* 7(3):e33291

- Petzold G, Fischer ES, Thoma NH (2016) Structural basis of lenalidomide-induced CK1alpha degradation by the CRL4(CRBN) ubiquitin ligase. *Nature* 532(7597):127–130
- Ranaivoson FM, Neiers F, Kauffmann B, Boschi-Muller S, Branlant G, Favier F (2009) Methionine sulfoxide reductase B displays a high level of flexibility. *J Mol Biol* 394(1):83–93
- Rao KV, Chen L, Gnanasekar M, Ramaswamy K (2002) Cloning and characterization of a calcium-binding, histamine-releasing protein from *Schistosoma mansoni*. *J Biol Chem* 277(34):31207–31213
- Rehmann H, Bruning M, Berghaus C, Schwarten M, Kohler K, Stocker H, Stoll R, Zwartkruis FJ, Wittinghofer A (2008) Biochemical characterisation of TCTP questions its function as a guanine nucleotide exchange factor for Rheb. *FEBS Lett* 582(20):3005–3010
- Rho SB, Lee JH, Park MS, Byun HJ, Kang S, Seo SS, Kim JY, Park SY (2011) Anti-apoptotic protein TCTP controls the stability of the tumor suppressor p53. *FEBS Lett* 585(1):29–35
- Rid R, Onder K, Trost A, Bauer J, Hintner H, Ritter M, Jakab M, Costa I, Reischl W, Richter K, MacDonald S, Jendrach M, Bereiter-Hahn J, Breitenbach M (2010) H<sub>2</sub>O<sub>2</sub>-dependent translocation of TCTP into the nucleus enables its interaction with VDR in human keratinocytes: TCTP as a further module in calcitriol signalling. *J Steroid Biochem Mol Biol* 118(1–2):29–40
- Robert X, Gouet P (2014) Deciphering key features in protein structures with the new ENDscript server. *Nucleic Acids Res* 42(Web Server issue):W320–W324
- Sanchez JC, Schaller D, Ravier F, Golaz O, Jaccoud S, Belet M, Wilkins MR, James R, Deshusses J, Hochstrasser D (1997) Translationally controlled tumor protein: a protein identified in several nontumoral cells including erythrocytes. *Electrophoresis* 18(1):150–155
- Seo EJ, Efferth T (2016) Interaction of antihistaminic drugs with human translationally controlled tumor protein (TCTP) as novel approach for differentiation therapy. *Oncotarget* 7(13):16818–16839
- Slomianny C (1990) Three-dimensional reconstruction of the feeding process of the malaria parasite. *Blood Cells* 16(2–3):369–378
- Stellfox ME, Nardi IK, Knippler CM, Foltz DR (2016) Differential binding partners of the Mis18alpha/beta YIPPEE domains regulate Mis18 complex recruitment to centromeres. *Cell Rep* 15(10):2127–2135
- Subramanian L, Medina-Pritchard B, Barton R, Spiller F, Kulasegaran-Shylini R, Radaviciute G, Allshire RC, Arockia Jeyaprakash A (2016) Centromere localization and function of Mis18 requires Yippee-like domain-mediated oligomerization. *EMBO Rep* 17(4):496–507
- Susini L, Besse S, Duflaut D, Lespagnol A, Beekman C, Fiucci G, Atkinson AR, Busso D, Poussin P, Marine JC, Martinou JC, Cavarelli J, Moras D, Amson R, Telerman A (2008) TCTP protects from apoptotic cell death by antagonizing bax function. *Cell Death Differ* 15(8):1211–1220
- Telerman A, Amson R, Cans C, Nancy-Portebois V, Passer BJ (2006) US Patent 20060140970 (06/29/2006)
- Teshima S, Rokutan K, Nikawa T, & Kishi K (1998) Macrophage colony-stimulating factor stimulates synthesis and secretion of a mouse homolog of a human IgE-dependent histamine-releasing factor by macrophages in vitro and in vivo. *J Immunol* 161(11):6356–6366
- Thaw P, Baxter NJ, Hounslow AM, Price C, Waltho JP, Craven CJ (2001) Structure of TCTP reveals unexpected relationship with guanine nucleotide-free chaperones. *Nat Struct Biol* 8(8):701–704
- Thebault S, Agez M, Chi X, Stojko J, Cura V, Telerman SB, Maillet L, Gautier F, Billas-Massobrio I, Birck C, Troffer-Charlier N, Karafin T, Honore J, Senff-Ribeiro A, Montessuit S, Johnson CM, Juin P, Cianferani S, Martinou JC, Andrews DW, Amson R, Telerman A, Cavarelli J (2016) TCTP contains a BH3-like domain, which instead of inhibiting, activates Bcl-xL. *Sci Rep* 6:19725
- Tonganunt M, Nupan B, Saengsakda M, Suklour S, Wanna W, Senapin S, Chotigeat W, Phongdara A (2008) The role of Pm-fortilin in protecting shrimp from white spot syndrome virus (WSSV) infection. *Fish Shellfish Immunol* 25(5):633–637
- Tsarova K, Yarmola EG, Bubb MR (2010) Identification of a cofilin-like actin-binding site on translationally controlled tumor protein (TCTP). *FEBS Lett* 584(23):4756–4760

- Tuynder M, Fiucci G, Prieur S, Lespagnol A, Geant A, Beaucourt S, Duflaut D, Besse S, Susini L, Cavarelli J, Moras D, Amson R, Teلمان A (2004) Translationally controlled tumor protein is a target of tumor reversion. *Proc Natl Acad Sci U S A* 101(43):15364–15369
- Vedadi M, Lew J, Artz J, Amani M, Zhao Y, Dong A, Wasney GA, Gao M, Hills T, Broxk S, Qiu W, Sharma S, Diassiti A, Alam Z, Melone M, Mulichak A, Wernimont A, Bray J, Loppnau P, Plotnikova O, Newberry K, Sundararajan E, Houston S, Walker J, Tempel W, Bochkarev A, Kozieradzki I, Edwards A, Arrowsmith C, Roos D, Kain K, Hui R (2007) Genome-scale protein expression and structural biology of *Plasmodium falciparum* and related Apicomplexan organisms. *Mol Biochem Parasitol* 151(1):100–110
- Wang X, Fonseca BD, Tang H, Liu R, Elia A, Clemens MJ, Bommer UA, Proud CG (2008) Re-evaluating the roles of proposed modulators of mammalian target of rapamycin complex 1 (mTORC1) signaling. *J Biol Chem* 283(45):30482–30492
- Wang F, Hu C, Hua X, Song L, Xia Q (2013) Translationally controlled tumor protein, a dual functional protein involved in the immune response of the silkworm, *Bombyx mori*. *PLoS One* 8(7):e69284
- Wu H, Gong W, Yao X, Wang J, Perrett S, Feng Y (2015) Evolutionarily conserved binding of translationally controlled tumor protein to eukaryotic elongation factor 1B. *J Biol Chem* 290(14):8694–8710
- Xiao B, Chen D, Luo S, Hao W, Jing F, Liu T, Wang S, Geng Y, Li L, Xu W, Zhang Y, Liao X, Zuo D, Wu Y, Li M, Ma Q (2016) Extracellular translationally controlled tumor protein promotes colorectal cancer invasion and metastasis through Cdc42/JNK/MMP9 signaling. *Oncotarget* 7(31):50057–50073
- Xu A, Bellamy AR, Taylor JA (1999) Expression of translationally controlled tumour protein is regulated by calcium at both the transcriptional and post-transcriptional level. *Biochem J* 342:683–689
- Xu Q, Hou YX, Langlais P, Erickson P, Zhu J, Shi CX, Luo M, Zhu Y, Xu Y, Mandarino LJ, Stewart K, Chang XB (2016) Expression of the cereblon binding protein argonaute 2 plays an important role for multiple myeloma cell growth and survival. *BMC Cancer* 16:297
- Yang Y, Yang F, Xiong Z, Yan Y, Wang X, Nishino M, Mirkovic D, Nguyen J, Wang H, Yang XF (2005) An N-terminal region of translationally controlled tumor protein is required for its antiapoptotic activity. *Oncogene* 24(30):4778–4788
- Yarm FR (2002) Plk phosphorylation regulates the microtubule-stabilizing protein TCTP. *Mol Cell Biol* 22(17):6209–6221
- Yoon T, Jung J, Kim M, Lee KM, Choi EC, Lee K (2000) Identification of the self-interaction of rat TCTP/IgE-dependent histamine-releasing factor using yeast two-hybrid system. *Arch Biochem Biophys* 384(2):379–382
- Yoon T, Kim M, Lee K (2006) Inhibition of Na,K-ATPase-suppressive activity of translationally controlled tumor protein by sorting nexin 6. *FEBS Lett* 580(14):3558–3564
- Zhang X (2014) Etude de complexes protéine-protéine impliquant la chaperone de bas poids moléculaire HSP27: Implications dans le cancer de la prostate. PhD Thesis, Aix-Marseille Université
- Zhang D, Li F, Weidner D, Mnjayan ZH, Fujise K (2002) Physical and functional interaction between myeloid cell leukemia 1 protein (MCL1) and Fortilin. The potential role of MCL1 as a fortilin chaperone. *J Biol Chem* 277(40):37430–37438
- Zhang J, de Toledo SM, Pandey BN, Guo G, Pain D, Li H, Azzam EI (2012) Role of the translationally controlled tumor protein in DNA damage sensing and repair. *Proc Natl Acad Sci U S A* 109(16):E926–E933
- Zhou Y, Li W, Xiao Y (2016) Profiling of multiple targets of artemisinin activated by hemin in cancer cell proteome. *ACS Chem Biol* 11(4):882–888



work was to test if isolated TCTP could present alternative structures in near-physiological or mild environmental pressure (salt, pH, urea...) in order to propose a comprehensive model that would describe the diversity of TCTP structures in solution (Sec. 1.4, 3). The second objective was to characterize the TCTP/Mcl-1 complex and to compare with the related TCTP/Bcl-xL complex in order to provide clues about the molecular basis of this TCTP-induced reinforcement of Bcl-xL and Mcl-1 antiapoptotic properties, in line with the particular BH3-like nature of TCTP protein (Sec. 1.4, 4). Especially, we paid attention to structure and dynamics changes that could occur in TCTP upon binding since we suggested that the BH3-like motif is likely to unpin from the globular core domain of the protein to bind Bcl-2 family partners. Our third objective was to explore TCTP interactome and beyond, by first characterizing interactions between TCTP and MDM2 in apoptosis and YB-1/RNA in nucleic acids processing pathways. We also wanted to use organic ligands in order to detect and map interactions on TCTP and also Mcl-1 protein (Sec. 1.4, 5) and their potential effect on the protein/protein complexes. In the current section, we present strategy to fulfill all three objectives by means of principles from biochemistry, molecular biology, analytical chemistry, biophysics and computational chemistry that we briefly present in the section (Sec. 1.4) with a more extensive description given in the next chapter of material and methods (Sec. 2).

### **Structural characterization of TCTP and alternative states**

TCTP interacts with many partners of various natures, functions and all share high structural heterogeneity [145] (Sec. 1.3). In the other hand, TCTP structure is relatively simple and the protein is small, which is counter-intuitive with its pleiotropic nature. Accordingly, we formulate the hypothesis that TCTP is prone to structural plasticity to explain how it can adapt to its myriad of partners. The first objective of the PhD was to test if isolated TCTP could present alternative structures in near-physiological or mild environmental pressure in order to propose a comprehensive model that would describe the diversity of TCTP structures (Sec. 3).

To do so, we first characterized native TCTP structure and dynamics and probed for the existence of non-covalent dimers in solution. We used site-directed mutagenesis and *in vitro* phosphorylation by Plk-1 to detect if changes in the primary sequence of TCTP could induce structure transition in the protein. To evaluate the possible role of TCTP IDR in remodeling the protein core domain, we studied phosphorylated TCTP and upon calcium binding using a combination of *in vitro* and *in silico* approaches. Finally, we wanted to question the existence of a minor, pre-existing TCTP state in solution that could further mediate binding to protein partners. To answer the question, we identified the determinants

of local (backbone stability) and global (buffer conditions of pH, salt) stability in TCTP. We tracked TCTP alternative states and thus we used environmental parameters such as salt, pH, urea or even hydrostatic pressure to populate minor states of the protein in solution. We extensively characterized the structure of TCTP alternative states at all primary, secondary and tertiary structure organization levels and we also assessed the oligomeric state.

## **Structural analysis of TCTP in interaction with Bcl-xL/Mcl-1**

Studies have highlighted that TCTP can inhibit apoptosis in cancer cells by binding to both Bcl-2 family members Bcl-xL [111] and Mcl-1 [172], thus promoting their antiapoptotic properties by distinct mechanisms (Sec. 1.2.3.2). Recently, the crystal structure of TCTP<sub>BH3</sub>/Bcl-xL complex was released [111] and the BH3-like peptide turned  $\alpha$ -helical in the BH3-binding groove of the protein, rising question about a structural transition for the  $\beta$ -sheet fold from free TCTP [145] (Sec. 1.3). Thus, the second objective of the PhD was to characterize the TCTP/Mcl-1 complex and to compare with the related TCTP/Bcl-xL complex in order to provide clues about both structure changes in TCTP and molecular basis of this TCTP-induced reinforcement of Bcl-xL and Mcl-1 antiapoptotic properties (Sec. 4).

We wanted to characterize the protein complexes at all organization levels, and we carefully looked at each TCTP, Mcl-1 and Bcl-xL proteins, isolated and in complex. To achieve the task, we estimated the hydrodynamic volume of TCTP and BH3-derived peptide in complex with Bcl-2 family partners. We looked for the apparent molecular weight of molecular species to gain informations on complex stoichiometry. In order to detect structure changes, we evaluated the secondary and tertiary structure content of isolated proteins and upon complex formation. Efforts were made at characterizing possible fluctuations in TCTP tertiary structure upon complex formation. We questioned if a stabilized folding intermediate of TCTP could change association kinetics with Mcl-1. Beyond the characterization of TCTP structure in complex with partners, we studied the impact of complex formation on the structure of Bcl-xL and Mcl-1. To do so, we first evaluated if the BH3-like peptide from TCTP could bind Mcl-1 and we looked to map the binding site on the protein. Then we went through full length TCTP and we extensively compared with the binding mode of the isolated BH3-like peptide in term of complex size, dynamics and binding interface to determine how the rest of TCTP structure impacts the interaction with Mcl-1. TCTP and Bcl-xL interaction was also studied and compared to Mcl-1/TCTP, considering that Bcl-xL is known to form 3D swapped dimer in solution. We also precisely deciphered the interaction mode of the two Bcl-xL and Mcl-1 with TCTP or BH3-like peptide to look for a transient association in parallel of the formation of the more stable complex. We also used

BH3-derived peptides from TCTP and Mule to bring clues about the importance of full length TCTP and the impact of aspartate residue at position h1 in the BH3-like sequence where a conserved hydrophobic amino-acid is found in canonical BH3s. Finally, we extensively compared BH3-derived peptides from Mule and TCTP to Mcl-1 to bring clues about the importance of h1 position and the differences between canonical and BH3-like sequence at Mcl-1 protein in term of binding site and complex dynamics. Finally, we computed molecular models of Mcl-1 complexes with BH3-derived sequences and estimated the binding affinity of all three TCTP<sub>BH3</sub>, TCTP<sub>BH3D16I</sub> and Mule<sub>BH3</sub> peptides.

### **TCTP complex with MDM2, YB-1/RNA, ligands and beyond**

The impact of TCTP in apoptosis was also described at MDM2 protein (Fig. 1.15) with unclear binding interface (Sec. 1.2.3.1). It was shown that ligands targeting TCTP such as sertraline and thioridazine disrupted the TCTP/MDM2 interaction, preventing p53 from degradation (Sec. 1.2.3.3). In TCTP interactome, the Mcl-1 protein is also a target of choice in cancer treatment (Sec. 1.1.2.2). Beyond apoptosis, a recent report found TCTP and YB-1 protein in complex and we speculate a putative role in the metabolism of RNA (Fig. 1.15) (Sec. 1.2.2.2). Consequently, our third objective was to explore TCTP interactome, by characterizing interactions between TCTP, MDM2 and YB-1/RNA. We also wanted to use organic ligands in order to detect and map interactions on TCTP and Mcl-1 (Sec. 5).

We aimed first at characterizing the interaction between TCTP and MDM2 N-terminal domain to latter discuss the binding mode compared to other TCTP complexes. Also, we could obtain from our collaborator D. Pastre (SABNP, INSERM/Université Paris-Saclay) full length YB-1 and variant 1-180 truncated for the C-terminal IDR. We tested if TCTP could bind RNA sequences in a direct manner. Next, we evaluated if YB-1 and TCTP could directly interact *in vitro* and tested the importance of the YB-1 C-terminal IDR for the interaction. We could finally measure the impact of RNA on TCTP/YB-1 complex and we investigated to know if a ternary complex could still assemble. Second, we used historical ligands and newly developed drugs targeting TCTP to investigate the impact of the molecule on TCTP structure and stability. Beyond TCTP, the team of our collaborator F. Roussi (ICSN, CNRS/Université Paris-Saclay) has developed ligands selective to Mcl-1 versus Bcl-xL and disposed of encouraging results in competition assays using ligands, BH3 peptides and Bcl-2 like proteins by fluorescence polarization. Thus, we finally characterized the interaction between these ligands and Bcl-xL plus Mcl-1 and mapped binding interface together with investigating the ligand selectivity for Mcl-1 compared to Bcl-xL.

## Methods

NMR was the main analytical method we used to monitor proteins and complexes structure and dynamics. NMR informs on all levels of structure organization in solution and thus is a tool of choice to study biomolecular systems, as reviewed in the next chapter (Sec. 2.3.1.2). We used 2D and 3D NMR experiments to characterize protein structure and binding affinity or interface at a residue resolution.  $^{15}\text{N}$ -spin relaxation,  $^1\text{H}\{-^{15}\text{N}\}$  heteronuclear NOEs, Chemical Exchange Saturation Transfer (CEST) and Carr-Purcell-Meiboom-Gill (CPMG) experiments were routinely used to evaluate the local and global dynamics of  $^{15}\text{N}$ -labeled proteins, isolated or upon complex formation. Diffusion-Ordered Spectroscopy (DOSY) NMR was also useful to estimate the translational diffusion coefficient (D) of proteins and complexes. We also probed the backbone stability of proteins toward amide hydrogen solvent-exchange by doing Hydrogen/Deuterium-eXchange (HDX) NMR experiments. Beyond NMR, we used other biophysical methods to study proteins and complexes structure and dynamics. To estimate protein stability and test interactions with ligands, we used the Thermal Shift Assay (TSA) protocol that allows to determine the melting temperature ( $T_m$ ) of a protein in given conditions. To modify proteins primary sequence, we used Plk-1 mediated *in vitro* phosphorylation and site-directed mutagenesis to obtain protein variants. We could detect modification in protein primary sequence by doing MS and Polyacrylamide Gel Electrophoresis (PAGE) experiments. The secondary structure content in proteins and complexes was estimated by far-UV Circular Dichroism (CD) experiments. For the tertiary structure evaluation, we used near-UV CD and limited proteolysis. 8-Anilinonaphthalene-1-sulfonic acid (ANS) fluorescence assay, that detects Molten-Globule (MG) states, was also used to determine how the tertiary structure in globular proteins could fluctuate, ultimately leading the ANS probe to enter in the core domain with raised fluorescence in hydrophobic environment. We could estimate tertiary structure and quaternary organization of proteins and complexes by doing Dynamic Light Scattering (DLS), Size Exclusion Chromatography (SEC), Multi-Angle Light Scattering (MALS) and Small-Angle X-ray Scattering (SAXS) experiments. DLS and SEC permit to estimate the hydrodynamic volume of proteins whereas MALS and SAXS experiments yield the apparent molecular weight of the molecular entity which is crucial to describe complex stoichiometry or self-association equilibrium. Finally, computational approaches such as molecular docking with HADDOCK web server [191] were used to compute structural models of protein-peptide complexes. We also used MST method to measure protein-protein and protein-peptide interaction affinity. Notably, MD via GROMACS software suite were used to compute conformational ensemble of proteins upon modification like phosphorylation or calcium binding. This work was facilitated by

a vast ensemble of home-made scripts and command-line processing routines. All the before-mentioned methods are more extensively described in the next chapter (Sec. 2).



# Chapter 2

## Materials and Methods

Our investigations in the molecular mechanisms by which TCTP and partners associate have required the use of a large panel of biophysical methods and principles from biochemistry and molecular biology. In the current chapter, we will report methods we used in terms of principles, objectives and practical aspects. Wetlab routines will be presented first and include protocols related to bacteria, sample integrity control and crystallization (Sec. 2.1). Second, we will report our rationale to design protein construct and protocols from protein expression and purification (Sec. 2.2). This work heavily relies on analytical, biophysical and computational methods and we will briefly describe all of them with the corresponding setups (Sec. 2.3). We will more extensively introduce NMR since we extensively used it in experiments we present in the manuscript.

### 2.1 Wetlab routines

Here, we report practical information and methods for small-scale preparation of bacteria incorporating a plasmid of interest. As part of the major routine techniques, PAGE and MS based experiments that report on the primary sequence integrity of a protein are also detailed in the section. Information on crystallization assays we carried out on TCTP and related complexes are also provided.

## 2.1.1 Bacterial transformation, storage and culture

### 2.1.1.1 Transformation protocols

Bacterial strains were genetically engineered using both thermal shock and electroporation methods. DNA fragments were controlled by commercial DNA sequencing (Eurofins Genomics). Competent *E. coli* for thermal shock were produced for daily use.

#### DH5 $\alpha$ and BL21 STAR production

DH5 $\alpha$  and BL21 STAR *E. coli* strains (code: DH5 $\alpha$ , BL21 (DE3) pLysS in [192]) are chemically competent and sensitive to the thermal shock transformation method. Both were obtained by regenerating bacteria in rich medium (2xYT) from a small (5 mL) to a large (100 mL) culture to Optical Density (OD)<sub>600</sub> 0.3-0.4. Bacterial pellet was isolated at 4 °C by slow (500 g, 5 min) centrifugation and resuspended in a cold calcium-rich buffer (5 mL of 0.1 M CaCl<sub>2</sub> and 15% glycerol). This process was repeated twice. Aliquots (100  $\mu$ L) were immediately flash-frozen. After the end of culture, all materials were kept on ice.

#### Thermal shock procedure

The aliquot of chemically competent *E. coli* cells (100  $\mu$ L) was kept on ice until melting. A small volume of plasmid (1-10 % v/v @ 100-1000 ng/ $\mu$ L) was gently mixed with the cell suspension and the sample was kept on ice for 30 min. Homogeneous samples were incubated at 42 °C during 90 s before putting the suspension back on ice. A minute later a volume of rich medium (2xYT) was added (900  $\mu$ L) and the sample incubated at 37 °C for 1-3 hours with vigorous agitation to prevent bacteria sedimentation. The resulting culture was centrifuged at low (500 g) speed to harvest bacteria and those were spread directly on a pre-heated agar plate of standard composition (LB, 2% (w/v) agar-agar and specific antibiotics).

#### Electroporation

In special cases, such as low efficiency transformation or low plasmid concentration, the electroporation method was used with associated commercial strains. The aliquot of *E. coli* cells competent for electroporation (50  $\mu$ L) was kept on ice until melting. A small volume of plasmid solution (1-10 % v/v @ 100-1000 ng/ $\mu$ L) was gently mixed with the cell suspension and the sample was transferred in an electroporation cuvette (EP-102, Cell projects). Current voltage was set at 2500 V according to the manufacturer specific recommendations (Eppendorf electroporator 2510). Bacterial transformation was then promoted by the application of a short (5 ms) electric current through the cell suspension. Rich medium (2xYT) was added (900  $\mu$ L) immediately after electric shock and the suspension was incubated at 37 °C for 1-3 hours before spreading on agar of standard composition (see above).

### 2.1.1.2 Glycerol stocks

The inoculation of agar plates by freshly transformed bacteria yielded colonies after 12-48 hours of incubation at 37 °C. Generally, a single colony was inoculated in rich medium (2xYT, 5 mL) and incubated at 37 °C until saturation of OD<sub>600</sub>. Glycerol stocks (1 mL) were then prepared by adding glycerol in the bacterial culture (25% v/v). Stocks were stored at -80 °C. Alternatively, minimal medium M9 or D<sub>2</sub>O can be used to prepare specific glycerol stocks. For M9 cultures in D<sub>2</sub>O the gradual increase in concentration during successive small cultures (5 mL) was employed to make the corresponding glycerol stocks. All available stocks with details are reported for DNA storage (Ann. 1) and expression strains (Ann. 2). On a daily basis, single-use glycerol stocks (20 µL) were preferred in order to preserve the master bank.

### 2.1.1.3 Preculture to main culture

Preculture were started 24 hours before main culture by inoculating a small (5 mL) volume of medium with a trace of the desired glycerol stock (Ann. 2). The relevant antibiotics were added and the flask incubated at 37 °C until the day after. Then the main culture was inoculated with a volume of saturated preculture to reach OD<sub>600</sub> = 0.05 in presence of the relevant antibiotics. Bacterial growth was monitored at OD<sub>600</sub> until next decision. 2xYT rich medium was preferred (NaCl, tryptone and yeast extract at 5, 16 and 10 g.L<sup>-1</sup> in milliQ water). Poor medium M9 was prepared for stable isotopic labeling needs (<sup>2</sup>H, <sup>15</sup>N, <sup>13</sup>C) using a classical recipe (M9 salts, 4 g.L<sup>-1</sup> glucose, 200 µM MgSO<sub>4</sub>, 10 µM CaCl<sub>2</sub>, 1 X MEM vitamins (invitrogen) 1 X oligoelements mix). For 1 L of medium, M9 salts were prepared as follow: Na<sub>2</sub>HPO<sub>4</sub>·7H<sub>2</sub>O (12.8 g), KH<sub>2</sub>PO<sub>4</sub> (3 g) and sodium chloride (1 g). Oligoelements recipe is as follow for 200 mL of 100 X preparation: 1 g EDTA, 0.9 g CaCl<sub>2</sub>, 88 mg CuSO<sub>4</sub>·5H<sub>2</sub>O, 240 mg MnCl<sub>2</sub>·4H<sub>2</sub>O, 4 mg H<sub>3</sub>BO<sub>3</sub>, 140 mg ZnSO<sub>4</sub>·7H<sub>2</sub>O, 1.2 g FeSO<sub>4</sub>·7H<sub>2</sub>O and 40 mg of reduced ascorbic acid in water (qsp 200 mL).

## 2.1.2 Protein analysis

### 2.1.2.1 PAGE experiments in various setup

Methods relying on PAGE look at the migration of a protein under an electric current through a polymer of variable density. Information about purity, molecular weight, isoelectric point and polydispersity can be derived from such experiments. PAGE technique was used in native, denaturing and reducing conditions in function of the specific need. Gel composition and setup are all recapitulated (Tab. 2.1). All PAGE-derived experiments were stained by

Type	Gel	%	Acrylamide (mL)	Water (mL)	Buffer (mL)	APS 10 % (μL)	TEMED (μL)	SDS 10 % (μL)	Urea (g)	Glycerol (% v/v)
SDS-PAGE	Stacking	4	0.4	2.6	1	5	50	5	-	-
	Resolving	9	2.7	6.3	3	12	120	12	-	-
		12	3.6	5.4	3	12	120	12	-	-
		15	4.5	4.5	3	12	120	12	-	-
		18	5.4	3.6	3	12	120	12	-	-
Native-PAGE	Stacking	4	0.4	2.6	1	5	50	No	-	-
	Resolving	12	3.6	5.4	3	12	120	No	-	-
Tris-tricine PAGE	Stacking	4	0.32	2.33	1.33	12	3	Run. Buffer	-	-
	Separation	20	4.85	0.2	4	40	9	Run. Buffer	5.76 (8 M)	1.2

**Table 2.1 Composition of gels for PAGE based experiments (2 gels 1 mm thickness).** For the preparation of 4 mL stacking and 12 mL resolving gels. Acrylamide refers to a 40 % w/v solution of 37.5:1 acrylamide:bisacrylamide ratio for SDS-PAGE or Native-PAGE and 49.5% w/v solution of 32:1 acrylamide:bisacrylamide ratio for Tris-tricine gels. Buffer refers to 1.5 M Tris-HCl pH 8.8 for stacking and 0.5 M Tris-HCl pH 6.8 for resolving gel in the SDS-PAGE and Native-PAGE section. Otherwise buffer refers to 3 M Tris-HCl pH 8.45 and 0.3% w/v SDS in the Tris-tricine section. For SDS-PAGE and Native-PAGE a unique running buffer was used for the anode and cathode: 25 mM Tris base pH 8.3, 192 mM glycine and finally 0.1% SDS for SDS-PAGE. For Tris-tricine gel the anode buffer (100 mM Tris-HCl pH 6.8) and the cathode buffer (0.1 M Tris-base pH 8.25, 0.1 M tricine and 0.1% (w/v) SDS) were used. pH of running buffer should never be adjusted. The sample buffer should contain 50 mM Tris-HCl pH 6.8, 25% (v/v) glycerol, 8% (w/v) SDS, 100 mM DTT and 0.02% (w/v) bromophenol blue. Concentrated solution of loading buffer was generally added to the sample prior to heating at 95 °C during 5 min and spotting on the gel. For Native-PAGE experiments, SDS, high DTT concentration and heating were prohibited. Typical running setup was 80 V at 20 mA for stacking and up to 600 V with max 80 mA for resolving gels in SDS-PAGE and Tris-tricine PAGE experiments. For Native-PAGE, gels were run at 80 V and 20 mA until desired migration.

using standard methods relying on Commassie blue (R250, with ethanol (30 % v/v) and acetic acid (10 % v/v) in milliQ water) or silver ions (SilverQuest, Invitrogen/Thermofisher). Gels of interest were conserved in 10% acetic acid at 4 °C.

### 2.1.2.2 Mass Spectrometry (MS) MALDI-TOF

An UltrafleXtreme mass spectrometer (Bruker) was used with Matrix-assisted laser desorption/ionization (MALDI) of the sample with Time Of Flight (TOF) analyzer to determine molecular weight of proteins. Samples were all readily crystallized with MALDI matrix (sinapinic acid) since they contained low NaCl concentration (< 150 mM). Acquisitions were performed in positive ion mode and laser intensity was set close to the ionization threshold to ensure the best signal to noise ratio. Mass calibration was achieved with Bovine Serum Albumin (BSA) protein prior to analysis to estimate uncertainty. All data were processed using FlexAnalysis (Bruker) and text file were further exported. The experiments were done at ICSN under the guidance of V. Guérineau (ICSN, CNRS/Université Paris-Saclay).

### 2.1.3 Cristallogenesis

Cristallogenesis assays were done on isolated Mcl-1 and in complex with TCTP<sub>BH3</sub> or TCTP FL. Mcl-1 and Mcl-1/TCTP<sub>BH3</sub> were prepared at neutral pH (Tris 5 mM pH 7, 50 mM NaCl) and high concentration (10 mg.mL<sup>-1</sup>). TCTP<sub>BH3</sub> peptide (3 eq.) was added to Mcl-1 to fully form the complex without further purification. Mcl-1/TCTP FL complex was prepared in alkaline conditions (50 mM CHES pH 9, 50 mM NaCl, 2 mM TCEP) due to limitation of the complex solubility at more acidic pH. For the latter complex, 20 min of incubation at 35 °C was required to accelerate complex formation. Crystallization assays were carried out via the I2BC crystallization platform (CNRS/Université Paris-Saclay) with a Mosquito system (TTP Labtech) using 1:1 and 2:1 mix ratio (protein:reservoir) for session 1 (PEGs, PEGs\_II, Classics) and session 2 (Protein\_Complex), respectively [193]. Online monitoring via the CRIMS system (EMBL-GR) allowed for drops observation and statistics over several months. The experiments were done under the guidance of A. Vigouroux and S. Plancqueel (I2BC, CNRS/Université Paris-Saclay) and P. Retailleau (ICSN, CNRS/Université Paris-Saclay).

## 2.2 Protein design, production and purification

In studying TCTP interactome, we needed several protein constructs and here we present corresponding procedures and methodology for protein production from gene design and cloning to expression and purification protocols. We list here several important elements such as DNA sequences for the major plasmid we used for protein production (Ann. 1), available glycerol stocks of bacteria for protein expression and DNA storage (Ann. 1, 2) but also general and specific information for protein expression and purification (Tab. 2.2.2). Finally, we summarize all primary sequences of protein we expressed and used in the study (Ann. 3).

### 2.2.1 Design and engineering of relevant proteins

#### 2.2.1.1 TCTP constructs and derivatives

TCTP protein (Fig. 2.1 A, C) is a 172 amino-acid single-domain protein encompassing an Intrinsically Disordered Region (IDR) in the 38-66 segment of the molecule, presumably important for protein function [145] and undergoing crucial phosphorylations at residues S46 and S64 for correct mitosis termination [33]. Moreover two conserved signatures TCTP1 and are present in the IDR region and helix  $\alpha_3$ .

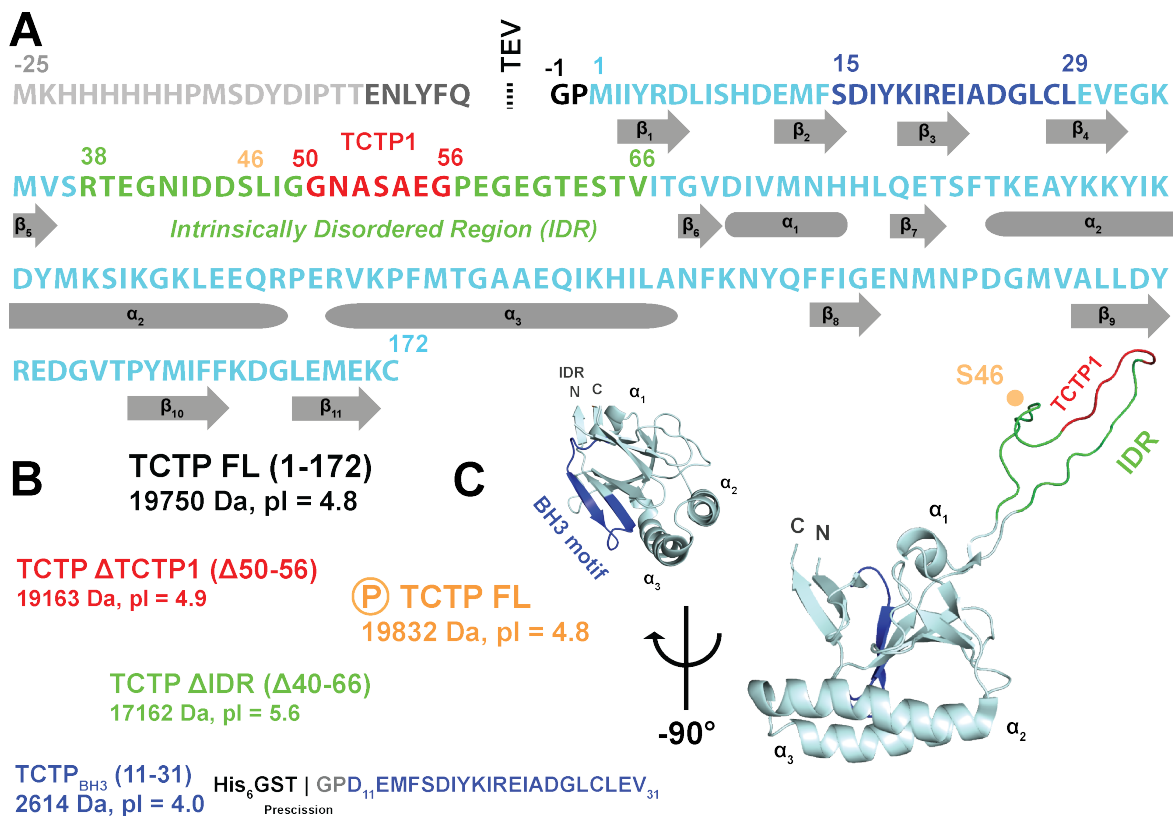


**Fig. 2.1 TCTP and variants.** (A) Primary sequence of human TCTP in fusion with a N-terminal His<sub>6</sub> tag. The sequence of the tag (lightgrey) and Tobacco Etch Virus protease (TEV) cleavage site (grey) are highlighted. TCTP is obtained with two extra N-terminal GP residues from TEV cleavage (black). On the sequence of the native TCTP (cyan), the conserved TCTP signature 1 (red) in the IDR region (green) and the phosphorylation site S46 are highlighted. The BH3-like motif is also shown (blue). Secondary structure elements are represented for  $\alpha$ -helix (rounded rectangle) and  $\beta$ -sheet (arrows). (B) TCTP constructs and properties. Full length TCTP (black) and variants lacking the TCTP signature 1 (TCTP1) (red) or the whole IDR (green) were expressed and purified. A recombinant peptide encompassing the BH3-like motif of the protein was also produced and purified (blue). (C) Representation of TCTP structure elements relevant to current protein constructs. On the protein structure (pdb code: 2HR9) the IDR region (40-66, orange), the TCTP1 signature (50-56, red) and the BH3-like motif (11-31, blue) are highlighted. Protein sequences are numbered according to the human canonical isoform.

TCTP FL and mutants were designed (Fig. 2.1 A, B) in order to question the role of the TCTP signature 1 and IDR region in the protein structure and interactions. Consequently, TCTP constructs lacking the conserved signature TCTP1 (50-56) (referred as TCTP  $\Delta$ TCTP1) or the whole disordered segment (40-66) (referred as TCTP  $\Delta$ IDR) were designed. We finally post-translationally modified TCTP FL by means of Plk-1 mediated phosphorylation to yield S46P-TCTP FL for evaluating the impact of IDR modification on protein structure, dynamics and interactions.

The DNA template encoding human TCTP was a pET-M11 plasmid [194] and we list the corresponding DNA sequence (Ann. 1). Deletion within TCTP sequence to obtain TCTP  $\Delta$ IDR ( $\Delta$ 40-66) and TCTP  $\Delta$ TCTP1 ( $\Delta$ 50-56) were done with partially overlapping primer using a single step of Polymerase Chain Reaction (PCR) amplification combined with DpnI mediated digestion of the original pET-M11 template [195]. Primers were designed paying attention to the GC content and melting temperature prediction from Serial Cloner software [196] (Ann. 2). For mutagenesis, PCR samples were prepared with the QuickChange kit (Agilent) and protocol [197]. PCR cycle was set as follow: 10-15-180 s for denaturation (98 °C), hybridation ( $\sim T_m - 5$  °C) and amplification (72 °C) of the template, respectively. The mixture was kept at 4°C after the end of the run until use. DNA sequences of PCR products were subcloned into expression vectors and amplified after transformation of DNA production bacterial strains to be further sequenced for control of the TCTP gene sequence (Eurofins Genomics). For TCTP<sub>BH3</sub>, the plasmid encoding His<sub>6</sub>-GST-TCTP<sub>BH3</sub> was commercially obtained (pRSETA vector, Invitrogen). In addition to the protein constructs for which expression was detected several others were successfully cloned but no protein expression could be detected (TCTP C27W, C27R,  $\Delta$ BH3  $\Delta$ IDR, and  $\Delta$ 1-10) (Ann. 1).

### 2.2.1.2 Bcl-xL constructs and derivatives

Bcl-xL protein (Fig. 2.2 A, C) is a single-domain protein predominantly anchored in the MOM through its C-terminal transmembrane  $\alpha$ -helix (TM). Otherwise, the protein is organized in a globular bundle of helices from which an IDR segment (32-87) projects away and samples a wide range of conformations (Fig. 1.5). In Bcl-xL, the BH3 binding region is shared between helices  $\alpha_3$ ,  $\alpha_4$ ,  $\alpha_5$  and  $\alpha_6$ . Bcl-xL protein construct and variants (Fig. 2.2 A, B) were designed in agreement with established sequences for IDR partial [198] or total [111] removal and deletion of the transmembrane part [199].

The DNA template encoding human Bcl-xL was a pUC-19 plasmid [200] from commercial gene synthesis. Cloning of Bcl-xL Open Reading Frame (ORF) in expression vector into pET-M11 was carried out through targeted amplification of Bcl-xL gene and integration via relevant restriction enzymes and ligase that was facilitated by the use of floating tail primers (Ann. 2). The final DNA sequence of the plasmid is listed (Ann. 1). To establish mutants, single-step targeted mutagenesis [195] was used on the pET-M11 template containing Bcl-xL ORF. Deletions of the C-terminal  $\alpha$ -helix and within the Bcl-xL IDR were then carried out as already described for the removal of TCTP IDR using floating tail primers and single PCR step to yield the desired plasmid. DNA sequence of PCR products were sequenced for

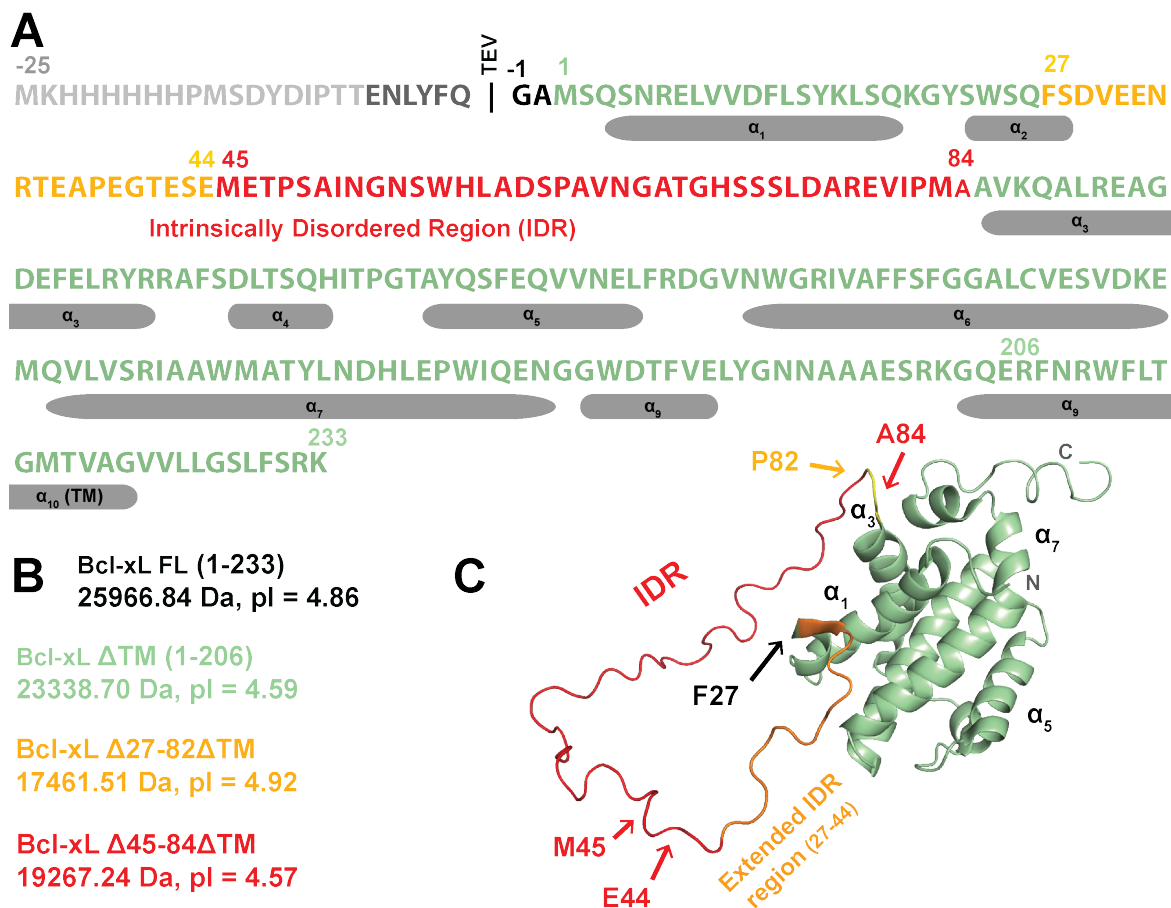


**Fig. 2.2 Bcl-xL and variants.** (A) Primary sequence of human Bcl-xL in fusion with a N-terminal His<sub>6</sub> tag. The sequence of the tag (lightgrey) and TEV cleavage site (grey) are highlighted. Bcl-xL is obtained with two extra N-terminal GA residues from TEV cleavage (black). On the sequence of the native Bcl-xL (green), the IDR region (red) and extended IDR region (orange) are highlighted. Secondary structure elements are represented for  $\alpha$ -helix (rounded rectangle). (B) Bcl-xL constructs and properties. Full length Bcl-xL (black) and variants lacking the IDR region (TCTP1) (red) plus the extended IDR region (27-44) (orange) were expressed and purified. (C) Representation of Bcl-xL structure elements relevant to current protein constructs. On the protein structure (pdb code: 2ME9) the IDR region (45-84, red) and the extended IDR region (27-44, orange) are highlighted. Protein sequences are numbered according to the human canonical isoform.

validation (Eurofins Genomics) after inclusion in the pET-M11 plasmid and bacteria-mediated amplification.

### 2.2.1.3 Other proteins Mcl-1, MDM2 and YB-1, peptides and proteases

#### Mcl-1 protein construct (172-329)

Mcl-1 protein is mostly anchored in the MOM through its C-terminal transmembrane  $\alpha$ -helix. Homologous to Bcl-xL, the protein is organized as a globular bundle of helices.

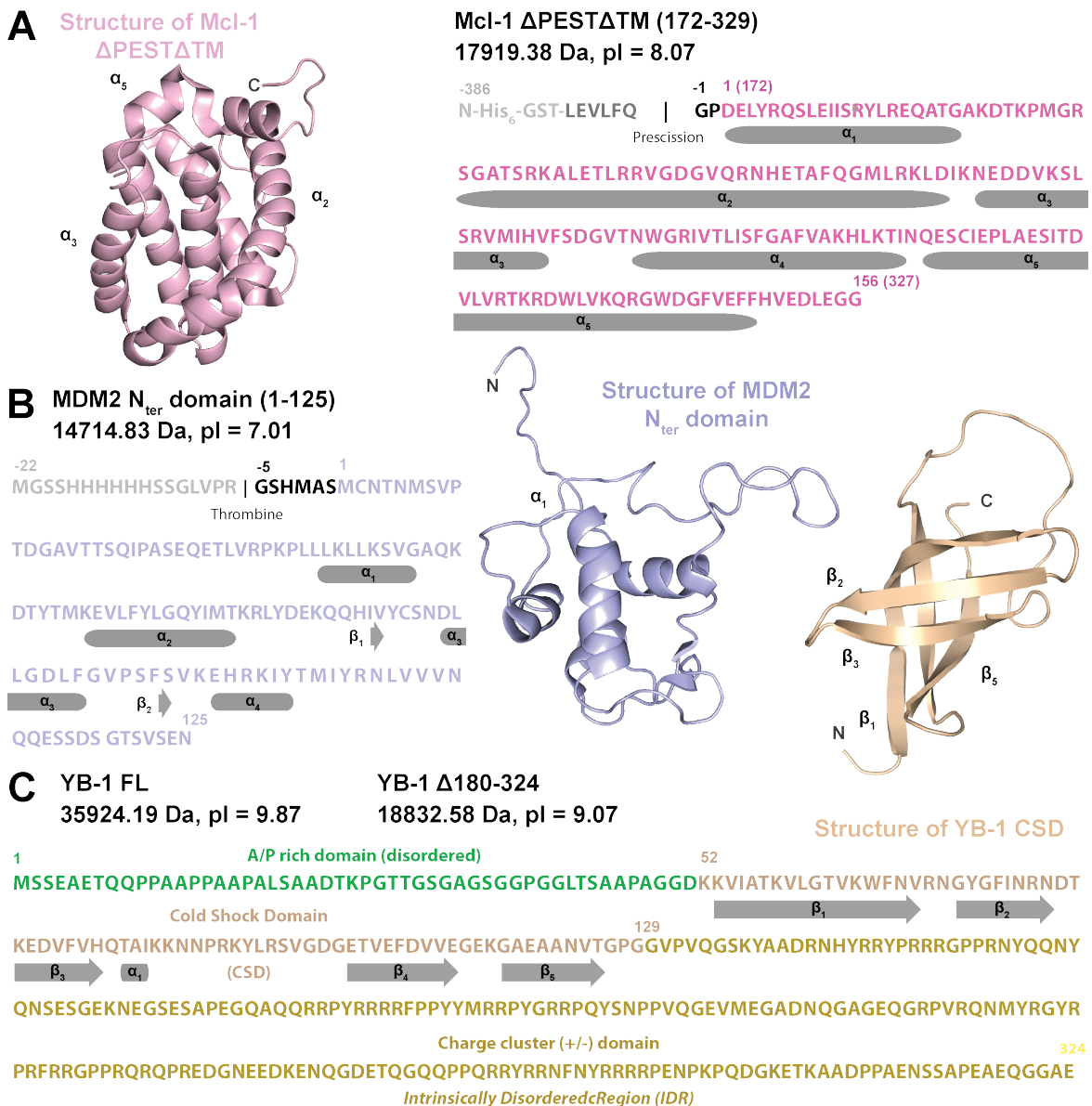


Fig. 2.3 Other protein variants. (A) Primary sequence of Mcl-1  $\Delta$ PEST  $\Delta$ TM with N-terminal His<sub>6</sub>-GST tag and precission cleavage site (right). Two extra N-terminal GP residues from precission cleavage site remain (black). (B) Sequence of MDM2 N-terminal domain in fusion with N-terminal His<sub>6</sub>-GST tag with thrombine cleavage site (left). Six N-terminal GSHMAS residues from thrombine cleavage remain after cleavage (black). (C) Sequence of YB-1 (bottom). The N-terminal A/P rich domain (green), the Cold Shock Domain (CSD) domain (maroon) and the clusters of charged residues (yellow) are highlighted. Below all sequences secondary structure elements are represented for  $\alpha$ -helix (rounded rectangle) and  $\beta$ -sheet (arrow). NMR structures of (A) Mcl-1  $\Delta$ PEST  $\Delta$ TM (pdb code: 2MHS), (B) MDM2 N-terminal domain (pdb code: 1Z1M) and (C) YB-1 CSD (pdb code: 1H95).

The N-terminal IDR region, known as the PEST domain, occupies 50% of Mcl-1 primary sequence. Here, the BH3 binding region is shared between helices  $\alpha_2$ ,  $\alpha_3$  and  $\alpha_4$ . Plasmid

pET15b (Amp<sup>R</sup>) encoding for the human Mcl-1 deleted for the PEST domain and C-terminal transmembrane segment (Fig. 2.3 A) in fusion with an N-terminal histidine tag followed by a Maltose Binding Protein (MBP) segment was generously shared by L. Carlier (LBM, CNRS/Sorbonne-Universités) and incorporated into BL21 Rosetta pLysS (Chlo<sup>R</sup>) using electroporation method.

#### **MDM2 N-terminal domain (1-125)**

MDM2 protein has E3 ubiquitin ligase activity in its C-terminal domain and a p53 binding domain in N-terminal extremity. TCTP was reported to interact either with the N- or C-terminal moiety of MDM2 [173, 150]. This interaction promotes p53 degradation by inhibiting MDM2 autoubiquitylation. To answer the question of where and how does TCTP bind to MDM2, a glycerol stock of *E. coli* BL21 STAR that contain pET28a (Kan<sup>R</sup>) encoding for human MDM2 N-terminal domain (Fig. 2.3) was generously shared by E. Jacquet (ICSN, CNRS/Université Paris-Saclay) for further binding assays (Fig. 2.3 B).

#### **The RNA binding protein YB-1 (1-324, full length)**

YB-1 protein binds to nucleic acids mostly through its central Cold Shock Domain (CSD). IDR regions span both moieties of the protein. Notably, the C-terminal extension is organized in clusters of charges. Human full length YB-1 and a truncated version in C-terminal region (1-180) (Fig. 2.3) were generously shared by D. Pastré (SABNP, INSERM/Université Paris-Saclay) to evaluate the interaction with TCTP recently proposed in the literature [145] (Fig. 2.3 C).

#### **BH3-derived peptides from TCTP and Mule**

In order to achieve binding studies with Bcl-2 family partners and BH3-derived peptides, we also ordered synthetic peptides (Proteogenix). Sequences of peptides derived from TCTP and Mule protein are all 22 amino-acids length and were designed paying attention to predicted solubility properties. Peptides were dialyzed against milliQ water using a 1 kDa Molecular Weight Cutoff (MWCO) membrane to remove residual contaminants from synthesis, prior to lyophilisation and further use. Alternatively, they could be readily used at low concentration without visible impact on buffer conditions (pH, conductivity...). Corresponding sequences are all listed (Ann. 3).

#### **TEV and prescission proteases for purification tag digestion**

We finally produced TEV and prescission proteases that cleave at ENLYFQ | [S/G] and LEVLFQ | GP sites, respectively, to use in tag digestion during purification processes. Glycerols stocks expressing the proteins were either available in our team (TEV) or generously shared by L. Carlier (LBM, CNRS/Sorbonne-Universités). TEV and prescission encoding plasmids were contained in BL21 Rosetta (Amp<sup>R</sup> + Chlo<sup>R</sup>) and SE1 cells (Amp<sup>R</sup>), re-

spectively. Proteases were produced by our own according to the later detailed protocols. Thrombine protease which cleaves at  $P_4P_3P[R/K] | P_1P_2$  with  $P_3, P_4$  hydrophobic and  $P_1, P_2$  non-acidic residues was obtained from commerce (Sigma-Aldrich).

### 2.2.2 Large-scale protein production protocols

Protein	Construct	Temp. induc. (°C)	IPTG conc. (μM)	Induct. time (hrs)	Base A urea - NaCl (M) - (M)	Wash/Elution (mM Imi.)	Protease	Protease conc. (% v/v)	Digest. temp. (°C)	Comments
TCTP	native ΔIDR ΔTCTP1	25	500	16	1 - 0.5	20-60/60+	TEV	5-10	34	N <sub>ter</sub> G G + M9 only N <sub>ter</sub> G
TCTP <sub>BH3</sub> peptide	TCTP <sup>15-29</sup>	10	500	48	1 - 0.5	70/500	pre-scission	0.1-1	4	His-GST-TCTP <sub>BH3</sub> Weak Expr. M9
Bcl-xL	ΔTM Δ45-84ΔTM Δ27-82ΔTM	25	1000	16	1 - 0.5	40-70/500	TEV	2-5	25	N <sub>ter</sub> GA N <sub>ter</sub> GA
Mcl-1	ΔPESTΔTM	15	250	16	1 - 0.5	0-20/20+	pre-scission	1	4	N <sub>ter</sub> GP
MDM2	N <sub>ter</sub> Domain	25	1000	16	0 - 0.3	70/250	Thrombine	1	4	N <sub>ter</sub> GP
Pre-scission	His-mC-HRV143C	37	1000	3-4	0 - 1	80/250	-	-	-	-
TEV	His-TEV	25	1000	3-4	0 - 0.2	80/250	-	-	-	-

**Table 2.2 Protein-specific information for the purification procedure.** Important parameters for the purification of proteins are presented.

About a dozen of protein constructs were expressed in a large-scale setup and further purified. We also produced accessory proteins such as proteases (TEV, pre-scission) to yield close to native proteins for biophysical studies. For all bacterial strains expressing protein constructs, rich medium (2xYT) and minimal medium (M9) were used. The IDR-truncated mutant of TCTP (TCTP ΔIDR) was produced in every case in minimal medium since it is particularly prone to proteolysis in rich medium culture (Tab. 2.2.2). For all expression protocols, the biomass was made in a 1 L culture under agitation (200 rpm) to an optical density of 0.6-0.9 prior to induction. Between four and height hours were necessary in rich medium to obtain a relevant biomass. In minimal medium, the same biomass takes longer to develop, yielding a 6-12 hours wait before induction. Induction of protein expression was carried out by adding isopropyl β-D-1-thiogalactopyranoside (IPTG) in the culture flask and setting up the protein specific induction temperature and time (Tab. 2.2.2). The culture was finally harvested (5000 g, 20 min) at 4°C and the bacterial pellet containing the protein of interest was collected. All bacterial pellets were stored at -80 °C until use.

### 2.2.3 General procedure for protein purification

The proteins we expressed share common and different purification steps. Here, we report the generic procedure for all proteins that consists in lysis, histidine-affinity chromatography, tag digestion and purification of the digested product. Specific informations are detailed

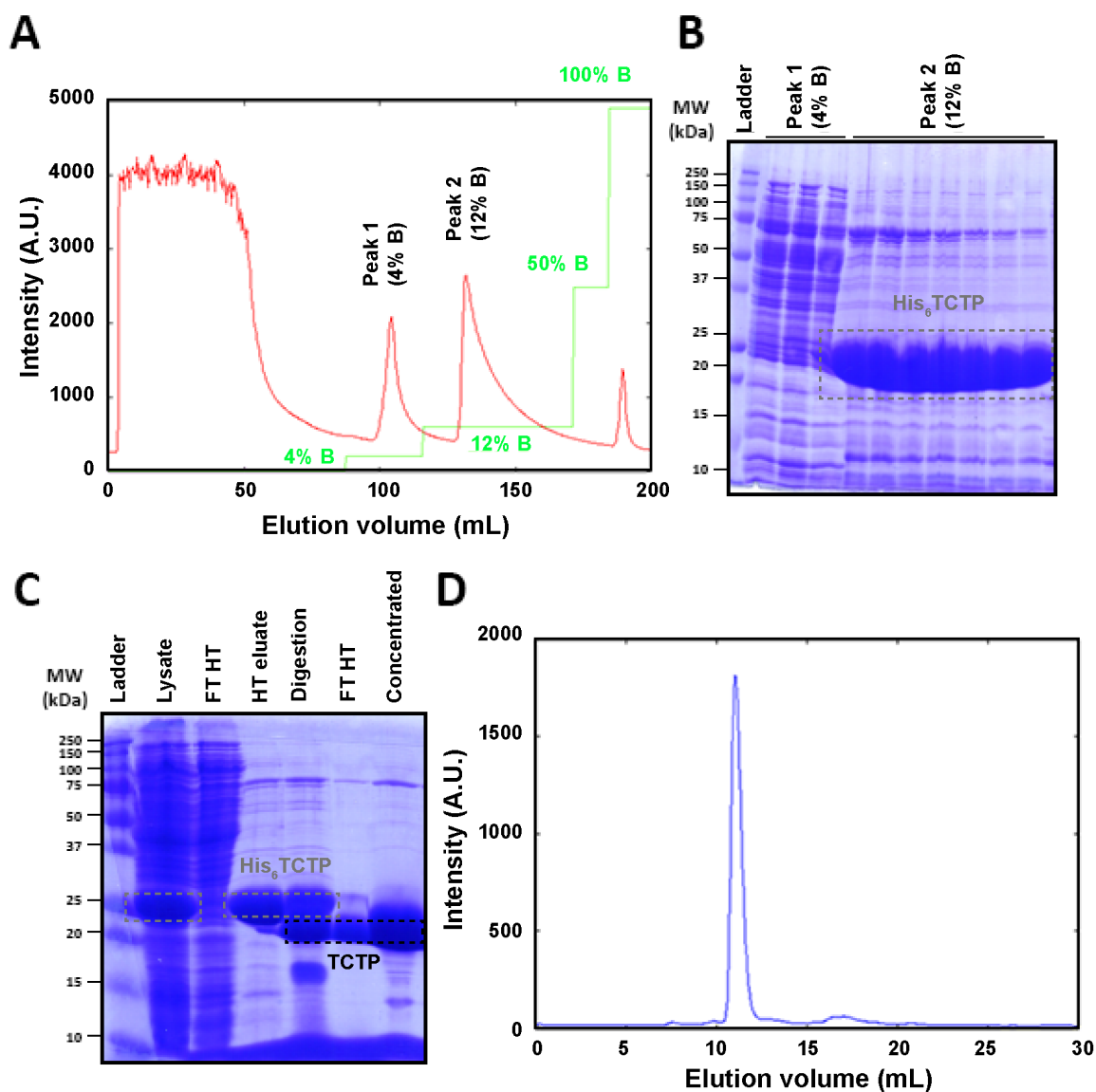


**Fig. 2.4 Protein purification workflow: example with TCTP.** (A) Histidine-affinity chromatography profile of lysate soluble fraction containing TCTP FL and obtained after centrifugation (red). Gradient of elution buffer is indicated with buffer B (500  $\mu$ M imidazole) (green). Starting 60 mM imidazole (peak 2, 12 % buffer B) TCTP FL is eluted while contaminants were partially eliminated at 20 mM imidazole (peak 1, 4 % buffer B). (B) SDS-PAGE profile of fractions from histidine-affinity chromatography. (C) SDS-PAGE profile of fractions from major purification steps. (D) SEC profile of digested, tag-free TCTP sample. Here TEV migrates at the same rate as cleaved TCTP so that this can hinder the interpretation of SDS-PAGE gels

for the purification of recombinant TCTP<sub>BH3</sub> peptide, phosphorylated TCTP and proteases we produced and used for tag digestion. The value of parameters such as temperature of induction and concentration of IPTG are all listed for specific proteins (Tab. 2.2.2).

**Bacterial lysis**

Bacterial pellet (4-8 g) was kept on ice during melting in presence of 10 volumes (w/v) of lysis buffer (50 mM Tris pH 8, 0-1 M NaCl, 0-1 M Urea, 2 mM DTT and 0.1 mg/mL lysozyme) (Tab. 2.2.2) supplemented with half a tab of protease inhibitors (Roche, EDTA-free). For TEV and prescission, urea, lysozyme and protease inhibitor were not present in the lysis buffer because we need active proteases and we proceed fast during the purification, thus limiting incubation times. prescission purification required higher (1 M) concentration of sodium chloride and the use of DNase to avoid DNA contamination. Bacterial pellet was resuspended in lysis buffer by magnetic agitation on ice until suspension homogeneity. To prevent excessive viscosity in the pressure-assisted lysis, the suspension was briefly sonicated when needed (20 s) at maximum power under agitation before the french press operation. Additional dilution can be envisaged prior to the first passage. After 3 cycles at 1500 bars the lysate was finally centrifuged at 12500 g during 30 min and the supernatant was collected, leaving small (<10 % of the original mass) residual pellet with dark inclusions. These two parameters indicate the lysis was successfully achieved.

**Histidine affinity chromatography procedure for all proteins**

The supernatant collected after lysis was loaded on a histidine affinity chromatography column (5 mL HisTrap FF crude, GE) equilibrated with imidazole-free buffer (50 mM Tris pH 8, 0-1 M NaCl, 0-1 M Urea and 2 mM DTT) (Tab. 2.2.2) with a flow-rate of 2.5 mL.min<sup>-1</sup> at 4 °C. The loaded column was washed with imidazole-free buffer (10 Column Volume (CV)) and by increasing imidazole concentration to specific values for washing steps (10 CV) and for protein elution (5 CV) (Tab. 2.2.2). For TEV and prescission purification, urea was prohibited. These did not need further purification and were stored at -20 °C in 25% glycerol (v/v).

**Digestion and tag removal: TCTP, Mcl-1 and Bcl-xL constructs**

The elution product (5-15 mL) from histidine-affinity chromatography was dialyzed against the digestion buffer for specific TEV (50 mM Tris base pH 8, 300 mM NaCl, 2 mM DTT) or prescission (50 mM Tris-HCl pH 7.4, 150 mM NaCl, 10 mM EDTA and 1 mM DTT) that also removes imidazole and urea (Tab. 2.2.2). After about two hours TEV or prescission were added to the sample for digestion at the required temperature and the sample was left in the dialysis buffer overnight (Tab. 2.2.2). The completion of protein digestion was checked through SDS-PAGE experiments. Once completed, the digestion product was concentrated with an adapted centrifugal filter (Amicon) to 10 mL and diluted with 5 X imidazole-free buffer (see HisTrap procedure) to reach 1 X concentration. The sample was loaded on a histidine affinity chromatography column (5 mL HisTrap FF crude, GE) equilibrated with

imidazole-free buffer 1 X. The column was washed with 3-4 CV of imidazole-free buffer and the flowthrough from loading and washing steps that contains the cleavage product were pooled together and concentrated (2 mL) prior to SEC purification.

#### **Size-exclusion chromatography and storage: TCTP, Mcl-1 and Bcl-xL**

The SEC purification step was done to ensure aggregate removal and sample polishing. S200 column (S200 10/300 GL, GE) was generally used since it allowed for larger differences in elution volume of aggregates and protein of interest. Flow-rate of 0.7 mL/min and maximal pressure of 1.5 MPa were considered as generic parameters for all protein purification by SEC. After equilibration of the FPLC system in the SEC buffer for TCTP, Bcl-xL (50 mM HEPES pH 7.4, 150 mM NaCl, 0.5 mM EDTA and 2 mM DTT) or Mcl-1 (with 20 mM Tris pH 7, 300 mM NaCl) and the samples (2 mL) were loaded into the column. Protein-containing fractions were analyzed by SDS-PAGE, pooled together and concentrated (1-2 mM range). Absorbance is measured at 280 nm for tryptophan and tyrosine residues with a NanoDrop device (ND-1000, Thermofisher) and we list all molar extinction coefficients (Ann. 3). Proteins are stable at -80 °C for years.

#### **Specific procedure for TCTP<sub>BH3</sub> purification**

The elution product from histidine-affinity chromatography was dialyzed against the digestion buffer for prescission (50 mM Tris-HCl pH 7.4, 150 mM NaCl, 10 mM EDTA and 1 mM DTT). After about two hours prescission was added to the sample (1 % v/v) in the dialysis membrane for digestion at 4 °C in a collection tube with no agitation overnight (Tab. 2.2.2). We took advantage of the low Molecular Weight (MW) of TCTP<sub>BH3</sub> (2.6 kDa) by using a centrifugal filtering device (10 kDa MWCO, Amicon) to isolate the peptide in the flowthrough since both purification tag and prescission have a MW above 2 MWCO and then were retained in the upper part of the filtering device. The collected flowthrough was collected and lyophilized. Lyophilized TCTP<sub>BH3</sub> was resuspended in a small volume (2 mL) of water and dialyzed against pure water using the relevant membrane (1 kDa MWCO) during 3 hrs. Concentration determination of the sample was done by measuring absorbance at 280 nm. Splitting and lyophilization of aliquots followed. Those were kept at room temperature in dark environment to prevent light-induced alteration until use.

#### **Specific procedure for the purification of pTCTP**

We also post-translationally modified TCTP FL by means of Plk-1 mediated phosphorylation. The kinase was generously shared by S. Zinn-Justin (LBSR, CEA Saclay/Université Paris-Saclay). TCTP (100 µM) was prepared in the reaction buffer (40 mM HEPES pH 8, 20 mM MgCl<sub>2</sub>, 5 mM ATP, 1 mM EDTA and 1 mM DTT) and the Plk-1 was added from the frozen stock (4 µL, 160 nM final) in the reaction tube at 303 K overnight. Sample was then incubated

with EDTA (100 mM) to sequester  $Mg^{2+}$  ions that are TCTP binders prior to filtration (0.2  $\mu M$ ) and injection on a SEC column (S75 10/300 GL, GE) equilibrated with the generic TCTP NMR buffer (50 mM HEPES pH 7.4, 150 mM NaCl, 2 mM TCEP) at 0.5 mL.min<sup>-1</sup>. Fractions of interest were pooled together and concentrated (200  $\mu M$ ) prior to storage at -80 °C.

## 2.3 Biophysical and computational methods

### 2.3.1 Nuclear Magnetic Resonance (NMR)

All NMR experiments were conducted using the following Bruker spectrometers: 600 MHz Avance III, 800 MHz Avance III and 950 MHz Avance III HD equipped with cryoprobes. Here, we present basics of NMR theory [201] and keys for analysis of protein spectra and characterization of molecular interactions. Sample preparation, experiment types and data processing routines are also detailed.

#### 2.3.1.1 Principles of NMR theory

##### Magnetic resonance of nuclear spins and vector model for 1D NMR

We briefly present core principles of the NMR theory and we detail the vector model which gives a theoretical description of simple 1D NMR experiments (Fig. 2.5). In absence of a static magnetic field  $B_0$  (T), the magnetic moment of spins orient in all possible directions. Upon application of  $B_0$ , the magnetic moment of non null spins orient parallel or anti-parallel to  $B_0$  direction (Fig. 2.5 A). The energy difference between the two orientations depends on  $B_0$  and on the gyromagnetic ratio  $\gamma$  (rad.s<sup>-1</sup>) of the considered nucleus. Populations are slightly unequal in both orientations under  $B_0$  and these are characterized by Boltzman's equations, with a weak energy difference between them which increases with the field strength. However, the net magnetization is still non-zero along the  $B_0$  axis due to the small population difference. In addition, spins precess around the  $B_0$  axis at a characteristic frequency described as the Larmor's frequency which depends of the gyromagnetic ratio and is modulated by the local environment and shielding as the basis for the chemical shift definition. In the classical pulse-acquire experiment, a radiofrequency pulse of short duration is applied to put the net magnetization from z-axis along the y-axis (Fig. 2.5 B). Spin-relaxation causes the transverse and longitudinal components of the net magnetization to decrease and increase over time, respectively. The precession of magnetization around  $B_0$  leads to time-domain data characterized by attenuated cos or sine wave along the x and y axes (Fig. 2.5 C). This signal contains information about environment in its frequency

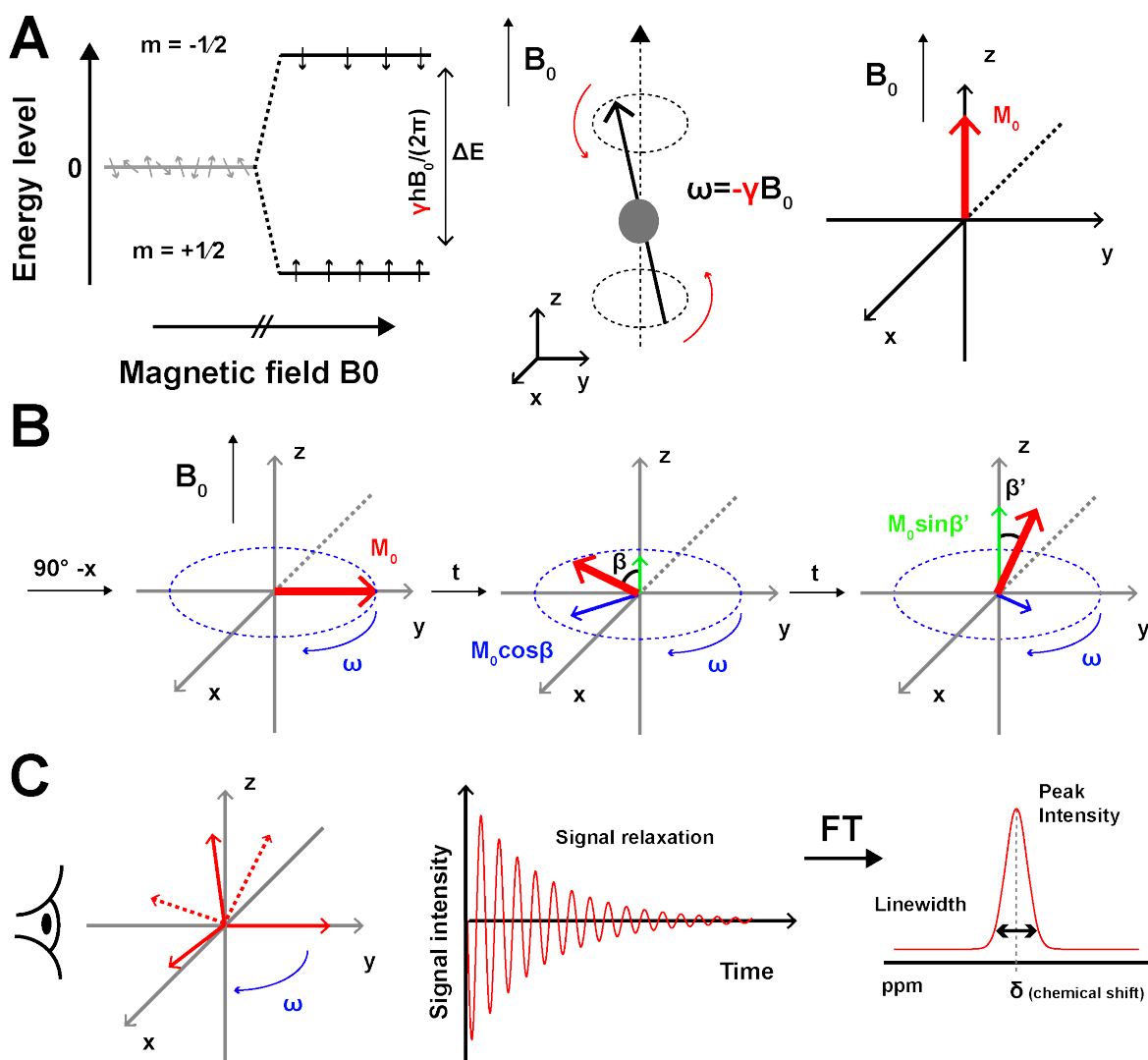


**Fig. 2.5 Basic theory of NMR: energy levels and vector model.** (A) Boltzmann energy levels of spin 1/2 in function of the strength of  $B_0$  magnetic field and resulting net magnetization. The nucleus specific gyromagnetic ratio ( $\gamma$ ,  $\text{rad}\cdot\text{s}^{-1}$ ) is highlighted (red). (B) Vector model for pulse-acquire experiment. A  $90^\circ$  -x pulse was applied to spin at equilibrium under  $B_0$ . Free precession of the spin is monitored in the xy spectrum until total decay of transversal magnetization. (C) The Free Induced Decay (FID) is a time-domain data that is readily converted into frequency-domain data by Fourier Transform (FT), yielding a resonance peak that owns chemical shift (parts per million (ppm)) and linewidth (Hz).

(chemical shift) and about dynamics (motion of atoms) that affects spin-relaxation as seen in the attenuation rate of the NMR signal. After FT in a single spin system, the frequency-domain data is a single lorentzian defined by chemical shift (position) and lineshape (broad or sharp). Using a 1 GHz NMR spectrometer, a chemical shift of 1 ppm means that 1 kHz difference is observed during the acquisition period between the precession rate of a given

spin around the z-axis in the xy plane compared to Larmor's frequency reference ( $10^6$  kHz for  $^1\text{H}$  at 1 GHz). This theoretically allows for probing every atom of a single molecule since they all have specific environment and dynamics, such providing specific NMR signatures (chemical shift, relaxation properties).

### Concepts in multidimensional NMR

Molecules can contain thousands of spins and all have close chemical shift in ppm. The capacity we have to distinguish and resolve two close resonances is directly linked to the strength of  $B_0$  field and peak lineshape. However, this still impedes detailed study of proteins and other large systems if only using 1D techniques because the many signals will inevitably overlap. Bidimensional NMR allows to correlate two same or different nuclei through spins coupling or spatial proximity to spread the original 1D data by one dimension, accordingly to the chemical shift of nucleus in the second, so-called indirect dimension of the NMR experiment. In the pulse-acquire experiment, only one time variable was used and corresponds to the acquisition time ( $t_1$ ). In 2D NMR, there is one more time variable ( $t_2$ ) but also a supplementary block called the mixing period. Time  $t_2$  is the evolution time between block p1 and the mixing period (p2) and  $t_1$  is still the acquisition time. 1D spectra series are recorded with variable evolution time ( $t_2$ ) for each 1D experiment, which results in  $t_2$ -modulated FID that are FT in the acquisition dimension first to yield as many 1D spectra as different evolution time  $t_2$ . Along the indirect,  $t_2$ -modulated dimension, this leads to cos/sin wave curves at given chemical shift in the direct dimension. These are also FT and the resulting spectrum is much simpler than the original 1D spectrum and consists in a 2D map on which there is, schematically, all the information present in the 1D counterpart, now made readable by filtering/selection of isotopic labels, coupling schemes and related dimensional splitting that spread signals on a multidimensional map.  $^1\text{H}$ - $^{15}\text{N}$  spectra are common representations of such 2D NMR since they contain one crosspeak for each HN in the protein which theoretically allows for probing along the backbone and side-chains of Asn, Gln, Trp residues. These spectra are often called NMR fingerprints because the distribution of signals are dependent on the primary and tertiary structure of the protein. In 2D NMR, other nuclei such as  $^{13}\text{C}$  can also be correlated to  $^1\text{H}$ . Beyond cross-nuclei correlation experiments, other types of parameters can be used in multidimensional NMR. For the simplest experiments, Heteronuclear NOEs experiments rely on  $^1\text{H}$ - $^{15}\text{N}$  correlation schemes and are pseudo-3D that detect flexible region in protein by means of  $^1\text{HN}$  saturation, yielding two different reference and saturated experiments. For spin-relaxation studies, a time variable is used in a pseudo-3D experiment to compute the corresponding relaxation parameters after examination of each 2D spectrum and extraction of peak intensities that decay over the increase of the relaxation time. Gradients in encoding/decoding combined

with diffusion delays in DOSY NMR permit to measure translational coefficient diffusion ( $D$ ) of molecules, also through pseudo-2D experiments in which the whole signal intensity from a single structural entity decreases with the gradient strength increasing. Relying on variable refocusing frequency and saturation offset, CEST and CPMG methods are two different approaches that also use pseudo-3D experiments for measuring chemical exchange kinetics.

### 2.3.1.2 NMR is useful to monitor protein structure, dynamics and interactions

The chemical shifts of NMR active spins such as  $^1\text{H}$ ,  $^{15}\text{N}$  or  $^{13}\text{C}$  are sensitive to the specific environment of the spin and thus inform on binding events at the protein surface since local spins have different environments and thus chemical shifts between free and bound state. The chemical shift analysis permits to delineate binding interfaces since the largest chemical shift perturbations observed in a protein spectrum upon addition of binding partner originate from residues located at the molecular interface and this can be mapped on a protein structure [202]. This is valid if we assume that no allosteric changes are present in both interacting partners upon complex formation and in the opposite case we should also observe chemical shifts perturbations from structure transition still related to molecular interaction but not defining the binding interface by itself. We extensively used the NMR titration method to evaluate the impact of proteins, drugs, ions and others on labeled proteins that were monitored to observe changes in the protein structure and dynamics upon environmental parameter variation. During the NMR titration experiment, we increase the concentration of a binding partner and we monitor the changes at the protein surface using  $^1\text{H}$ - $^{15}\text{N}$  Heteronuclear Simple-Quantum Correlation (HSQC) experiments, typically.

Different exchange regimes (fast, intermediate, slow) relative to the exchange rate between free and bound state ( $k_{\text{ex}}$ ,  $\text{s}^{-1}$ ), expressed as  $k_{\text{ex}} = k_{\text{on}}[L] + k_{\text{off}}$ , are seen in spectra series and generally indicate affinity (low-medium-high) considering that the dissociation constant is  $K_{\text{d}} = \frac{k_{\text{off}}}{k_{\text{on}}}$  (Fig. 2.6). For two interacting molecules, when the exchange rate  $k_{\text{ex}}$  is greater than the chemical shift difference between resonances from the free and bound state, then exchange is fast ( $\mu\text{s}$ ) on the chemical shift timescale and a unique peak tend to represent both free and bound state at averaged position regarding population fraction. This means that populations and dissociation constant  $K_{\text{d}}$  can be readily computed by fitting a single-parameter model in the most simple case upon titration and analysis of spectra series. Also, crosspeaks undergoing rapid exchange perturbations can be more easily followed in the multidimensional map upon perturbation. When  $k_{\text{ex}}$  is equivalent to the chemical shift difference, severe line broadening leads to signal disappearing and exchange is said intermediate (ms). When  $k_{\text{ex}}$  is weaker than the chemical shift difference, the exchange



NMR spectrum upon titration can bring crucial elements to describe a protein structure in complex with partners. Moreover, carbon backbone resonances ( $C\alpha$ ,  $C\beta$ , CO,  $C'$ ) reliably inform on the local secondary structure environment of a given residue, which is useful to provide information about structural transitions upon complex formation or to map the topology of a protein.

In conclusion, chemical shifts in NMR are essential to distinguish species in solution and to characterize interactions in term of binding affinity and interface. Upon full formation of a molecular assembly,  $^{15}\text{N}$ -spin relaxation and lineshape analysis of spectra series can be used together to delineate the respective impact of global size and local interaction on line broadening, thus refining interaction-specific perturbation set from a dynamics perspective.

### 2.3.1.3 NMR Experiments to study protein structure and dynamics

Dim.	Nucleus	Gen. name	Pulse prog.	Use	Ref
1D	$^1\text{H}$	$^1\text{H}$	zg	Control	-
	$^1\text{H}$	$^1\text{H}$ with water sup.	zgesgp	Proteins	-
	$^1\text{H}$	$^1\text{H}$ with $^{15}\text{N}$ and $^{13}\text{C}$ filter	ELzgesgp_filt15N13C	Ligands	-
	$^1\text{H}$	$^1\text{H}$ DOSY	ID_DOSY_MET	Diffusion	Mori [203] adapted by Schanda
2D	$^1\text{H}$ , $^{15}\text{N}$	SOFAST HMQC $^{15}\text{N}$	SOFAST HMQC $^1\text{H}$ - $^{15}\text{N}$	Fingerprint	Schanda [204]
	$^1\text{H}$ , $^{13}\text{C}$	SOFAST HMQC $^{13}\text{C}$	SOFAST HMQC $^1\text{H}$ - $^{13}\text{C}$	Fingerprint	Amero [205]
	$^1\text{H}$ , $^{15}\text{N}$	HetNOE ( $^1\text{H}$ )- $^{15}\text{N}$	hsqcnoef3gpsi	Local flexibility	-
	$^1\text{H}$ , $^{15}\text{N}$	$^1\text{H}$ - $^{15}\text{N}$ DOSY	ELHSQC_XSTE_2D	Diffusion	-
	$^1\text{H}$ , $^1\text{H}$	NOE Spectroscopy (NOESY) $^1\text{H}$ - $^1\text{H}$	noesyegpph	Correlation through space	-
3D	$^1\text{H}$ , $^{15}\text{N}$ , $^{13}\text{C}$	HNCO	HNCO	Backbone Ass.	-
	$^1\text{H}$ , $^{15}\text{N}$ , $^{13}\text{C}$	HNCA	BEST-Transverse Relaxation-Optimized Spectroscopy (TROSY)-HNCA	Backbone Ass.	-
	$^1\text{H}$ , $^{15}\text{N}$ , $^{13}\text{C}$	HNCACB	BEST-TROSY-HNCACB	Backbone Ass.	-
	$^1\text{H}$ , $^{15}\text{N}$ , $^{13}\text{C}$	HN(CO)CACB	BEST-TROSY-HN(CO)CACB	Backbone Ass.	-
	$^1\text{H}$ , $^{15}\text{N}$ , $^{13}\text{C}$	HN(CO)CA	BEST-TROSY-HN(CO)CA	Backbone Ass.	-
	$^1\text{H}$ , $^{15}\text{N}$ , $^{13}\text{C}$	HN(CA)CO	BEST-TROSY-HN(CA)CO	Backbone Ass.	-
	$^1\text{H}$ , $^{15}\text{N}$ , $^{13}\text{C}$	HN(CA)NH	BEST-TROSY-HNCANH	Backbone Ass.	-
	$^1\text{H}$ , $^{15}\text{N}$ , $^1\text{H}$	HNHA	BEST-TROSY-HNHA	Dihedral angle	-
	$^1\text{H}$ , $^{15}\text{N}$ , Time	$^{15}\text{N}$ T1	hsqct1etf3gpsitc3d	Local dynamics	-
	$^1\text{H}$ , $^{15}\text{N}$ , Time	$^{15}\text{N}$ T2	hsqct2etf3gpsitc3d	Local dynamics	-
	$^1\text{H}$ , $^{15}\text{N}$ , Freq.	$^{15}\text{N}$ CPMG	hsqcrexetf3gpsitc3d	Exchange	Tollinger [206]
	$^1\text{H}$ , $^{15}\text{N}$ , Freq.	$^{15}\text{N}$ CEST	n15cest_gb_v2.4	Exchange	Vallurupalli [207]

**Table 2.3 Routine NMR experiments.** Experiments are ordered by increasing dimension number. Related names refer to Bruker notation system and local pulse-program names.

NMR is unique among spectroscopic techniques because it informs on both protein structure and dynamics at atomic resolution. They were used for investigating the structural and dynamics properties of our molecular systems are recapitulated (Tab. 2.3). For 1D  $^1\text{H}$  experiments, the *zgesgp* (Fig. 5) was preferred for its better water suppression through gradients use. Filtered 1D  $^1\text{H}$  results from its adaptation to remove signals from  $^{15}\text{N}$  and or  $^{13}\text{C}$  bound  $^1\text{H}$ .

Bidimensional (2D) NMR was carried out to correlate  $^1\text{H}$  and either  $^{15}\text{N}$  or  $^{13}\text{C}$  nuclei. For recording  $^1\text{H}$ -X spectra, the SOFAST Heteronuclear Multiple-Quantum Correlation (HMQC) experiments (Fig. 5) from NMRLib [208], a library of NMR experiments from IBS Grenoble, were preferred for their superior sensitivity. 2D  $^1\text{H}$ - $^{15}\text{N}$  correlation experiments (HSQC, HMQC) are useful to inform on the local environment at the protein backbone

which changes upon interaction with partners and thus we extensively used them for NMR titration to map binding interfaces and to estimate binding affinity. The  $^1\text{H}$ - $^{15}\text{N}$  HSQC also yields information about local and global dynamics by analyzing the lineshape of the residue-specific crosspeaks. Bidimensional DOSY with selection of  $^{15}\text{N}$  bound protons was adapted from *hsqct1etf3gpsi3d.2* to measure of translational diffusion coefficient (D) in protein mixtures with heterogeneous labeling.

Tridimensional (3D) NMR was carried out between  $^1\text{H}$ ,  $^{15}\text{N}$  and a third nucleus ( $^{13}\text{C}$ ,  $^{15}\text{N}$ ) or a third parameter of variable nature. For backbone assignment the BEST-TROSY [209] (Fig. 5) series of experiments from NMRlib [208] was preferred for its excellent sensitivity due to the combination of BEST and TROSY-based recovery of multiple coherence pathways. Protein backbone assignments and NMR titrations relied on such experiments. We measured global and local dynamics along the protein backbone using  $^{15}\text{N}$  longitudinal ( $T_1$ ) and transverse ( $T_2$ )  $^{15}\text{N}$ -spin relaxation experiments. Both experiments consist in applying increasing delays before in which  $^{15}\text{N}$ -spin relaxation occurs along the z-axis or in the xy plane for  $T_1$  and  $T_2$ , respectively. At the end of the relaxation delay, the residual magnetization along z-axis ( $T_1$ ) is detected in the xy plane by applying a  $90^\circ$  pulse whereas it can be readily detected at the end of the relaxation period for  $T_2$  experiments. The exponential decay of the residue-specific signal intensity in function of increasing relaxation delay ( $\tau$ ) can be fitted from the  $^{15}\text{N}$ -relaxation spectra series and the decay rate informs on the local and global dynamics. For example, for a globular protein with a flexible tail ( $\sim 20$  kDa), we expect higher longitudinal ( $T_1$ ) and lower transverse ( $T_2$ ) relaxation time in structured regions whereas the opposite is expected for flexible residues, thus informing on dynamics on a fast timescale (ps-ns) and also yielding information about chemical exchange at slower timescales.  $\{^1\text{H}\}$ - $^{15}\text{N}$  Heteronuclear NOEs experiment also informs on local dynamics through bond saturation transfer increased for mobile backbone NH bond vectors, yielding a greater loss of intensity in crosspeaks upon saturation compared to more rigid segments. When the intensity ratio between saturated and reference experiments is in the range 0.8-1 (depends of  $B_0$ ), the specific residue is very rigid whereas lower ratios down to -1 indicate more to extremely flexible regions with corresponding mobility of the residue-specific backbone NH bond vectors. For local dynamics,  $^{15}\text{N}$ -spin relaxation informs on motions at fast to slow timescales (ps-ms) and can be combined with Heteronuclear NOEs derived parameters for treatment via the Lipari-Szabo or model-free formalism [210] to obtain the amplitude ( $S^2$ ) and timescale of internal motions as well as the global motion of the protein. The model-free is based on the spectral density spin-relaxation theory that explains NMR relaxation and yields local parameters related to molecular motions in models of increasing complexity. It also serves to compute global information on dynamics such as the rotational

diffusion of the protein, expressed as the correlation time ( $\tau_c$ ), which describes is a tumbling time usually higher with the MW of the protein. Methodology for CPMG experiment in investigating chemical exchange at intermediate timescale ( $\mu\text{s}$ - $\text{ms}$ ) results from the original scheme [206] and the CPMG block consists in applying refocusing pulses at increasing CPMG frequency ( $\nu_{\text{CPMG}}$ , 0-1600 Hz) before starting the acquisition period. By increasing  $\nu_{\text{CPMG}}$ , the dephasing of signal is reduced and the residue-specific  $^{15}\text{N}$  transverse  $R_{2\text{eff}}$  parameter decreases for residues undergoing chemical exchange at intermediate timescales, enabling kinetics and thermodynamics parameters determination. CEST experiments were adapted from a sequence shared by the developers of the method (G. Bouvignies, CNRS/ENS and L. Kay in Toronto) to detect chemical exchange at slower timescale (5-50 ms) [207] compared to CPMG experiments. This scheme involves irradiating various regions of the spectrum with a weak  $B_1$  field while monitoring the effect on the visible resonances from the major state. Indeed, irradiating invisible peaks from minor states exchanging with the major one results in signal loss in the latter upon saturation at the minor peak offset. This allows to detect and characterize in solution invisible species that are slowly exchanging with the major, NMR-visible state.

#### 2.3.1.4 Sample preparation and material for NMR

For NMR measurements, all samples were desalted in the experimental buffer prior analysis. The latter usually contained a suited buffer molecule regarding the experiment specific pH (mainly 10-50 mM HEPES pH 7.4, EPPS pH 8, MES pH 6.5) and sodium-chloride (0-500 mM) with TCEP (0-2 mM) often used as reducing agent. Here TCEP helped to keep the two cysteins C28 and C172 in their reduced state, and to prevent the formation of covalent TCTP dimers. Importantly, no anti-protease cocktail (Complete or EDTA-free Protease Inhibitor Cocktail (PIC)) should be added in the NMR tube in order to preserve proteins stability. Indeed, we have observed that such agents chemically evolved during our NMR experiments and influenced crosspeaks position with patterns characteristic of protein degradation. A standard amount of  $\text{D}_2\text{O}$  (5 % with a cryo-probe) was finally diluted in the sample. Experiments were generally done using a 3 mm NMR tube to ensure the best signal to noise ratio using a limited amount of protein sample (200  $\mu\text{L}$ ,  $\geq 50 \mu\text{M}$  protein concentration).

For NMR titration of proteins by ligands, aliquots of organic molecules were prepared as follow. A mass of solid molecule was dissolved in a volatile buffer (acetonitrile, methanol, chloroform...) according to the specific solubility of the compound. Relevant volumes were transferred in collection tubes and those were lyophilized to remove the solvent. The NMR

sample containing the protein to be titrated was added onto the dried aliquot with vigorous and extended mixing. Comparison with liquid addition from stock solution of ligand was done to validate the protocol. For NMR sample preparation and titration of proteins by proteins, dried aliquots were prepared as follow. Proteins were desalted in pure water at high ( $\geq 200 \mu\text{M}$ ) concentration and immediately put on ice. For Mcl-1, a quick (30 s) centrifugation (16000 g) ensures the removal of the species that aggregate upon desalting. Relevant volumes were transferred in collection tubes and those were lyophilized. The resulting white solid will be dissolved in the NMR sample when needed.

High-Pressure NMR (HP-NMR) [211] experiments were conducted on the 800 MHz Avance III spectrometer with the use of an hydrostatic pumping system (Daedalus Inc.) providing up to 2500 bars in the dedicated NMR tube containing the protein of interest. Mineral oil was used to ensure impermeability between water from the pump coil and the aqueous protein sample. Separately, HDX experiments report on the strength of H-bond, and thus assess tertiary and secondary structure stability. In the HDX experiment we resuspend a dried aliquot of protein initially prepared in an acidic buffer with protonated solvent ( $\text{H}_2\text{O}$ ) into  $\text{D}_2\text{O}$  buffer and  $^1\text{H}$ - $^{15}\text{N}$  fingerprint of the protein sample were measured at regular intervals at 288 K during 24 hrs. HDX exchange was monitored by following intensities on the  $^1\text{H}$ - $^{15}\text{N}$  spectrum of the protein and fast (slow) exchanging  $^1\text{HN}$  indicates weak (strong) H-bonds or water accessibility. Exponential decays could be fitted for each residue-specific resonance and extrinsic H/D exchange rates were computed. Intrinsic exchange rates were gained using ClntX server [212] and Protection Factor (PF) were calculated as the ratio of the intrinsic and extrinsic rates ( $k_{\text{int}}/k_{\text{rc}}$ ) [213] to remove the amino-acid type contribution to the exchange.

### 2.3.1.5 NMR data processing and extraction

NMR processing of raw Bruker data and spectra analysis were achieved with Topspin 3.5 pl 5 (Bruker) and CcpNmr [214] when looking at chemical shifts and NMRpipe [215] when looking at intensities and volumes. For NMRpipe [215] processing of 2D and 3D spectra, samples of script *fid.com* (Ann. 4) and *nmrproc.com* (Ann. 5) are presented. NMRpipe peak-lists were built with *ipap.tcl* module in combination with a protein assignment list exported from CcpNmr in nmrDraw format. For intensities extraction and non-linear modelling the procedures *autofit.tcl* and *modelExp.tcl* were applied. Data visualization was permitted by the homemade *fitPlotListXYdYinPDF.py* script which also refits the data for comparison. This general procedure is detailed in *fitModPlot.csh* (Ann. 7). Specific script for CPMG treatment *getR2eff.sh* (Ann. 8) was developed whereas CEST experiments were treated with the generic routine for pseudo-3D experiments which include intensity extraction with NMRpipe and

the script *fitPlotListXYdYinPDF.py* to plot and visualize CEST profiles for each residue in a single PDF file. For accurate intensities comparison between two peaklists, *calcHetNoe.sh* (Ann. 9) was used with *nlin.tab* files (output from *autofit.tcl*) from two spectra as inputs.  $^{15}\text{N}$  relaxation and  $^1\text{H}$ - $^{15}\text{N}$  heteronuclear NOEs experiments were analyzed by relying on the model-free formalism [210] integrated in the TENSOR2 program [216] after parameters extraction. Using this approach we fitted the data with an isotropic diffusion tensor to estimate the correlation time ( $\tau_c$ ) of protein and complex. The model-free formalism was also used to compute local order parameters  $S^2$ , describing the local dynamics of the amide backbone NH vector on a fast timescale ( ns) from very rigid ( $S^2 \sim 0$ ) to extremely mobile ( $S^2 \sim 1$ ).

### 2.3.2 Biophysical methods for investigation of proteins structure

For all methods listed below, samples were systematically centrifuged (16 000 g, 5 min) prior to measurement in order to remove aggregates which could interfere with the signal of interest.

#### 2.3.2.1 Dynamics Light Scattering (DLS)

DLS measurements were carried out using a Zetasizer Nano ZS (Malvern Panalytical) machine to evaluate hydrodynamic radius and polydispersity of proteins. In the method, the sample is illuminated by a laser beam and fluctuations of the scattered light at fixed scattering angle over time ( $\Theta$ ) permit to estimate the hydrodynamic volume of species in solution since light scattering is higher for big particles and it fluctuates slower due to smaller translational diffusion coefficient (D) compared to small entities. After centrifugation (16 000 g, 5 min), samples (60  $\mu\text{L}$ ) were disposed in the cuvette and measurements were done in the 25-35  $^\circ\text{C}$  range. Protein concentrations were variable (1-20  $\text{mg}\cdot\text{mL}^{-1}$ ) but all allowed for a correct signal to noise ratio to be further considered. Constant parameters were set as follows: scattering angle  $90^\circ$ , wavelength 632.8 nm refractive index 1.33. Experiments results are analyzed predominantly through *distribution by intensity* and *distribution by volume* plots in the Zetasizer software (Malvern Panalytical).

#### 2.3.2.2 Size-Exclusion Chromatography (SEC)

SEC experiments allow to separate proteins using a column matrix that discriminates hydrodynamic volumes by means of nanoporous material. Routine SEC was performed using the FPLC system Akta Explorer (ÄKTAexplorer, GE) with S75 and S200 10/300 GL columns for globular proteins in the range 3-70 kDa and 10-600 kDa, respectively. Room temperature was maintained at 18  $^\circ\text{C}$  and flow adjusted (0.5-1  $\text{mL}\cdot\text{min}^{-1}$ ) to limit the system pressure

below 1.8 MPa and 1.5 MPa for the S75 and S200 columns, respectively. Proteins were monitored at 260 nm and 280 nm. Text files were exported for further processing. System was systematically equilibrated with the sample buffer prior to each session.

### 2.3.2.3 Small Angle X-Ray Scattering (SAXS)

The Synchrotron SOLEIL facility (Saint-Aubin, France) and the SWING beamline were used to measure SAXS profile of proteins and complexes thereof. Those inform on the MW, radius of gyration and they allow to compute the 3D envelope of the molecular entity. Temperature was set to 25 °C and samples were detected after passing through a SEC column (S200 Increase, GE) at 0.5 mL.min<sup>-1</sup>. In-line SAXS measurement on elution fractions was done and data were processed using ATSAS software suite [217] and US-SUMO processing tool for signal deconvolution. The experiments were done under the guidance of A. Thureau (Synchrotron SOLEIL).

### 2.3.2.4 Circular Dichroism (CD)

The far-UV (180–260 nm) and near-UV (260–320 nm) CD spectra were recorded at 25 °C under N<sub>2</sub> atmosphere using a JASCO J-810 spectropolarimeter to observe secondary structure content and 3D folding of proteins. The method relies on polarized light and absorption by the protein chromophores to yield a deviation of light that is measured to estimate structure properties. Protein concentrations were kept in the range 2-5 mg.mL<sup>-1</sup>. Path lengths were 0.1 mm and 1 mm for the far-UV and near-UV CD, respectively. Ten accumulations at 100 nm.min<sup>-1</sup> with data pitch 0.2 nm and digital integration time (DIT) 1 s were recorded for each sample. Detector voltage never exceeded 700 V in the work presented. Text file were further exported for plotting. For simulation of CD spectra, the BeStSel [218] online software was used. All experiments were conducted in EPPS or MES buffers, low salt concentration (< 50 mM) and with TCEP (1 mM). For accuracy in low wavelengths, phosphate buffer (2.5 mM) and no salt were preferred with low TCEP concentration (100 μM).

### 2.3.2.5 Tyrosine and ANS fluorescence spectroscopy

To identify changes in tertiary structure of proteins upon conformational transition or complex formation, we used fluorescence-based methods. Using a temperature-regulated F-2500 fluorescence spectrophotometer (Hitachi), we measured the emission spectrum of protein with focus on the intrinsic fluorescence of Tyr residues since TCTP has no Trp in its primary sequence. Excitation wavelength was determined by first determining maxima on the absorbance spectrum of TCTP ( $\lambda_{Abs}$ ). Then an emission spectrum of TCTP at excitation

wavelengths corresponding to maxima of absorption (280 nm) were recorded to identify the electronic transitions that yield the strongest relative fluorescence signal in the emission spectrum. The corresponding peak apex was used to record an excitation spectrum at fixed  $\lambda_{Em}$  (303 nm) which yields the refined  $\lambda_{Exc}$  (277 nm). In all experiments, protein samples were prepared at 5  $\mu$ M and complexes at equimolar ratio in the following buffer: 50 mM EPPS pH 8, 50 mM NaCl, 2 mM TCEP. For urea-based experiments, different samples in specific buffers were prepared to prevent dilution upon addition of solid urea in the sample tube. Samples were all incubated overnight at 37 °C and measurement of Tyr fluorescence was recorded at the same temperature with the following setup:  $\lambda_{Exc}$  = 277 nm,  $\lambda_{Em}$  = 220-700, scan speed = 500 nm.min<sup>-1</sup>, delay = 1 s, Ex and Em split = 10 nm, response = 0.08 s). We also used the fluorescent hydrophobic probe ANS since it binds to hydrophobic surfaces that are overexposed in MG proteins with strong enhancement of fluorescence emission from the bound probe [219]. After incubation at 37°C overnight, ANS was added at 1 mM which correspond to 1:200 or 1:100 protein:ANS ratio for sample of protein and complex, respectively. Samples were kept at 37°C (2 hrs) prior to the measurement of ANS fluorescence in same setup than listed above excepted for  $\lambda_{Exc}$  which was set to 342 nm and fluorescence emission from ANS was broad over the 500-600 nm region of the emission spectrum. We corrected all spectrum with baseline separately recorded on buffers and upon ANS addition at the  $\lambda_{Exc}$  of Tyr and ANS.

### 2.3.2.6 Thermal Shift Assay (TSA)

TSA is a biophysical method that quantifies the change in protein folding using an hydrophobic and fluorescent probe that preferentially binds to the unfolded state compared to the folded state of the protein, thus increasing fluorescence intensity upon unfolding [220]. The TSA method detects such change in the probe fluorescence, thus allowing to measure the melting temperature ( $T_m$ ) of proteins. Interactions between a protein and partners can modify the melting temperature and thus TSA can also describe such interactions. TSA experiments were done by monitoring the fluorescence of SYPRO probe when applying a temperature gradient from 25 °C to 95 °C at 3 °C.min<sup>-1</sup> speed. A real-time PCR instrumentation (StepOne-Plus, Applied Biosystems) was used to measure the fluorescence along the gradient. Samples were prepared in various buffers according to the considered session: TCTP\_buffers (diverse), TCTP\_ligands (10 mM HEPES pH 7.4, 150 mM NaCl, 2 mM TCEP and 5 mM EDTA), TCTP\_proteins (50 mM EPPS pH 8, 50 mM NaCl, 2 mM TCEP) and TCTP\_urea (50 mM EPPS pH 8, 50 mM NaCl, 2 mM TCEP, 2.5 M urea). For experiments involving urea or protein complexes, samples were all incubated 12 hrs at 25 °C or 1 hr at 35 °C prior to measurement, respectively. All measurements were done in triplicate by a robot. Raw results

were analyzed (StepOne software, Applied Biosystems) and the melting temperature ( $T_m$ ) was computed as the derivative of the SYPRO raw fluorescence curve in function of the temperature. The experiments were done by E. Jacquet (ICSN, CNRS/Université Paris-Saclay) from our team at ICSN and we list all tested buffer conditions (Ann. 11) with variable pH (6-8.5) and salt concentration (0-500 mM) or type (NaCl, KCl).

### 2.3.2.7 Microscale Thermophoresis (MST)

MST is based of the thermophoresis of molecules, which provides informations about molecule size, charge, and hydratation shell [221]. Thermophoresis properties are affected upon interactions and the method monitors the changes to estimate binding affinities and interaction modes. MST experiments were carried out on a Monolith NT.115 (Nanotemper Technology) to determine affinity of protein-partner complexes. Standard capillaries (for Monolith NT.115, Nanotemper Technology) were used with "green" labeling of Mcl-1 protein at lysine residue and 1:1 protein:label in average. Labeling was achieved with the manufacturer recommendation [222] and materials. Raw fluorescence of the labeling product was measured and sample subsequently diluted before storing for further MST measurement. Samples were prepared according to the manufacturer comment [222]. In brief, serial 1:1 dilution of a partner stock solution over 16 collection tubes previously filled with analysis buffer (10  $\mu$ L) was done. Then an equivalent volume of labeled protein (10  $\mu$ L) was added in each collection tube. All samples were made in triplicates and incubated 1 hr at 35 °C prior to MST run. The experiments were done under the guidance of P. Llinas (I2BC, CNRS/Université Paris-Saclay).

## 2.3.3 Informatics, software routines and modelling tools

Bioinformatics and more generally computer-based strategy in molecular sciences and data management have allowed to greatly accelerate research and were used on a daily basis in the work presented in the manuscript. Here, we recapitulate the essential of publicly available tools we used and to report on the original algorithms and codes we developed to speed up data processing during the project.

### 2.3.3.1 Hardware & Desktop environment

The current work was supported by an ACER laptop equipped with an Intel-i7 7700HQ @ 3.4GHz, 24 GB of RAM DDR4 and both Hard Disk Drive (HDD) and Solid State Drive (SSD) disks. Gnu's Not Unix (GNU)/Linux Debian [223] Stretch was the main operating system and Mac OS X / Windows 7 were run with virtualization tools when needed. The GNU [224] software

suite provides a scientist-friendly environment and open-source tools of great interest. For data processing and treatment, programming language such as Bash [225], awk [226] and Python [227] were extensively used. For text processing, LaTeX [228] was preferred and WPS Office suite was used to ensure an optimal compatibility with MS Office. Graphic plots were obtained using Grace [229], Gnuplot [230] or Python with Matplotlib library [231]. All the figures were retreated through Adobe Illustrator CS6 running on Win7/VMWare. Tridimensional structures of molecules were visualized through PyMOL software [232].

### 2.3.3.2 Bioinformatic tools

Molecular docking was carried out with HADDOCK [191] for protein-peptide modelling, respectively. We also used PTools [233] to achieve TCTP-TCTP docking [234]. Finally we used the open-source GROMACS [235] molecular dynamics software to compute conformational ensemble of native TCTP and upon modifications. This work was done under the guidance of T. Ha-Duong (BioCIS/CNRS, Université Paris-Saclay). For common tasks such as getting the protein properties via its primary sequence, treating nucleic acid sequences (reverse, complement...), predicting and modelling, the ExPASy [236] online suit was used on a monthly basis. For computation of hydrodynamics radius and  $^{15}\text{N}$  relaxation parameters of a protein the HydroNMR [237] program was executed.

### 2.3.3.3 Algorithms for data processing and bibliography

#### Routines for data processing, treatment and visualization

Numerical data were processed automatically most of the time by the use of scripting facilities in Bash, awk and Python. As example, peaklists exported from 2D experiments in CcpNmr [214] were formatted via *XYnFT.py* (Ann. 12). Between two XY data files such as peaklists, computation of parameters relative to chemical shifts and intensities was made possible by *calc.sh* (Ann. 13). The same principle was applied for XY files from any origin when arithmetic operation were needed for comparison between the two files. Figures were quickly created by means of *plotXY.sh* (Ann. 14) with its associated gnuplot *plotXY.conf* file (Ann. 15). Generation of pymol command for selecting particular residues with respect to user-defined cutoffs was achieved by the *grpXY.sh* script (Ann. 16). This example of procedure is recapitulated in *analyze.sh* (Ann. 17). Importantly, scripting for systematic representation and fitting of XY files database was extensively used by executing *fitPlotListXYdYinPDF.py* (Ann. 10). Such database of XY files can be easily generated with series experiments and appropriate few lines of code for pre-processing.

**Management of bibliography by *2Pmed.py* script**

Downloading papers and retrieving metadata in PDF files using classical bibliography softwares can be source of mistakes and it is time consuming. From an input file containing a list of Pubmed Central ID (PMID), the *2Pmed.py* outputs blocks of bibliography citation data in word text and in the *.bib* format with associated call commands for LaTeX [228] text-processing (Ann. 18). On purpose, *2Pmed.py* can manage bibliography in a given path by creating PMID-specific folders (e.g. AuthorName\_year\_Pmid) containing the downloaded paper and specific word, *.bib* and *.tex* citation information with automatic compilation in a PDF file. This for all entries in the PMID input file, allowing to download and reliably manage many papers at time on a fully custom mode. The user can read papers and add notes in a text file that will be automatically included in the PDF file upon re-run of *2Pmed.py* and this for each single paper folder detected in the choosen path. An alternative version of the script called *2Gpat.py* was also developed to retrieve patent-specific metadata in a similar approach (Ann. 19).



# Chapter 3

## Research for alternative TCTP states

The large and diverse TCTP interactome is intriguing since the protein is a single-domain entity with a relatively simple tertiary organization. Accordingly, our main working hypothesis in the whole thesis is that TCTP is prone to structural plasticity to explain how it can adapt to its myriad of partners [145]. Before the characterization of TCTP complexes with partners, it is important to accumulate observations regarding the isolated protein, to further delineate binding specific perturbations from those that occur in the context of the isolated TCTP protein.

Here, we will first describe the structures of isolated TCTP by means of NMR prior to test if the protein could form non-covalent dimers since this could interfere when monitoring interactions with partners. Then, we know that phosphorylations of TCTP, which is mediated by Plk-1 in cells, is a marker of aggressive tumors and it abolishes the interaction with the  $\alpha$ -tubulin, possibly modifying the structure of TCTP. Thus, we performed the *in vitro* phosphorylation of TCTP and we will report here our characterization of the phosphorylated TCTP state (Sec. 3.1). We will also introduce our published paper where we report a combination of MD and NMR to study the conformational landscape of TCTP IDR under phosphorylation and calcium binding in order to evaluate at which extent the modifications could impact the protein structure (Sec. 3.2). In order to test further if TCTP could change its structure or exist in a minor state that we could promote, we applied stress of different natures (temperature, urea, pressure...) and we could detect and stabilize an alternative state of the protein. We will show in the next chapter that this state is crucial for interactions with Bcl-2 family proteins (Sec. 4). Thus, here we will extensively describe the structural organization of this alternative state by means of a vast panel of analytical (NMR, SAXS, DLS, CD, SEC, ANS and tyrosine fluorescence...) methods (Sec. 3.3). At the end of the chapter, we will



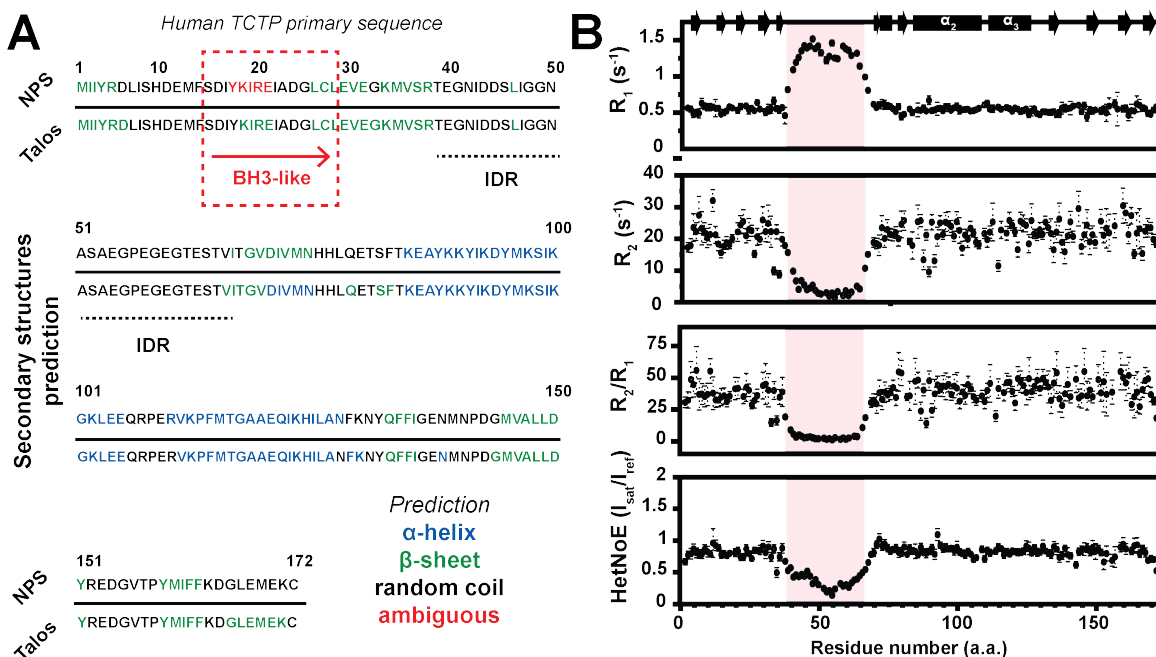


**Fig. 3.2 Secondary structures and dynamics in TCTP protein.** (A) Statistical and data-driven prediction of secondary structures in TCTP. Network Protein Server (NPS) [238] uses three different statistical approaches to predict consensus secondary structures from the TCTP primary sequence and Talos+ software uses experimental chemical shifts of TCTP backbone heavy atoms as input. The TCTP sequences are colored according to the prediction results from each methods. With *ab initio* prediction using NPS [238], the ambiguous result for the BH3-like motif is highlighted. (B) <sup>15</sup>N-spin  $R_1$  and  $R_2$  and {<sup>1</sup>H}-<sup>15</sup>N Heteronuclear NOEs experiments for studying TCTP dynamics. The TCTP IDR is highlighted (pink background). Experiments were recorded at 950 MHz and 25 °C in the following buffer: 20 mM HEPES pH 7.4, 150 mM NaCl, 2 mM TCEP in 95 % H<sub>2</sub>O / 5 % D<sub>2</sub>O.

NMR is a method of choice for studying protein structure, dynamics and interactions at atomic resolution. During the PhD, we mainly used NMR to gain insights into the molecular features of proteins and associated complexes. Routine experiments largely include the so-called <sup>1</sup>H-<sup>15</sup>N SOFAST HMQC or protein fingerprint which is a SOFAST HMQC containing signals termed as crosspeaks or resonances that report on the environment and dynamics at a residue resolution. For proteins, rigid segments are less visible as they have higher local correlation time ( $\tau_c$ ), yielding broader crosspeaks with respect to the size (MW) and shape of the rigid region. Flexible residues are strongly visible and the signal intensity is not related to the MW of the flexible region, allowing to probe such segments in proteins of any size. Typically, we expect as much crosspeaks in the SOFAST HMQC as stable <sup>1</sup>H-<sup>15</sup>N bonds in the protein backbone and side-chains. Notably, we can not observe proline residues in the typical 2D <sup>1</sup>H-<sup>15</sup>N HSQC/HMQC experiments since the residue has no NH bond in its structure.

In the  $^1\text{H}$ - $^{15}\text{N}$  fingerprint of full length human TCTP (Fig. 3.1), we counted more resonances than residues in the protein due to side-chains contribution. All crosspeaks were well dispersed in both  $^1\text{H}$  and  $^{15}\text{N}$  dimensions, indicating that the visible protein is well folded in our conditions. For the TCTP IDR (residues 38 to 66), corresponding signals are grouped in the center of the spectrum ( $\sim 8$  ppm in  $^1\text{H}$  dimension) which is typical of unstructured, flexible segments. Indeed, signal dispersion is low for resonances from disordered and solvent-exposed regions in a protein since they have no stable structure and thus limited differences in their averaged environment, leading to small dispersion of chemical shifts. For flexible residues, such as in the TCTP IDR, the signal intensity is higher due to slower transverse relaxation time that sharpens lines and is typical from flexible regions with faster tumbling compared to structured regions. Within the globular core of TCTP, the intensity is weaker since it is rigid with slower rotational tumbling and thus higher correlation time ( $\tau_c$ ). We have recorded 3D NMR experiments such as HNCO, HNCA and HNCACB (Sec. 2.3.1.3) to achieve the backbone assignment of TCTP to further probe the protein structure and dynamics at residue-resolution upon various conditions. These experiments rely on inter- and intra-residues correlation of backbone nuclei and allow to sequentially link each crosspeak in the  $^1\text{H}$ - $^{15}\text{N}$  fingerprint to the corresponding amino-acid in TCTP sequence. Following this principle and using a previously published assignment [176], we have assigned most of the 172 residues in TCTP excepted proline residues that lack backbone HN (P57, P108, P113, P142, P158) and the two extra-residues in C-terminal (G-1, P0) from the TEV digestion during TCTP purification (Sec. 2.2.3) since they both have no backbone amide HN. The residue N51 could not be assigned, likely due to overlapping signals or intermediate exchange at the chemical shift timescale (ms) which broadens lines in the NMR spectrum. Residues arginine, asparagine and glutamine have a NMR-visible HN in their side-chains and these were also assigned and can report on interaction within the protein structure and also with an interacting molecule. Using all types of backbone chemical shifts ( $^1\text{H}$ ,  $^{15}\text{N}$  and  $^{13}\text{C}$ ) we could predict and well reproduce the secondary structure definition found in both crystal [149] and solution [176] structures of TCTP protein using the software Talos+ (Fig 3.2 A). Alternatively, we used NPS [238] secondary structure prediction server that uses three different statistic methods to report on the consensus topology predicted from TCTP sequence without experimental data (Fig 3.2 A). Even though the secondary structure pattern obtained by NPS [238] was essentially similar to the experimental pattern determined using Talos+, we found that the BH3-like region (15-29) was predicted to form either  $\beta$ -sheet,  $\alpha$ -helix or random coil depending of the algorithm used by NPS, yielding a consensus with ambiguous score. This means that the primary sequence of the BH3-like motif does not contain strong sequence discriminants for neither of random coil or stable ( $\alpha$ -helix,  $\beta$ -sheet)

structure elements and that the rest of the TCTP sequence is likely to help the folding of the BH3-like region into a  $\beta$ -strand.

Beyond TCTP structure, we used NMR to characterize the protein dynamics in various conditions. We have measured  $^{15}\text{N}$ -spin  $R_1$  and  $R_2$  and  $\{^1\text{H}\}$ - $^{15}\text{N}$  Heteronuclear NOEs experiments performed on native TCTP that yield information on both local and global dynamics. Individually,  $^{15}\text{N}$ -spin rates  $R_1$  and  $R_2$  yield information on motion in a wide range of timescales (ps-ms) (Fig 3.2 B). We found higher  $R_1$  and lower  $R_2$  in TCTP IDR compared to the rest of the protein which mostly includes well structured segments. These differences from  $^{15}\text{N}$ -spin relaxation rates in TCTP IDR are typical signatures of a disordered region in which accelerated motions (ps-ns) induce longer transverse and shorter longitudinal  $^{15}\text{N}$ -spin relaxation time. Finally, parameters extracted from  $\{^1\text{H}\}$ - $^{15}\text{N}$  Heteronuclear NOEs experiments are a different source of information on the local mobility of the H-N vector in the protein backbone. By using a principle based on NOE-mediated saturation transfer, we could discriminate rigid from not rigid backbone H-N since the efficiency of the saturation transfer is greater for H-N vectors reorienting fast as in flexible regions with no stable structure and fast dynamics (ps-1 ns). Most of the TCTP structured parts had heteronuclear NOEs values close to 1, indicating that the H-N vector in these residues is rigid and likely engaged in hydrogen-bonding and related stable structure elements. In the TCTP IDR, we observe a decrease of values from each extremity to reach a minima at position E55. This confirms that the IDR is highly dynamic with maximal mobility of H-N bonds in the central region of the protein segment.

For assessing the global dynamics of the protein, the  $R_2/R_1$  ratio can serve to estimate the correlation time ( $\tau_c$ ) using the Lipari-Szabo formalism [210]. The correlation time ( $\tau_c$ ) represents the rotational diffusion time of the protein and was computed to  $10.1 \pm 0.12$  ns for TCTP at 500  $\mu\text{M}$ . The  $\tau_c$  depends on the MW and protein shape. The Lipari-Szabo formalism also allows to compute models that explain  $^{15}\text{N}$ -spin  $R_1$  and  $R_2$  and  $\{^1\text{H}\}$ - $^{15}\text{N}$  Heteronuclear NOEs experiments in term of local mobility at different timescales and under chemical exchange. We will present such this analysis for native TCTP and upon modification later in the manuscript (Sec. 3.2).

### 3.1.2 TCTP forms salt- and IDR- dependent dimers

We wanted to establish if TCTP could form dimers in solution since it could cause spectral perturbations non-related to binding events with partners. To test if the native human TCTP could exist as non-covalent dimers in our conditions of buffer and salt (pH 7.4, 150 mM NaCl), we have proceeded with dilution experiment of the protein from 1 mM to 50  $\mu\text{M}$

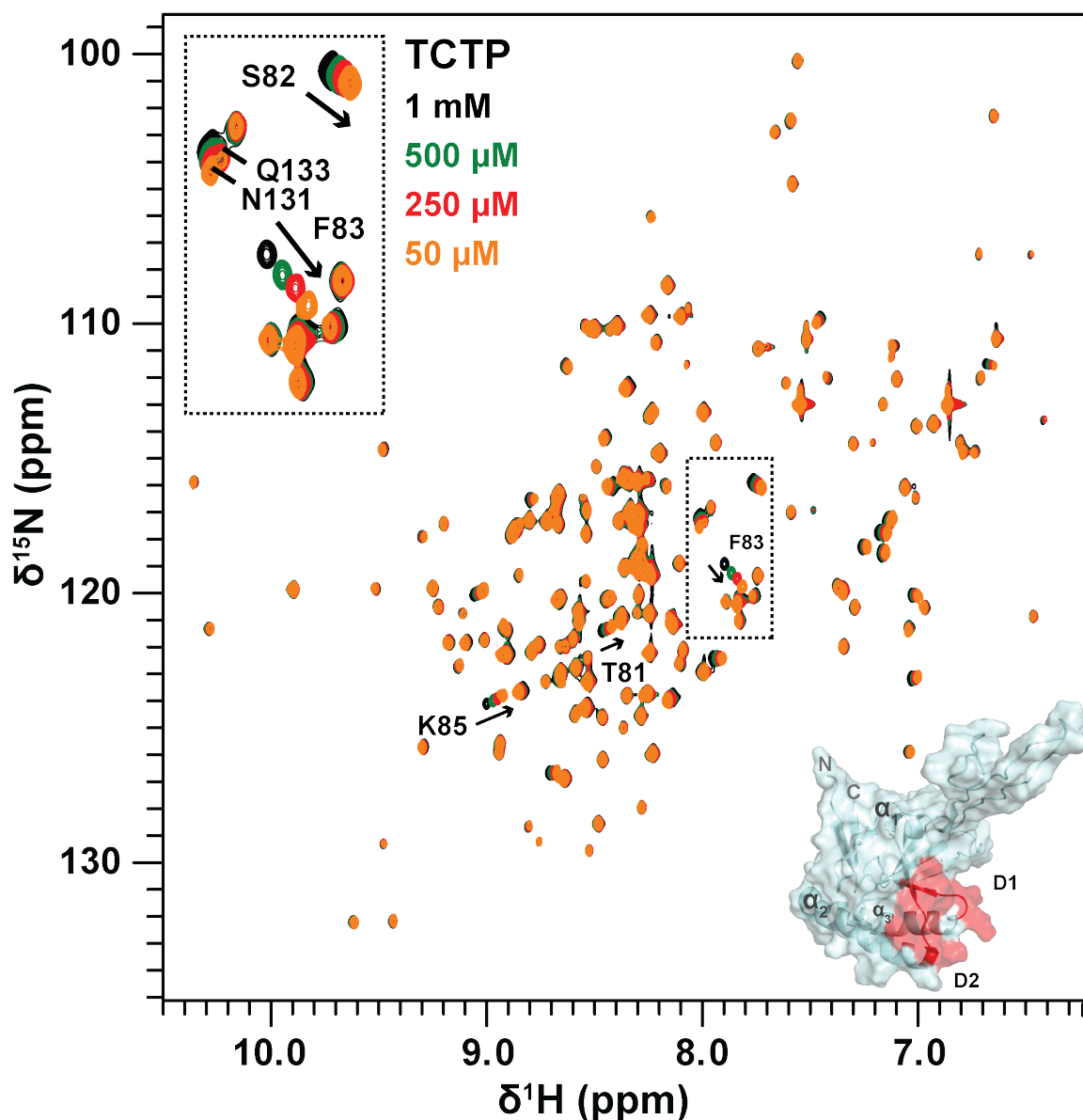
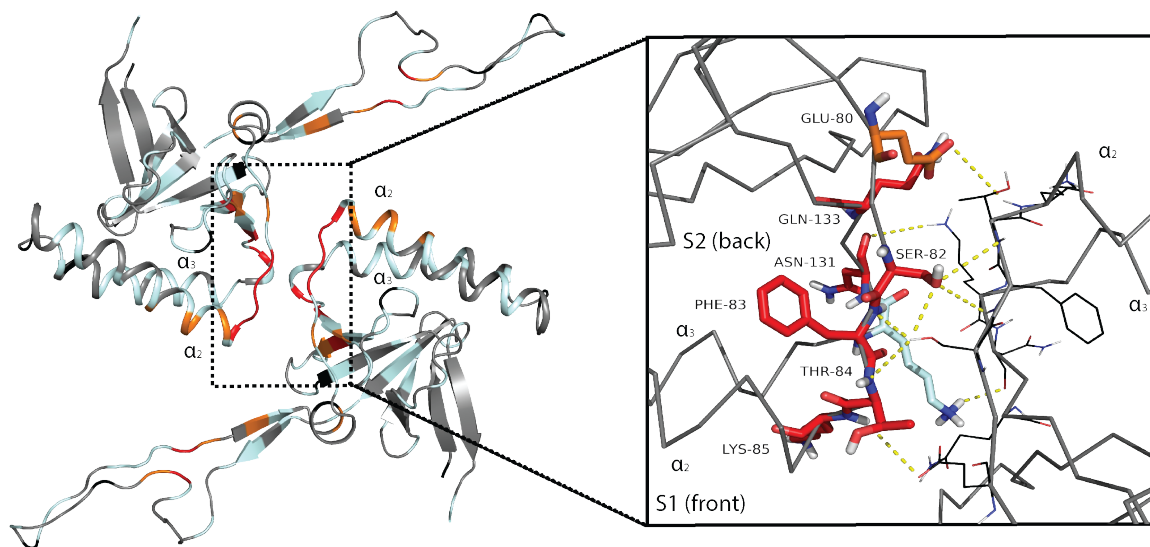
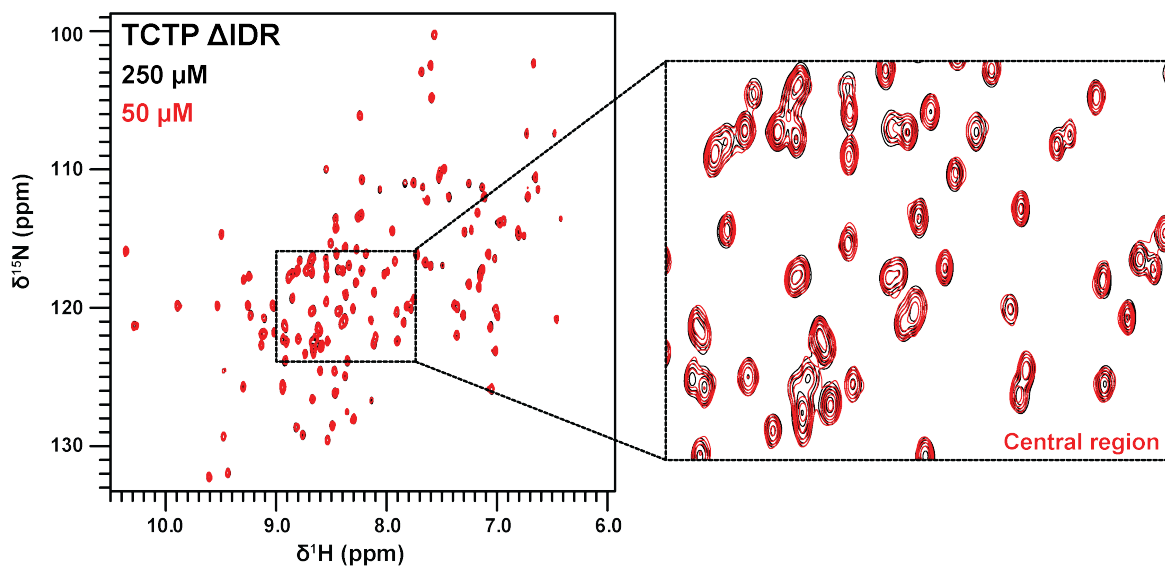


Fig. 3.3 **The concentration-dependent monomer-dimer equilibrium in TCTP.** (A) Overlay of  $^1\text{H}$ - $^{15}\text{N}$  SOFAST HMQC spectra from TCTP upon dilution from high (1 mM) (black) to low (50  $\mu\text{M}$ ) (orange) concentration. Spectra were scaled arbitrarily. Residue F83 shows the largest perturbation upon dilution and forms with residues S82, T81, K85, N131 and Q133 a group of dimer-sensitive amino-acids (black labels). Segments D1 (80-85) and D2 (130-135) are shown (red) on the structure of TCTP (pdb code: 2HR9) (bottom-right). Experiments were recorded at 950 MHz and 25  $^\circ\text{C}$  in the following buffer: 50 mM HEPES pH 7.4, 150 mM NaCl, 2 mM TCEP in 95 %  $\text{H}_2\text{O}$  / 5 %  $\text{D}_2\text{O}$ .

concentration. We have recorded  $^1\text{H}$ - $^{15}\text{N}$  SOFAST HMQC spectra of the protein upon dilution to observe the sensitivity of  $^1\text{H}$ ,  $^{15}\text{N}$  chemical shifts toward TCTP concentration. Interestingly, we have detected  $^1\text{H}$ ,  $^{15}\text{N}$  chemical shift dependence for several residues



**Fig. 3.4 Model of TCTP dimerization interface.** The NMR structure [176] (pdb code: 2HR9) and crystal structure [149] (pdb code: 1YZ1) of TCTP were used to propose a structural model at the dimer interface. The TCTP monomer from NMR structure was aligned on the asymmetric unit in the crystal structure. The operation was repeated with another monomeric TCTP from NMR data to assemble the dimer interface. Residues for which  $^1\text{H}$ - $^{15}\text{N}$  resonances are strongly (red  $\geq$  orange) and weakly (grey) affected by TCTP dimerization are highlighted.



**Fig. 3.5 Importance of TCTP IDR for dimer formation.** Overlay of  $^1\text{H}$ - $^{15}\text{N}$  SOFAST HMQC spectra from TCTP  $\Delta\text{IDR}$  at high (250  $\mu\text{M}$ ) (black) and low (50  $\mu\text{M}$ ) (red) concentration. Spectral intensity were scaled arbitrarily. Experiments were recorded at 950 MHz and 25  $^\circ\text{C}$  in the following buffer: 50 mM HEPES pH 7.4, 150 mM NaCl, 2 mM TCEP, EDTA 0.5 mM in 95 %  $\text{H}_2\text{O}$  / 5 %  $\text{D}_2\text{O}$ .

to the concentration of TCTP (Fig. 3.3). We computed combined  $^1\text{H}$ - $^{15}\text{N}$  chemical shift perturbations and mapped these residues within the poorly defined segments D1 (80-85) and D2 (130-135) of the protein. Residue F83 exhibited by far the largest  $^1\text{H}$ - $^{15}\text{N}$  chemical shift perturbation. The surface drawn by D1 and D2 segments on the structure of TCTP was similar to the electrostatic TCTP-TCTP interface described in the crystal structure of the protein [149] (Fig. 3.4) which suggest that D1/D2 is a hotspot in the protein for dimerization, possibly favored in the crystallisation process. We conclude that native TCTP form concentration-dependent non-covalent dimers in solution.

We computed the self-dissociation constant ( $K_{\text{d-self}}$ ) for the TCTP dimer to estimate populations in solution (150 mM NaCl, pH 7.4) and found  $1.36 \pm 0.26$  mM but the value is extremely sensitive to salt concentration. Our methodology is explained in the paper we will present in the next section (Sec. 3.2). We could estimate that TCTP dimer is poorly populated (3 %) at low concentration of protein but is significantly enriched (30 %) at higher concentration (500  $\mu\text{M}$ ). In addition to protein concentration, we searched for other parameters balancing the monomer-dimer equilibrium in TCTP to further predict the dimer content relative to the experimental setup. In the NMR sample of protein, we used variable salt concentration and pH to show that the TCTP dimer is predominant ( $\geq 95$  %) in absence of NaCl and is promoted at alkaline pH (Ann. 7).

We then tested how the TCTP IDR could participate in TCTP dimer formation using the TCTP  $\Delta\text{IDR}$  mutant. We recorded  $^1\text{H}$ - $^{15}\text{N}$  SOFAST HMQC of the protein variant at different concentrations.  $^1\text{H}$ ,  $^{15}\text{N}$  chemical shifts from the TCTP  $\Delta\text{IDR}$  mutant were not sensitive toward protein concentration anymore (Fig. 3.5). The monomer-dimer equilibrium in TCTP was abolished upon IDR removal and only monomeric TCTP  $\Delta\text{IDR}$  could be detected, indicating that the IDR is required for dimer formation. This is surprising considering that the IDR does not overlap with segments D1/D2 that we proposed for the inter-TCTP interface. Furthermore, we could have expected that the TCTP IDR would inhibit self-association rather than allowing it since it represents a mobile lid that evolves close to the dimerization interface. Hypothetically, TCTP IDR could bring protein units closer from each other to decisively increase the local concentration and to promote self-association. Further discussions about the putative role of TCTP IDR in dimer formation are reported in the next section (Sec. 3.2).

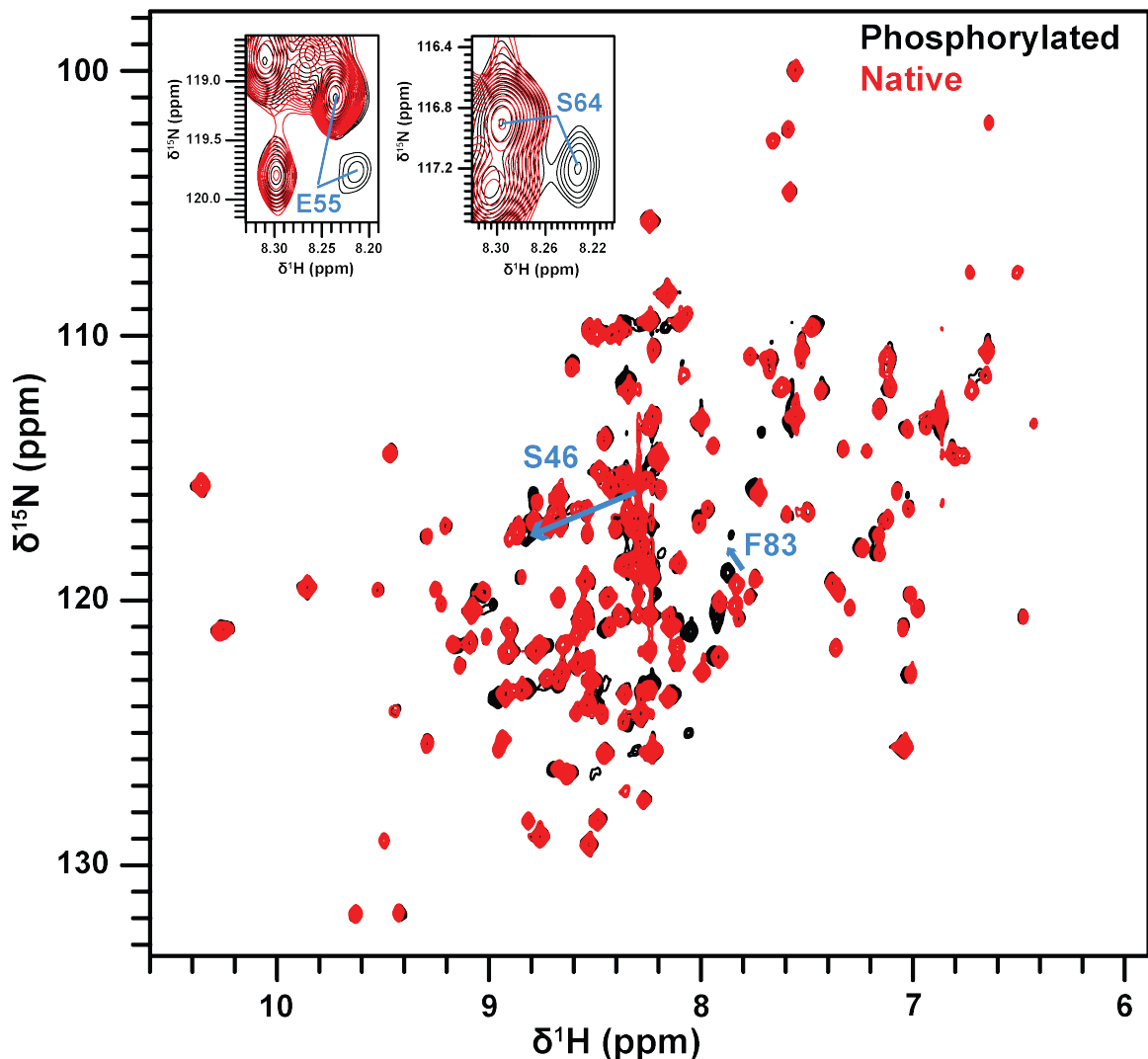
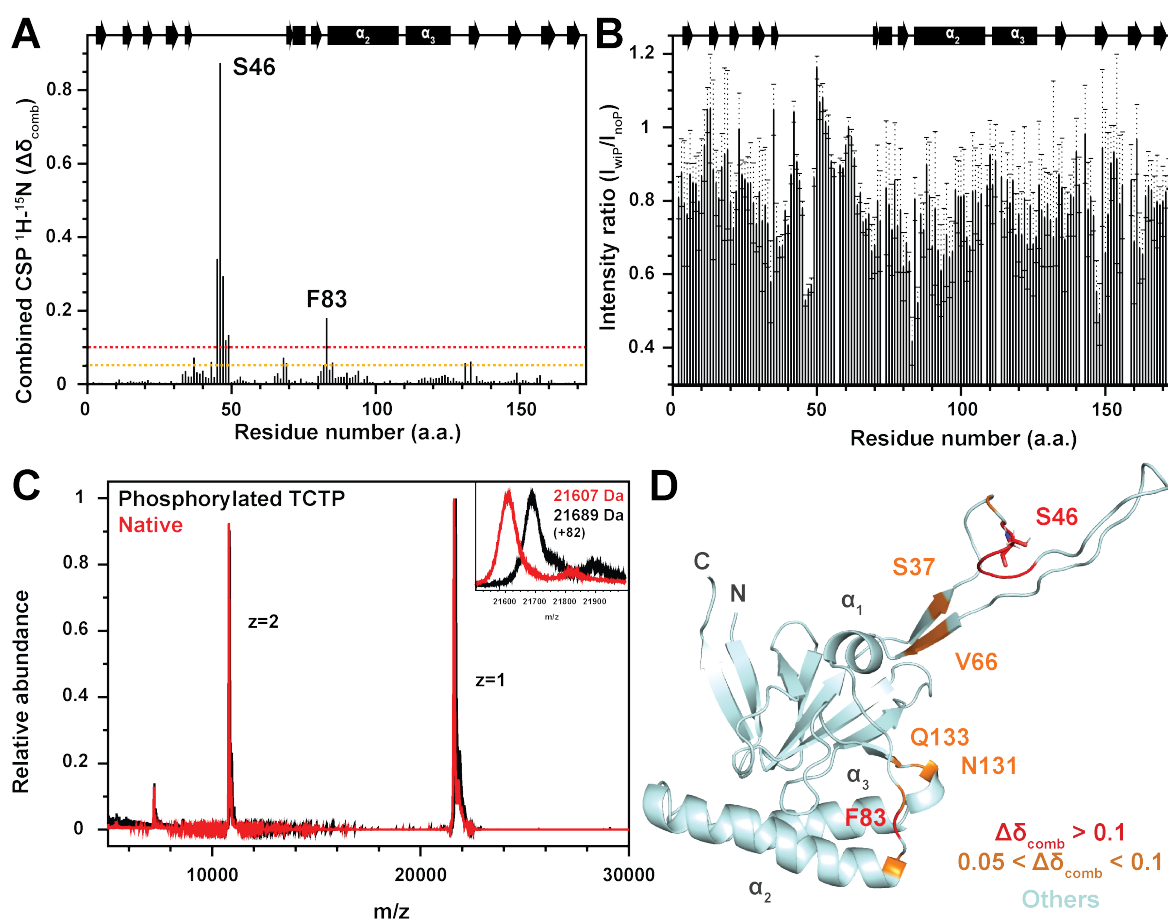


Fig. 3.6 **Overview of TCTP phosphorylation by Plk-1.** Overlay of  $^1\text{H}$ - $^{15}\text{N}$  SOFAST HMQC spectra from phosphorylated (black) and native (red) TCTP (100  $\mu\text{M}$ ). Residue S46 exhibits the largest perturbation upon phosphorylation. The dimer-sensitive residue F83 is also affected. Both are highlighted (light blue). Examples of TCTP IDR residues for which multiple resonances were matched are given with E55 and S64 (top-left). Experiments were recorded at 950 MHz and 25  $^\circ\text{C}$  in the following buffer: 50 mM HEPES pH 7.4, 150 mM NaCl, 2 mM TCEP in 95 %  $\text{H}_2\text{O}$  / 5 %  $\text{D}_2\text{O}$ .

### 3.1.3 Phosphorylation in TCTP IDR by Polo-like kinase 1 (Plk-1)

#### 3.1.3.1 Monitoring of TCTP phosphorylation and structural characterization

TCTP was reported to stabilize microtubules (MTs) upon binding to  $\alpha$ -tubulin units, stabilizing the mitotic spindle during the metaphase in mitotic cells. The Plk-1 phosphorylates TCTP both *in vivo* and *in vitro* at positions S46/S64 and lead to the dissociation of TCTP from the  $\alpha$ -tubulin [31], leading to mitotic spindle destabilization and mitosis completion [33].



**Fig. 3.7 Characterization of the phosphorylation site in TCTP.** (A) Combined  $^1\text{H}$ - $^{15}\text{N}$  chemical shift perturbations and (B) intensity ratios computed between  $^1\text{H}$ - $^{15}\text{N}$  SOFAST HMQC spectra from native and phosphorylated TCTP. (C) MALDI-TOF spectra from native (red) and phosphorylated (black) TCTP. (D) Mapping of combined  $^1\text{H}$ - $^{15}\text{N}$  chemical shift perturbations (red  $\geq 0.1$ , orange  $\geq 0.05$ , cyan  $\geq 0.015$ , grey  $\geq 0.015$ ) on TCTP structure (pdb code: 2HR9). Residue S46 is highlighted (sticks). Experiments were recorded at 950 MHz and 25 °C in the following buffer: 50 mM HEPES pH 7.4, 150 mM NaCl, 2 mM TCEP in 95 %  $\text{H}_2\text{O}$  / 5 %  $\text{D}_2\text{O}$ .

Since phosphorylation is often reported to modulate protein interactions [239], we tested if we could detect an alternative TCTP state upon Plk-1 mediated phosphorylation, that could explain why it dissociates from MTs upon phosphorylation. Furthermore, obtaining the phosphorylated state of TCTP could be used to test the effect of the phosphorylation on interactions with molecules like sertraline since the phosphorylation of TCTP is supposed to abolish such interactions, possibly providing chemoresistance to cancer cells (Sec. 1.2.3.3).

We obtained a pre-activated Plk-1 from Sophie Zinn-Justin (LBSR, CEA/Université Paris-Saclay) and proceeded with the *in vitro* phosphorylation of TCTP with real-time monitoring of the reaction by NMR (Sec. 2.2.3). Briefly, we prepared native  $^{15}\text{N}$ -TCTP protein in a

buffer containing ATP and we added a small concentration ratio (1:1000) of Plk-1 in the NMR tube. The reaction started immediately after addition of Plk-1 and we did not observe significant spectral variations after two hours of monitoring, suggesting that it was 100 % completed (Fig. 3.6). Comparison between native and phosphorylated TCTP (pTCTP) was best achieved after a SEC of the reaction mixture to separate pTCTP from magnesium ions that bind the protein and ATP/ADP molecules. The phosphorylation homogeneity in TCTP was established by MS MALDI-TOF experiments with both native and phosphorylated proteins (Fig. 3.7 C). We have measured a difference of 82.4 Da between the mono-charged species from native and phosphorylated TCTP when expecting a positive difference of 81 Da between the two structural isoforms (perdeuterated sample) due to the gain of the phosphate group. The uncertainty of measurement ( $\pm 5$  Da) covered the difference. This indicates that TCTP is affected by a unique phosphorylation event. In the  $^1\text{H}$ - $^{15}\text{N}$  SOFAST HMQC spectra of TCTP during the phosphorylation reaction, about ten resonances from TCTP IDR characteristic of the native protein progressively disappeared, while new intense crosspeaks progressively became visible, likely from residues at the phosphorylation site. Interestingly, minor resonances were also visible and they were located close to major crosspeaks from the IDR in the spectrum of pTCTP, which could suggest modification in the IDR dynamics and possibly new stable conformations upon phosphorylation. Nevertheless, the  $^1\text{H}$ - $^{15}\text{N}$  SOFAST HMQC spectra globally remained highly similar suggesting limited change of the protein structure upon phosphorylation. Notably, a slight decrease in the whole signal intensity from structured parts of the protein can be observed, which might indicate that phosphorylated TCTP is more prone to dimerization.

3D NMR experiments were recorded to precisely assign the most shifted crosspeaks and to assess local structure and dynamics variations upon phosphorylation: BEST TROSY for pTCTP backbone assignment (HNCO, HNCA, HNCACB), longitudinal ( $T_1$ ), transverse ( $T_2$ )  $^{15}\text{N}$  relaxation and  $\{^1\text{H}\}$ - $^{15}\text{N}$  Heteronuclear NOEs (Sec. 2.3.1.3). The backbone assignment of pTCTP allowed to map the phosphorylation-induced spectral perturbations on the protein structure. 96 % of pTCTP residues (99 % if excluding proline) were matched with a corresponding crosspeak in the  $^1\text{H}$ - $^{15}\text{N}$  SOFAST HMQC with missing assignment for residues M1 and I73 in both native and phosphorylated protein. In order to locate the phosphorylation site and to identify phosphorylation-sensitive elements along TCTP primary sequence, we analyzed combined  $^1\text{H}$ - $^{15}\text{N}$  chemical shift perturbations (Fig. 3.7 A) and intensity ratios (Fig. 3.7 B) computed from  $^1\text{H}$ - $^{15}\text{N}$  fingerprint of native or phosphorylated TCTP. Overall, the largest perturbations were located in the 45-49 segment of the protein IDR. This segment contains the residue S46, a known target of Plk-1 [33]. Consistently,  $^1\text{H}$ - $^{15}\text{N}$  crosspeak from residue S46 exhibited the largest perturbation and is the unique phosphorylation site

detected in TCTP upon Plk-1 mediated phosphorylation. In a lesser extent, surrounding residues were also affected (D45, L47, I48, G49). Residues S46-L47-I48 also showed a significant decrease in signal intensity ( $\geq 50\%$ ) possibly induced by a slower dynamics on a fast timescale (ps-ns) upon phosphorylation of residue S46. Long-range modifications were seen through modest but significant variations at the dimer interface (F83, K85, N131, Q133) which are consistent with a slight but significant increase ( $\sim 10\%$ ) in dimer content upon phosphorylation. Consequently, the dimer interface is preserved in pTCTP compared to TCTP. Finally, N- and C- terminal extremities of the TCTP IDR which arrange together as a  $\beta$ -sheet in the non-phosphorylated protein are affected in term of chemical shift at residues S37 and V66 upon phosphorylation. It is likely that this segment transiently interacts with the IDR in the native state considering their close proximity, and this interaction is expected to be modified upon phosphorylation, possibly explaining these residual perturbations at S37 and V66 residues. In our experiments, we could not detect phosphorylation at residue S64 which raises questions about the activity of our Plk-1 or a permissive TCTP state toward phosphorylation at this residue position.

In order to inform on the conformations of TCTP that are promoted upon phosphorylation, we assigned minor  $^1\text{H}$ - $^{15}\text{N}$  resonances seen appearing close from IDR crosspeaks. The NMR assignment has permitted to distinguish conformations populated in the TCTP IDR upon phosphorylation at residue S46 and this is exemplified for S64 and E55 residues (Fig. 3.7 D). Secondary chemical shifts for these residues in the phosphorylation-promoted TCTP IDR conformations were still characteristic of random coil as for the major state, indicating that the micro states populated in pTCTP IDR do not have propensity to form  $\alpha$ -helix or  $\beta$ -strand. However, they could still have an impact on partner binding and might represent relevant targets for drug development which would aim to target phosphorylated TCTP.

### 3.1.3.2 The monomer-dimer equilibrium in phosphorylated TCTP

We then wanted to investigate more precisely the impact of TCTP phosphorylation at residue S46 on both TCTP IDR dynamics and the oligomeric state of the protein (Fig. 3.8). We measured parameters related to local and global dynamics from  $^{15}\text{N}$ -spin  $R_1$  and  $R_2$  and  $\{^1\text{H}\}$ - $^{15}\text{N}$  Heteronuclear NOEs experiments. The averaged  $^{15}\text{N}$  longitudinal ( $R_1$ ) and transverse ( $R_2$ ) relaxation rates over the structured parts of native TCTP were  $\langle R_1 \rangle = 1.00 \pm 0.06 \text{ s}^{-1}$  and  $\langle R_2 \rangle = 22.41 \pm 1.78 \text{ s}^{-1}$ , respectively. For pTCTP over the same structured parts, the averaged longitudinal  $^{15}\text{N}$  relaxation rate  $\langle R_1 \rangle = 1.00 \pm 0.11 \text{ s}^{-1}$  was identical compared to the native protein and also we did not find significant differences considering the pTCTP transverse  $^{15}\text{N}$  relaxation rate  $\langle R_2 \rangle = 21.84 \pm 1.15 \text{ s}^{-1}$ .  $R_2/R_1$  ratio were logically similar

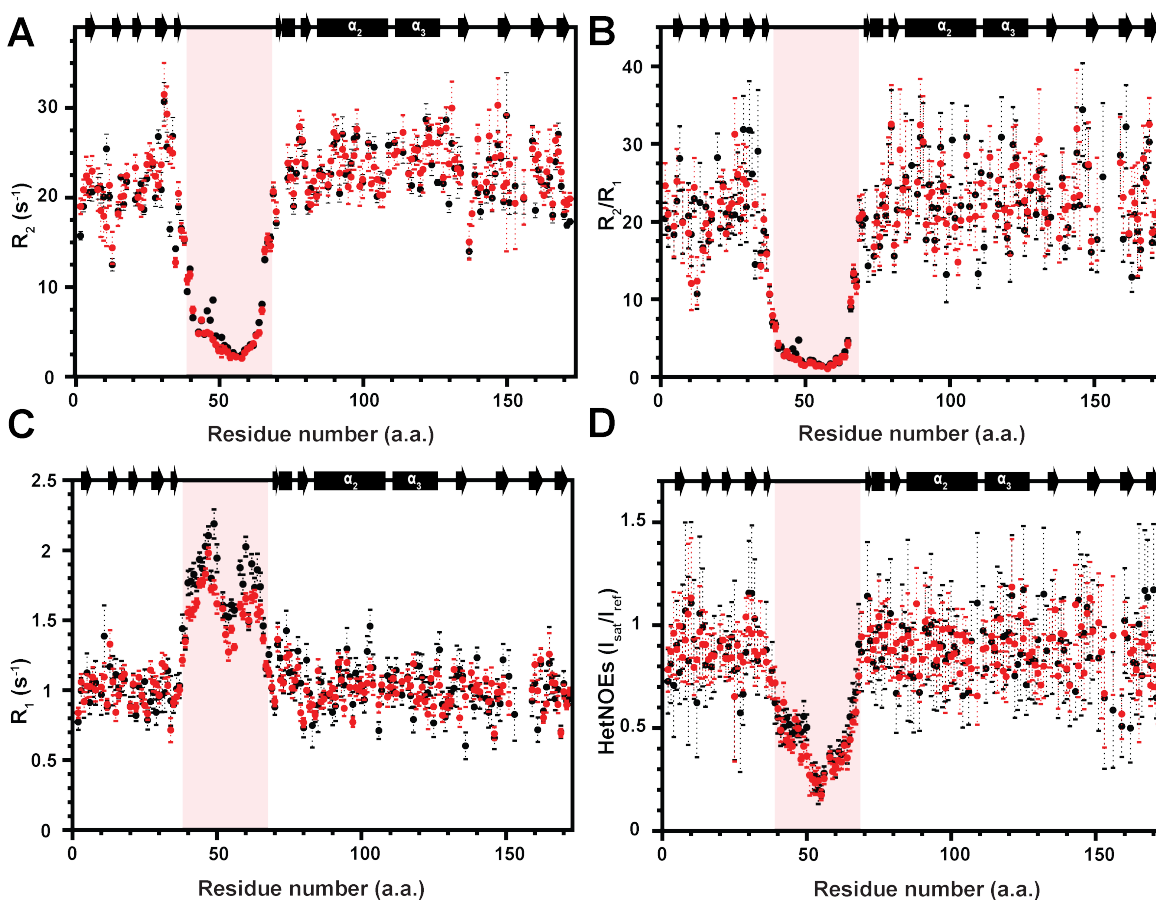


**Fig. 3.8 Impact of phosphorylation on TCTP backbone dynamics.** (A) Longitudinal ( $R_1$ ), (B) transverse  $R_2$   $^{15}\text{N}$  relaxation rates and (C)  $R_2/R_1$  ratios and (D)  $\{^1\text{H}\}$ - $^{15}\text{N}$  heteronuclear NOEs were measured for both native (red) and phosphorylated (black) TCTP. All data were obtained using same experimental conditions (pH 7.4, 25 °C). Relaxation delays were set for  $T_1$  (from 1 ms to 3000 ms) and  $T_2$  (from 1 ms to 138 ms) experiments. Experiments were carried out at 25 °C in the following buffer: 50 mM HEPES pH 7.4, 150 mM NaCl and 1 mM TCEP. Samples were injected into a pre-equilibrated S200 10/300 Increase (GE Healthcare) column prior to SAXS measurement.

for native TCTP  $\langle R_2/R_1 \rangle = 21.93 \pm 3.85$  and phosphorylated TCTP  $\langle R_2/R_1 \rangle = 21.78 \pm 3.46$  over the structured parts of the protein states. In the TCTP IDR, we expect local variations in  $^{15}\text{N}$ -spin  $R_1$  and  $R_2$  since phosphorylation is likely to impact local interactions of phosphorylated S46 with neighbors in the primary sequence and possibly in the whole disordered region.  $^{15}\text{N}$   $R_1$  and  $R_2$  within TCTP IDR were  $1.46 \pm 0.04 \text{ s}^{-1}$  and  $\langle R_2 \rangle = 5.29 \pm 0.26 \text{ s}^{-1}$ , respectively.  $^{15}\text{N}$   $R_1$  and  $R_2$  in phosphorylated TCTP were both higher with  $1.64 \pm 0.07 \text{ s}^{-1}$  and  $5.76 \pm 0.11 \text{ s}^{-1}$ , respectively. The slight but significant increase in averaged  $R_1$  and transverse  $R_2$  revealed slower motions (ns) in TCTP IDR upon phosphorylation since we expect both relaxation rates to increase if very mobile segments with small "local" correlation time (1 ns) have slower tumbling upon phosphorylation. More specifically for

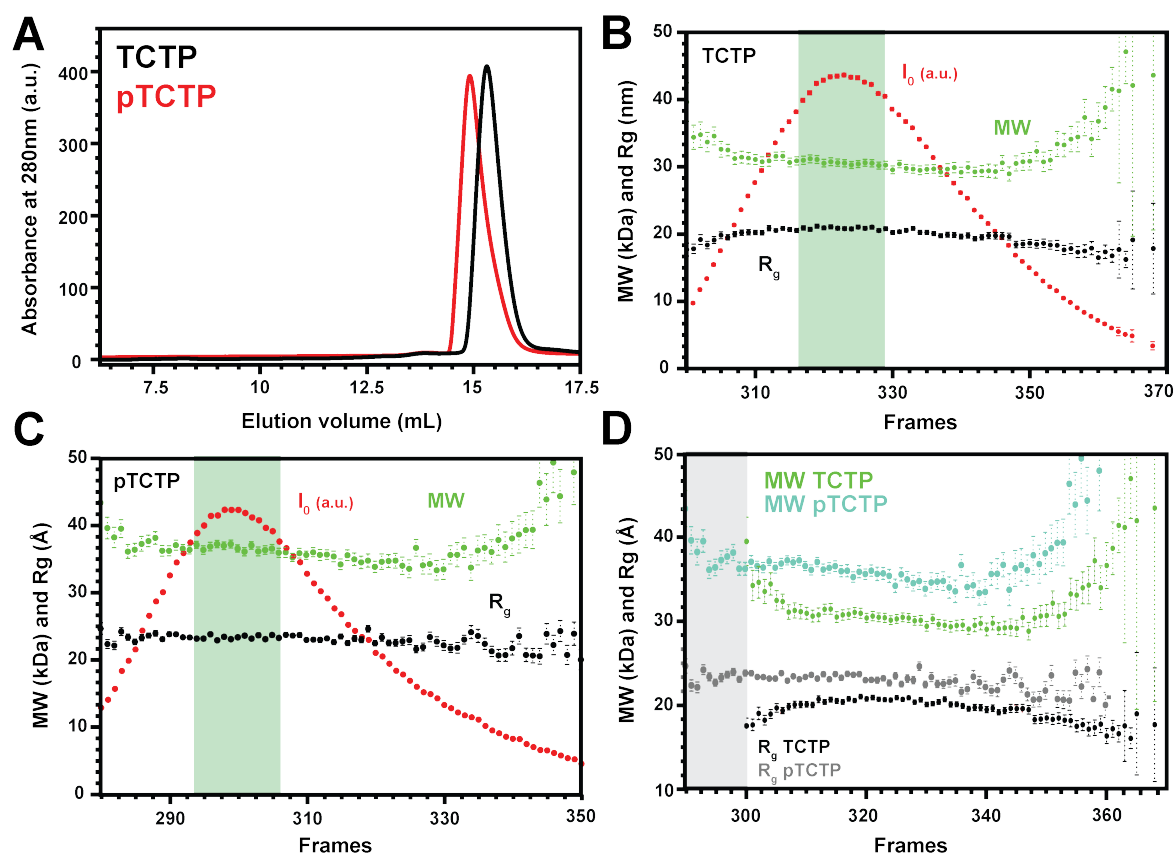


**Fig. 3.9 Oligomeric state of native and phosphorylated TCTP.** (A) SEC profiles of native (black) and phosphorylated (red) TCTP (top-left) and representation of estimated MW (kDa) and gyration radius ( $R_g$ ) (nm) along the elution peaks from (B) native and (C) phosphorylated TCTP (top-right, bottom-left) as estimated from SAXS experiments and Guinier analysis. (D) Overlays of MW and  $R_g$  curves corresponding to the frames with high SAXS signal ( $I_0$ ) for each native and phosphorylated TCTP in SEC elution fractions. Experiments were carried out at 25°C in the following buffer: 50 mM EPPS pH 8, 50 mM NaCl and 2 mM TCEP. Samples were injected into a pre-equilibrated S200 10/300 Increase (GE Healthcare) column prior to SAXS measurement.

residues D45-S46-L47, local  $R_1$  and  $R_2$  values indicate that motions in the residue stretch are slower upon phosphorylation [240]. Here, we can interpret the relaxation data by proposing that TCTP IDR is slightly rigidified upon phosphorylation whereas so significant differences can be found regarding the structured core both TCTP and pTCTP.

To determine if phosphorylation could induce variation in TCTP dimer fraction, the apparent correlation time ( $\tau_c$ ) of the protein, which can probe a change in protein oligomeric state, was measured and is  $9.09 \sim 0.07$  ns for pTCTP compared to  $9.19 \sim 0.07$  ns for native TCTP, which is not consistent if we consider that phosphorylation promotes dimer formation which should increase  $\tau_c$  due to the slower rotational diffusion of the populated dimer compared to monomer. This means that phosphorylation of residue S46 in TCTP IDR does not seem

to significantly enrich TCTP dimer at medium concentration of protein (100  $\mu\text{M}$ ) in our  $^{15}\text{N}$ -spin relaxation experiments. However, the TCTP dimer is weakly populated (5-10 %) in the present setup (150 mM NaCl) and even an important relative increase (100 %) in dimer versus monomer could be difficult to detect considering that it would still represent a minor fraction of the total protein with minor contribution to the whole signal, limiting the possibility to detect such little variations in the absolute concentration of dimer.

Finally, we used SEC-SAXS experiments to determine precisely if the non-covalent TCTP dimer could be promoted upon phosphorylation (Fig. 3.9). The apparent gyration radii ( $R_g$ ) were of 2.15 nm and 2.34 nm for both native and phosphorylated isoforms, respectively. The elution volume from SEC (29.8 mL) consistently showed that pTCTP has higher apparent hydrodynamic radius since it was eluted before native TCTP (30.6 mL) (Fig. 3.9 A). The estimated molecular weight of both species was estimated to be 33.8 kDa and 36.1 kDa, respectively (Fig. 3.9 B, C). This apparent MW for native TCTP reflects the relative population of monomer (30 %) and dimer (70 %) in the experimental setup (50 mM NaCl) since the MW of monomeric TCTP is  $\sim 20$  kDa. For pTCTP, the apparent MW is found 16 % higher than for native TCTP, meaning that the relative populations of monomer and dimer for the phosphorylated protein are 15 % and 85 %, respectively. We conclude that phosphorylation at S46 residue promotes TCTP dimerization and we established that dimer is enriched by  $\sim 20$  % upon phosphorylation in a dimer-permissive setup (500  $\mu\text{M}$  protein, 50 mM NaCl, pH 8). In the next section, we will discuss more about the impact of phosphorylation on the IDR conformational space and its putative influence in modulating the monomer-dimer equilibrium in TCTP, based on MD (Sec. 3.2).

## 3.2 *Research paper* TCTP IDR upon phosphorylation and calcium binding

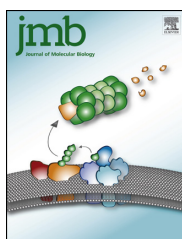
The IDR in native TCTP projects far away from the globular core of the protein. This segment modulates protein-protein interactions with partners such as MDM2 [173] or  $\alpha$ -tubulin [33] via phosphorylation or mimetics at residues S46 and S64. Binding of sertraline and thioridazine, drugs targeting TCTP in cancer context, was abolished upon phosphorylation mimetics [173]. Moreover, the TCTP IDR region (38-66) was shown to bind calcium with strong enough affinity (10  $\mu\text{M}$ ) to inhibit thapsigargin-induced apoptosis [175]. To understand how calcium binding and phosphorylation in TCTP IDR can modify interactions with partners, we measured the impact of phosphorylation (*in silico*, pTCTP was not available yet at the moment of the study) and calcium binding (*in silico*, *in vitro*) on TCTP structures

to explain how interactions capabilities could be modified upon IDR modification. More precisely, we computed conformational ensemble of mono- and di- phosphorylated TCTP in presence and in absence of calcium by MD simulations. Experimental data regarding calcium binding were also combined with computational approaches. We also characterized the conformational ensemble of the free protein and compared with experimental data from NMR in order to validate the simulation protocol. We also report in this publication our work about the identification of a non-covalent dimer equilibrium in TCTP and describe the molecular interface and possible structure. Overall, this study brings clues about the putative mechanism by which phosphorylation and calcium binding in TCTP IDR could modify interaction capabilities for the whole protein.

## **Conformational Ensemble and Biological Role of the TCTP Intrinsically Disordered Region: Influence of Calcium and Phosphorylation**

Florian Malard, Nadine Assrir, Mouad Alami, Samir Messaoudi, Ewen Lescop and Tâp Ha-Duong

Consult supplementary data in appendix (App. 6.3)



## Conformational Ensemble and Biological Role of the TCTP Intrinsically Disordered Region: Influence of Calcium and Phosphorylation

Florian Malard<sup>1</sup>, Nadine Assrir<sup>1</sup>, Mouad Alami<sup>2</sup>, Samir Messaoudi<sup>2</sup>, Ewen Lescop<sup>1</sup> and Tâp Ha-Duong<sup>2</sup>

1 - Institut de Chimie des Substances Naturelles, CNRS UPR 2301, Université Paris-Saclay, 1 avenue de la Terrasse, 91198 Gif-sur-Yvette, France

2 - BIOCIS, Université Paris-Sud, CNRS UMR 8076, Université Paris-Saclay, 5 rue Jean-Baptiste Clément, 92290 Châtenay-Malabry, France

Correspondence to Ewen Lescop and Tâp Ha-Duong: [ewen.lescop@cnr.fr](mailto:ewen.lescop@cnr.fr); [tap.ha-duong@u-psud.fr](mailto:tap.ha-duong@u-psud.fr).  
<https://doi.org/10.1016/j.jmb.2018.04.024>

Edited by Monika Fuxreiter

### Abstract

The translationally controlled tumor protein (TCTP) is a multifunctional protein that may interact with many other biomolecules, including itself. The experimental determinations of TCTP structure revealed a folded core domain and an intrinsically disordered region, which includes the first highly conserved TCTP signature, but whose role in the protein functions remains to be elucidated. In this work, we combined NMR experiments and MD simulations to characterize the conformational ensemble of the TCTP intrinsically disordered loop, in the presence or not of calcium ions and with or without the phosphorylation of Ser46 and Ser64. Our results show that these changes in the TCTP electrostatic conditions induce significant shifts of its conformational ensemble toward structures more or less extended in which the disordered loop is pulled away or folded against the core domain. Particularly, these conditions impact the transient contacts between the two highly conserved signatures of the protein. Moreover, both experimental and theoretical data show that the interface of the non-covalent TCTP dimerization involves its second signature which suggests that this region might be involved in protein–protein interaction. We also show that calcium hampers the formation of TCTP dimers, likely by favoring the competitive binding of the disordered loop to the dimerization interface. All together, we propose that the TCTP intrinsically disordered region is involved in remodeling the core domain surface to modulate its accessibility to its partners in response to a variety of cellular conditions.

© 2018 Elsevier Ltd. All rights reserved.

### Introduction

Abundantly found in eukaryotes, the translationally controlled tumor protein (TCTP) has a very conserved sequence through evolution but a poor amino acid homology to other proteins. TCTP is actually a multifunctional protein involved in several biological processes, including cell growth, cell division, cell survival, and immune response [1]. It has notably a crucial role in tumorigenesis and is up-regulated in many cancer cell lines [2]. TCTP is also an important player in the complex process of somatic cell phenotypic reprogramming into embryonic-stem-like cells. Interestingly, it is involved in the tumor reversion process that makes cancer cells lose their malignant phenotype [3,4]. Thus, TCTP represents a promising biomolecular target for cancer therapy [5].

To exert its various functions, TCTP may interact with many other biomolecules, including itself [6,7]. A recent study using coimmunoprecipitation and mass spectrometry identified 98 potential interacting partners for TCTP [8]. At least 33 proteins were previously shown to bind TCTP by yeast two-hybrid screenings [4]. In addition, TCTP is known to sequester calcium ions [9–11], presumably to block the Ca<sup>2+</sup>-dependent apoptosis process [12]. However, very little information on the structures of TCTP–ligand complexes is available, which impedes the full understanding of the mechanisms by which TCTP performs its functions.

Several groups attempted to determine the TCTP binding regions on which its partners interact, using, in most cases, the domain mapping technique that consists in testing if different truncated domains of

the protein can bind an identified ligand. To our knowledge, the TCTP binding region of 12 protein partners and calcium ions is reported in the literature (Fig. S1 of the Supporting Information). Despite the limitations of the domain mapping approach, we can roughly distinguish three binding regions, each of them being able to interact with several TCTP partners: the N-terminal region (1–80) encompassing the disordered long loop and the TCTP first signature (TCTP1), the central segment (81–130) which is structured in helical hairpin, and the C-terminal region (131–172) containing the protein second signature TCTP2 (the amino acid numbering used in this report comes from the human sequence). However, the three-dimensional structures of TCTP [11,13,14] reveal that its N-terminal and C-terminal segments do not form two separated domains but are interlaced in a  $\beta$ -barrel-like architecture whose accessible surface is composed of patches from both N-terminal and C-terminal residues. Besides the fact that truncated segments of TCTP do not necessarily fold like the full-length protein, this makes the domain mapping results even more difficult to be interpreted in terms of protein–protein interfaces. Therefore, experimental and theoretical studies carried out on the native full-length protein should provide more reliable information regarding the TCTP interactome.

Importantly, the highly conserved signature TCTP1 (consensus sequence IG[A-G]N[A-P]SAE) is located in the middle of the protein disordered region (residues 37–68) and probably plays a pivotal role in the TCTP recognition by its multiple partners. To illustrate this, TCTP1 contains the residue Ser53 which was found to be phosphorylated in human cell line during mitosis [15], and can therefore be involved in TCTP functional regulation. Furthermore, it is often highlighted that dynamic intrinsically disordered regions can transiently adopt various secondary structures which are recognized by different ligands [16–18]. Another possible role of the disordered loop is to transiently interact with different parts of the structured core domain, potentially hampering the binding of ligands on these regions (competitive binding) [19–21]. More generally, these loop–core intramolecular interactions could modify the physical–chemical properties of the protein binding surfaces, regulating the binding of other partners. Among the possible binding sites on the TCTP core domain, the second signature TCTP2 is located at the region 129–151 and contains the largely conserved residues Phe134, Phe135, Gly137, Glu138, Met140, Asp143, and Tyr151. These solvent-exposed residues delineate an extended area on TCTP surface that can be decomposed into two patches formed by residues 129–133 in strand  $\beta$ 8 with residues 150–151 in strand  $\beta$ 9 (TCTP2a) and by the  $\beta$ 8 –  $\beta$ 9 loop residues 138–143 (TCTP2b).

To add complexity to the TCTP structure–activity relationship, residues Ser46 and Ser64, both located in the intrinsically disordered loop, were shown to be hierarchically phosphorylated by the polo-like kinase Plk1 [22]. These post-translational modifications might impact the TCTP conformational ensemble and its binding activity with other proteins. Likewise, the disordered region having many negatively charged residues (Glu40, Asp44, Asp45, Glu55, Glu58, Glu60, Glu63), the binding of  $\text{Ca}^{2+}$  ions on TCTP surface is likely to influence the conformational dynamics of its long loop. All these considerations call attention to the possible role of the disordered region in modulating the recognition of TCTP by multiple other proteins. In that context, the present study aims at exploring and characterizing the TCTP conformational ensemble, with a particular focus on its disordered loop. Notably, the impacts of calcium binding and of Ser46 and Ser64 phosphorylation on its structures and surface accessibility will be scrutinized and related to the TCTP activity. For this purpose, we investigated the TCTP structural ensemble under four conditions: no calcium and no phosphorylation (noCa–noPhos), with calcium and no phosphorylation (wiCa–noPhos), no calcium and with phosphorylated Ser46 (noCa–pS46), and lastly no calcium and with both Ser46 and Ser64 phosphorylated (noCa–diPhos).

## Results and Discussion

### NMR backbone resonance assignment

The 173-amino-acid construct of the human TCTP used in this study corresponds to the native sequence of the protein with an extra N-terminal Gly residue (Gly0) due to the TEV cleavage site. The  $^1\text{H}$ – $^{15}\text{N}$  SOFAST-HMQC spectrum of the protein was of excellent quality with very well dispersed signals in agreement with a properly folded protein. This spectrum was very similar to that previously published [11] with a slightly different TCTP construct (native N-terminal and extra C-terminal Leu and Glu residues) in different experimental conditions. We confirmed and adjusted the backbone resonance assignment using BEST-TROSY type triple resonance correlation experiments [23]. All 173 amino acids of TCTP except Gly0, Met1, and Asn51 could be assigned to a  $^1\text{H}$ – $^{15}\text{N}$  cross-peak. All HSQC cross-peaks could be assigned suggesting that Met1 and Asn51 likely suffer from severe line broadening. The analysis of the secondary structures by TALOS+ software revealed, as expected, a very good agreement between predicted secondary structures and the NMR [11] and crystal [24] structures of the protein.

### Analysis of $^{15}\text{N}$ -relaxation

$^{15}\text{N}$  spin relaxation rates depend mostly on the reorientation of the N–H bonds, thus providing rich information about local and global dynamics of the protein. We measured residue-specific  $^{15}\text{N}$   $R_1$  and  $R_2$  relaxation rates and  $\{^1\text{H}\}$ – $^{15}\text{N}$  heteronuclear nuclear Overhauser effect (NOE) values at 950-MHz  $^1\text{H}$  frequency, 298 K, and 50  $\mu\text{M}$  protein concentration. Extracted parameters show that relaxation rates were very homogeneous along the structured regions of the protein. Over the structured parts of TCTP, averaged  $^{15}\text{N}$   $R_1$ ,  $R_2$ , and  $R_2/R_1$  values were  $0.63 \pm 0.07 \text{ s}^{-1}$ ,  $18.4 \pm 2.4 \text{ s}^{-1}$  and  $29.1 \pm 6.7$ , respectively. Within the segment 38–66, elevated  $^{15}\text{N}$   $R_1$  and decreased values of  $^{15}\text{N}$   $R_2$  and heteronuclear NOE were observed, which is typical of significant mobility in the fast timescale (picosecond to nanosecond). To further analyze  $^{15}\text{N}$ -relaxation and  $\{^1\text{H}\}$ – $^{15}\text{N}$  heteronuclear NOE, we computed the global correlation time ( $\tau_c$ ) of the protein and the residue-specific order parameters  $S^2$  by using the Lipari–Szabo formalism [25] and an isotropic rotational diffusion tensor. The apparent correlation time was  $10.1 \pm 0.12 \text{ ns}$  which is largely consistent with the value predicted by HYDRONMR [26] for a monomeric TCTP (9.82 ns). The averaged order parameter  $S^2$  were  $0.86 \pm 0.08$  along the structured parts, in agreement with restricted motions in the core domain of TCTP, whereas much lower values of  $S^2$  were obtained within the disordered loop of TCTP, in agreement with its mobility at the ps–ns timescale.

### Conformational ensemble of the non-phosphorylated TCTP in the absence of calcium

In this section, the noCa–noPhos TCTP conformational ensemble was first assessed by comparing several observable parameters computed from MD simulations with those measured by NMR experiments (Fig. 1). These include the coupling constants  $^3J_{H_N-H\alpha}$  and the N–H order parameter  $S^2$  which give information about the protein backbone conformations and dynamics, and secondary chemical shifts which indicate the backbone propensity to form secondary structures. More specifically, we compared the secondary structure propensity (SSP) score that combines the three  $C\alpha$ ,  $C\beta$  and  $H\alpha$  secondary chemical shifts as proposed by Marsh *et al.* [27]. Figure 1 shows that the residue SSP score calculated from MD simulations is in very good agreement with those derived from NMR chemical shifts. Despite a slight offset of the theoretical  $J$ -couplings toward higher values when compared to NMR data, the  $^3J_{H_N-H\alpha}$  values from simulations correlate well with experimental one. Both SSP score and  $J$ -coupling profiles confirm that the region

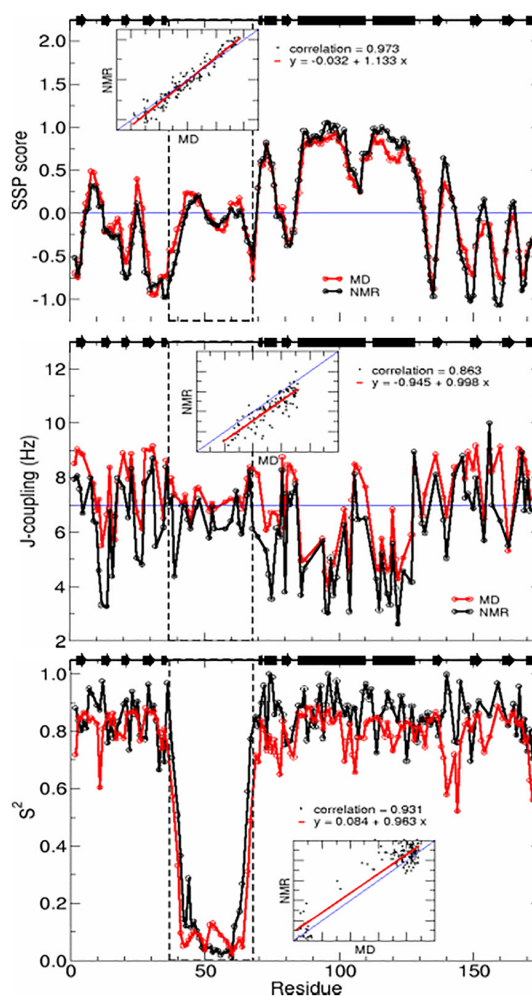


**Fig. 1.** Comparison between NMR (black) and noCa–noPhos MD (red) SSP scores calculated from  $C\alpha$ ,  $C\beta$  and  $H\alpha$  chemical shifts (top), coupling constants  $^3J_{H_N-H\alpha}$  (middle), and N–H bond order parameters  $S^2$  as a function of residue number. NMR experiments were done at 50  $\mu\text{M}$  TCTP concentration in the buffer Hepes 50 mM (pH 7.4), 150 mM NaCl, and 2 mM TCEP at 298 K.

37–68 has no stable secondary structure, as indicated by their values around 0.0 and 7 Hz, respectively. Finally, the theoretical order parameters  $S^2$  appear quite close to those measured by NMR. Notably, in both MD and NMR ensembles, the long loop 37–68 is very mobile, with  $S^2$  values below 0.2 for residues 45–65 indicating very large amplitude fluctuations. Interestingly, some residues exhibit lower order parameter in MD than observed by NMR, notably residues Asp11, His77, Glu138, and Asn139 which are in close spatial proximity in the three-dimensional structure, suggesting possible correlated motions on timescales slower than the protein correlation time ( $\sim 10 \text{ ns}$ ), and hence not detectable

by NMR. All together, these comparisons indicate that the TCTP conformational ensemble explored by MD simulations is fairly consistent with the experimental one.

The noCa–noPhos TCTP conformational ensemble was further analyzed to investigate the possible roles of its intrinsically disordered region. We noticed that the long loop containing the signature TCTP1 tends to contact the core domain on the surface defined with the signature TCTP2. In order to gain insight into this propensity, a free energy surface of the protein was computed as a function of its radius of gyration and the ratio of the distance between the centers of mass of segment 48–58 (TCTP1) and of residues 129–133 and 150–151 (TCTP2a) over the distance between the centers of mass of TCTP1 and of residues 138–143 (TCTP2b). The latter parameter was chosen to highlight the inclination of the TCTP first signature to preferentially bind the solvent

accessible regions defined by either the patches TCTP2a or TCTP2b. The free energy surface displayed in Fig. 2 shows that the TCTP intrinsically disordered loop can adopt various extended conformations more or less distant from the folded core domain, conferring a protein radius of gyration larger than 1.8 nm. But in addition, this long loop can fold toward the bottom of the core domain resulting in a more compact protein with a radius of gyration lower than 1.8 nm. In the latter case, it is observed that the residues of the TCTP first signature are close to either the residues 129–133 and 150–151 (TCTP2a) or residues 138–143 (TCTP2b).

To specify these contacts, the fraction of the simulation time for which each residue of the TCTP core domain is distant by less than 3 Å to the disordered region are shown in Fig. 3. It can be seen that the disordered loop is able to transiently but significantly contact the three segments 73–82, 130–

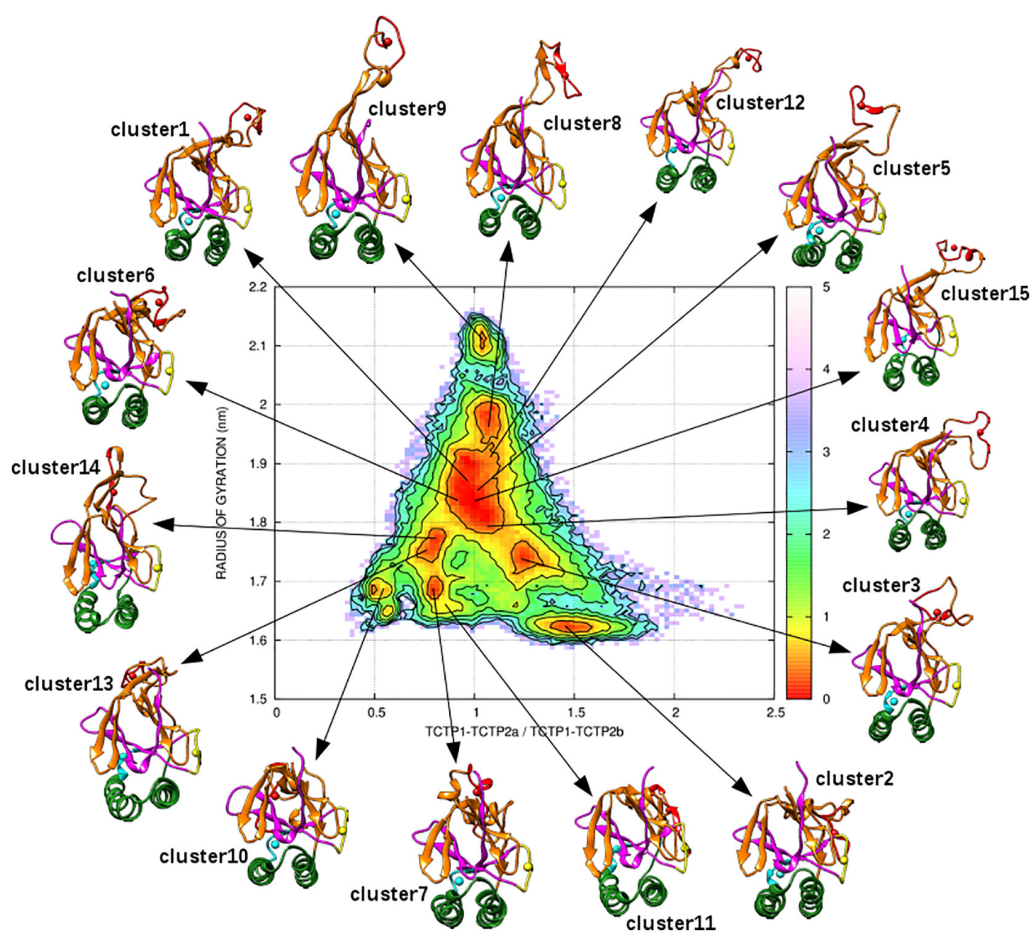


**Fig. 2.** Free energy surface (kcal/mol) of the non-phosphorylated TCTP in the absence of calcium calculated as a function of its radius of gyration and the ratio of the distance between the centers of mass of the signature TCTP1 (region 48–58, red ball) and of residues 129–133, 150–151 (TCTP2a, cyan ball) to the distance between the centers of mass of TCTP1 and of residues 138–143 (TCTP2b, yellow ball). The representative conformation of the 15 most populated clusters is displayed in top view.

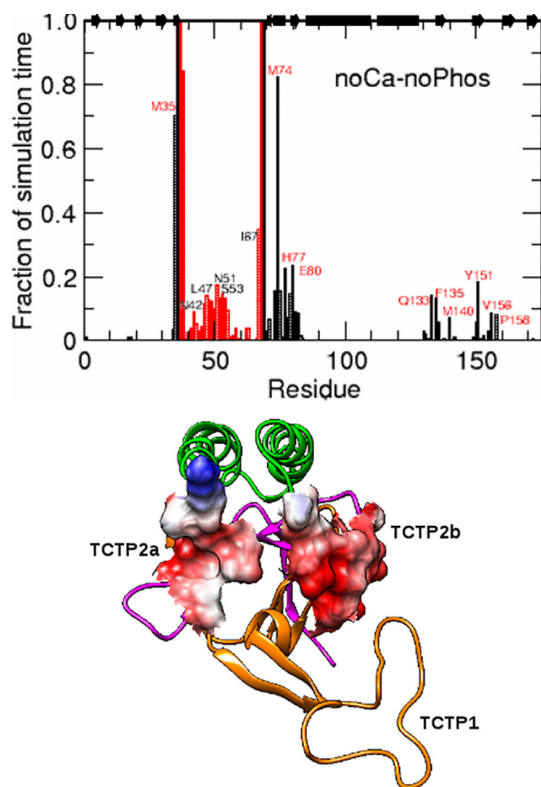


**Fig. 3.** Top: Fraction of the simulation time for which each residue of the TCTP core domain (black), or of the disordered loop (red), is contacted (distance  $< 3 \text{ \AA}$ ) by the long loop or the core domain, respectively. Bottom: Bottom view of the two areas on the TCTP core domain which are the most affected by the binding of its intrinsically disordered loop. The first patch is composed of segments 77–82 and 138–141 (TCTP2b). The second one is composed of residues 130–133 and 150–151 (TCTP2a). These surfaces are colored as a function of their local charge density (red: negative, white: neutral, and blue: positive). The loop structure displayed here is only one of many conformations of the TCTP ensemble.

142, and 150–158 of the folded core domain. Among these latter, it should be noted that residues His77, Leu78, Gln79, Glu80, Thr81, and Ser82 form with residues Glu138, Asn139, Met140, and Asn141 (TCTP2b) a continuous patch, rather negatively charged, on one side of the protein core domain (Fig. 3). Similarly, residues Lys130, Asn131, Tyr132, and Gln133 form with Asp150 and Tyr151 a continuous area (TCTP2a), at the bottom of the core domain, but less negatively charged due to the presence of the conserved residue Lys130 (Fig. 3). These two patches at the surface of the TCTP core domain are among the most affected areas by the transient binding of its disordered loop. To highlight the residues of the TCTP core domain which make contacts with the disordered loop, we first performed

a clustering of the TCTP conformations based on their pairwise RMSD, and then, for the 10 most populated clusters (Fig. 2), we computed the distance matrix between the residues 48–58 and 129–151. Among the top 10 clusters, only cluster2 and cluster10 clearly exhibit contacts between the signature segment TCTP1 and the second signature TCTP2 (Fig. S2 of Supporting Information). In cluster2, the predominant contacts are observed between residues Gly50 and Ala54 of the disordered loop and the residues Phe135, Ile136, and Met140 of the segment TCTP2b. The nature of these interactions is clearly hydrophobic. In cluster10, residues Ile48, Gly49, Gly50, and Asn51 make contacts with the residues Lys130, Asn131, Gln133, and Tyr151 of the region TCTP2a. A visual inspection of cluster10 indicates that, in contrast to cluster2, the core–loop contacts mostly involved polar interactions between the amide group of the Asn51, Asn131, and Gln133 side chains and those of the Gly49, Gly50, and Tyr151 backbone. In none of the TCTP clusters, the signature TCTP1 binds both regions TCTP2a and TCTP2b at the same time.

### Calcium binding and impact on TCTP conformational ensemble

As mentioned in Introduction, TCTP is known to sequester calcium, but the protein regions that bind the  $\text{Ca}^{2+}$  ions are not unambiguously determined. Indeed, using domain mapping techniques, Kim *et al.* [10] located the  $\text{Ca}^{2+}$  binding sites in region 81–112. With the same approaches, Graidist *et al.* [12] identified two high affinity and several low affinity binding sites in the regions 43–62, 57–76, and 127–146, with a particular emphasis on residues Glu58 and Glu60 of the TCTP disordered loop. On the other hand, Feng *et al.* [11] found a single weak affinity calcium binding site in the vicinity of residues Asn131, Gln133, and Asp150 by analyzing NMR chemical shift perturbations in TCTP  $^1\text{H}$ – $^{15}\text{N}$  SOFAST-HMQC spectra. To resolve these ambiguities, we measured and analyzed sets of calcium-induced chemical shift perturbations in light of MD simulations of the non-phosphorylated TCTP in the presence of calcium (wiCa–noPhos). Before, it should be reminded that  $^1\text{H}$ – $^{15}\text{N}$  SOFAST-HMQC NMR spectra can only detect N–H signals from backbone or from asparagine and glutamine side chains. Thus, these experiments may not reveal changes in the chemical environment of long side chain bearing no N–H group. Therefore, for a fair comparison of NMR and MD data, we first compared residues with chemical shift perturbations detected by NMR spectroscopy (top row of Fig. 4) to residues having an N–H group distant by less than  $5 \text{ \AA}$  from a calcium ion in our wiCa–noPhos simulations (middle row of Fig. 4). Recovering the observations reported by Feng *et al.*, our NMR data show that the N–H groups which are the most affected by calcium

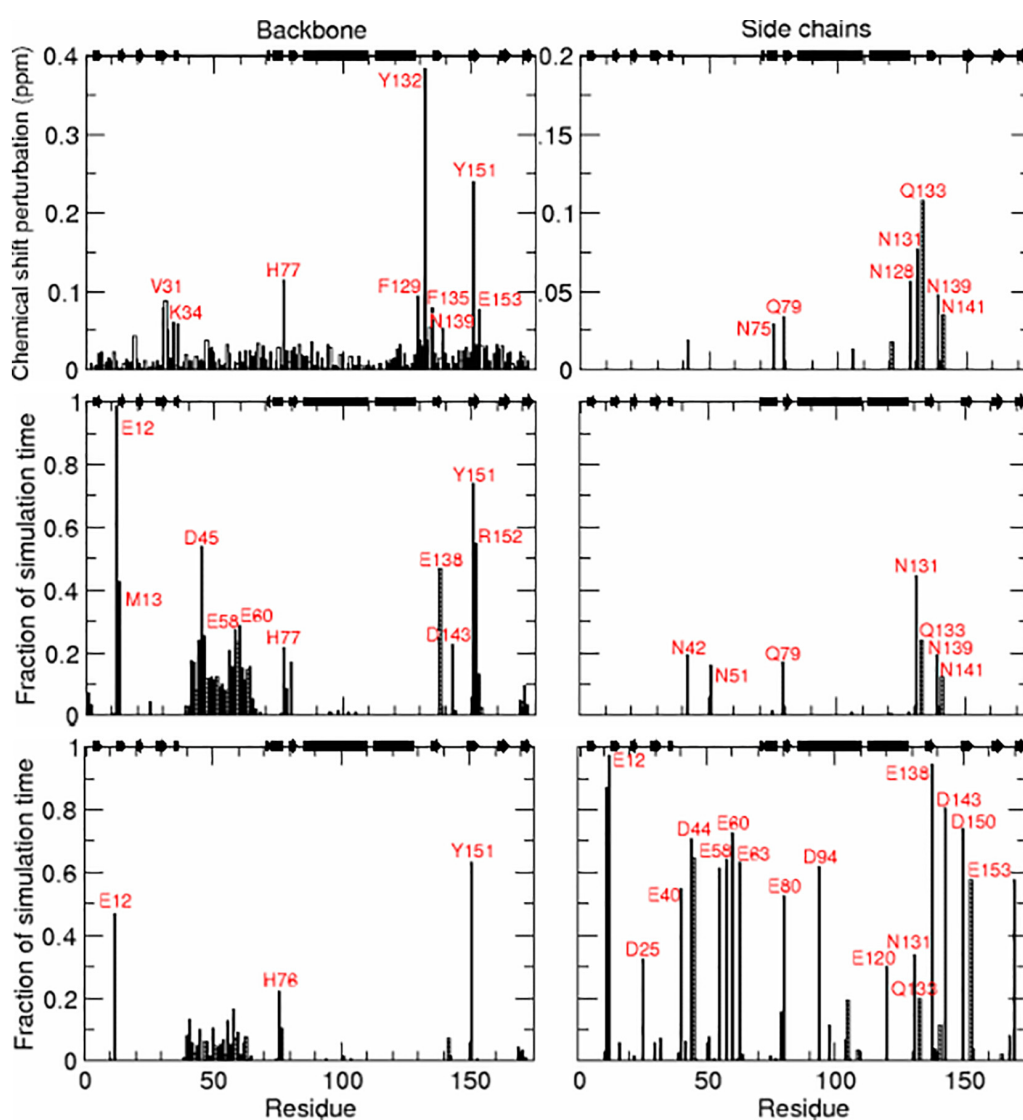


**Fig. 4.** Top: NMR  $^1\text{H}$ - $^{15}\text{N}$  chemical shift perturbations of TCTP backbone (left) and Asn or Gln side chain (right) amide protons induced by the presence of 20 mM calcium ions. Middle: Fraction of simulation time for which calcium ions are distant by less than 5 Å to the TCTP backbone (left) and Asn or Gln side chain (right) amide protons. Bottom: Fraction of simulation time for which calcium ions are distant by less than 3 Å to the TCTP backbone (left) and side chains (right) atoms.

belong to residues His77, Gln79, Asn128, Asn131, Tyr132, Gln133, Asn139, Asn141, Tyr151, and Glu153. In a fairly good agreement, these residues were retrieved in MD simulations, although additional residues contacted by calcium ions, including Glu12, Asp45, Glu58, Glu60, Glu138, and Arg152, were also identified (middle row of Fig. 4). Moreover, MD simulations revealed many other binding sites, most of which are the negatively charged carboxylate groups of Asp or Glu side chains which cannot be captured by NMR  $^1\text{H}/^{15}\text{N}$  chemical shift perturbation measurements (bottom row of Fig. 4). However, we

detected a dramatic diminishing of the backbone  $^1\text{H}$ - $^{15}\text{N}$  resonance intensities in the loop (38–66) upon calcium addition (Fig. S3) which was not reported by Feng *et al.* [11]. We attribute this observation to a change in loop mobility upon calcium binding. To this regard, multiple calcium binding sites were detected within the loop, as demonstrated by MD simulations, and might explain the effect of calcium on the loop dynamics.

In order to visually describe the preferential binding sites of calcium on TCTP, we superimposed the representative structure of the 10 most populated

clusters of the wiCa–noPhos conformational ensemble, and displayed the ions when at least three calcium were located at the same site (Fig. 5). Combined with previous NMR chemical shift perturbations and MD frequent contacts, this visual inspection allows to identify seven calcium binding sites constituted by residues listed in Fig. 5. The two most occupied calcium binding sites are made up by at least five residues, and the other ones by less than four residues. Interestingly, the TCTP disordered loop is often observed folded toward the core domain in such way that Glu58 and Glu60, which were shown as critical for calcium binding by mutagenesis studies [12], contribute to strengthen the fourth and fifth binding sites made up by residues Gln79, Glu80,

and Gln133, confirming the important role of Glu58 and Glu60 in calcium sequestration.

Strikingly, the two most occupied calcium binding regions coincide with the two previously identified patches on the TCTP core domain which are transiently contacted by the disordered loop (Fig. 3). Since the disordered loop is composed of several negatively charged residues, this suggests that the presence of calcium should shift the TCTP conformational ensemble toward structures in which the loop is folded over the calcium ions bound to the core domain. This is indeed what can be observed in the plot of the free energy surface of the wiCa–noPhos TCTP as a function of its radius of gyration and the ratio of the distance TCTP1–TCTP2a over the

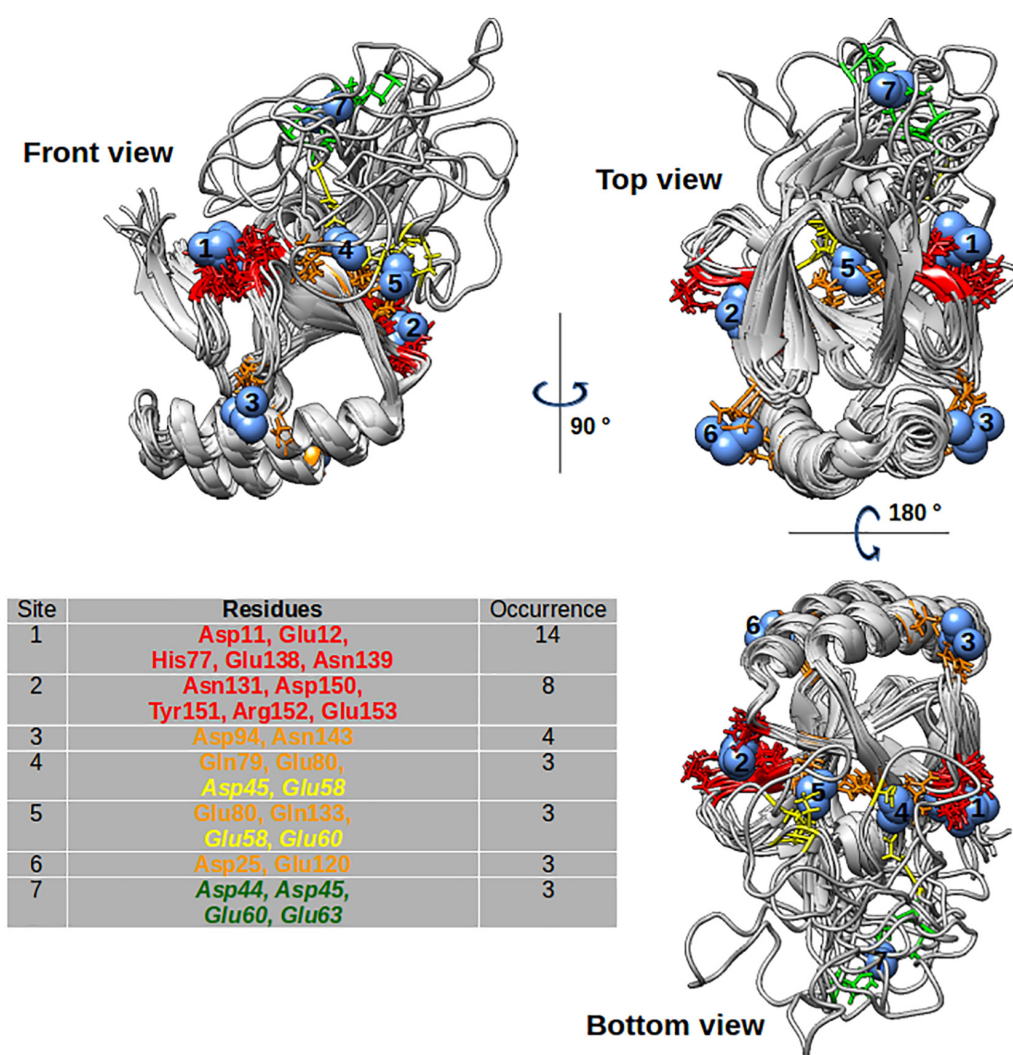


**Fig. 5.** Front, top, and bottom views of the seven preferential binding sites of calcium on TCTP. These illustrations were obtained by superimposing the representative structures of the 10 most populated clusters of the wiCa–noPhos conformational ensemble. The bottom left table lists the residues that compose each binding site and the total number of calcium found there in these 10 most populated clusters (occurrence).

distance TCTP1–TCTP2b (top graph of Fig. 6). When compared to the noCa–noPhos conformational ensemble (Fig. 2), the TCTP intrinsically disordered loop adopts significantly less extended conformations in presence of calcium, the protein radius of gyration of the most populated structures being below 1.7 nm. The presence of calcium induces a more restricted conformational ensemble of the disordered loop, with three major conformations, the first one with TCTP1 in

contact with TCTP2a, the second one with TCTP1 close to TCTP2b, and the third one characterized by a proximity of TCTP1 with regions 11–12 and 76–77. In the first two cases, the residues involved in these contacts were identified using distance matrix between the residues 48–58 and 129–151 computed for the 10 most populated clusters of TCTP in the presence of calcium. The most significant core–loop contacts were detected for cluster5 and cluster10 (Fig. S4). In the former, hydrophobic interactions were observed between residues Ile48, Gly49, and Ala52 (TCTP1) and residue Pro142 (TCTP2b). In the latter, residues Pro57 and Glu58 (TCTP1) rather make polar contacts with residues Gln133 and Tyr151 (TCTP2a). These two modes of interaction of the disordered loop to the core domain are similar to those previously described for the non-phosphorylated TCTP in the absence of calcium, but are favored over the detached conformations of the loop by the binding of calcium ions on the surface of the core domain.

### Influence of phosphorylations on TCTP conformational ensemble

Several cellular and molecular studies indicate that TCTP is involved in the regulation of the dynamics of microtubules and/or microfilaments by binding to tubulin and/or actin [28–31]. This biological activity was shown to depend on the hierarchical phosphorylation by polo-like kinase Plk1 of the TCTP Ser46 and Ser64 which are located in the intrinsically disordered loop [22,30–32]. In addition, two pharmacological molecules, sertraline and thioridazine, were shown to bind directly to TCTP and prevent its association to MDM2, but these two compounds were unable to bind TCTP when introducing mutations S46E or S64E which mimic phosphorylated amino acids [33]. These considerations led us to study the influence of the single phosphorylation pS46 and di-phosphorylation pS46 and pS64 on the TCTP disordered loop conformational ensemble, to gain insight into the role of these post-translational modifications. MD simulations of the modified TCTP, in the same conditions as the non-phosphorylated protein in the absence of calcium, yielded the free energy surfaces displayed in Fig. 6. When compared with Fig. 2, it can be observed that the single phosphorylation pS46 overall induces a slight shift of the TCTP conformational ensemble toward less extended structures among which the disordered loop can fold toward the bottom of the TCTP core domain, but preferentially closer to the TCTP2a segment 129–133 than to the TCTP2b region 138–143 which is more negatively charged. When TCTP is diphosphorylated, its conformational ensemble is also slightly shifted toward less extended structures, but in contrast with the non- and mono-phosphorylated protein, the two phosphate groups reduce the propensity of the disordered loop to bind

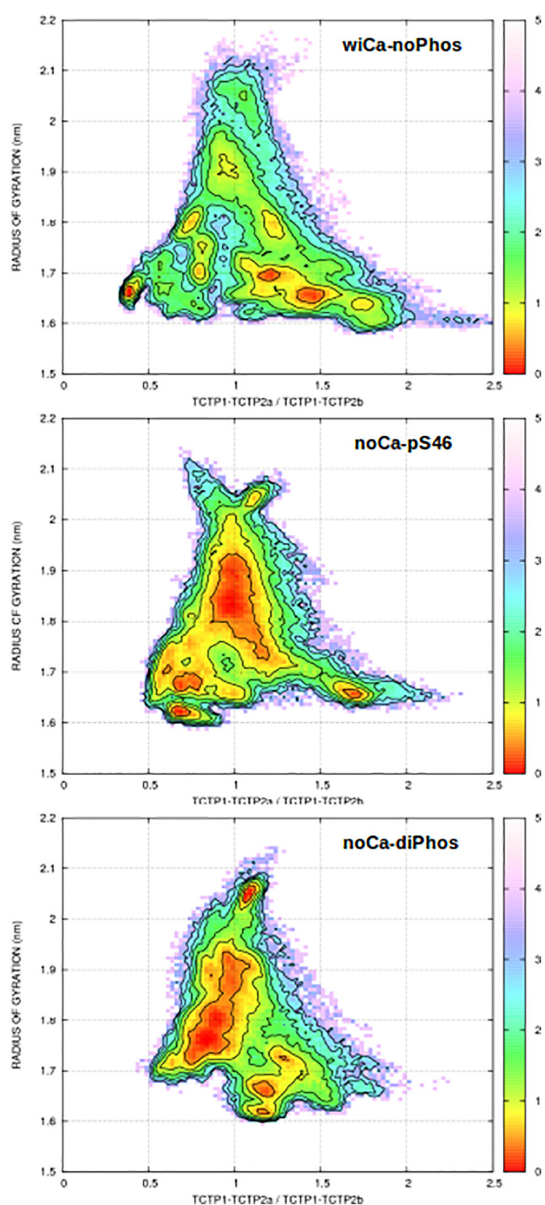


**Fig. 6.** Same free energy surface (kcal/mol) as in Fig. 2 but for the non-phosphorylated TCTP in the presence of calcium (top), the phosphorylated pS46 (middle) and the di-phosphorylated pS46 and pS64 protein in the absence of calcium (bottom).

both the TCTP2a and TCTP2b regions and keep it detached from the core domain.

A quantitative analysis of the contacts between residues of the TCTP core domain and its disordered loop confirmed that the contacts made by the region 130–160 with the disordered loop are reduced in number and duration in the di-phosphorylated TCTP with respect to the non-phosphorylated one (Fig. S5). In the case of the mono-phosphorylated pS46 protein, it can be noted that the residues 80–82, 135, and 140 (TCTP2b) are less often contacted by the disordered loop, whereas the segments 71–75 and 129–130 have longer contacts than in the non-phosphorylated TCTP (Fig. S5). Among the 10 most populated clusters of the phosphorylated pS46-TCTP, we found again two clusters with the two signatures TCTP1 and TCTP2 in spatial proximity (Fig. S6): cluster4 in which residues Ser53, Glu55, Gly56, and Pro57 make contacts with residues Lys130, Gln133, Phe135, and Tyr151 (TCTP2a), and cluster5 in which residues Asn51 and Ser53 are close to the residue Glu138 (TCTP2b). For the di-phosphorylated protein, we retrieved similar contacts in cluster6 (Asn51 with Glu138) and cluster8 (Asn51, Ala52, and Ser53 with Gln133 and Tyr151) but to a significantly less extent (Fig. S7). It could be noticed that the hydrophobic contacts between TCTP1 and TCTP2b previously observed in the non-phosphorylated protein are not recovered in the phosphorylated TCTP. The phosphorylation-induced weakening of the core–loop contacts might increase the solvent accessibility of some patches at the surface of the TCTP core domain, in particular TCTP2, which could potentially modulate the TCTP binding to other molecular partners.

At the local level, we also examined the impact of the phosphorylation of TCTP residues Ser46 and Ser64 upon the propensity of the disordered loop to form secondary structures. As displayed in Fig. S8, the percentages of TCTP structures, in which  $\alpha$ -helix or  $\beta$ -strand conformations are observed in the disordered region, remain overall similar (less than 20–25%) in the four conditions of simulation. Nevertheless, it can be noted that, upon phosphorylation, the helical propensity of segment 44–48 is decreased, whereas it is slightly increased in region 56–60 with respect to the non-phosphorylated TCTP. More strikingly, TCTP phosphorylation significantly increases the percentage of simulation time in random coil for the phosphorylated serines and adjacent residues when compared to the non-phosphorylated protein. Besides the enhanced electrostatic repulsions between the two highly conserved signatures TCTP1 and TCTP2, serine phosphorylation seems also to favor some local structures of the disordered loop which disadvantage its bridging to the TCTP core domain.

As mentioned above, it was demonstrated that phosphorylations of Ser46 and Ser64 or mimics of

these phosphorylations impact the binding of TCTP with tubulin and MDM2 proteins [22,33] and with TCTP inhibitors [33]. However, as far as we know, the quaternary structures of these TCTP-tubulin, TCTP-MDM2, and TCTP-inhibitor complexes are not yet experimentally determined. Some domain mapping studies can suggest the TCTP regions that are involved in binding these proteins but with ambiguity related to this method [28,33,34]. In the absence of unambiguous structural information, it is therefore difficult to estimate the implication of TCTP phosphorylations in the interactions with its partners. Nevertheless, we believe that our theoretical results provide some clues that might help to rationalize future experimental studies about the structures of TCTP-ligand complexes.

### Experimental evidence of a monomer-dimer equilibrium of TCTP in solution

Dimerization of TCTP was previously reported in the literature [35–39]. In this section, we assessed the ability of TCTP to form a concentration-dependent non-covalent dimer through dilution experiments from high (1 mM) to low (6.25  $\mu$ M) concentration of protein using several NMR methods: chemical shift perturbation mapping, diffusion ordered spectroscopy (DOSY),  $^{15}$ N-relaxation as well as their further treatment using Lipari–Szabo formalism via TENSOR2 program. When comparing relaxation parameters over the structured parts at two protein concentrations (50  $\mu$ M and 500  $\mu$ M), we observed lower averaged  $^{15}$ N  $R_1$  values at high concentration ( $\langle R_1 \rangle = 0.55 \pm 0.04 \text{ s}^{-1}$ ) compared to low concentration ( $\langle R_1 \rangle = 0.63 \pm 0.07 \text{ s}^{-1}$ ). In addition, the averaged  $^{15}$ N transverse relaxation rate was higher at high concentration ( $\langle R_2 \rangle = 21.3 \pm 2.8 \text{ s}^{-1}$ ) than at low concentration ( $\langle R_2 \rangle = 18.4 \pm 2.4 \text{ s}^{-1}$ ) for the TCTP structured parts. Consequently, a higher  $R_2/R_1$  ratio was observed at high concentration ( $\langle R_2/R_1 \rangle = 38.6 \pm 7.6$ ) compared to low concentration ( $\langle R_2/R_1 \rangle = 29.0 \pm 6.7$ ) (Fig. 7a). By using the Lipari–Szabo formalism, we computed an apparent correlation time ( $\tau_c$ ) that was significantly higher at 500  $\mu$ M concentration (11.57  $\pm$  0.06 ns) than at 50  $\mu$ M concentration (10.10  $\pm$  0.12 ns), suggesting that a dimer population is enriched when increasing concentration of TCTP. We also performed DOSY experiments in order to measure the translational diffusion coefficient of TCTP as a function of its concentration. We found that the diffusion coefficient gradually decreased from  $1.453 \pm 0.008 \times 10^{-10} \text{ m}^2 \cdot \text{s}^{-1}$  at low concentration (100  $\mu$ M) to  $1.273 \pm 0.003 \times 10^{-10} \text{ m}^2 \cdot \text{s}^{-1}$  at high concentration (1 mM) of protein (Fig. S9). This change in TCTP diffusion properties could not be attributed to a change in solution viscosity because other solutes, such as the buffer Hepes, had constant diffusion properties over the studied TCTP concentration range (Fig. S9). Hence, this slower translational diffusion at higher concentration is consistent with an

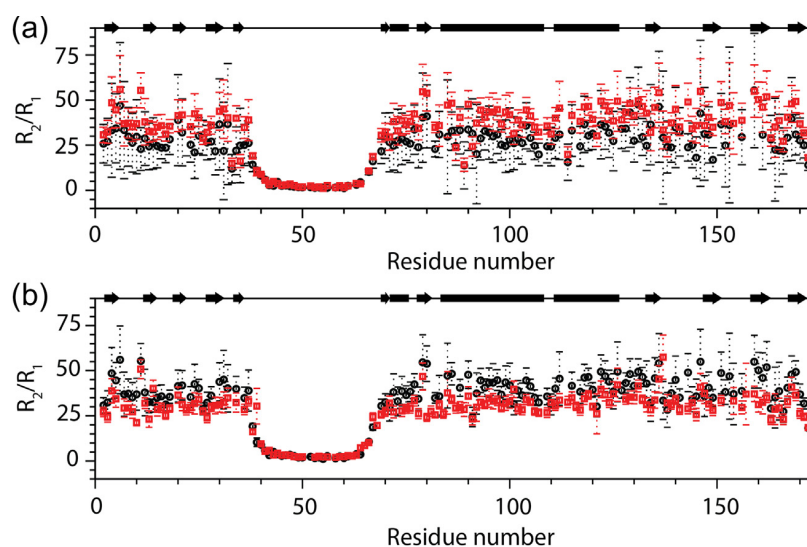


**Fig. 7.** Comparison of  $^{15}\text{N}$   $R_2/R_1$  ratio between low (50  $\mu\text{M}$ , black) and medium (500  $\mu\text{M}$ , red) concentrations of TCTP in the absence of calcium (a), and for medium concentration of TCTP (500  $\mu\text{M}$ ) in the absence (black) or in the presence of 50 mM calcium ions (red) (b).

increase in the population of TCTP oligomers. The recent native mass analysis of TCTP [40] which revealed the existence of a TCTP dimer together with the limited increase in rotational and translational diffusion properties of TCTP at high concentration suggests that the populated oligomeric form is most likely a dimer in solution.

The  $^1\text{H}$ - $^{15}\text{N}$  SOFAST-HMQC spectra for TCTP concentrations from 1 mM to 6.25  $\mu\text{M}$  showed clear concentration-dependent chemical shift variations for a subset of residues, including the segment 81–85 which contains the most affected residue (Phe83), the segment 131–135 with residues Asn131, Gln133 and Phe135 showing significant perturbations, and in a lesser extent the segment 149–150. Residues Ile48 and Thr65 in the intrinsically disordered loop were also noticeably disturbed by the dilution. Based on the  $^1\text{H}$  and  $^{15}\text{N}$  chemical shift variations of the most affected residue Phe83, we could estimate the dissociation constant of the dimer to  $1.36 \pm 0.26$  mM (Fig. S10). This indicates that TCTP is mostly monomeric at low concentration, the dimer population being lower than 4% at 50  $\mu\text{M}$ , whereas this population increases up to 20% and 30% at 500  $\mu\text{M}$  and at 1 mM, respectively. All together, these data strongly evidence the tendency of TCTP to self-associate *in vitro* in the mM concentration range. It could be noted that non-covalent dimers of TCTP were also detected *in cellulo* [35], where a high protein concentration could favor the dimeric form, which might have a biological function.

#### Quaternary structure of TCTP dimer and impact of calcium binding

To get deeper insight into the structure of the dimer formed in solution, we analyzed the concentration-dependent NMR chemical shifts information with

interfaces derived from several structural models of the dimer. To generate structural models of the TCTP dimer, we considered the representative conformation of the 10 most populated clusters from the MD simulations of the non-phosphorylated monomer in the absence of calcium (Fig. 2), and we performed a docking calculation of each of these structure-against each of them, using the program PTools and the force field SCORPION. The statistical analysis of the interaction energy of the generated TCTP complexes (Fig. S11) allows to identify five quaternary structures with significantly lower energy than all the other associations. Among this top five, four complexes (dimer1, dimer2, dimer4, and dimer5) exhibit a similar mode of binding in which one of the two TCTP is located at the bottom of the core domain of the other one, these structures differing from each other by the orientation of the first partner (Fig. 8). In order to determine which of these four complexes is the most probable, we computed the number of contacts per residue between the two TCTP of each complex and compared these contact profiles with the NMR chemical shift perturbations upon protein dilution (Fig. 9). This analysis shows that dimer1 and dimer2 have contact profiles in good agreement with NMR chemical shift perturbations, indicating that they are among the most probable structures of the TCTP dimer, but without ruling out dimer5 whose contact profile remains fairly consistent with NMR data. All the more so dimer5 is interestingly the most symmetric complex among the top five and its dimerization interface is highly similar to that observed in the crystallographic structures solved by Susini *et al.* [24] for the human wild-type TCTP (Fig. 8), but also for the human E12V mutant [41] and the murine TCTP [42], which might reveal that this interface plays a major role in TCTP crystallization. It could be noted that, in these three most probable

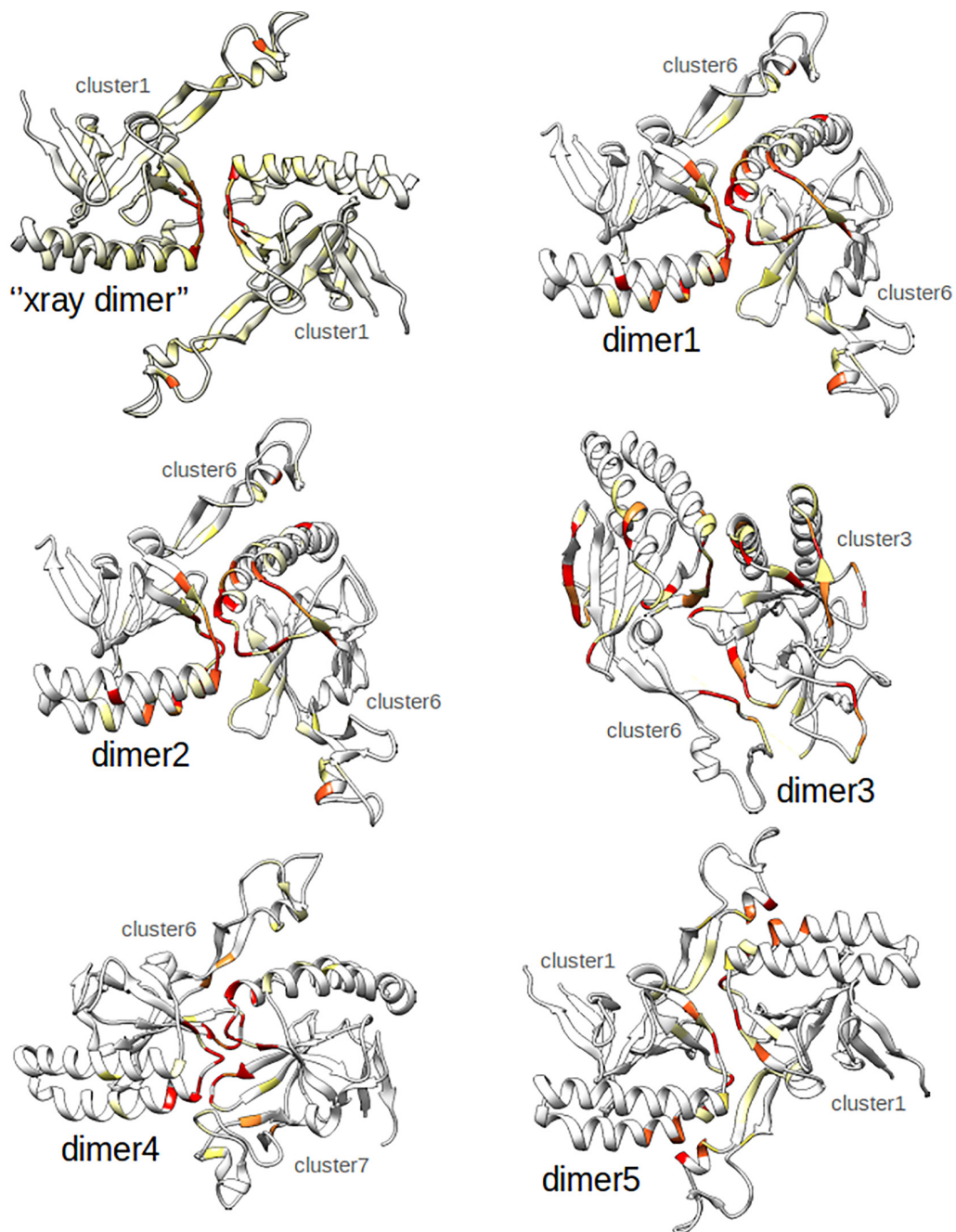


**Fig. 8.** Top left: Structural model of a TCTP dimer built by superimposing the cluster1 on the dimer observed between chains A and D of the PDB structure 1YZ1 [24]. Top right, middle, and bottom: Structures of the five lowest energy TCTP dimers obtained by docking calculations. Residues that exhibit large, medium, or low chemical shift perturbation in NMR dilution experiment or number of contacts in docked complexes are highlighted in red, orange, and yellow, respectively.

complexes, one of the two partners is either cluster6 or cluster1 which both have the disordered loop in a rather extended conformation, with a short  $\alpha$ -helix at segment 59–63. In the modeled dimer1, dimer2, and dimer5, this transient helix is in contact with the  $\alpha$ -

hairpin of the interacting partner, contributing to stabilize the TCTP dimer. This latter remark is in line with far-UV CD experiments which indicate a gain of  $\alpha$ -helical content upon hemin-induced TCTP dimerization [39].

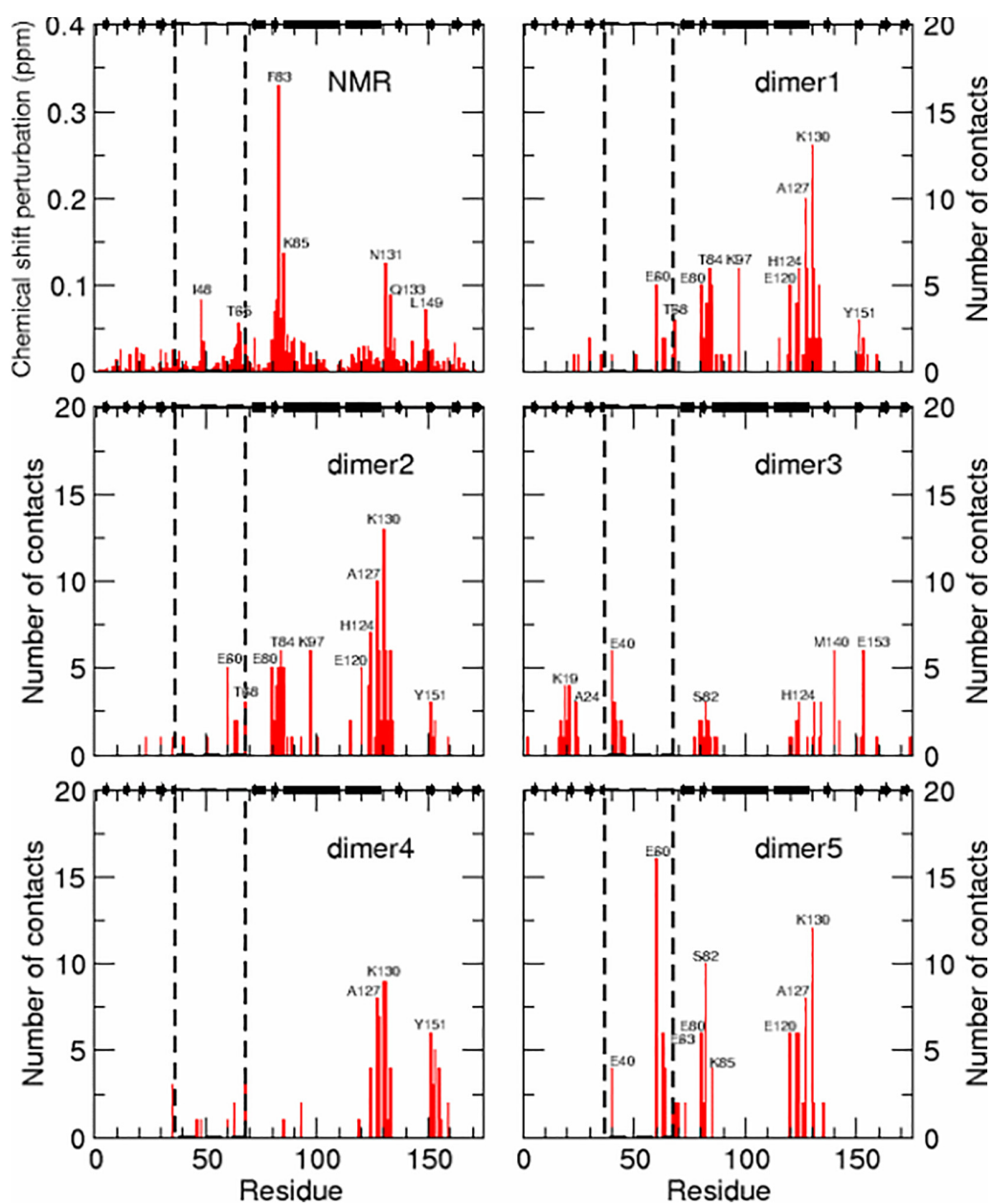


**Fig. 9.** Top left:  $^1\text{H}$ - $^{15}\text{N}$  chemical shift perturbations observed upon TCTP dilution from 1 mM to 50  $\mu\text{M}$ . Top right, middle, and bottom: Number of contacts made by TCTP residues in the five lowest energy complexes.

Strikingly, the interface of TCTP dimerization partially overlaps several calcium binding sites previously identified (sites 2, 4, and 5 of Fig. 5), suggesting that calcium ions could hinder protein self-association. To verify this hypothesis, we compared the TCTP  $^1\text{H}$ - $^{15}\text{N}$  HSQC spectra at low (50  $\mu\text{M}$ ) or medium (500  $\mu\text{M}$ ) protein concentration, without or with 50 mM calcium ions. More specifically, we closely examined the positions of the

$^1\text{H}$ - $^{15}\text{N}$  cross-peaks of residues Phe83 and Lys85 which were previously shown to be sensitive to dimerization. As shown in Fig. 10, an important shift in cross-peak positions of these residues can be noticed between low and medium protein concentration, in the absence of calcium (top panels). In contrast, in the presence of calcium, the cross-peak positions of Phe83 and Lys85 do not depend on the protein concentration (in this concentration range)

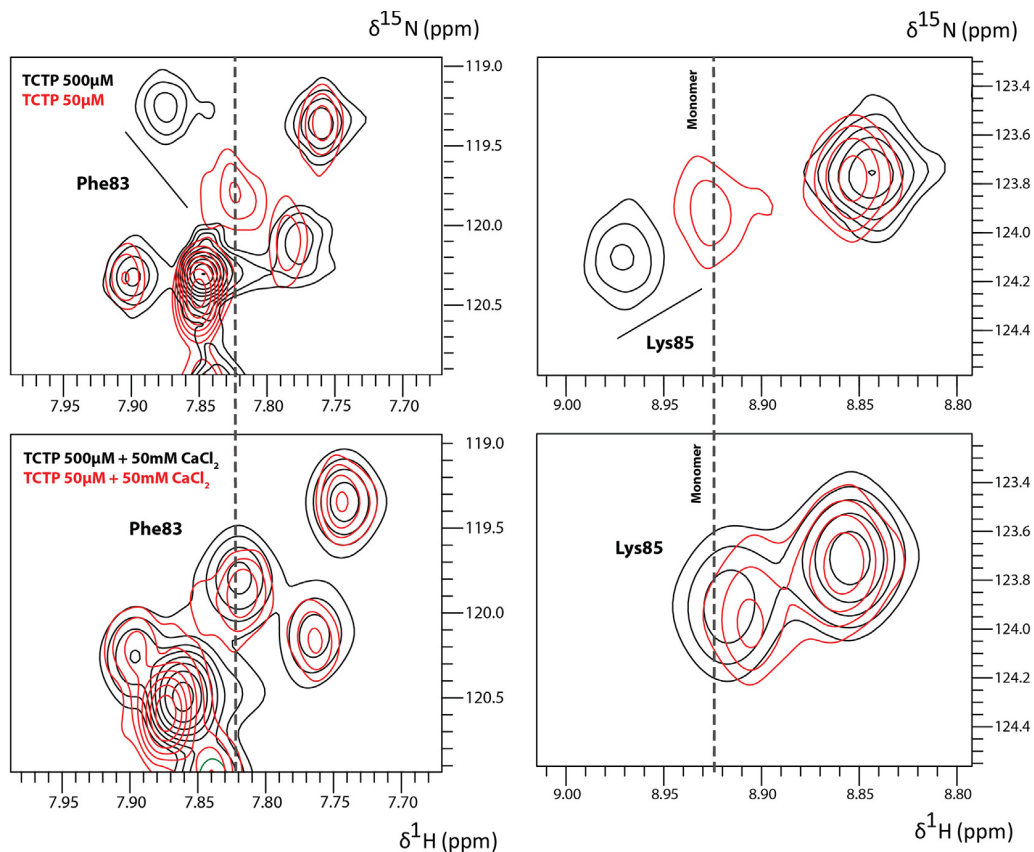


**Fig. 10.** NMR cross-peaks of dimer-sensitive residues Phe83 (left) and Lys85 (right) at low ( $50 \mu\text{M}$ ) or medium ( $500 \mu\text{M}$ ) concentration of protein, without (top) or with  $50 \text{ mM}$  calcium (bottom). The NMR spectra were otherwise collected in the buffer Hepes  $50 \text{ mM}$  (pH 7.4),  $150 \text{ mM}$  NaCl, and  $2 \text{ mM}$  TCEP at  $298 \text{ K}$ .

and are typical of monomeric TCTP (bottom panels). Taken together, this suggests that calcium prevents the formation of TCTP dimer. To confirm this, we compared  $^{15}\text{N}$  relaxation experiments collected at low ( $50 \mu\text{M}$ ) and medium ( $500 \mu\text{M}$ ) TCTP concentration in the absence or in the presence of  $50 \text{ mM}$  calcium (Fig. 7). In the presence of calcium, the averaged  $^{15}\text{N}$   $R_2/R_1$  ratio over the structured regions of TCTP at medium ( $500 \mu\text{M}$ ) concentration ( $\langle R_2/R_1 \rangle = 31.0 \pm 6.9$ ) was close to the value observed for the protein at lower ( $50 \mu\text{M}$ ) concentration ( $\langle R_2/R_1 \rangle = 29.1 \pm 6.7$ ). This turned into similar apparent correlation times at  $500 \mu\text{M}$  ( $\tau_c = 10.62 \pm 0.03 \text{ ns}$ ) and at  $50 \mu\text{M}$  ( $\tau_c = 10.10 \pm 0.12 \text{ ns}$ ) for TCTP in the presence of calcium. Moreover, we observed a significant increase in the translational coefficient diffusion of TCTP ( $500 \mu\text{M}$ ) from  $D = 1.320 \pm 0.004 \times 10^{-10} \text{ m}^2 \cdot \text{s}^{-1}$  to  $D = 1.370 \pm 0.003 \times 10^{-10} \text{ m}^2 \cdot \text{s}^{-1}$  when adding calcium ions. All together, these data confirm that the presence of calcium ions prevents the TCTP dimerization at medium protein concentration. Our results are in

agreement with those reported by Lucas *et al.* [39], which demonstrated that the hemin-induced dimeric form of TCTP is destabilized by the addition of calcium ions. We propose that in both situations (in the presence or absence of hemin), calcium ions favor the TCTP monomeric form by a similar mechanism which involves calcium-induced increased interactions between the disordered loop and the core domain. The competitive binding of the loop to the TCTP dimerization interface may contribute to disfavor its self-association, thus exemplifying the potential role of the disordered loop in regulating the TCTP protein-protein interactions.

## Conclusion

The role of the intrinsically disordered region in TCTP biological activities was poorly studied so far, partly because its conformations were not exhaustively characterized. However, this long loop should probably play an important role since it contains a

highly conserved amino acid signature of TCTP. In the present study, we combined NMR experiments and MD simulations to better characterize its conformational ensemble and investigate its potential role in TCTP functions. We showed that the non-phosphorylated TCTP disordered loop can adopt extended conformations detached from the core domain, but can also fold toward the latter in such way that the protein first signature segment (TCTP1) directly binds to one of the two extreme parts of its second signature region (TCTP2). These long-range transient interactions between TCTP1 and TCTP2 might reveal an underlying mechanism connecting the two signatures. Such mechanism, which still needs to be elucidated, might be a driving force that contributes to the signature sequence conservation. When the two Ser46 and Ser64 of the disordered loop are phosphorylated, the TCTP conformations in which the loop is attached to the core domain are less populated than in the non-phosphorylated protein. In contrast, the presence of calcium ions induces a significant shift of the TCTP conformational ensemble toward structures in which the disordered loop folds against the core domain and contributes to the binding of calcium ions on TCTP surface. In the protein dimers, the disordered loops are pulled away from the core domains to allow TCTP self-association. They also contribute in the stabilization of the protein–protein interface by interacting with the partner  $\alpha$ -hairpin. All together, we propose that the TCTP intrinsically disordered region could play an important role in participating to the interactions with other proteins and non-peptidic ligands, in remodeling the core domain surface, and modulating its accessibility to its partners in response to a variety of cellular conditions, in particularly the presence of calcium ions, or to chemical modifications, such as phosphorylations. We conclude that the TCTP disordered region conformational dynamics must be carefully taken into account when using TCTP structure as a biomolecular target for drug development, particularly for *in silico* screening.

## Materials and Methods

### Expression and purification of the human TCTP

The open reading frame of human TCTP was cloned into pET-M11 vector. A His<sub>6</sub> tag followed by a TEV protease cleavage site was inserted at the N-terminus of TCTP (His-TCTP). <sup>15</sup>N and <sup>15</sup>N–<sup>13</sup>C labeled TCTP were expressed in *Escherichia coli* BL21 star (DE3) (Life Technologies) grown in M9 minimal medium containing <sup>15</sup>N-labeled NH<sub>4</sub>Cl (1 g/L) and <sup>12</sup>C –  $\alpha$ -D-glucose (4 g/L) or <sup>15</sup>N-labeled NH<sub>4</sub>Cl (1 g/L) and <sup>13</sup>C-labeled  $\alpha$ -D-glucose (4 g/L), respectively. Overexpression was induced when

OD<sub>600</sub> reached 0.9 by addition of 0.2 mM IPTG and lasted 20 h at 25 °C. Cell pellets were resuspended at 1:10 w/v in lysis buffer [50 mM Tris (pH 8), 300 mM NaCl, 10 mM imidazole, 2 mM DTT] supplemented with 0.3 mg/mL lysozyme and protease inhibitor cocktail (Roche) and lysed using a French press system (1500 bars, 3 cycles). After centrifugation (12,500g, 60 min), supernatant was loaded on a Hisrap Fast Flow crude column (GE Healthcare life sciences) and His-TCTP was eluted with 150 mM imidazole. The N-Terminal His<sub>6</sub> tag was removed by digesting the His-TCTP protein with home-made His-TEV protease (1:50 w/w ratio) and simultaneously dialyzed against imidazole-free buffer [50 mM Tris (pH 8), 300 mM NaCl, 2 mM DTT] for 15 h at 34 °C. TCTP was separated from His-TCTP and His-TEV by passing the digest products on a Hisrap Fast Flow crude column (GE Healthcare life sciences) and further purified on a Superdex 75 10/300 GL column (GE Healthcare Life Sciences) equilibrated with storing buffer [50 mM Hepes (pH 7.4), 150 mM NaCl, 2 mM TCEP, 0.5 mM EDTA]. Human TCTP was concentrated at 2 mM and stored at –80 °C.

### NMR spectroscopy

NMR spectroscopy measurements were performed at 298 K in the following buffer: 50 mM Hepes (pH 7.4), 150 mM NaCl, and 2 mM TCEP. Measurements were done using Bruker AVIII 950 MHz and 800-MHz spectrometers equipped with a TCI cryoprobe. Sequence-specific backbone assignment of human TCTP was achieved using a classical approach [43] and on the basis of the published assignment [11]. All NMR data, except <sup>15</sup>N-relaxation measurements, were processed with Topspin 3.5 (Bruker) and analyzed with CCPNMR software [44]. Coupling constants <sup>3</sup>J<sub>H<sub>N</sub>–H $\alpha$</sub>  were measured from a 3D HNHA experiment [45]. The intensities of the diagonal (S<sub>diag</sub>) and off-diagonal (S<sub>cross</sub>) cross-peaks were extracted and coupling constants were computed according to the following equation: S<sub>cross</sub>/S<sub>diag</sub> = –tan<sup>2</sup>(2 $\pi$ J<sub>H<sub>H</sub>ζ) with  $\zeta$  = 13.05 ms. For calcium binding studies and TCTP dilution experiments, combined <sup>1</sup>H–<sup>15</sup>N chemical shift perturbations ( $\Delta\delta_{\text{comb}}$ ) were calculated according to the equation  $\Delta\delta_{\text{comb}} = (\Delta\delta^1\text{H} + 0.14\Delta\delta^{15}\text{N})^{1/2}$ , where  $\Delta\delta^1\text{H}$  and  $\Delta\delta^{15}\text{N}$  are the chemical shift perturbations (in ppm) for <sup>1</sup>H and <sup>15</sup>N resonances, respectively. Such calculation was done by recording series of <sup>1</sup>H–<sup>15</sup>N SOFAST-HMQC spectra [46]. TCTP self-dissociation constant K<sub>d</sub> was estimated by fitting the <sup>1</sup>H and <sup>15</sup>N chemical shift perturbation of Phe83 cross-peak upon protein dilution from 1 mM to 6.25  $\mu$ M with the following equation:  $\Delta\delta^A X = \Delta\delta^A X_0 + \Delta\delta^A X_{\text{max}} * F_d$ , where <sup>A</sup>X denotes either <sup>1</sup>H or <sup>15</sup>N nucleus, and F<sub>d</sub> the fraction of dimer which is related to K<sub>d</sub> and TCTP total concentration according to the</sub>

following equation:

$$F_d = \frac{4 * [TCTP] + K_d - \sqrt{8 * [TCTP] * K_d + K_d^2}}{4 * [TCTP] - K_d + \sqrt{8 * [TCTP] * K_d + K_d^2}} \quad (1)$$

### <sup>15</sup>N relaxation measurement

Relaxation experiments were performed using a Bruker AVIII HD 950 MHz spectrometer at 298 K with a <sup>15</sup>N-labeled TCTP at low (50 μM) and medium (500 μM) concentration, in the absence and in the presence of CaCl<sub>2</sub> (50 mM), and processed using NMRPipe software [47]. The <sup>15</sup>N relaxation experiments were recorded in interleaved pseudo-3D fashion to attenuate the effects of sample and/or conditions changes during the collection time. The <sup>15</sup>N *R*<sub>1</sub> values were determined from series of 2D <sup>1</sup>H–<sup>15</sup>N correlation spectra recorded with the following delays (ms): 10, 3000, 200, 2500, 400, 2000, 600, 1500, 800, and 1000 (in this order). The <sup>15</sup>N *R*<sub>2</sub> values were determined with different relaxation delays (ms): 17, 170, 34, 102, 0, 51, 85, and 68 (in this order). {<sup>1</sup>H}–<sup>15</sup>N heteronuclear NOE experiments were recorded using one reference and one proton-saturated 2D <sup>1</sup>H–<sup>15</sup>N correlation experiment. <sup>15</sup>N *R*<sub>1</sub>, *R*<sub>2</sub>, and {<sup>1</sup>H}–<sup>15</sup>N heteronuclear NOE were recorded with an interscan delay of 5, 3.5, and 4.8 s, respectively. Intensities from *R*<sub>1</sub>, *R*<sub>2</sub>, and {<sup>1</sup>H}–<sup>15</sup>N heteronuclear NOE experiments were extracted using the nlinLS routine in NMRPipe and *R*<sub>1</sub> and *R*<sub>2</sub> values were obtained by fitting intensities with a two-parameter exponential model with the modelXY tool in NMRPipe. Further analysis of <sup>15</sup>N relaxation parameters and {<sup>1</sup>H}–<sup>15</sup>N heteronuclear NOE in terms of rotational diffusion tensor was achieved by using TENSOR2 program [48].

### MD simulation

The TCTP conformational ensembles were explored under four conditions: no calcium and no phosphorylation (noCa–noPhos), with calcium and no phosphorylation (wiCa–noPhos), no calcium and with phosphorylated Ser46 (noCa–pS46), and lastly no calcium and with both Ser46 and Ser64 phosphorylated (noCa–diPhos). For each condition, the TCTP conformational space was sampled using 20 independent simulations starting from the 20 NMR structures of the PDB file 2HR9 [11]. The phosphorylations of residues Ser46 and Ser64 were done using the *Structure Editing* tools of the UCSF Chimera package [49]. All initial conformations were solvated in a triclinic box type with a minimum distance of 1.4 nm between the solute and the box sides. The total charges were neutralized by adding sufficient sodium and chloride ions to reach the salt concentration of 100 mM. In simulations with calcium, 10 Ca<sup>2+</sup> ions were randomly

placed in the solvent bulk, corresponding to a calcium concentration of 30 mM in average.

MD simulations were performed using the GROMACS-4.5.5 software [50,51], at the all-atom level in explicit solvent. We used for this study the AMBER-99SB-ILDN force field [52] and the TIP3P water model [53]. The non-bonded interactions were treated using the smooth PME method [54] for the electrostatic terms and a cutoff distance of 1.2 nm for the van der Waals potentials. The covalent bond lengths were kept constant using the LINCS [55] and SETTLE [56] procedures for the protein and water molecules, respectively. A leap-frog algorithm was used to integrate the equations of motion with a 2-fs time step. Each MD simulation was run for 200 ns in the NPT ensemble, at *T* = 310 K and *P* = 1 bar, using the Nose–Hoover and Parrinello–Rahman algorithms [57–59], with the time coupling constants  $\tau_T = 0.5$  ps and  $\tau_P = 2.5$  ps.

Molecule coordinates were saved every 20 ps for subsequent analysis, using mainly the tools implemented in the GROMACS package. Notably, we made principal component analyses of the protein conformational ensembles using *g\_covar* and projected the trajectories onto the first two eigenvectors with *g\_anaeig*, yielding for the four TCTP ensembles the reduced free energy surfaces displayed in Fig. S12. These analyses allowed to identify and objectively separate the most populated sub-ensembles or clusters of the TCTP conformations. However, it is not straightforward to interpret the eigenvectors of a principal component analysis in terms of geometrical quantities. Moreover, the first two principal axes are not necessarily identical for the four TCTP conformational ensembles (noCa–noPhos, wiCa–noPhos, noCa–pS46, and noCa–diPhos), which makes comparisons between the four systems very difficult. For these reasons, we chose to analyze the TCTP conformational ensembles in terms of the more intuitive radius of gyration and distances between the two signatures TCTP1 and TCTP2. More specifically, we used the ratio of the distance TCTP1–TCTP2a over TCTP1–TCTP2b in order to highlight the propensity of the TCTP loop to bind either one or another area of the TCTP core domain.

Theoretical chemical shifts were calculated using the SHIFTS program [60,61]. Multiple secondary chemical shifts were subsequently combined into a single SSP score following the Marsh *et al.* [27] approach. Coupling constants <sup>3</sup>*J*<sub>H<sub>N</sub>–H<sub>α</sub></sub> were calculated from the dihedral angles  $\varphi$  and  $\psi$  using the Karplus equation [62] and the Vuister and Bax empirical parameters [45].

### Bootstrap analysis of the TCTP conformational ensembles

In order to assess the reliability of our theoretical results, particularly the significance of the differences between the four TCTP conformational ensembles

(noCa–noPhos, wiCa–noPhos, noCa–pS46, and noCa–diPhos), a bootstrap analysis was performed on the protein radius of gyration and the distance between the two signatures TCTP1 and TCTP2. The bootstrapping consisted in reconstructing 4- $\mu$ s-long trajectories with 20 short 200-ns trajectories randomly selected with replacement among the performed 20 MD simulations. This resampling was iterated 1000 times and the statistics on the TCTP radius of gyration and the TCTP1–TCTP2 distance (averages and standard deviations) were calculated over the 1000 reconstructed trajectories.

The bootstrap analysis yielded the probability distributions displayed in Fig. 11. It is observed that the distributions of both the radius of gyration and the TCTP1–TCTP2 distance are clearly shifted toward lower values in the presence of calcium when compared to simulations without calcium. The error bars show that this difference is significant and reliable. In contrast, the differences between the conformational ensembles of the phosphorylated and non-phosphorylated proteins are less marked. Nevertheless, in the distributions of the TCTP1–

TCTP2 distance, one can detect a higher probability of distances below 0.5 nm for the pS46 TCTP and a more subtle higher probability of distances between 0.5 and 1.0 nm for the di-phosphorylated protein than for the non-phosphorylated one.

### Protein–protein docking

Structures of the TCTP dimer were generated using the molecular modeling library PTools [63]. This toolbox enables to perform protein–protein docking at a coarse-grained level by multiple energy minimizations without any bias, using possibly various force fields. We used in this study the coarse-grained force field SCORPION which was able to successfully reproduce the quaternary structure of several protein–protein complexes, starting from the bound conformation of the two partners [64,65]. PTools performs systematic rigid-body docking, starting from initial regular positions and orientations of the ligand around the receptor surface, at a distance slightly larger than its largest dimension. The docking procedure consists in minimizing the interaction energy

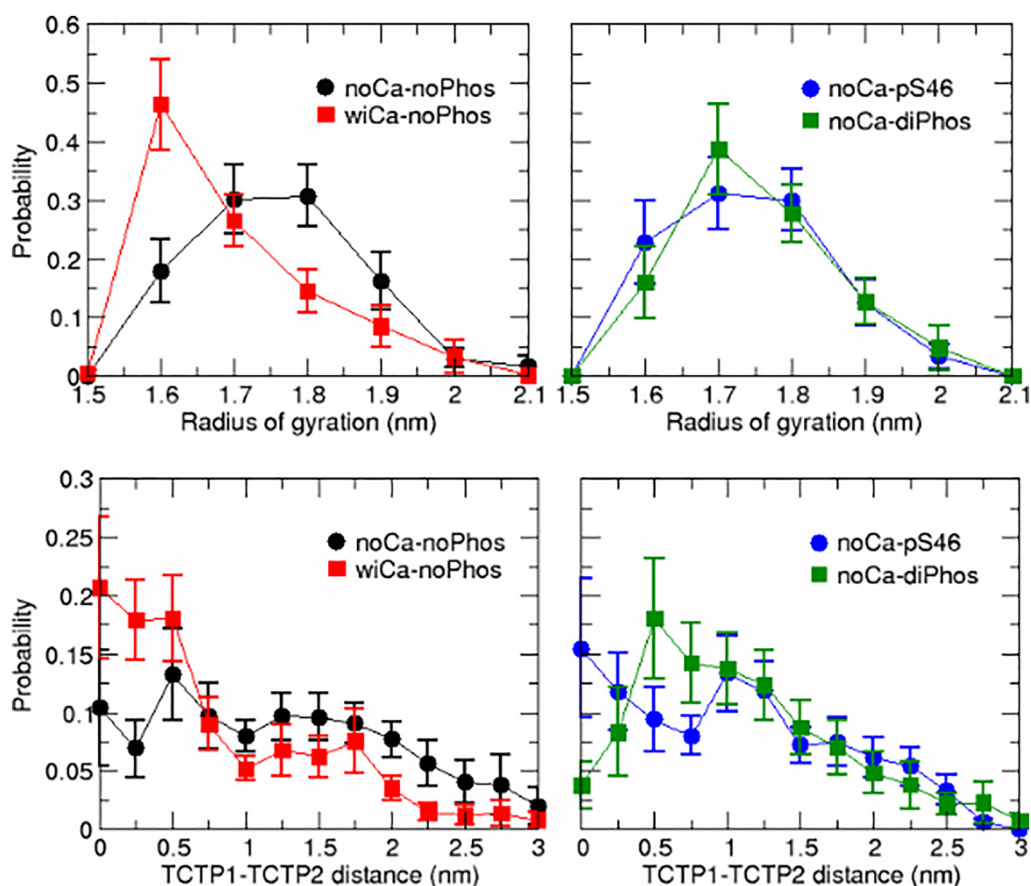


**Fig. 11.** Probability distributions of the TCTP radius of gyration and of the distance between the centers of mass of the two protein signatures TCTP1 and TCTP2. The mean values and standard deviations were calculated by using the bootstrap approach.

between the two partners, using the ligand six translational and rotational degrees of freedom. The minimized complex conformations were finally clustered by similarity and ranked according to their interaction energies.

## Acknowledgments

This work was supported by the LabEx LERMIT (Grant ANR-10-LABX-33) and by the project IDI 2016 funded by the IDEX Paris-Saclay (Grant ANR-11-IDEX-0003-02). Financial support from the TGIR-RMN-THC FR3050 CNRS for conducting the research is gratefully acknowledged. Simulations were performed using HPC resources from GENCI-CINES (Grant c2015077390). T.H.D. is also thankful for the support from the French Ministry of Foreign Affairs (Grant Bio-Asia-2015 34058UC). Lastly, the authors are warmly grateful to François Bontems for sharing the equation relating the fraction of dimer to the self-dissociation constant.

**Conflicts of Interest:** The authors declare no conflicts of interest regarding the publication of this article.

## Appendix A. Supplementary data

Supplementary data to this article can be found online at <https://doi.org/10.1016/j.jmb.2018.04.024>.

*Received 20 February 2018;*

*Received in revised form 19 April 2018;*

*Accepted 22 April 2018*

Available online 30 April 2018

### Keywords:

nuclear magnetic resonance;  
molecular dynamics;  
intrinsically disordered protein;  
TCTP–calcium interaction;  
TCTP dimerization

### Abbreviations used:

TCTP, translationally controlled tumor protein; SSP, secondary structure propensity; NOE, nuclear Overhauser effect; MD, molecular dynamics.

## References

- [1] U.-A. Bommer, Cellular function and regulation of the translationally controlled tumour protein TCTP, *Open Allergy J.* 5 (2012) 19–32.
- [2] M. Nagano-Ito, S. Ichikawa, Biological effects of mammalian translationally controlled tumor protein (TCTP) on cell death, proliferation, and tumorigenesis, *Biochem. Res. Int.* 2012 (2012) 1–7.
- [3] A. Telerman, R. Amson, The molecular programme of tumour reversion: the steps beyond malignant transformation, *Nat. Rev. Cancer* 9 (2009) 206–216.
- [4] R. Amson, S. Pece, J.-C. Marine, P.P.D. Fiore, A. Telerman, TPT1/TCTP-regulated pathways in phenotypic reprogramming, *Trends Cell Biol.* 23 (2013) 37–46.
- [5] J. Acunzo, V. Baylot, A. So, P. Rocchi, TCTP as therapeutic target in cancers, *Cancer Treat. Rev.* 40 (2014) 760–769.
- [6] T. Kawakami, T. Ando, Y. Kawakami, HRF-interacting molecules, *Open Allergy J.* 5 (2012) 41–46.
- [7] N. Assrir, F. Malard, E. Lescop, Structural insights into TCTP and its interactions with ligands and proteins, in: A. Telerman, R. Amson (Eds.), *TCTP/tpt1—Remodeling Signaling from Stem Cell to Disease*, vol. 64, Springer International Publishing 2017, pp. 9–46.
- [8] S. Li, M. Chen, Q. Xiong, J. Zhang, Z. Cui, F. Ge, Characterization of the translationally controlled tumor protein (TCTP) interactome reveals novel binding partners in human cancer cells, *J. Proteome Res.* 15 (2016) 3741–3751.
- [9] J.-C. Sanchez, D. Schaller, F. Ravier, O. Golaz, S. Jaccoud, M. Belet, M.R. Wilkins, R. James, J. Deshusses, D. Hochstrasser, Translationally controlled tumor protein: a protein identified in several nontumoral cells including erythrocytes, *Electrophoresis* 18 (1997) 150–155.
- [10] M. Kim, Y. Jung, K. Lee, C. Kim, Identification of the calcium binding sites in translationally controlled tumor protein, *Arch. Pharm. Res.* 23 (2000) 633–636.
- [11] Y. Feng, D. Liu, H. Yao, J. Wang, Solution structure and mapping of a very weak calcium-binding site of human translationally controlled tumor protein by NMR, *Arch. Biochem. Biophys.* 467 (2007) 48–57.
- [12] P. Graidist, M. Yazawa, M. Tonganunt, A. Nakatomi, C.C.-J. Lin, J.-Y. Chang, A. Phongdara, K. Fujise, Fortilin binds Ca<sup>2+</sup>-dependent apoptosis in vivo, *Biochem. J.* 408 (2007) 181–191.
- [13] P. Thaw, N.J. Baxter, A.M. Hounslow, C. Price, J.P. Waltho, C.J. Craven, Structure of TCTP reveals unexpected relationship with guanine nucleotide-free chaperones, *Nat. Struct. Mol. Biol.* 8 (2001) 701–704.
- [14] O.F. Lange, P. Rossi, N.G. Sgourakis, Y. Song, H.-W. Lee, J.M. Aramini, A. Ertekin, R. Xiao, T.B. Acton, G.T. Montellione, D. Baker, Determination of solution structures of proteins up to 40 kDa using CS-Rosetta with sparse NMR data from deuterated samples, *Proc. Natl. Acad. Sci.* 109 (2012) 10873–10878.
- [15] N. Dephoure, C. Zhou, J. Villén, S.A. Beausoleil, C.E. Bakalarski, S.J. Elledge, S.P. Gygi, A quantitative atlas of mitotic phosphorylation, *Proc. Natl. Acad. Sci.* 105 (2008) 10762–10767.
- [16] M. Fuxreiter, I. Simon, P. Friedrich, P. Tompa, Preformed structural elements feature in partner recognition by intrinsically unstructured proteins, *J. Mol. Biol.* 338 (2004) 1015–1026.
- [17] A. Mohan, C.J. Oldfield, P. Radivojac, V. Vacic, M.S. Cortese, A.K. Dunker, V.N. Uversky, Analysis of molecular recognition features (MoRFs), *J. Mol. Biol.* 362 (2006) 1043–1059.
- [18] D.D. Boehr, R. Nussinov, P.E. Wright, The role of dynamic conformational ensembles in biomolecular recognition, *Nat. Chem. Biol.* 5 (2009) 789–796.

- [19] H.R.A. Jonker, R.W. Wechselberger, R. Boelens, R. Kaptein, G.E. Folkers, The intrinsically unstructured domain of PC4 modulates the activity of the structured core through inter- and intramolecular interactions, *Biochemistry* 45 (2006) 5067–5081.
- [20] K. Stott, M. Watson, F.S. Howe, J.G. Grossmann, J.O. Thomas, Tail-mediated collapse of HMGB1 is dynamic and occurs via differential binding of the acidic tail to the a and B domains, *J. Mol. Biol.* 403 (2010) 706–722.
- [21] H.-Y. Li, J. Wang, F. Meng, Z.-K. Jia, Y. Su, Q.-F. Bai, L.-L. Lv, F.-R. Ma, L.A. Potempa, Y.-B. Yan, S.-R. Ji, Y. Wu, An intrinsically disordered motif mediates diverse actions of monomeric C-reactive protein, *J. Biol. Chem.* 291 (2016) 8795–8804.
- [22] F. Yarm, Plk phosphorylation regulates the microtubule-stabilizing protein TCTP, *Mol. Cell. Biol.* 22 (2002) 6209–6221.
- [23] Z. Solyom, M. Schwarten, L. Geist, R. Konrat, D. Willbold, B. Brutscher, BEST-TROSY experiments for time-efficient sequential resonance assignment of large disordered proteins, *J. Biomol. NMR* 55 (2013) 311–321.
- [24] L. Susini, S. Besse, D. Duffaut, A. Lespagnol, C. Beekman, G. Fiucci, A. Atkinson, D. Busso, P. Poussin, J. Marine, J. Martinou, J. Cavarelli, D. Moras, R. Amson, A. Telerman, TCTP protects from apoptotic cell death by antagonizing bax function, *Cell Death Differ.* 15 (2008) 1211–1220.
- [25] G. Lipari, A. Szabo, Model-free approach to the interpretation of nuclear magnetic resonance relaxation in macromolecules. 1. Theory and range of validity, *J. Am. Chem. Soc.* 104 (1982) 4546–4559.
- [26] J. Garcia de la Torre, M. Huertas, B. Carrasco, HYDRONMR: prediction of NMR relaxation of globular proteins from atomic-level structures and hydrodynamic calculations, *J. Magn. Reson.* 147 (2000) 138–146.
- [27] J.A. Marsh, V.K. Singh, Z. Jia, J.D. Forman-Kay, Sensitivity of secondary structure propensities to sequence differences between  $\alpha$ - and  $\gamma$ -synuclein: implications for fibrillation, *Protein Sci.* 15 (2006) 2795–2804.
- [28] Y. Gachet, S. Tournier, M. Lee, A. Lazaris-Karatzas, T. Poulton, U.A. Bommer, The growth-related, translationally controlled protein P23 has properties of a tubulin binding protein and associates transiently with microtubules during the cell cycle, *J. Cell Sci.* 112 (1999) 1257–1271.
- [29] F. Bazile, A. Pascal, I. Arnal, C. Le Clainche, F. Chesnel, J. Kubiak, Complex relationship between TCTP, microtubules and actin microfilaments regulates cell shape in normal and cancer cells, *Carcinogenesis* 30 (2009) 555–565.
- [30] M. Lucibello, S. Adanti, E. Antelmi, D. Dezi, S. Ciafre, M. Carcangiu, M. Zonfrillo, G. Nicotera, L. Sica, F. De Braud, P. Pierimarchi, Phospho-TCTP as a therapeutic target of dihydroartemisinin for aggressive breast cancer cells, *Oncotarget* 6 (2015) 5275–5291.
- [31] H. Jeon, S. You, Y. Park, J. Chang, J. Kim, J. Oh, TCTP regulates spindle microtubule dynamics by stabilizing polar microtubules during mouse oocyte meiosis, *Biochim. Biophys. Acta* 1863 (2016) 630–637.
- [32] U. Cucchi, L.M. Gianellini, A. De Ponti, F. Sola, R. Alzani, V. Patton, A. Pezzoni, S. Troiani, M.B. Saccardo, S. Rizzi, Others, phosphorylation of TCTP as a marker for polo-like kinase-1 activity in vivo, *Anticancer Res.* 30 (2010) 4973–4985.
- [33] R. Amson, S. Pece, A. Lespagnol, R. Vyas, G. Mazzarol, D. Tosoni, I. Colaluca, G. Viale, S. Rodrigues-Ferreira, J. Wynendaele, O. Chaloin, J. Hoebeke, J.-C. Marine, P.P. Di Fiore, A. Telerman, Reciprocal repression between P53 and TCTP, *Nat. Med.* 18 (2011) 91–99.
- [34] G. Funston, W. Goh, S.J. Wei, Q.S. Tng, C. Brown, L. Jiah Tong, C. Verma, D. Lane, F. Ghadessy, Binding of translationally controlled tumour protein to the N-terminal domain of HDM2 is inhibited by Nutlin-3, *PLoS One* 7 (2012), e42642.
- [35] T. Yoon, J. Jung, M. Kim, K.M. Lee, E.C. Choi, K. Lee, Identification of the self-interaction of rat TCTP/IgE-dependent histamine-releasing factor using yeast two-hybrid system, *Arch. Biochem. Biophys.* 384 (2000) 379–382.
- [36] J. Bhisutthibhan, S. Meshnick, Immunoprecipitation of [3H] dihydroartemisinin translationally controlled tumor protein (TCTP) adducts from plasmodium falciparum-infected erythrocytes by using anti-TCTP antibodies, *Antimicrob. Agents Chemother.* 45 (2001) 2397–2399.
- [37] M. Gnanasekar, K. Rao, L. Chen, R. Narayanan, M. Geetha, A. Scott, K. Ramaswamy, P. Kaliraj, Molecular characterization of a calcium binding translationally controlled tumor protein homologue from the filarial parasites *brugia malayi* and *wuchereria bancrofti*, *Mol. Biochem. Parasitol.* 121 (2002) 107–118.
- [38] M. Kim, H.J. Min, H.Y. Won, H. Park, J.-C. Lee, H.-W. Park, J. Chung, E.S. Hwang, K. Lee, Dimerization of translationally controlled tumor protein is essential for its cytokine-like activity, *PLoS One* 4 (2009), e6464.
- [39] A. Lucas, X. Fu, J. Liu, M. Brannon, J. Yang, D. Capelluto, C. Finkielstein, Ligand binding reveals a role for heme in translationally-controlled tumor protein dimerization, *PLoS One* 9 (2014), e112823.
- [40] S. Thébault, M. Agez, X. Chi, J. Stojko, V. Cura, S.B. Telerman, L. Maillet, F. Gautier, I. Billas-Massobrio, C. Birck, N. Troffer-Charlier, T. Karafin, J. Honoré, A. Senff-Ribeiro, S. Montessuit, C.M. Johnson, P. Juin, S. Cianférani, J.-C. Martinou, D.W. Andrews, R. Amson, A. Telerman, J. Cavarelli, TCTP contains a BH3-like domain, which instead of inhibiting, activates Bcl-xL, *Sci. Rep.* 6 (2016), 19725.
- [41] X. Dong, B. Yang, Y. Li, C. Zhong, J. Ding, Molecular basis of the acceleration of the GDP–GTP exchange of human Ras homolog enriched in brain by human translationally controlled tumor protein, *J. Biol. Chem.* 284 (2009) 23754–23764.
- [42] K.A. Doré, J. ichi Kashiwakura, J.M. McDonnell, H.J. Gould, T. Kawakami, B.J. Sutton, A.M. Davies, Crystal structures of murine and human histamine-releasing factor (hrf/tctp) and a model for hrf dimerisation in mast cell activation, *Mol. Immunol.* 93 (2018) 216–222.
- [43] M. Sattler, J. Schleucher, C. Griesinger, Heteronuclear multidimensional NMR experiments for the structure determination of proteins in solution employing pulsed field gradients, *Prog. Nucl. Magn. Reson. Spectrosc.* 34 (1999) 93–158.
- [44] W. Vranken, W. Boucher, T. Stevens, R. Fogh, A. Pajon, M. Llinas, E. Ulrich, J. Markley, J. Ionides, E. Laue, The CCPN data model for NMR spectroscopy: development of a software pipeline, *Proteins* 59 (2005) 687–696.
- [45] G.W. Vuister, A. Bax, Quantitative J correlation: a new approach for measuring homonuclear three-bond J(HNH $\alpha$ ) coupling constants in <sup>15</sup>N-enriched proteins, *J. Am. Chem. Soc.* 115 (1993) 7772–7777.
- [46] P. Schanda, B. Brutscher, Very fast two-dimensional NMR spectroscopy for real-time investigation of dynamic events in proteins on the time scale of seconds, *J. Am. Chem. Soc.* 127 (2005) 8014–8015.
- [47] F. Delaglio, S. Grzesiek, G.W. Vuister, G. Zhu, J. Pfeifer, A. Bax, NMRPipe: a multidimensional spectral processing system based on UNIX pipes, *J. Biomol. NMR* 6 (3) (1995) 277–293.

- [48] P. Dosset, J.-C. Hus, M. Blackledge, D. Marion, Efficient analysis of macromolecular rotational diffusion from heteronuclear relaxation data, *J. Biomol. NMR* 16 (2000) 23–28.
- [49] E.F. Pettersen, T.D. Goddard, C.C. Huang, G.S. Couch, D.M. Greenblatt, E.C. Meng, T.E. Ferrin, UCSF chimera? A visualization system for exploratory research and analysis, *J. Comput. Chem.* 25 (2004) 1605–1612.
- [50] D. Van Der Spoel, E. Lindahl, B. Hess, G. Groenhof, A.E. Mark, H.J.C. Berendsen, GROMACS: fast, flexible, and free, *J. Comput. Chem.* 26 (2005) 1701–1718.
- [51] B. Hess, C. Kutzner, D. van der Spoel, E. Lindahl, GROMACS 4: algorithms for highly efficient, load-balanced, and scalable molecular simulation, *J. Chem. Theory Comput.* 4 (2008) 435–447.
- [52] K. Lindorff-Larsen, S. Piana, K. Palmo, P. Maragakis, J.L. Klepeis, R.O. Dror, D.E. Shaw, Improved side-chain torsion potentials for the Amber ff99sb protein force field, *Proteins* 78 (2010) 1950–1958.
- [53] W.L. Jorgensen, J. Chandrasekhar, J.D. Madura, R.W. Impey, M.L. Klein, Comparison of simple potential functions for simulating liquid water, *J. Chem. Phys.* 79 (1983) 926–935.
- [54] U. Essmann, L. Perera, M.L. Berkowitz, T. Darden, H. Lee, L.G. Pedersen, A smooth particle mesh Ewald method, *J. Chem. Phys.* 103 (1995) 8577–8593.
- [55] B. Hess, P-LINCS: a parallel linear constraint solver for molecular simulation, *J. Chem. Theory Comput.* 4 (2008) 116–122.
- [56] S. Miyamoto, P.A. Kollman, SETTLE: an analytical version of the SHAKE and RATTLE algorithm for rigid water models, *J. Comput. Chem.* 13 (1992) 952–962.
- [57] S. Nosé, A unified formulation of the constant temperature molecular dynamics methods, *J. Chem. Phys.* 81 (1984) 511–519.
- [58] W.G. Hoover, Canonical dynamics: equilibrium phase-space distributions, *Phys. Rev. A* 31 (1985) 1695–1697.
- [59] M. Parrinello, A. Rahman, Polymorphic transitions in single crystals: a new molecular dynamics method, *J. Appl. Phys.* 52 (1981) 7182–7190.
- [60] K. Ósapay, D.A. Case, Analysis of proton chemical shifts in regular secondary structure of proteins, *J. Biomol. NMR* 4 (1994) 215–230.
- [61] X.-P. Xu, D.A. Case, Automated prediction of  $^{15}\text{N}$ ,  $^{13}\text{C}$   $\alpha$ ,  $^{13}\text{C}$   $\beta$  and  $^{13}\text{C}$  chemical shifts in proteins using a density functional database, *J. Biomol. NMR* 21 (2001) 321–333.
- [62] M. Karplus, Contact electron  $\gamma$ -spin coupling of nuclear magnetic moments, *J. Chem. Phys.* 30 (1959) 11–15.
- [63] A. Saladin, S. Fiorucci, P. Poulain, C. Prévost, M. Zacharias, PTools: an opensource molecular docking library, *BMC Struct. Biol.* 9 (2009) 27.
- [64] N. Basdevant, D. Borgis, T. Ha-Duong, A coarse-grained protein–protein potential derived from an all-atom force field, *J. Phys. Chem. B* 111 (2007) 9390–9399.
- [65] N. Basdevant, D. Borgis, T. Ha-Duong, Modeling protein–protein recognition in solution using the coarse-grained force field SCORPION, *J. Chem. Theory Comput.* 9 (2013) 803–813.

### 3.3 The molten-globule state TCTP\*

In the current section, we present our efforts to detect and characterize alternative states of the free TCTP protein since we will show in the next chapter that such states are crucial for TCTP to achieve its interactions (Sec. 4). Here, we first evaluated the protein stability toward buffer (Sec. 3.3.1.1) conditions and also tested the backbone stability of TCTP by HDX NMR (Sec. 3.3.1.2). Second, we tried to populate potential alternative states of TCTP using urea and pressure and we extensively report changes observed in the protein structure and dynamics under these conditions (Sec. 3.3.2).

#### 3.3.1 Evaluation of protein stability in diverse conditions

##### 3.3.1.1 Stability of TCTP toward experimental conditions

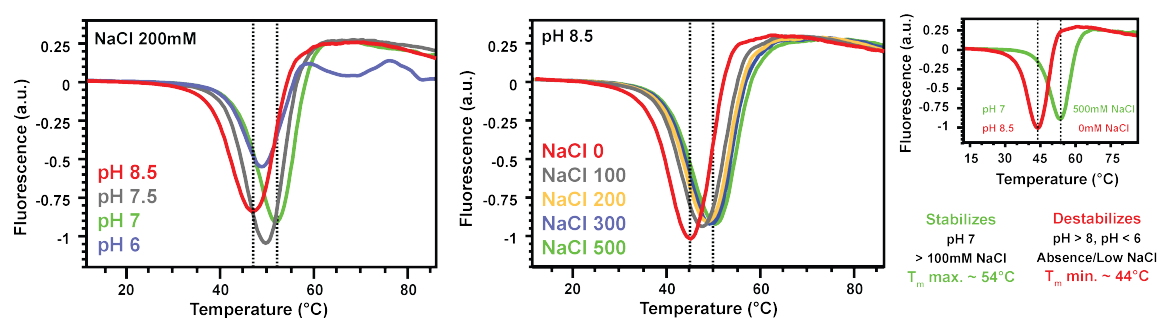


**Fig. 3.10 Evaluation of TCTP thermal stability toward buffer conditions using the TSA method.** Salt- (center) and pH- (left) dependence of the TCTP melting temperature ( $T_m$ ). Minima of curves correspond to  $T_m$ . Comparison of the TSA curves from the conditions that promote either the lowest (pH 8.5, 0 mM NaCl) or highest (pH 7, 500 mM NaCl)  $T_m$  (right). Experiments were done by applying a temperature gradient from 25 °C to 95 °C at 3 °C.min<sup>-1</sup> on TCTP sample (5  $\mu$ M) in various buffer conditions and detecting SYPRO fluorescence.

TSA is a well established method for the determination of the melting temperature ( $T_m$ ) of proteins by means of an hydrophobic fluorescent probe (SYPRO) that emits more fluorescence when bound to the unfolded tested protein which exposes more hydrophobic surface compared to the native counterpart. The melting temperature depends on several parameters but is generally used to optimize the buffer conditions for structural studies to keep the protein as stable as possible under a given condition. We used the method for evaluating TCTP stability under 48 different combinations of salt (0-500 mM) and pH (pH 6 to pH 8.5) in buffer solutions (Sec. 3.10). Such parameters are known to influence the TCTP monomer-dimer equilibrium (Sec. 3.1.2), thus also informing on the relative stability of both monomer and dimer. The melting temperature ( $T_m$ ) of TCTP in a standard experimental setup (50 mM

HEPES pH 7.4, 150 mM NaCl, 2 mM TCEP and 5 mM EDTA) was  $\sim 50^\circ\text{C}$ . When screening the buffers, the thermal stability of the protein reached a maximum at neutral pH (pH 7) and high salt concentration (500 mM) to yield a  $T_m$  of  $\sim 54^\circ\text{C}$ . Absence or low salt concentration and alkaline pH have a destabilizing effect on the protein and yield to a  $T_m$  value of  $\sim 44^\circ\text{C}$  for the more marked decrease (pH 8.5, 0 mM NaCl).  $T_m$  was maximal at  $54^\circ\text{C}$  in neutral conditions with high salt-content (pH 7, 500 mM NaCl). No folding intermediate could be detected since only a monophasic change in fluorescence was observed under the temperature gradient. Minimum and maximum  $T_m$  correlate with maximum and minimum dimer content in solution, respectively. Beyond the intrinsic effect of salts in stabilizing protein structures in solution, we can envisage that the TCTP dimer is intrinsically less stable toward temperature compared to TCTP monomer, possibly explaining why the  $T_m$  decreases in high-dimer content conditions. Moreover, these conditions correspond to the optimal setup we report in the next chapter (Sec. 4) for interactions with Bcl-2 family proteins, which raises interest in studying the relationship between TCTP dimer and interactions capabilities of the protein.

### 3.3.1.2 Local instability in TCTP backbone

Hydrogen-bonding plays an important role in proteins by mediating secondary structure elements formation [241, 242] and involves the backbone amide bond which hosts an hydrogen-donor H(N) and hydrogen-acceptor O(C). The engagement of these in bonding networks commonly results in  $\alpha$ -helix and  $\beta$ -sheet stabilization and this can be quantified through HDX [243] NMR (Sec. 2.3.1.4) since structured segments in a protein are more likely to have their backbone amide hydrogen protected from exchange compared to flexible or solvent-exposed parts. Moreover, this is useful to detect segments that partially unfold in protein, even though they have a very weak population. Indeed, we expect in such a case that backbone HN are less protected from solvent-exchange compared to the rest of the protein. Thus, we tested if the globular domain of TCTP was stable over time by doing HDX experiments and we aimed at detecting segments of the protein, as the BH3-like motif, that could regularly unfold from the TCTP core to be possibly available for partners.

After resuspension of a dry TCTP aliquot in 100 % deuterated water in acidic condition (pH 6.5) to reduce solvent exchange of backbone HN with water,  $^1\text{H}$ - $^{15}\text{N}$  fingerprints were recorded over 18 hours (Fig. 3.11 A). Signals from TCTP either disappeared during the first measurement or gradually decreased in intensity along the kinetics with partial or total signal disappearing at the end of the measurement time.  $^1\text{H}$ - $^{15}\text{N}$  resonances from TCTP IDR and extensions disappeared immediately after sample resuspension, as expected from the IDR fast dynamics (Sec. 3.1.1) and solvent-exposed location seen in the NMR structure [43] of

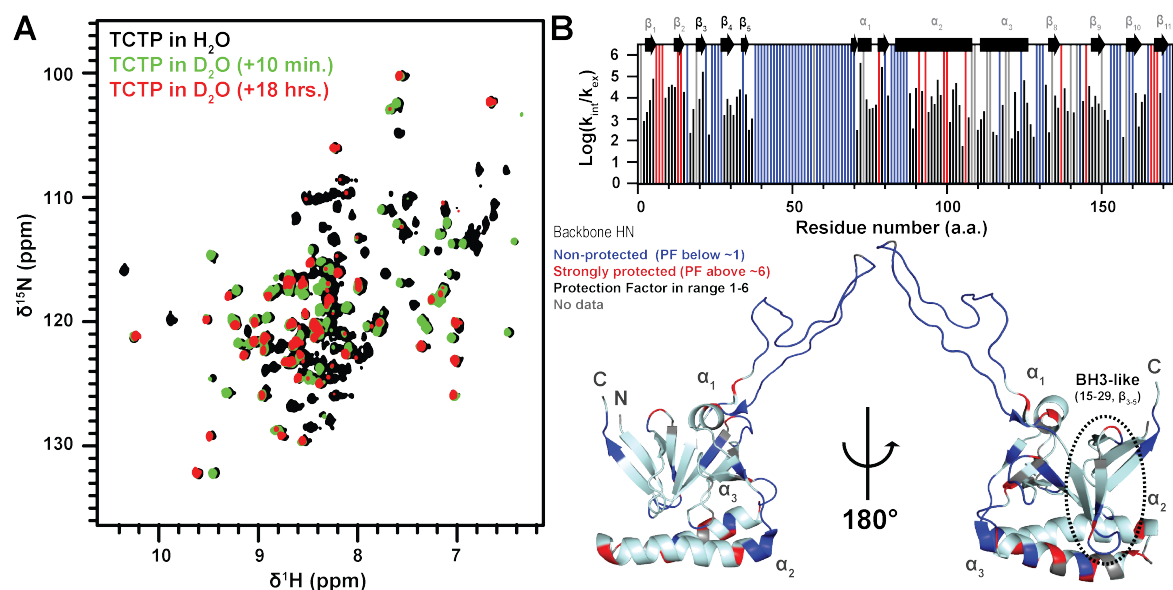


**Fig. 3.11 HDX mapping of labile amide hydrogen in TCTP backbone.** (A) Overview of the H/D exchange kinetics in TCTP. Overlay of  $^1\text{H}$ - $^{15}\text{N}$  SOFAST HMQC spectra from TCTP (100  $\mu\text{M}$ ) in buffer containing 95 %  $\text{H}_2\text{O}$  / 5 %  $\text{D}_2\text{O}$  (black) or 100 %  $\text{D}_2\text{O}$  a few minutes (green) and hours (red) later. (B) PF computed for residues in TCTP upon H/D-Exchange (up). The BH3-like region (D11-K34) is highlighted (down). Bars indicate either the computed PF value (black), no significant exchange at the end of experiment (magenta) corresponding to very protected amide protons, total exchange at the beginning of experiment (blue) corresponding to weakly-protected amide protons or finally residues excluded from analysis due to crosspeaks overlap (grey). (C) Mapping of residues for which signal immediately disappeared (blue) or did show a weak PF ( $\leq 2.5$ ) (red) are highlighted on TCTP structure (pdb code: 2HR9). Experiments were recorded at 800 MHz and 25  $^\circ\text{C}$  in the following buffer: 50 mM MES pH 6.5, 250 mM NaCl, 2 mM TCEP in relevant  $\text{H}_2\text{O}$  /  $\text{D}_2\text{O}$  ratio. The pH value was measured in buffer with 100 %  $\text{H}_2\text{O}$ .

the protein. Similarly, crosspeaks from residues in loops connecting secondary structure elements also disappeared. However, several other crosspeaks out from this set (E22, K34, G69, V70, E80, T84, K85, E86, Q106, G117, H124, Y159, M160, E170 and K171) also disappeared readily during the first measurement after sample resuspension in deuterated water. These are from residues essentially located within  $\beta$ -sheet and  $\alpha$ -helix that form the globular TCTP domain and we surprisingly observed that several of them are engaged in hydrogen-bonding network in the solution structure of the protein. Moreover, these residues have some spatial proximity when plotted on the TCTP structure and draw a surface that is also affected upon calcium binding or non-covalent dimer formation (Fig. 3.11 B). This means that there is flexibility in parts of TCTP backbone and indicates hotspot of structural divergence with possible roles in sensing and propagation of molecular signals in the whole protein as we think that TCTP is prone to structural plasticity. Over the whole

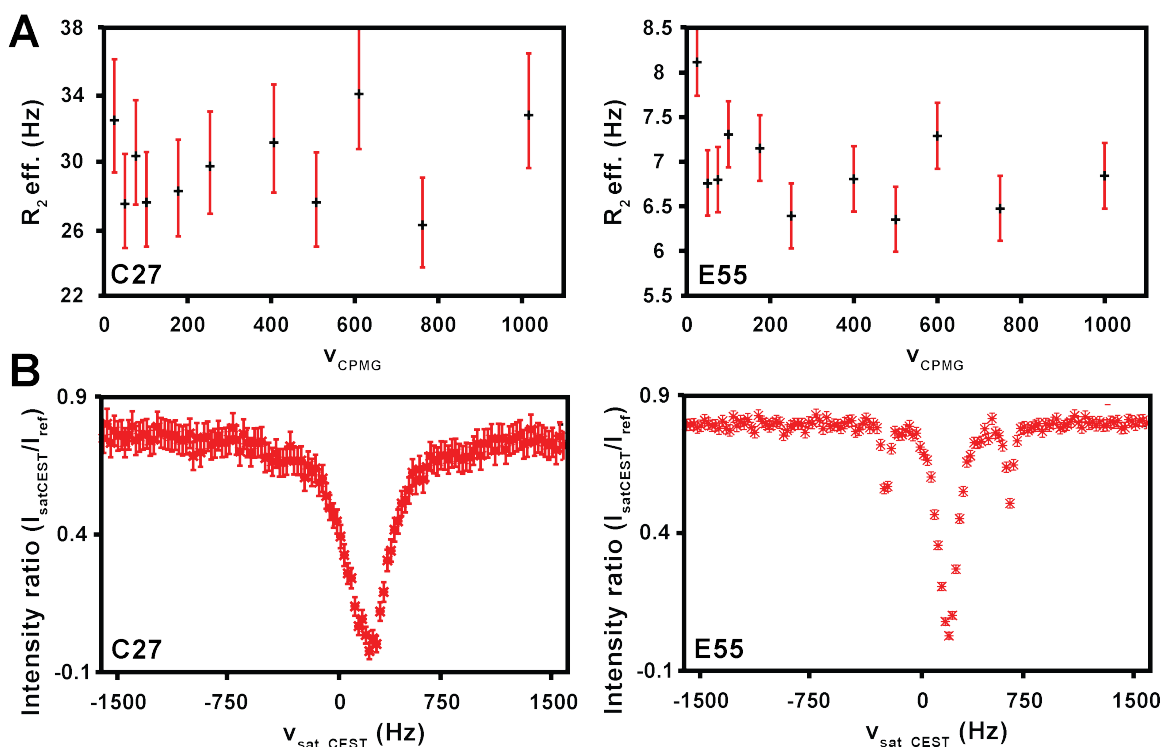


Fig. 3.12 **Typical CPMG and CEST profiles in TCTP.** (A) CPMG and (B) CEST profiles for residues C27 (left) and E55 (right) from the BH3-like motif and IDR part, respectively. Experiments were recorded at 950 MHz and 25 °C in the following buffer: 20 mM HEPES pH 6.5, 150 mM NaCl, 2 mM TCEP in 95 % H<sub>2</sub>O / 5 % D<sub>2</sub>O.

protein, we observed crosspeaks for which the intensity decrease over time was too small at the end of the experiments (18 hrs) which impedes the fit of exponential decay functions since it leads to important error interval in the exchange model. Also we did not perform a linear fit to still rank these residues since we are more interested into labile segments in the current perspective. An arrangement of three  $\beta$ -strands, namely  $\beta_2$ ,  $\beta_1$  and  $\beta_{11}$  hosts the majority of residues for which no significant intensity decrease is observed during the experiment. The poor solvent exchange property in this region reveals strong H-bonds in agreement with a strong  $\beta$ -sheet packing between the N- and C- terminal moieties of the protein. Corresponding residues are all engaged in secondary structure elements via their backbone HN and this suggests that they could be key for the protein structure stability, with possible perspectives for site-directed mutagenesis that would aim at destabilizing the TCTP structure to induce alternative states. Residue-specific PF [213] were computed in the case of residues for which signal intensity gradually and significantly decreased and they report on the strength of local hydrogen-bonding as well as the solvent accessibility, permitting to detect more labile structural segment in a protein fold (Fig. 3.11 B). As it is represented using

a logarithmic scale, there is up to 1000 X difference between the backbone HN exchange rates from residues from the globular domain of the protein with strong sequential variations along a given residue stretch. However, we can still observe that lower PF is more often computed for residues HN close from residues that readily exchange their backbone HN, thus having very low PF. This is consistent since hotspots of flexibility in TCTP backbone are likely to have an impact at surrounding residues by propagating structure instability. In the BH3-like segment of TCTP, we find three  $\beta$ -strands from  $\beta_2$  to  $\beta_4$ , all spaced by short loops. Strand  $\beta_2$  exhibits a strong engagement with  $\beta_1$  as described above. In the structure of TCTP, strand  $\beta_3$  is packed against strand  $\beta_4$  and the latter also contacts strand  $\beta_{10}$  in the globular core of the protein. We consistently observed reduction of H/D exchange for residues engaged in hydrogen-bonding from observation of TCTP structure. Finally, about 50 % of residues in the BH3-like region are included in loop segments and mostly disappeared during the first measurement, as expected from their flexible nature and solvent-exposed location. Overall, the BH3-like motif contains residues with lower PF since it is composed of short loops connecting short  $\beta$ -strands and thus intrinsically contains less hydrogen-bonding interactions compared to other protein structured regions. If we compare with the N-terminal segment that precedes the BH3-like motif and is also composed of loops and  $\beta$ -strands, we observe that higher mean PF values, which suggests that the BH3-like motif can be relatively more fragile in the protein compared to the rest of the globular domain.

Since HDX experiments detects flexibility preferentially in solvent-exposed regions and is not resolved for backbone HN with exchange rates below the experiment time (min.), we performed CPMG and CEST measurements in order to detect conformational exchange at intermediate and slower (100  $\mu$ s-500 ms) timescales. CPMG relaxation dispersion curves were all flat along the protein backbone with no exponential decay in the value of computed  $R_{2\text{eff}}$  parameters at greater CPMG pulse frequency ( $\nu_{\text{CPMG}}$ ). This means that we could not observe significant chemical exchange at intermediate timescale (100  $\mu$ s-10 ms) in free TCTP protein. At slower timescales (1-500 ms), CEST profiles were all showing a single minima, indicating that no minor state exchanging with the major, visible state of TCTP could be detected. Typical CPMG and CEST profiles are exemplified with residues C27 and E55 (Fig. 3.12). For flexible residue E55 the up- and down- fielded satellite minima are artefactual and arise from an excessive strength of CEST pulse regarding the relaxation properties of the TCTP IDR. This setup was used to ensure best signal to noise ratio for CEST response in structured regions of the protein. We therefore conclude that visible TCTP does not undergo detectable conformational exchange in the 100  $\mu$ s-500 ms second timescale. In combination with results from HDX experiments, we can finally say that the globular TCTP core is stable at intermediate and slower timescales (100  $\mu$ s-500 ms). However, we can not exclude that

sensitivity could be limiting in detecting very weakly populated states ( $\leq 1\%$ ) or very slowly exchanging conformations ( $\geq s$ ) that could still represent structural variants of interest.

### 3.3.2 Identification of TCTP\* and structural characterization

#### 3.3.2.1 Slow kinetics conversion from TCTP to TCTP\*

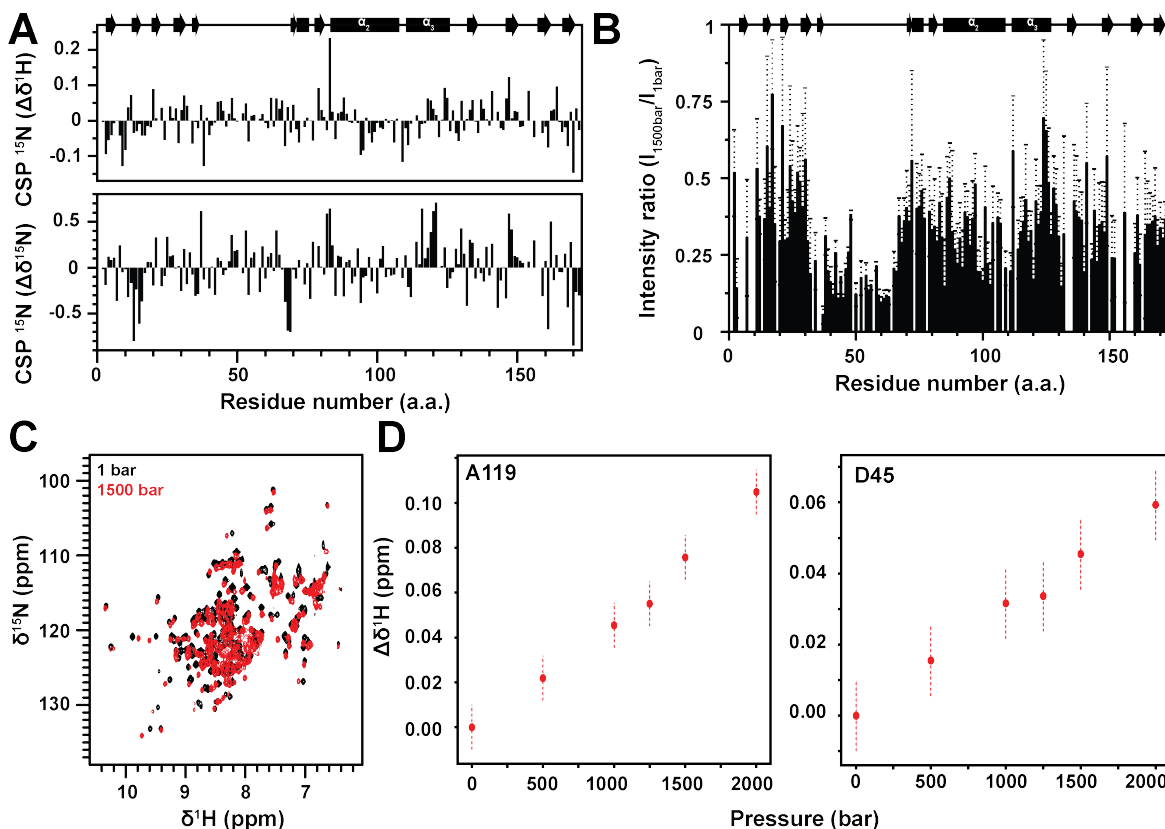


Fig. 3.13 **Impact of high-pressure on TCTP structure monitored by NMR.** (A)  $^1\text{H}$  (top) and  $^{15}\text{N}$  (bottom) chemical shift perturbations and (B) intensity ratios computed between  $^1\text{H}$ - $^{15}\text{N}$  SOFAST HMQC spectra from TCTP at atmospheric (1 bar) (black) and high (1500 bars) (red) pressure. (C) Overlay of  $^1\text{H}$ - $^{15}\text{N}$  SOFAST HMQC spectra from TCTP (300  $\mu\text{M}$ ) at atmospheric (1 bar) (black) and medium (1500 bars) (red) pressure. (D) Representation of the variation in  $^1\text{H}$  chemical shift ( $\Delta^1\text{H}$ ) upon pressure gradient for residues D45 and A119 to illustrate the strong linear correlation observed for all well separated resonances with optimal signal to noise ratio. Errors bars for  $^1\text{H}$  chemical shift determination are indicated (0.01 ppm, red dash). Experiments were recorded at 800 MHz and 25  $^\circ\text{C}$  in the following buffer: 50 mM HEPES pH 7.4, 150 mM NaCl, 2 mM TCEP in 95 %  $\text{H}_2\text{O}$  / 5 %  $\text{D}_2\text{O}$ .

#### Impact of pressure on TCTP structure

HP-NMR has emerged as a promising technique for balancing an equilibrium from a major to a minor state, thus increasing the population of an excited or lowly-populated state of a

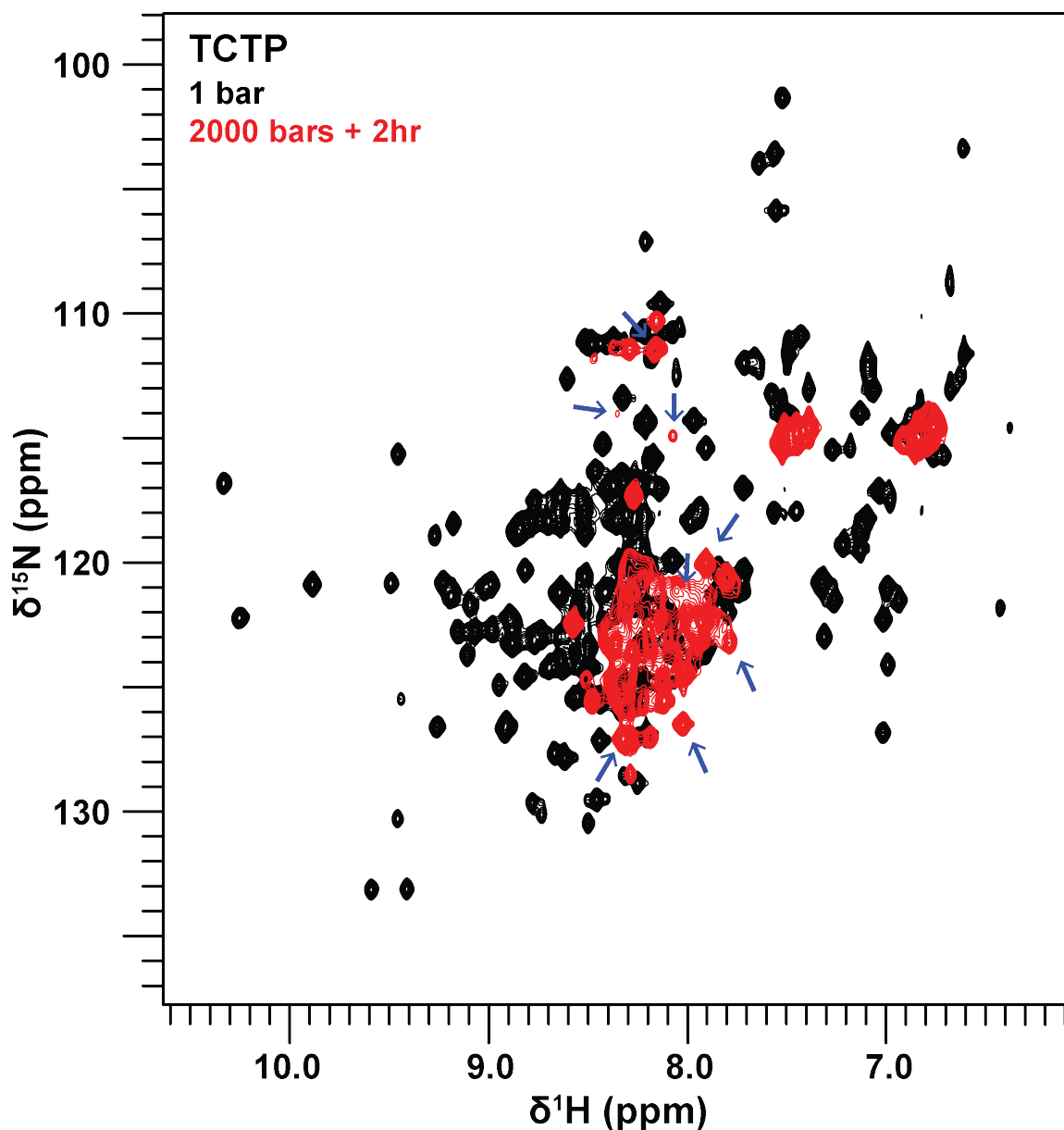


Fig. 3.14 **Comparison of TCTP and TCTP\* upon pressure induction.** Overlay of  $^1\text{H}$ - $^{15}\text{N}$  SOFAST HMQC spectra from TCTP (black) and TCTP\* (red) upon pressure induction. TCTP\* signatures are highlighted (arrows). Experiments were recorded at 800 MHz and 25 °C in the following buffer: 50 mM HEPES pH 7.4, 150 mM NaCl, 2 mM TCEP and 5%  $\text{D}_2\text{O}$ .

protein that might exist at atmospheric pressure [244, 245]. We applied HP-NMR on TCTP from atmospheric (1 bar) to high (2500 bars) pressure in order to highlight a potential minor TCTP state at ambient pressure. We therefore recorded series of  $^1\text{H}$ - $^{15}\text{N}$  spectra and exchange experiments (CPMG, CEST, ZZ exchange) under various pressure values. Protein response to pressure was monitored by looking at resonances in each  $^1\text{H}$ - $^{15}\text{N}$  spectra [246, 247] at

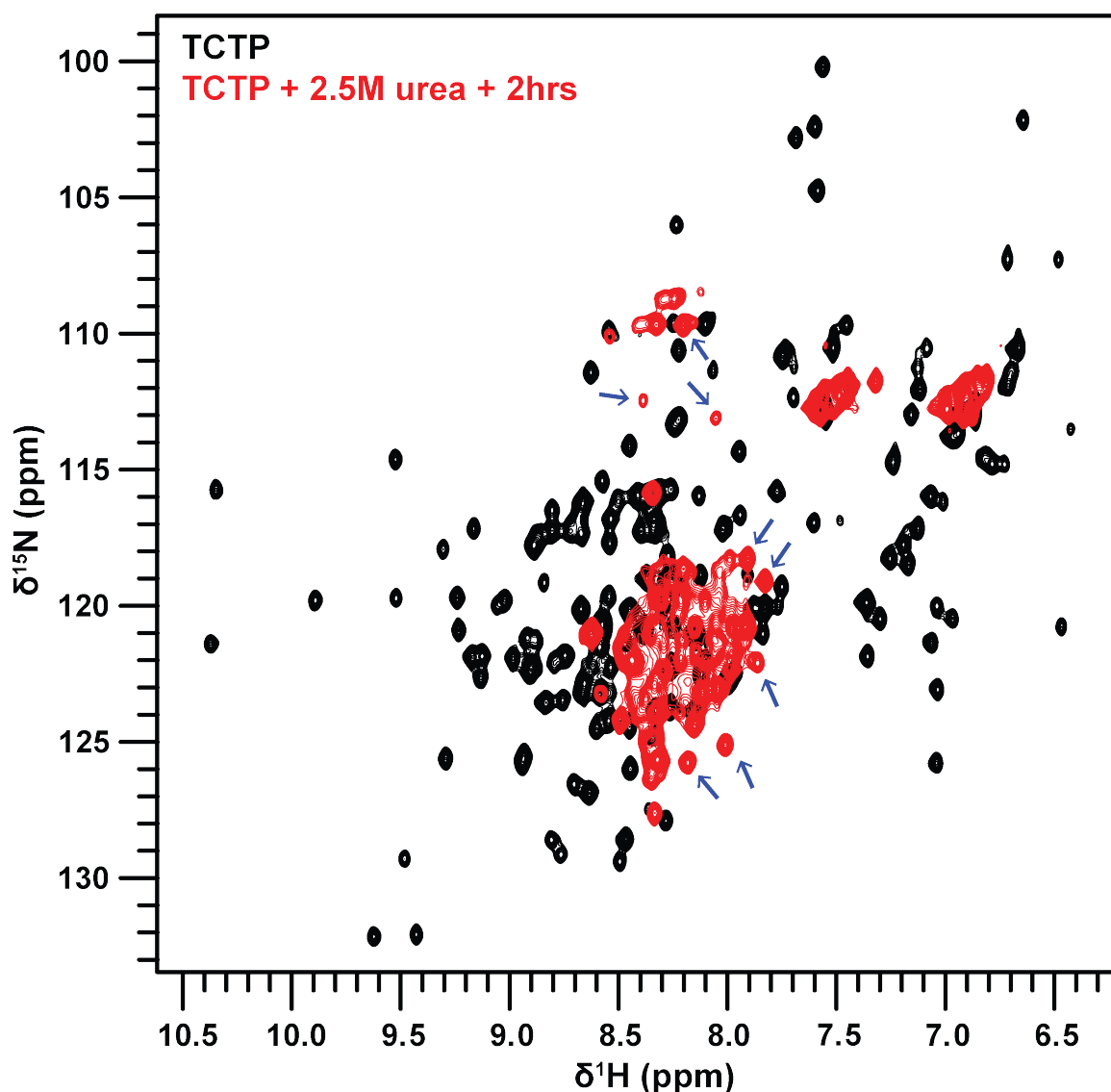


Fig. 3.15 **Comparison of TCTP and TCTP\* upon urea induction.** Overlay of  $^1\text{H}$ - $^{15}\text{N}$  SOFAST HMQC spectra from TCTP (black) and TCTP\* (red) upon urea induction (2.5 M). TCTP\* signatures are highlighted (arrows). Experiments were recorded at 950 MHz and 25 °C in the following buffer: 50 mM EPPS pH 8, 50 mM NaCl, 2 mM TCEP in 95 %  $\text{H}_2\text{O}$  / 5 %  $\text{D}_2\text{O}$ .

atmospheric (1 bar), medium-high (1500 bars) and high (2000 bars) pressure. Combined  $^1\text{H}$ - $^{15}\text{N}$  chemical shift perturbations between atmospheric and medium-high pressure (1500 bars) did spread along the primary sequence of the protein (Fig. 3.13 A, C). Analysis of the linearity of  $^1\text{H}$ - $^{15}\text{N}$  chemical shift perturbations upon pressure gradient from 0 bar to 2500 bars did show unambiguous linear fits along the whole primary sequence of the protein (Fig. 3.13 D), suggesting no local unfolding in TCTP prior to the major structural transition seen between atmospheric and high-pressure (2500 bars). In term of crosspeaks intensity, the signal from

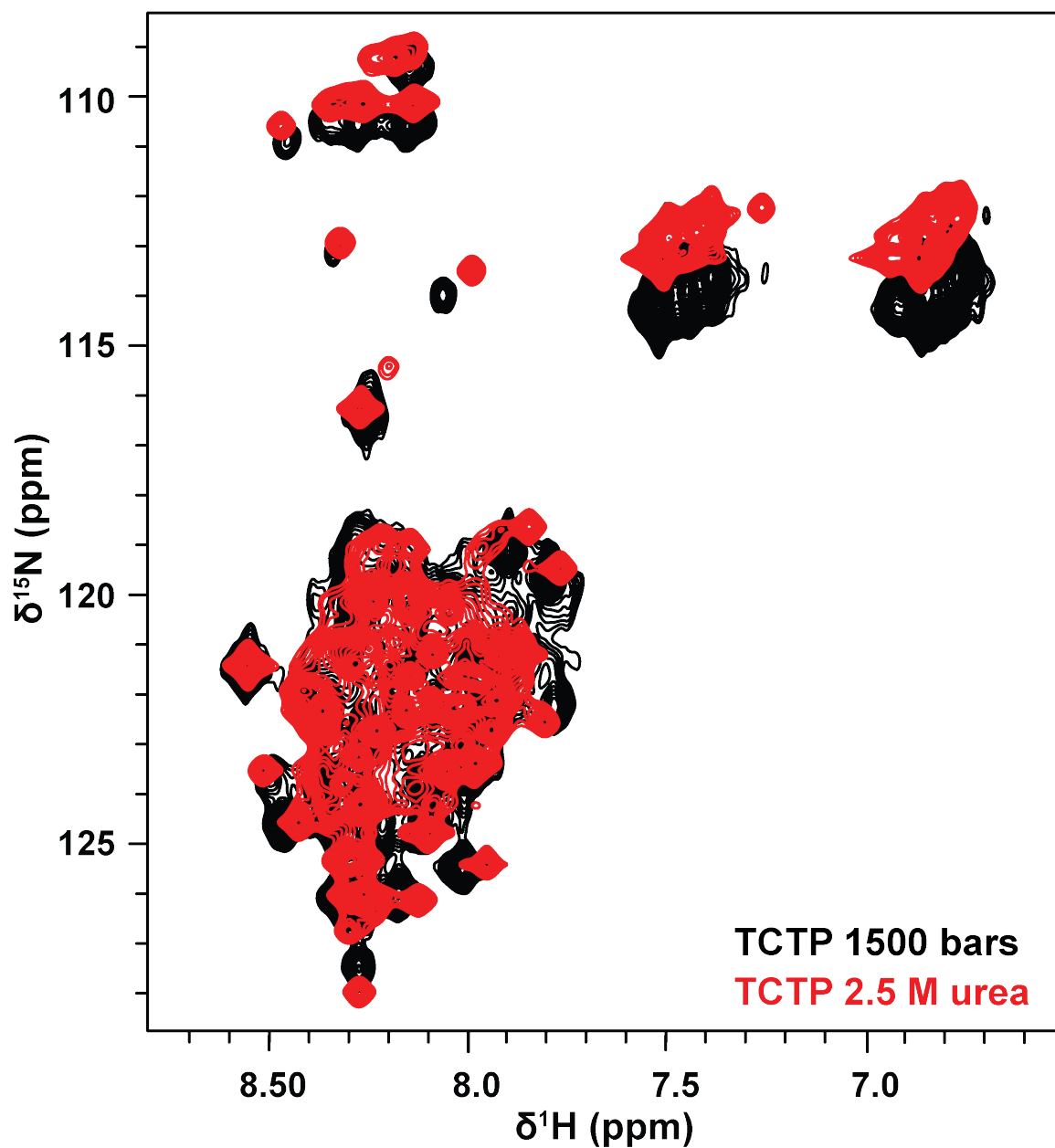


Fig. 3.16 **Comparison of SOFAST HMQC spectra from TCTP\* upon pressure or urea induction.** Overlay of  $^1\text{H}$ - $^{15}\text{N}$  SOFAST HMQC spectra of TCTP\* under pressure (2000 bars) (black) and mild urea concentration (2.5 M) (red). Spectral intensity were scaled arbitrary to ensure the optimal comparison of crosspeak patterns in both spectra. Experiments were recorded at 25 °C and 800 MHz or 950 MHz for pressure and urea experiments, respectively. Experimental conditions were as follow: 50 mM HEPES pH 7.4, 150 mM NaCl, 2 mM TCEP for pressure experiments and 50 mM EPPS pH 8, 50 mM NaCl, 2 mM TCEP for urea experiments. 5%  $\text{D}_2\text{O}$  was added in the NMR tube in both cases. TCTP was present at higher (300  $\mu\text{M}$ ) concentration in pressure experiments compared to urea (100  $\mu\text{M}$ ) experiments.

TCTP structured parts gradually disappeared when increasing pressure with no preference regarding the location in the protein structure (Fig. 3.13 B, C). However, it should be noted that signals from TCTP IDR underwent a much stronger intensity decrease compared to the rest of the protein, probably due to the increased solvent exchange rate induced by pressure. This could also be explained by the pressure-mediated unfolding of the protein and by reduced dynamics of the IDR in fast timescale (ps-ns) or increased exchange contribution ( $R_{ex}$ ) at the millisecond timescale under pressure application. Spectral signatures of a new TCTP state that we populated using pressure (0-2000 bars) were seen appearing starting low pressure (500 bars) and we could estimate this alternative state to be populated at about 50 % to 100 % at 1500 bars and 2000 bars, respectively, and it took time to equilibrate the system (2 hrs) upon each pressure change. At 2000 bars, the signals from the native TCTP state completely vanished. TCTP is a protein that unfolds at relatively low pressure compared to other proteins which suggests that the protein contains large cavities or many small cavities. The inspection of the structure and the prediction of cavities by KVfinder [248] plugin for Pymol software did not reveal obvious large cavities, indicating that many small cavities are present or that transient interactions between the IDR and the protein core surface contribute to water exclusion.

Experiments permitting to detect and characterize chemical exchange (CPMG, CEST, ZZ-exchange) were done with the aim to detect the transition from the native to unfolded state but could not detect such events at intermediate and slower timescales (ms-s). In the  $^1\text{H}$ - $^{15}\text{N}$  SOFAST HMQC of the pressure-induced state of TCTP we could not detect more than a third of resonances seen at atmospheric pressure. This indicates that oligomerization or intermediate exchange (ms) in the protein core domain take place in the TCTP alternative state we unveiled here by applying hydrostatic pressure. Overall, we demonstrated by using HP-NMR that TCTP can convert from its native to a pressure-induced alternative state at pressure starting from 500 bars which is usually not reported for proteins having a stable, well structured globular domain and this suggests that the energy difference or conversion kinetics between native and alternative states is modified by means of pressure. Importantly, we name this protein state TCTP\* herein and we consider its  $^1\text{H}$ - $^{15}\text{N}$  SOFAST HMQC (Fig. 3.14) as containing all necessary signatures to further compare with other alternative states that could be induced using different modes of perturbation.

#### **Induction of TCTP\* by means of urea**

HP-NMR is not suited for daily experiments since it requires a specific hardware and includes pressure-related dangers for both people and spectrometers. Thus, we tested to induce TCTP\* by using a chemical reagent, urea, at low (500 mM) to moderate (2-3 M) concentration. Urea

is a classical chaotropic agent which destabilizes secondary structures in proteins, leading to tertiary and quaternary structure disorganization and ultimately full unfolding of the protein [249]. Interestingly, urea was reported to destabilize  $\beta$ -sheet preferentially compared to  $\alpha$ -helix [250, 251] and thus we tried to selectively unpin the BH3-like motif from the core domain since it is organized as an hairpin of  $\beta$ -strands where a single strand ( $\beta_3$ ) anchors the protein BH3-like segment into the globular core of TCTP. Thus, we hypothesized that a limited destabilization by means of urea at strand  $\beta_3$  could be sufficient to yield an alternative TCTP state with unpinned and solvent-exposed BH3-like motif as we expect that to be crucial to make the motif readily accessible for partners. In addition, the use of TCTP primary sequence to predict secondary structure in this region did not yield reliable results, suggesting that the sequence itself has no clear property at being structured or unfolded and thus we envisage it could be more easily unpinned upon urea addition compared to other well structured and predicted regions in the protein.

After the first urea increment (500 mM), an immediate disappearing of a subset of crosspeaks was observed and was not changed at higher (1 M) urea concentration, meaning that TCTP and urea molecules should interact together with important dynamics (ms) at the molecular interfaces between TCTP and urea molecules (Fig. 11 A). The disappearing crosspeaks were spread in different segments of the protein (L7, M35, V36, T68, G69, Q79, F83, I136, G137 and G143) without drawing a clear continuum on the protein structure (Fig. 11 B). A large set of small chemical shifts perturbations were also seen in the protein spectrum and were essentially located in solvent-exposed loops connecting secondary structure elements in TCTP, suggesting that urea could bind in these regions. Over time (2 hrs), spectral signatures found in the spectrum of TCTP\* induced by pressure appeared and stabilized, meaning that we could induce an alternative TCTP state that slowly converts from native TCTP state and this starting from low urea concentration (500 mM). Higher concentration of urea (2-3 M) has permitted to recover most of the  $^1\text{H}$ - $^{15}\text{N}$  spectra measured for the pressure-induced state, including reliable spectral signatures (Fig. 3.16). After addition of urea (2.5 M) and about two hours of equilibration time, we observed the full conversion from the native protein to an urea-induced state that we also refer to as TCTP\* since both urea- and pressure- induced states have strikingly similar  $^1\text{H}$ - $^{15}\text{N}$  fingerprint (Fig. 3.15). As with pressure use, this urea-induced state should have a slow tumbling rate related to oligomeric state or undergo conformational exchange at intermediate timescale (ms) since we observed severe line broadening with only a third of crosspeaks visible compared to the  $^1\text{H}$ - $^{15}\text{N}$  spectra of native TCTP. Among the remaining crosspeaks, a large part overlap with crosspeaks from the IDR in the native state, suggesting that the protein segment is marginally affected upon structural transition of TCTP to TCTP\*. Higher temperatures ( $\geq 35$  °C) on the 2.5 M urea containing

sample did not increase the crosspeaks number but led to the irreversible protein unfolding or aggregation as judged by the fast decrease in the whole spectral intensity over time (min.) with no recovery if lowering the temperature to 5 °C. With native TCTP, the protein was stable in these conditions and we think that TCTP\* is intrinsically more prone to aggregate compared to the native state. Moreover, for crosspeaks overlapping resonances from the IDR in the reference spectrum, the rate at which intensity decreases was significantly slower, suggesting that the urea-induced TCTP conformer oligomerizes in soluble assembly in which the IDR is still exposed to solvent prior to aggregation. This indicates that TCTP\* could be the folding intermediate from native to unfolded or aggregated states that finally precipitate in our NMR tube. Notably, the experimental conditions of salt (50 mM pH) and alkaline pH 8 that promotes the conversion from native to TCTP\* state at lower urea concentration were also reported to lower the melting temperature of the protein in urea-free conditions. This strengthens the hypothesis that TCTP\* could be a relevant intermediate in the folding pathway of the TCTP protein.

In conclusion, both pressure and urea use have yielded alternative states of TCTP with very similar  $^1\text{H}$ - $^{15}\text{N}$  spectra, suggesting that they have close structure and dynamics (Fig. 3.16). We consider that such degree of resemblance allow to propose that both states represent TCTP\*, a folding intermediate that has striking structure and dynamics differences compared to the native form and that is likely showing flexible segments in the  $^1\text{H}$ - $^{15}\text{N}$  of the protein.

### 3.3.2.2 Characterization of the BH3-like motif and IDR in TCTP\*

To identify and characterize the NMR-visible protein segments in TCTP\*, we assigned the resonances found in the  $^1\text{H}$ - $^{15}\text{N}$  fingerprint of the protein in presence of 3 M urea to reduce background of residual resonances from native TCTP state that remain at 2.5 M urea ( $\sim 5$ -10 %). Overall 35 % (61/172 residues) of the protein backbone amide hydrogen and nitrogen were assigned corresponding to  $\sim 80$  % of the visible crosspeaks in TCTP\* spectrum. Assignment was carried out using standard experiments such as HNCOCACB, HNCACB and HNCANH (Sec. 2.3.1.3) and is fully reported (Fig. 3.17 A). Backbone resonances from the BH3-like (15-29) and IDR (38-66) regions were assigned and included in a continuous segment spanning from residues F14 to M74 (61 aa) (Fig. 3.17 B). Several crosspeaks ( $\sim 20$  % of total) from the SOFAST HMQC spectra could not be assigned due to missing signals in the 3D spectra, presumably due to line-broadening from chemical exchange (ms) or protein oligomerization. We did not considered isolated short residue stretches ( $\leq 5$  residues) we found in the final assignment since low variability is expected for backbone HN chemical shifts in flexible segments, thus increasing the probability of errors.

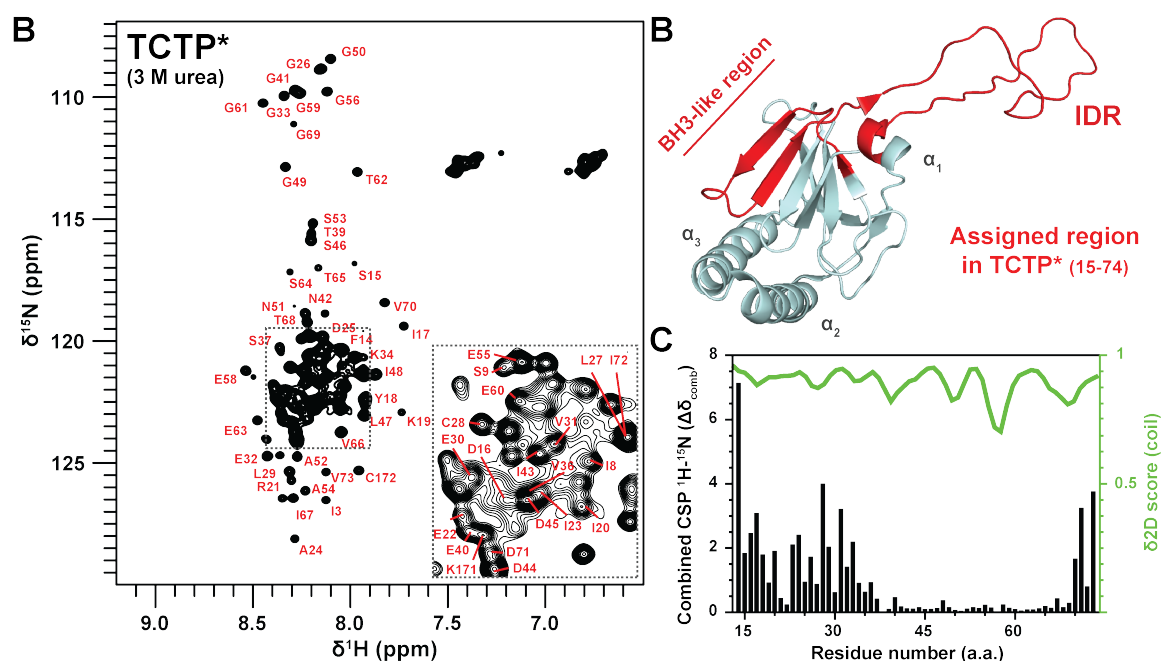


**Fig. 3.17 NMR characterization of TCTP\* and secondary structure prediction.** (A) Backbone assignment of TCTP\*.  $^1\text{H}$ - $^{15}\text{N}$  SOFAST HMQC from TCTP\* (600  $\mu\text{M}$ ) and  $^1\text{H}$ - $^{15}\text{N}$  backbone assignment (red labels). (B) Completion of TCTP\* assignment (red) represented on TCTP structure (pdb code: 2HR9) with highlight of the BH3-like region. (C) Combined  $^1\text{H}$ - $^{15}\text{N}$  chemical shift perturbations computed between  $^1\text{H}$ - $^{15}\text{N}$  fingerprint from TCTP and TCTP\*. The result of  $\delta 2\text{D}$  software analysis for the random coil structure prediction based on backbone chemical shifts from carbon atoms is represented (green curve) on the same panel. Experiments were recorded at 800 MHz and 5  $^\circ\text{C}$  in the following buffer: 50 mM EPPS pH 8, 50 mM NaCl, 2 mM TCEP, 3 M urea in 95 %  $\text{H}_2\text{O}$  / 5 %  $\text{D}_2\text{O}$ .

This strongly increases the possibility of errors because the NMR backbone assignment lies on differences between chemical shifts from backbone atoms in the protein. We could still assign the C-terminal residue C172 that yields the strongest signal at higher temperature ( $\geq 35$   $^\circ\text{C}$ ) in the  $^1\text{H}$ - $^{15}\text{N}$  SOFAST HMQC of TCTP\*. In consequence, we report C172 to be a useful probe for further detecting traces of TCTP\* in urea-free conditions and at room temperature. All others assigned resonances were sharper at low temperature (5  $^\circ\text{C}$ ) compared to room temperature (25  $^\circ\text{C}$ ), suggesting that most of NMR-visible TCTP\* residues are flexible and solvent-exposed. Combined  $^1\text{H}$ - $^{15}\text{N}$  chemical shifts perturbations could be computed between  $^1\text{H}$ - $^{15}\text{N}$  fingerprint from TCTP and TCTP\* after subtracting the average  $^1\text{H}$  and  $^{15}\text{N}$  perturbations seen upon urea addition to each residue-specific  $^1\text{H}$  and  $^{15}\text{N}$  chemical shift perturbation, respectively (Fig. 3.17 A). Resonances from the extended BH3-like region of the protein (F14-V36) and in the C-terminal of the IDR (65-68) were severely affected upon conversion from TCTP to TCTP\*. These segments contain  $\beta$ -strands ( $\beta_2$ ,  $\beta_3$ ,  $\beta_4$  and

$\beta_5$ ) and an  $\alpha$ -helix ( $\alpha_1$ ) in the native structure, respectively, and the amplitude of spectral perturbations reports on a large structural reorganization in the region upon conversion from the native protein to TCTP\*.

To get further insights in the structure of TCTP\*, the chemical shifts from C', C(O), C $\alpha$  and C $\beta$  were used through  $\delta$ 2D [252] online tool to compute the secondary structure propensity in the F14-M74 segment (Fig. 3.17 A) and the analysis showed that all assigned residues in TCTP\* (F14-M74, 61 over 172 residues) organize as random coil. This in particular has demonstrated the unstructured nature of the BH3-like segment in TCTP\* and this also showed that the region could be selectively unpinned from the globular domain upon urea stress. We also noticed that the short  $\beta$ -sheet that is formed at the bottom of the IDR (residues 34-37 and 67-70) is also unfolded in TCTP\*. In contrast, the invisible signals in TCTP\* mostly correspond to the well structured core in the native TCTP. The absence of signal for this region can be explained potentially by protein oligomerization or conformation exchange at intermediate timescale (ms). The two possibilities will be explored in the next sections to better characterize the TCTP\* state.

### 3.3.2.3 Secondary and tertiary structure definition of TCTP\*

Since signal loss in TCTP\* can be attributed to molecular size, conformational exchange or unfolding considering solvent-exchange at alkaline pH, we have further characterized the secondary and tertiary structure organization of the protein by doing CD spectroscopy in the Far-UV (205-260 nm) and Near-UV (240-310 nm) regions [253]. The Far-UV region informs on the secondary structure content in a protein. For the native protein, the far-UV CD spectrum contains contributions of both  $\alpha$ -helical and  $\beta$ -sheet segments (Fig. 3.18), as expected from the solution [176] and crystal [149] structures of the protein. Upon TCTP\* induction with 2.5 M urea, the far-UV CD spectrum did show a slight but reproducible decrease between 210 nm and 230 nm which is compatible with a limited unfolding of the BH3-like region. At denaturing concentration (8 M), urea totally unfolded the protein, yielding a flat curve in the spectral regions above 215 nm and meaning that no stable secondary structure elements were present in TCTP<sub>U</sub>. Urea use was judged responsible for the poorer sensitivity at low wavelength ( $\leq$  205 nm) and here we only conclude that the whole secondary structure content is generally conserved in TCTP\* when compared to native TCTP. At higher structural level, the Near-UV region in CD spectra informs on the tertiary organization of the protein by measuring light deviation from aromatic (Phe, Tyr) residues. In TCTP protein, residues F14, F114, F134, F162, F163, Y88, Y91 and Y95 structure the globular core of TCTP via a network of hydrophobic interactions. Residues Y4, Y18, Y132,

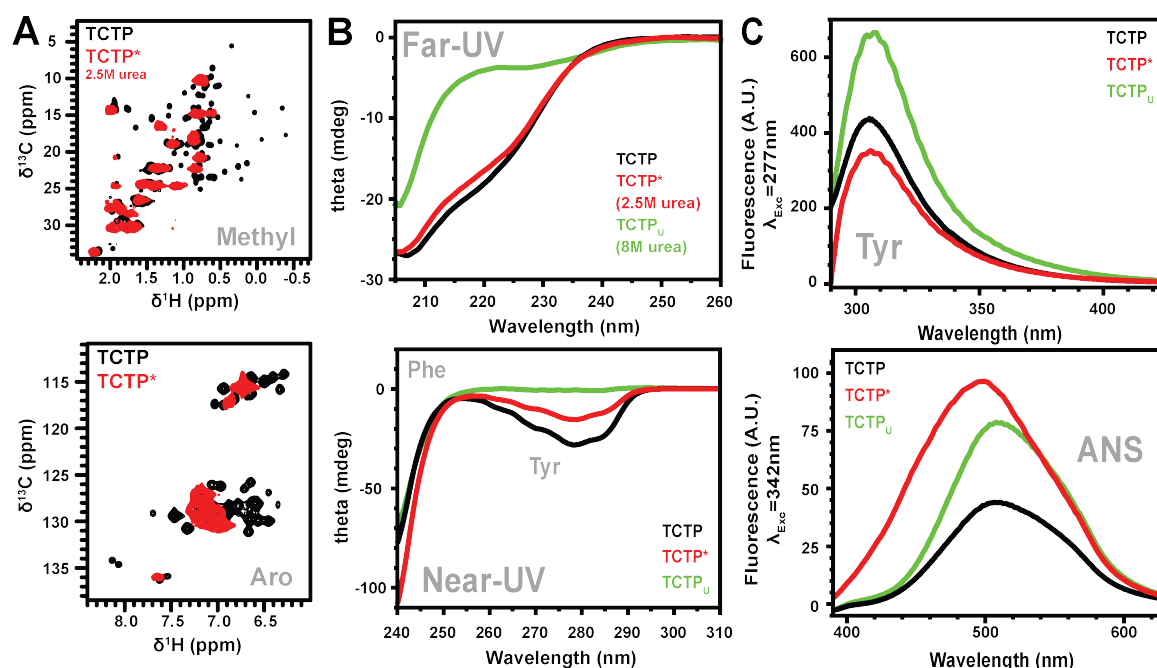


**Fig. 3.18 Tertiary structure content in TCTP\*.** (A) Methyl and aromatic fingerprint of TCTP\*. Overlay of  $^1\text{H}$ - $^{13}\text{C}$  SOFAST HMQC spectra from urea-free TCTP (100  $\mu\text{M}$ ) (black) and upon addition of urea (2.5 M) and after system equilibration (2 hrs) (red). Both methyl (left) and aromatic (right) regions are shown. Experiments were recorded at 800 MHz and 25  $^\circ\text{C}$ . (B) (top) Far-UV (205-260 nm) circular dichroism spectra from native TCTP (150  $\mu\text{M}$ ) (black) and upon addition of 2.5 M (red) or 8 M (green) urea and (bottom) Near-UV (240-310 nm) circular dichroism experiment spectra from native TCTP (150  $\mu\text{M}$ ) (black) and upon addition of 2.5 M (red) or 8 M (blue) urea. Contribution regions of Phe and Tyr residues are highlighted (grey labels). (C) TCTP fluorescence and (D) ANS fluorescence emission spectra from native TCTP (5  $\mu\text{M}$ ) (black) and upon addition of 2.5 M (red) or 8 M (green) urea after subtraction of background.  $\lambda_{\text{Exc}}$  was set to 277 nm and 342 nm for recording Tyr and ANS fluorescence spectra, respectively. The contribution region of the Tyr residues and ANS probe are highlighted (grey labels). Samples were all incubated at 37  $^\circ\text{C}$  overnight prior to experiment. For ANS fluorescence assays, the probe was then added and samples were re-incubated 2 hours at 37  $^\circ\text{C}$ . Experiments were carried out at the same temperature in the following buffer: 50 mM EPPS pH 8, 50 mM NaCl, 1 mM TCEP supplemented with 2.5 M (TCTP\*) or 8 M urea (TCTP<sub>U</sub>). For NMR, 5 %  $\text{D}_2\text{O}$  (v/v) was added in the sample before measurement.

Y151, Y159, F83 and F129 are solvent-exposed and do not contribute in the packing of the core domain. Overall, Phe residues are principal mediators of the bonding network in the globular domain compared to Tyr residues. The Near-UV region from TCTP with no, mild (2.5 M) and fully denaturing (8 M) urea concentration (Fig. 3.18 B) showed variations in both Phe (240-260 nm) and Tyr (260-300 nm) regions. Phe residues induced a stronger light deviation within TCTP\* compared to both native and unfolded TCTP states. Light-deviation induced by Tyr residues gradually decreased to finally disappear during the conversion from native TCTP to TCTP\* and final TCTP<sub>U</sub>. We conclude that TCTP\* retains an hydrophobic

core organization despite major changes in its tertiary structure. Unfortunately, near-UV CD spectra do not allow for further reliable interpretation about the nature of structural changes. Indeed, tyrosine transitions are not sensitive to the polarity of the environment [254]. However, when looking at the  $^1\text{H}$ - $^{13}\text{C}$  fingerprint of TCTP\* (Fig. 3.18 A) in the methyl and aromatic regions we observed a gradual and total disappearing of resonances from residues buried in the hydrophobic core of the native protein. Resonances from flexible parts underwent line broadening, particularly pronounced in the aromatic region. The remaining visible signals in the NMR spectra of TCTP\* were all with random coil  $^1\text{H}$ ,  $^{13}\text{C}$  chemical shift values and they correspond to the residues for which amide HN were visible and assigned to the random coil F14-M74 regions.

The tertiary structure change in TCTP\* was further characterized by using intrinsic fluorescence-based methods. Since TCTP contains 7 Tyr residues we could measure the intrinsic fluorescence of the protein by recording emission spectra upon urea addition to convert native TCTP to TCTP\* (2.5 M) and then TCTP<sub>U</sub> (8 M) (Fig. 3.18 C). The tyrosine emission spectra from native TCTP and TCTP\* were similar with a moderate difference when compared to the larger variation seen for TCTP<sub>U</sub> spectrum. We conclude that TCTP\* retains a tertiary structure closer from the native protein compared to the fully unfolded protein. Finally, we used the hydrophobic fluorescent probe ANS to determine if the folding intermediate TCTP\* could be described as a MG state (Fig. 3.18 D). MG states are compact folding intermediates [255] with generally conserved secondary structures from the native state but fluctuating tertiary organization [256] and are very distinct from the unfolded state. The fluorescent probe ANS is useful to detect molten-globule state in proteins since the probe binds to MG stronger because MG have a more loosen tertiary structure and the ANS probe can penetrate in globular domains and bind to hydrophobic surfaces, raising its fluorescence [219]. Here, ANS fluorescence was increased by a factor of two upon TCTP\* conversion with 2.5 M urea. Strikingly, the fluorescence diminished upon unfolding of TCTP, indicating that TCTP\* exposes by far more hydrophobic surfaces in cavities than native or unfolded TCTP. Interestingly, urea was shown to compete with ANS at high concentration (8 M) to bind proteins and thus it could explain the decrease in ANS fluorescence for unfolded TCTP, together with the disappearing of the main cavity in the core domain of TCTP\*. These NMR and CD data are collectively compatible with a compact core region in TCTP\* with largely preserved secondary structure content. Consequently, the signal loss observed in TCTP\* NMR spectrum likely originate from chemical exchange at intermediate timescales (ms) and the protein state has typical characteristics of MG state.

## 3.3.2.4 Oligomeric state of TCTP\* and molecular envelope

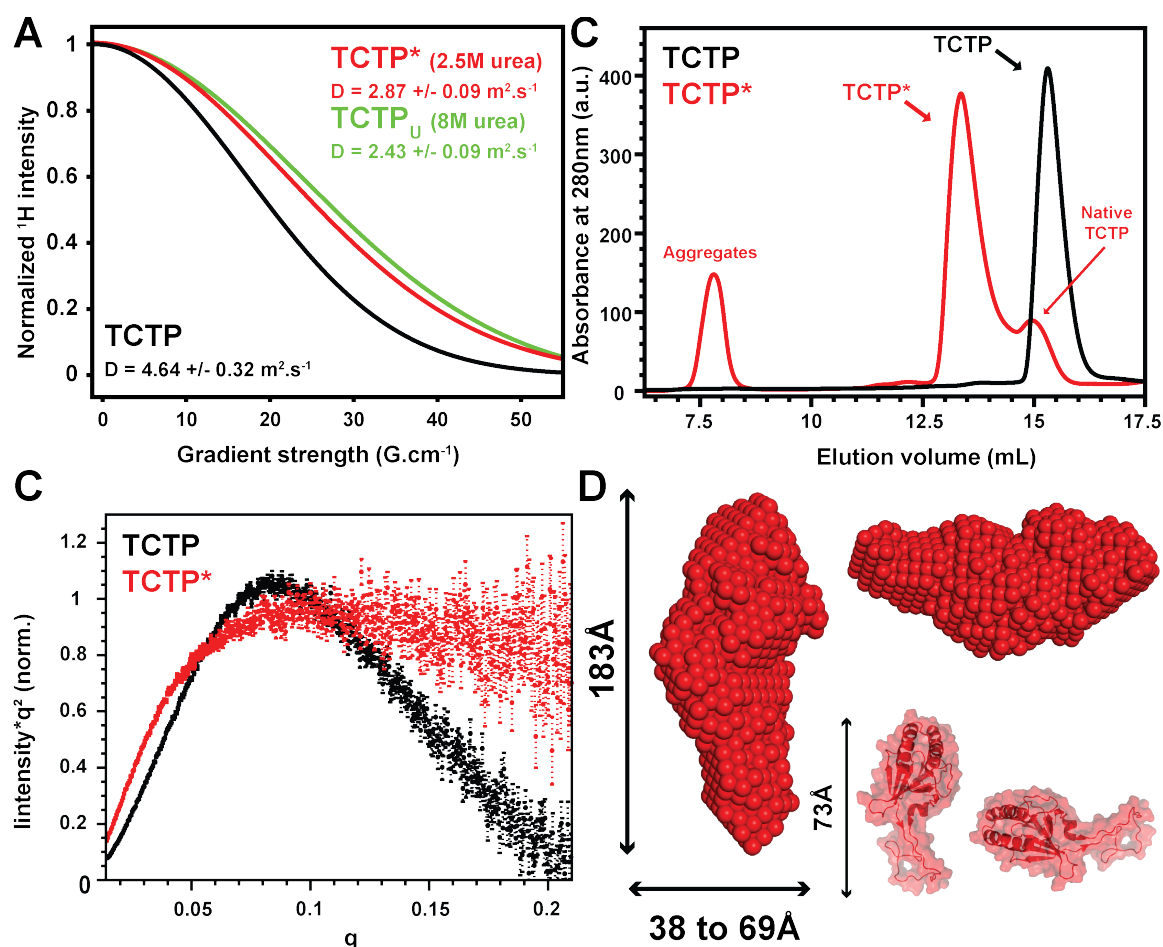


**Fig. 3.19 Oligomeric state of TCTP\* and molecular envelope.** (A)  $^1\text{H}$ - $^{15}\text{N}$  HSQC-DOSY experiments from native TCTP (100  $\mu\text{M}$ ) (black), TCTP\* (2.5 M urea) (red) and unfolded TCTP (8 M urea) (green). DOSY curves were corrected for the modification of viscosity induced by urea. The variation of the diffusion coefficient for EPPS buffer in function of urea concentration was used as baseline for correction with the protein samples. Experiments were recorded at 800 MHz and 5  $^\circ\text{C}$ . The fitted translational diffusion coefficient ( $D$ ) is reported for TCTP at various urea concentrations. (B) SEC elution profiles of TCTP and TCTP\*. Species that absorb light at 280 nm are indicated (arrows), including soluble aggregates of proteins. For SEC analysis, the sample was more concentrated (500  $\mu\text{M}$ ) and injected into a S200 Increase column (GE Healthcare) pre-equilibrated with the sample buffer (25  $^\circ\text{C}$ ). (C) Kratky plot ( $q^2 I_q(q)$ ) from in-line SAXS experiments done with native TCTP (black) and upon conversion to TCTP\* (red). (D) Molecular envelope computed from SAXS data and generated with DAMMIF from ATSAS software [217] and in-built module primusqt (left). Solution structure of native TCTP (pdb code: 2HR9) with cartoon and surface representation. Experiments were done using the following buffer: 50 mM EPPS, 50 mM NaCl, 2 mM TCEP for TCTP plus 2.5 M (TCTP\*) or 8 M (TCTP<sub>U</sub>) urea. For NMR, the buffer was complemented with 5 %  $\text{D}_2\text{O}$  (v/v).

We reported the assignment of TCTP\* and could match a crosspeak with a residue in the protein for the majority of resonances. This indicates that C-terminus of TCTP\* state undergoes severe line broadening and we proposed that either oligomerization or intermediate exchange (ms) could contribute in that particular behavior. Thus, we performed  $^1\text{H}$ - $^{15}\text{N}$  HSQC-DOSY on native TCTP and both urea-induced TCTP\* (2.5 M) and in the 8 M urea condition where we expect TCTP to be totally unfolded (TCTP<sub>U</sub>) (Fig. 3.19 A). Indeed, DOSY experiments yield the translational diffusion coefficient (D) and permit to estimate the oligomeric state since D depends on the hydrodynamic radius ( $R_h$ ) of the protein. Diffusion properties strongly depend on the viscosity ( $\eta$ ) and thus on the concentration of urea. Thus, we computed the variation (%) of the translational diffusion coefficient for EPPS buffer with respect to urea concentration and corrected values for TCTP, TCTP\* and TCTP<sub>U</sub>. We have demonstrated that TCTP has a greater diffusion coefficient compared to TCTP\* and TCTP<sub>U</sub> with  $4.64 \pm 0.32 \cdot 10^{-10} \text{ m}^2 \cdot \text{s}^{-1}$ ,  $2.87 \pm 0.09 \cdot 10^{-10} \text{ m}^2 \cdot \text{s}^{-1}$  and  $2.43 \pm 0.09 \cdot 10^{-10} \text{ m}^2 \cdot \text{s}^{-1}$ , respectively. This shows that the native TCTP state diffuses faster than the other states. Since TCTP has an IDR part it can not be properly considered as a globular protein and the estimation of the hydrodynamic radius  $R_h$  from the Stokes-Einstein equation expressed as  $\frac{k_B T}{6\pi\eta R_h}$  gives less reliable values because it assumes spherical particle shape. We could still estimate that TCTP and TCTP\* have  $R_h$  of  $4.70 \pm 0.54 \text{ nm}$  and  $7.61 \pm 0.27 \text{ nm}$ , respectively. We could confirm this difference without baseline correction for urea in  $^1\text{H}$ - $^{15}\text{N}$  HSQC DOSY experiments with half native TCTP and TCTP\* (1.5 M urea) but do not report more extensively since low signal to noise ratio raised the uncertainty. For unfolded TCTP we estimated a greater  $R_h$  at  $8.98 \pm 0.26 \text{ nm}$ . These differences in diffusion properties of TCTP and TCTP\* are in the range of what expected considering the unfolding of the BH3-like region and/or a possible preference of TCTP\* to form dimers in solution. In the latter cases, the fact that TCTP\* and TCTP<sub>U</sub> have similar translational diffusion properties would logically be explained by the dissociation of TCTP\* dimer upon conversion to TCTP<sub>U</sub> at higher urea concentration.

To further establish the oligomeric state and shape of TCTP\*, we measured SEC-SAXS experiments by running the samples of native TCTP at 0 M urea and TCTP\* at 2.5 M urea concentration in the buffer. We first show SEC profiles of TCTP and TCTP\* (Fig. 3.19 B). We demonstrated that TCTP\* was eluted first (26.7 mL) whereas residual non-converted TCTP came at greater elution volume (30.6 mL), consistently with profile from the native TCTP control in urea-free conditions. We expect urea not to critically impact the protein elution if we consider that residual non-converted TCTP (2.5 M urea) is eluted at close volume compared with native TCTP in urea-free condition. This difference in the elution volume and related  $R_h$  is also compatible with the unfolding of the BH3-like region and a tendency of

TCTP\* to form dimers. Interestingly, TCTP\* forms soluble aggregates ( $V_{\text{elution}} = 7.75$  mL) whereas native TCTP does not. This strengthens the hypothesis that TCTP\* could be an unfolding intermediate which mediates the protein full unfolding or aggregation as reported for the molten-globule states in proteins [257]. It should be noted that lowering the pH down to 6-7 (at 2.5M urea) also lead to the precipitation of TCTP\*, reinforcing the tendency of TCTP\* to self-association and aggregation. To definitely establish the oligomeric state of TCTP\* and to know at which extent TCTP\* gains flexible parts compared to native TCTP, we measured in-line SAXS experiments on the two distinct protein states and we computed the molecular envelope of TCTP\* using ATSAS software suite [217].

We first compared the kratky plots ( $q^2 I_q(q)$ ) obtained from the SAXS signal intensity ( $I_0$ ) in function of the diffusion angle ( $q$ ) which qualitatively assess the degree of unfolding in protein samples (Fig. 3.19 C). As expected from the limited unfolding of the BH3-like motif in TCTP\*, we observed a significant increase in  $q^2 I_q$  at higher values of  $q$ . This confirms that more flexible residues are present in TCTP\* state compared to native. The degree of difference is important and thus could suggest that the IDR in TCTP\* is more mobile than in native TCTP, as a cooperative effect from the unfolded BH3-like at the IDR (or vice-versa) in TCTP\*. To definitely establish the oligomeric state of TCTP\*, we have computed the radius of gyration ( $R_g$ ) and apparent MW of the protein state from the Guinier plot ( $\ln(I) (q^2)$ ) using ATSAS/Primus software [217]. From frames 19-65 we estimated a  $R_g$  of  $3.95 \pm 0.2$  nm and a apparent MW of  $40.2 \pm 2.9$  kDa for TCTP\* whereas we found 2.15 nm and 33.8 kDa for native TCTP (Sec. 3.1.3.2). These parameters clearly establish that TCTP\* is a fully populated dimer in solution as seen from a two fold increase in the apparent MW of TCTP\* compared to monomeric, theoretical MW of TCTP (monomer = 19.7 kDa, dimer = 39.3 kDa). Experimentally, native TCTP had apparent MW between the two values since it is an equilibrium between monomer and dimer with comparable populations. The  $R_g$  of the TCTP\* state is increased almost by a factor of two, which is consistent with the increase in unfolded regions and the formation of a fully populated dimer upon conversion. This also explains why TCTP\* has similar hydrodynamic properties compared to fully unfolded TCTP (Fig. 3.19 A). To estimate the structure of TCTP\* dimer, we have computed the molecular envelope of this particular TCTP state (Fig. 3.19 D). TCTP\* has a prolate type of structure organisation with cylindrical shape. In its larger dimension, the protein model is 18.3 nm long whereas the diameter of the model sections are in the range 3.8-6.9 nm. By analogy, we compared the surface representation of the TCTP high-resolution structure and we could measure half than TCTP\* for the largest dimension (7.3 nm) whereas the mean diameter was roughly estimated similar between TCTP and TCTP\*. Thus, it is possible that TCTP\* is organized as two units interacting in the central region of the molecular envelope,

and both units would project their disordered BH3-like and IDR segments toward the solvent away from the central region of the molecular envelope.

In conclusion, TCTP\* has limited increase in its hydrodynamic radius compared with native TCTP and we established that both unfolding of the BH3-like region and dimerization were responsible for these differences. The size of TCTP\* dimer is still largely amenable for high-field NMR studies and thus we can reasonably exclude that signal extinction for most crosspeaks from the C-terminal TCTP\* region (80-172) originates from the slower molecular tumbling due to self-association. This suggests that intermediate exchange (ms) rather strongly contribute in the line broadening seen in TCTP\*  $^1\text{H}$ - $^{15}\text{N}$  fingerprint. Finally, the molecular envelope of TCTP\* gives an idea of how both protein units could arrange together in a prolate and cylindrical structure organization. Altogether our results strongly support the classification of TCTP\* as a MG state.

### 3.3.3 Evidences for the pre-existing character of TCTP\*

Structural organization of proteins can fluctuate under temperature variation and be monitored by NMR [258–260]. Since we want to detect or induce alternative TCTP states in solution we monitored the protein from low (5 °C) to high (40 °C) temperature in order to promote structural transitions and to observe spectral signatures of TCTP\* (Fig. 3.20). Signals in  $^1\text{H}$ - $^{15}\text{N}$  fingerprint from structured and flexible parts of TCTP showed increasing and decreasing intensity, respectively, when increasing the temperature (Fig. 3.20). Such effects are easily explained through the decrease of global correlation time ( $\tau_c$ ) and the resulting longer transverse relaxation time for structured regions and also by the increase of solvent-exchange at higher temperatures for flexible regions accessible to water. We compared  $^1\text{H}$ - $^{15}\text{N}$  SOFAST HMQC from TCTP at 35 °C and 20 °C and computed combined  $^1\text{H}$ - $^{15}\text{N}$  chemical shift perturbations. These were stronger within the flexible segments of the protein but otherwise spread along the primary sequence (Ann. 8). The analysis of  $^1\text{H}$ ,  $^{15}\text{N}$  chemical shifts changes essentially showed raw linear variations. But still we observed a slight unimodal curving along the temperature gradient as exemplified for residues G101 and A127 (Ann. 9) and this reports on energetics of backbone amide H-N related to engagement in hydrogen bonding networks. This means that no structure transition could be detected in the major TCTP state prior to the protein melting at the melting temperature of 40 °C.

Interestingly, minor peaks appeared on TCTP spectrum above 25 °C. These crosspeaks gradually increased in intensity (up to 40 °C) and were found similar to those identified as TCTP\* signatures. The C-terminal residue C172 best reports on the temperature-promoted conversion to TCTP\* since the signature appears from 25 °C and is the strongest among

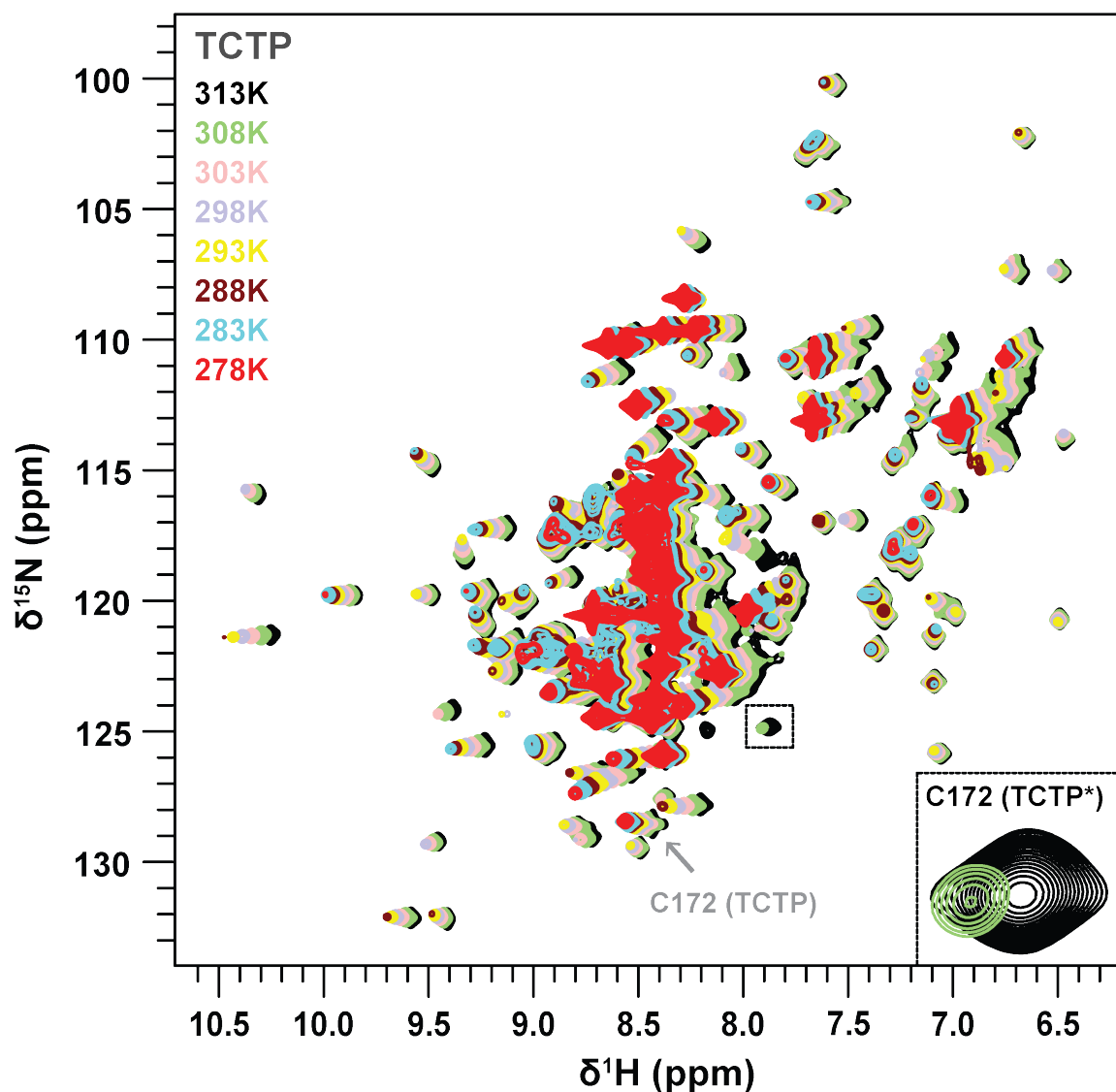


Fig. 3.20 **Impact of temperature on TCTP structure with SOFAST HMQC.** Overlay of  $^1\text{H}$ - $^{15}\text{N}$  SOFAST HMQC spectra from TCTP (1 mM) at different temperatures (278-40 °C). Temperatures are indicated (colors). The crosspeak from C172 from the native TCTP as well as an alternative crosspeak from the same residue appearing at higher temperature are highlighted (close-up). Experiments were recorded at 800 MHz in the following buffer: 50 mM EPPS pH 8, 50 mM NaCl, 1 mM TCEP in 95 %  $\text{H}_2\text{O}$  / 5 %  $\text{D}_2\text{O}$ .

TCTP\* signatures at higher temperatures. At 40 °C, the whole spectral intensity including the newly converted TCTP\* decreased over time due to protein unfolding or aggregation. A slower loss of intensity is observed for the flexible parts of the protein (Ann. 10), which suggests that limited oligomerization precedes protein aggregation or unfolding. This raises the question to know if TCTP\* represents a necessary route or not in the unfolding pathway

of the protein. Indeed, all three temperature, pressure and urea lead to alternative states that we said they correspond to TCTP\* description. From apart HP-NMR, where protein aggregates were likely not representing the more compact state for a protein, we could demonstrate that TCTP\* is intrinsically more sensitive to unfolding or aggregation than the native protein from which the molten-globule state TCTP\* originates.

Strikingly, the apparent melting temperature ( $T_m$ ) of the protein is lower than expected regarding before-mentioned TSA experiments (46 °C) done in similar conditions (Sec. 3.3.1.1). A longer equilibration time in NMR experiments compared to TSA setup can explain the difference if considering that a minor protein state, presumably TCTP\*, is part of the route for full protein temperature denaturation. Indeed, temperature promotes the minor state in a time-dependent manner (hrs) and TSA experiments use short temperature gradient step time (s), yielding overestimated melting temperatures. Overall, we exposed lines of experimental evidence regarding the pre-existing nature of TCTP\* in native-like conditions and its place in the protein unfolding/aggregation pathway.

## 3.4 Discussion

In the chapter, we have accumulated experimental and theoretical evidences that the TCTP protein can remodel upon a wide range of stimuli. We reported the use of many parameters (temperature, protein concentration, phosphorylation, mutation, calcium binding, urea and pressure) to induce structural transitions in TCTP that were monitored by means of an integrated panel of biophysical methods (NMR, SAXS, far- and near- UV CD, ANS and tyrosine fluorescence, TSA, SEC, MS) and computational approaches (MD, docking). In the next paragraphs we summarize and discuss our results and we also introduce a model to describe the diversity of TCTP structures and related equilibrium.

To briefly summarize our results, we have described TCTP in its native state (TCTP) (Sec. 3.1.1) and confirmed that the protein is well structured and contains an IDR segment (Fig. 3.21). We have demonstrated that native TCTP can form non-covalent dimers (TCTP<sub>D</sub>) in reducing conditions and common salt and buffer conditions (Sec. 3.1.2) (Fig. 3.21). Together with the characterization of TCTP dimer, we published our work about TCTP IDR modifications (phosphorylation, calcium binding) in which we proposed that the IDR could remodel the globular part of TCTP upon modifications which should involve conserved signature TCTP1 and TCTP2 in the IDR and core domain, respectively (Sec. 3.2) (Fig. 3.21). So far it was unknown how the conserved signatures TCTP1/TCTP2 could play a role in the protein interaction and we proposed that it could serve as a switch to enable or disable

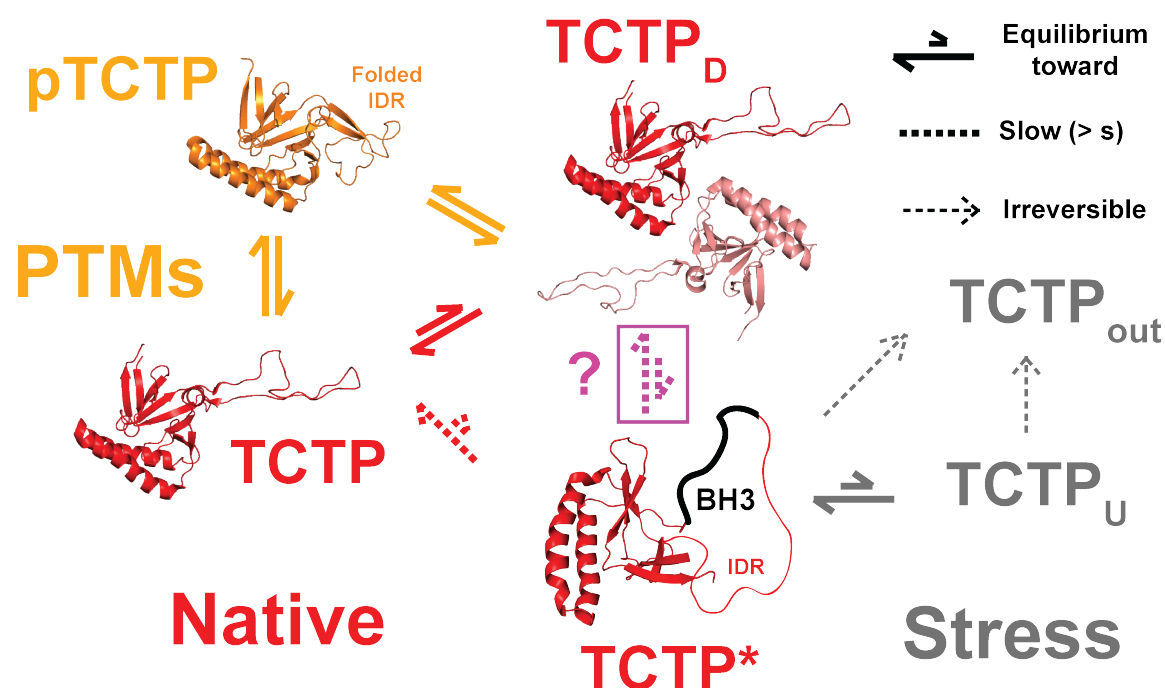


**Fig. 3.21 The diversity of TCTP structure: current model.** TCTP exists as native (TCTP), as dimer (TCTP<sub>D</sub>) and as being phosphorylated (pTCTP) with biological relevance. pTCTP is likely to have a more compact shape due to the IDR preference for contacting the protein core upon modifications. The protein also pre-exists as a minor ( $\leq 1\%$ ), slowly exchanging molten-globule state TCTP\* that is promoted by temperature, urea and pressure. In TCTP\*, the residue stretch including the BH3-like motif and IDR part are unstructured and solvent-exposed. TCTP can also totally unfold (TCTP<sub>U</sub>) and the protein finally aggregates over time (hrs) if incubated at higher temperatures ( $\geq 40\text{ }^\circ\text{C}$ ) or low pH in the TCTP\* state (TCTP<sub>out</sub>).

protein-protein interaction. We reported additional work to characterize Plk-1 mediated phosphorylation of TCTP and its impact on the IDR structure and dynamics as well as on TCTP dimer equilibrium (Sec. 3.1.3). Indeed, we show that S46 phosphorylation promotes the non-covalent TCTP dimer.

Decisively, we have demonstrated that the protein also pre-exists as a minor ( $\leq 1\%$ ), slowly exchanging molten-globule state TCTP\* that is promoted by temperature, urea and pressure (Fig. 3.21). We also demonstrated that TCTP\* was an exclusive dimer in our conditions. That could open the door to propose TCTP<sub>D</sub> as a promoter of TCTP\* conversion, since the latter is promoted in high TCTP<sub>D</sub> content setups. Conversion between TCTP structures occurs immediately upon covalent modification (phosphorylation), ligand binding and protein concentration changes. Most interestingly, conversion between TCTP and TCTP\* takes about 2 hrs to complete at generally non-denaturing urea concentration for most proteins (2.5 M). This slow, limiting step in the conversion routes of TCTP structures is the door to

---

full protein unfolding and aggregation. In TCTP\*, the residue stretch including the BH3-like and IDR part are unstructured and solvent-exposed, questioning how the order-to-disorder transition in the BH3-like motif could enhance interactions with Bcl-2 family proteins that target the sequence. We answer this question in the next chapter of the manuscript.



## Chapter 4

# TCTP & Bcl-2 family proteins Bcl-xL and Mcl-1

In the context of apoptosis, the BH3-like motif in TCTP protein has antiapoptotic function via interactions with the Bcl-2 family proteins Bcl-xL and Mcl-1. TCTP promotes Bcl-xL/Bax association, preventing from MOMP, cytochrome c release and thus apoptosis activation. The crystal structure of TCTP<sub>BH3</sub> in complex with Bcl-xL was published [111], revealing a canonical arrangement for the BH3-like peptide in the BH3-binding groove of Bcl-xL. To fit this structure, the BH3-like motif of TCTP would have to, at least, unpin from the globular domain. Regarding TCTP/Mcl-1, different reports say that TCTP does stabilize Mcl-1 (or vice-versa) or that both proteins stabilize each other [181, 172, 182, 261], also this could be cell-specific. TCTP was proposed to prevent the proteasome-mediated degradation of Mcl-1. Importantly, the binding site of TCTP in Mcl-1 is unknown and the TCTP protein could either mask ubiquitination sites or compete with Mcl-1 partners that would promote the protein destabilization, such as the E3 ligase Mule which has a canonical BH3 motif in its sequence that interacts in the BH3 binding groove of Mcl-1 (Sec. 1.2.3.2).

In the current chapter, we will investigate to get clues about structure and dynamic changes in TCTP and Bcl-2 family proteins upon complex formation and we will assess the molecular basis for the TCTP-induced reinforcement of Bcl-xL and Mcl-1 antiapoptotic properties. We will first report the characterization of TCTP structure and dynamics upon complex formation with Bcl-2 family partners Mcl-1 and Bcl-xL (Sec. 4.1). We will also describe binding interfaces and structure reorganization in Bcl-xL and Mcl-1 upon binding of both TCTP FL and BH3-like peptide from native TCTP (Sec. 4.2). In addition to TCTP<sub>BH3</sub>, we used the D16I variant which restores the hydrophobic residue in position h1 and Mule<sub>BH3</sub> peptide to compare binding profiles and affinity of canonical and BH3-like sequences (Sec. 4.3). At

the end of the chapter, we will finally propose a model for TCTP/Bcl-xL and TCTP/Mcl-1 interaction (Sec. 4.4) that is fairly consistent with all data.

## 4.1 Structure and dynamics of TCTP upon complex formation

TCTP complexes with Bcl-2 family proteins Bcl-xL and Mcl-1 were reported to form efficiently in particular setups. Alkaline (pH 8-9) conditions, low salt content (50 mM) and high temperature (37 °C) plus incubation time (18 hrs) were necessary to fully assemble TCTP/Bcl-xL complex [111]. In another study, the truncated TCTP  $\Delta$ 1-10 was demonstrated to enhance the interaction with Mcl-1 protein [172], possibly by freeing the BH3-like motif (15-29) in TCTP. However, the atomic details regarding full length TCTP in complex with Bcl-2 family partners Mcl-1 and Bcl-xL are unknown.

In this first section, we report experiments to control protein integrity (considering the harsh conditions to assemble TCTP complexes) and to estimate the hydrodynamic radius of proteins and complexes as well as stoichiometry (Sec. 4.1.1). Then, we describe TCTP in complex with Bcl-xL and Mcl-1 in terms of secondary and tertiary structure by using NMR, CD and limited proteolysis experiments (Sec. 4.1.2). We finally assess if minor state TCTP\* that we characterized in the last chapter (Sec. 3.3) could enable interactions with Mcl-1 (Sec. 4.1.3).

### 4.1.1 Stoichiometry and quaternary structure of TCTP complexes

#### 4.1.1.1 Integrity and hydrodynamic properties of TCTP complexes

Protein degradation can occur in the NMR sample and complex formation can make proteins more sensitive to residual protease by exposition of backbone amide bonds to solvent. To evaluate if protein degradation occurred in  $^{15}\text{N}$ -TCTP complex with Mcl-1  $\Delta$ PEST  $\Delta$ TM (Mcl-1) during the NMR experiments (hrs-days) that we will report in the chapter, we used MS, MALDI-TOF and SDS-PAGE experiments to compare protein integrity in fresh samples and after the measurement time (18 hrs, 35 °C) (Fig. 4.1 A). The MS spectrum of the TCTP/Mcl-1 complex superimposed fairly with both free protein controls. For the mono-charged ion of isolated, fresh TCTP FL and Mcl-1, we estimated a molecular weight of  $19648 \pm 5$  Da and  $18138 \pm 5$  Da, respectively. For both proteins upon complex formation and data acquisition time, these were of  $19645 \pm 5$  Da and  $18134 \pm 5$  Da for fresh  $^{15}\text{N}$ -TCTP FL and Mcl-1, respectively. We could not detect MS peaks significantly raised in intensity upon complex formation or the appearance of other MS peaks after incubation time (18 hrs).

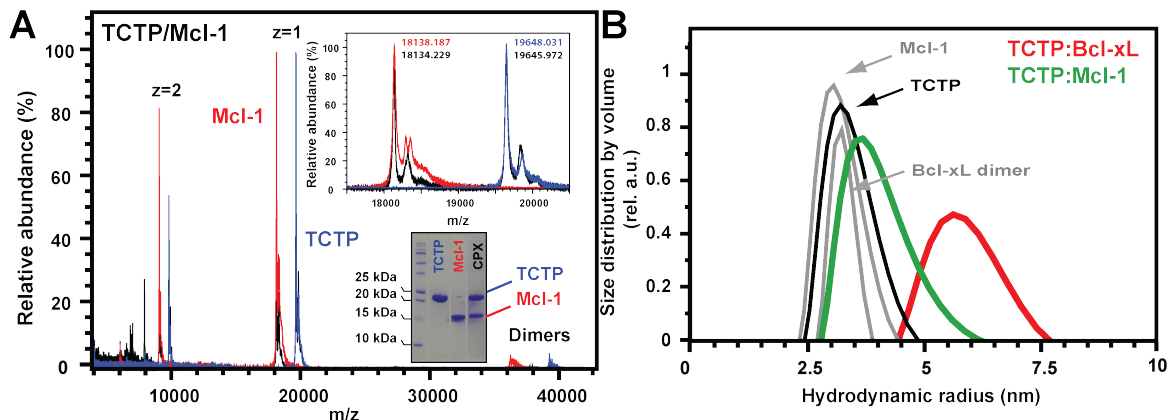


**Fig. 4.1 Evaluation of the integrity and hydrodynamic radius of TCTP/Mcl-1 complex by MS and SDS-PAGE.** (A) Experiments carried out with isolated TCTP (blue curve, first lane), isolated Mcl-1 (red curve, second lane) or a mix of the two (black curve, third lane). Samples were prepared in 50 mM HEPES pH 7.4, 250 mM NaCl and 2 mM TCEP. (B) DLS curves of isolated TCTP FL (black), Mcl-1 ( $\Delta$ PEST  $\Delta$ TM) and Bcl-xL ( $\Delta$ TM) protein (grey) and upon TCTP/Bcl-xL (red) or TCTP/Mcl-1 (green) complex formation. Samples were prepared in 50 mM EPPS pH 8, 50 mM NaCl and 2 mM TCEP. All samples were incubated overnight at 35 °C and complex formation was controlled by NMR prior to analysis.

SDS-PAGE analysis of the samples showed that bands corresponding to isolated proteins are found correspondingly when looking at the protein complex lane. Consequently, TCTP and Mcl-1 do not degrade at detectable levels upon complex formation and after several hours (18 hrs) at high temperature (35 °C).

Experimental conditions were optimized to ensure efficient TCTP complex formation and stability in solution. Higher salt content were shown to result in higher energetic barrier for the complex formation, thus requiring the use of higher temperatures ( $\geq 40$  °C) to efficiently form the complex which possibly impact protein stability. Acidic to neutral conditions (pH 6-7) were not suitable for experiments with full length TCTP, since the related TCTP/Mcl-1 complexes have weak solubility in this condition. After screening of other buffer-agents (detergents, glycerol, ions...) we established that sample conditions of proteins (100  $\mu$ M) with low sodium chloride content (50 mM) in EPPS buffer (pH 8) at 35 °C were optimal to efficiently form the complex between TCTP FL and Bcl-xL or Mcl-1 partners with acceptable lifetime (days) and complex solubility ( $\sim 100$   $\mu$ M). In order to estimate the hydrodynamic radius ( $R_h$ ) of the TCTP complex with Bcl-2 family proteins Bcl-xL  $\Delta$ 27-82  $\Delta$ TM (Bcl-xL) and Mcl-1 in these conditions, we performed DLS experiments. Indeed, such information is important when further doing NMR studies since we want to know size-related parameters of the molecular entity to delineate the impact of molecular size ( $\tau_c$ ) and chemical exchange on line broadening. The DLS experiments were low signal to noise ratio since all three isolated

TCTP, Mcl-1 and Bcl-xL constructs are at the low size limit for DLS measurement. The  $R_h$  of isolated TCTP and Mcl-1 were similar at  $\sim 3$  nm with low reliability regarding the poor sensitivity of DLS experiments at small molecular size. Upon complex formation we measured a  $R_h$  of 5.2 nm and 3.6 nm for TCTP/Bcl-xL and TCTP/Mcl-1, respectively. The TCTP complex with Mcl-1 is likely to be heterodimeric whereas we expect an heterotetramer with Bcl-xL considering the volume difference and the heterotetrameric TCTP<sub>BH3</sub>/Bcl-xL complex [111]. Qualitatively, the polydispersity was greater with TCTP/Bcl-xL complex, suggesting more conformational heterogeneity or different complex stoichiometry. The analysis of the scattering profiles of TCTP/Mcl-1 complex using intensity or volume related distribution representation did not show the presence of high molecular weight ( $> 80$  kDa) assembly upon complex formation and filtering of particle aggregates ( $0.22 \mu\text{m}$ ). Despite poor precision at low  $R_h$  in the DLS measurement, we can conclude that TCTP/Bcl-xL complex is likely to have a higher oligomeric state than TCTP/Mcl-1, for which data suggest a heterodimeric complex predominantly forming in the current experimental setup ( $100 \mu\text{M}$ , pH 8).

#### 4.1.1.2 Heterogeneity of TCTP complexes with Bcl-xL or Mcl-1

We questioned the heterogeneity of the TCTP/Bcl-2 family protein assemblies in term of stoichiometry by doing SEC coupled with SAXS on isolated TCTP and upon complex formation at two increasing ratios (1:2, 1:4, TCTP:partner) with Bcl-xL  $\Delta 45-84 \Delta\text{TM}$  (Bcl-xL) (SEC) or Mcl-1 (SEC-SAXS). The SEC profile of isolated TCTP showed the characteristic single peak at  $t_{\text{elution}} = 9.8$  min (pH 9, Agilent Bio SEC-5) and  $V_{\text{elution}} = 15.7$  mL (pH 8, S200 10/300 Increase) (Fig. 4.2 A, B). At pH 9, two peaks from TCTP complex with Bcl-xL are seen at lower elution volume  $t_{\text{elution}} = 8.25$  min. (\*\*) and  $t_{\text{elution}} = 9.1$  min. (\*). Aggregates were also eluted at  $t_{\text{elution}} = 5.5$  min) (Fig. 4.2 A). It is likely that the peak (\*) originates from an heterotetramer whereas the peak (\*\*) is possibly an higher oligomer. With Mcl-1 protein, we detected only two peaks, presumably including free TCTP since one peak from TCTP/Mcl-1 sample is at same elution volume than isolated TCTP (Fig. 4.2 A). However, Mcl-1 complex with TCTP is detected in this fraction with  $V_{\text{elution}} = 15.7$  mL at pH 8 and  $t_{\text{elution}} = 9.8$  min. at pH 9, also suggesting that the assembly is a compact heterodimer in the elution fraction (\*) (Fig. 4.2 B). The major peak (\*\*) at pH 9 with  $t_{\text{elution}} = 8.5$  mL also contains both TCTP and Mcl-1 and it is likely an higher or a mix of complex oligomers as seen by the lower elution volume that indicates higher apparent hydrodynamic radius. At pH 8, which corresponds to the alkaline condition in NMR experiments reported latter, the presumably heterodimeric TCTP/Mcl-1 was predominantly found whereas higher soluble oligomers were markedly less soluble. We can propose that higher complex oligomers

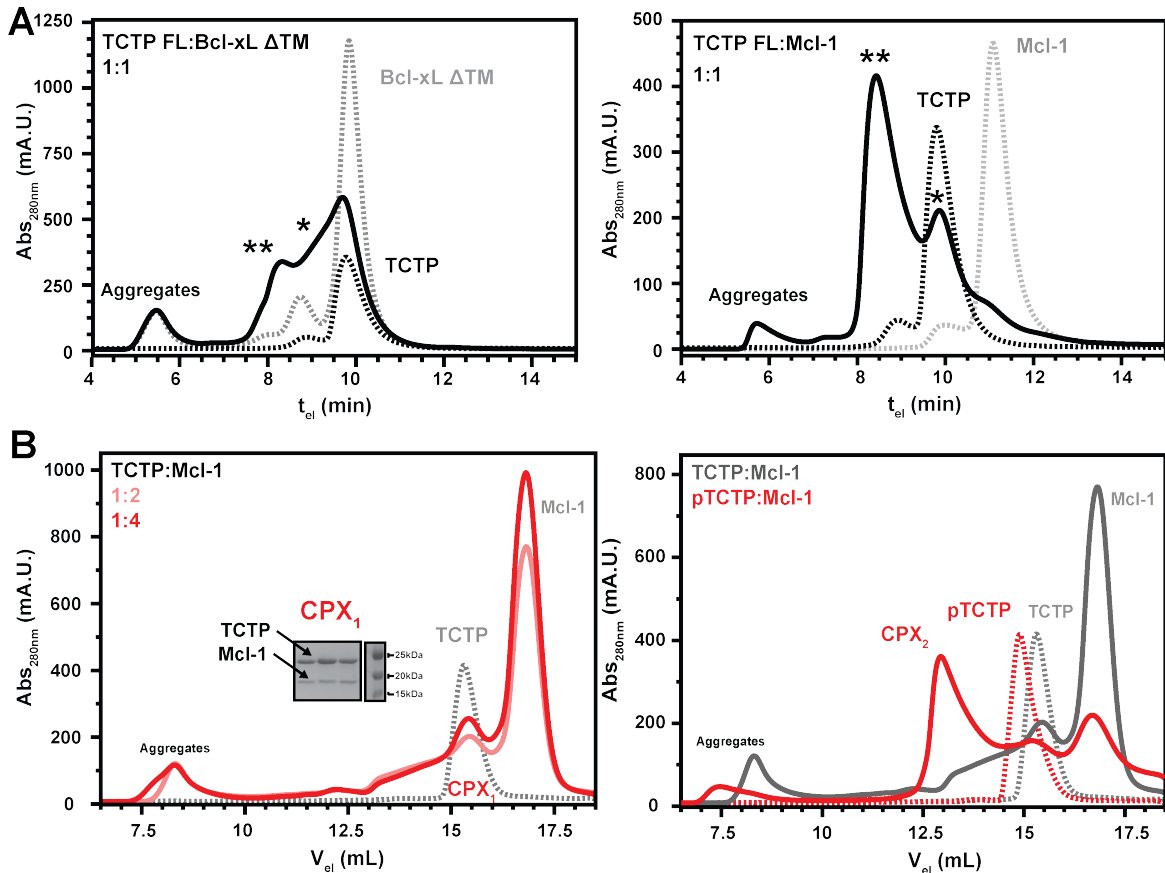


**Fig. 4.2 Heterogeneity of TCTP/Bcl-xL and TCTP/Mcl-1 complexes by SEC.** (A) SEC elution profiles from isolated TCTP (500  $\mu$ M) (black, dashed), isolated (grey, dashed) Bcl-xL  $\Delta$ TM (left) or Mcl-1 (right) and an equimolar mix of each with TCTP (black). Samples were prepared at pH 9 in CHES buffer (50 mM) for this particular experiment and samples injected into a Agilent Bio SEC-5 column. (B) SEC elution profiles from isolated (500  $\mu$ M) (black, dashed) (left) TCTP or (right) pTCTP and from 1:2 (pink) to 1:4 (red) TCTP:Mcl-1 ratio. Samples were prepared in 50 mM EPPS pH 8, 50 mM NaCl, 2 mM TCEP and all incubated 2 hrs at 37°C prior to SEC injection into S200 Increase column.

predominantly aggregate in less alkaline condition (pH 8), improving sample homogeneity for further NMR studies. We also found that phosphorylated TCTP promotes the solubility of higher oligomeric states of the TCTP/Mcl-1 complex (Fig. 4.2 B). Indeed, these higher oligomeric states were minor at pH 8 with non-phosphorylated TCTP whereas they turned major with pTCTP in the same conditions. Truncation of TCTP1 signature and TCTP IDR led to less soluble complexes with Bcl-xL (Ann. 12) and Mcl-1 (Ann. 13). These complexes form with no major difference regarding efficiency and experimental setup. Together with DLS experiments, we can conclude that TCTP forms heterogeneous complexes with Bcl-xL and

Mcl-1, with possibly major heterotetrameric and heterodimeric stoichiometry, respectively and in alkaline condition (50 mM NaCl, pH 8).

#### 4.1.1.3 Molecular size and stoichiometry of the major TCTP/Mcl-1 complex

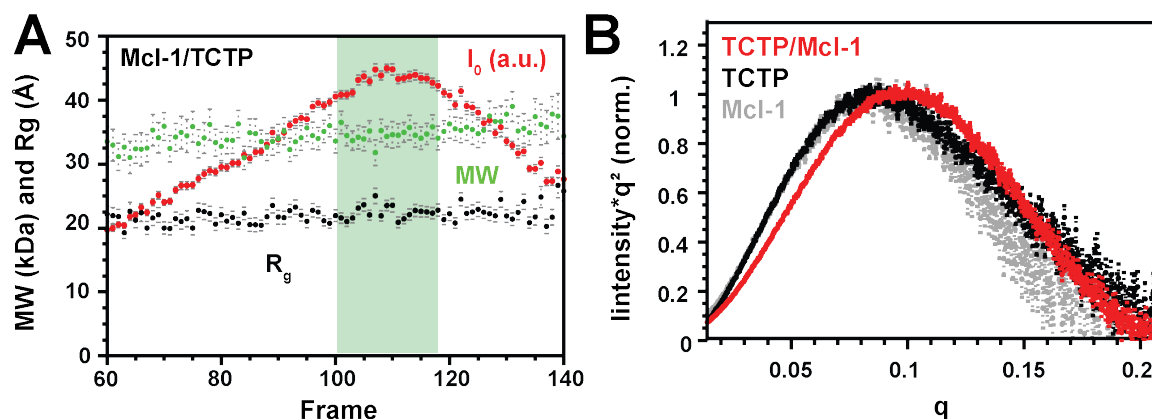


**Fig. 4.3 Molecular size and stoichiometry of TCTP/Mcl-1 complex.** (A) SAXS profile of TCTP/Mcl-1 complex with initial signal intensity ( $I_0$ ) (red), MW (green) and radius of gyration ( $R_g$ ) (black) along the frames that correspond to elution time from SEC separation. The frame interval where MW and  $R_g$  are stable (green background) was used to compute effective MW and  $R_g$  and correspond to maximum  $I_0$  values, with optimal signal to noise ratio. (B) Kratky plot ( $q^2 I_q(q)$ ) from SAXS experiments done with TCTP (black), Mcl-1 (grey) and TCTP/Mcl-1 (red). Experiments were done at 25 °C in the following buffer: 50 mM EPPS pH 8, 50 mM NaCl, 2 mM TCEP and SAXS run was coupled with SEC separation (Fig. 4.2 B, left) prior to measurement.

In order to be decisive regarding the stoichiometry of the predominant TCTP/Mcl-1 complex in alkaline conditions used in NMR (pH 8), we coupled SEC with on-line SAXS and we determined all three radii of gyration ( $R_g$ ), MW and flexibility (Kratky plot) in the TCTP/Mcl-1 complex (Fig. 4.1.1.3). The estimated MW for the TCTP/Mcl-1 complex was  $34.7 \pm 1.9$  kDa whereas we expect 37.4 kDa from the sum of MW for each protein (Fig. 4.1.1.3 A). The small difference can be explained by the residual free TCTP (< 5 %) that is co-eluted with the complex since they both have similar hydrodynamic properties. Indeed, this could lead to a slight decrease of the apparent MW by population average, explaining the small difference between experimental and theoretical values of MW for TCTP/Mcl-1 complex. The corresponding radius of gyration ( $R_g$ ) was  $2.22 \pm 0.09$  nm which is consistent with typical values for a  $\pm 35$  kDa, globular protein or complex. By comparison, we reported isolated TCTP having a  $R_g$  of 2.15 nm (Sec. 3.1.3.2) which is consistent with the presence of the flexible loop in the protein and very similar to the value computed for the complex. This is fairly consistent with previous observations from DLS and SEC experiments that all show similar diffusion-related properties for free TCTP and complex with Mcl-1. This

is an indication that the protein complex is compact and does not contain long disordered segments. To further evaluate the flexibility in TCTP/Mcl-1 complex, we compared the Kratky plots from isolated TCTP and Mcl-1 to TCTP/Mcl-1 complex (Fig. 4.1.1.3 B). With a bell shape and near to zero values at high diffusion angle ( $q$ ), the Kratky plot of Mcl-1 protein was typical of a globular, well folded protein. This means that no significant flexibility was found in the protein backbone, consistently with the NMR structure of the protein (pdb code: 2MHS). The Kratky plot from TCTP was similar but higher values were computed at higher  $q$ , consistently with the IDR segment found in the protein. When looking at the Kratky plot from TCTP/Mcl-1 complex, we observe a roughly similar shape, meaning that the complex is essentially globular. TCTP/Mcl-1 had smaller flexible residues fraction than TCTP but greater than Mcl-1, which simply indicates that no major unfolding event took place upon complex formation. Still, significant differences were observed at lower  $q$ , usually informing on protein sample polydispersity. That might be an indication about the heterogeneity of the hydrodynamic volumes from all TCTP/Mcl-1 complexes that co-exist in solution. Such heterogeneity was lower in this case compared to isolated TCTP or Mcl-1. In conclusion, TCTP and Mcl-1 assemble to form a tight, compact heterodimeric complex that we will further study in the next two sections.

## 4.1.2 Structure of TCTP upon binding to Bcl-2 family partners

### 4.1.2.1 Slow complex formation and consequence on structure and dynamics

We then wanted to describe TCTP structure and dynamics upon complex formation with Bcl-xL or Mcl-1. To do so, we first recorded  $^1\text{H}$ - $^{15}\text{N}$  SOFAST HMQC spectra of isolated  $^{15}\text{N}$ -TCTP FL and upon addition of unlabeled Bcl-2 family partners (1.5 eq.). We tested each Bcl-xL construct ( $\Delta\text{TM}$ ,  $\Delta 45\text{-}84\Delta\text{TM}$ ,  $\Delta 27\text{-}82\Delta\text{TM}$ ) (Bcl-xL) and Mcl-1  $\Delta\text{PEST}$   $\Delta\text{TM}$  (Mcl-1). Protein complexes were efficiently formed ( $> 95\%$ ) at  $35\text{ }^\circ\text{C}$  after about 2 hours of equilibration time. Upon each increment of Bcl-xL or Mcl-1 we observed a similar progressive decrease in the intensity of TCTP spectrum from structured parts and the slow appearing of a limited number of resonances from bound TCTP ( $\sim 10\text{-}15$ ), mostly broadened which is likely due to conformational exchange (ms) or increased correlation time ( $\tau_c$ ). Significant rapid exchange shift could be observed from TCTP residues such as F83 at the TCTP dimer interface upon addition of partner in TCTP sample (Fig. 4.4). To confirm that these chemical shift perturbations were not related to TCTP interaction with partners, we used TCTP  $\Delta\text{IDR}$  which does not form dimer and observed that all perturbations were canceled upon complex formation, as expected (Fig. 4.5). Thus, the chemical shift variation observed in TCTP spectra upon complex formation with Bcl-xL and Mcl-1 is due to the

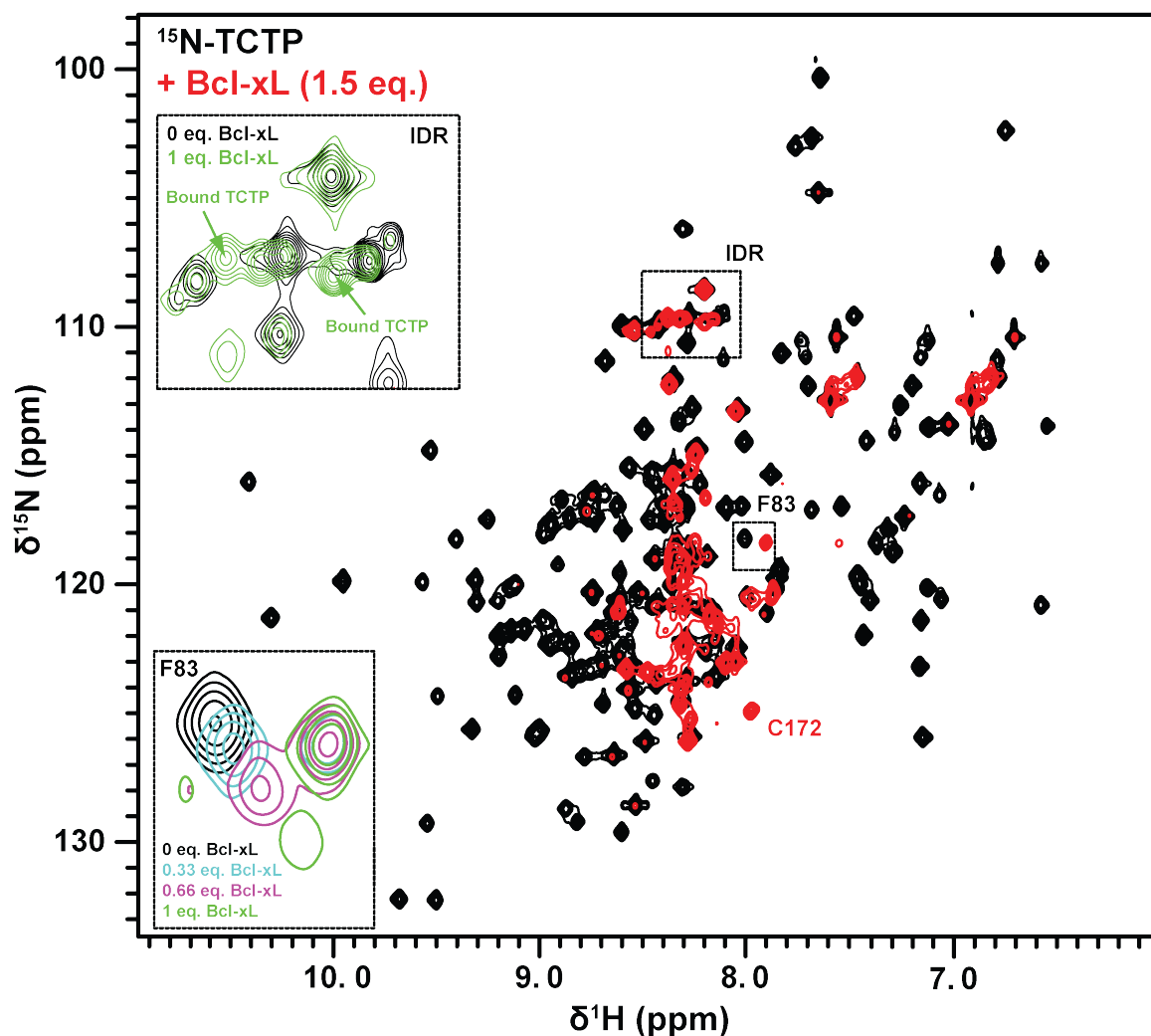


Fig. 4.4 **TCTP upon complex formation with Bcl-xL.** Overlay of  $^1\text{H}$ - $^{15}\text{N}$  SOFAST HMQC spectra from isolated  $^{15}\text{N}$ -TCTP FL (500  $\mu\text{M}$ ) (black) and in presence of unlabeled Bcl-xL  $\Delta 45\text{-}84\Delta\text{TM}$  (1.5 eq.) (red). The frame (top-left) represents the spectra of free and bound TCTP at intermediate Bcl-xL concentration (1 eq.) (green), allowing to estimate the relative population of free/bound TCTP ( $\pm 50\%$ ) at this ratio. The second frame (bottom-left) depicts the spectral change corresponding to TCTP monomer-dimer re-equilibration upon complex formation. Experiments were recorded at 950 MHz and 35  $^\circ\text{C}$  in the following buffer: 50 mM HEPES pH 7.4, 50 mM NaCl, 2 mM TCEP and 5%  $\text{D}_2\text{O}$  / 95%  $\text{H}_2\text{O}$ .

reduced free TCTP concentration and subsequent dissociation of TCTP dimer. Together, only  $\sim 60$  crosspeaks over the expected  $\sim 160$  crosspeaks were visible in the spectrum of TCTP complex with Bcl-xL or Mcl-1. These crosspeaks were in the typical region for unfolded proteins or loops and show similar patterns as the IDR in the free TCTP protein. Overall, this indicates that only a single binding event with slow kinetics could be detected in TCTP  $^1\text{H}$ - $^{15}\text{N}$  SOFAST HMQC upon Bcl-xL or Mcl-1 addition. This leads to dramatic changes in

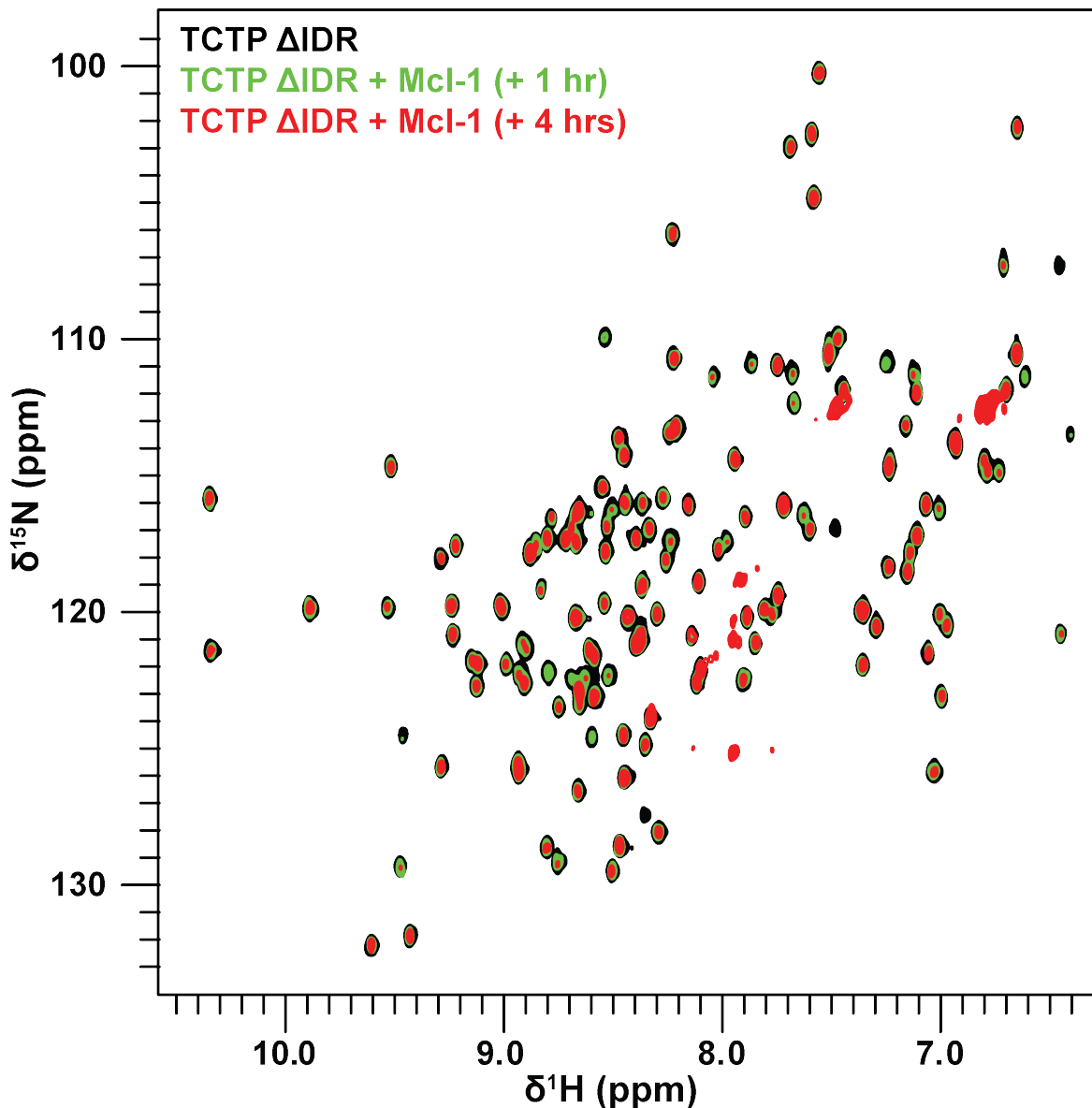
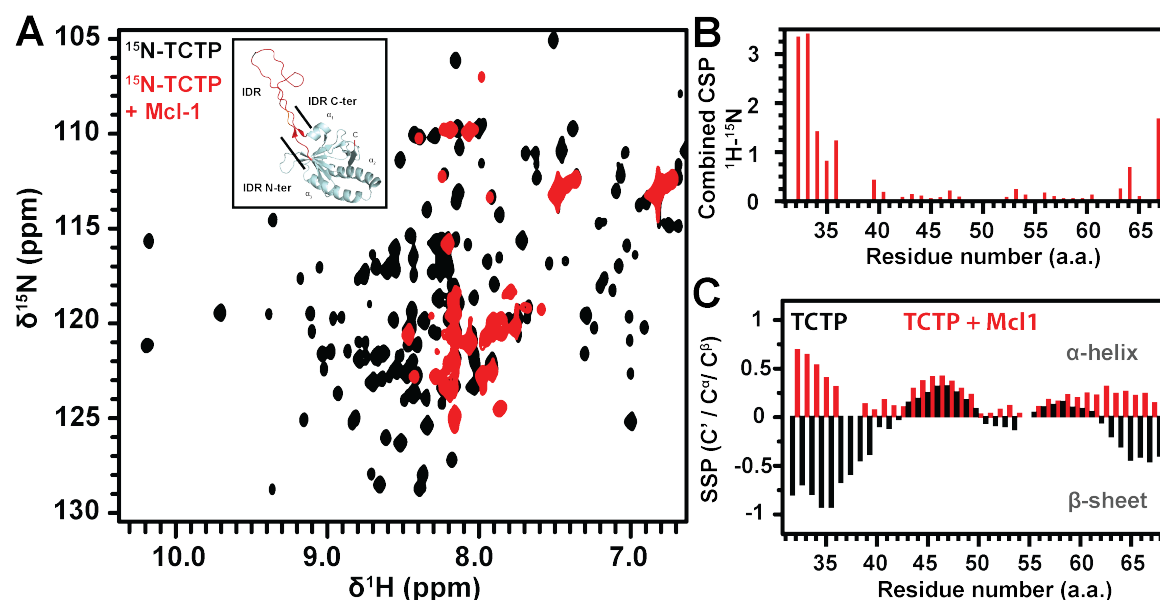


Fig. 4.5 **Binding of TCTP  $\Delta$ IDR to Mcl-1.** Overlay of  $^1\text{H}$ - $^{15}\text{N}$  SOFAST HMQCs from isolated TCTP  $\Delta$ IDR (50  $\mu\text{M}$ ) (black), upon addition of Mcl-1 (3 eq.) after short (1 hr) (green) and long (4 hrs) (red) system equilibration. Experiments were recorded at 950 MHz and 25  $^\circ\text{C}$  in the following buffer: 50 mM EPPS pH 8, 50 mM NaCl, 1 mM TCEP and 5 %  $\text{D}_2\text{O}$ .

protein structure and dynamics, as judged from the severe line broadening in bound TCTP spectrum that can not be only linked with the molecular size for the heterodimeric TCTP/Mcl-1 complex (Sec. 4.1.1.3). For the heterotetrameric TCTP/Bcl-xL complex ( $\sim 80$  kDa), it is possible that the molecular size, through the correlation time ( $\tau_c$ ), contributes in the line broadening seen in bound TCTP spectrum. For this reason, we mainly worked with

TCTP/Mcl-1 complex since we can eliminate a  $\tau_c$  related explanation for the line broadening TCTP spectrum upon complex formation.

#### 4.1.2.2 NMR assignment and structure near the BH3-like region



**Fig. 4.6 Backbone assignment and structure in TCTP FL complex with Mcl-1.** (A) Overlay of  $^1\text{H}$ - $^{15}\text{N}$  SOFAST HMQC spectra from isolated  $^{15}\text{N}$ -TCTP FL (250  $\mu\text{M}$ ) (black) and in complex with unlabeled Mcl-1 (1.5 eq., red). The residue stretch we could assign in bound TCTP is highlighted (red) in TCTP structure (pdb code: 2HR9). (B) Combined  $^1\text{H}$ - $^{15}\text{N}$  chemical shift perturbations calculated between  $^1\text{H}$ - $^{15}\text{N}$  spectra from free and bound TCTP in the residue stretch (V31-V70) we assigned. (C) Secondary Structure Propensity (SSP) [262] computed for isolated TCTP (black) and in complex with Mcl-1 (red). Positive values indicate  $\alpha$ -helix propensity whereas negative values indicate  $\beta$ -sheet propensity. Experiments were recorded at 950 MHz and 25  $^\circ\text{C}$  in the following buffer: 50 mM EPPS pH 8, 50 mM NaCl and 2 mM TCEP in 95 %  $\text{H}_2\text{O}$  / 5 %  $\text{D}_2\text{O}$ .

#### Liquid-state NMR

In order to characterize bound TCTP structure and dynamics, we used experiments such as HNCOCACB and HNCACB (Sec. 2.3.1.3) to assign the visible part of the protein backbone. The NMR assignment was completed up to 40 residues (V31-V70) that correspond to the TCTP IDR and extensions (Fig. 4.6 A). Although the BH3-like motif was not visible in the bound TCTP spectrum, this still allows to probe the structure of the motif (15-29) since V31 is localized right upstream of the residue stretch (V31-V70) we could assign. We used temperature to probe solvent-exposed regions or intermediate exchange (ms) in bound TCTP that could be advantageously modulated by temperature variation. Indeed, we can use temperature to obtain more resolved crosspeaks since lower

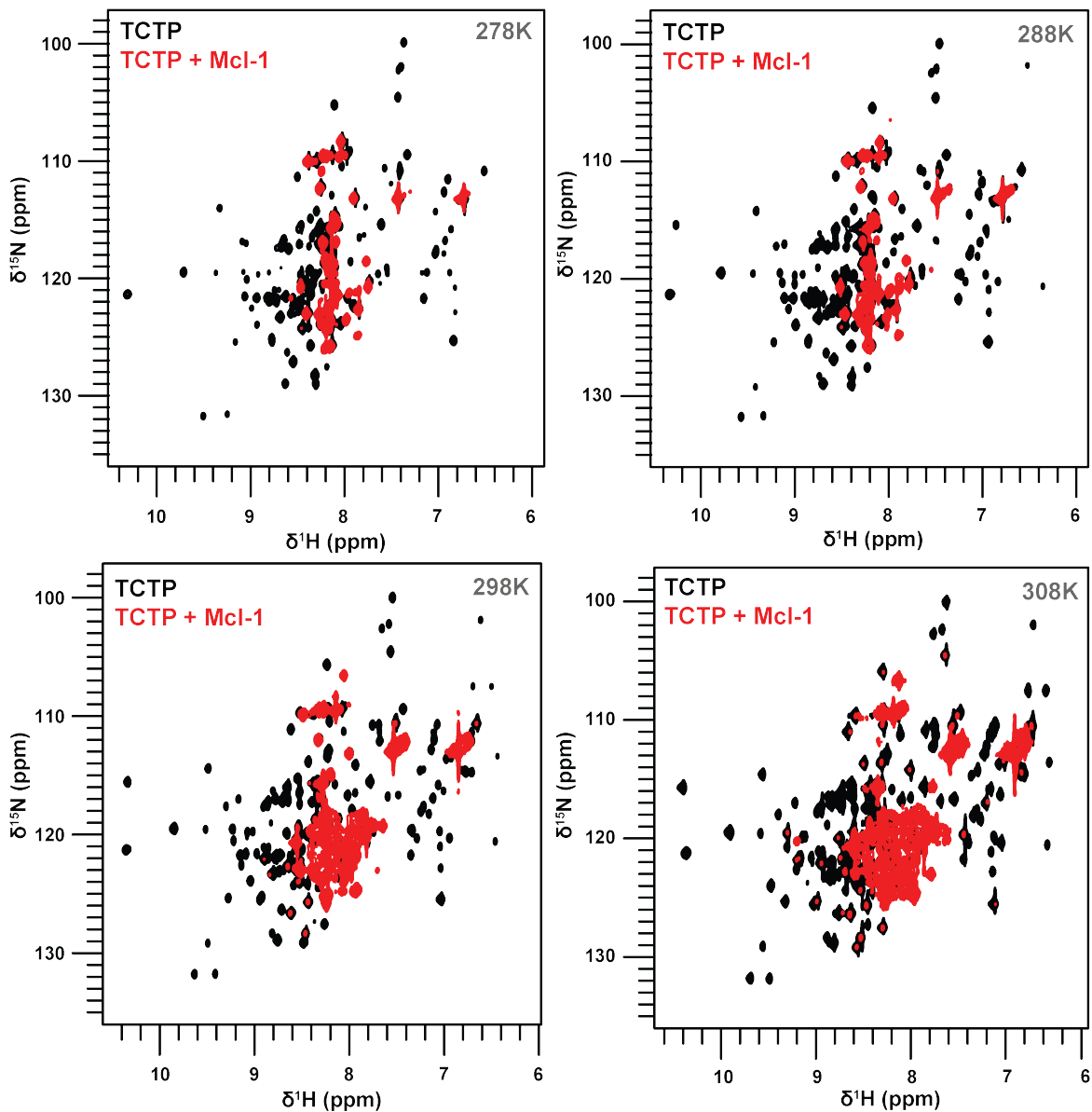


**Fig. 4.7 TCTP in complex with Mcl-1: impact of temperature.** Overlay of  $^1\text{H}$ - $^{15}\text{N}$  SOFAST HMQC spectra from isolated  $^{15}\text{N}$ -TCTP (black) and in complex with unlabeled Mcl-1 (red) at different temperatures. Tested temperatures are explicated (grey). Experiments were recorded at 950 MHz in the following buffer: 50 mM EPPS pH 8, 50 mM NaCl and 2 mM TCEP in 95 %  $\text{H}_2\text{O}$  / 5 %  $\text{D}_2\text{O}$ .

temperatures slow down both solvent and chemical exchange, sharpening crosspeaks. Thus, we recorded  $^1\text{H}$ - $^{15}\text{N}$  SOFAST HMQC spectra of isolated  $^{15}\text{N}$ -TCTP FL and upon addition of unlabeled Mcl-1  $\Delta\text{PEST } \Delta\text{TM}$  (Mcl-1) from low (5 °C) to high (35 °C) temperature (Fig. 4.7). Residues from the C-terminal extension of the bound TCTP IDR (V66-V70) were only visible at low temperature, suggesting that conformational exchange (ms) or

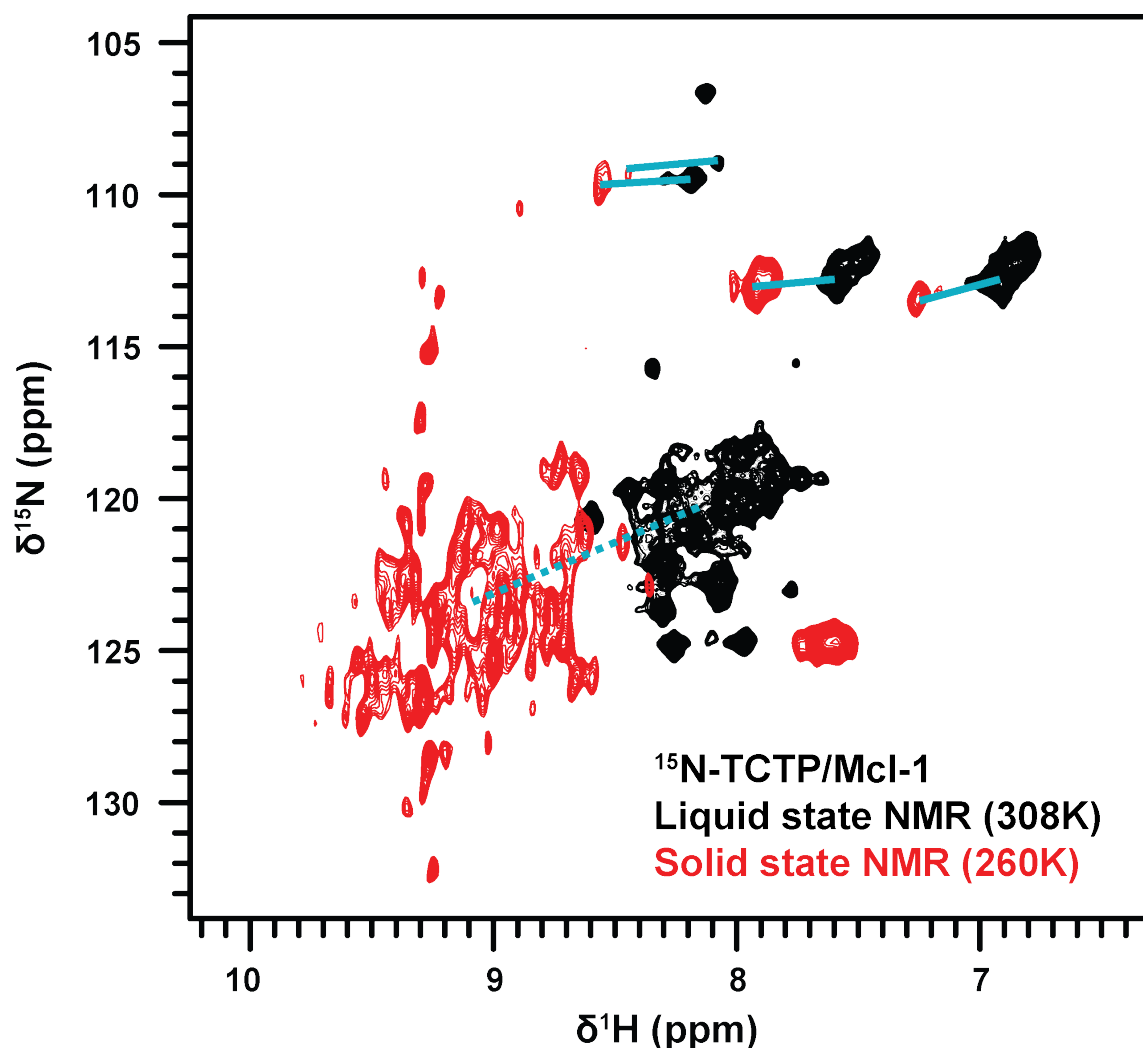


Fig. 4.8 TCTP in complex with Mcl-1: solid state NMR. Overlay of  $^1\text{H}$ - $^{15}\text{N}$  SOFAST HMQC from  $^{15}\text{N}$ -TCTP in complex with unlabeled Mcl-1 (35 °C, liquid state) (black) and INEPT HSQC  $^1\text{H}$ - $^{15}\text{N}$  from the same sample after precipitation in acidic conditions (pH 6.5) and preparation of the 1.3 mm rotor for solid state NMR (260 K, 55 kHz) (red). Experiments were recorded at 800 MHz (liquid state NMR) and 600 MHz (solid state NMR) and the sample was initially prepared in the following buffer: 50 mM EPPS pH 8, 50 mM NaCl and 2 mM TCEP in 95 %  $\text{H}_2\text{O}$  / 5 %  $\text{D}_2\text{O}$ .

solvent exchange takes place at 25 °C in the short residue stretch that consists in a  $\alpha$ -helix in the free TCTP structure (Fig. 4.7). Globally, the TCTP IDR is also best visible at low temperature, especially in the TCTP1 signature (49-55) from which resonances could mostly not be found at higher temperature (35 °C). The slower solvent-exchange rate at lower temperature probably increases the spectral quality for the IDR region while the very rapid solvent exchange rate at 35 °C (and pH 8) leads to poor spectral quality. Differently, the N-terminal extension of TCTP IDR downstream the BH3-like motif of the protein was only

visible at higher temperature ( $> 25$  °C), suggesting that the segment (31-38) is included in a more rigid structure with backbone HN protected from solvent exchange.

To further describe the structure of NMR-visible bound TCTP, we computed combined  $^1\text{H}$ - $^{15}\text{N}$  chemical shift perturbations and intensity ratios between  $^1\text{H}$ - $^{15}\text{N}$  SOFAST HMQC spectra of isolated TCTP FL and upon complex formation with Mcl-1 (Fig. 4.6 B). The TCTP IDR did not show important perturbations in terms of chemical shift and relative intensity upon complex formation, indicating the IDR has similar dynamics and environment in both free and bound TCTP. Large perturbations could be observed in the segments V31-R38 and V66-V70 from the N- and C- terminal IDR extension, respectively, that form a short  $\beta$ -sheet at the bottom of the IDR (Fig. 4.6 C). Considering the sequence proximity of segment V31-R38 and the BH3-like motif (15-29), we expect the V31-R38 segment to probe the possible structure change in the BH3-like region upon complex formation with Mcl-1, even though we could not directly characterize the BH3-like motif of TCTP in its bound state.

To deeper characterize the structural transition ongoing in TCTP upon complex formation with Mcl-1, we analyzed  $^{13}\text{C}$  chemical shifts from carbon (C, C', C $\alpha$  and C $\beta$ ) in free and bound TCTP protein spectra since they inform on the chemical environment and secondary structure definition at the residue-scale. We used that precisely to detect the expected  $\beta$ -sheet to  $\alpha$ -helix structure transition in the BH3-like region (15-29) and we computed Secondary Structure Prediction (SSP) that quantify the susceptibility of a given amino-acid to contribute in  $\alpha$ -helix,  $\beta$ -sheet (Fig. 4.6 B) or random coil (SSP close to 0). Above an absolute value of two, SSP score indicates a fully formed secondary structure element whereas below it depicts a tendency to form either  $\alpha$ -helix ( $> 0$ ) or  $\beta$ -sheet ( $< 0$ ). SSP score showed that N- and C- terminal extensions of TCTP IDR (residues V31-R38, V66-V70) have high  $\beta$ -sheet propensity in the isolated protein whereas this turned to  $\alpha$ -helix propensity in the bound TCTP. For the V31-R38 segment, it is likely that we probe here the structure transition in the BH3-like motif (15-29) that is expected to convert from  $\beta$ -sheet to  $\alpha$ -helix upon complex formation.

We can conclude that  $\beta$ -strands  $\beta_5$  and  $\beta_6$  separate in TCTP upon complex formation with Mcl-1 and form more helical structures. The BH3-like region itself was not visible in the NMR spectra at any temperature. This could originate from line-broadening due to intermediate exchange on the chemical shift timescale (ms) inside the complex, at the molecular interface. Finally, most of the residues from D71-K171 remained not visible in the NMR spectrum, which is going to be further investigated.

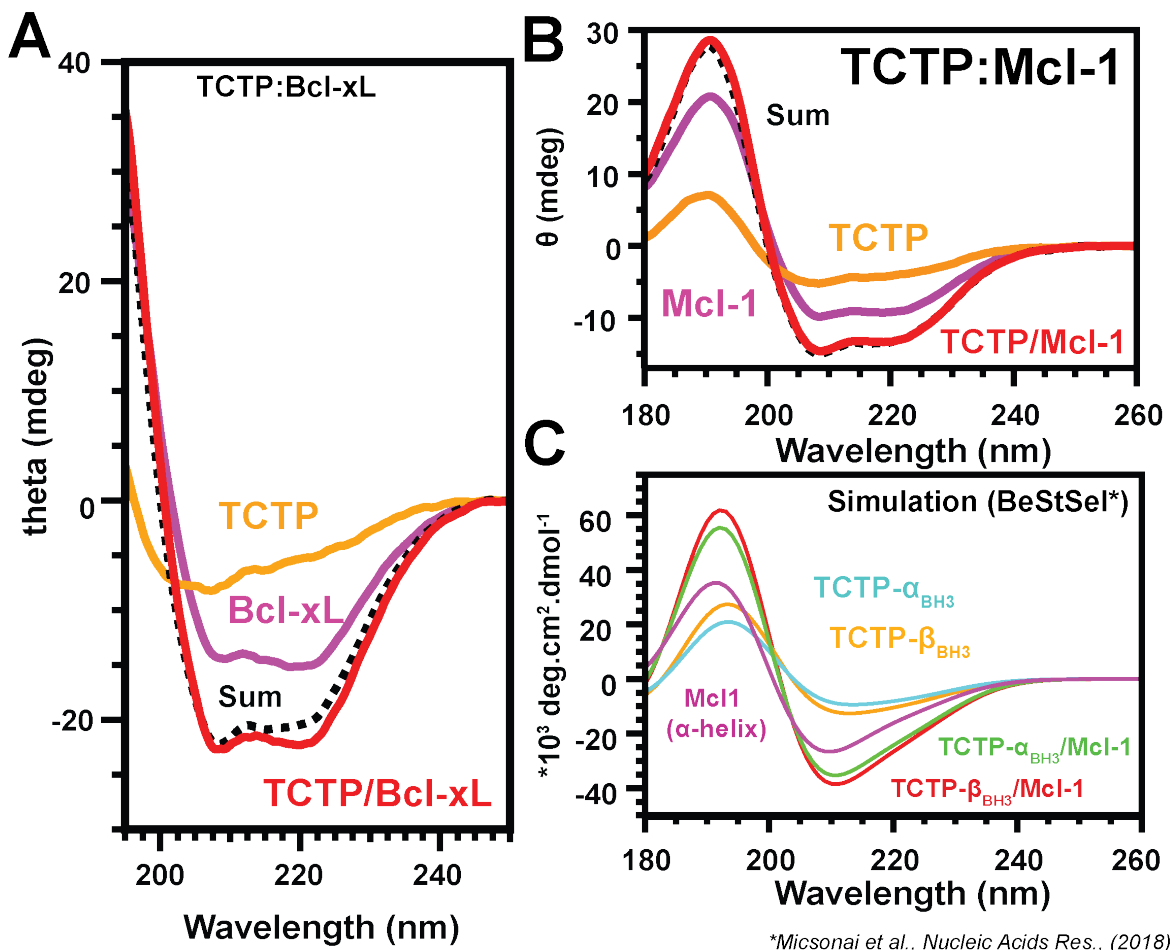
### Solid-state NMR

In order to both recover signals from bound  $^{15}\text{N}$ -TCTP and to test if the protein dynamics in complex with Mcl-1 could be modulated in solid state, we also worked with A. Vallet (IBS, CNRS/Université Grenoble Alpes) who led solid state NMR (ssNMR) experiments on the TCTP complex with Mcl-1. The sample of  $^{15}\text{N}$ ,  $^{13}\text{C}$ -labeled TCTP complex with Mcl-1 was precipitated in acidic conditions (pH 6.5) and washed with pure water prior to the measurement of  $^1\text{H}$ - $^{15}\text{N}$ ,  $^1\text{H}$ - $^{13}\text{C}$  Cross Polarization (CP) and Inensitive Nuclei Enhanced by Polarization Transfer (INEPT) HSQC experiments with a BCUII airflow set to 260 K (sample temperature  $\sim 295$  K) and using a 1.3 mm rotor and MAS rotation of  $\sim 55$  kHz at 600 MHz (Bruker Avance III HD). We report a comparison between the liquid state  $^1\text{H}$ - $^{15}\text{N}$  SOFAST HMQC spectrum of the complex as reference and the  $^1\text{H}$ - $^{15}\text{N}$  INEPT HSQC obtained by solid state NMR (Fig. 4.8). Despite the temperature ( $\sim 13$  K), acidic conditions (pH 6.5) and the solid nature of the sample, the overall ssNMR spectra was rather similar to the liquid state reference experiment considering the crosspeaks position relative to each other. Indeed, we also observed very broad resonances in the central region of the ssNMR spectrum with poor signal dispersion. Moreover, we could identify a pattern of crosspeaks from TCTP IDR residues that is found in both liquid and solid state NMR spectra, indicating that these residues have similar environment in both conditions. Thus, it is unlikely that TCTP could be included in large, spherical oligomers in solid state since the IDR is solvent-exposed in solution. Interestingly, we could observe in ssNMR experiments a fast transverse ( $T_2$ ) relaxation time for TCTP in complex with Mcl-1 partner. Indeed, most of the whole spectral intensity was lost by applying a 2 ms relaxation delay in the xy plane before acquisition. This signifies either that TCTP undergoes conformational exchange ( $\mu\text{s}$ -ms) in the complex with Mcl-1, as also seen in liquid state NMR. In conclusion, we showed that TCTP complexes with Bcl-2 family proteins assemble slowly and the TCTP protein undergoes a dramatic structure and dynamics change upon complex formation with rearrangement from  $\beta$ -sheet to  $\alpha$ -helix near the BH3-like region.

#### 4.1.2.3 Molten-globule properties of TCTP in complex

##### Far-UV CD experiments

We have further characterized the secondary and tertiary structure organization of TCTP/Mcl-1 complex by doing CD spectroscopy in far-UV (205-260 nm) that inform on the secondary structure definition in a protein, respectively (Fig. 4.9). The far-UV CD spectrum of isolated TCTP contains contributions from  $\alpha$ -helix,  $\beta$ -sheet and random coil elements in the protein and consequently it does not fit either of the three templates for secondary structure types ( $\alpha$ -helix,  $\beta$ -sheet, random coil). CD theta values were positive at low wavelength ( $< 200$  nm)



\*Micsonai et al., *Nucleic Acids Res.*, (2018)

**Fig. 4.9 Secondary structures in TCTP and complexes with Bcl-xL or Mcl-1.** (A) Far-UV CD experiments on isolated TCTP (orange), isolated Bcl-xL  $\Delta 27-82 \Delta \text{TM}$  (magenta), sum of the two previous CD experiments (black, dashed) and experimental CD of the equimolar mix of the two proteins (red). (B) Far-UV CD experiments on isolated TCTP (orange), isolated Mcl-1  $\Delta \text{PEST} \Delta \text{TM}$  (magenta), sum of the two previous CD experiments (black, dashed) and experimental CD of the equimolar mix of the two proteins (red). All samples were pre-incubated at 50  $\mu\text{M}$  each overnight at 37  $^\circ\text{C}$  in 5 mM phosphate buffer pH 8. (C) Theoretical prediction of CD curves for native TCTP (cyan), TCTP with BH3 transition to  $\alpha$ -helix (orange), Mcl-1 (magenta). Sum of Mcl-1 curve plus native TCTP curve (red) or with BH3 refolding (green) are shown. The difference between the two last ones illustrates the required sensitivity to gain experimental insights in the refolded state.

and negative above 200 nm, as sign of well defined secondary structures in isolated TCTP. The CD spectrum of Bcl-xL  $\Delta 27-82 \Delta \text{TM}$  (Bcl-xL) (Fig. 4.9 A) and Mcl-1 (Fig. 4.9 B) are simpler because they only contain the contributions of  $\alpha$ -helices with a major band at 214 nm in the 210-250 nm wavelength interval that corresponds to structured segments. Higher CD theta values for Mcl-1 compared to TCTP at lower wavelength ( $< 200$  nm) are due to the absence of long flexible regions in Mcl-1. Hypothetical CD spectra of the TCTP complex

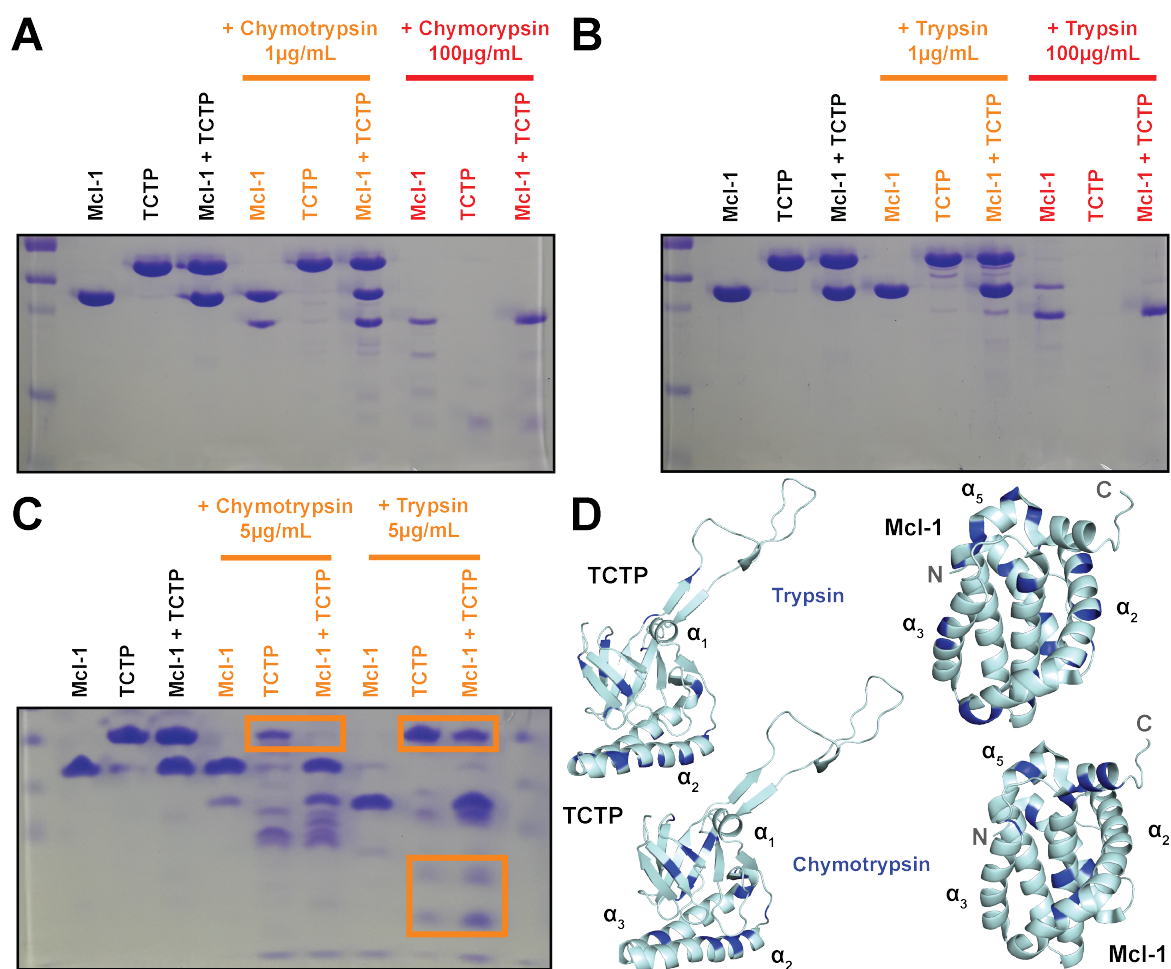


**Fig. 4.10 Control of tertiary structure integrity by limited proteolysis.** Experiments were carried out on concentrated samples (500  $\mu\text{M}$  each protein) considering both isolated TCTP and Mcl-1 as well as an equimolar mix of the two. Limited proteolysis was achieved at low concentration (1  $\mu\text{g}\cdot\text{mL}^{-1}$ ) of chymotrypsin (A) and trypsin (B). Complete digestion as control was achieved at high protease concentration (100  $\mu\text{g}\cdot\text{mL}^{-1}$ ). (C) With intermediate concentration of protease (5  $\mu\text{g}\cdot\text{mL}^{-1}$ ). The orange rectangle highlights the region where the complex formation speeds up protein proteolysis. (D) Representation of theoretical cleavage sites for trypsin and chymotrypsin on TCTP (pdb code: 2HR9) and Mcl-1 (pdb code: 2MHS) structures. Samples were prepared in 50 mM EPPS pH 8, 50 mM NaCl, 2 mM TCEP and all incubated 6 hrs at 37°C.

with Bcl-xL or Mcl-1 were calculated by summing the experimental spectra from separated proteins. Assuming no or limited secondary structure change upon complex formation, the experimental CD spectrum of the complex would be simply the sum of the individual spectra. In contrast, a significant change in secondary structure upon complex formation would be revealed by differences between the experimental spectrum and the sum of individual spectra. Here, the summed CD curves were fairly similar to the experimental CD curves for each TCTP/Mcl-1 and TCTP/Bcl-xL complex, suggesting no or limited secondary structure

change upon complex formation (Fig. 4.9 A, B). Nevertheless, a slight difference in the spectrum region specific of folded elements (210-250 nm) was observed in a reproducible manner, suggesting that a small part of one or both TCTP and Bcl-xL/Mcl-1 partner could slightly change its secondary structure definition upon complex formation. Because the NMR study of Mcl-1 in the complex did not reveal significant secondary structure reorganization (Sec. 4.2.1.2), this difference probably originates from TCTP and more precisely from the BH3-like region that should rearrange from free to bound TCTP, as already suggested (Sec. 4.1.2.2).

We encouraged this hypothesis by simulating far-UV CD spectra of native TCTP and upon BH3-like motif structure transition to  $\alpha$ -helix in the context of both isolated and bound protein. To do so, we used BestSel [218] server and submitted native TCTP structure (TCTP- $\beta_{\text{BH3}}$ ) and upon replacement of the  $\beta$ -sheet BH3-like by an helical motif with same sequence and length (TCTP- $\alpha_{\text{BH3}}$ ) (Fig. 4.9 C). The theoretical difference from  $\alpha$ -helix and  $\beta$ -sheet contribution was small at 200-220 nm, typical of structured regions, and comparable to our experimental data. In conclusion, far-UV CD experiments have demonstrated that both proteins retains high degree of secondary structure definition upon TCTP/Mcl-1 complex formation and are compatible with a refolding of the BH3-like region in TCTP upon interaction with Mcl-1 or Bcl-xL.

### Limited proteolysis

Protein susceptibility to proteolytic cleavage is widely used to map secondary structure elements, molecular interfaces and structural transitions. Such experiments can also inform on fluctuation in a protein tertiary structure, as a characteristic trait of MG state in proteins. Thus, we tested if TCTP and Mcl-1 could exhibit different susceptibility toward proteases in their bound compared to their free states by performing limited proteolysis experiments with trypsin and chymotrypsin, separately. For both TCTP and Mcl-1 proteins, the predicted cleavage sites (at the C-terminus K/R or Y/F/W residues for trypsin or chymotrypsin, respectively) were spread in the whole protein structures (Fig. 4.10 D). Notably, TCTP IDR does not contain cleavage site for any of the two proteases. The SDS-PAGE analysis of all samples first established the stability of protease-free controls under incubation conditions (Fig. 4.10 A-C). Neither isolated proteins or TCTP/Mcl-1 complex did degrade in absence of enzyme. Fully digested control samples at high protease concentration ( $100 \mu\text{g.mL}^{-1}$ ) did yield only one low molecular weight band ( $\sim 10 \text{ kDa}$ ) and no band at all left for chymotrypsin and trypsin mediated degradation of TCTP, respectively. The full digestion of TCTP/Mcl-1 complex contains visible signatures from both digested TCTP and Mcl-1 (chymotrypsin) (Fig. 4.10 A) or only TCTP (trypsin) (Fig. 4.10 B). We achieved limited proteolysis at two

concentrations of protease in the samples ( $1-5 \mu\text{g.mL}^{-1}$ ) in order to prevent from excessive or insufficient protein digestion. At low chymotrypsin concentration ( $1 \mu\text{g.mL}^{-1}$ ) we observed slightly more degradation bands for TCTP/Mcl-1 complex compared to isolated proteins (Fig. 4.10 A), as with low concentration of trypsin (Fig. 4.10 B). Higher concentration of chymotrypsin ( $5 \mu\text{g.mL}^{-1}$ ) amplified the difference with clear disappearing of bands from TCTP upon digestion of the protein complex compared to control (Fig. 4.10 C). Indeed, the native TCTP band completely disappeared in presence of chymotrypsin while it is intense in the isolated TCTP control (orange frame). By contrast, the Mcl-1 degradation is not as sensitive to the presence or absence of TCTP. A similar effect is observed with trypsin mediated limited proteolysis (Fig. 4.10 C).

In conclusion, both proteins retain a packed tertiary structure organization in TCTP/Mcl-1 complex but TCTP either does expose unfolded segments or has a fluctuating tertiary structure since it is more sensitive to proteolysis in complex compared to isolated, a variation also described for MG states in proteins upon transition from a native state.

### 4.1.3 Molten-globule TCTP\* readily interacts with Mcl-1

Interestingly, the spectrum of TCTP in the TCTP\* state (Sec. 3.3.2) has strong similarities with the spectrum of TCTP in complex with Mcl-1: only a subset of residues ( $\sim 80$  in TCTP\*,  $\sim 60$  in complex with Mcl-1) were visible, all of them in the central regions of the  $^1\text{H}-^{15}\text{N}$  SOFAST HMQC spectrum. However, they differ in that more crosspeaks were visible in the spectrum of TCTP\* and they do correspond to the residues F14 to E30 that encompass the BH3-like motif. In TCTP\* this region is unfolded while it is involved in the complex formation with Bcl-xL and presumably Mcl-1. Because the formation of the complexes between the well-folded TCTP and Mcl-1 or Bcl-xL is very slow (min.-hrs), we hypothesized that Mcl-1 or Bcl-xL could interact with TCTP\* in which the BH3-like motif is unpinned and readily accessible to partners rather than with the well-folded TCTP. As we demonstrated, conversion from TCTP to TCTP\* takes similar time compared to the formation of TCTP/Mcl-1 and TCTP/Bcl-xL complexes (2 hrs) and we expect that pre-stabilized TCTP\* could suppress the time requirement to assemble the protein complexes.

In order to prove this hypothesis, we tested the ability of TCTP, initially stabilized in the TCTP\* state with 2.5 M urea, to bind Mcl-1. We first verified that the  $^1\text{H}-^{15}\text{N}$  spectrum of  $^{15}\text{N}$ -Mcl-1 did not show major changes in presence of 2.5 M urea. Then, the  $^1\text{H}-^{15}\text{N}$  SOFAST HMQC spectra of isolated  $^1\text{H},^{15}\text{N}$ -TCTP\* and upon successive additions of unlabeled Mcl-1  $\Delta\text{PEST } \Delta\text{TM}$  (Mcl-1) showed that TCTP\* readily interacts with Mcl-1 and is saturated at equimolar ratio with fast kinetics complex formation, by contrast with what we reported

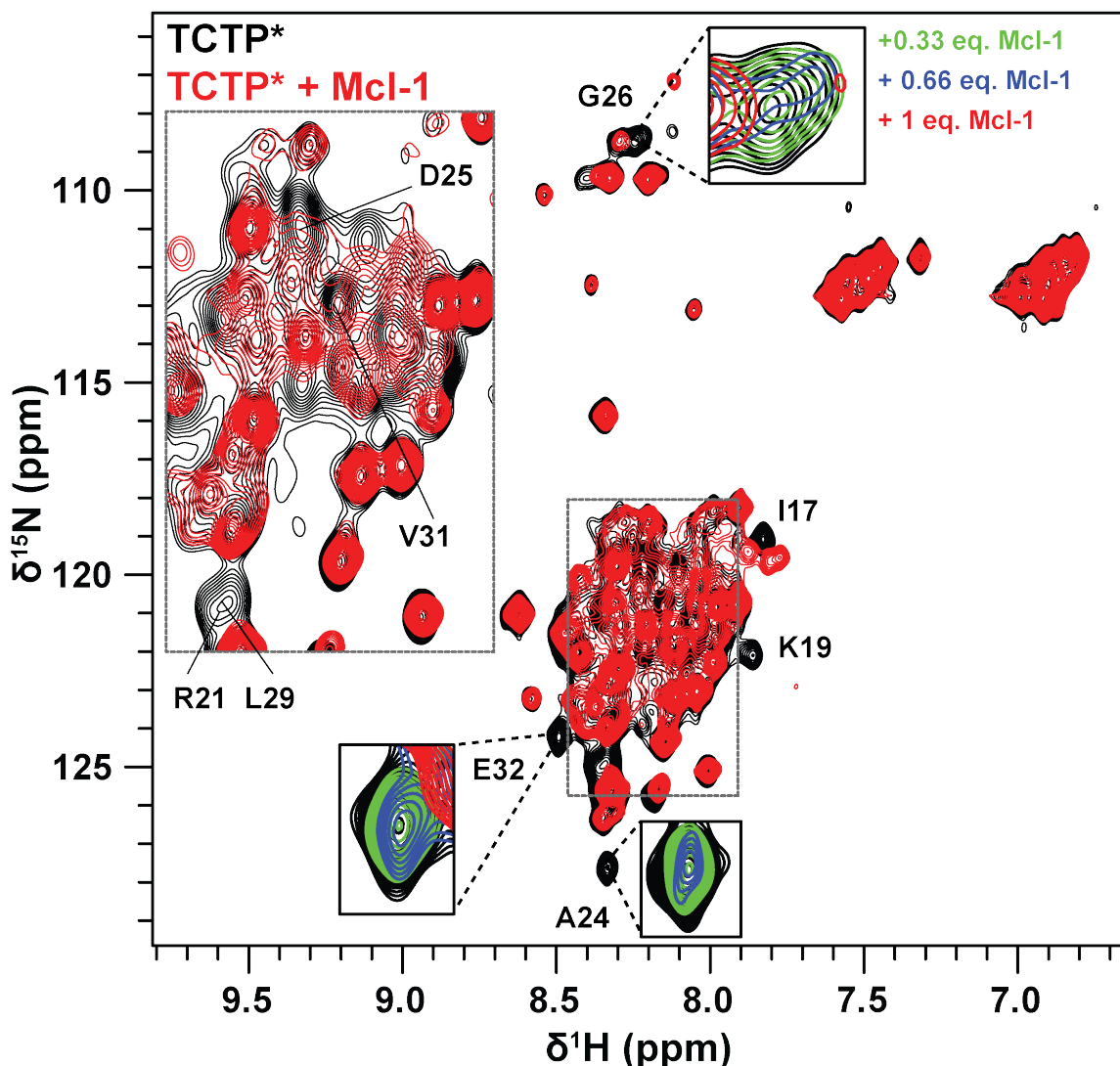


Fig. 4.11 **Comparison of free TCTP\* and in the complex with Mcl-1.** Overlay of  $^1\text{H}$ - $^{15}\text{N}$  SOFAST HMQC spectra from isolated  $^{15}\text{N}$ -TCTP in TCTP\* state (100  $\mu\text{M}$ ) (black) and upon addition of unlabeled Mcl-1 (1 eq.) (red). Intermediate titration points are shown (green, blue) for residues E32 and A24. Residues I17, K19 and G26 which are part of the BH3-like motif in TCTP\* are labeled. Experiments were recorded at 950 MHz and 35  $^\circ\text{C}$  in the following buffer: 50 mM EPPS pH 8, 50 mM MES, 50 mM NaCl, 2 mM TCEP, 2.5 M urea and 5%  $\text{D}_2\text{O}$  / 95 %  $\text{H}_2\text{O}$ .

with the well-folded TCTP state (2 hrs) (Fig. 4.11). Indeed, upon each Mcl-1 addition in the sample, we observed an immediate decrease in signal intensity for a specific subset of  $^1\text{H}$ - $^{15}\text{N}$  resonances corresponding to the BH3-like region (15-29) in TCTP\*. This indicates that the motif directly associates with Mcl-1. The full formation of TCTP\*/Mcl-1 complex resulted in full extinction of the well-resolved resonances from residues I17, K19, A24 and G26, all located within the BH3-like motif that is completely unfolded in the free TCTP\*

state. We could also reliably track E32 residues which did also disappear and is located near the BH3-like region (15-29), validating that residues spanning in C-terminal of the BH3-like motif can sense the binding of the region to Mcl-1 partner at great extent, echoing with the assumption we did in urea-free condition (Sec. 4.1.2.2).

The crosspeaks corresponding to other residues between I17 and G26 in the BH3-like motif were overlapped with other crosspeaks in the central region and we could not reliably monitor them. But from a qualitative perspective, they seem to disappear since the whole intensity in the central, crowded region of the spectrum diminished with no obvious recovery. Moreover, these residues are part of the BH3-like motif and if our urea-promoted interaction mimics well the urea-free condition in the final TCTP/Mcl-1 complex, we should not observe crosspeaks for these residues D17 to G26 in the spectrum of bound TCTP\*. Finally, several broad resonances of weaker intensity simultaneously built-up on the  $^1\text{H}$ - $^{15}\text{N}$  SOFAST HMQC spectrum of TCTP\* upon Mcl-1 additions to yield a near-identical pattern compared to the urea-free complex, indicating that TCTP structure and dynamics are similar in complex with Mcl-1, regardless the presence or absence of urea (2.5 M).

Interestingly, we have demonstrated before that TCTP\* is a dimer with unfolded BH3-like motif (15-29) in solution using the SEC-SAXS protocol (Sec. 3.3.2.4) and NMR (Sec. 3.3.2.2). However, the MW of the TCTP/Mcl-1 complex we obtained in urea-free conditions did correspond to an heterodimer ( $\sim 37$  kDa). Since TCTP\* enables the interaction with Mcl-1 in our growing model, the TCTP\* dimer should dissociate upon complex formation to fit the MW computed for heterodimeric TCTP/Mcl-1 complex. To confirm, we would have to measure a very small population of TCTP\* found in urea-free conditions to detect dimers and thus reject the possibility that the dimeric state of TCTP\* is linked to urea use.

Overall, TCTP\* readily interacts with Mcl-1 using its unfolded BH3-like motif and did suppress the time-requirement to form the complex. Conformational exchange (ms) is present at the binding interface between the BH3-like motif of TCTP\* and the BH3 binding groove of Mcl-1. Crucially, the demonstration that TCTP\* abolishes the time requirement (2 hrs) for the complex to assemble is a strong element to propose that the TCTP\* state is the active TCTP state at Bcl-2 family proteins Bcl-xL and Mcl-1. This will be further discussed in the chapter (Sec. 4.2.3, 4.3.3.3).

## 4.2 Study of Bcl-xL and Mcl-1 in complex with TCTP and BH3 peptides

Here, we observe interactions between TCTP and Bcl-2 family proteins from Bcl-xL and Mcl-1 sides, essentially by means of NMR. We first expose results concerning binding studies between Mcl-1 and the BH3-like peptide from native TCTP. This includes an extensive characterization of free and bound Mcl-1 structure and dynamics by NMR (Sec. 4.2.1). Then, we describe the binding interface of TCTP FL at Bcl-xL and Mcl-1 and compare the binding mode and kinetics to the BH3-like peptide (Sec. 4.2.2). Finally, we share observations regarding the formation of a transient complex between TCTP and Bcl-xL or Mcl-1 (Sec. 4.2.3).

### 4.2.1 Complex between Mcl-1 and the native BH3-like peptide from TCTP

#### 4.2.1.1 NMR characterization of Mcl-1

In the present study we used a soluble construct of human Mcl-1 truncated for both N-terminal PEST and C-terminal transmembrane anchor (TM). This variant corresponds to the 172-327 segment of full length human Mcl-1 with native C286 residue. In the manuscript, residues are numbered according to the native, full length human Mcl-1 protein (List. 3). Since there is no published structure or NMR data about this specific Mcl-1 construct, we extensively characterized the free protein before to perform binding studies with TCTP and BH3-derived peptides.

#### Backbone assignment of free Mcl-1

Mcl-1  $\Delta$ PEST  $\Delta$ TM (Mcl-1) was described using NMR and we first present a  $^1\text{H}$ - $^{15}\text{N}$  SOFAST HMQC spectrum of the protein (Fig. 4.12). Crosspeaks were dispersed over the spectrum with a marked crowding in the central area (Fig. 4.14 A). This pattern is consistent with an  $\alpha$ -helical and globular protein [263], as expected for Mcl-1 protein. We then proceeded with  $^1\text{H}$ ,  $^{15}\text{N}$  backbone resonances assignment of Mcl-1 in acidic (pH 6.5) and alkaline (pH 8) conditions since experiments with TCTP FL complex necessitated an alkaline setup to keep proteins soluble during NMR data acquisition (hrs-days). We recorded classical 3D NMR experiments in BEST-TROSY version to achieve backbone assignment of Mcl-1: HNC(O), HNCACO, HNCA, HNCOCACB and HNCACB (Sec. 2.3.1.3). We used a partial assignment generously shared by A. Bourafai (COBRA, CNRS/Université de Rouen Normandie) to speed up the task and to improve our assignment robustness. In

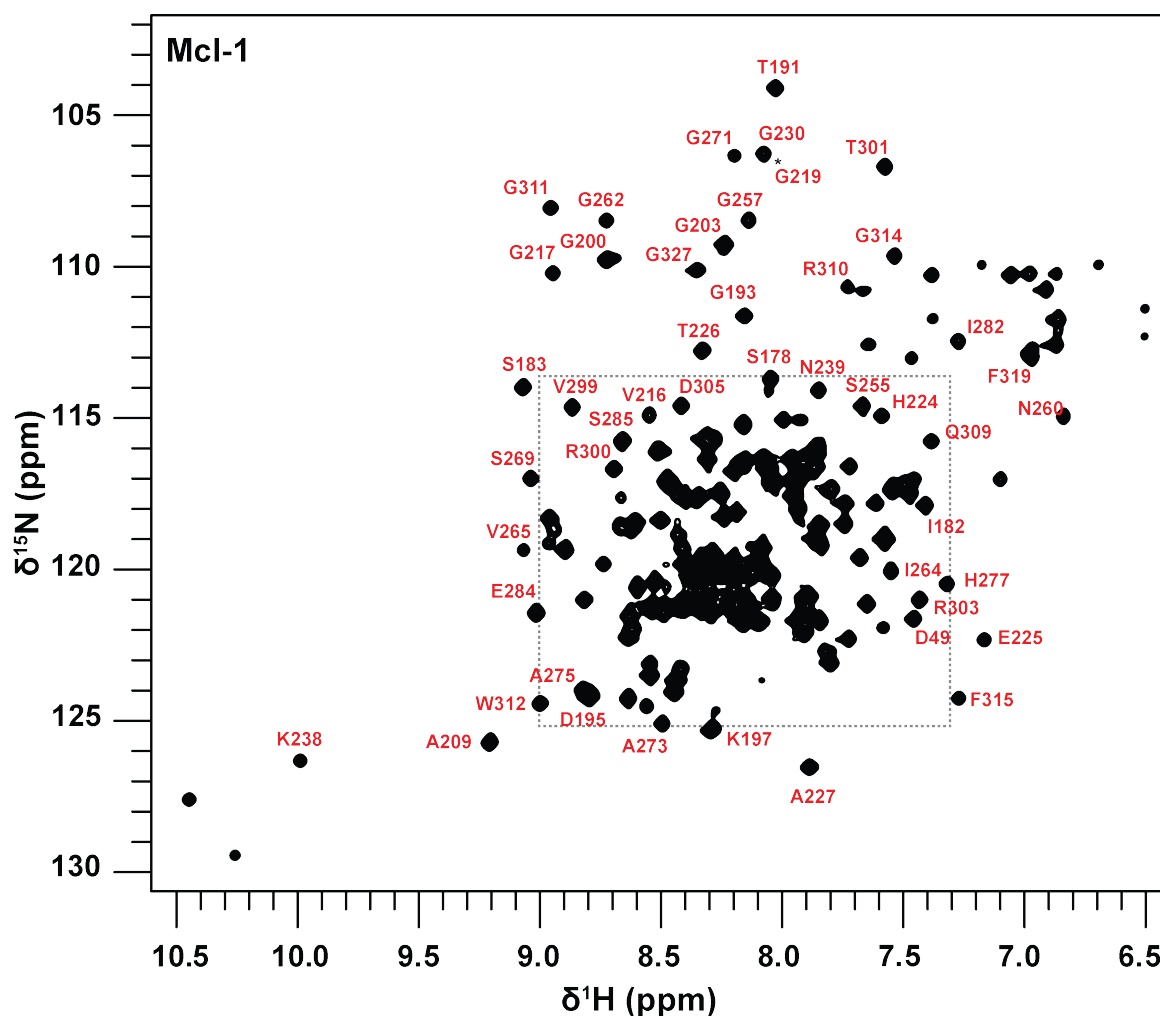
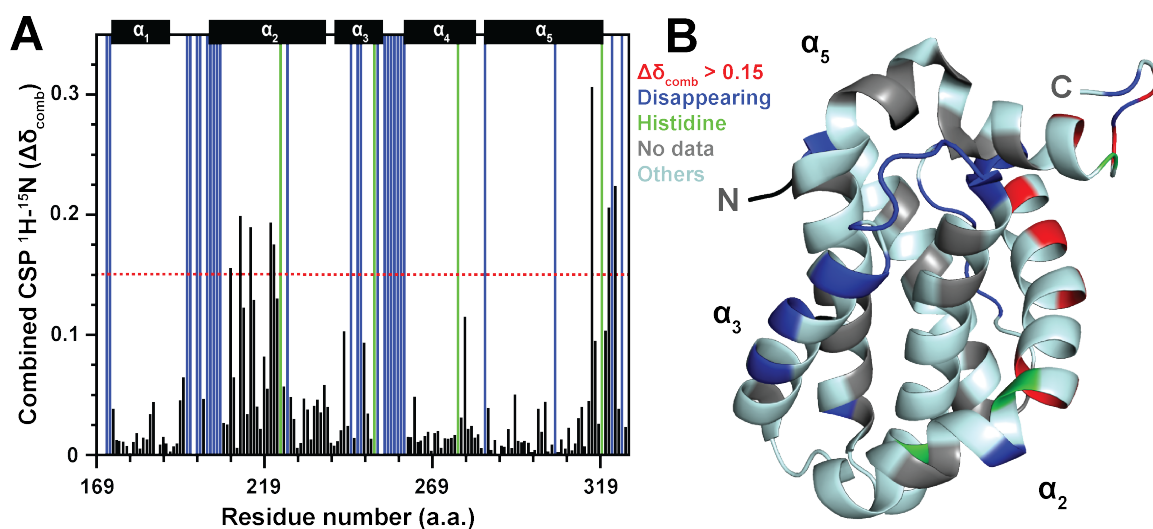


Fig. 4.12 **NMR fingerprint of Mcl-1 and overview of backbone assignment.**  $^1\text{H}$ - $^{15}\text{N}$  SOFAST HMQC from  $^{15}\text{N}$ -Mcl-1 (500  $\mu\text{M}$ ) and corresponding  $^1\text{H}$ - $^{15}\text{N}$  backbone assignment (red labels). A close-up view of the central, crowded region is shown in (Fig 4.14 A). Experiments were recorded at 950 MHz and 35  $^\circ\text{C}$  in the following buffer: 50 mM MES pH 6.5, 50 mM EPPS, 50 mM NaCl, 1 mM TCEP and 5%  $\text{D}_2\text{O}$  / 95 %  $\text{H}_2\text{O}$ . MES/EPPS was used to efficiently prevent from pH variation in both acidic ( $\text{pK}_{\text{aMES}} = 6.10$ ) and alkaline ( $\text{pK}_{\text{aEPPS}} = 8$ ) conditions.

acidic condition (pH 6.5), 152 from the 158 protein residues matched a  $^1\text{H}$ - $^{15}\text{N}$  crosspeak on the Mcl-1  $^1\text{H}$ - $^{15}\text{N}$  SOFAST HMQC spectrum, yielding 96.2 % completion and 98.7 % if excluding proline residues (P198, P289) plus the N-terminal, non-native GP residues from PreScission cleavage site (Fig. 4.12, 4.14 A). G219 and F254 could not be matched with any  $^1\text{H}$ - $^{15}\text{N}$  crosspeak probably because of vanishing intensity. They are located in helix  $\alpha_2$  and the loop connecting  $\alpha_3, \alpha_4$ , respectively. Reduced intensity is probably due to backbone instability in  $\alpha_2$  and increased solvent exchange for the flexible F254 under the current conditions.



**Fig. 4.13 Impact of transition from acidic (pH 6.5) to alkaline (pH 8) condition on Mcl-1.** (A) Combined  $^1\text{H}$ - $^{15}\text{N}$  chemical shift perturbations calculated between  $^1\text{H}$ - $^{15}\text{N}$  SOFAST HMQC spectra from  $^{15}\text{N}$ -Mcl-1 in acidic (pH 6.5) or alkaline (pH 8) condition. (B) Mapping of combined  $^1\text{H}$ - $^{15}\text{N}$  chemical shift perturbations for lowest (grey  $\leq 0.01$ ) and highest (red  $\geq 0.15$ ) values. Coloring of disappearing residues at alkaline pH (blue) on Mcl-1 structure (pdb code: 2MHS). Histidine are highlighted (green) since they are sensitive to pH. Experiments were recorded at 950 MHz and 35 °C in the following buffer: 50 mM EPPS pH 8, 50 mM MES, 50 mM NaCl, 1 mM TCEP and 5%  $\text{D}_2\text{O}$  / 95 %  $\text{H}_2\text{O}$ .

In alkaline condition (pH 8), we have assigned 125 of the  $^1\text{H}$ - $^{15}\text{N}$  resonances to specific residues in Mcl-1 backbone, thus representing a 81 % completion. Many crosspeaks from residues located in flexible parts of the protein did disappear upon transition to alkaline pH due to rapid solvent exchange (Fig. 4.13). These include the short loop (254-259) connecting helices  $\alpha_3$ ,  $\alpha_4$  in the BH3 binding region of the protein. We then computed combined  $^1\text{H}$ - $^{15}\text{N}$  chemical shifts perturbations between  $^1\text{H}$ - $^{15}\text{N}$  SOFAST HMQC spectra of Mcl-1 at either acidic or alkaline pH (Fig. 4.13 A). The largest perturbations were seen in the C-terminal tail of the protein and helix  $\alpha_2$  in close proximity. These contain histidine residues (H224, H320) and it is likely that perturbations originate from changes in histidine protonation state upon pH transition (Fig. 4.13 B). In both acidic and alkaline conditions, intensities of  $^1\text{H}$ - $^{15}\text{N}$  crosspeaks along the Mcl-1 primary sequence (Fig. 4.14 B) were stronger in the short loop (193-202) connecting helices  $\alpha_1$ ,  $\alpha_2$  and at the C-terminal tail of the protein. These segments are flexible in the NMR structure of Mcl-1 and have sharper lines due to increased dynamics at faster timescales (ps-ns). Over the helical part, the BH3-binding groove of the protein composed of helices  $\alpha_2$ ,  $\alpha_3$  and  $\alpha_4$  had weaker average intensity compared to the rest of the helix bundle, suggesting conformational exchange (ms) or anisotropic protein tumbling with

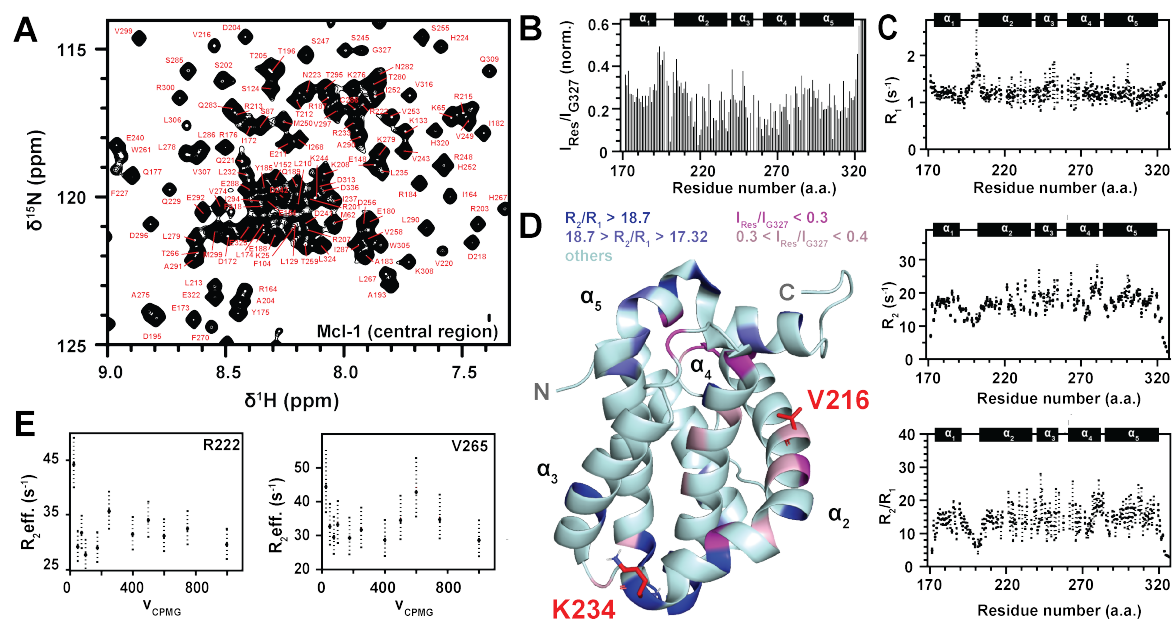


**Fig. 4.14 Characterization of Mcl-1 structure and dynamics** (A) Crowded central region of  $^1\text{H}$ - $^{15}\text{N}$  SOFAST HMQC from  $^{15}\text{N}$ -Mcl-1 (500  $\mu\text{M}$ ) with backbone assignment (red labels) and (B) intensities from resonances along the protein primary sequence. Intensities were normalized by using C-terminal G327 residue resonance intensity as reference ( $I_{\text{Res}}/I_{\text{G327}}$ ). (C)  $^{15}\text{N}$  longitudinal ( $R_1$ ), transverse ( $R_2$ ) relaxation rates with  $R_2/R_1$  ratios along Mcl-1 (400  $\mu\text{M}$ ) primary sequence. Representation of residues with higher  $R_2/R_1$  ratio (blue  $\geq 18.7$ ,  $18.7 > R_2/R_1 \geq 17.3$ ) compared to average on Mcl-1 structure (pdb code: 2MHS). Residues for which relative signal intensity  $I_{\text{Res}}/I_{\text{G327}}$  is lower (magenta  $\leq 0.3$ ,  $0.45 \geq \text{lightpink} \geq 0.3$ ) are also highlighted. (E) Example of CPMG experiment profiles for residues R222 and V265 with  $R_2^{\text{eff}}$  plotted in function of the CPMG pulse frequency ( $\nu_{\text{CPMG}}$ ).

different helix orientations but we show in the next paragraph that the latter explanation was ruled out from the  $^{15}\text{N}$   $R_2/R_1$  ratio.

### Dynamics at the BH3 interface in Mcl-1

We tested Mcl-1 for fast-slow dynamics (ns-ms) by doing  $^{15}\text{N}$ -spin relaxation experiments and probed slower (ms) dynamics by CPMG and spectral lineshape analysis in acidic conditions (pH 6.5).  $^{15}\text{N}$ -spin relaxation rates depend mostly on the local and global reorientation of the backbone NH bonds, thus providing rich information about local and global motions in the protein. Residue-specific  $^{15}\text{N}$   $R_1$  and  $R_2$  relaxation rates of  $^{15}\text{N}$ -Mcl-1 (500  $\mu\text{M}$ ) protein were computed along Mcl-1 primary sequence (Fig. 4.14 C). Relaxation rates were generally homogeneous along the structured regions of the protein. Over these, averaged  $^{15}\text{N}$   $R_1$ ,  $R_2$ , and  $R_2/R_1$  values were  $1.21 \pm 0.15 \text{ s}^{-1}$ ,  $17.24 \pm 1.03 \text{ s}^{-1}$  and  $14.51 \pm 2.59$ , respectively. Within the short loop (193-202) connecting helices  $\alpha_1\alpha_2$ , elevated  $^{15}\text{N}$   $R_1$  and decreased values of  $^{15}\text{N}$   $R_2$  were observed, as expected for a flexible segment with fast

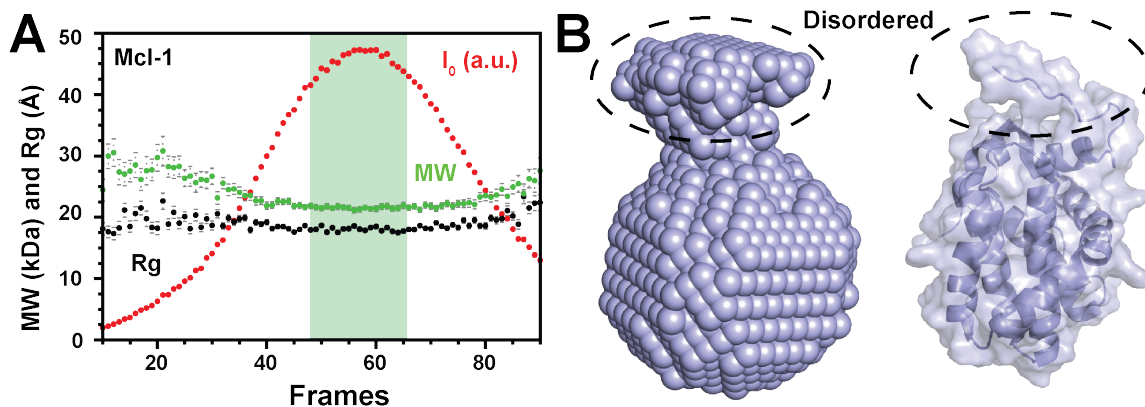


**Fig. 4.15 Structural envelope of Mcl-1 from SEC-SAXS experiments.** (A) SAXS profile of Mcl-1 with initial signal intensity ( $I_0$ ) (red), MW (green) and radius of gyration ( $R_g$ ) (black) along the frames that correspond to elution time from SEC separation. The frame interval where MW and  $R_g$  were stable (green background) was used to compute effective MW and  $R_g$  and correspond to maximum  $I_0$  values, with optimal signal to noise ratio. Experiments were done at 25 °C in the following buffer: 50 mM EPPS pH 8, 50 mM NaCl, 2 mM TCEP. Prior to SAXS run, the sample containing TCTP and Mcl-1 (1:2 ratio) was injected into a S200 Increase (GE) column to separate free Mcl-1 from the protein complexes and to latter proceed with TCTP/Mcl-1 using same protocol, sample and run (B) Molecular envelope computed from SAXS data and generated with ATSAS software [217] and in-build modules (left). Representation of the solution structure of Mcl-1 (pdb code: 1MHS) with cartoon and surface representation.

backbone HN bond reorientation (ps-1 ns). This pattern in  $^{15}\text{N}$   $R_1$  and  $R_2$  values along Mcl-1 primary sequence confirms the structural definition observed in the NMR [264] structure of the protein but still we find a stretch of residues showing larger ( $> 25\%$ )  $R_2/R_1$  ratios compared to mean from all residues in structured parts of Mcl-1.

We have mapped the amino-acids on Mcl-1 structure for which the corresponding  $^1\text{H}$ - $^{15}\text{N}$  crosspeak intensity and  $R_2/R_1$  ratio were significantly lower ( $I_{\text{Res}}/I_{\text{G327}} \leq 0.3$ ) or higher ( $R_2/R_1 \geq 18.7$ ) than the mean for all residues in the structured segments of the protein, respectively. Higher  $R_2/R_1$  values were computed for residues in helix  $\alpha_2$  in Mcl-1 and that includes positively charged K234 and V216 residues as well as others in helices  $\alpha_3$  and  $\alpha_4$ . This suggests that the BH3 binding interface (helices  $\alpha_2$ ,  $\alpha_3$ ,  $\alpha_4$ ) is sampling different conformations in intermediate regime at the NMR chemical shift timescale (ms). Interestingly, the stretch from residue L298 to D304 (helix  $\alpha_5$ ) is seen to move backwards upon binding of BH3 ligands and has also more dynamics (ms) compared to mean for structured residues in the isolated Mcl-1 protein. However, we failed to detect chemical exchange (ms) in Mcl-1 in CPMG experiments since related profiles were all flat after data processing and visualization, as exemplified for residues R222 and V265 (Fig. 4.14 E). This means that conformational dynamics of NMR-visible residues in free Mcl-1 is likely not

occurring at the millisecond timescale, but probably a level below. Altogether these data indicates that conformational exchange is present in the BH3-binding site prior to complex formation with BH3 ligands.

### **Diffusion properties and correlation time of Mcl-1**

To confirm the monomeric nature of Mcl-1 and to probe for possible weak self-association equilibrium, we estimated the hydrodynamic radius of the protein using  $^1\text{H}$  DOSY experiments. We found a translational diffusion coefficient of  $1.17 \pm 0.03 \cdot 10^{-10} \cdot \text{m}^2 \cdot \text{s}^{-1}$  which corresponds to a  $R_h$  of 2.3 nm if assuming a spherical hydrated Mcl-1 and considering the Stokes-Einstein equation.

By comparison, we simulated a translational diffusion coefficient  $D$  with HYDRONMR [237] software to  $1.09 \cdot 10^{-10} \cdot \text{m}^2 \cdot \text{s}^{-1}$  using the Mcl-1 structure (pdb code: 2HR9) as a template. Both experimental and theoretical values were very similar and confirm that Mcl-1 is predominantly a monomer in solution. Then we used  $^{15}\text{N}$ -spin relaxation data and the Lipari-Szabo formalism [210] to compute the rotational correlation time ( $\tau_c$ ) of Mcl-1 and this was  $10.88 \pm 0.55$  ns assuming an isotropic tumbling. With HYDRONMR [237], we predicted the  $\tau_c$  from monomeric Mcl-1 NMR structure (pdb code: 2MHS) and we found 9.95 ns, which is fairly similar to the experimental parameter. This strongly suggests that Mcl-1 is predominantly monomeric in solution but does not exclude the possibility for Mcl-1 weak self-association, since the experimental apparent  $\tau_c$  is slightly higher (+ 0.93 ns) and thus could be, among other reasons, a mean value from an underlying monomer-dimer equilibrium.

### **Molecular envelope of Mcl-1 protein**

To further estimate the shape of TCTP/Mcl-1 complex, we used SEC-SAXS experiments to compute the molecular envelope of isolated Mcl-1 protein in order to later locate the protein in the molecular envelope of the complex. We consistently found an averaged MW of  $21.7 \pm 0.4$  kDa and a radius of gyration ( $R_g$ ) of  $1.81 \pm 0.03$  nm along the frames we used to compute the model, which corresponds well to the small and globular Mcl-1 protein construct. The difference with the theoretical value (17.9 kDa) is significant (+ 21 %) but this likely originates from the small fraction (< 5 %) of digested tag (His<sub>6</sub>-MBP, 42 kDa) that remains at the end of the purification and co-elutes with the protein in SEC-SAXS experiments. Notably, we detected a structural signature that we attribute to the C-terminal and disordered tail of Mcl-1 seen as a protuberance pointing out from the main core. This can allow to further locate and orient the high-resolution structure of Mcl-1 in the molecular envelope of the Mcl-1/TCTP complex from SAXS.



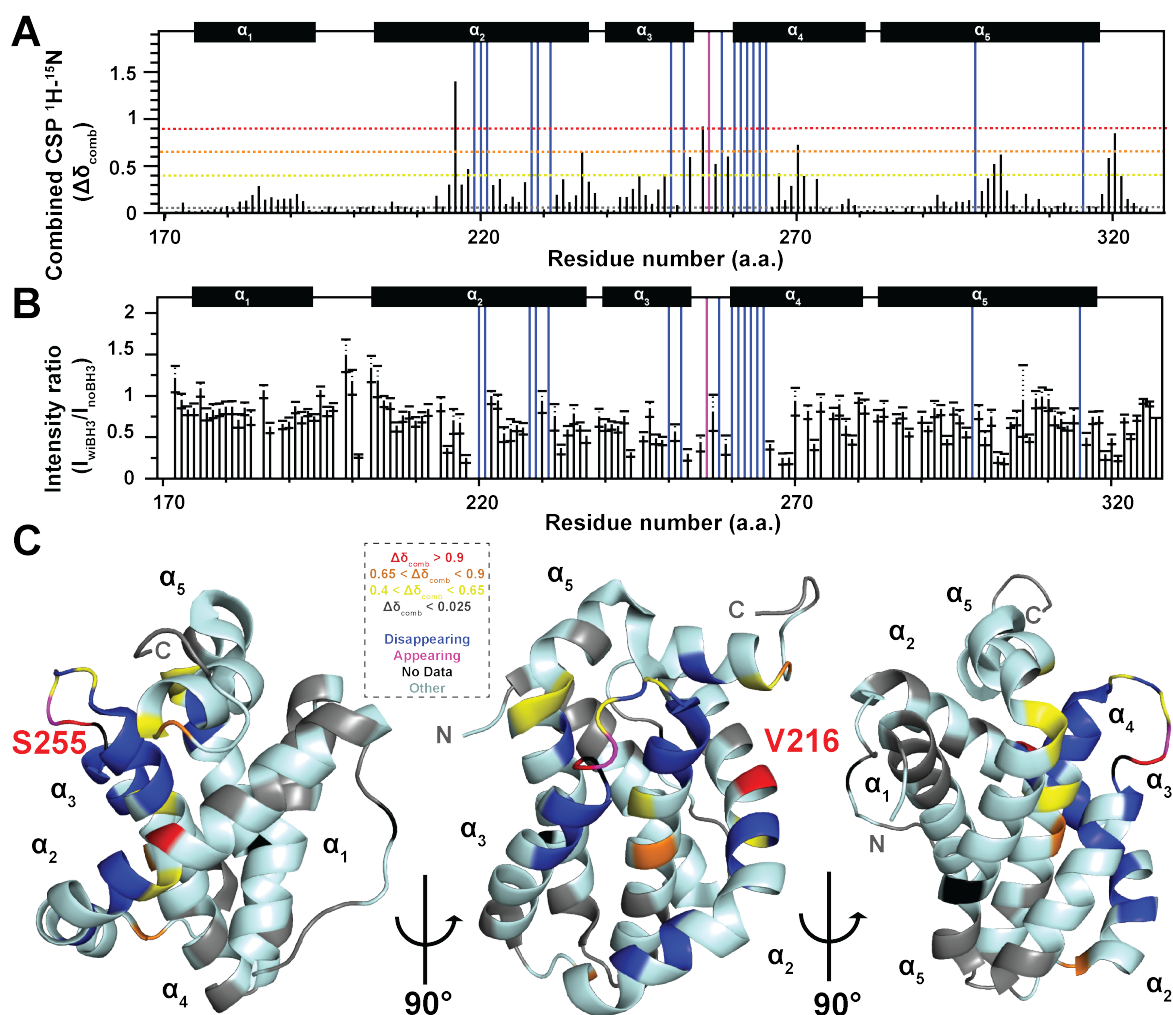


Fig. 4.17 NMR mapping of TCTP<sub>BH3</sub> binding site in Mcl-1. (A) Combined <sup>1</sup>H-<sup>15</sup>N chemical shift perturbations and (B) intensity ratios computed between <sup>1</sup>H-<sup>15</sup>N SOFAST HMQC spectra from isolated Mcl-1 (100 μM) and upon addition of TCTP<sub>BH3</sub> (5 eq.). Disappearing (blue bar) or appearing (magenta bar) residues are shown. Dotted colored bars indicate thresholds for mapping. (C) Mapping of combined <sup>1</sup>H-<sup>15</sup>N chemical shift perturbations (red ≥ 0.9, 0.9 ≥ orange ≥ 0.65, 0.65 ≥ yellow ≥ 0.4, 0.05 ≥ grey) and <sup>1</sup>H-<sup>15</sup>N signal disappearing (blue) or appearing (magenta) on Mcl-1 structure. Residues for which no data were available are highlighted (black).

of <sup>15</sup>N-Mcl-1 up to several hours (2 hrs), meaning that equilibrium seems to be reached immediately between Mcl-1 protein and the TCTP<sub>BH3</sub> peptide, in sharp contrast with the slow formation of the Mcl-1/TCTP complex but in a rather similar way compared to TCTP\* and Mcl-1 titration experiment. To estimate the  $K_d$ , we used the well known Hill-Langmuir equation considering a unique binding pocket and assuming no cooperative binding. Also in the current case, ligand concentration is of the same order compared to protein concentration and  $K_d$ . Thus, we used the extended equation model to estimate the  $K_d$  between TCTP<sub>BH3</sub>

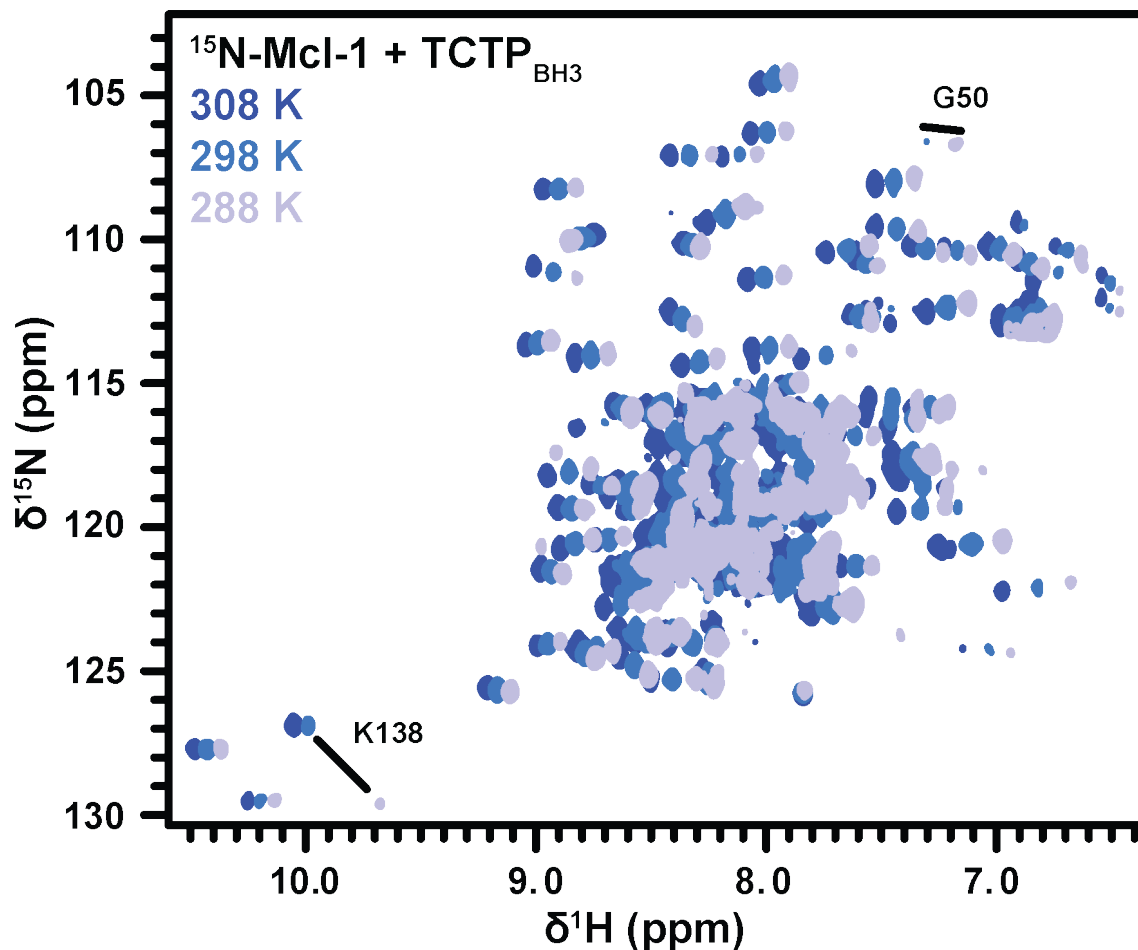


Fig. 4.18 **Impact of temperature on Mcl-1/TCTP<sub>BH3</sub> complex.** Overlay of  $^1\text{H}$ - $^{15}\text{N}$  SOFAST HMQC spectra from  $^{15}\text{N}$ -Mcl-1 (100  $\mu\text{M}$ ) in complex with TCTP<sub>BH3</sub> at 288 K (lightblue), 25  $^\circ\text{C}$  (blue) or 35  $^\circ\text{C}$  (darkblue). Experiments were recorded at 950 MHz and 35  $^\circ\text{C}$  in the following buffer: 50 mM MES pH 6.5, 50 mM EPPS, 50 mM NaCl, 1 mM TCEP in 95 %  $\text{H}_2\text{O}$  / 5 %  $\text{D}_2\text{O}$ .

and Mcl-1:  $f_{\text{bound}} = \frac{[P] + [L] + K_d - \sqrt{([P] + [L] + K_d)^2 - 4[P][L]}}{2[P]}$  with  $[L]$  and  $[P]$  total ligand and protein concentration, respectively. This equation is valid at any given ligand concentration whereas it drops to the hyperbolic binding function  $f_{\text{bound}} = \frac{[L]}{[L] + K_d}$  if  $[L] \gg [P]$ . Considering the concentration of Mcl-1 (100  $\mu\text{M}$ ) and the ligand concentration for 95 % complex formation with Mcl-1, we can estimate that the  $K_d$  is smaller than 25  $\mu\text{M}$  for the Mcl-1/TCTP<sub>BH3</sub> peptide interaction by modulating  $K_d$  in the equation above and observe the threshold value for which the bound fraction is greater than 0.95. This method has arguable reliability and we could prefer a classical fit of bound Mcl-1 fraction in function of TCTP<sub>BH3</sub> concentration but here we can not reliably estimate the bound Mcl-1 fraction after each TCTP<sub>BH3</sub> addition since we observed different exchange regimes from slow to intermediate on the chemical shift timescale before saturation. Moreover, we will show latter

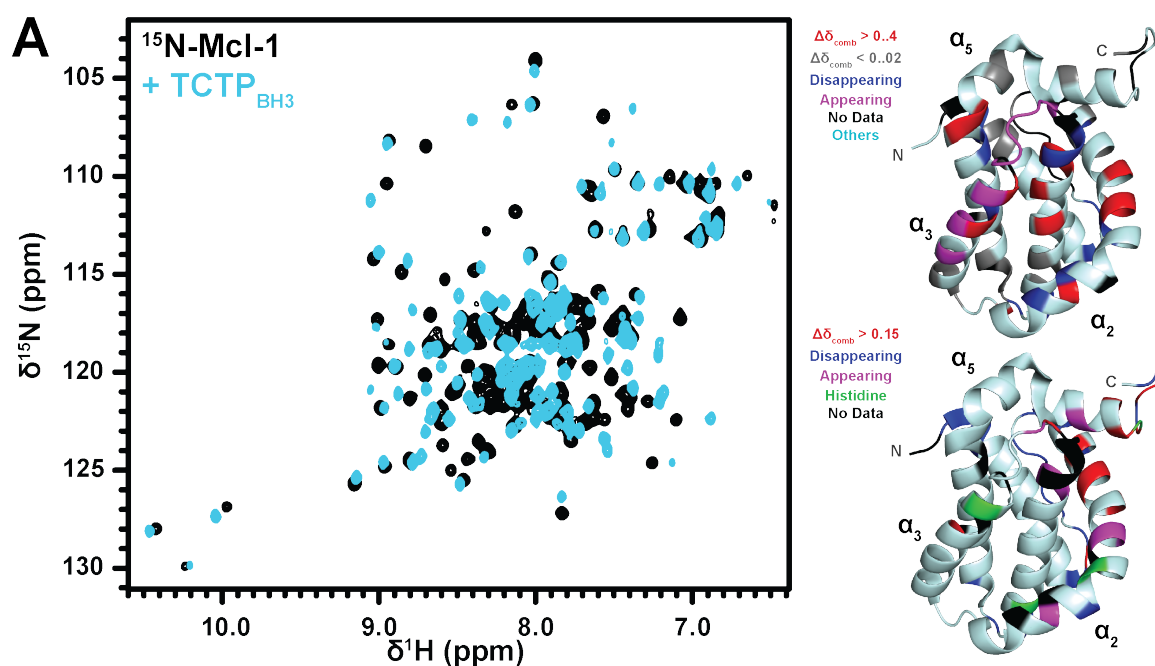


Fig. 4.19 Comparison of free Mcl-1 complex with TCTP<sub>BH3</sub> at pH 8. (A) Overlay of <sup>1</sup>H-<sup>15</sup>N SOFAST HMQC spectra from isolated Mcl-1 (100 μM) (black) in complex with TCTP<sub>BH3</sub> (cyan). Experiments were recorded at 950 MHz and 35 °C in the following buffer: 50 mM EPPS pH 8, 50 mM MES, 50 mM NaCl, 1 mM TCEP in 95 % H<sub>2</sub>O / 5 % D<sub>2</sub>O. (B) NMR mapping of TCTP<sub>BH3</sub> binding site in Mcl-1 in acidic conditions via combined <sup>1</sup>H-<sup>15</sup>N chemical shift perturbations computed between <sup>1</sup>H-<sup>15</sup>N SOFAST HMQC spectra from <sup>15</sup>N-Mcl-1 complex with TCTP<sub>BH3</sub> in acidic (pH 6.5) or alkaline (pH 8) conditions and (C) Between NMR spectra of Mcl-1 complex with TCTP<sub>BH3</sub> at alkaline versus acidic pH, computation and mapping of large combined <sup>1</sup>H-<sup>15</sup>N chemical shift perturbations (red  $\geq 0.15$ ) and disappearing (blue) or appearing (magenta) residues. Histidine residues are highlighted (green) as well as residues for which no data are available (black).

that the main binding event between Mcl-1/TCTP<sub>BH3</sub> we describe here proceeds in parallel of another event (Sec. 4.2.3), thus impairing the proper calculation of the bound Mcl-1 fraction before saturation by the TCTP derived peptide. Anyway, when the affinity is strong, with slow exchange we cannot measure the  $K_d$  from titrations, only estimate the minimal affinity.

In the <sup>1</sup>H-<sup>15</sup>N SOFAST HMQC spectrum of <sup>13</sup>C,<sup>15</sup>N-Mcl-1, strong differences were observed between the free and bound protein in terms of chemical shifts, line broadening and crosspeaks number. A new set of crosspeaks did appear upon successive additions of the BH3-like peptide until saturation of the protein. We could assign up to 87 % of the bound Mcl-1 (134/154 residues, excluding N-terminal GP from precision cleavage and proline residues) using experiments such as HNCOCACB and HNCACB (Sec. 2.3.1.3) and we report the full assignment of Mcl-1 complex with TCTP<sub>BH3</sub> in acidic conditions (pH 6.5) (Fig. 4.16). Next, we computed combined <sup>1</sup>H-<sup>15</sup>N chemical

shift perturbations and intensity ratios between  $^1\text{H}$ - $^{15}\text{N}$  SOFAST HMQC spectra of isolated Mcl-1 and upon formation of the saturated Mcl-1/TCTP<sub>BH3</sub> complex (Fig. 4.17 B, C) with the representation of the most affected residues on Mcl-1 structure (Fig. 4.17 C) in order to locate the TCTP<sub>BH3</sub> binding site at Mcl-1 protein. Largest perturbations were observed for residues V216 and S255 within helix  $\alpha_2$  and in the loop connecting  $\alpha$ -helices  $\alpha_3\alpha_4$ .  $^1\text{H}$ - $^{15}\text{N}$  resonances from residues within the BH3-binding groove of Mcl-1 were largely affected upon complex formation with TCTP<sub>BH3</sub>. Also, the region contains most of the residues for which severe line broadening and signal extinction were observed upon peptide addition. Indeed, disappearing residues include F228, Q229 and M231 from the C-terminal segment of helix  $\alpha_2$ . Moreover, several crosspeaks (G220, L238) present in the  $^1\text{H}$ - $^{15}\text{N}$  SOFAST HMQC spectrum of bound Mcl-1 were distinctively sharper at high temperature (35 °C) compared to the average for crosspeaks from structured region, indicating that conformational exchange exists at the BH3 interface and is accelerated by temperature (Fig. 4.19 A). In conclusion, we have shown that the conformational dynamics ( $\mu\text{s}$ - $\text{ms}$ ) observed in free Mcl-1 still exists in Mcl-1 complex with TCTP<sub>BH3</sub> at the molecular interface with the BH3-like motif. This mirrors the signal extinctions of the BH3 signal in the TCTP FL spectrum when in complex with Mcl-1.

We also achieved the assignment in alkaline conditions (pH 8) to further perform experiments involving TCTP FL and requiring higher pH for the solubility (100  $\mu\text{M}$ ) of associated complexes (Fig. 4.19 A). We completed 89 % assignment (141/154, excluding N-terminal GP and proline) of bound Mcl-1 backbone which is better than reported for acidic conditions (pH 6.5). Surprisingly, considering that alkaline conditions should reduce the number of crosspeaks through increased exchange with water, as observed for the free Mcl-1, several  $^1\text{H}$ - $^{15}\text{N}$  resonances were only observed in alkaline and not acidic condition in Mcl-1/TCTP<sub>BH3</sub> complex (Fig. 4.19 C). These were assigned to residues G219, V220, Q229, H252, V257, I263, V264 and F315. These particular residues were essentially not reported to be affected by pH transition in the free Mcl-1 and are located at the BH3 interface, suggesting that they have faster dynamics or reduced exchange contribution in complex at alkaline compared to acidic pH. It is likely that peptide binding quenched the chemical exchange or reduced the solvent exchange rates for these residues. In conclusion, we have established that the TCTP<sub>BH3</sub> peptide binds to Mcl-1 in the BH3-binding groove of the protein with conformational exchange (ms) at the molecular interface in the saturated complex

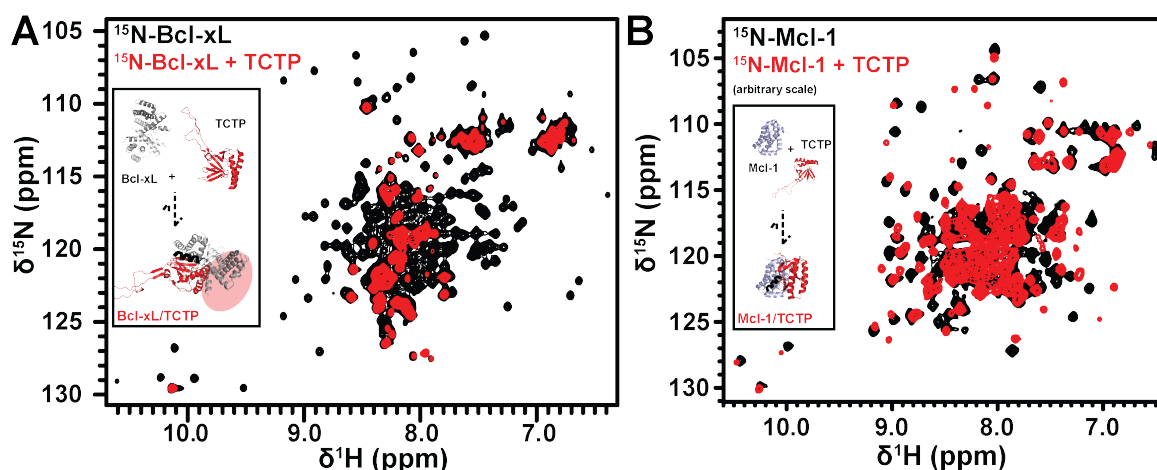


Fig. 4.20 **Mcl-1 and Bcl-xL in complex with TCTP** (A) Overlay of  $^1\text{H}$ - $^{15}\text{N}$  SOFAST HMQC spectra from isolated  $^{15}\text{N}$ -Bcl-xL  $\Delta\text{TM}$  (100  $\mu\text{M}$ ) (black) and upon addition of unlabeled TCTP FL (2 eq.) (red). The whole signal from structured parts of bound Bcl-xL could not be detected at all in the corresponding spectrum of the complex after equilibration time (2 hrs) while signals from flexible regions were still visible. (B) Overlay of  $^1\text{H}$ - $^{15}\text{N}$  SOFAST HMQC spectra from isolated  $^{15}\text{N}$ -Mcl-1 (100  $\mu\text{M}$ ) (black) and upon addition of unlabeled TCTP FL (2 eq.) (red). Because Mcl-1 intensity dropped upon TCTP addition, the spectral intensity was scaled arbitrary in this panel. Experiments were recorded at 950 MHz and 35  $^\circ\text{C}$  in the following buffer: 50 mM EPPS pH 8, 50 mM MES, 50 mM NaCl, 2 mM TCEP and 5%  $\text{D}_2\text{O}$  / 95 %  $\text{H}_2\text{O}$ .

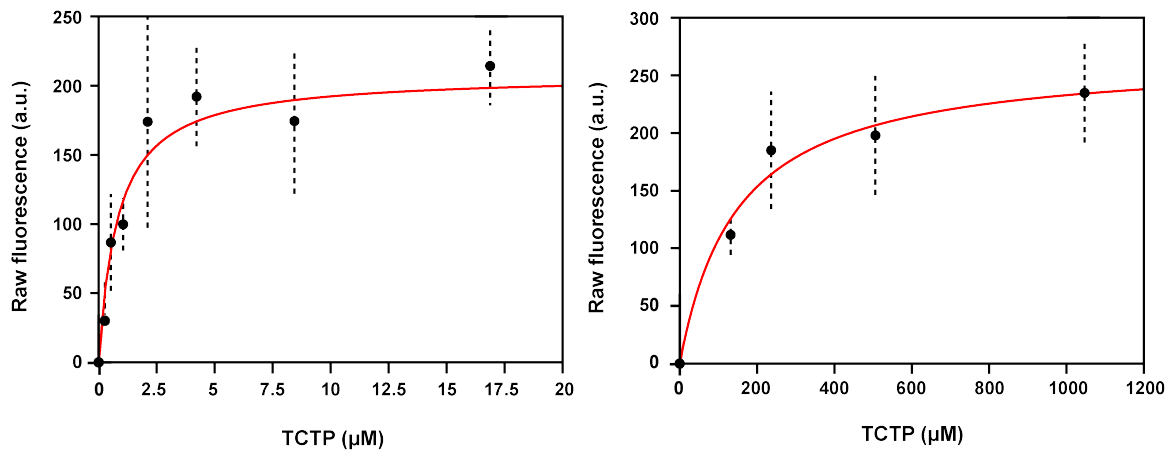


Fig. 4.21 **Determination of TCTP/Mcl-1 dissociation constant ( $K_d$ ) by MST.** (A) High and (B) low affinity binding events. We used the raw fluorescence detection mode since binding-related variations of the baseline from the fluorescent MST label on Mcl-1 protein ( $\sim 20\text{nM}$ ) were observed during the titration and did allow for this raw fluorescence analysis.

## 4.2.2 Binding studies of Mcl-1 and Bcl-xL with full length TCTP

### 4.2.2.1 NMR fingerprint of Bcl-xL and Mcl-1 in complex with TCTP

In order to determine where TCTP FL could associate with Bcl-xL and Mcl-1 since the literature did not identify the binding interfaces in the context of full length TCTP, we recorded  $^1\text{H}$ - $^{15}\text{N}$  SOFAST HMQC spectra of isolated  $^{15}\text{N}$ -Mcl-1  $\Delta\text{PEST}$   $\Delta\text{TM}$  (Mcl-1) or each Bcl-xL construct ( $\Delta\text{TM}$ ,  $\Delta 45\text{-}84\Delta\text{TM}$ ,  $\Delta 27\text{-}82\Delta\text{TM}$ ) (Bcl-xL) and upon addition of unlabeled TCTP FL (2 eq.) with 2 hours equilibration time required to stabilize the system (Fig. 4.20). At saturation with unlabeled TCTP, no signal from either free Bcl-xL (Fig. 4.20 A) or Mcl-1 (Fig. 4.20 B) constructs could be detected, indicating that complexes with TCTP did form efficiently during the equilibration time. Higher protein concentrations in the assay did accelerate the complex formation. In the Bcl-xL/TCTP complex, we expect a predominantly heterotetrameric [111] assembly in solution whereas we showed that Mcl-1/TCTP complex is likely heterodimeric (Sec. 4.1.1.3). Consistently, we could not detect signals from the structured parts of Bcl-xL upon complex formation with TCTP whereas Mcl-1 was still visible in the smaller complex with TCTP (Fig. 4.20 A). The signal disappearance of structured parts of Bcl-xL in the complex can be first explained by the expected increase in the apparent  $\tau_c$  from monomeric, free Bcl-xL to the bound form included in an heterotetrameric assembly. It can also possibly originate from exchange between two or more conformations in the Bcl-xL/TCTP complex at the millisecond. However, in absence of NMR signal, it was difficult to estimate the relative contributions of the two mechanisms. With Mcl-1/TCTP complex, the whole spectral intensity of the Mcl-1 bound state was severely diminished compared to the free Mcl-1, typically by a factor of 2-3, but the heterodimeric complex remained small enough to make Mcl-1 visible by NMR. Because the complex with Bcl-xL was more difficult to characterize, we next focused on the Mcl-1/TCTP.

We tried to measure the binding affinity between TCTP FL and Mcl-1 by using the MST method. Indeed, since slow kinetics characterizes the complex formation, the Isothermal Titration Calorimetry (ITC) protocol should not be suited, due to the diluting impact of slow kinetics on heat release over time and then the low signal to noise ratio that we can expect in such situation. We obtained ambiguous results in term of binding events we could detect. In the majority of the assays, we could detect only one binding event between TCTP FL and labeled, fluorescent Mcl-1 which proceeds with dissociation constant ( $K_d$ ) in the range 20-100  $\mu\text{M}$ . However, we could measure in some experiments two binding events detected by raw fluorescence changes from labeled Mcl-1 since the signal baseline fluctuated upon TCTP addition (Fig. 4.21). At lower concentration of TCTP ( $\mu\text{M}$ ), we detected a binding event with higher affinity and the dissociation constant  $K_d$  was computed

to  $0.82 \sim 0.27 \mu\text{M}$  (Fig. 4.21 A). However, this result has to be considered very carefully since it was not reproduced reliably. At higher concentrations of TCTP ( $> 100 \mu\text{M}$ ), we detected a low affinity event with  $K_d$  computed at  $146.62 \sim 38.42 \mu\text{M}$  and we suppose that it could correspond to the formation of oligomers of TCTP/Mcl-1 complex at higher TCTP concentrations (Fig. 4.21 B). In conclusion, we mostly showed that MST was not suited to reliably estimate the binding affinity between TCTP and Mcl-1 and thus we will rely on NMR-based estimations for binding affinity limits in the next sections.

#### 4.2.2.2 NMR characterization of Mcl-1 complex with full length TCTP

To further describe Mcl-1 in the complex with TCTP FL and the molecular interface, we assigned the backbone of bound  $^{15}\text{N}, ^{13}\text{C}$ -Mcl-1 protein. Classical 3D-NMR methods for protein backbone assignment did not yield signal in 3D-planes of Mcl-1 in Mcl-1/TCTP complex despite intense efforts. Indeed, the fast relaxation induced in part by the supposed large molecular weight of the complex combined with rapid solvent exchange at pH 8 and  $35^\circ\text{C}$  lead to severe line broadening in the triple resonance experiments. We also attempted to use HA-based triple resonance without further success, suggesting that the high molecular weight of the assembly predominated the enhanced transverse relaxation. No significant improvements could be gained by increasing temperature up to  $328\text{ K}$ , possibly because the decrease in correlation time  $\tau_c$  is compensated by higher solvent-exchange rate. Therefore, we mainly relied on the assignment of Mcl-1 complex with the TCTP<sub>BH3</sub> peptide to propose a structural description in the context of TCTP FL since the two spectra were very similar (Fig. 4.23 A). Over 158 residues in Mcl-1, we matched 78 % of Mcl-1 backbone  $^1\text{H}$ - $^{15}\text{N}$  with crosspeaks in the  $^1\text{H}$ - $^{15}\text{N}$  spectrum of  $^{15}\text{N}, ^{13}\text{C}$ -Mcl-1 in Mcl-1/TCTP FL (Fig. 4.22).

In order to locate the TCTP FL binding site in Mcl-1 upon the slow kinetics formation of Mcl-1/TCTP FL complex, we computed combined  $^1\text{H}$ - $^{15}\text{N}$  chemical shift perturbations and intensity ratios between  $^1\text{H}$ - $^{15}\text{N}$  SOFAST HMQC spectra of isolated  $^{15}\text{N}$ -Mcl-1 and upon complex formation with TCTP FL (Fig. 4.24 A).  $^1\text{H}$ - $^{15}\text{N}$  resonances from residues S245, R248, H252, V253, S255, D256, G257, V258 and T259 did appear in Mcl-1 spectrum upon formation of Mcl-1/TCTP FL while absent in free Mcl-1. These are all located in helix  $\alpha_3$  and its C-terminal extension which are included in the BH3-binding groove definition of Mcl-1. This suggests that TCTP FL protects these residues from solvent-exchange. By contrast, residues K194, R207, V220, Q221, F228, M231, M250, G262 and L298 disappeared in Mcl-1 spectrum after complex formation. These are located in the BH3-binding groove of Mcl-1 (helices  $\alpha_2, \alpha_3, \alpha_4$ ) for all but not residue L298 that is in the helix  $\alpha_5$  which should move backwards upon complex formation with peptides. Finally, residues V216, D218,

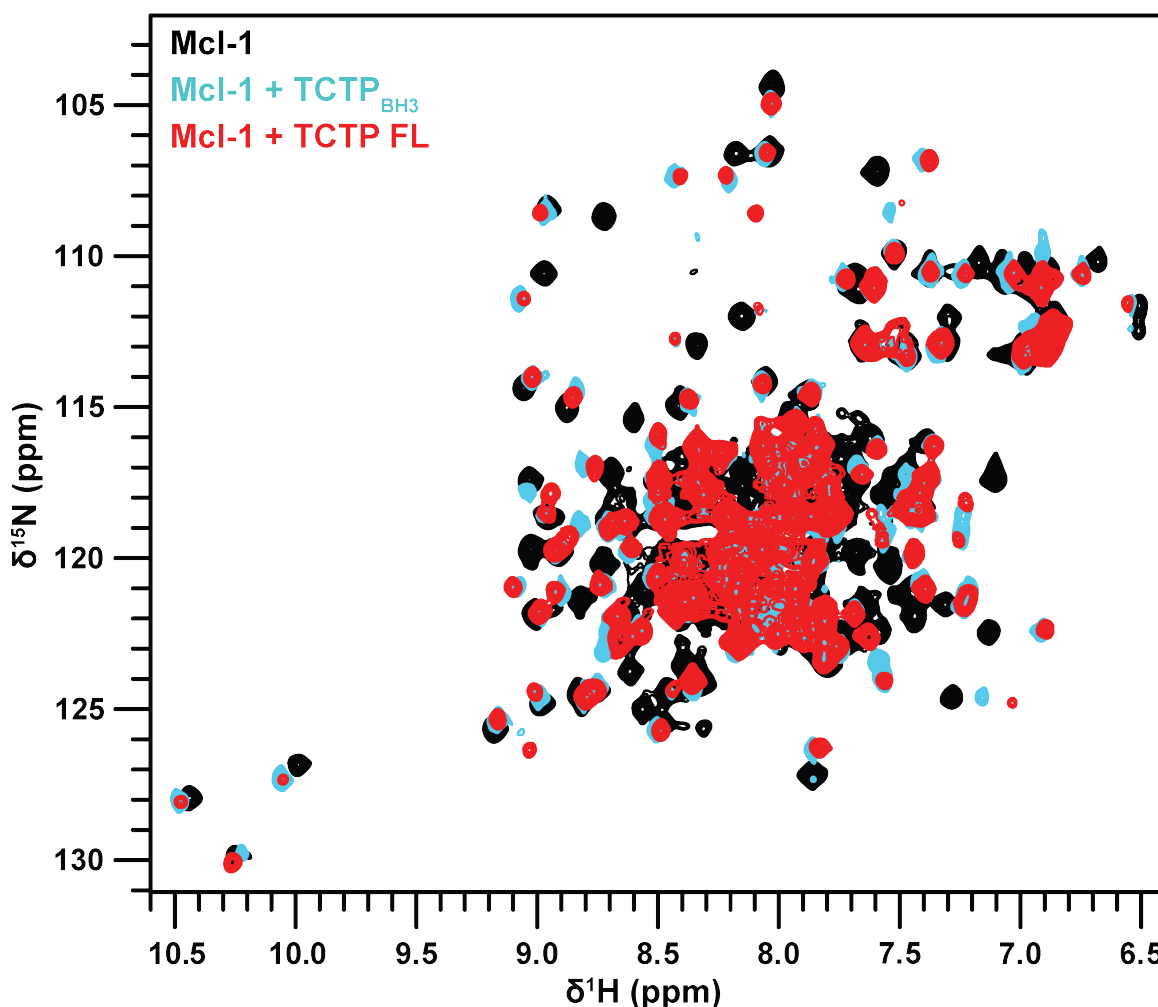


Fig. 4.22 Comparison of free Mcl-1 and in complex with TCTP FL or TCTP<sub>BH3</sub>. Overlay of <sup>1</sup>H-<sup>15</sup>N SOFAST HMQC spectra from isolated <sup>15</sup>N-Mcl-1 (100 μM) (black) and upon addition of TCTP<sub>BH3</sub> (5 eq.) (blue) or TCTP FL (2 eq.) (red). Contours were scaled arbitrary to best observe chemical shift related perturbations. Experiments were recorded at 950 MHz and 35 °C in the following buffer: 50 mM EPPS pH 8, 50 mM MES, 50 mM NaCl, 2 mM TCEP and 5% D<sub>2</sub>O / 95 % H<sub>2</sub>O.

G219, D236, R263, I264, V265, F270, F273, R300, T301 and K302 showed chemical shift perturbations above threshold and these are consistently located in the BH3-binding groove of Mcl-1 and surrounding binding sensitive regions. All three types of reported spectral perturbations unambiguously demonstrated that TCTP FL binds to the BH3-binding groove of Mcl-1 upon formation of Mcl-1/TCTP FL (Fig.4.24 B).

## 4.2.2.3 Impact of full length TCTP compared to BH3-like peptide

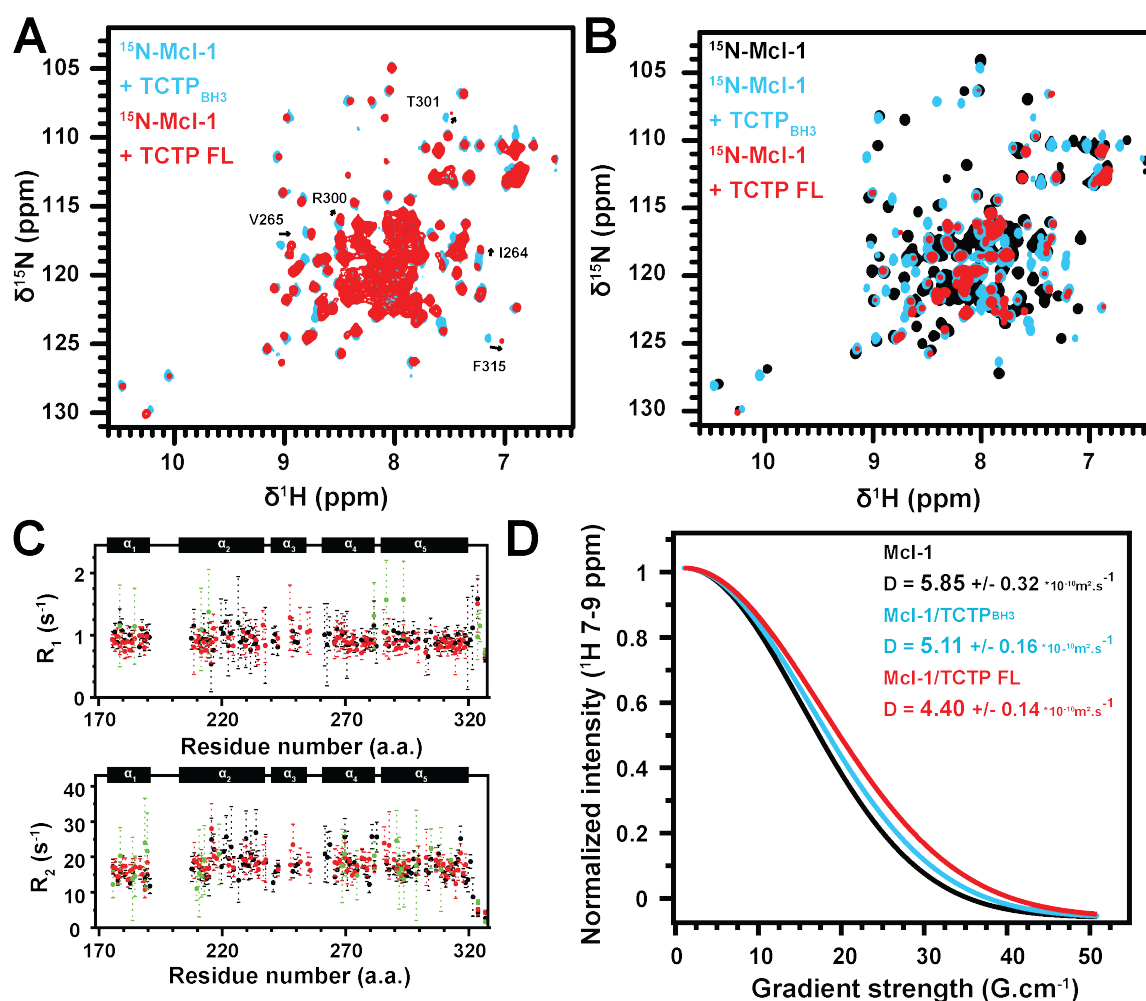
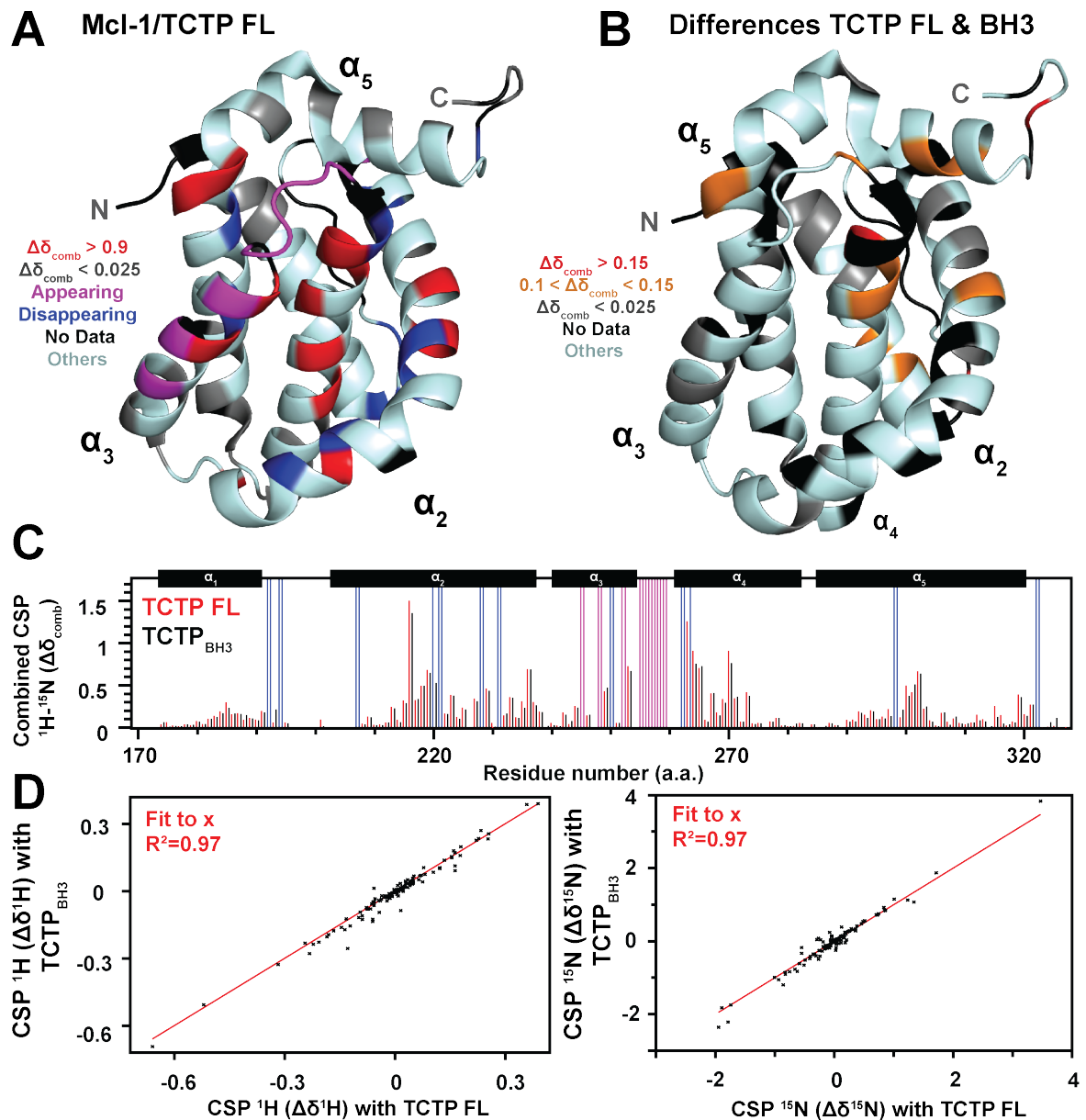


Fig. 4.23 **Comparison of Mcl-1 complexes with TCTP FL or TCTP<sub>BH3</sub> by NMR.** (A) Overlay of <sup>1</sup>H-<sup>15</sup>N SOFAST HMQC spectra from <sup>15</sup>N-Mcl-1 (100 μM) complex with TCTP<sub>BH3</sub> (5 eq.) (blue) or TCTP FL (2 eq.) (red). Contours were scaled arbitrary to best observe chemical shift related perturbations. (B) Overlay of <sup>1</sup>H-<sup>15</sup>N SOFAST HMQC spectra from isolated <sup>15</sup>N-Mcl-1 (100 μM) (black) and upon complex formation with TCTP<sub>BH3</sub> (5 eq.) (blue) or TCTP FL (2 eq.) (red). (C) <sup>15</sup>N longitudinal ( $R_1$ ) and transverse ( $R_2$ ) relaxation parameters from isolated Mcl-1 (black) and upon complex formation with TCTP<sub>BH3</sub> (5 eq.) (red) or TCTP FL (2 eq.) (green). (D) <sup>1</sup>H-<sup>15</sup>N HSQC-DOSY intensity curves versus gradient strength from isolated <sup>15</sup>N-Mcl-1 and upon complex formation with TCTP<sub>BH3</sub> or TCTP FL (blue). Experiments were recorded at 950 MHz and 35 °C in the following buffer: 50 mM EPPS pH 8, 50 mM NaCl, 2 mM TCEP and 5% D<sub>2</sub>O / 95 % H<sub>2</sub>O.

### Binding profiles of TCTP FL and BH3-like peptide at Mcl-1 protein

We compared <sup>1</sup>H-<sup>15</sup>N SOFAST HMQC spectra spectra from isolated <sup>15</sup>N-Mcl-1 ΔPEST ΔTM (Mcl-1) and in complex with TCTP<sub>BH3</sub> or TCTP FL in terms of chemical shifts (Fig. 4.22, 4.23 A) and signal intensity (Fig. 4.23 B). We also determined <sup>15</sup>N-spin relaxation



**Fig. 4.24 Mapping of TCTP FL binding site on Mcl-1 by NMR** (A) Combined  $^1\text{H}$ - $^{15}\text{N}$  chemical shift perturbations calculated between isolated  $^{15}\text{N}$ -Mcl-1 (100  $\mu\text{M}$ ) and in presence of 2 eq. TCTP FL after equilibration. (B) Mapping of combined  $^1\text{H}$ - $^{15}\text{N}$  chemical shift perturbations (red  $\geq 0.4$  and grey  $\leq 0.05$ , cyan). In (A) and (B), disappearing (blue bars) and appearing (magenta) residues are highlighted with those for which no data are available (black). (C) Alignment of combined  $^1\text{H}$ - $^{15}\text{N}$  chemical shift perturbations calculated between isolated  $^{15}\text{N}$ -Mcl-1 (100  $\mu\text{M}$ ) and in complex with TCTP FL (red) or TCTP<sub>BH3</sub> (black). Disappearing (blue bars) and appearing (magenta bars) residues are highlighted. (D) Bi-dimensional correlation of  $^1\text{H}$  (left) and  $^{15}\text{N}$  (right) chemical shifts perturbations from Mcl-1 in complex with TCTP<sub>BH3</sub> or TCTP FL.

parameters (Fig. 4.23 C) and diffusion properties (Fig. 4.23 D) of the isolated Mcl-1 and bound to either TCTP<sub>BH3</sub> or TCTP FL. Overall, <sup>1</sup>H and <sup>15</sup>N chemical shifts of Mcl-1 in complex with either TCTP FL or the BH3-like peptide were strongly correlated for most residues that could be assigned in both conditions (Fig. 4.24 D). Logically, residues that appear or disappear and <sup>1</sup>H-<sup>15</sup>N combined chemical shift perturbation profiles in Mcl-1 were similar comparing both complexes (Fig. 4.24 C). This means that Mcl-1 adapts similarly to both TCTP FL and TCTP<sub>BH3</sub> even though we do not know about residues undergoing line broadening or severe crowding that can not be reliably followed in a quantitative perspective. Spectral perturbations still have slightly higher average value for Mcl-1/TCTP complex but with no preference regarding the location in the protein. However, a subset of crosspeaks did not overlap well and moderate <sup>1</sup>H-<sup>15</sup>N combined chemical shifts differences could be computed between Mcl-1 in complex with TCTP FL or TCTP<sub>BH3</sub>. More than 90 % of residues for which we observed differences above threshold were located in the BH3-binding pocket of Mcl-1 or in helix  $\alpha_5$  which is supposed to displace backwards upon complex formation with both TCTP FL and peptide. These residues were T259, I264, V265, T266 in the BH3-binding groove and R300, T301, F315, V316 in helix  $\alpha_5$ . Also, signal intensity much decreased upon complex formation with TCTP FL compared to TCTP<sub>BH3</sub> which is linked to the slower correlation time  $\tau_c$  of the Mcl-1 complex with TCTP FL compared to BH3-like peptide (Fig. 4.23 B). Overall, we could not detect strong discriminant at the molecular interface between Mcl-1 and TCTP FL or BH3-like peptide. This indicates that the rest of the TCTP structure has limited impact at the molecular interface with Mcl-1.

### **Dynamics and size of Mcl-1 complex with TCTP FL or TCTP<sub>BH3</sub>**

Regarding local and global dynamics, <sup>15</sup>N-spin relaxation parameters were homogeneous along the structured regions of Mcl-1 complex with BH3-like peptide compared to the free protein (Fig. 4.23 C). Over these, averaged <sup>15</sup>N  $R_1$  and  $R_2$  values were  $0.88 \pm 0.19 \text{ s}^{-1}$  and  $17.73 \pm 3.31 \text{ s}^{-1}$ , respectively. For the free protein, values were of  $0.93 \pm 0.33 \text{ s}^{-1}$  and  $16.31 \pm 2.91 \text{ s}^{-1}$  and  $17.30 \pm 0.20 \text{ s}^{-1}$  for <sup>15</sup>N  $R_1$  and  $R_2$  averaged parameters, respectively. This is consistent with the formation of the Mcl-1/TCTP<sub>BH3</sub> complex for which we expect slightly slower longitudinal ( $T_1$ ) and faster transverse ( $T_2$ ) relaxation time due to the increase in the gyration radius of bound Mcl-1 with the BH3-like peptide. Based on the  $R_2/R_1$  ratio, we have computed the translational correlation time ( $\tau_c$ ) of Mcl-1 and this was  $7.99 \pm 0.19 \text{ ns}$  for the free protein and  $8.23 \pm 0.12 \text{ ns}$  in complex with TCTP<sub>BH3</sub> in the current experimental setup (100  $\mu\text{M}$  protein, 50 mM NaCl, pH 8). Unfortunately, and in line with the poor signal to noise ratio in triple resonance experiments, <sup>15</sup>N-spin relaxation properties of Mcl-1 upon stable complex formation with TCTP FL were very unfavorable and most signals disappeared at the first relaxation delay in both  $T_1$  (10 ms) and  $T_2$  (7.7 ms) dimensions, suggesting

severe conformational exchange in Mcl-1 protein since we demonstrated the complex to be heterodimeric and with a suitable MW for NMR ( $\sim 37$  kDa). To further describe the contribution of Mcl-1 complex with TCTP FL or BH3-like peptide, we performed  $^1\text{H}$ - $^{15}\text{N}$  HSQC-DOSY to estimate the diffusion coefficient ( $D$ ) of isolated Mcl-1 and upon complex formation with TCTP FL or TCTP<sub>BH3</sub> peptide (Fig. 4.23 D). Isolated Mcl-1 and in complex with TCTP<sub>BH3</sub> share a similar diffusion coefficient of  $5.85 \pm 0.32 * 10^{-10} \text{ m}^2 \cdot \text{s}^{-1}$  and  $5.11 \pm 0.16 * 10^{-10} \text{ m}^2 \cdot \text{s}^{-1}$ , respectively. As expected, the diffusion coefficient of Mcl-1 in complex with TCTP FL was lower at  $4.40 \pm 0.14 * 10^{-10} \text{ m}^2 \cdot \text{s}^{-1}$ .

In conclusion, this comparison analysis suggests that from Mcl-1 point of view, the intermolecular interfaces between Mcl-1 and TCTP<sub>BH3</sub> peptide or TCTP FL are very similar and is dominated by the BH3 region of TCTP. The rest of the structure of TCTP does not significantly contribute to other binding area but does contribute to slow down the translational and rotational diffusion of Mcl-1. Keeping in mind that the BH3-like region of TCTP FL is engaged in a restrained  $\beta$ -strand in TCTP FL, and considering that the BH3-like motif likely adopts an helical conformation when bound to Mcl-1, the situation appears to be a paradox if we do not make the assumption that TCTP undergoes a conformational change upon binding, at least to free BH3 sequences from the  $\beta$ -strand. The simplest explanation to explain this is to assume that upon interaction with Mcl-1 in the BH3 region unpins from the folded part of TCTP to create a new molecular interface on Mcl-1 as we proposed in the first section of the chapter (Sec. 4.1.2). Finally, Mcl-1 complex with the BH3-like peptide did form readily whereas Mcl-1 complex with TCTP FL required time (2 hrs) to stabilize. Here, the BH3-like peptide behaves as TCTP\* does in term of fast association kinetics, and in both cases the short motif is unstructured and solvent accessible prior to binding partners. Also since we observe chemical exchange (ms) at the molecular interface in Mcl-1 upon saturation by TCTP<sub>BH3</sub>, we expect the subsequent line broadening to be also observed in the TCTP<sub>BH3</sub> peptide and the BH3-like region in the full length protein, which was demonstrated in the context of both full length native and TCTP\*.

#### 4.2.2.4 Molecular envelope of TCTP and Mcl-1 complex

Until now, we extensively characterized TCTP and Mcl-1 structures and dynamics both in their isolated or bound states. The complex is heterodimeric, compact and secondary structures are essentially preserved in the bound proteins compared to their free states, as well as tertiary structure for Mcl-1. By contrast, TCTP has molten-globule state in its globular domain which implies tertiary structure fluctuation at the millisecond timescale. In order to illustrate these results and learn about the body shape of the TCTP/Mcl-1 complex, we

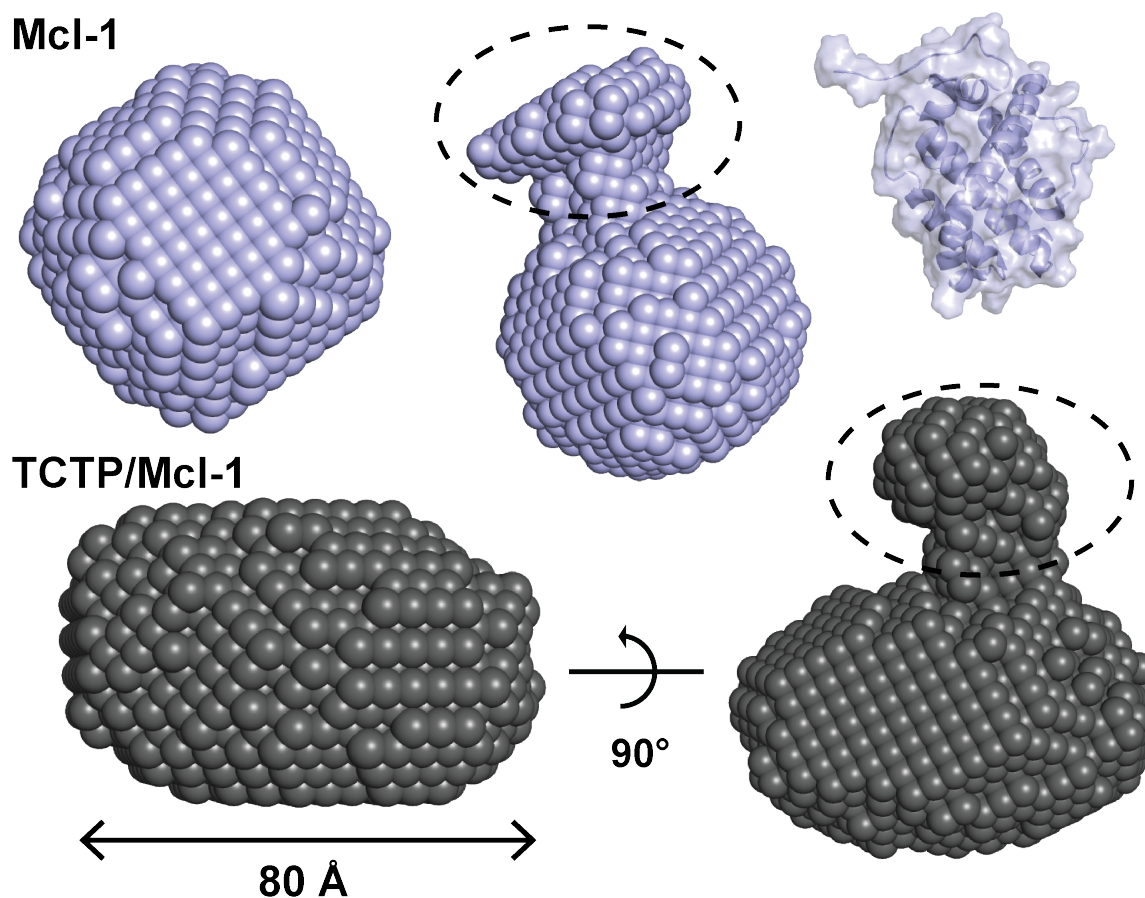
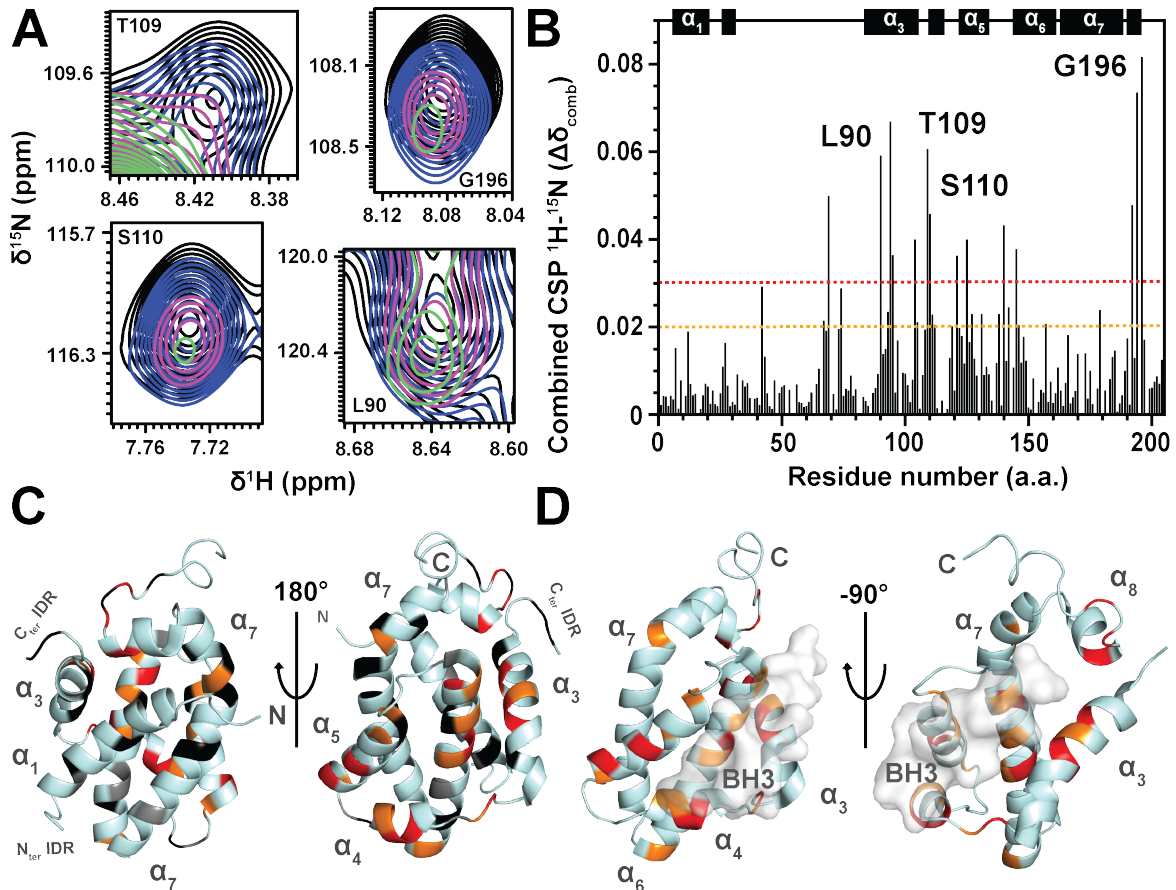


Fig. 4.25 **Molecular envelopes of Mcl-1 and complex Mcl-1/TCTP.** (A) Molecular envelope of Mcl-1 from SEC-SAXS experiment presented already presented (Sec. 4.1.1.3) and US-SUMO deconvolution routine. (B) Molecular envelope of Mcl-1/TCTP complex. The model was obtained from the same sample and SEC-SAXS run than the reported molecular envelope of Mcl-1. Same routines were used for data processing.

computed a low quality molecular envelope from SEC-SAXS since peaks overlap in SEC and the limited complex concentration made difficult to obtain deconvoluted data with optimal signal to noise ratio. However, we still obtained a molecular envelope compatible with all the observations we mentioned so far (Fig. 4.25). The TCTP/Mcl-1 complex has prolate type of organization and the model has a tightly packed organization as we expected. Strikingly, a structural signature characteristic of the molecular envelope from free Mcl-1 and seen as a protuberance pointing out likely from helix  $\alpha_5$  in C-terminal of the protein. Thus, we could locate Mcl-1 in the molecular envelope of the complex with TCTP. The space left could accommodate the globular domain of TCTP but density would be clearly missing considering the IDR in the protein, which suggests that the IDR samples a much more restricted volume upon complex formation compared to in the free TCTP protein.

### 4.2.3 Transient association of TCTP with Bcl-2 partners

#### 4.2.3.1 NMR mapping of TCTP binding site on Bcl-xL



**Fig. 4.26 NMR characterization of Bcl-xL in the transient complex with TCTP.** (A) Overlay of  $^1\text{H}$ - $^{15}\text{N}$  SOFAST HMQC spectra from isolated  $^{15}\text{N}$ -Bcl-xL  $\Delta\text{TM}$  (500  $\mu\text{M}$ ) (black) and in presence of 0.25 eq. (blue), 0.50 eq. (purple) or 0.75 eq. (green) His<sub>6</sub>-TCTP. Close-up views from residues T109, G196, S110 and L90 are shown. (B) Combined  $^1\text{H}$ - $^{15}\text{N}$  chemical shift perturbations calculated between isolated  $^{15}\text{N}$ -Bcl-xL  $\Delta\text{TM}$  and in presence of TCTP (0.75 eq.). (C) Mapping of combined  $^1\text{H}$ - $^{15}\text{N}$  chemical shift perturbations (red  $\geq 0.03$ ,  $0.03 > \geq 0.02$ , grey  $\leq 0.002$ ). Residues for which no data were available (overlap, line broadening...) are highlighted (black). (D) Same as (C) with representation of the TCTP<sub>BH3</sub> peptide in the BH3-binding groove of Bcl-xL from the crystal structure of the complex (pdb code: 4Z9V) with color code (red  $\geq 0.03$ ,  $0.03 > \geq 0.02$ ). Experiments were recorded at 800 MHz and 35 °C in the following buffer: 50 mM HEPES pH 7.4, 50 mM NaCl, 2 mM TCEP and 5% D<sub>2</sub>O / 95 % H<sub>2</sub>O.

Even though we could not characterize the structured parts of Bcl-xL in the stable complex with TCTP by means of NMR, we observed that both proteins also interact via a transient, weak affinity complex, and we report our characterization of this complex to first identify a binding interface between TCTP FL and Bcl-xL. We have recorded  $^1\text{H}$ - $^{15}\text{N}$  SOFAST HMQC

spectra of isolated  $^{15}\text{N}$ -Bcl-xL  $\Delta\text{TM}$  (Bcl-xL) and upon successive additions of unlabeled TCTP FL. We have detected the formation of a transient complex between TCTP FL and Bcl-xL through subtle  $^1\text{H}$ - $^{15}\text{N}$  chemical shift perturbations in rapid exchange regime (ns- $\mu\text{s}$ ) on the chemical shift timescale (Fig. 4.26 B) in Bcl-xL straight after addition of TCTP. This rapid exchange regime observed on Bcl-xL can be explained by a weak affinity complex between Bcl-xL and TCTP (thereafter called “transient complex”) and differs with the “stable complex”. Indeed, the latter is obtained at high TCTP concentration and after equilibration time (2 hrs) whereas the transient complex is readily observed upon TCTP FL addition starting from low protein concentration equivalent (0.25 eq.).

We have computed combined  $^1\text{H}$ - $^{15}\text{N}$  chemical shift perturbations between  $^1\text{H}$ - $^{15}\text{N}$  SOFAST HMQC spectra from isolated Bcl-xL  $\Delta\text{TM}$  and upon TCTP addition (Fig. 4.26 B) to locate the TCTP binding site on Bcl-xL in this transient complex. Along the primary sequence of Bcl-xL, the most significant perturbations were observed in  $\alpha$ -helical segments defining the BH3-binding groove ( $\alpha_3$ ,  $\alpha_4$ ,  $\alpha_5$  and  $\alpha_6$ ) and marginally at the C-terminal of the protein ( $\alpha_8$ ) (Fig. 4.26 C). When considering the crystal structure of Bcl-xL bound to TCTP<sub>BH3</sub> peptide, it is clear that these segments form the essential of the protein-peptide interface (Fig. 4.26 D). Notably, residue E179 in helix  $\alpha_7$  showed a significant perturbation upon TCTP addition. This can be attributed to a structural adjustment ongoing in Bcl-xL since helix  $\alpha_7$  is far from the BH3-binding pocket and is seen to also move backwards upon binding of canonical or non canonical BH3 sequences (e.g. with p53 [265]). It is interesting to note that this helix  $\alpha_7$  is affected upon both transient and stable complexes, which means that even weak interactions can induce structure changes through the Bcl-xL structure. Under similar conditions, but with  $^{15}\text{N}$ -TCTP, we did not observe any chemical shift variation for the visible  $^{15}\text{N}$ - TCTP signals. We therefore consider that the transient complex corresponds to Bcl-xL bound to a minor state of TCTP that is competent for interacting with Bcl-xL, while the main TCTP state is not able to interact with Bcl-xL. Here is one element more that makes the minor TCTP\* state a key and it helps to understand the formation of this weak affinity, transient complex.

#### 4.2.3.2 NMR characterization of transient TCTP/Mcl-1

We previously discussed the NMR spectra of Mcl-1 in absence of TCTP and in excess of TCTP. Here we described the spectral change at intermediate TCTP concentration. We recorded  $^1\text{H}$ - $^{15}\text{N}$  SOFAST HMQC spectra of isolated  $^{15}\text{N}$ -Mcl-1  $\Delta\text{PEST}$   $\Delta\text{TM}$  (Mcl-1) and upon addition of unlabeled TCTP FL protein (2, 3, 4 eq.) in acidic conditions (pH 6.5). Upon increasing TCTP FL concentration in the NMR tube, we observed rapid exchange shifts

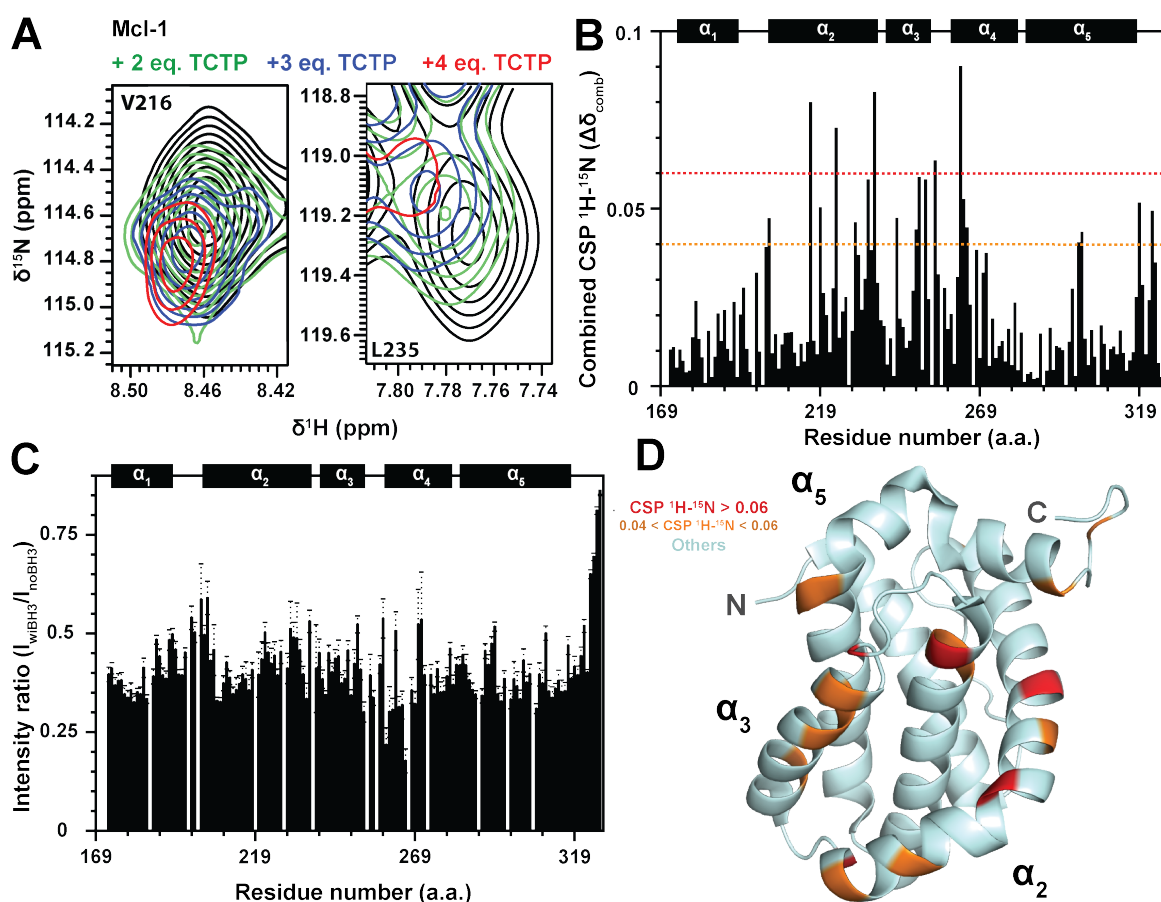


**Fig. 4.27 NMR characterization of Mcl-1/TCTP transient complex.** (A) Close-up views from overlay of  $^1\text{H}-^{15}\text{N}$  SOFAST HMQC spectra from isolated  $^{15}\text{N}$ -Mcl-1 (150  $\mu\text{M}$ ) (black) and upon increments of TCTP concentration (green, blue, red). (B) Combined  $^1\text{H}-^{15}\text{N}$  chemical shift perturbations and (C) intensity ratios calculated between  $^1\text{H}-^{15}\text{N}$  SOFAST HMQC spectra from isolated Mcl-1 (150  $\mu\text{M}$ ) and in presence of TCTP (3 eq.). (D) Mapping of large combined  $^1\text{H}-^{15}\text{N}$  chemical shift perturbations (red  $\geq 0.06$ ,  $0.04 \leq \text{CSP } ^1\text{H}-^{15}\text{N} < 0.06$ , cyan  $\leq 0.04$ ). Experiments were recorded at 950 MHz and 303 K in the following buffer: 20 mM HEPES pH 6.5, 2 mM TCEP and 5%  $\text{D}_2\text{O}$  / 95 %  $\text{H}_2\text{O}$ .

in the  $^1\text{H}-^{15}\text{N}$  SOFAST HMQC spectra from  $^{15}\text{N}$ -Mcl-1 (Fig. 4.27 A). This indicates the formation of a transient complex between Mcl-1 and TCTP. Information at the residue-level was gained through analysis of combined  $^1\text{H}-^{15}\text{N}$  chemical shift perturbations and intensity ratios computed between  $^1\text{H}-^{15}\text{N}$  SOFAST HMQC spectra of isolated Mcl-1 and in transient Mcl-1/TCTP complex (Fig. 4.27 B, C). Intensity changes were significant in the whole protein with more than half of loss at the maximum concentration of TCTP, consistently with the observation of material precipitating in the NMR tube due to the low solubility at acidic pH of the slow forming, TCTP/Mcl-1 stable complex that assembles in parallel. The largest chemical shift perturbations we observed upon TCTP FL addition were for residues

V216, H224, D236, S255 and R263 (Fig. 4.27 D). These residues were all located within the BH3-binding groove of Mcl-1 in helices  $\alpha_2$ ,  $\alpha_3$  and  $\alpha_4$ . In the C-terminal extremity of the protein, residues F319 and D323 showed moderate perturbations and they contribute in the structural continuum defining the BH3-binding groove in Mcl-1 structure. Perturbations of medium amplitude were also reported for residues R300, T301 and F315, V316 in helix  $\alpha_5$  as we also described the region to be affected upon stable complex formation but with perturbations of much higher amplitude ( $\Delta\delta_{\text{comb}} \sim 1$ ). Compared to residues in the BH3 binding region, the perturbations in helix  $\alpha_5$  have similar relative amplitude in both transient and stable complexes, which means that motions in helix  $\alpha_5$  do not necessitate a strong complex to proceed. In conclusion, as with Bcl-xL, the TCTP protein forms an transient, weak relative affinity complex with Mcl-1 by contacting its BH3-binding groove. We also interpret this weak relative affinity complex as the direct interaction between the lowly populated TCTP\* state and Mcl-1, made possible by the accessibility of the BH3-like region of TCTP\* to Mcl-1.

#### 4.2.3.3 The BH3-like peptide enhances the transient complex formation

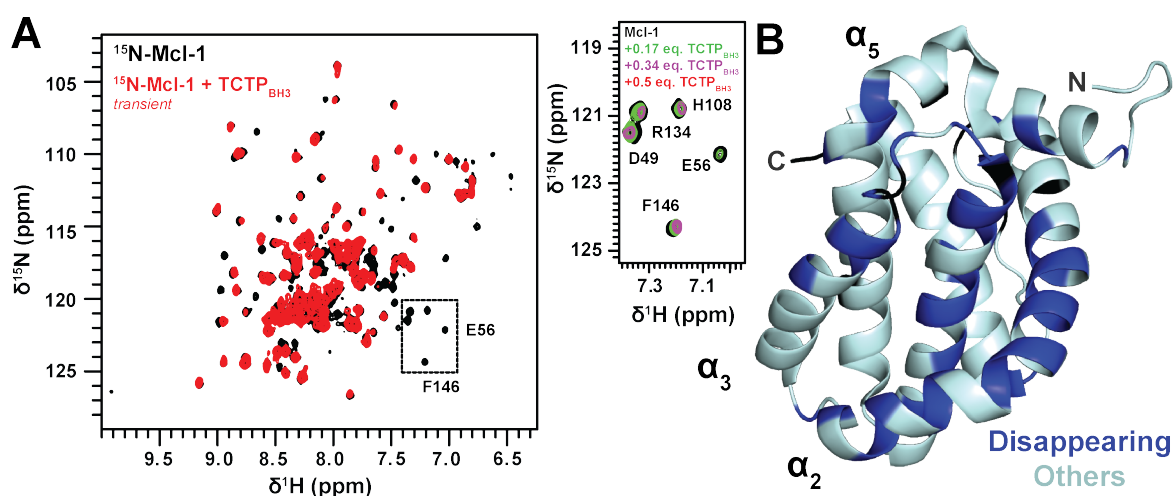


Fig. 4.28 **NMR characterization of Mcl-1 in the transient complex with TCTP<sub>BH3</sub>**. (A) Overlay of  $^1\text{H}$ - $^{15}\text{N}$  SOFAST HMQC spectra from isolated  $^{15}\text{N}$ -Mcl-1 (100  $\mu\text{M}$ ) (black) and upon addition of TCTP<sub>BH3</sub> (0.5 eq.) (red). (B) Missing  $^1\text{H}$ - $^{15}\text{N}$  resonances in  $^1\text{H}$ - $^{15}\text{N}$  SOFAST HMQC after TCTP<sub>BH3</sub> addition (0.5 eq.) were mapped on Mcl-1 structure (blue) (pdb code: 2MHS). Experiments were recorded at 950 MHz and 25  $^\circ\text{C}$  in the following buffer: 50 mM MES pH 6.5, 50 mM EPPS, 50 mM NaCl, 1 mM TCEP and 5%  $\text{D}_2\text{O}$  / 95 %  $\text{H}_2\text{O}$ .

If TCTP\* interacts with Bcl-xL and Mcl-1 in the transient complex as we suggest, we should observe much stronger perturbations in Mcl-1 spectrum using the BH3-like peptide since

we suppose it is 100 % active at the Bcl-2 family proteins by opposite to TCTP\* which represents a very little fraction (< 1%) of the whole TCTP in urea-free conditions.

To answer this question, we recorded  $^1\text{H}$ - $^{15}\text{N}$  SOFAST HMQC spectra of  $^{15}\text{N}$ -Mcl-1 and upon addition of half equivalent of unlabeled TCTP<sub>BH3</sub> peptide. We observed the disappearing of a subset of resonances in the  $^1\text{H}$ - $^{15}\text{N}$  SOFAST HMQC spectra of  $^{15}\text{N}$ -Mcl-1 in presence of BH3-like peptide, suggesting conformational exchange in intermediate timescale (ms) (Fig. 4.28 A) either between the free and the bound state, or within the formed complex. We also observed rapid exchange chemical shift perturbations of small amplitude by looking at the same crosspeaks before the line broadening was too severe. Despite that free Mcl-1 could not be detected anymore, no resonance from bound Mcl-1 in the stable complex described before (Sec. 4.2.1.2) was identified, indicating that another, transient complex of weaker affinity is formed. To confirm the TCTP<sub>BH3</sub> binding site in Mcl-1 in this transient complex, we have mapped all disappearing residues at half equivalent of TCTP<sub>BH3</sub> and the BH3-binding region ( $\alpha_1$ ,  $\alpha_2$  and  $\alpha_3$ ) of the Mcl-1 protein hosted 88 % of the disappearing residues (30/34) (Fig. 4.28 B). Other residues were located in the helix  $\alpha_5$  and as we described the helix is supposed to move backward upon complex formation (Sec. 1.2.3.2). In conclusion, TCTP<sub>BH3</sub> also forms a transient, weak affinity complex with Mcl-1 by contacting its BH3-binding groove. This complex was much more populated at equivalent ratio compared to transient Mcl-1/TCTP complex which is a strong indication that TCTP\* could mediate the formation of this transient complex in the context of the full length protein. Indeed, TCTP\* and the BH3-like motif have same unstructured nature prior to complex formation with partners and both are 100 % available for interactions.

### 4.3 Canonical and BH3-like motifs at Mcl-1 protein

In this section, we will first establish the binding mode of TCTP<sub>BH3D16I</sub> variant at Mcl-1 protein since the mutation D16I restores the conserved hydrophobic residue at position h1 in the h1-4 consensus sequence that defines the canonical BH3 motif (Sec. 4.3.1). We will also test the interaction of the canonical Mule<sub>BH3</sub> motif with Mcl-1 in order to discuss the differences between the canonical BH3s (Mule<sub>BH3</sub> and TCTP<sub>BH3D16I</sub>) and the BH3-like peptide from TCTP in terms of binding interface and dynamics at Mcl-1 protein (Sec. 4.3.2). Finally, we estimate the relative affinity of BH3 peptides and TCTP FL in competition experiments at Mcl-1 protein (Sec. 4.3.3). We also report a crucial experiment that illustrates the importance of TCTP\* to efficiently form complexes with Mcl-1.

### 4.3.1 Complex of Mcl-1 with BH3 peptides from TCTP and Mule

#### 4.3.1.1 Structure of BH3 peptides from TCTP and Mule

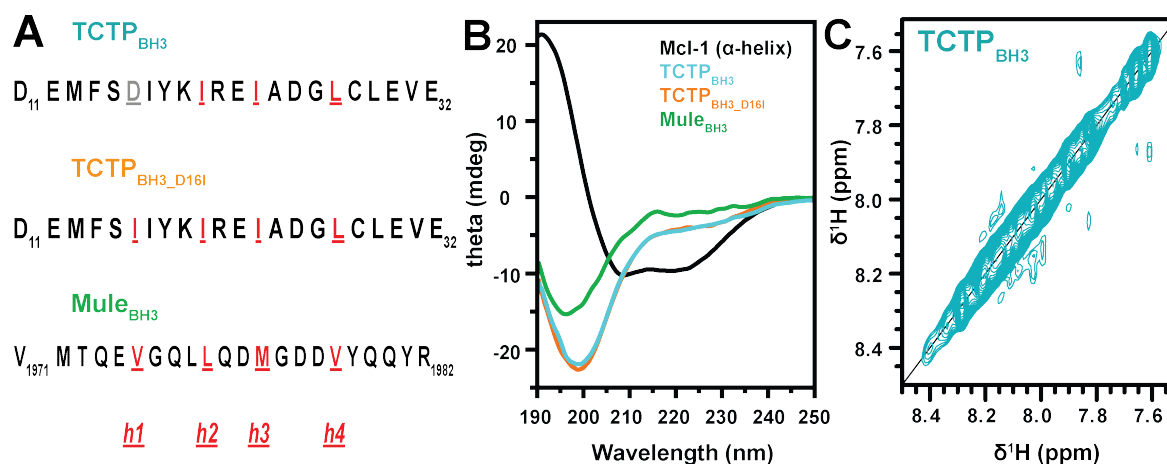


**Fig. 4.29 Primary sequences and structural characterization of BH3 peptides related to TCTP and Mule.** (A) Primary sequence of the BH3 peptides TCTP<sub>BH3</sub>, TCTP<sub>BH3D16I</sub> and Mule<sub>BH3</sub>. Conserved position h1, h2, h3, h4 typical of BH3 motifs are highlighted (red). (B) Far-UV (190-250 nm) CD experiments from TCTP<sub>BH3</sub>, TCTP<sub>BH3D16I</sub>, Mule<sub>BH3</sub> and an  $\alpha$ -helical template (Mcl-1) (blue). Experiments were carried out at 25°C in NaPO<sub>4</sub> 2.5 mM and pH 6.5 with 100  $\mu$ M protein or peptides.

Canonical BH3 motifs contained in BH3-only proteins are either unstructured or  $\alpha$ -helical in the context of the full length proteins [91]. Peptidic approaches have demonstrated that BH3 motifs fold in  $\alpha$ -helix upon binding to Bcl-2 family proteins as exemplified in the crystal structure of Bcl-xL/TCTP<sub>BH3</sub> [111] and Mcl-1/Mule<sub>BH3</sub> (pdb code: 5C6H) complexes. To evaluate the structural state of our three BH3-derived peptides in their free states (Fig. 4.29 A), we have used homonuclear <sup>1</sup>H-<sup>1</sup>H NOESY experiments and CD in the far-UV region (190-250 nm) on all TCTP<sub>BH3</sub>, TCTP<sub>BH3D16I</sub> and Mule<sub>BH3</sub> peptides. The far-UV CD spectrum is compared to the spectrum of Mcl-1  $\Delta$ PEST  $\Delta$ TM (Mcl-1) as template for  $\alpha$ -helix since this protein is  $\alpha$ -helical (Fig. 4.29 B). Ellipticity had strongly negative values at low wavelength (190-210 nm) for BH3-derived peptides whereas these were strongly positive for the  $\alpha$ -helical template. At higher wavelength (210-250 nm) the CD spectra of the peptides were flat whereas the curve from the  $\alpha$ -helical template showed the typical signature of  $\alpha$ -helix type of secondary structure. Thus, all three TCTP<sub>BH3</sub>, TCTP<sub>BH3D16I</sub> and Mule<sub>BH3</sub> peptides are unstructured prior to bind Mcl-1.

To confirm using a different method, we used <sup>1</sup>H-<sup>1</sup>H NOESY experiment on TCTP<sub>BH3</sub> and looked in the amide region of the spectrum since it informs about stable contacts between backbone <sup>1</sup>H with patterns characteristic of  $\alpha$ -helix (Fig. 4.29 C). We could not observe



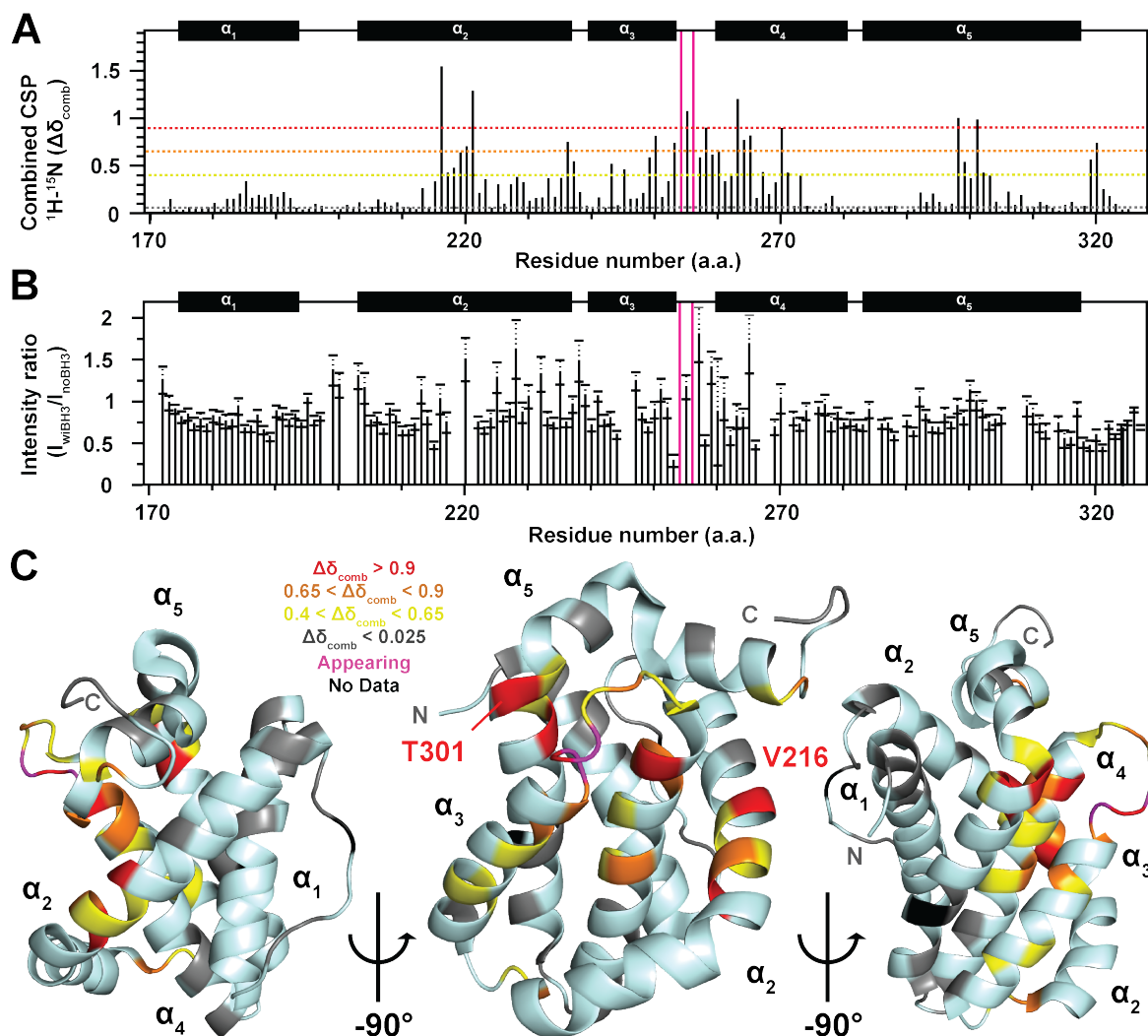


Fig. 4.31 NMR mapping of TCTP<sub>BH3D16I</sub> binding site in Mcl-1. (A) Combined  ${}^1\text{H}-{}^{15}\text{N}$  chemical shift perturbations and (B) intensity ratios computed between  ${}^1\text{H}-{}^{15}\text{N}$  SOFAST HMQC spectra from isolated  ${}^{15}\text{N}$ -Mcl-1 (100  $\mu\text{M}$ ) and upon addition of TCTP<sub>BH3D16I</sub> (5 eq.). Appearing (magenta bar) residues upon complex formation are shown. Dotted colored bars indicate thresholds for mapping. (C) Mapping of combined  ${}^1\text{H}-{}^{15}\text{N}$  chemical shift perturbations (red  $\geq 0.9$ ,  $0.9 \geq$  orange  $\geq 0.65$ ,  $0.65 \geq$  yellow  $\geq 0.4$ ,  $0.025 \geq$  grey) and  ${}^1\text{H}-{}^{15}\text{N}$  signal appearing (magenta) on Mcl-1 structure. Residues for which no data are available (overlap, line broadening...) are highlighted (black).

compared to the native BH3-like sequence (1:5) as confirmed by increasing again peptide content without observing significant changes in the  ${}^1\text{H}-{}^{15}\text{N}$  spectrum of bound Mcl-1. The NMR spectra of the titration of Mcl-1 with BH3D16I was typical of a slow exchange process between the free and bound Mcl-1 state and no additional Mcl-1 state was detectable. Indeed, the crosspeaks of free Mcl-1 decreased in intensity while the crosspeaks of the complex increased in intensity with increasing concentration of TCTP<sub>BH3D16I</sub>. This further indicates a

rather strong affinity. Considering Mcl-1 concentration (100  $\mu\text{M}$ ) and that the complex is almost fully formed in our conditions (> 95 %) but not at lower concentration of proteins, this indicates that the  $K_d$  is 10  $\mu\text{M}$  or below for the interaction Mcl-1/TCTP<sub>BH3D16I</sub> which is stronger than for the limit value estimated for TCTP<sub>BH3</sub> (25  $\mu\text{M}$ ). The NMR assignment of Mcl-1 complex with TCTP<sub>BH3D16I</sub> was completed up to 100 % if excluding proline residues and the N-terminal GP residues by carrying out standard experiments such as HNCOCACB and HNCACB (Sec. 2.3.1.3). Residues F254 and D256 were not visible in the free Mcl-1 whereas they turned visible upon formation of Mcl-1/TCTP<sub>BH3D16I</sub> complex, thus allowing for the full assignment of bound Mcl-1 backbone.

To characterize the binding site of TCTP<sub>BH3D16I</sub> in Mcl-1, we computed combined  $^1\text{H}$ - $^{15}\text{N}$  chemical shift perturbations and intensity ratios between  $^1\text{H}$ - $^{15}\text{N}$  SOFAST HMQC spectra of isolated Mcl-1 and upon complex formation with TCTP<sub>BH3D16I</sub> peptide (Fig. 4.31 A, B). The largest chemical shift perturbations were observed for residues V216, Q221, S255 and R263 in the BH3-binding groove of Mcl-1 (helices  $\alpha_2$ ,  $\alpha_3$  and  $\alpha_4$ ). Residues L298 and T301 in helix  $\alpha_5$  also exhibited strong perturbations and were already described as originating from the motion of helix  $\alpha_5$  to accommodate BH3 motifs (Sec. 1.2.3.2). Weak perturbations were observed in helix  $\alpha_1$  and surrounding surfaces, at the opposite of the BH3-binding region which is expected if we consider that the TCTP<sub>BH3D16I</sub> peptide binds the BH3-binding groove. Crosspeaks intensity from Mcl-1 decreased upon TCTP<sub>BH3D16I</sub> binding to Mcl-1, attributable to a slight decrease in correlation time ( $\tau_c$ ) and possible conformational exchange upon complex formation. In conclusion, the canonical variant of the BH3-like sequence still binds to the BH3-binding groove of Mcl-1 (Fig. 4.31 C) in a tighter complex compared to native TCTP<sub>BH3</sub>. The impact of TCTP<sub>BH3D16I</sub> in the complex dynamics compared to TCTP<sub>BH3</sub> will be discussed later.

#### 4.3.1.3 Mcl-1 complex with BH3 peptide from Mule

The E3 ubiquitin ligase Mule is necessary for proteasome-mediated degradation of Mcl-1. It owns a canonical BH3 motif with valine at position h1 that binds to Mcl-1 as seen in the crystal structure of the Mcl-1/Mule<sub>BH3</sub> complex (pdb code: 5C6H) (Fig. 1.12 C). To inhibit ubiquitylation of Mcl-1, one hypothesis is that TCTP could bind to the BH3-binding groove of Mcl-1, possibly competing with Mule. Moreover, Mule<sub>BH3</sub> is also a tool to compare respective behaviors of BH3-like and canonical motifs at the binding interface. To answer these questions, we recorded  $^1\text{H}$ - $^{15}\text{N}$  SOFAST HMQC spectra of isolated  $^{13}\text{C}$ ,  $^{15}\text{N}$ -Mcl-1  $\Delta\text{PEST}$   $\Delta\text{TM}$  (Mcl-1) and upon addition of unlabeled Mule<sub>BH3</sub> peptide (Fig. 4.32). We

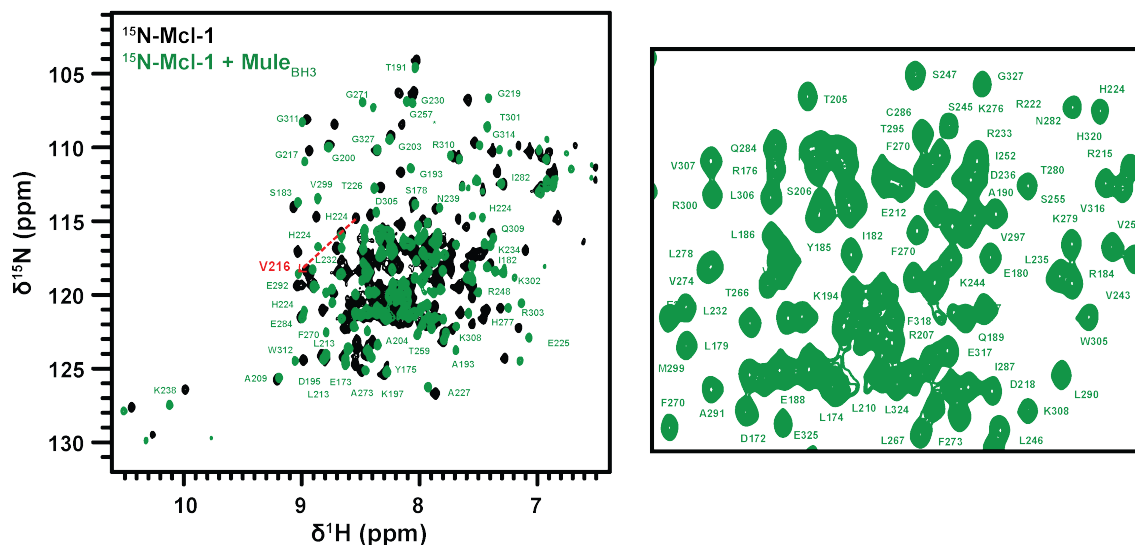


Fig. 4.32 **Comparison of free Mcl-1 and in the complex with Mule<sub>BH3</sub>**. Overlay of <sup>1</sup>H-<sup>15</sup>N SOFAST HMQC spectra from isolated <sup>15</sup>N-Mcl-1 (100 μM) (black) and upon addition of Mule<sub>BH3</sub> (green) (2 eq.). A close-up view of the central, crowded region of Mcl-1 spectrum is shown. Backbone assignments of bound Mcl-1 are also reported (labels). Experiments were recorded at 950 MHz and 35 °C in the following buffer: 50 mM MES pH 6.5, 50 mM EPPS, 50 mM NaCl, 2 mM TCEP and 5% D<sub>2</sub>O / 95 % H<sub>2</sub>O.

confirmed that Mcl-1 and Mule<sub>BH3</sub> readily assemble to form a complex at the lowest ratio (1:2) among the three peptides, suggesting relative affinity greater ( $K_d \sim 5 \mu\text{M}$ ) than for native and D16I variant of the TCTP BH3-like sequence. In the context of peptides at equivalent concentrations, this does not encourage to propose a competition mechanism with Mule to explain the inhibitory effect of TCTP on Mcl-1 ubiquitinylation levels. However, the cellular levels of the different BH3 might be very different, and thus  $K_d$  is not the unique parameters when considering competition effects.

To describe the molecular interface of Mcl-1/Mule<sub>BH3</sub> complex in solution, we computed combined <sup>1</sup>H-<sup>15</sup>N chemical shift perturbations between <sup>1</sup>H-<sup>15</sup>N SOFAST HMQC spectra of isolated <sup>15</sup>N-Mcl-1 and upon complex formation with Mule<sub>BH3</sub> peptide and we plotted the results on Mcl-1 structure (Fig. 4.35 A). We have found large perturbations between the two conditions and these were maximal for residues V216, V220, N260 and I264, all located in the BH3-binding region of Mcl-1. Additionally, residue D256 did appear upon complex formation. By contrast, the helix  $\alpha_1$ , the linker  $\alpha_1$ - $\alpha_2$ , the N-terminal of helix  $\alpha_3$  and the C-terminus of helix  $\alpha_2$  were not significantly affected upon complex formation and they are not part of the BH3-binding groove of the protein. Thus, we could confirm that Mule<sub>BH3</sub> binds into the BH3-binding groove of Mcl-1, consistently with the crystal structure of the protein complex (Fig. 1.12). When comparing structures of Mcl-1 and in complex with

Mule<sub>BH3</sub>, we observe that residues showing the largest combined chemical shift perturbations are located close to the BH3 peptide. Finally, we observed that residues R300, T301 in helix  $\alpha_5$  of Mcl-1 are also affected upon Mule<sub>BH3</sub> binding as for the two TCTP-derived peptides.

### 4.3.2 Canonical and BH3-like sequences at Mcl-1 protein

#### 4.3.2.1 BH3-like sequence promotes conformational dynamics (ms)

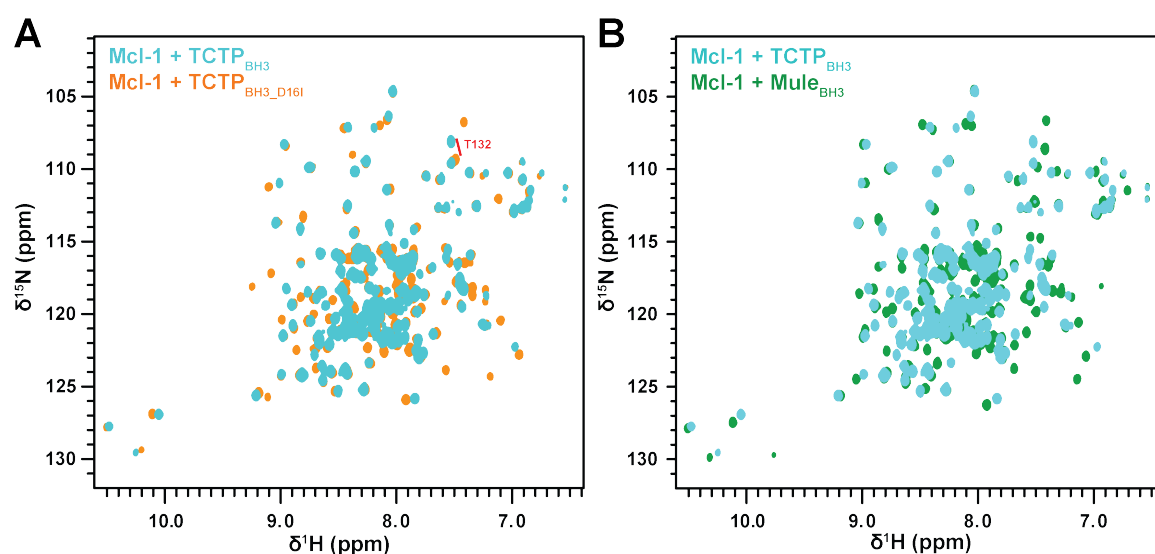


**Fig. 4.33 Comparison Mcl-1 in complex with TCTP<sub>BH3</sub> and with D16I or Mule<sub>BH3</sub>.** (A) Overlay of <sup>1</sup>H-<sup>15</sup>N SOFAST HMQC spectra from <sup>15</sup>N-Mcl-1 in Mcl-1/TCTP<sub>BH3</sub> (cyan) or Mcl-1/TCTP<sub>BH3D16I</sub> (orange) complexes. (B) Overlay of <sup>1</sup>H-<sup>15</sup>N SOFAST HMQC spectra from <sup>15</sup>N-Mcl-1 in Mcl-1/TCTP<sub>BH3</sub> (cyan) or Mcl-1/Mule<sub>BH3</sub> (green) complexes. Experiments were recorded at 950 MHz and 35 °C in the following buffer: 50 mM MES pH 6.5, 50 mM EPPS, 50 mM NaCl, 1 mM TCEP and 5% D<sub>2</sub>O / 95 % H<sub>2</sub>O.

We have characterized Mcl-1 complexes with native BH3-like TCTP<sub>BH3</sub> and D16I variant TCTP<sub>BH3D16I</sub> at position h1 that restores the canonical BH3 sequence. When we compare <sup>1</sup>H-<sup>15</sup>N spectra from bound Mcl-1 in both complexes, it is clear that a single amino-acid mutation dramatically changed dynamics at the molecular interface. In term of chemical shift perturbations, differences were modest. But surprisingly, line broadening was canceled upon D16I mutation in bound Mcl-1 spectrum, indicating that D16 residue promotes conformational exchange (ms) at the molecular interface of the Mcl-1/TCTP<sub>BH3</sub> complex. D16I variant at h1 position strongly reduced the dynamics, leading to a more rigid complex. The same observation can be made by comparing with <sup>1</sup>H-<sup>15</sup>N spectrum from Mcl-1 complex with canonical Mule<sub>BH3</sub> peptide, reinforcing the idea that the BH3-like nature confers ability to promote conformational dynamics at the millisecond timescale on Mcl-1 protein. Moreover,

the nature of spectral perturbations was similar for Mcl-1 complex with Mule<sub>BH3</sub> compared with the canonical variant TCTP<sub>BH3D16I</sub> peptide and no major line broadening in Mcl-1 spectrum was observed upon complex formation. This strengthens the idea that the D16 residue in h1 is critical to induce dynamics at the molecular interface at the millisecond timescale. This also parallels the fact we could never observe NMR signals for the BH3-like region whether from TCTP FL or from the derived BH3 peptide, suggesting that the BH3-like region also suffers from extensive line broadening in the complex.

#### 4.3.2.2 Signatures of canonical and BH3-like motifs

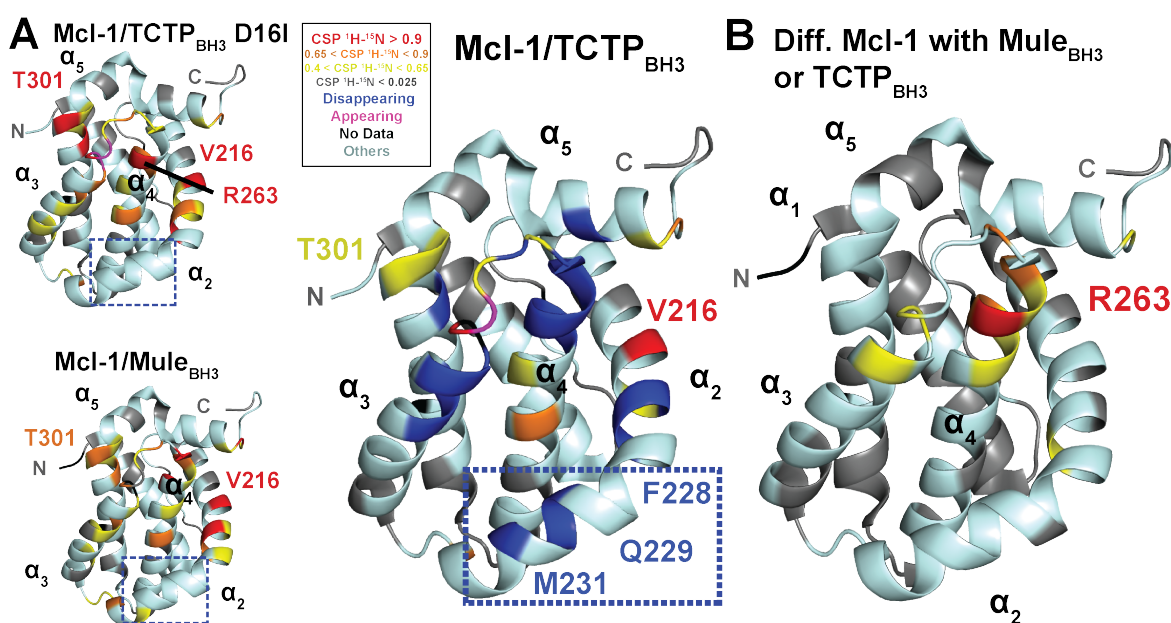


**Fig. 4.34 Binding interface of BH3-derived peptides at Mcl-1 protein.** (A) Representation of spectral perturbation in Mcl-1 spectrum upon complex formation with TCTP<sub>BH3D16I</sub>, Mule<sub>BH3</sub> and TCTP<sub>BH3</sub>. (B) Differences in terms of  $^1\text{H}$ - $^{15}\text{N}$  combined chemical shift perturbations between bound spectra of Mcl-1 in complex with TCTP<sub>BH3D16I</sub> or with Mule<sub>BH3</sub>. Colors indicate large  $^1\text{H}$ - $^{15}\text{N}$  combined chemical shift perturbations (red  $\geq$  orange  $\geq$  yellow  $\geq$  palecyan  $\geq$  grey, see legend for thresholds) or disappearing (blue) and appearing (magenta) residues. Residues for which no data were available are also highlighted (black). Experiments were recorded at 950 MHz and 35 °C in the following buffer: 50 mM MES pH 6.5, 50 mM EPPS, 50 mM NaCl, 1 mM TCEP and 5% D<sub>2</sub>O / 95 % H<sub>2</sub>O.

#### Binding mode of canonical and BH3-like sequences at Mcl-1 protein

We compared  $^1\text{H}$ - $^{15}\text{N}$  spectra of isolated Mcl-1 and in complex with native BH3-like peptide from TCTP or with canonical TCTP<sub>BH3D16I</sub> or Mule<sub>BH3</sub> and we described dynamics and binding sites in each Mcl-1 complex. Beyond the conformational dynamics promoted by the BH3-like sequence, we looked for structure determinant of Mcl-1 complex with BH3-like

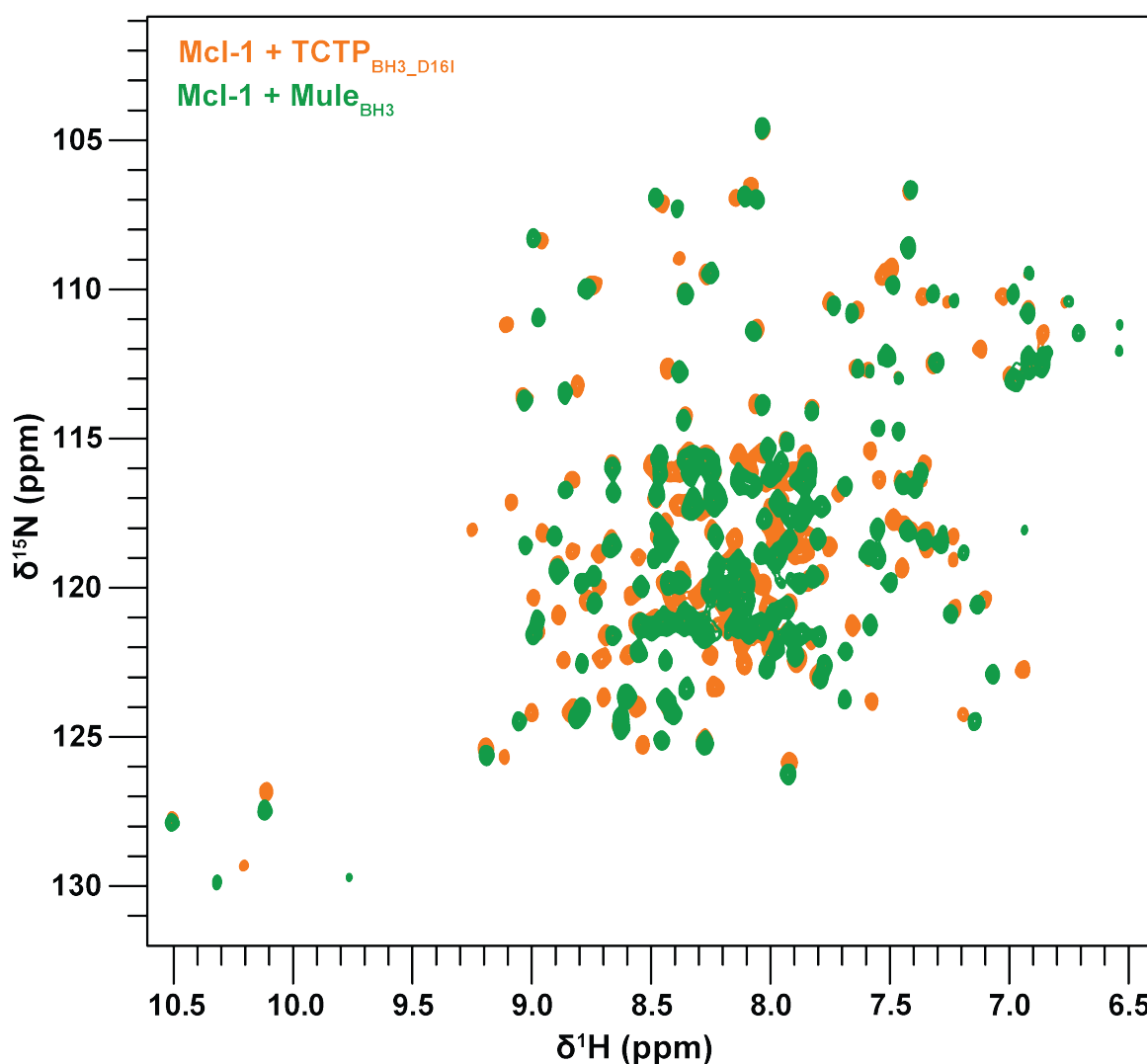


Fig. 4.35 **Comparison between Mcl-1 in complex with TCTP<sub>BH3D16I</sub> or Mule<sub>BH3</sub>** Overlay of <sup>1</sup>H-<sup>15</sup>N SOFAST HMQC spectra from <sup>15</sup>N-Mcl-1 (100 μM) in complex with TCTP<sub>BH3D16I</sub> (yellow) or Mule<sub>BH3</sub> (green). Experiments were recorded at 950 MHz and 35 °C in the following buffer: 50 mM MES pH 6.5, 50 mM EPPS, 50 mM NaCl, 1 mM TCEP and 5% D<sub>2</sub>O / 95 % H<sub>2</sub>O.

compared to canonical and thus we compared all three molecular interfaces with peptides at Mcl-1 protein (Fig. 4.34 A). Decisively, the C-terminal segment of helix  $\alpha_2$  encompassing residues F228, Q229 and M231 is affected with TCTP<sub>BH3</sub> with signal extinction whereas no significant perturbations could be detected with TCTP<sub>BH3D16I</sub> and Mule<sub>BH3</sub> in terms of both <sup>1</sup>H-<sup>15</sup>N chemical shifts and intensity. In the structure of Mcl-1/TCTP<sub>BH3</sub>, residue D16 could contact K234 residues in Mcl-1, as K234 side-chain is close from h1 position and in C-terminal of helix  $\alpha_2$ , where specific resonances are broadened upon binding of the native BH3-like sequence. Residues F254 and D256 in a connecting loop between helix  $\alpha_3$  and  $\alpha_4$

were not visible in the free Mcl-1 whereas they turned visible upon formation of the complex with TCTP<sub>BH3D16I</sub>, possibly protected from solvent-exchange. Apart from the final Mcl-1 complex with peptides, we have shown that the BH3-like sequence from TCTP induces a transient complex with Mcl-1 whereas this was not seen with canonical BH3 sequences.

### **Sensitive residues in Mcl-1 regarding the sequence of canonical BH3 motifs**

TCTP<sub>BH3D16I</sub> and Mule<sub>BH3</sub> are canonical BH3 in that all residues in positions h1-4 are hydrophobic but they strictly differ in their amino-acid composition (h1: I-V, h2: I-L h3: I-M h4: L-V). In addition they also strictly differ in the rest of their primary sequence and thus differences in the direction of <sup>1</sup>H, <sup>15</sup>N chemical shift perturbations between Mcl-1 complex with TCTP<sub>BH3D16I</sub> or Mule<sub>BH3</sub> inform on sequence-specific sensors of the BH3 motif at the binding interface in Mcl-1, if we do the hypothesis that the structures of the complexes are strictly the same. To further define active residues using HADDOCK docking algorithm, a software classically used to create structural models on the basis of sparse NMR data, such as chemical shift perturbations, we used this principle and compared <sup>1</sup>H-<sup>15</sup>N SOFAST HMQC spectra of <sup>13</sup>C, <sup>15</sup>N-Mcl-1 in complex with unlabeled TCTP<sub>BH3D16I</sub> or Mule<sub>BH3</sub> peptide (Fig. 4.35).

We have computed combined <sup>1</sup>H-<sup>15</sup>N chemical shift perturbations between the spectrum of bound Mcl-1 with TCTP<sub>BH3D16I</sub> or Mule<sub>BH3</sub> and plotted the result on the structure of Mcl-1 protein (Fig. 4.34 B). We have observed that a short stretch of amino-acids spanning on helices  $\alpha_3$ ,  $\alpha_4$  and the loop connecting them (252-266), hosted the vast majority of residues largely sensitive to the primary sequence of the BH3 peptide upon complex formation. These are consistently found at the molecular interface in the crystal structure of Mcl-1/Mule<sub>BH3</sub> but does not define the major part of the hydrophobic cleft in Mcl-1, with helix  $\alpha_2$  and parts of  $\alpha_3$  and  $\alpha_4$  that remain non significantly affected by the variation in the BH3 primary sequence. This indicates that the interface in Mcl-1 that contacts conserved h1-4 residues in canonical BH3 motifs is not significantly sensitive to the rest of the BH3 sequence. In other words, the structure and environment in this interface remains similar regardless the primary sequence of the BH3 peptide. Others areas on the protein surface were left weakly or not affected by the nature of the primary sequence of the BH3 peptide.

Finally, we did not observe significant differences in terms of chemical shift perturbations away from the BH3 interface. This means that Mcl-1 is likely to rearrange its  $\alpha$ -helix  $\alpha_5$ , or any other parts away from the molecular interface, in similar ways upon complex formation with TCTP<sub>BH3D16I</sub> or Mule<sub>BH3</sub>. In consequence, the differences we observed are expected to originate from Mcl-1 surfaces adapting to the peptides in a sequence-specific manner and with direct interaction.

## 4.3.2.3 Models of Mcl-1 complex with canonical and BH3-like motifs

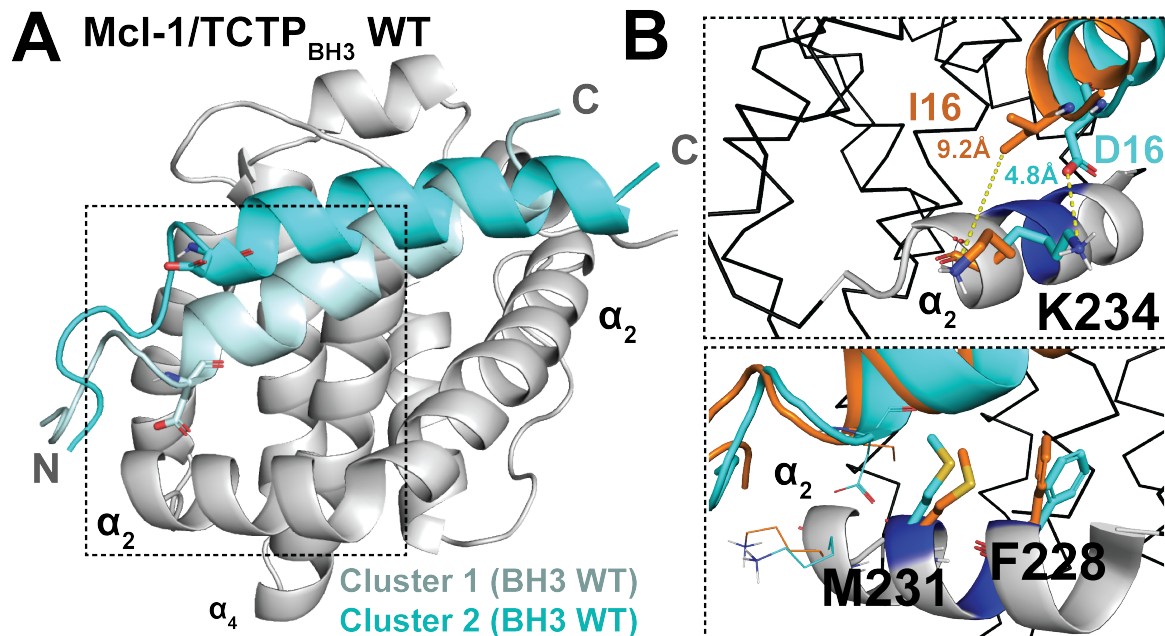


**Fig. 4.36 HADDOCK models of Mcl-1 complex with TCTP<sub>BH3</sub> and D16I variant.** (A) Representation of TCTP<sub>BH3</sub> poses in the more (palecyan) and second more (cyan) populated clusters generated using HADDOCK web server. (B) Side-chain rotations in helix  $\alpha_2$  for residue F228, M231 and K234 upon binding of either native BH3-like (cyan) from TCTP or D16I variant (orange). Residues D16 and I16 at position h1 are highlighted. For modeling we used the crystal structure of Mcl-1/Mule<sub>BH3</sub> complex and *in silico* mutants from the bound and helical Mule<sub>BH3</sub> to the TCTP-derived peptides with same length and secondary structure properties.

In order to obtain an experimental structure of the Mcl-1 in complex with TCTP or derived peptide, we first performed crystallogenesis assays on Mcl-1 complex with TCTP FL and BH3-like peptide. Despite several plates and hundreds of tested conditions, we could not obtain crystals convenient for X-Ray structure determination, this likely due to the high dynamics at the molecular interface between Mcl-1 and the BH3-like sequence both in TCTP FL and the derived BH3 peptide.

Thus, we used the crystal structure of Mcl-1/Mule<sub>BH3</sub> complex to separately submit structures of Mcl-1, Mule<sub>BH3</sub> peptide and *in silico* mutants (pdb file of bound and  $\alpha$ -helical Mule<sub>BH3</sub> in which all amino-acids were modified) for TCTP<sub>BH3</sub> and TCTP<sub>BH3D16I</sub>. We used active residues at the molecular interface for Mcl-1 (221, 252, 254, 255, 259, 261, 262, 263, 264, 265 and 266) as obtained from the previous analysis (Sec. 4.3.2.2) and for all three BH3 peptides (positions h1, h2, h3 and h4) with automatic definition of passive residues using the web interface of HADDOCK server which generates a set of clusters that represent possible

arrangements for each Mcl-1/peptide complex. Within the set of clusters of Mcl-1/TCTP<sub>BH3</sub>, the BH3-like peptide was more fluctuating in the BH3 binding groove of Mcl-1 compared with canonical TCTP<sub>BH3D16I</sub> or Mule<sub>BH3</sub>.

In all models, one cluster had significantly lower energy compared to others in each set, and the corresponding representative structures are more likely to be populated since they have the lowest Gibbs free energy. First, we observe two different poses of TCTP<sub>BH3</sub> in Mcl-1 groove for the two lowest energy clusters from HADDOCK (Fig. 4.36 A). We compared the different lowest energy clusters from Mcl-1/TCTP<sub>BH3</sub> and Mcl-1/TCTP<sub>BH3D16I</sub> to describe how Mcl-1 could arrange at helix  $\alpha_2$  to accommodate D16 residue at position h1 in TCTP<sub>BH3</sub> compared to the hydrophobic I16 in TCTP<sub>BH3D16I</sub>. We found out that side-chain of positively charged K234 residue contacts residue D16 by electrostatic interaction in native BH3-like peptide from TCTP (Fig. 4.36 B, top). By comparison, the terminal nitrogen atom of K234 was measured at less than 5 Å for Mcl-1/TCTP<sub>BH3</sub> whereas it was 9.2 Å for Mcl-1/TCTP<sub>BH3D16I</sub> complex, with the lysine side-chain pointing in opposite direction. This motion from side-chain of residue K234 can explain line broadening at close residues F228 and M231 since side-chains of those are also displaced in the conformation where D16 and K234 residues are close from each other in Mcl-1/TCTP<sub>BH3</sub> complex (Fig. 4.36 B, bottom). In the TCTP<sub>BH3D16I</sub> and Mule<sub>BH3</sub> this salt bridge with K234 in Mcl-1 can not form since D16 is replaced by an isoleucine or valine, respectively, thus quenching the conformational sampling. The pose in the second lowest energy cluster of Mcl-1/TCTP<sub>BH3</sub> corresponds to the first lowest energy cluster with TCTP<sub>BH3D16I</sub> (Fig. 4.36). By contrast the two lowest energy clusters of Mcl-1/TCTP<sub>BH3D16I</sub> are in the salt-bridge free conformation. We assume that this observation is the structural basis that explains why the BH3-like motif from TCTP with D16 residue promotes conformational heterogeneity at the molecular interface with Mcl-1 compared to canonical BH3s.

### 4.3.3 Relative affinity of BH3 peptides and TCTP protein for Mcl-1

#### 4.3.3.1 Relative affinity of TCTP<sub>BH3</sub>, D16I variant and Mule<sub>BH3</sub> at Mcl-1 protein

To estimate the relative affinity of native BH3-like peptide, D16I variant and BH3 motifs from Mule, we mixed an equal amount of each peptide (5 eq.) with free Mcl-1 (100  $\mu$ M) and measured  $^1\text{H}$ - $^{15}\text{N}$  spectra over hours (Fig. 4.37 A). In such competition experiments, we would expect Mcl-1 to “choose” to preferentially bind with the peptide(s) with highest affinity. System did equilibrate readily (> min.) and we measured crosspeaks intensity ratio ( $I_{\text{bound}}/I_{\text{free}}$ ) for reporter signals of all three distinct Mcl-1 complexes with BH3-derived peptide. Since we know the intensity ratio to expect between bound and free Mcl-1 consider-

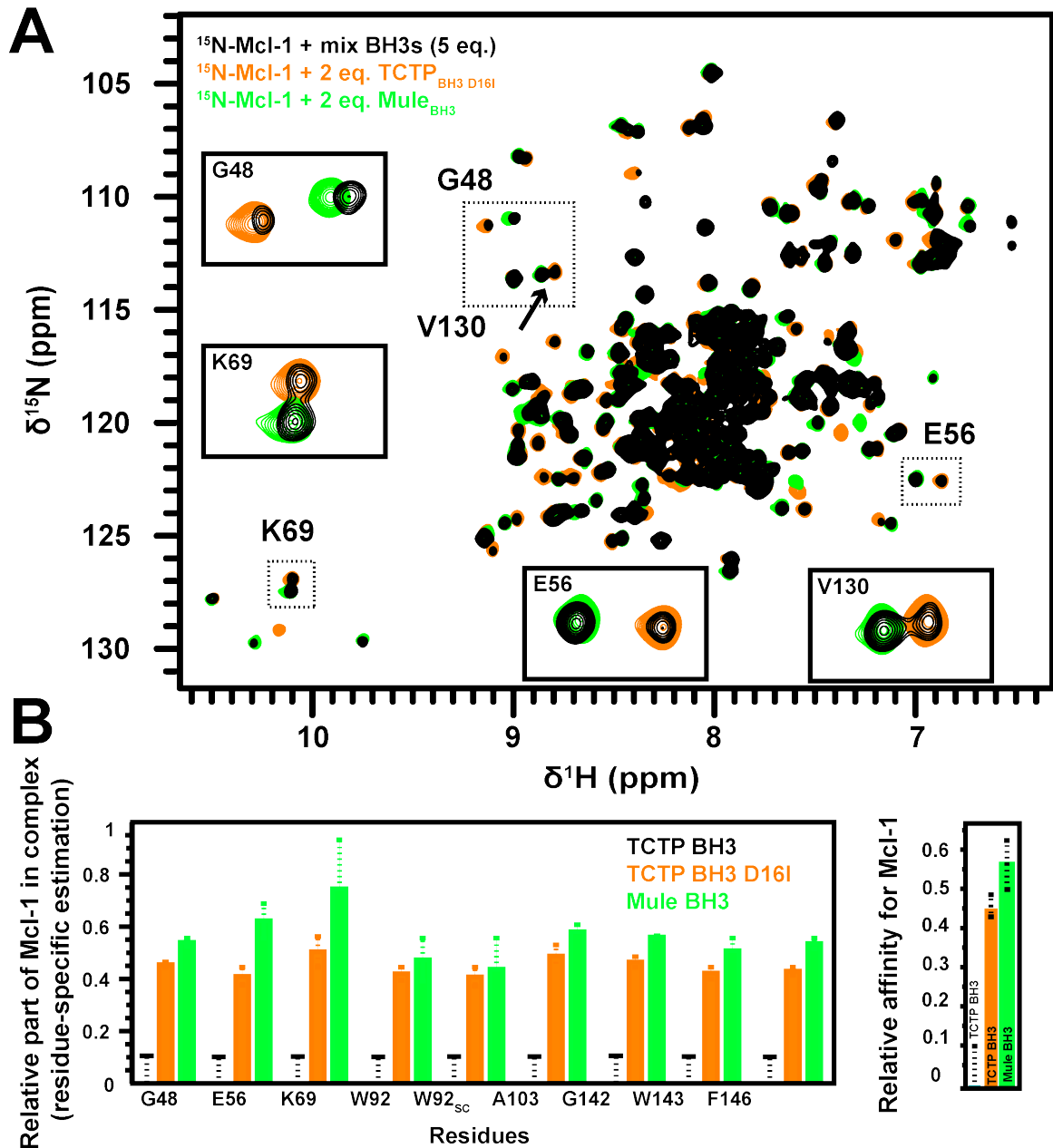


**Fig. 4.37 Relative affinity of TCTP<sub>BH3, BH3D16I</sub> and Mule<sub>BH3</sub> for Mcl-1.** (A) Overlay of <sup>1</sup>H-<sup>15</sup>N SOFAST HMQC spectra from <sup>15</sup>N-Mcl-1 (100 μM) in complex with TCTP<sub>BH3D16I</sub> (orange), Mule<sub>BH3</sub> (green) and with equimolar mix (5 eq. each) of the three peptides (black). (B) Relative population of <sup>15</sup>N-Mcl-1 bound to TCTP<sub>BH3</sub>, TCTP<sub>BH3D16I</sub> or Mule<sub>BH3</sub>. Ratios represent  $R_{Exp}/R_{Ref}$ , where  $R_{Exp}$  is, for example, equal to  $I_{bound}/I_{free}$ . Data are shown for all separated reported residues (left) and also the average (right). Experiments were recorded at 25 °C and 950 MHz in the following buffer: 50 mM EPPS pH 8, 50 mM NaCl, 2 mM TCEP and 5 % D<sub>2</sub>O / 95 % H<sub>2</sub>O.

ing 100 % complex formation, we can estimate the fraction of each complex in the sample by dividing intensity ratio of reporters in competition experiment by the intensity ratio in

the reference experiments (Fig. 4.37 B) that are  $^1\text{H}$ - $^{15}\text{N}$  spectra of 100 % bound Mcl-1 to either TCTP or Mule derived peptides. This complication in the calculation mode comes from expected differences in the relaxation properties and chemical exchange for Mcl-1 in complex with each peptide. For example, since line broadening is seen in the  $^1\text{H}$ - $^{15}\text{N}$  spectrum of Mcl-1 complex with TCTP<sub>BH3</sub> due to conformational exchange (ms) at the molecular interface, we expect less intensity from these residues upon complex formation compared with other Mcl-1/peptides complexes, for the same complex population fraction. Thus, rather than doing a simple ratio of intensities ( $I_{\text{bound}}/I_{\text{free}}$ ), we need to compute a ratio of ratio to obtain reliable parameters.

About ten reporters residues were chosen since they were well above the spectral noise and did not overlap in spectra from free Mcl-1 and in complex with all three different BH3 peptides (Fig. 4.37 A). On all reporter residues, we could not detect an unambiguous signal characteristic of  $^{15}\text{N}$ -Mcl-1 complex with native BH3-like peptide from TCTP. However, we could detect signals from the protein in complex with the D16I variant TCTP<sub>BH3D16I</sub> and Mule<sub>BH3</sub>. This indicates that TCTP<sub>BH3</sub> peptide has at least 5 times less affinity for Mcl-1 than the two canonical BH3 motifs. Indeed, in a simple competitive binding model and considering the estimated  $K_d$  for each Mcl-1/peptide complex, less than 10 % of the Mcl-1/TCTP<sub>BH3</sub> complex should be formed in our conditions (with 100  $\mu\text{M}$  Mcl-1 protein). This is below our detection level considering the reporter crosspeaks and intermediate exchange regime specific of resonances from Mcl-1/TCTP<sub>BH3</sub> complex.

Mule<sub>BH3</sub> has slightly higher relative affinity for Mcl-1 compared to TCTP<sub>BH3D16I</sub> since 55 % of Mcl-1 was bound to Mule<sub>BH3</sub> at equilibrium compared to 45 % bound to TCTP<sub>BH3D16I</sub> (Fig. 4.37 C). This correlates with the lower ratio for saturation of Mcl-1 by Mule<sub>BH3</sub> (1:2) compared to TCTP<sub>BH3D16I</sub> (1:3) and allows to conclude that Mule has comparable but slightly greater relative affinity to Mcl-1 compared to TCTP<sub>BH3D16I</sub>, consistently with the absolute values of  $K_d$  we reported before. In contrast, the presence of D16 in the BH3-like motif significantly reduced the affinity by at least a factor of at least 5 compared to TCTP<sub>BH3D16I</sub>. We finally tested if dissociation kinetics could allow for displacement of TCTP<sub>BH3D16I</sub> by Mule<sub>BH3</sub>. In order to remove free peptides from the sample containing bound Mcl-1 and the free peptides that remain, we desalted the sample to remove free peptides, checked that Mcl-1 was still fully bound and we added a large excess (10 eq.) of Mule<sub>BH3</sub> and observed the dissociation of the Mcl-1/TCTP<sub>BH3D16I</sub> over several hours, yielding only Mcl-1/Mule<sub>BH3</sub> at equilibrium (> 95 %). This shows the competitive binding of the two peptides at the BH3 binding groove of Mcl-1. Similarly, the competition experiments precluded the

binding of TCTP<sub>BH3</sub> to Mcl-1, reinforcing the structural model where peptides can only form heterodimeric complexes since their binding interfaces all largely overlap at Mcl-1 protein.

#### 4.3.3.2 Mule<sub>BH3</sub> at the transient Mcl-1/TCTP<sub>BH3</sub> complex

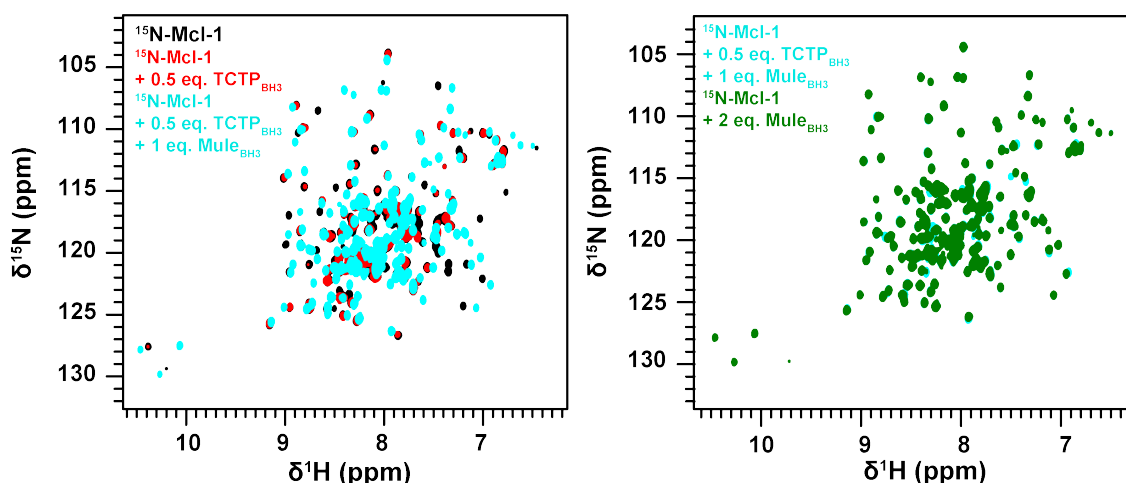


Fig. 4.38 **Dissociation of transient Mcl-1/TCTP<sub>BH3</sub> by Mule<sub>BH3</sub>.** (A) Overlay of <sup>1</sup>H-<sup>15</sup>N SOFAST HMQC spectra from isolated <sup>15</sup>N-Mcl-1 (100 μM) (black), in transient complex with TCTP<sub>BH3</sub> (red) and upon addition of Mule<sub>BH3</sub> (2 eq.) (cyan). (B) Overlay of <sup>1</sup>H-<sup>15</sup>N SOFAST HMQC spectra from <sup>15</sup>N-Mcl-1 with the TCTP<sub>BH3</sub> (0.5 eq.) and Mule<sub>BH3</sub> (1 eq.) (cyan) and reference spectrum of <sup>15</sup>N-Mcl-1 bound to Mule<sub>BH3</sub> (green). Experiments were recorded at 35 °C and 950 MHz in the following buffer: 50 mM MES pH 6.5, 50 mM NaCl, 2 mM TCEP and 5 % D<sub>2</sub>O / 95 % H<sub>2</sub>O.

Since we observed that the BH3-like motif in TCTP promotes a transient complex with Bcl-2 family partners in solution, we tested if the transient Mcl-1/TCTP<sub>BH3</sub> complex could prevent Mule<sub>BH3</sub> from binding to Mcl-1, even though this hypothesis lacks strong rationale since the transient complex appears to have much lower affinity compared to stable Mcl-1/Mule<sub>BH3</sub> complex. We prepared the transient complex with half equivalent of TCTP<sub>BH3</sub> peptide in Mcl-1 sample and recorded <sup>1</sup>H-<sup>15</sup>N spectrum of the protein (Fig. 4.38 A). Signals from the BH3-binding groove of Mcl-1 did totally disappear, as described before (Sec. 4.2.3.3). We added 2 eq. of Mule<sub>BH3</sub> peptide in the sample and measured <sup>1</sup>H-<sup>15</sup>N experiment to test if Mcl-1/Mule<sub>BH3</sub> complex could be readily formed or inhibited by the pre-formed transient Mcl-1/TCTP<sub>BH3</sub> complex. We immediately (min.) observed that transient Mcl-1/TCTP<sub>BH3</sub> complex was dissociated upon addition of Mule<sub>BH3</sub> peptide. We nearly recovered the reference <sup>1</sup>H-<sup>15</sup>N spectrum of Mcl-1 complex with Mule<sub>BH3</sub> (Fig. 4.38 B). This indicates that the native BH3-like sequence from TCTP can not protect Mcl-1 from Mule<sub>BH3</sub> binding, as expected considering the faster exchange regime seen in transient Mcl-1/TCTP<sub>BH3</sub> which suggests lower relative affinity compared to Mcl-1/Mule<sub>BH3</sub> complex.

#### 4.3.3.3 Full length TCTP protein and its BH3-like peptide

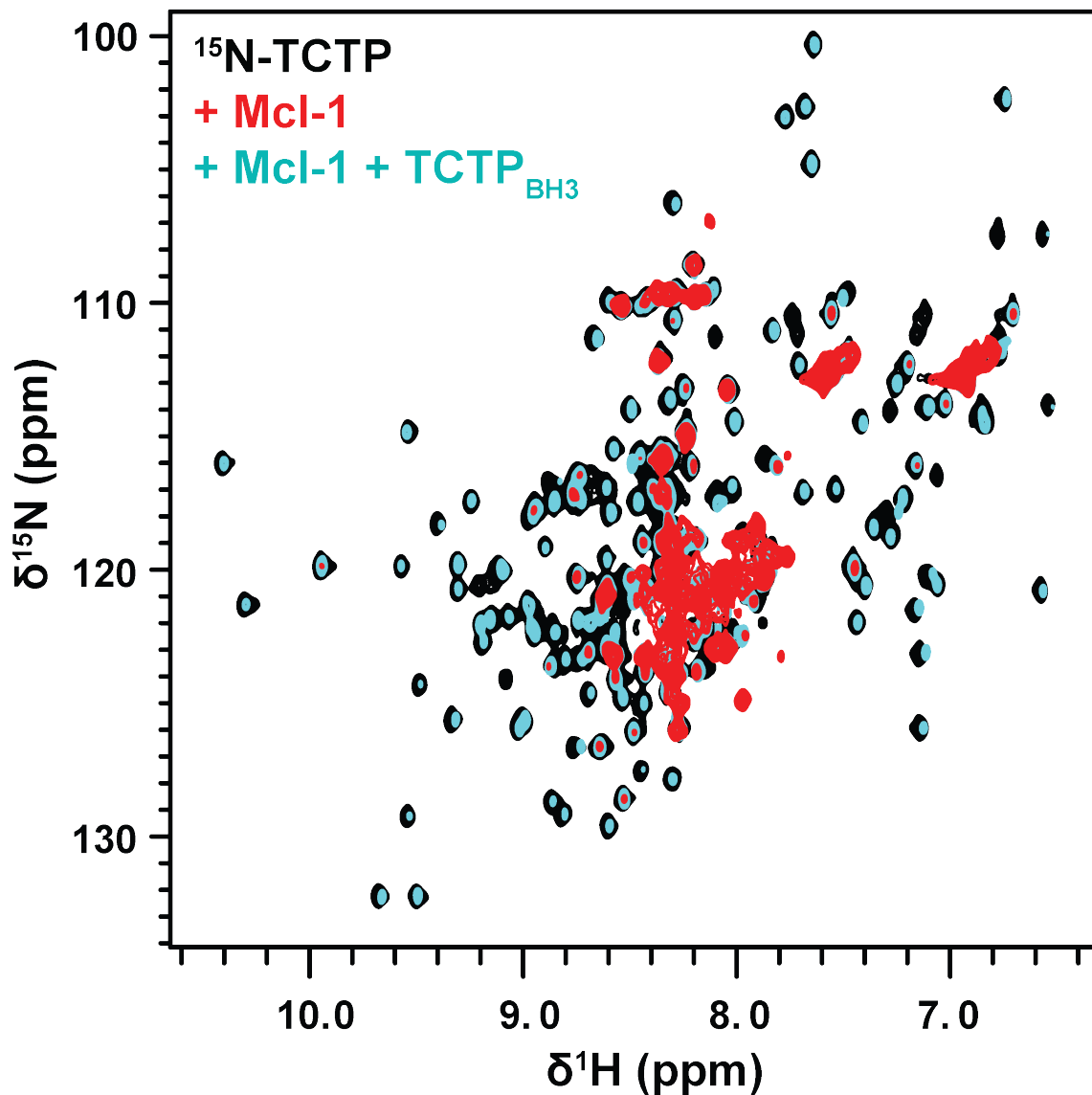


Fig. 4.39 **Impact of pre-formed TCTP/Mcl-1 complex on TCTP<sub>BH3</sub> binding.** Overlay of  $^1\text{H}$ - $^{15}\text{N}$  SOFAST HMQC spectra from isolated  $^{15}\text{N}$ -TCTP (100  $\mu\text{M}$ ) (black), in complex with unlabeled Mcl-1 (2 eq.) (red) and upon addition of TCTP<sub>BH3</sub> peptide (2 eq.) (cyan). Experiments were recorded at 35  $^\circ\text{C}$  and 950 MHz in the following buffer: 50mM MES pH 6.5, 50 mM NaCl, 2 mM TCEP and 5 %  $\text{D}_2\text{O}$  / 95 %  $\text{H}_2\text{O}$ .

#### **BH3-like peptide at TCTP/Mcl-1 complex**

We could not identify a significant contribution of full length TCTP versus the BH3-like peptide at the molecular interface with Mcl-1 protein. Both full length protein and peptide did bind Mcl-1 with very similar modes, including binding site definition and dynamics (ms)

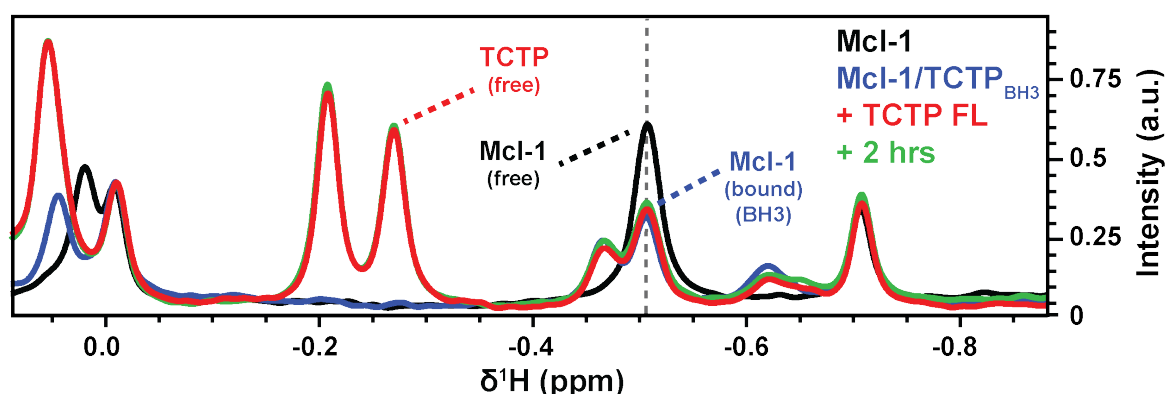


Fig. 4.40 **Impact of pre-formed TCTP<sub>BH3</sub>/Mcl-1 complex on TCTP FL binding.** Overlay of <sup>1</sup>H spectra from isolated Mcl-1 (100 μM) (black) and upon addition of TCTP<sub>BH3</sub> (4 eq., 2 hrs) (blue) and TCTP FL (2 eq.) (cyan) after incubation time (2 hrs) (red). Experiments were recorded at 35 °C and 950 MHz in the following buffer: 50 mM EPPS pH 8, 50 mM NaCl, 2 mM TCEP and 5 % D<sub>2</sub>O / 95 % H<sub>2</sub>O.

inside the complexes. Thus, we wanted to test if the affinity of full length TCTP for Mcl-1 protein was significantly different than the affinity between the BH3-like peptide and the same Mcl-1 protein. We first pre-formed <sup>15</sup>N-TCTP complex with unlabeled Mcl-1 ΔPEST ΔTM (Mcl-1) (2 eq.) and we obtained a populated complex (> 90 %) after equilibration time (2 hrs) (Sec. 4.39). Then, we added an excess of TCTP<sub>BH3</sub> peptide (4 eq.) and we progressively observed over time (2 hrs) a gradual increase of free full length TCTP protein in the NMR tube as seen in the corresponding <sup>1</sup>H-<sup>15</sup>N SOFAST HMQC spectrum (Sec. 4.39).

However, we commonly observe a loss of intensity from flexible residues and solvent-exposed side-chains in the spectrum of <sup>15</sup>N-TCTP bound to Mcl-1. Upon dissociation of TCTP/Mcl-1 by the TCTP<sub>BH3</sub> peptide we could not recover the whole spectral intensity from native TCTP. Then, upon addition of a large excess of Mcl-1/BH3 peptide we could recover Mcl-1/Mcl-1/BH3 complex, as seen in the corresponding <sup>1</sup>H experiment, but still we did not recover significantly more free TCTP protein. However, we could not detect significant crosspeak patterns corresponding to bound TCTP anymore upon addition of a large excess of peptides. This means that a significant fraction of TCTP turns in a dead angle for NMR upon complex formation with Mcl-1 or dissociation. We know that TCTP/Mcl-1 can still form oligomers in these conditions, and this can first explain at least part of the observation. Moreover, we do not know at which extent bound TCTP could refold to the native TCTP state upon dissociation. We have shown that TCTP\* state is more prone to aggregation than the native state, especially at high temperature as we use 35 °C in the current experiment. If dissociation and refolding to the native TCTP state involves the TCTP\* state, as we strongly think, then we do not expect to recover all the spectral intensity present at the beginning of the

experiment with native TCTP. The consequence of this is the impossibility to reliably quantify the relative affinity between TCTP FL and the BH3-like peptide. However, we can still affirm that the peptide dissociates TCTP FL from Mcl-1 when used at similar concentration regarding full length TCTP. This suggests, as we expected, that the affinity of both full length protein and peptide for Mcl-1 protein is likely in the same order of magnitude. That fits with the poor differences we could observe in the behavior of TCTP FL or the BH3-like peptide at the molecular interface with TCTP. Another more practical explanation is that the TCTP\* (free or in complex) is more prone to proteases than native TCTP, and the cleaved TCTP\* probably cannot refold properly.

### **Full length TCTP at Mcl-1/TCTP<sub>BH3</sub> complex**

Even though we demonstrated that TCTP<sub>BH3</sub> can dissociate Mcl-1/TCTP at near equimolar TCTP:peptide ratio, we could not quantify the relative affinity of the BH3-like peptide and full length TCTP protein for Mcl-1 and thus thought to proceed with the reverse competition experiment.

On September 29<sup>th</sup> of this year, at night (2-3 in the morning), whereas my PhD contract was going to end a few hours ahead, I thought it was important to spend a bit more time with the 950 MHz to have a last moment of intimacy with my favorite machine. The first intention was to observe the dissociation of Mcl-1 and TCTP<sub>BH3</sub> upon full length TCTP addition to get the relative affinity information by canceling the problem of intensity recovery we mentioned in the previous paragraph. Since I could not find any <sup>15</sup>N-labeled Mcl-1 protein left in the lab I followed the informed recommendation of my PhD supervisor, E. Lescop, and I used unlabeled Mcl-1  $\Delta$ PEST  $\Delta$ TM (Mcl-1), TCTP<sub>BH3</sub> and TCTP FL to perform a last series of spectra, a last experiment before a long time out of the lab. Using unlabeled Mcl-1 protein, I measured <sup>1</sup>H spectrum and this was characteristic of the free protein (Sec. 4.40). Upon TCTP<sub>BH3</sub> addition, we obtained the <sup>1</sup>H spectrum with characteristic signatures of bound Mcl-1 to the BH3-like peptide. Then, we added TCTP in the tube. And strictly nothing happened when looking at unlabeled TCTP signatures over time (Sec. 4.40). Whereas the TCTP<sub>BH3</sub> peptide did dissociate TCTP FL over time, the reverse effect could not be observed. This is even more surprising considering that the affinity of rather full length TCTP or BH3-like peptide for Mcl-1 protein were similar in experiments with separated binary systems Mcl-1/TCTP or Mcl-1/TCTP<sub>BH3</sub>.

Finally, I realized that this was maybe the more significant and undeniable proof of the existence of TCTP\* as a concept in urea-free conditions. It is not possible to explain what we observed if we do not invoke a minor TCTP state in solution. Indeed, since TCTP\* would be a very minor state (< 1 %), the concentration of "active" full length TCTP would always be

negligible compared to the active concentration of  $\text{TCTP}_{\text{BH3}}$ . These experiments therefore informed us that the peptide has a much greater affinity compared to the full length protein due to the small fraction of  $\text{TCTP}^*$  in the whole TCTP content.

## 4.4 Discussion

### Model for TCTP interactions with Bcl-xL and Mcl-1

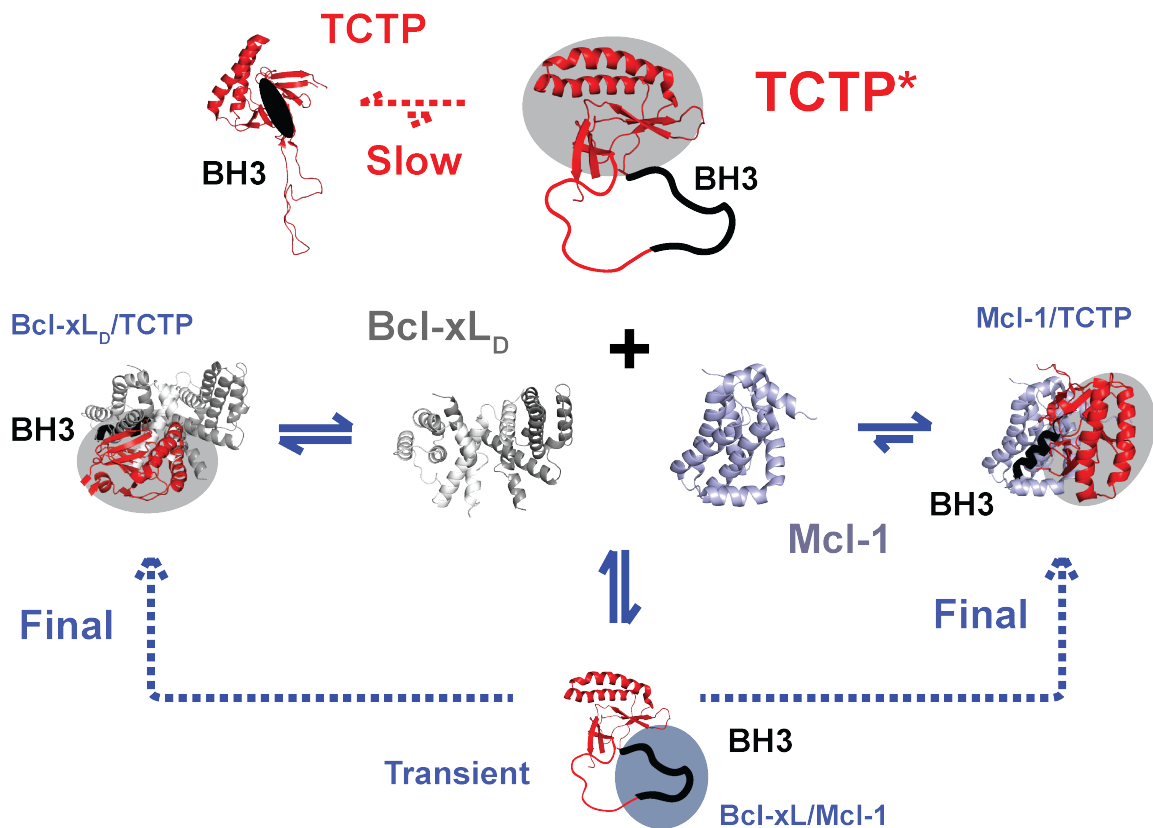


Fig. 4.41 **Model for TCTP interactions with Bcl-2 family proteins Bcl-xL and Mcl-1.** TCTP (red) exists with major (TCTP) and minor (TCTP\*) (< 1 %) states. Native TCTP slowly convert to TCTP\* state (> min.). TCTP\* has molten-globule organization in the globular domain (grey sphere) with unpinned, solvent-exposed BH3-like motif (black line). Bcl-xL exists as a mixture of monomer and dimer and we represent Bcl-xL as dimer (lightgrey) with Mcl-1 as monomer (mauve). TCTP complex with partners are transient (bottom) or more stable (sides). TCTP complex with Bcl-xL is shown with 1:2 stoichiometry, possibly leaving a free binding interface in Bcl-xL for Bax. TCTP/Mcl-1 complex is shown as heterodimer.

As we demonstrated, TCTP exists as major, native TCTP and in the minor (< 1 %), molten-globule TCTP\* state, slowly converting from TCTP (> min.). Bcl-xL exists as a mixture

of monomer and dimer and we confirmed that heterotetramers were mostly forming with TCTP [111]. Moreover it was reported that TCTP affinity for Bcl-xL dimers is higher compared to monomers [111]. Thus, we simplified by only considering Bcl-xL dimers, but not monomer, in our model (Fig. 4.41). Mcl-1 is known to be as a monomeric protein in solution and we confirmed this (Sec. 4.2.1.1). TCTP and Bcl-2 family proteins slowly assemble together because the native TCTP takes time to convert into TCTP\*, which is the only species forming complexes with partners. If TCTP\* is also a dimer in native conditions of population (< 1 %), temperature (25-35 °C) and buffer (pH 7-8, 50-150 mM NaCl) and considering that we established that it corresponds to the active state of TCTP protein, it is seducing to envisage that interactions with Bcl-2 family partners dissociate the dimer of TCTP\*, since we know that major TCTP/Mcl-1 complex contains a single TCTP unit. Upon conversion, TCTP\* forms a weak affinity, transient complex with Bcl-xL and Mcl-1, that is overridden by a more stable, stable complex that form predominantly at high TCTP:partners ratios or long (2 hrs) equilibration time. It is unclear if the transient interaction represents an encountering complex that proceeds to final TCTP complex with Bcl-2 family partners. It can also be forming off pathway and then could represent the TCTP complexes when Bcl-xL/Mcl-1 are in less permissive conformations, preventing TCTP to lock into the BH3 binding groove. In the final TCTP complex with Mcl-1, heterodimers are thought to be predominant. With Bcl-xL, heterotetramers were suggested. Interestingly, TCTP dissociates fast (< min.) from Bcl-xL under lower temperature, dilution or any change that modify populations at equilibrium. Compared to TCTP complex with Mcl-1, it is likely that TCTP in complex with Bcl-xL dissociates faster considering that it can be reversed upon non favorable conditions. This raises the possibility for conformational selection by BH3 ligands such as Bax at the free Bcl-xL unit from the dimer. Indeed, dissociation of TCTP could release a 1:2 TCTP/Bcl-xL complex with exposition of a specific interface (Fig. 4.41).

## Chapter 5

# Exploration and frontiers in TCTP interactome

Dozens of partners were reported to interact directly with TCTP [145]. They are diverse by nature and the list is regularly updated [145], as for the newly identified TCTP partner YB-1, a pleiotropic protein originally discovered as a transcription factor. In the context of cancer, anti-TCTP drugs such as sertraline are thought to break protein-protein interactions with specific partners, such as MDM2 protein, leading to the restoration of p53 levels. At the *frontiers* of TCTP interactome, the TCTP/Mcl-1 interaction can also be abolished, in principle, by targeting Mcl-1 protein with small molecules. Our collaborator F. Roussi (ICSN, CNRS/Université Paris-Saclay) develops molecules targeting Mcl-1 protein but lacked a structural description to further improve them.

In this last chapter of results, we will examine the interplay between TCTP, YB-1 and RNA molecules. To discuss the molecular interface in TCTP/MDM2 complex and related bound TCTP structure, we will investigate the interaction between the full length TCTP and MDM2 N-terminal domain (Sec. 5.1). Then we will report our binding studies with TCTP inhibitors, sertraline and related, known to break TCTP/MDM2 complex with efficiency in clinical assays for cancer treatment (Sec. 5.2). At the *frontiers* of TCTP interactome, we will map binding sites and confirm selectivity for ligands targeting preferentially Mcl-1 compared to Bcl-xL in line with medicinal chemistry need (Sec. 5.3). Finally, we will discuss our finding at the end of the chapter (Sec. 5.4).

## 5.1 TCTP complex with proteins and RNA

### 5.1.1 The E3 ubiquitin ligase MDM2

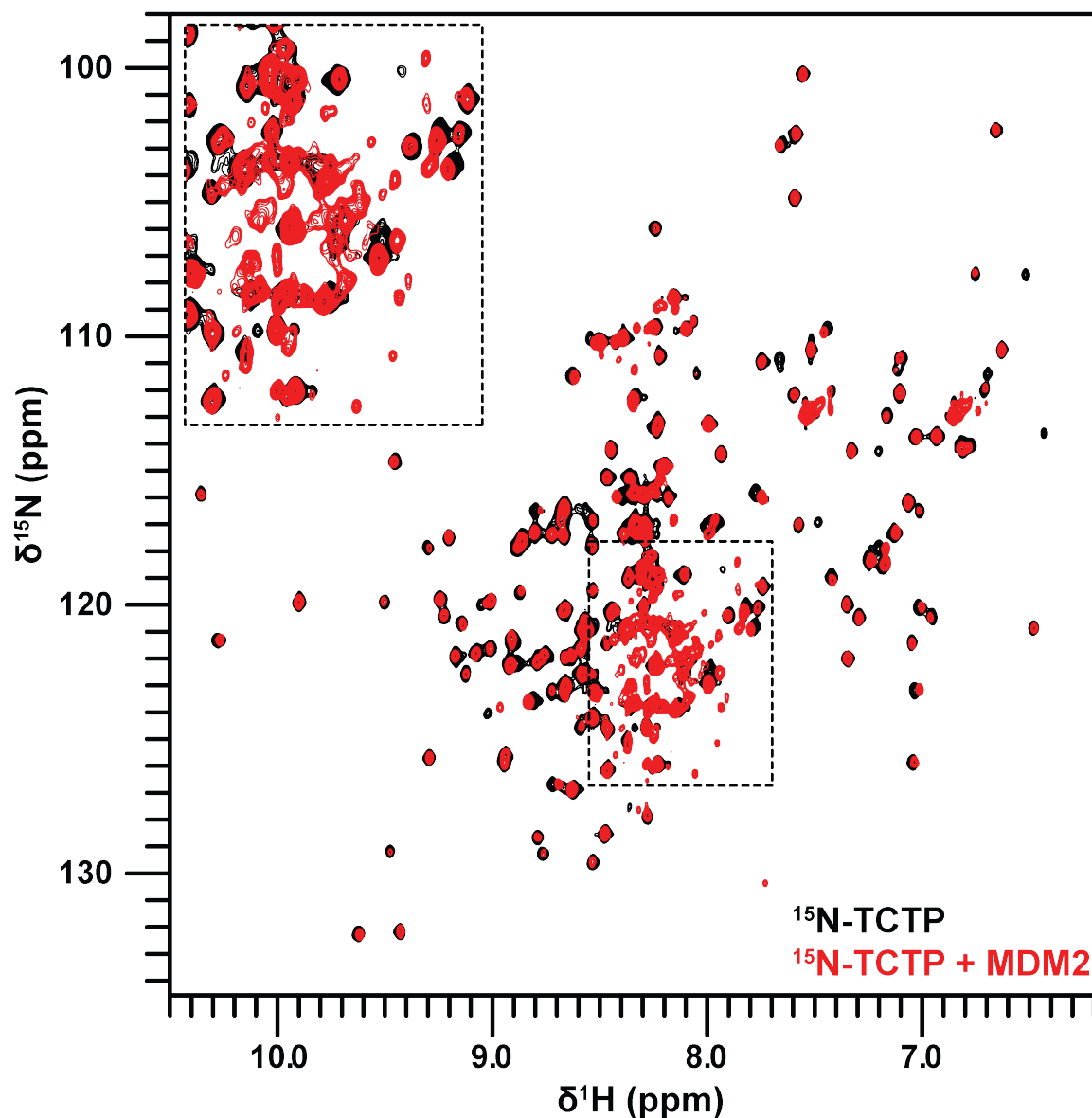
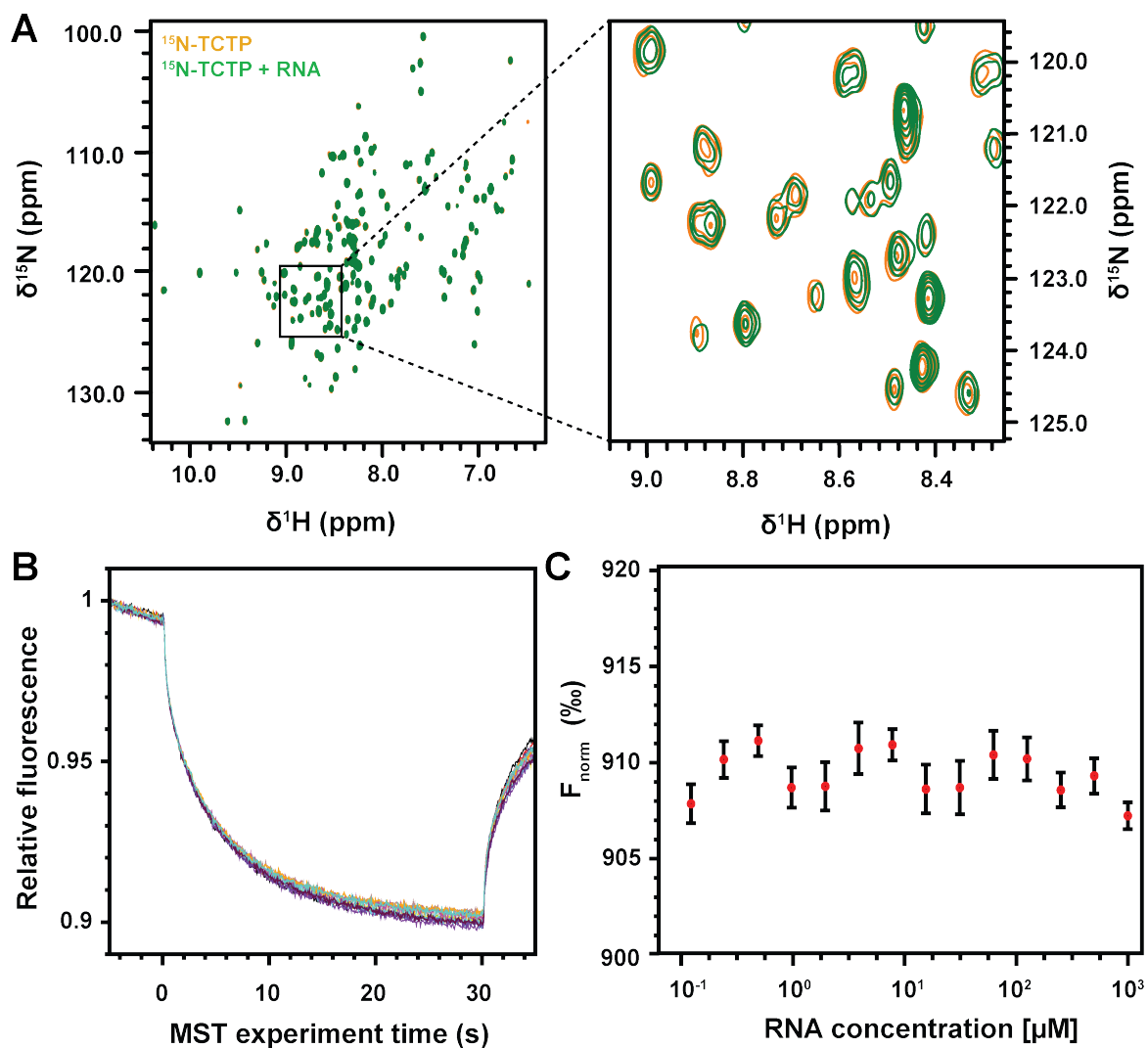


Fig. 5.1 TCTP upon partial complex formation with MDM2 N-terminal domain. Overlay of  $^1\text{H}$ - $^{15}\text{N}$  SOFAST HMQC spectra from isolated  $^{15}\text{N}$ -TCTP (50  $\mu\text{M}$ ) (black) and upon addition of unlabeled MDM2 (3.5 eq.) and system equilibration (2 hrs) (red). A close-up view of the central region is shown (top-left). Experiments were recorded at 950 MHz and 25  $^\circ\text{C}$  in the following buffer: 50 mM  $\text{NaPO}_4$  pH 6.8, 12.5 mM KCl, 2 mM TCEP and 5%  $\text{D}_2\text{O}$  / 95 %  $\text{H}_2\text{O}$ .

The interaction between TCTP and the E3 ubiquitin ligase MDM2 was reported to induce decreased p53 levels in cancer cells. Indeed, TCTP stabilizes MDM2 and thus promotes

proteasome-mediated p53 degradation [173]. This promotes cancer cell survival and constitutes part of TCTP antiapoptotic mode of action. TCTP was proposed to bind MDM2 N-terminal domain [150] through its  $\alpha$ -helices  $\alpha_2$  and  $\alpha_3$  (residues 68-133) or, alternatively, MDM2 C-terminal domain [173] through its N-terminal segment (residues 1-68). Drugs targeting MDM2/partners association are of great interest to promote higher levels of tumor suppressors such as p53 [266]. Moreover, we introduced before anti-TCTP drugs such as sertraline and thioridazine (Sec. 1.2.3.3) that target TCTP/MDM2 interaction at TCTP protein. Overall, it is of great interest to decipher the molecular basis for this interaction in order to improve our knowledge about two pharmacological targets of choice. Thus, we decided to test if the full length TCTP could bind to the N-terminal domain of MDM2 protein and to get details of the interaction mode and surfaces.

As preliminary studies, the interaction between full length  $^{15}\text{N}$ -TCTP and the unlabeled MDM2 N-terminal domain (1-125) (MDM2) was monitored by recording  $^1\text{H}$ - $^{15}\text{N}$  SOFAST HMQC spectra of TCTP upon successive additions of MDM2 (Fig. 5.1). The whole spectral intensity from the structured parts of TCTP gradually decreased upon addition of MDM2 but no significant diminishing in intensity could be observed in TCTP IDR, meaning that the loop dynamics remains unaffected upon complex formation. However, a small set of crosspeaks in the  $^1\text{H}$ - $^{15}\text{N}$  SOFAST HMQC spectra from TCTP appeared with slow kinetics after each partner addition and these were strengthened until system stabilization (2 hrs). Protein degradation can be excluded from SDS-PAGE analysis of samples and the usual very long lifetime of free and bound TCTP samples, typically days at 35 °C. Similarly to what observed with Bcl-2 family partners (Sec. 4.2.2), several hours were required to reach the equilibrium. However, no signatures from TCTP\* like C172 could be identified concerning the visible part of the protein upon complex formation. But we could only characterize TCTP\* in more alkaline conditions (pH 8) and thus we can not say how this particular state behaves at more acidic pH (pH 6.8) which impairs for the detection of specific signatures. Finally, visible TCTP does not seem to form a fast forming, transient complex with MDM2 even though we could only detect it by looking at TCTP bound partners  $^1\text{H}$ - $^{15}\text{N}$  spectra in the last chapter with Bcl-2 family proteins (4.2.3). Thus, we can not exclude that such transient complex exists if it also involves a minor, non NMR-visible TCTP. In conclusion, TCTP interacts with MDM2 N-terminal domain (MDM2) in one slow kinetics step and the structure of TCTP is likely to undergo major structure and dynamics changes upon complex formation.



**Fig. 5.2 Interaction of TCTP with RNAs from yeast by NMR and MST experiments.** (A) Overlay of  $^1\text{H}$ - $^{15}\text{N}$  SOFAST HMQC spectra from isolated  $^{15}\text{N}$ -TCTP (50  $\mu\text{M}$ ) (orange) and upon addition of unlabeled RNA extract from yeast (0.3  $\text{mg}\cdot\text{mL}^{-1}$ ) (green). A close-up view of part of the central region is shown (right). Experiments were recorded at 950 MHz and 25  $^\circ\text{C}$  in the following buffer: 10 mM HEPES pH 7.4, 150 mM NaCl, 2 mM TCEP and 5%  $\text{D}_2\text{O}$  / 95 %  $\text{H}_2\text{O}$ . (B) MST traces and (C) normalized MST signals ( $F_{\text{norm}}$ ) from labeled TCTP (20-40 nM) in function of RNA concentration (0.1-1000  $\mu\text{M}$ ) calculated from average MW for single ribonucleotides. For MST experiments, 100 %  $\text{H}_2\text{O}$  and 0.005 % Tween20 were used for buffer preparation.

### 5.1.2 Interaction studies between TCTP and RNAs

Our collaborators A. Telerman and R. Amson (IGR, INSERM/Université Paris-Saclay) have identified that TCTP plays a role in RNA fate, and more specifically the subcellular and extracellular distribution of RNA. For confidentiality reasons we cannot describe more this in

more details (yet unpublished results). In order to provide a molecular basis to this biological function of TCTP, we aimed at characterizing if TCTP could directly interact with RNA.

To test if TCTP could interact with RNA sequences, we recorded  $^1\text{H}$ - $^{15}\text{N}$  SOFAST HMQC spectra of the  $^{15}\text{N}$ -labeled protein (50  $\mu\text{M}$ ) in absence or in presence of increasing of RNA concentration from yeast RNA extracts to reach 1:65 protein:RNA molar ratios. The RNA concentration was calculated as nucleotide equivalents. In case of interaction between TCTP and RNA, we typically expect chemical shift or intensity changes in the spectrum of the protein upon RNA addition. These perturbations usually reflect a change in the very close environment of the protein or in the molecular tumbling. Here, we compared spectra from isolated TCTP and in the presence of RNA in a 1:65 molar ratio (Fig. 5.2 A). We could not observe significant perturbation in the  $^1\text{H}$ - $^{15}\text{N}$  spectrum of  $^{15}\text{N}$ -TCTP. Indeed, no rapid exchange chemical shift perturbations could be reliably observed and we could not detect a new TCTP state since the total of crosspeaks remained unchanged upon RNA addition in  $^{15}\text{N}$ -TCTP spectrum. In term of spectral intensity, we did not observe significant variations neither. This indicates that the oligomeric state of the TCTP is unaffected by the presence of RNA and that no interaction at the surface of the protein giving rise to intermediate exchange is present.

To confirm that TCTP does not interact with RNA sequences from yeast extract, MST experiments were performed with TCTP (20-40 nM) at increasing concentrations of RNAs (0.1-1000  $\mu\text{M}$  eq. nucleotides) (Fig. 5.2 B, C). We could record MST curves and observe that all were slightly different but regardless the concentration of RNA, suggesting that the variations originate from the measurement error (Fig. 5.2 B). When calculating the normalized MST response ( $F_{\text{norm}}$ ), we confirmed that the small variations (5 %) observed were meaningless regarding the RNA concentration in solution (Fig. 5.2 C). This indicates that we could not detect a change in TCTP oligomeric state or association with RNA since the diffusion properties of the protein remain unchanged upon addition of the yeast extract.

In conclusion, we have shown using NMR and MST experiments that TCTP does not interact with RNAs sequences from yeast extract. However and despite the variety of RNA sequences in the extract, we can not exclude that TCTP does present a low to moderate affinity ( $K_d > \mu\text{M}$ ) for a specific pattern that would not be sufficiently present in the mix ( $[\text{RNA}] < \mu\text{M}$ ). This result is part of a paper in preparation with our collaborators and suggested that the observed RNA-related biological event they observed is likely not due to direct interaction between TCTP and RNA but most probably due to the regulation of RNA binding protein by TCTP.

### 5.1.3 TCTP and the RNA binding YB-1 protein

#### 5.1.3.1 TCTP interacts with full length YB-1

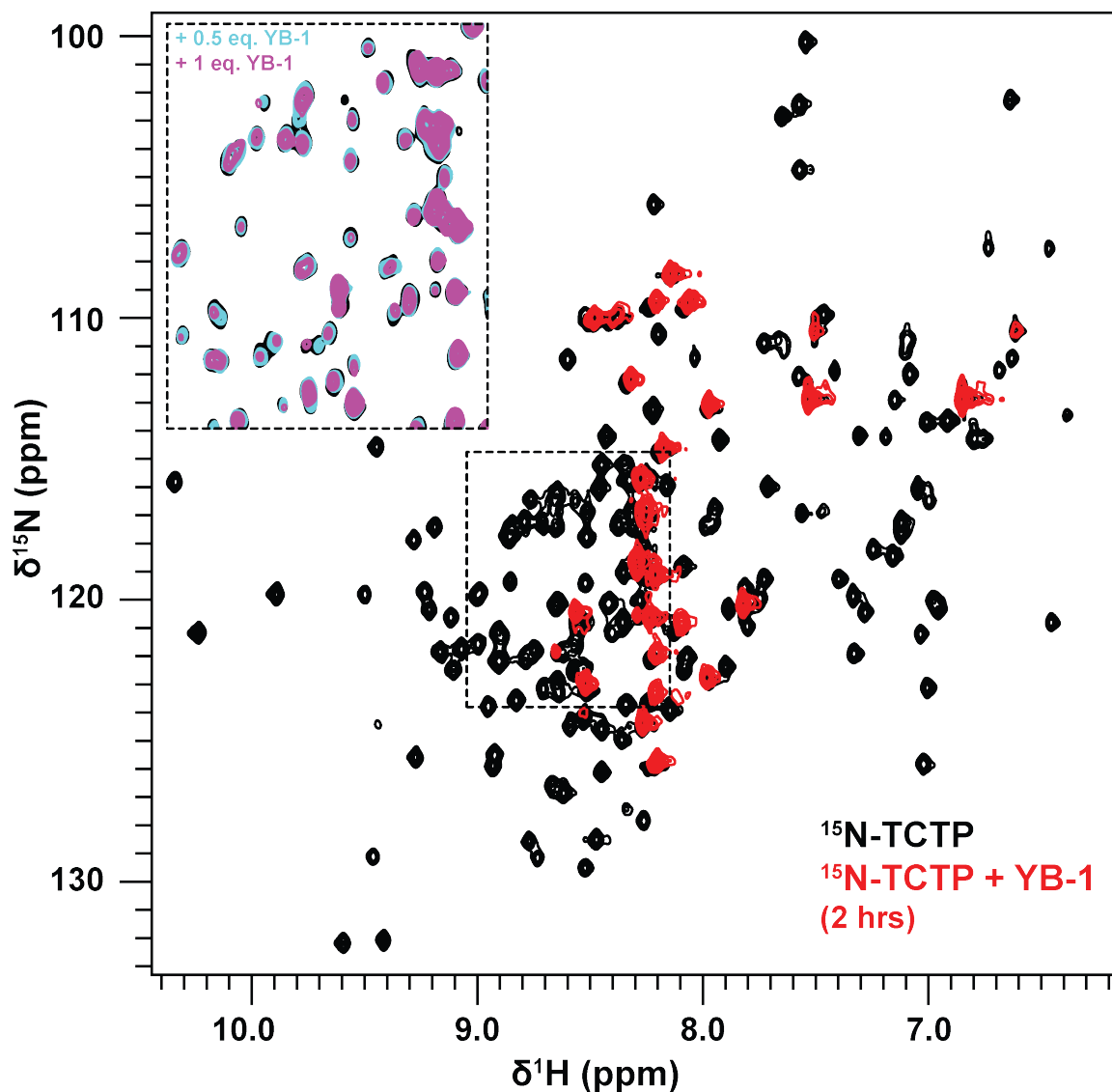
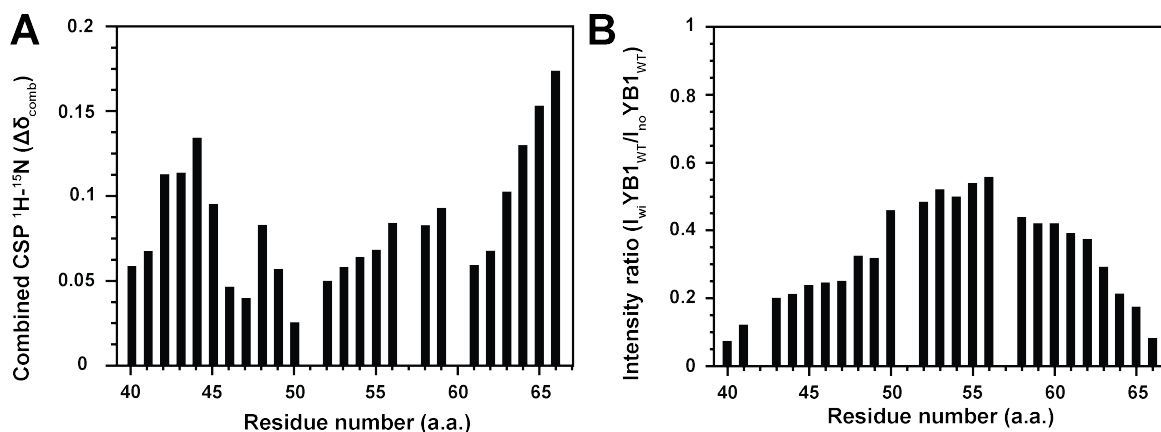


Fig. 5.3 **Comparison of free TCTP and in complex with YB-1.** Overlay of  $^1\text{H}$ - $^{15}\text{N}$  SOFAST HMQC spectra from isolated  $^{15}\text{N}$ -TCTP (50  $\mu\text{M}$ ) (black) and upon addition of YB-1 (1 eq.) after equilibration time (2 hrs) (red). A close-up view of the central region at intermediate YB-1 ratios is shown (top-left). Experiments were recorded at 950 MHz and 25  $^\circ\text{C}$  in the following buffer: 50 mM  $\text{NaPO}_4$  pH 6.8, 12.5 mM KCl, 2 mM TCEP and 5%  $\text{D}_2\text{O}$  / 95 %  $\text{H}_2\text{O}$ .

YB-1 is a pleiotropic protein originally described for its role in DNA transcription but has recently emerged as a potential biomarker and novel therapeutic target [160]. The protein is 324 amino-acid long with N-terminal A/P rich domain, CSD domain and C-terminal



**Fig. 5.4 Description of TCTP upon slow complex formation with YB-1.** (A) Combined  $^1\text{H}$ - $^{15}\text{N}$  chemical shift perturbations and (B) Intensity ratios computed between  $^1\text{H}$ - $^{15}\text{N}$  spectra from free TCTP and upon slow complex formation with YB-1 are shown along the IDR region. Other parts of the protein could not be observed.

disordered region composed of clusters of charged residues (Sec. 2.2.1.3). The interaction between TCTP and YB-1 was first reported in Co-IP experiments [151] in HeLa cells. Even though the method could not distinguish between direct or indirect interaction in this context the authors have demonstrated the dependence of the interaction toward segments of YB-1 (1-129) and TCTP (42-83). Additionally, they have calculated a structural model of the complex in direct interaction through MD experiments. However, no information regarding the interplay of YB-1/TCTP and RNAs was explicated. Thus, we decided to test if TCTP could directly interact with YB-1 protein and if we could confirm predicted data concerning the complex arrangement. We also searched for validating the suggested ternary complex between TCTP, YB-1 and RNAs.

In order to test if both full length TCTP and YB-1 proteins could directly interact together, we have recorded  $^1\text{H}$ - $^{15}\text{N}$  SOFAST HMQC spectra of  $^{15}\text{N}$ -TCTP (50  $\mu\text{M}$ ) upon successive increments of unlabeled YB-1 concentration (0-50  $\mu\text{M}$ ). Immediately after addition of the unlabeled YB-1 the whole spectral intensity from the structured parts of TCTP significantly decreased until system stabilization (2 hrs). No signal from free TCTP could be detected anymore at one equivalents of protein partner, indicating a medium-strong binding affinity ( $K_d < 5 \mu\text{M}$ ) for the complex formation. In the spectrum of bound TCTP, we could not detect signals from structured parts of the protein (Fig. 5.3). Rapid exchange shifts of small amplitude could be measured along the protein primary sequence during the NMR titration but these were explained by the dissociation of the weak TCTP dimer upon diminishing of free TCTP in solution. Despite acidic conditions that generally sharpen  $^1\text{H}$ - $^{15}\text{N}$  crosspeaks by reducing backbone amide hydrogen exchange with water, no spectral signature from

structured parts of bound TCTP could be found in the spectrum.  $^1\text{H}$ - $^{15}\text{N}$  resonances from TCTP IDR were still visible upon complex formation and we could still compute combined  $^1\text{H}$ - $^{15}\text{N}$  chemical shift perturbations along this specific protein segment. These were stronger in the N- and C- terminal parts of the IDR (Fig. 5.4 A) compared to the central part. Corresponding intensity ratios showed similar pattern with more marked decrease of signal intensity in N- and C- terminal of the IDR (Fig. 5.4 B). The whole protein core domain was not visible upon complex formation and we can presume that TCTP IDR extremities have spectral perturbations because they feel the strong structure or dynamics changes in the globular part of TCTP. This is seen from the disappearing of crosspeaks, meaning either complex oligomerization or conformational exchange (ms) in the core domain. These global variations in TCTP core do not allow to map the interaction surface with YB-1 in the current setup. Finally, we could not detect signatures of TCTP\* in the  $^1\text{H}$ - $^{15}\text{N}$  spectrum of TCTP bound to YB-1. This means that the protein has a distinct structure and dynamics in complex with YB-1 compared to previously described complexes with Bcl-2 family proteins or MDM2. The most likely explanation is that the highly negatively charged TCTP interacts with YB-1 to form large oligomers, without major reorganization of TCTP core structure. In conclusion, we have demonstrated *in vitro* that TCTP does interact with YB-1 with medium-strong affinity in a slow kinetics process. Also, the current experiment was carried out in presence of 12.5 mM KCl. It should be noted that at high salt concentration (100 mM NaCl) no interaction was detectable between TCTP and YB-1 by NMR, suggesting an electrostatic interaction mode between the two proteins.

### 5.1.3.2 TCTP transiently interacts with YB-1/RNAs

To test if TCTP could still interact with YB-1 in presence of RNA, we have added an excess of RNAs from yeast extract (1 mg) to the previous sample containing  $^{15}\text{N}$ -TCTP and YB-1. Whereas all crosspeaks from structured parts of TCTP disappeared upon complex formation with YB-1 (Fig. 5.3), a flagrant recovery was observed upon RNA addition to yield a spectrum resembling to free TCTP (Fig. 5.5 A). However, several  $^1\text{H}$ - $^{15}\text{N}$  crosspeaks were left shifted between isolated TCTP and upon YB-1 and RNAs addition (Fig. 5.5 B). We computed  $^1\text{H}$ - $^{15}\text{N}$  combined chemical shift positions and intensities were computed between the isolated TCTP and in presence of YB-1/RNA (Fig. 5.6 A, B). We observed local differences along TCTP primary sequence and this signifies that TCTP still transiently interacts with either YB-1 or RNA or complexes thereof in fast kinetics ( $< \mu\text{s}$ ). The long  $\alpha$ -helices  $\alpha_2$  and  $\alpha_3$  hosted the majority of residues for which a significant perturbation was observed in presence of YB-1/RNAs compared to isolated  $^{15}\text{N}$ -TCTP. Thus, this  $\alpha$ -helical segment in TCTP mediates the transient complex formation with YB-1/RNA, demonstrating

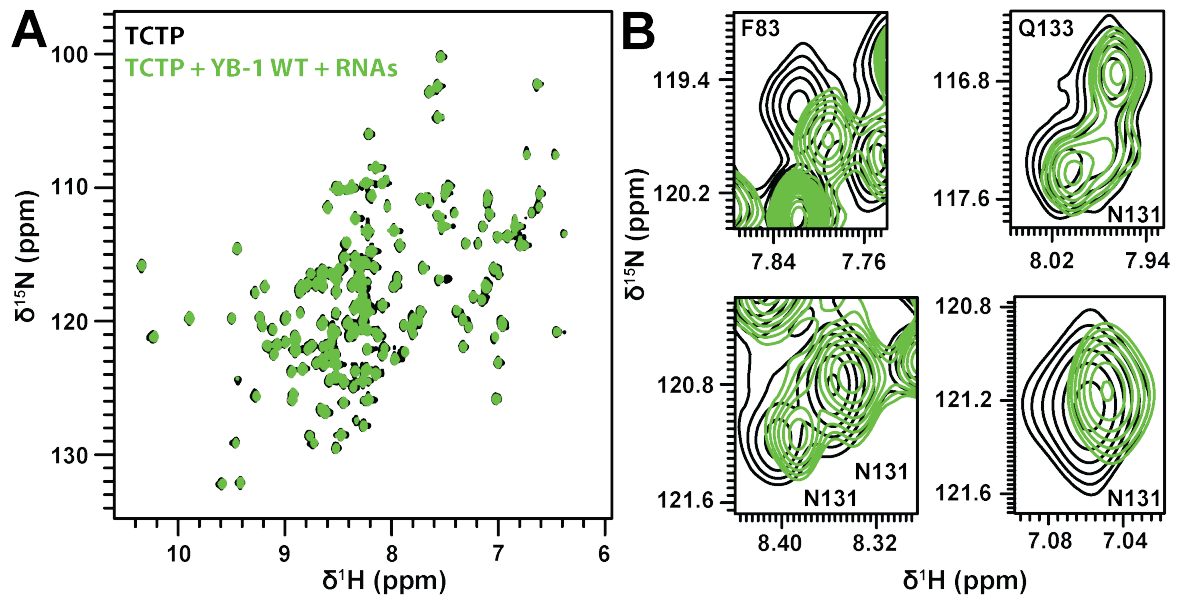
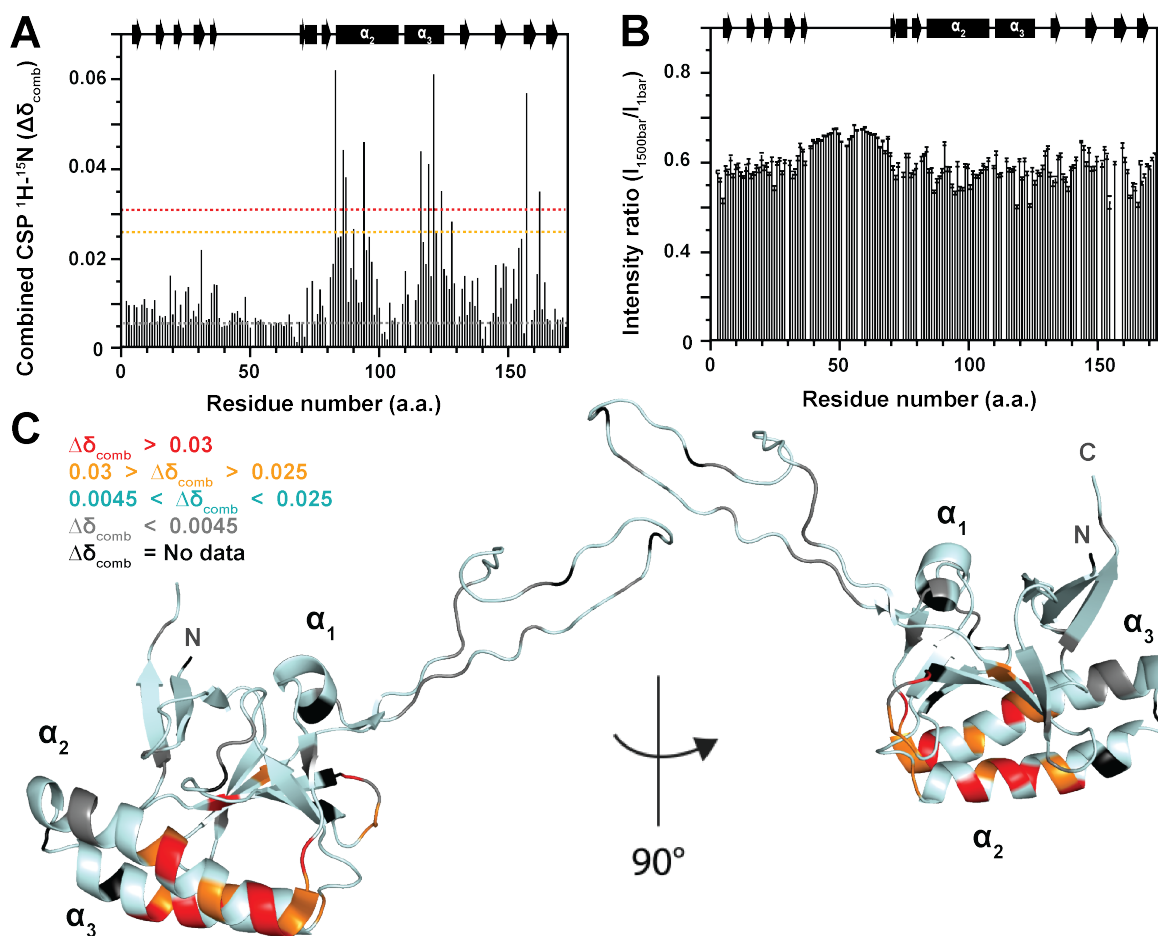


Fig. 5.5 **TCTP upon fast complex formation with YB-1/RNAs.** Overlay of  $^1\text{H}$ - $^{15}\text{N}$  SOFAST HMQC spectra from isolated  $^{15}\text{N}$ -TCTP (50  $\mu\text{M}$ ) (black) and in presence of YB-1 (1 eq., red) plus an excess of RNAs from yeast (green). Experiments were recorded at 950 MHz and 25  $^\circ\text{C}$  in the following buffer: 50 mM  $\text{NaPO}_4$  pH 6.8, 12.5 mM KCl, 2 mM TCEP and 5%  $\text{D}_2\text{O}$  / 95 %  $\text{H}_2\text{O}$ .

that the three molecules retain the capability to assemble together (Fig. 5.6 C). We have shown that TCTP does not directly interact with the same RNA extract from yeast (Sec. 5.1.2) and this encourages to propose that TCTP contacts mainly YB-1 in the transient complex with RNAs. The RNA could also impact the oligomerization state of YB-1 bound to TCTP, possibly leading to signal recovery in TCTP spectrum. Perturbations in the N-terminal region of TCTP IDR were abolished in the transient TCTP complex YB-1/RNA compared to the TCTP/YB-1 complex, suggesting that the TCTP/YB1 interface is largely disrupted in presence of RNA.

We then wanted to assess which component of YB-1/RNAs complex did interact with TCTP in the transient interaction between TCTP and YB-1/RNAs. We have compared  $^1\text{H}$ - $^{15}\text{N}$  spectra of isolated  $^{15}\text{N}$ -TCTP, in presence of unlabeled YB-1 (1-180) and upon addition of RNAs from yeast extract (Fig. 5.7 A). As already described for YB-1 full length protein,  $^1\text{H}$ - $^{15}\text{N}$  resonances were affected upon slow kinetics, partial complex formation with C-terminally truncated YB-1 (1-180). These were either reversed or prolonged co-linearly upon RNAs addition, indicating that two different populations decrease and increase, respectively. This could signify that TCTP and YB-1 IDR form two complexes with different interfaces or a single one with an extended interaction surface. In any cases, RNA addition disrupts one interface to only allow the helices  $\alpha_2$  and  $\alpha_3$  to interact with YB-1 (1-180). Moreover, we



**Fig. 5.6 Description of TCTP in the fast forming complex with YB-1/RNAs.** (A) Combined  $^1\text{H}-^{15}\text{N}$  chemical shift perturbations calculated between isolated TCTP and in presence of YB-1 (1 eq.) plus a large excess of RNAs from yeast extract (1 mg). (B) Mapping of large (red  $> 0.03$ ,  $0.03 >$  orange  $> 0.025$ ) and low (grey  $< 0.0045$ ) combined  $^1\text{H}-^{15}\text{N}$  chemical shift perturbations on TCTP structure (pdb code: 2HR9). Residues for which no value was computed (black) are highlighted.

could not detect a new interface in TCTP upon RNA addition, suggesting that the protein does not directly interact with RNA in the transient ternary complex with YB-1 (1-180), in agreement with previously reported experiments showing that TCTP does not interact with the same RNA extract from yeast (Sec. 5.1.2). To confirm that the same observation can be made with full length YB-1/RNA, we compared  $^1\text{H}-^{15}\text{N}$  perturbation profiles computed between isolated TCTP and transient complex with YB-1 (1-180)/RNA or full length YB-1/RNA. We could not detect significant differences, indicating the YB-1 IDR does not seem to participate in the binding interface between TCTP and YB-1/RNAs.

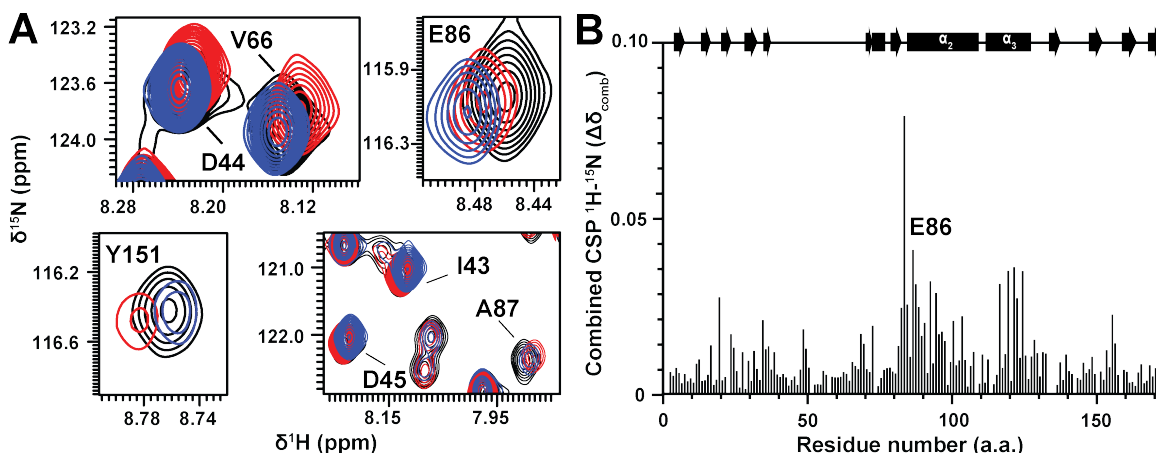


**Fig. 5.7 Impact of RNA on TCTP and YB-1 (1-180) complex.** (A) Overlay of  $^1\text{H}$ - $^{15}\text{N}$  SOFAST HMQC spectra from isolated  $^{15}\text{N}$ -TCTP (100  $\mu\text{M}$ ) (black) and in presence of 1.5 eq. YB-1 (1-180) (1.5 eq.) (blue) plus an excess of RNAs from yeast extract (1 mg) (red). Close-up views are shown for residues I43, D44, D45, V66, E86, A87 and Y151. (B) Combined  $^1\text{H}$ - $^{15}\text{N}$  chemical shift perturbations computed between  $^1\text{H}$ - $^{15}\text{N}$  spectra from isolated TCTP and in presence of YB-1 (1-180) (1.5 eq.) plus an excess of RNAs from yeast extract (1 mg). Experiments were recorded at 950 MHz and 25  $^\circ\text{C}$  in the following buffer: 50 mM  $\text{NaPO}_4$  pH 6.8, 12.5 mM KCl, 2 mM TCEP and 5%  $\text{D}_2\text{O}$  / 95 %  $\text{H}_2\text{O}$ .

In conclusion, TCTP transiently interacts with YB-1/RNA complex via its helical segment composed of helices  $\alpha_2$ ,  $\alpha_3$  and is likely to only contact YB-1 via a pre-existing interface detected in TCTP/YB-1 without RNA.

### 5.1.3.3 YB-1 C-terminal IDR mediates stronger affinity

To identify the structural determinants for the medium-strong interaction between TCTP and YB-1 ( $K_d < 5 \mu\text{M}$ ), we used a variant of YB-1 protein truncated for the C-terminal part. YB-1 (1-180) excludes a region from the C-terminal of YB-1 which arranges as clusters of charged residues in the native protein. We have recorded  $^1\text{H}$ - $^{15}\text{N}$  spectra of  $^{15}\text{N}$ -TCTP FL upon successive increments of unlabeled YB-1 (1-180) concentration (2 eq.) (Fig. 5.8 A). After addition of the unlabeled YB-1 (1-180) the whole spectral intensity from the structured parts of the TCTP protein progressively decreased until system stabilization (2 hrs). Since about half of the signal from structured parts in free TCTP was left at the end of the titration, we can presume that the affinity of the interaction is weaker ( $K_d > 100 \mu\text{M}$ ) with YB-1 (1-180) compared to YB-1. This highlights the importance of the IDR region in YB-1 for the interaction strength. We could compute combined  $^1\text{H}$ - $^{15}\text{N}$  chemical shift perturbations and intensity ratios between  $^1\text{H}$ - $^{15}\text{N}$  spectra of isolated TCTP and upon YB-1 (1-180) addition (Fig. 5.9 A, B). We corrected for perturbations induced by the re-equilibration of TCTP monomer-dimer upon interaction with YB-1 (1-180) by applying a  $^1\text{H}$ ,  $^{15}\text{N}$  chemical shift

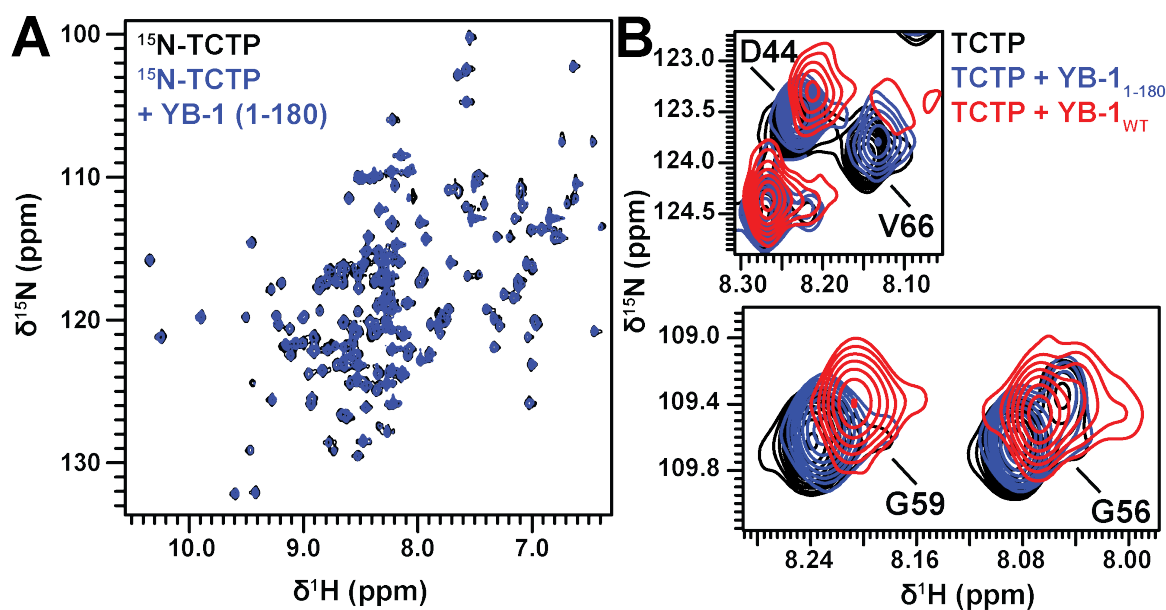
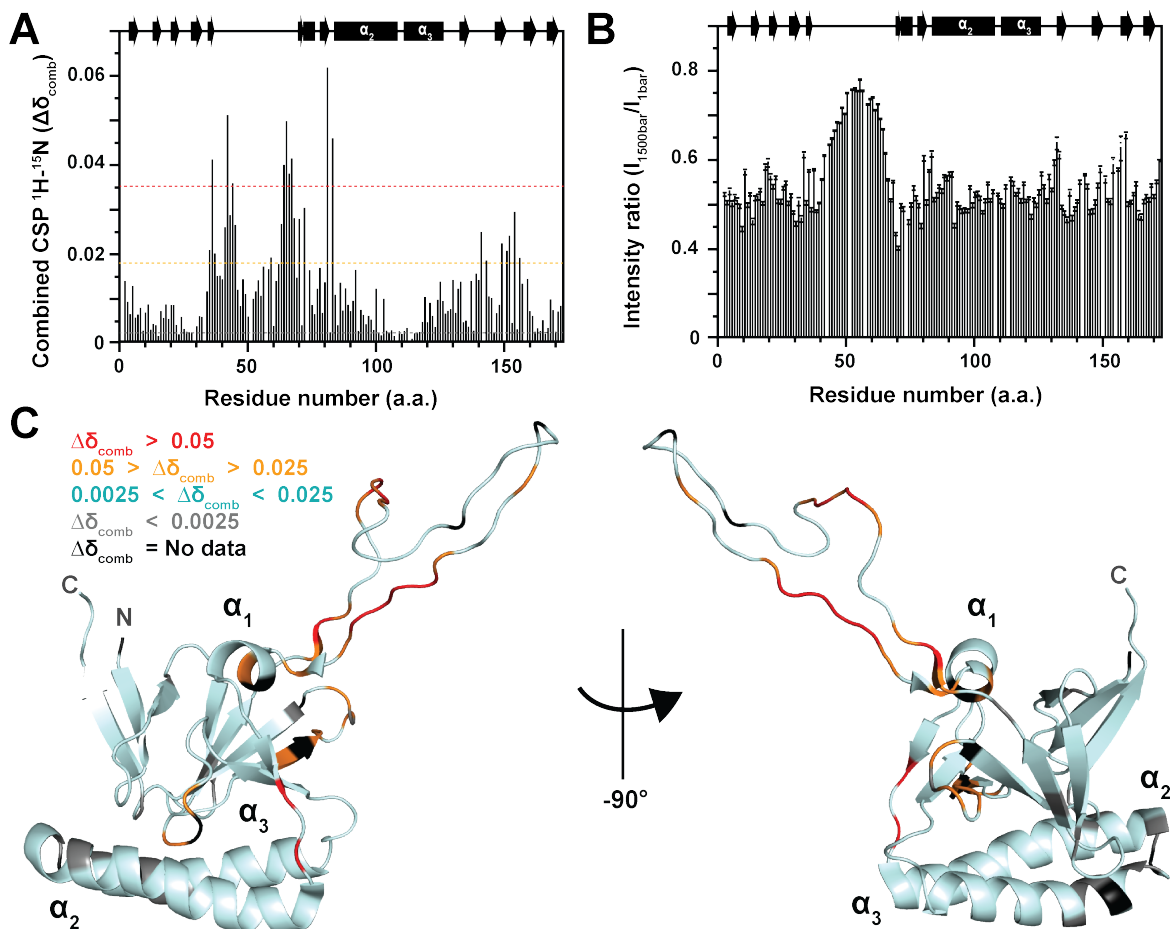


Fig. 5.8 **TCTP upon partial complex formation with YB-1 IDR.** (A) Overlay of  $^1\text{H}$ - $^{15}\text{N}$  SOFAST HMQC spectra from free TCTP (100  $\mu\text{M}$ ) (black) and upon partial, slow kinetics complex formation with YB-1 (1-180) (2 eq., red) and equilibration time (6 hrs). (B) Close-up view for residues D44, G59, G56 and V66 with superimposition of the  $^1\text{H}$ - $^{15}\text{N}$  spectrum of the fully formed TCTP/YB-1 complex. Experiments were recorded at 950 MHz and 25  $^\circ\text{C}$  in the following buffer: 50 mM  $\text{NaPO}_4$  pH 6.8, 12.5 mM KCl, 2 mM TCEP and 5%  $\text{D}_2\text{O}$  / 95%  $\text{H}_2\text{O}$ .

baseline calculated from dilution experiments. First,  $\beta$ -strands and connecting loops in the C-terminal extremity of the TCTP globular core did show perturbations above threshold (Fig. 5.9 C). This could either originate from a transient contact with YB-1 (1-180) or be due to residual perturbation from the monomer-dimer related shifts since the protein segment hosts residues such as Y151 which is sensitive to the dimer content. For residue F83 and F85 it is clear that residual perturbations arise from the monomer-dimer equilibrium whose they are the main probes. However, we could still detect chemical shift perturbations specific of the complex formation with YB-1 (1-180). For  $^1\text{H}$ - $^{15}\text{N}$  resonances from residues spanning the TCTP IDR, chemical shift perturbations were smaller but co-linear with those observed in the same region in interaction studies with full length YB-1 (Fig. 5.8 B). Intensity ratios in TCTP IDR showed a similar pattern upon complex formation with full length YB-1 or YB-1 (1-180) whereas structured parts from bound TCTP were non-visible in both complexes. These similarities between chemical shift perturbations and intensity ratios led to propose that TCTP interacts comparably with full length and  $\Delta\text{IDR}$  YB-1 constructs. However, since most of bound TCTP is not visible in complex with full length YB-1, we have to be careful regarding this assessment. In conclusion, we have demonstrated the importance of YB-1 IDR



**Fig. 5.9 Description of TCTP upon partial, slow complex formation with YB-1 (1-180).** (A) Combined  $^1\text{H}-^{15}\text{N}$  chemical shift perturbations and (B) Intensity ratios computed between  $^1\text{H}-^{15}\text{N}$  spectra from isolated TCTP and in presence of YB-1 (1-180) (1.5 eq.) after system equilibration (6 hrs). (C) Mapping of large (red  $> 0.05$ , orange  $0.05 > \Delta\delta_{\text{comb}} > 0.025$ ) and low (grey  $< 0.0025$ ) combined  $^1\text{H}-^{15}\text{N}$  chemical shift perturbations on TCTP structure (pdb code: 2HR9). Residues for which no value was computed (black) are highlighted.

in mediating the medium-high affinity ( $K_d < 5 \mu\text{M}$ ) of the complex formation with TCTP and is likely important for oligomerization related process.

## 5.2 Inhibitors of TCTP for anti-cancer therapy

In this section, we present our binding studies with ligands that target TCTP protein (Sec. 5.2). Several molecules were demonstrated to bind TCTP and one of them, sertraline, has even proved clinical efficiency in cancer treatment [188, 173] (Fig. 1.14). Binding affinities between these ligands and TCTP were established using the SPR method and found a micromolar range of affinity ( $K_d \sim 10\text{-}100 \mu\text{M}$ ) for sertraline, thioridazine and other molecules

developed by our collaborator S. Messaoudi (BioCIS, CNRS/Université Paris-Saclay) and based on the same molecular scaffold with sertraline. For patenting reasons, we can not show the molecular structure of these herein. Even though TCTP is a recognized pharmacological target in cancer treatment, structural data describing these interactions [184] are still very limited, making difficult the rationale optimization of these compounds. Thus, we used NMR to locate the ligands binding site on TCTP surface experimentally and in solution. We used native and phosphorylated TCTP since phosphorylation mimetics S46E and S64E were shown to abolish interaction with sertraline (Sec. 5.2). TSA and PAGE were combined with NMR to challenge results from SPR studies first established (Sec. 5.3).

### 5.2.1 Sertraline and other ligands at TCTP protein

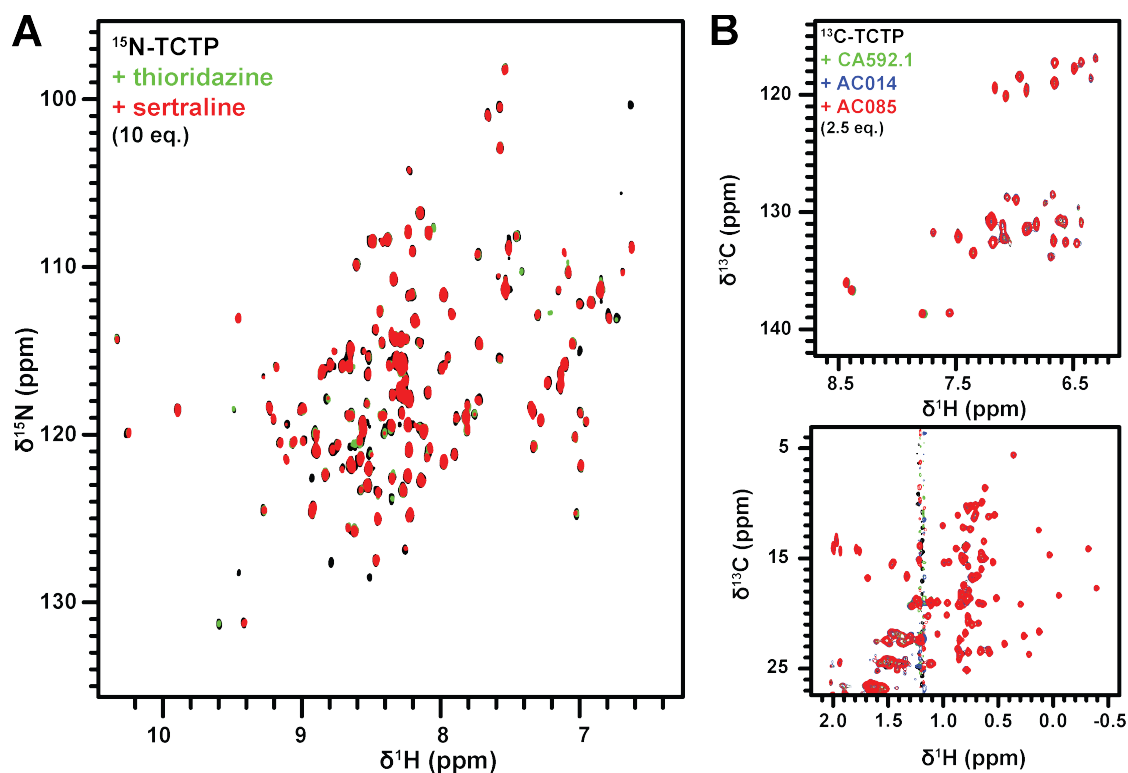


Fig. 5.10 NMR evaluation of ligands ability to target TCTP. (A) Overlay of  $^1\text{H}$ - $^{15}\text{N}$  SOFAST HMQC spectra from isolated  $^{15}\text{N}$ -TCTP (50  $\mu\text{M}$ ) (black) and in presence of thioridazine (10 eq.) (green) or sertraline (red). (B) Overlay of  $^1\text{H}$ - $^{13}\text{C}$  SOFAST HMQC spectra from isolated  $^{15}\text{N}$ -TCTP (50  $\mu\text{M}$ ) (black) and in presence of CA592.1 (2.5 eq.) (green), AC014 (2.5 eq.) (blue) or AC085 (2.5 eq.) (red). The aromatic (top) and methyl (bottom) region are shown. Experiments were recorded at 950 MHz and 25  $^\circ\text{C}$  in the following buffer: HEPES 10 mM pH 7.4, 150 mM NaCl, 3 mM EDTA, 0.005% Tween20, 5% DMSO, 2 mM TCEP and 5%  $\text{D}_2\text{O}$  / 95 %  $\text{H}_2\text{O}$ .

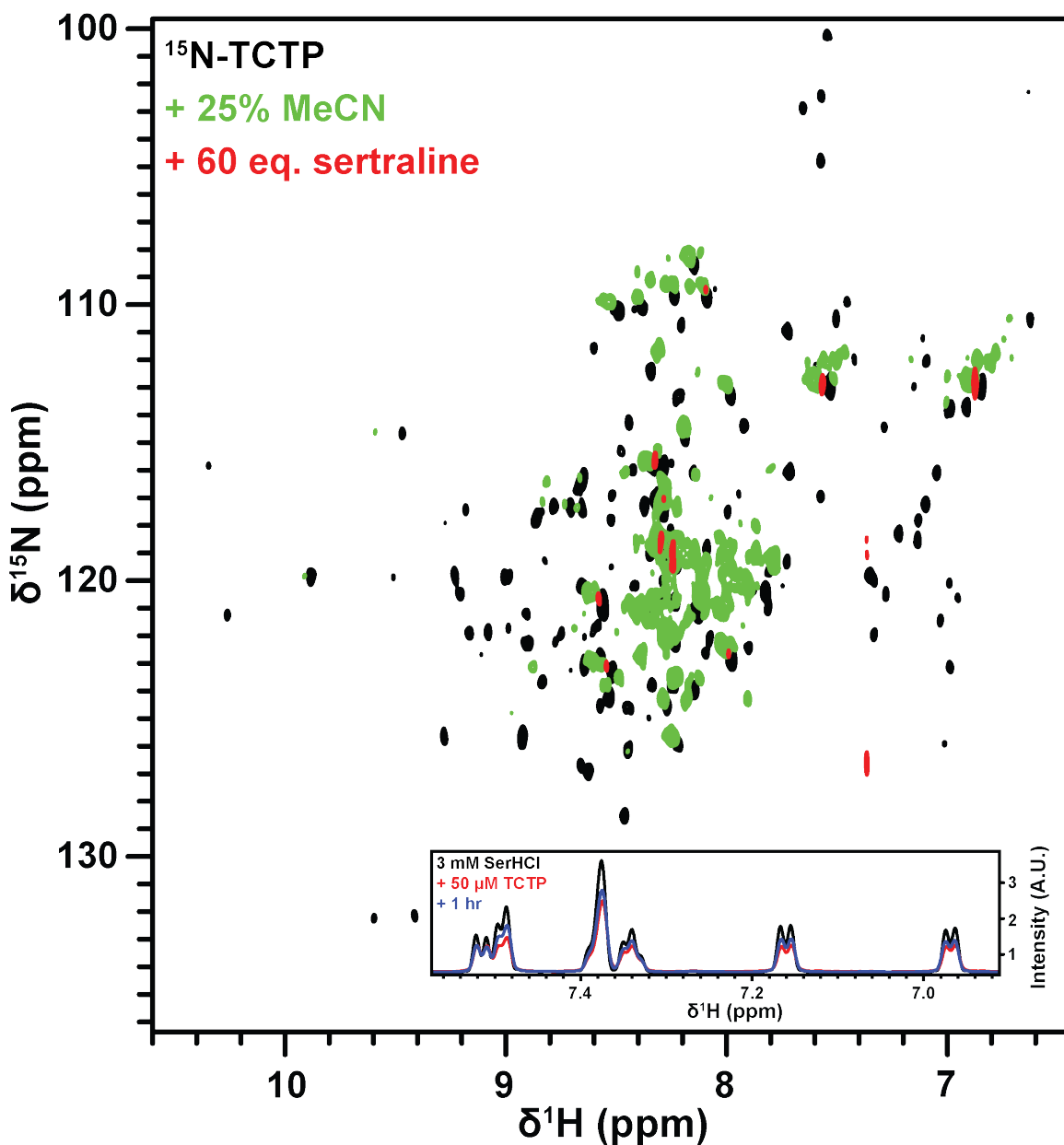
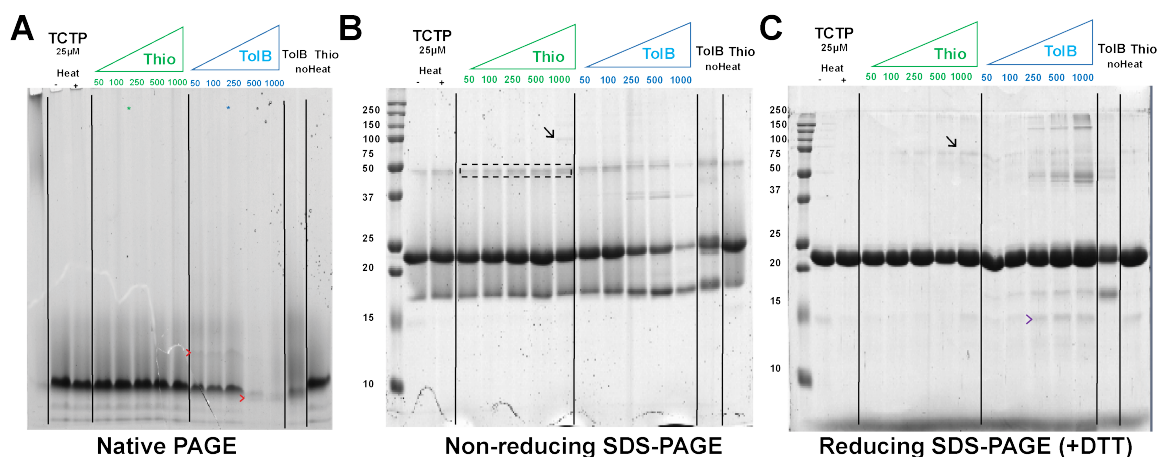


Fig. 5.11 **Effect of sertraline at high concentration on TCTP.** Overlay of  $^1\text{H}$ - $^{15}\text{N}$  SOFAST HMQC spectra from isolated  $^{15}\text{N}$ -TCTP (50  $\mu\text{M}$ ) (black) and in presence of 25% acetonitrile (green) plus 60 eq. sertraline hydrochloride (3 mM) (red). A close-up view of 1D  $^1\text{H}$  spectra focusing on sertraline signals from aromatics protons is shown (bottom). Signal decrease upon TCTP addition before recovery within an hour to reach a partial recovery. Experiments were recorded at 800 MHz and 25  $^\circ\text{C}$  in the following buffer: 10 mM HEPES pH 7.4, 150 mM NaCl, 3 mM EDTA, 0.005% Tween20, 2 mM TCEP and 25 % acetonitrile / 5 % DMSO / 65 %  $\text{H}_2\text{O}$  / 5 %  $\text{D}_2\text{O}$ .

First, we verified that all ligands were soluble in our experimental conditions (5 % DMSO included in buffer). We recorded  $^1\text{H}$  spectra of each ligand at increasing concentration and



**Fig. 5.12 Thioridazine and toluidine blue induce covalent TCTP oligomers.** (A) Native BisTris PAGE, (B) Non-reducing and (C) reducing SDS-PAGE experiments (4-16 %) done on isolated TCTP (25  $\mu$ M) and upon incubation with increasing concentration of thioridazine or toluidine blue (TolB) (0-1 mM) during 24 hrs at 37  $^{\circ}$ C. Experiments were done in the following buffer: 50 mM HEPES pH 7.4, 150 mM NaCl and 2 mM TCEP.

compared to the increase in signal intensity to estimate that the solubility is at least 100  $\mu$ M for all ligands. Prior to proceed with interaction studies, the effect of DMSO (5 %) on TCTP was also tested and we did not observe major change in the  $^1\text{H}$ - $^{15}\text{N}$  spectrum of the protein, suggesting that TCTP structure remains largely unchanged in presence of DMSO. Then we recorded  $^1\text{H}$ - $^{15}\text{N}$  and  $^1\text{H}$ - $^{13}\text{C}$  SOFAST HMQC of isolated  $^{13}\text{C}$ ,  $^{15}\text{N}$ -TCTP FL and in presence of increasing concentrations of the different molecules from dry aliquots resuspended in the NMR sample. Systems were free to evolve during several hours (6 hrs) before the last measurement. At low concentration of ligands (125  $\mu$ M), no significant  $^1\text{H}$ - $^{15}\text{N}$  and  $^1\text{H}$ - $^{13}\text{C}$  spectral perturbations could be detected upon addition of the molecules in the NMR samples containing TCTP. This is exemplified by the  $^1\text{H}$ - $^{13}\text{C}$  spectra from TCTP in both methyl and aromatic regions recorded upon addition of different ligands (Fig. 5.10 B). However, at higher concentration of ligands, the comparison of  $^1\text{H}$ - $^{15}\text{N}$  spectra from isolated TCTP and upon ligand (sertraline or thioridazine) addition (Fig. 5.10 A) showed that both thioridazine and sertraline induced a global decrease in spectral intensity without chemical shift variation excepted for the monomer-dimer equilibrium. The protein did aggregate in the NMR tube, diminishing the free TCTP concentration. The effect was more marked with sertraline. This clearly indicates that these ligands have a destabilizing effect on TCTP by inducing oligomer formation or protein aggregation. In conclusion, ligands did not show any significant effect on TCTP structure at reasonable (125  $\mu$ M), biologically relevant concentration. Higher concentrations led to protein aggregation and that might be due to destabilization of TCTP

via ligand aggregates or stabilization of an alternative state of the protein that is prone to aggregation.

We decided to clarify the impact of sertraline on TCTP and we have optimized the experimental setup to allow very high ligand concentrations in order to accelerate and reinforce the aggregation-related effect mentioned above. We used acetonitrile since it was already used at high concentration for protein NMR and sertraline is largely soluble in the solvent. We recorded  $^1\text{H}$ - $^{15}\text{N}$  SOFAST HMQC spectra of TCTP in buffer (5 % DMSO), supplemented with acetonitrile and later with sertraline (Fig. 5.11). The impact of high acetonitrile concentration on TCTP were visible through the global diminishing of signal from structured parts of the protein. However the protein was still largely visible through the flexible parts and resonances from the protein core. Strikingly, almost all signal present in the spectrum disappeared immediately after sertraline addition (3 mM) in the sample, meaning that sertraline readily induced TCTP aggregation nor precipitation. Informations on the interaction can still be derived by looking at the evolution of sertraline  $^1\text{H}$  crosspeaks before, after TCTP addition and following equilibration time (2 hrs) (Fig. 5.11). Sertraline signals were visible in the  $^1\text{H}$  spectrum before TCTP addition. Immediately after addition of TCTP about 50 % of the signal intensity disappeared, with no line broadening for sertraline signals left in the spectrum. A few hours later about 75 % of the initial intensity was recovered. This means that sertraline molecules are released from TCTP/sertraline aggregates over time. Overall TCTP did interact immediately with sertraline to readily aggregate in the NMR tube. Considering that almost 30 molecules of sertraline did aggregate with 1 molecule of TCTP straight after ligand addition, we can expect this interaction to be mediated by oligomers of ligands rather than single molecules.

Finally, we decided to assess the nature of the aggregate of TCTP that is induced upon ligand addition at high concentration. To do so, we achieved PAGE experiments in native, denaturing and reducing/denaturing conditions (Fig 5.12). We used thioridazine and another phenothiazine we identified as a TCTP binder, the toluidine blue. After incubation time overnight at room temperature in presence of reducing agent as in the NMR conditions (2 mM TCEP), we observed a strong effect with toluidine blue whereas which was much less marked with thioridazine. Both thioridazine and toluidine blue started to induce the disappearing of the native TCTP band starting 250-500  $\mu\text{M}$  ligand (Fig 5.12 A, B). This means that the TCTP protein aggregated in a molecular assembly that contains strong chemical bond, most likely covalent bond. In reducing conditions, we recovered most of TCTP signals and observed several bands of high molecular weight (Fig 5.12 C). That confirms the ligands did induce disulfide bonding between TCTP and TCTP, or between TCTP and the ligands molecules.

So far we do not know how that could be relevant in a biological context, especially when considering the reducing environment of the intracellular space, which makes quite unlikely that the molecules could act by such a way *in vivo*. Moreover, we showed that the toluidine blue itself reacts with reducing agents in solution, most likely interfering with the experiments and explaining why we observed a strong induction of disulfide bonded oligomers using this particular ligand compared to thioridazine.

### 5.2.2 Binding of sertraline on phosphorylated TCTP

Since phosphorylation mimetic S46E and S64E were reported to abolish the interaction between TCTP and sertraline, we have tested if phosphorylated TCTP at S46 position was still affected upon sertraline addition at high concentration ( $> 500 \mu\text{M}$ ). We titrated pTCTP from low ( $50 \mu\text{M}$ ) to high ( $1050 \mu\text{M}$ ) concentration of sertraline by recording  $^1\text{H}$ - $^{15}\text{N}$  SOFAST HMQC spectra of the  $^{15}\text{N}$ -labeled pTCTP in absence and in presence of ligand. We could not see significant changes in the spectrum of pTCTP until  $550 \mu\text{M}$  of sertraline. After equilibration time overnight, we observed a gradual decrease in the whole spectral intensity from pTCTP, indicating that the phosphorylated protein did also aggregate in presence of ligand, as observed for the non-phosphorylated form. At higher concentration ( $1050 \mu\text{M}$ ), the phenomenon was strengthened right after ligand addition and after equilibration time overnight. At the end of the experiment, about 75 % of pTCTP did aggregate in the NMR sample, as judged from the intensity loss. We could not detect a binding site in pTCTP and only monitored the rapid exchange shifts from the monomer-dimer of TCTP. In conclusion, sertraline induces the aggregation of phosphorylated TCTP in a concentration-dependent manner with significant effect starting at  $\sim 500 \mu\text{M}$ .

### 5.2.3 Impact of sertraline on the melting temperature of TCTP

Ligand-induced destabilization of TCTP was recurrently suggested in the previous paragraphs. Thus, we have used TSA to detect such effect through the variation of the protein melting temperature ( $T_m$ ) possibly induced upon ligand addition. Thus, we measured the  $T_m$  of TCTP in presence of increasing concentrations of sertraline. The latter molecule destabilized TCTP to yield a  $5.1 \text{ }^\circ\text{C}$  decrease in the  $T_m$  of the protein upon ligand addition, albeit at high ligand concentration ( $500 \mu\text{M}$ ) (Fig. 5.14 A). At lower concentration, the decrease is more modest with  $2.6 \text{ }^\circ\text{C}$  at  $250 \mu\text{M}$  sertraline. Below the difference with isolated TCTP is weak ( $< 1 \text{ }^\circ\text{C}$ ). We compared with control proteins and we show the denaturation curves for three proteins in absence and in presence ( $500 \mu\text{M}$ ) of sertraline (Fig. 5.14 B). We also observed a destabilizing effect of sertraline for all three controls. For control no 1, 2 and 3 a decrease

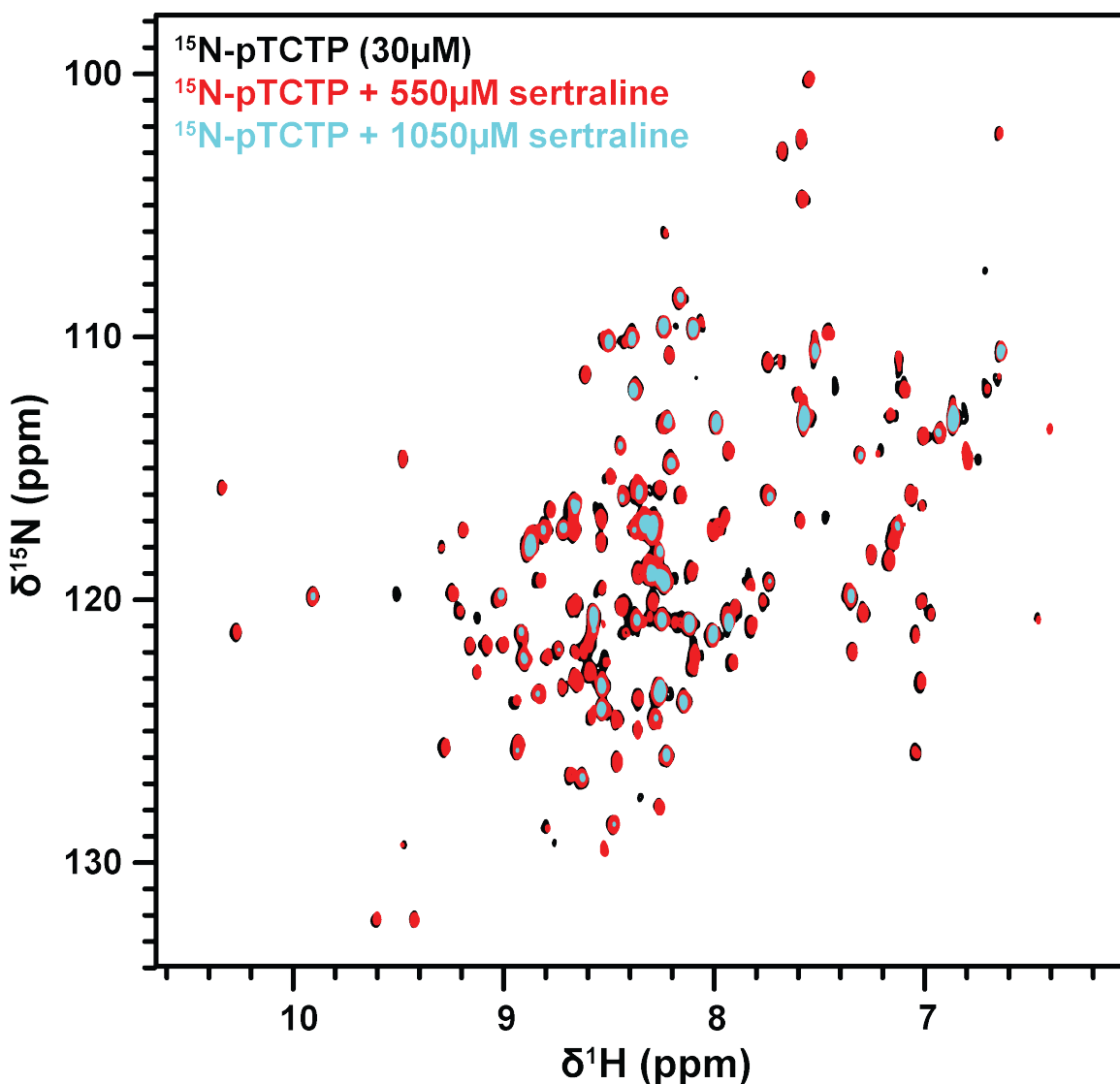
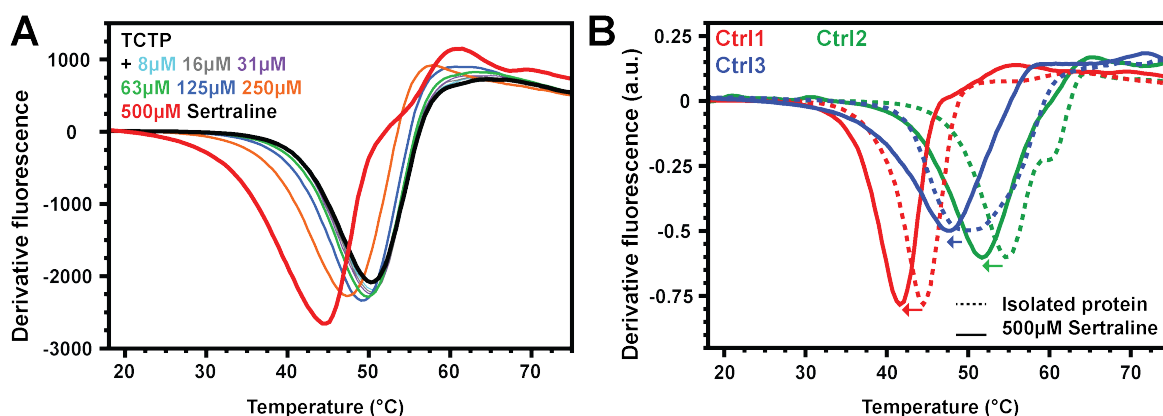


Fig. 5.13 NMR titration of phosphorylated TCTP (pTCTP) by sertraline ligand. Overlay of  $^1\text{H}$ - $^{15}\text{N}$  SOFAST HMQC spectra from isolated  $^{15}\text{N}$ -labeled pTCTP (30  $\mu\text{M}$ ) (black) and in presence of 550  $\mu\text{M}$  (red) or 1050  $\mu\text{M}$  (cyan) sertraline after equilibration time (> 6 hrs). Experiments were recorded at 800 MHz and 25  $^\circ\text{C}$  in the following buffer: 50 mM HEPES pH 7.4, 150 mM NaCl, 0.5 mM EDTA, 2 mM TCEP and 5 % DMSO / 5 %  $\text{D}_2\text{O}$  / 90 %  $\text{H}_2\text{O}$ .

in melting temperature of 3.2  $^\circ\text{C}$ , 2  $^\circ\text{C}$  and 2.4  $^\circ\text{C}$  were observed upon sertraline addition, respectively (Fig. 5.14 B). This indicates that the impact of sertraline on TCTP stability is not specific of the protein, even though the decrease of TCTP melting temperature is about twice stronger at 500  $\mu\text{M}$  sertraline compared to controls. In conclusion, we demonstrated the destabilizing effect of sertraline on proteins, especially TCTP, leading to protein unfolding and aggregation. It is important to note that TSA experiments do not let the system evolving



**Fig. 5.14 Evaluation of TCTP thermal stability toward ligands.** (A) Dependence of the TCTP melting temperature ( $T_m$ ) regarding sertraline concentration (0–500  $\mu\text{M}$ ). Minima of curves cross the x axis at  $T_m$ . (B) Comparison with control proteins in absence or presence of sertraline (500  $\mu\text{M}$ ). Experiments were done by applying a temperature gradient from 25  $^{\circ}\text{C}$  to 95  $^{\circ}\text{C}$  at 3  $^{\circ}\text{C}\cdot\text{min}^{-1}$  on TCTP sample (5  $\mu\text{M}$ ) in the following buffer: 10 mM HEPES pH 7.4, 150 mM NaCl, 2 mM TCEP, 5 mM EDTA and 2.5 % DMSO.

toward equilibrium due to the fast temperature ramp (3 min.). Thus, the impact of sertraline on the  $T_m$  of TCTP might be under-evaluated in these conditions.

### 5.3 Selective Mcl-1 inhibitors

Exploring protein-protein interactions is important for the rational design of drugs for anti-cancer therapy, especially for *in silico* workflows [267]. Correspondingly, the description of drug and protein complexes at the binding interface allows for the identification of structural determinants and further drug optimization. Both TCTP [183] and Mcl-1 [72] represent targets of therapeutic interest in anti-cancer therapy. Here, we report our collaboration work with F. Roussi (ICSN, CNRS/Université Paris-Saclay) who is developing ligands showing selectivity for Mcl-1 in fluorescence polarization assays with preformed Bcl-2 family protein and BH3 peptide complex. Selectivity for Mcl-1 compared to Bcl-xL is important in AML for example, where Mcl-1 is overexpressed but where Bcl-xL is constitutively present and should not be removed to prevent healthy immune cells from death, with obvious consequences in the whole organism. Even though not strictly part of TCTP interactome, the interaction Mcl-1/ligands represent the *frontiers* we refer to in the title of the current chapter. Ligands targeting Mcl-1 are likely to have an impact on TCTP/Mcl-1 interaction and we can start learning by establishing binding sites of these ligands on Mcl-1 protein, to further compare with the interfaces found for TCTP/Mcl-1 and TCTP<sub>BH3</sub>/Mcl-1 complexes. Thus, we document binding interfaces of ligands Na-1-115-7 (Sec. 5.3.1) and FD-24-3 (Sec. 5.3.2) at both Mcl-1

and Bcl-xL proteins. Moreover, we report experiments to confirm the selectivity of the molecules toward Mcl-1 compared to Bcl-xL (Sec. 5.3.3).

### 5.3.1 Solubility of Na-1-115-7 and FD-24-3

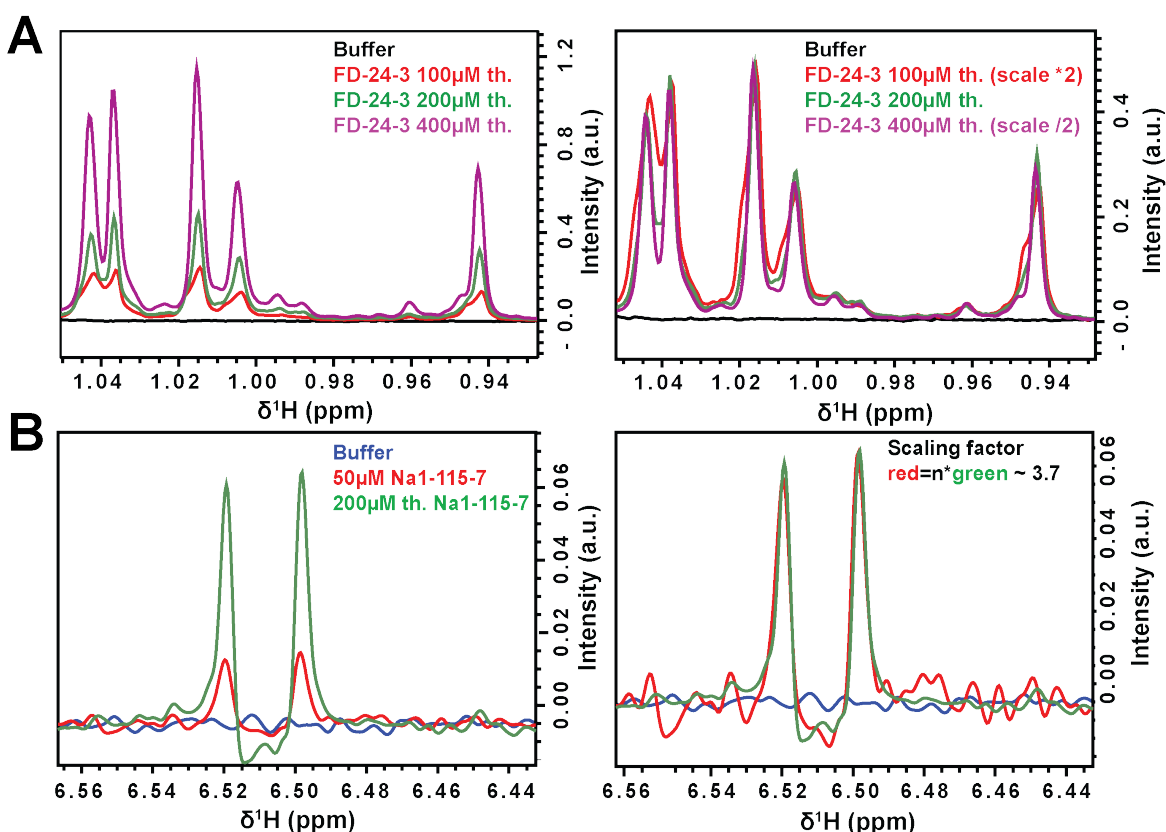
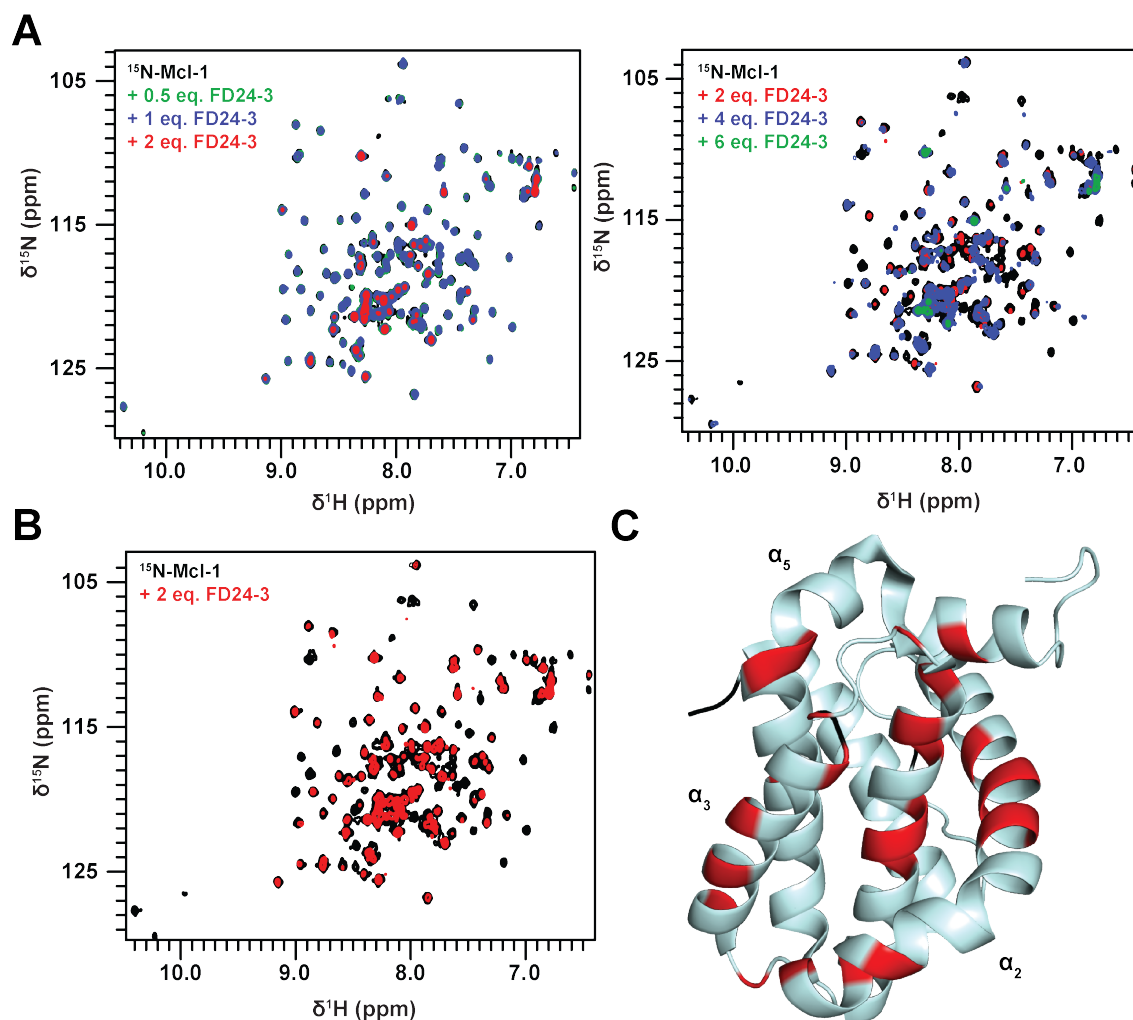


Fig. 5.15 Solubility of Mcl-1 selective ligands Na-1-115-7 and FD-24-3. Overlay of  $^1\text{H}$  spectrum from buffer (black) and in presence of increasing concentration of (A) FD-24-3 (0-400  $\mu\text{M}$ ) and (B) Na-1-115-7 (0-200  $\mu\text{M}$ ). Experiments were recorded at 800 MHz and 25  $^\circ\text{C}$  in the following buffer: 20 mM  $\text{NaPO}_4$  pH 7.4, 50 mM NaCl, 2  $\mu\text{M}$  EDTA, 2 mM TCEP, 0.005% pluronic acid, 3.5% DMSO, and 5%  $\text{D}_2\text{O}$  / 95 %  $\text{H}_2\text{O}$ .

We first tested the solubility of both Na-1-115-7 and FD-24-3 ligands by recording  $^1\text{H}$  spectra of the molecules at increasing concentrations. From 0  $\mu\text{M}$  to 400  $\mu\text{M}$  we observed sharp resonances for methyl hydrogen from FD-24-3 (Fig. 5.15 A). Signal intensity was proportional to ligand concentration in this range, with no major modification of peak shape. This indicates that FD-24-3 is soluble up to at least 400  $\mu\text{M}$ . With Na-1-115-7, we used a similar protocol to demonstrate that the molecule was soluble up to at least 200  $\mu\text{M}$  (Fig. 5.15 B). In conclusion, both molecules are soluble enough (200-400  $\mu\text{M}$ ) in presence of organic co-solvent (3.5 % DMSO) for interaction studies with Mcl-1 and Bcl-xL proteins.

### 5.3.2 Binding study with Mcl-1 selective FD-24-3

#### 5.3.2.1 FD-24-3 binding study with human Mcl-1



**Fig. 5.16 FD-24-3 binds to human Mcl-1 with strong affinity.** (A) Overlay of SOFAST  $^1\text{H}$ - $^{15}\text{N}$  HMQC spectra from isolated Mcl-1 (50  $\mu\text{M}$ ) (black) and in presence of increasing number (0-2, left; 2-6, right) of FD-24-3 equivalents. (B) Overlay of  $^1\text{H}$ - $^{15}\text{N}$  SOFAST HMQC spectra from isolated Mcl-1 (50  $\mu\text{M}$ ) (black) and in presence of FD-24-3 (2 eq.) (red). (C) Mapping of disappearing  $^1\text{H}$ - $^{15}\text{N}$  resonances and corresponding residues in presence of FD-24-3 (2 eq.) on Mcl-1 structure. Experiments were recorded at 800 MHz and 25  $^\circ\text{C}$  in the following buffer: 20 mM  $\text{NaPO}_4$  pH 7.4, 50 mM NaCl, 2  $\mu\text{M}$  EDTA, 2 mM TCEP, 0.005% pluronic acid, 3.5% DMSO, and 5%  $\text{D}_2\text{O}$  / 95 %  $\text{H}_2\text{O}$ .

In order to first locate the binding pocket of FD-24-3 on human Mcl-1  $\Delta\text{PEST}$   $\Delta\text{TM}$  (Mcl-1) we recorded  $^1\text{H}$ - $^{15}\text{N}$  spectra of isolated  $^{15}\text{N}$ -labeled Mcl-1 and in presence of increasing

concentrations of the molecule (Fig. 5.18 A). Along the titration and in a concentration-dependent manner, ligand induced two successive events in the protein. The first event is characterized by the progressive decrease in intensity, but without chemical shift variation, from a consequent set of  $^1\text{H}$ - $^{15}\text{N}$  resonances ( $\sim 15$ ) (Fig. 5.18 B). When increasing ligand concentration toward higher ratios ( $> 2$  eq.) the whole signal from Mcl-1 decreased and almost no resonances anymore could be seen at maximum ligand concentration (300  $\mu\text{M}$ , 6 eq.). The first event was described through computation of  $^1\text{H}$ - $^{15}\text{N}$  intensity ratios. Disappearing residues were mapped on Mcl-1 structure (Fig. 5.18 C) and these were located within the BH3-binding groove of the protein composed by  $\alpha$ -helices  $\alpha_2$ ,  $\alpha_3$  and  $\alpha_4$ . Additional perturbations could be observed in  $\alpha$ -helix  $\alpha_5$  that does not directly interact with the ligand in most crystal structures. The helix  $\alpha_5$  likely underwent a displacement upon ligand binding, as reported before for Mcl-1 complex with BH3-derived peptides and full length TCTP (Sec. 4.2). Considering that resonances from the BH3 binding groove did totally disappear at 2 eq. ligand, establishing the saturation of Mcl-1, we estimated a  $K_d$  of 5  $\mu\text{M}$  between FD24-3 and human Mcl-1. In conclusion, FD-24-3 binds to Mcl-1 in the BH3-binding pocket and likely induces the oligomerization of Mcl-1 at high concentration ( $> 100$   $\mu\text{M}$ ). It is important to note that FD24-3 is a dialdehyde molecule which could react at lysine residues and in N-terminal of the protein, predominantly, possibly inducing covalent protein-ligand complexes and oligomerization.

### 5.3.2.2 FD-24-3 selectivity for Mcl-1 compared to Bcl-xL

FD-24-3 was designed for selectivity toward Mcl-1 compared to Bcl-xL. We have done competition experiments to compare the relative affinity of FD-24-3 for human Mcl-1  $\Delta\text{PEST}$   $\Delta\text{TM}$  (Mcl-1) and human Bcl-xL  $\Delta 45-84$   $\Delta\text{TM}$  (Bcl-xL). The  $^1\text{H}$ - $^{15}\text{N}$  SOFAST HMQC spectrum of isolated  $^{15}\text{N}$ -labeled Mcl-1 was compared with the  $^1\text{H}$ - $^{15}\text{N}$  spectra of Mcl-1 in presence of ligand (1 eq.) or in presence of ligand (1 eq.) and Bcl-xL (1 eq.). In these conditions, about 75 % of Mcl-1 is bound to FD24-3 in absence of Bcl-xL as seen from the partial disappearing of resonances from residues in the BH3 binding groove of the protein (Fig. 5.17 A). Upon addition of Bcl-xL, no significant change was observed in the spectrum of  $^{15}\text{N}$ -labeled Mcl-1 in term of both  $^1\text{H}$ - $^{15}\text{N}$  chemical shifts and intensity (Fig. 5.17 B). This means that the protein remained bound to the ligand until 2 hours of equilibration time and confirms the selectivity of FD24-3 for human Mcl-1 compared to Bcl-xL in our experimental setup with pre-formed Mcl-1/FD24-3 complex. Considering the relative concentration of the two proteins, this suggests that the relative affinity of FD24-3 for Bcl-xL is at least 20 lower ( $K_d > 100$   $\mu\text{M}$ ) compared to Mcl-1 ( $K_d \sim 5$   $\mu\text{M}$ ). We can explain the difference since the BH3 binding groove of Bcl-xL and Mcl-1 differ in size and amino-acids composition.

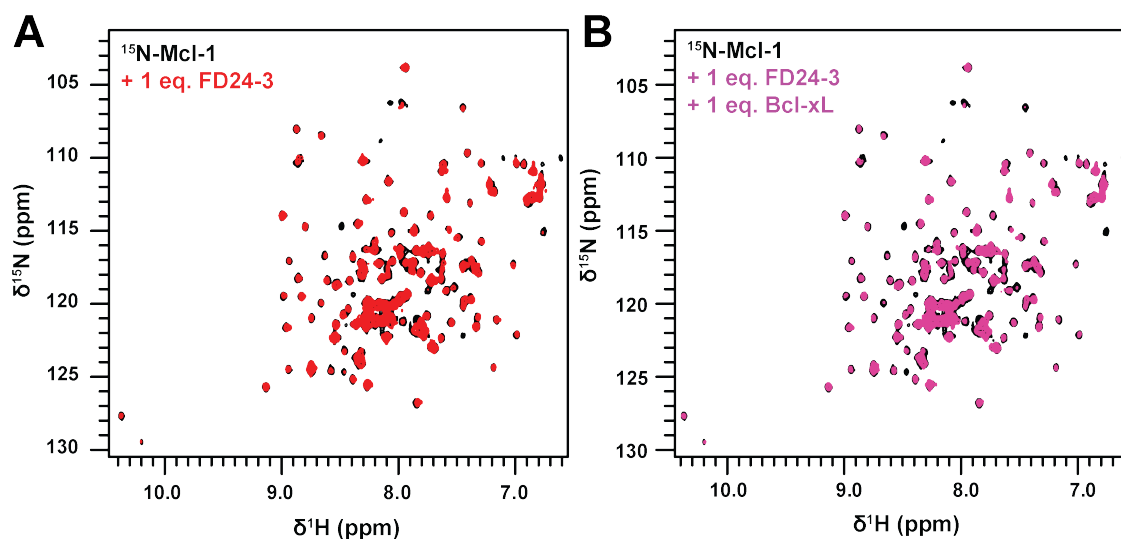


**Fig. 5.17 Relative affinity of FD-24-3 for Mcl-1 and Bcl-xL evaluated by NMR.** (A) Overlay of  $^1\text{H}$ - $^{15}\text{N}$  SOFAST HMQC from isolated Mcl-1 (50  $\mu\text{M}$ ) (black) and in presence of 1 eq. FD-24-3. (B) Overlay of SOFAST  $^1\text{H}$ - $^{15}\text{N}$  HMQC from isolated Mcl-1 (50  $\mu\text{M}$ ) (black) and in presence of 1 eq. FD-24-3 plus 1 eq. Bcl-xL. Experiments were recorded at 800 MHz and 25  $^\circ\text{C}$  in the following buffer: 20 mM  $\text{NaPO}_4$  pH 7.4, 50 mM NaCl, 2  $\mu\text{M}$  EDTA, 2 mM TCEP, 0.005% pluronic acid, 3.5% DMSO, and 5%  $\text{D}_2\text{O}$  / 95 %  $\text{H}_2\text{O}$ .

Indeed, the space between C-terminal of helix  $\alpha_2$  and helix  $\alpha_3$  in Mcl-1 is more extended (10.6  $\text{\AA}$  between residues M231-V249) compared to the homologous region in Bcl-xL (6.2  $\text{\AA}$  between residues L108-V126) at helices  $\alpha_3$  and  $\alpha_4$ .

### 5.3.3 Binding study with Mcl-1 selective Na-1-115-7

#### 5.3.3.1 Binding site of Na-1-115-7 in human Mcl-1

In order to first locate the binding pocket of Na-1-115-7 on human Mcl-1  $\Delta\text{PEST}$   $\Delta\text{TM}$  (Mcl-1) we recorded  $^1\text{H}$ - $^{15}\text{N}$  SOFAST HMQC spectra of isolated  $^{15}\text{N}$ -labeled Mcl-1 and in presence of increasing concentrations of the molecule until the solubility limit (250  $\mu\text{M}$ , 4.5 eq.). At maximum concentration of ligand, the protein was not fully saturated (Fig. 5.18 A). Along the titration, spectral perturbations were clearly visible through progressive shifts of several resonances, predominantly in intermediate exchange regime (Fig. 5.18 B, C). After each ligand increment, several hours were necessary to reach an apparent system equilibrium. Despite heterogeneity in perturbations regime we could estimate that most of Mcl-1 (60-70%) was bound to Na-1-115-7 at maximum ligand concentration (250  $\mu\text{M}$ ). Considering that the protein concentration (50  $\mu\text{M}$ ), this corresponds to a dissociation constant of  $\sim 100$   $\mu\text{M}$  describing a medium affinity interaction. Then we have computed  $^1\text{H}$ - $^{15}\text{N}$  chemical shifts per-

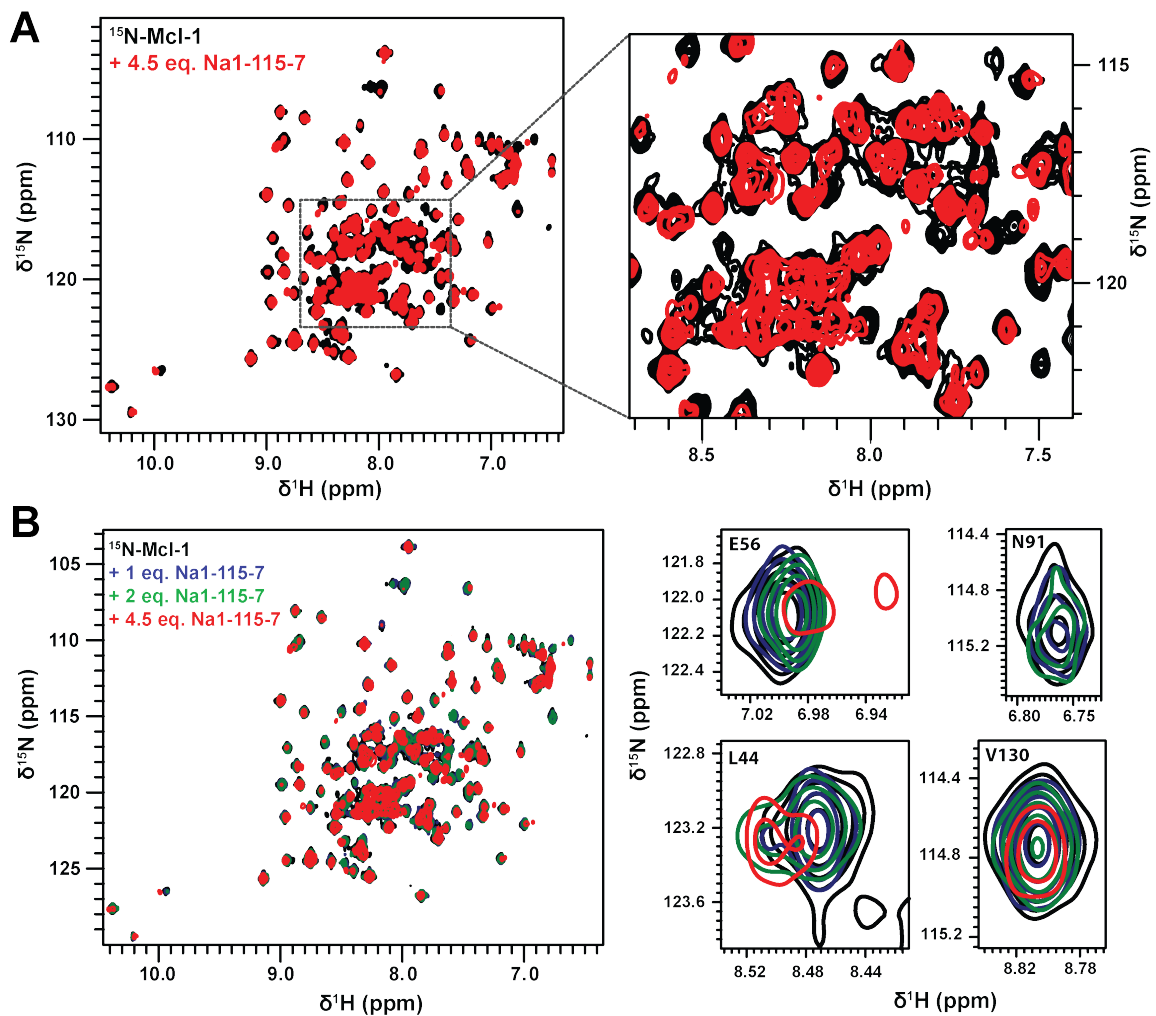


**Fig. 5.18 Na-1-115-7 binds to human Mcl-1 with medium affinity.** (A) Overlay of  $^1\text{H}$ - $^{15}\text{N}$  SOFAST HMQC spectra from isolated Mcl-1 (50  $\mu\text{M}$ ) (black) and in presence of Na-1-115-7 (4.5 eq.) (red). A close-up view of the central region is shown (right). (B) Overlay of SOFAST  $^1\text{H}$ - $^{15}\text{N}$  HMQC spectra from isolated Mcl-1 (50  $\mu\text{M}$ ) (black) and in presence of increasing concentrations of Na-1-115-7 (blue, green, red). A close-up view of residues experiencing spectral perturbations is shown (right). Experiments were recorded at 950 MHz and 25  $^\circ\text{C}$  in the following buffer: 20 mM  $\text{NaPO}_4$  pH 7.4, 50 mM NaCl, 2  $\mu\text{M}$  EDTA, 2 mM TCEP, 0.005% pluronic acid, 3.5% DMSO, and 5%  $\text{D}_2\text{O}$  / 95 %  $\text{H}_2\text{O}$ .

turbations between  $^1\text{H}$ - $^{15}\text{N}$  spectra from isolated Mcl-1 and in presence of ligand. Residues located in helical regions ( $\alpha_1$ ,  $\alpha_2$  and  $\alpha_3$ ) forming the BH3-binding groove of the protein were predominantly affected upon ligand addition. This indicates that Na-1-115-7 and BH3 motifs do share a common binding pocket in the protein. Notably, no residue from helix

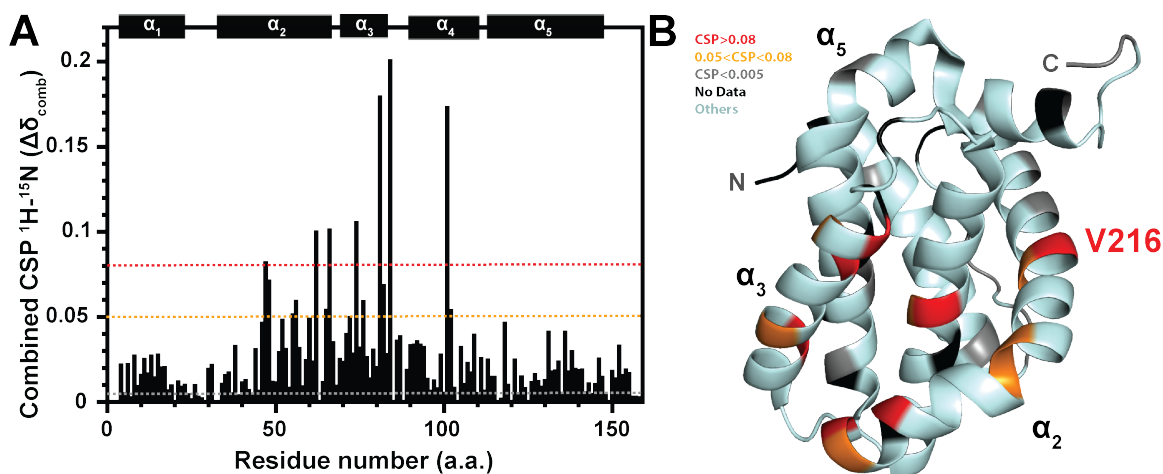


Fig. 5.19 **Mapping of Na-1-115-7 binding site on Mcl-1** (A) Combined  $^1\text{H}$ - $^{15}\text{N}$  chemical shift perturbations calculated between isolated Mcl-1 (50  $\mu\text{M}$ ) and in presence of Na-1-115-7 (4.5 eq.). (B) Mapping of combined  $^1\text{H}$ - $^{15}\text{N}$  chemical shift perturbations (red  $> 0.08$ ,  $0.08 > \text{orange} > 0.05$ , grey  $< 0.005$ ) on Mcl-1 structure. Residues for which no data are available are highlighted (black).

$\alpha_1$  was affected above threshold as reported for BH3-motifs, consistently since helix  $\alpha_1$  is located at the opposite of the BH3 binding groove.

Ligands targeting Mcl-1 including Na-1-115-7 were originally developed using mouse Mcl-1  $\Delta\text{PEST } \Delta\text{TM}$  (mMcl-1) since it was the only model available for decades, despite striking differences [264] in the BH3-binding groove organization between both orthologous human and mouse proteins. To bridge past development of Na-1-115-7 to the current circumstances and to experimentally validate the importance of using a human protein, binding experiments were repeated using the mouse  $^{15}\text{N}$  Mcl-1  $\Delta\text{PEST } \Delta\text{TM}$  (mMcl-1) (Fig. 5.22). Results have shown that mMcl-1 is saturated at equivalence (1-1.25 eq.) with an estimated affinity rather high ( $K_d < 1 \mu\text{M}$ ) for Na-1-115-7 complex formation with mMcl-1 compared to human Mcl-1. This confirms that human and murine sequence have distinct binding properties, probably due to the divergence in the width of the BH3 binding groove [264], the murine protein having 100 higher affinity for Na-1-115-7 than the human counterpart. Consistently, spectral perturbations were visible through slow and, marginally, intermediate exchange shifts on the protein spectrum and also located on the BH3 binding site.

### 5.3.3.2 Evaluation of Na-1-115-7 binding to Bcl-xL

Na-1-115-7 was designed for Mcl-1 selectivity compared to Bcl-xL protein based on the fluorescence competition experiment. Our collaborators F. Roussi (ICSN, CNRS/Université Paris-Saclay) used a binding assay of ligands on pre-formed complexes Mcl-1/Bak<sub>BH3</sub> and

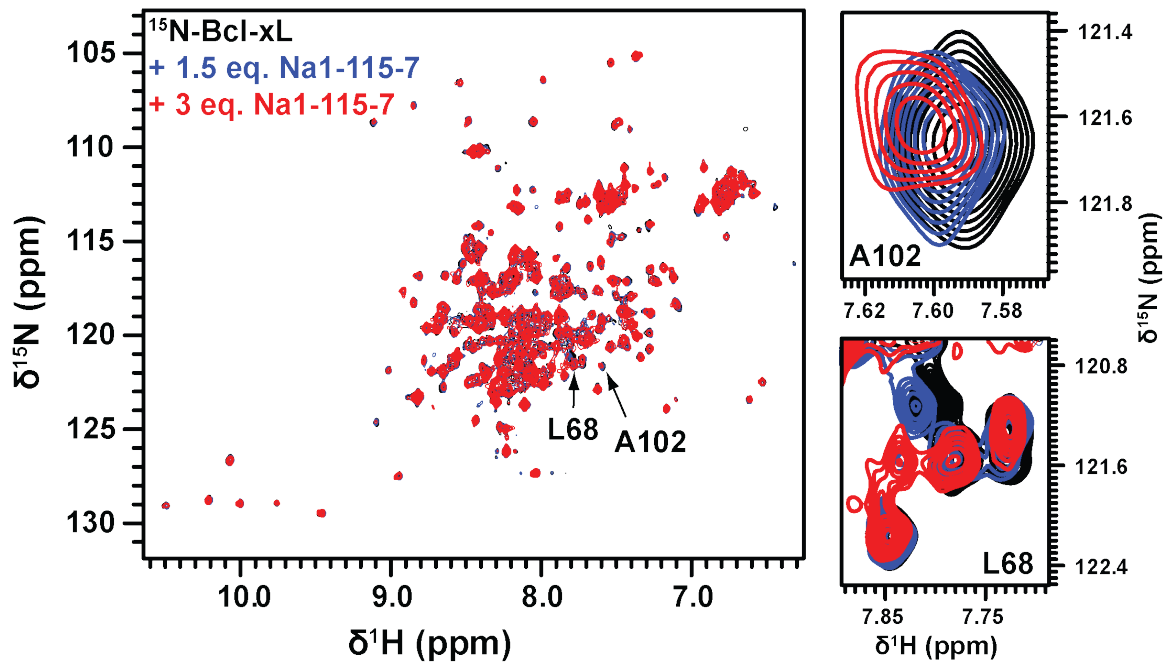


Fig. 5.20 Na-1-115-7 binds to human Mcl-1 with low affinity. (A) Overlay of  $^1\text{H}$ - $^{15}\text{N}$  SOFAST HMQC spectra from isolated Bcl-xL (50  $\mu\text{M}$ ) (black) and in presence of Na-1-115-7 (1.5 eq.) (blue), (3 eq.) (red). A close-up view of selected crosspeaks is shown (right). Experiments were recorded at 950 MHz and 25  $^\circ\text{C}$  in the following buffer: 20 mM  $\text{NaPO}_4$  pH 7.4, 50 mM NaCl, 2  $\mu\text{M}$  EDTA, 2 mM TCEP, 0.005% pluronic acid, 3.5% DMSO, and 5%  $\text{D}_2\text{O}$  / 95 %  $\text{H}_2\text{O}$ .

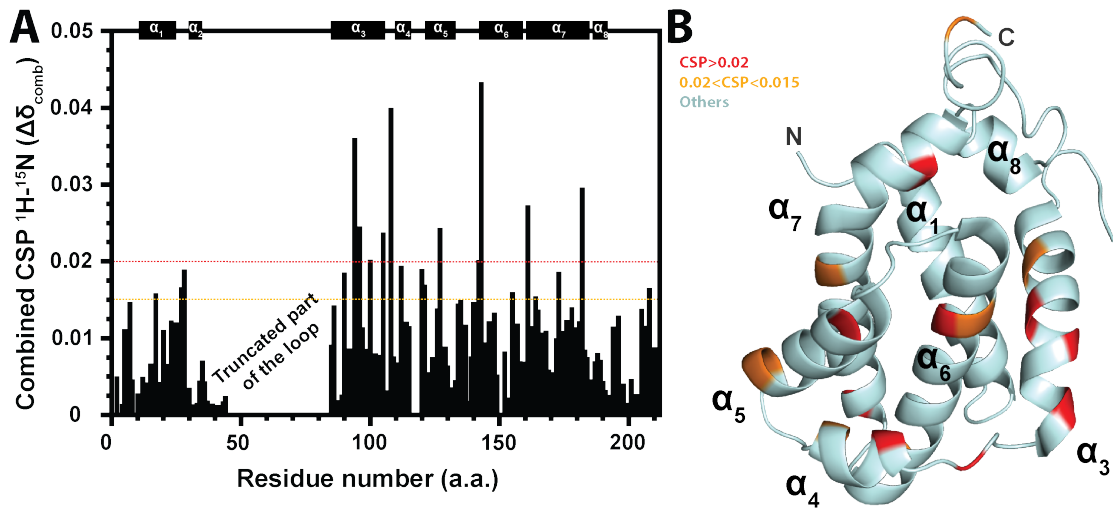


Fig. 5.21 Mapping of Na-1-115-7 binding site on Bcl-xL. (A) Combined  $^1\text{H}$ - $^{15}\text{N}$  chemical shift perturbations calculated between isolated Bcl-xL (50  $\mu\text{M}$ ) and in presence of Na-1-115-7 (4.5 eq.). (B) Mapping of largest combined  $^1\text{H}$ - $^{15}\text{N}$  chemical shift perturbations (red  $> 0.02$ ,  $0.02 >$  orange  $> 0.015$ ) on Bcl-xL structure. Residues for which no data are available are highlighted (black).

Bcl-xL/Bax<sub>BH3</sub>, originally with the murine Mcl-1. Since Bcl-2 family proteins undergo structure changes upon complex formation, it is unclear how the ligands could be selective of Mcl-1 compared to Bcl-xL in the context of both human, free proteins. Thus we first wanted to test if the ligand Na1-115-7 could still bind to human Bcl-xL  $\Delta 45-84 \Delta TM$  (Bcl-xL). Binding was tested by recording successive  $^1H$ - $^{15}N$  spectra of isolated  $^{15}N$ -labeled Bcl-xL and upon addition of ligand (3 eq.) (Fig. 5.20). Along the titration, spectral perturbations were modest but still visible through small but progressive shifts of several resonances (10-15), predominantly in rapid exchange regime. However, for a very limited number of residues (< 5), intermediate and slow exchange regime shifts could be observed. Bcl-xL was far (< 50%) from being saturated at the maximum concentration of ligand (150  $\mu M$ ) since the rapid exchange shifts are linear regarding the concentration of ligand along the whole titration. Spectral perturbations were of small amplitude but sufficient to compute  $^1H$ - $^{15}N$  chemical shifts perturbations (Fig. 5.21) upon ligand addition. In Bcl-xL, several residues from the BH3-binding groove of the protein ( $\alpha_3$ ,  $\alpha_4$  and  $\alpha_5$ ) were affected upon ligand addition. Overall we conclude that Na-1-115-7 binds to Bcl-xL in the BH3-binding groove of the protein with rather low affinity ( $K_d > 150 \mu M$ ).

### 5.3.3.3 Na-1-115-7 selectivity at Mcl-1 compared to Bcl-xL

In order to test if Na-1-115-7 also binds the BH3 binding groove of murine Mcl-1 (mMcl-1), we recorded  $^1H$ - $^{15}N$  SOFAST HMQC spectra of the free protein and upon saturation by the ligand (1.25 eq.) (Fig. 5.22). Major spectral changes are observed between both conditions. First, numerous signals disappeared upon addition of the ligand. Second, an important number of new peaks are observed within the bound mMcl-1 state. Signal broadening was also seen. Overall, these slow and intermediate exchange spectral perturbations are in agreement with a medium-strong ( $K_d \sim 1 \mu M$ ) binding affinity of the ligand for mMcl-1.

To assess the relative affinity of murine Mcl1 (mMcl-1) and human Bcl-xL for Na1-115-7, a competition experiment was done. Overlay of isolated mMcl-1 and bound to Na1-115-7 is shown (Fig. 8) as well as an overlay of mMcl-1 bound to Na-1-117-7 in absence and in presence of 3 eq. Bcl-xL  $\Delta 45-84 \Delta TM$  (Bcl-xL). Spectral differences were very important between free and bound mMcl-1, as described before. When comparing both mMcl-1 bound spectra in absence and in presence of Bcl-xL, minor changes were observed. Several crosspeaks with low intensity disappeared upon Bcl-xL addition and very small shifts were observed for several resonances. Such minor spectral changes were not significant compared to the major changes observed between free and bound Mcl-1. Considering that we added 3 eq. of Bcl-xL, we can say that mMcl-1 has a much greater affinity for Na1-115-7 than Bcl-xL.

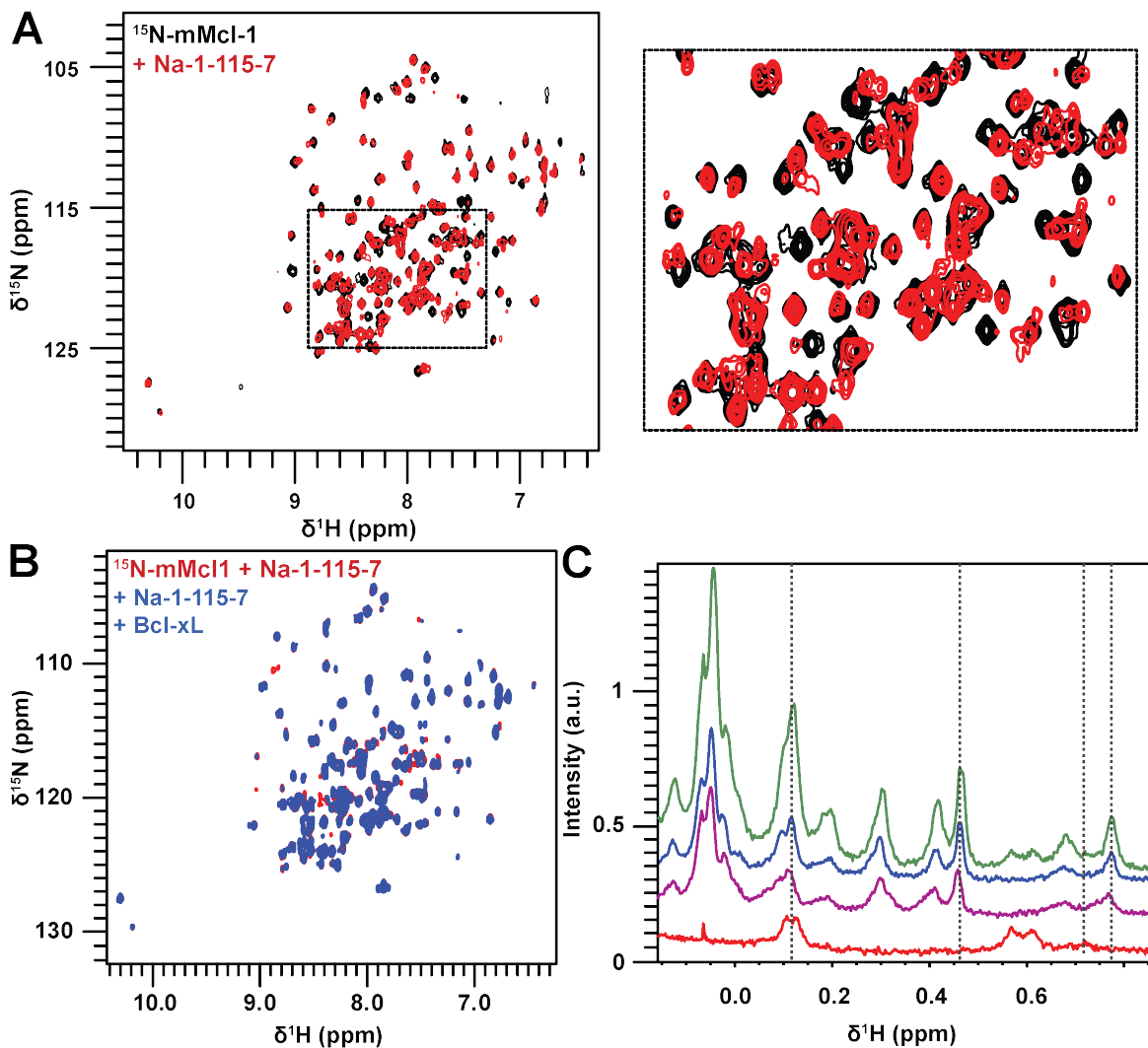


Fig. 5.22 **Comparison of free mMcl-1 and bound to Na-1-115-7.** Overlay of  $^1\text{H}$ - $^{15}\text{N}$  SOFAST HMQC spectra from isolated mouse Mcl-1 (50  $\mu\text{M}$ ) (black) and in presence of Na-1-115-7 (4.5 eq.) (red). Experiments were recorded at 800 MHz and 25  $^\circ\text{C}$  in the following buffer: 20 mM  $\text{NaPO}_4$  pH 7.4, 50 mM NaCl, 2  $\mu\text{M}$  EDTA, 0.005% pluronic acid, 3.5% DMSO, 2 mM TCEP in 95 %  $\text{H}_2\text{O}$  / 5 %  $\text{D}_2\text{O}$ .

We can estimate a  $K_d$  difference if we consider that less than 5 % of mMcl-1 is displaced from the ligand upon Bcl-xL addition. By doing the hypothesis we can deduce that the  $K_d$  of Na1-115-7 for mMcl-1 is at least 50 times lower than for Bcl-xL. Overall, Na1-115-7 appears to be mMcl-1 selective. This result will complement other results in an article.

## 5.4 Discussion

### Sertraline and other ligands at TCTP protein

Sertraline is a well-known TCTP inhibitor used to target AML. First clinical trials carried out under mono-therapy and led to promising results despite adverse side effect on CNS at the dose used, mainly due to its main usage as a SSRI. The current strategy is a bi-therapy combining cytarabine (Ara-C) with low dose of sertraline to recover apoptosis in cancer cells, under clinical phase I evaluation. Despite these very promising clinical results, the detection of molecular interaction between TCTP and sertraline is limited to SPR technique. By NMR, we revealed that sertraline did not bind TCTP with micromolar affinity as reported in the SPR assay (34  $\mu\text{M}$ ). SPR is based on crosslinking reactions between a protein and a sensor chip. This can impact protein structure and SPR was often reported to induce a high level of false positive. By contrast, solution-state NMR ensures optimal conservation of relevant protein structure and dynamics. Nevertheless one cannot rule out the hypothesis that SPR captured the sertraline-induced TCTP aggregation. This further strengthened the idea that one needs to validate molecular interaction by multiple techniques.

The very low, if any, affinity of sertraline to TCTP (> mM) detected under our conditions and leading to protein aggregation questions the molecular target of sertraline in cells. This also questions if the native well-folded TCTP state is the actual state in cells, which would be inconsistent with being the main component of sertraline effect. Interestingly, sertraline decreased the melting temperature of TCTP, suggesting that it stabilizes a folding intermediate on the aggregation route. Also, ligands were shown to induce the formation of disulfide covalent TCTP-TCTP dimers, questioning the relevance of this for biological systems. The destabilizing effect of sertraline on TCTP might also be linked to the decrease in protein levels observed under treatment, with increase in p53 levels and recovery of apoptosis. Thus, the mode of action of sertraline can be linked to cellular turnover of TCTP rather than direct inhibition of protein-protein interaction. Indeed, a simple model whereby sertraline interacts with a protein to perturb its molecular network does not imply a change in the protein level. Nothing occurs *in vitro* at less than 100  $\mu\text{M}$  sertraline. So another very probable mechanism, consistent with the low dosage at which sertraline has effects on cells (<10 $\mu\text{M}$ ) is that sertraline does not touch TCTP directly but controlled TCTP levels through mTOR pathway

### **TCTP and MDM2 N-terminal domain**

The overall preliminary study carried out on TCTP/MDM2 show strong similarities with the previous TCTP interaction with Mcl-1 and Bcl-xL. Slow kinetics and both dynamics and conformational change in TCTP suggest that the protein undergoes a significant remodeling upon interaction with MDM2. This firmly indicates that TCTP/MDM2 interaction is not a simple complex bringing two rigid-body in proximity and undoubtedly, the proposed model is likely not correct. Further work will be needed to characterize the competent structural isoform of TCTP when bound to MDM2, and how this is similar or dissimilar to TCTP\* and where the binding interface is located.

However, our preliminary work contradicts SPR experiments reported by our collaborators A. Telerman and R. Amson (IGR, CNRS/Université Paris-Saclay) since they could not detect an interaction between TCTP and MDM2 N-terminal domain (1-134) but they rather proposed that the C-terminal or central MDM2 domain could bind TCTP protein with a  $K_d$  of 370 nM and 290 nM, respectively. This difference finally makes no naive surprise since we already reported striking differences in binding studies with sertraline and other ligands when using TCTP in solution or immobilized on the SPR chip by covalent cross-linking. Thus, we think that SPR should not be used if one wants to study the interaction between MDM2 and TCTP from its native structure (2HR9). Indeed, it is likely that the protein structure is strikingly different between both solution and immobilized states.

### **Interplay between TCTP, YB-1 and RNA**

We validated the direct interaction between TCTP and YB-1 and have shown that TCTP does not interact with RNAs extracted from yeast. TCTP and YB-1 likely form soluble oligomer upon complex formation. The C-terminal IDR in YB-1 was responsible for greater affinity for complex formation with TCTP. It is interesting to note that the YB-1 C-terminal IDR has crucial role in the binding affinity with TCTP since it is also important to allow high affinity association with RNA. Indeed, the CSD itself has significantly lower affinity for RNA which illustrates the importance of the YB-1 C-terminal IDR in mediating high affinity interactions. In presence of RNA, the TCTP/YB-1 complex dissociated but the TCTP protein was found to still transiently and weakly interact with YB-1 in YB-1/RNA complexes. The binding mode was rather different compared to TCTP/YB-1 complex but we surprisingly recovered a spectral pattern that resemble to TCTP bound to YB-1 construct truncated for the C-terminal IDR. Thus, this might be the interface with the CSD domain of YB-1. Consequently, we can expect TCTP to bind YB-1 at either YB-1 CSD or C-terminal IDR, with the latter interface likely broken upon RNA addition. It is clear that the interaction

between TCTP and YB-1 N-terminal fragment (1-180, A/P rich domain and CSD) does not induce major modifications of TCTP structure, dynamics and oligomeric state. However, we do not know how the C-terminal YB-1 IDR since TCTP could induce oligomerization upon complex formation with YB-1. In any case, the RNA sequences and TCTP definitely interfere at YB-1 protein and its possible that RNA could regulate TCTP/YB-1 association or the opposite, which could make TCTP as also involved in RNA fate. To demonstrate such hypothesis, our preliminary work should be extended further.

Although the *in vitro* data were promising, the group of our collaborator D. Pastré tried to reproduce the interaction between TCTP and YB1 in HeLa cells but failed (same cells as in the original paper). Therefore whether this interaction is biologically relevant is not clear yet, and the *in vitro* interaction could be facilitated by the low salt concentration.

# Chapter 6

## General discussion

In the first chapter of the manuscript, we introduced the tumor reversion program and the associated TCTP protein in term of structure, function and interaction in the context of apoptosis and beyond (Sec. 1). All the methods we used to study structure and dynamics of TCTP interactome were presented in the second chapter with practical considerations and brief theoretical description, with a more extensive focus on NMR (Sec. 2). In the first part of results, we demonstrated that TCTP can adapt different tertiary and quaternary organization upon IDR modification or non-covalent dimer formation and we also unveiled TCTP\*, a molten-globule state of the protein (Sec. 3). In the second part of results we characterized TCTP complex with Bcl-2 family proteins Bcl-xL/Mcl-1 and we established the molten-globule nature for TCTP structure in the complexes. We mapped binding interfaces of TCTP and BH3-derived peptides on Bcl-xL/Mcl-1 proteins and we identified discriminant of the BH3-like motif compared to the canonical BH3 sequence in term of structure and dynamics at the molecular interface with Mcl-1 (Sec. 4). In the last part of results, we identified TCTP complex with YB-1, YB-1/RNA and we confirmed that TCTP associates with MDM2 N-terminal domain but we could not reproduce the TCTP/sertraline interaction reported by SPR ( $K_d = 34 \mu\text{M}$ ). Regarding ligands, we could still map binding sites of Mcl-1 selective molecules at Bcl-xL/Mcl-1 and confirmed the Mcl-1 selective nature of the drugs compared to Bcl-xL (Sec. 5).

As general discussion topics, we first extend the description of the molten-globule state and discuss the putative impact for TCTP function (Sec. 6.1). Then we propose a functional model that explains, from our structural work, the mechanistic basis for the TCTP-induced reinforcement of the antiapoptotic properties of Bcl-xL and Mcl-1 (Sec. 6.2). Finally, we compare BH3-like and canonical BH3 sequences in term of binding mode specificity and nature, and discuss the particular role of the BH3-like TCTP protein (Sec. 6.3).

## 6.1 Molten-globule states

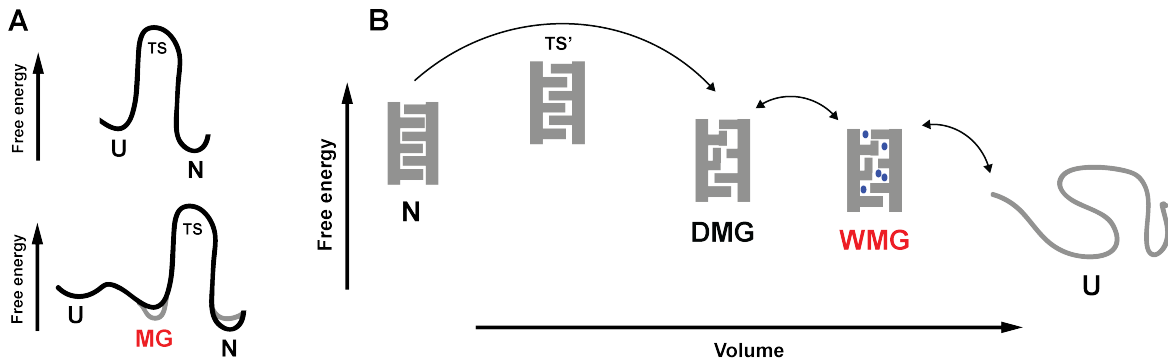


**Fig. 6.1 Energetic model for the molten-globule state.** (A) Energy diagrams representing a two-step folding pathway (top) and including a molten-globule intermediate (bottom). Upon variation of environmental conditions, relative energy levels between protein states can evolve (grey) and possibly balance the thermodynamic equilibrium toward the molten-globule state. The energy of activation between native and molten-globule state is annotated (TS). (B) Model for the molten-globule. From a native protein a limiting step with high energetic cost (TS') convert into a dry molten-globule. The folding intermediate could easily convert into wet molten-globule upon water insertion in the hydrophobic core of the protein. Equilibrium with the unfolded form of the protein is likely to happen.

In the history, protein folding was first theorized as an univocal path in which a single unfolded amino-acids chain adopts a single and unique tridimensional structure, which represents the global minimum in the free energy diagram of the protein [268–270] (Fig. 6.1). Over time, accumulating evidences of additional structural states for a single protein were gained mainly through improvements in solution-structure determination by NMR, thus challenging the dominant model of protein folding. The description of stable folding intermediates, such as the Molten-Globule (MG) state [257], irreversibly triggered a shift of the dogma in that multivocal sequence-structure relationship can also drive protein folding and be the physical basis for molten-globule states and metamorphic proteins [271]. These alternative states were demonstrated to be functionally important in a wide range of cellular processes and are commonly found in proteins having a large interactome, like TCTP, to adapt with their partners.

We have compiled experimental results on TCTP structure in TCTP\* and bound state to Bcl-2 family partners Bcl-xL and Mcl-1. Since the literature reports structures of MG from many different proteins we could compare and establish that TCTP\* and bound TCTP have a molten-globule organization in the core domain. In general, MG state of a protein is weakly populated at neutral pH and medium salt concentration, as in this case. We used urea and pressure to balance the energy levels of both native and MG state [272–274], thus allowing

for the formation of an equilibrium MG. One of the most important features of the MG state is the similarity of the compactness compared to the native state. In term of secondary structure, it is often accepted that the MG retains a far-UV CD spectrum as pronounced as in the native protein as we observed between native TCTP and bound or TCTP\* states [275]. In contrast, the near-UV spectrum of the MG state differ substantially and is strongly reduced compared to the native one suggesting the absence of a rigid tertiary structure organization, consistently with our observations. By NMR, people have demonstrated that MG have much simpler spectra resembling to those of unfolded proteins [276–279] due tertiary structure fluctuation with similar appearance compared to our data.

The MG can be Dry (DMG) or Wet (WMG) in that it disallows or allows for water to insert inside the hydrophobic core of the protein [280, 281] (Fig. 6.1 B). The increase in large-scale fluctuation can lead to a substantial increase in MG susceptibility to proteases [282] and we could also detect such effect in bound TCTP with Mcl-1 protein. Similarly, the WMG should expose more hydrophobic surface to solvent, thus allowing for binding of hydrophobic ligands. Such principle was used with the ANS probe which strongly binds to WMG leading to a large increase in the fluorescence properties of the probe [283]. We could confirm using this test that the bound TCTP state and TCTP\* have wet molten-globule core domains.

Interestingly, the MG can present stronger affinity for membranes [282] as shown with liposomes [284] or phospholipids [285] which can be important in case of membrane-inserting proteins as suggested for TCTP. Indeed, it was proposed that the MG state could be involved in the translocation of proteins across membranes [286]. In line with TCTP/Bcl-xL/Bax, such membrane insertion could be facilitated by the molten-globule state of the protein. As a general property the MG state of proteins tend to aggregate as recently illustrated by the MG state of p53 protein [287]. We also demonstrated that TCTP\* and the bound protein tend to precipitate at lower concentration and temperature compared to the native protein. The existence of the MG state *in vivo* has also been demonstrated in several studies [274], making relevant to study this particular TCTP state. Considering that MG state have more labile tertiary structures and are more prone to degradation by proteases and the ubiquitin-proteasome system, this would mean that upon interaction with Bcl-xL or Mcl-1 the MG nature of TCTP could lead to increased TCTP degradation in cells, unless some specific mechanisms protect TCTP from degradation.

## 6.2 TCTP in complex with Bcl-xL and Mcl-1: functional hypothesis

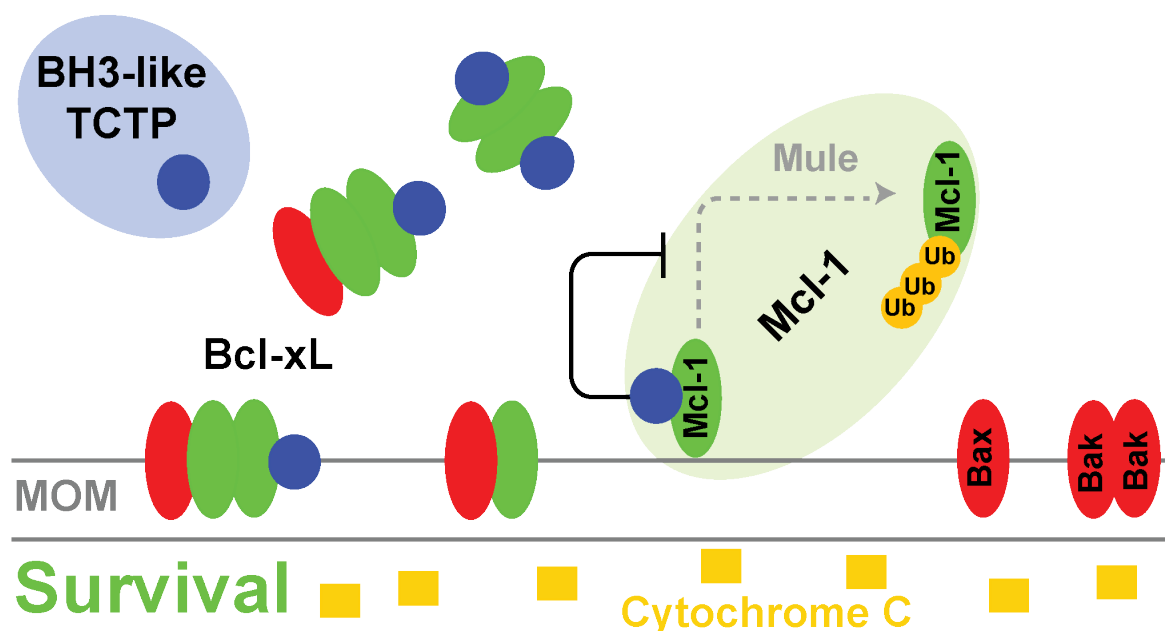


**Fig. 6.2 Impact of the BH3-like TCTP on MOMP via Bcl-xL and Mcl-1.** In presence of TCTP, pro-survival signaling through Bcl-xL and Mcl-1 inhibits MOMP, cytochrome c release and thus apoptosis which contributes to cancer cells maintenance and progression. By interacting with Bcl-xL, the BH3-like protein TCTP promotes Bcl-xL/Bax interaction even though both TCTP and Bax share the same binding pocket on Bcl-xL. TCTP and Bax have potentiating and inhibiting impact on Bcl-xL, respectively. An hypothesis is that TCTP binds nor induces Bcl-xL dimers to expose a modified BH3-binding groove of greater affinity for Bax. Alternatively, TCTP could prepare Bcl-xL for binding to Bax with greater affinity. Complementary, TCTP inhibits ubiquitinylation and proteasome-mediated degradation of Mcl-1. It is possible that TCTP competes with the E3 ubiquitine ligase Mule for binding to the protein. This could also be mediated by binding interference with other E3 ubiquitine ligase, even though Mule was reported to be necessary for proteasome-mediated degradation of Mcl-1.

We have shown that TCTP complex with Mcl-1 are smaller in size compared to TCTP complex with Bcl-xL. Using SEC, DLS and  $^{15}\text{N}$ -spin relaxation plus DOSY experiments we could estimate that TCTP/Mcl-1 and TCTP/Bcl-xL were predominantly forming stable heterodimers and heterotetramers with equimolar ratios. An underlying equilibrium in both complexes with higher n-mers was suggested from our failure to establish reliable complex stoichiometry in MALS and SAXS, despite prior separation by SEC. Interestingly, cytosolic Bcl-xL dimers were described to be dissociated upon ligand binding and membrane insertion [83]. This was also observed with other Bcl-2 family proteins [288]. The fact that ligand binding dissociates Bcl-xL dimers means that BH3 ligands can tune the monomer-

dimer equilibrium in Bcl-xL. In consequence, the BH3 binding groove from Bcl-xL monomer is promoted. By opposite, we showed that TCTP did stabilize Bcl-xL dimers, consistently with reports indicating that TCTP preferentially binds the Bcl-xL dimer [111], thus likely shifting the equilibrium toward complete Bcl-xL dimerization. TCTP promotes the BH3 binding groove from Bcl-xL dimer, with possibly different binding properties toward Bax or other BH3 ligands. However, we do not know the consequence of such observations regarding TCTP and Bcl-xL oligomeric state in the context of the cytosolic or membrane environment. Still, we can propose a model to explain how TCTP potentiates Bcl-xL and strengthens Bcl-xL/Bax interaction. By stabilizing Bcl-xL dimer, TCTP promotes a specific binding interface since the BH3-binding groove organization slightly differs between Bcl-xL monomer and dimer. We showed that TCTP/Bcl-xL complex still has heterogeneous stoichiometry and thus, we expect Bcl-xL dimers to bind one or two TCTP units, leaving the opportunity for Bax to compete for binding to the dimer state of Bcl-xL, as a putative mechanism to explain membrane permeabilization assays [111]. This interplay would be more likely to occur in cytosolic complexes since membrane insertion usually competes with Bcl-xL oligomerization. Also, TCTP levels can be very high (500  $\mu$ M) in the cytosolic fraction of cancer cells.

The study of the heterodimeric TCTP/Mcl-1 complex permitted to unveil the binding site of TCTP on Mcl-1 and this was located to the BH3 binding groove, at the opposite of the ubiquitinylation sites K194 and K197. The E3 ubiquitin ligase Mule was reported to be required for the poly-ubiquitinylation [85] and proteasome-dependent degradation of Mcl-1. The protein includes a BH3 motif that specifically interacts with Mcl-1 but not with Bcl-2, Bcl-xL or Bax. Interestingly, Bcl-2 family proteins can modulate the interaction between Mcl-1 and Mule. Phosphorylations in the PEST domain also serve to tune the association. Conceptually, it is interesting to note that BH3-only proteins such as Bim, Puma and Noxa were shown to inhibit [289, 290] and promote [291, 292] proteasome-dependent degradation of Mcl-1, respectively, in a Mule dependent manner [293]. Other things being equal, this means that the activity of Bim and Puma is a mix with an antiapoptotic fraction at Mcl-1 protein with functional significance regarding Mule activity. Compared to canonical BH3-only proteins, the Mule<sub>BH3</sub> peptide was reported to have very low binding affinity for Mcl-1, as for TCTP<sub>BH3</sub>. Thus, TCTP and Mule could possibly compete to bind the BH3 binding groove of Mcl-1, as possible basis for explaining how TCTP contributes in reducing the ubiquitinylation of the protein. This should be further tested in membrane environment with more native protein constructs since we showed that Mule<sub>BH3</sub> has significantly greater affinity for Mcl-1 than TCTP<sub>BH3</sub> using a soluble truncate of Mcl-1 protein, contradicting this hypothesis. TCTP is also likely to be present at higher concentrations in cancer cells

compared to the massive Mule E3 ubiquitin ligase (481 kDa, 4374 residues), which could still allow TCTP to protect Mcl-1 from Mule. Also, one cannot exclude that the stabilization of Mcl-1 by TCTP can be explained by Mule-dependent but BH3-independent mechanisms or by Mule-independent degradation.

### 6.3 Toward a representative definition for all natural BH3 motifs

		h1				h2				h3				h4				
Canonical BH3 motif	Antiapoptotic	Bcl-2	P	V	V	H	L	T	L	R	Q	A	G	D	D	F	S	R
		Bcl-xL	A	A	V	K	Q	A	L	R	E	A	G	D	E	F	E	L
		Bcl-w	D	P	L	H	Q	A	M	R	A	A	G	D	E	F	E	T
		Mcl-1	R	K	A	L	E	T	L	R	R	V	G	D	G	V	Q	R
	Proapoptotic	Bax	K	K	L	S	E	C	L	K	R	I	G	D	E	L	D	S
		Bak	G	Q	V	G	R	Q	L	A	I	I	G	D	D	I	N	R
		Bok	A	E	V	C	A	V	L	L	R	L	G	D	E	L	E	M
		Bid	R	N	I	A	R	H	L	A	Q	V	G	D	S	M	D	R
		Bim	I	W	I	A	Q	E	L	R	R	I	G	D	E	F	N	A
		Bik	D	A	L	A	L	R	L	A	C	I	G	D	E	M	D	V
		Hrk	Q	L	T	A	A	R	L	K	A	L	G	D	E	L	H	Q
		Noxa	V	E	C	A	T	Q	L	R	R	F	G	D	K	L	N	F
		Puma	R	E	I	G	A	Q	L	R	R	M	A	D	D	L	N	A
		Bmf	V	Q	I	A	R	K	L	Q	C	I	A	D	Q	F	H	R
Bad	Q	R	Y	G	R	E	L	R	R	M	S	D	E	F	V	D		

Fig. 6.3 Primary sequence alignment of BH3 motifs from BH3-only proteins. All sequences were retrieved from the uniprot ID present in BCL2DB [66] for the corresponding proteins. Low (blue) to high (red) sequence entropy for similar residues are shown.

BH3 and BH3-like sequences are predominantly proapoptotic, as reported for 92 % (3/37) of the human proteins containing the sequences that we compiled from BCL2DB [66]. Canonical BH3 sequences were first identified in BH3-only proteins [294]. Over a 12 residues stretch, the consensus sequence was established as the h1-X<sub>2-4</sub>-h2-X<sub>6-7</sub>-h3-X<sub>9-11</sub>-h4

		L                    GD																
BH3-like motif	Proapoptotic	MULE	Q	E	V	G	Q	L	L	Q	D	M	G	D	D	V	Y	Q
		RAD9A	G	K	A	V	H	S	L	S	R	I	G	D	E	L	Y	L
		CHMP5	D	D	L	E	A	E	L	D	A	L	G	D	E	L	L	A
		BOP	W	L	L	D	R	F	L	A	Q	L	G	D	Y	M	S	F
		ATG12	K	K	I	D	I	L	L	K	A	V	G	D	T	P	I	M
		SEC20	N	L	E	K	A	E	L	L	Q	G	G	D	L	L	R	K
		ERBB4	R	D	P	Q	R	Y	L	V	I	Q	G	D	D	R	M	K
		APOL6	G	N	I	D	K	K	L	R	A	L	A	D	D	I	D	K
		BNIP3	K	E	V	E	S	I	L	K	K	N	S	D	W	I	W	D
		APOL1	E	D	N	I	R	R	L	R	A	L	A	D	G	V	Q	K
		BNI3L	E	K	E	V	E	A	L	K	K	S	A	D	W	V	S	D
		ERBB2	E	D	P	T	V	P	L	P	S	E	T	D	G	Y	V	A
		CLUS	N	P	S	Q	A	K	L	R	R	E	L	D	E	S	L	Q
		SPHK2	H	E	V	L	N	G	L	L	D	R	P	D	W	E	E	A
		APOL2	E	D	H	I	R	K	L	R	A	L	A	E	E	V	E	Q
HEBP2	L	T	L	A	S	I	L	R	E	D	G	K	V	F	D	E		
TGM2	D	V	N	P	K	F	L	K	N	A	G	R	D	C	S	R		
AMRA	S	T	S	R	G	L	L	P	E	A	G	Q	L	A	E	R		
BH3-like motif	Antiapoptotic	AVEN	T	D	F	S	V	L	L	S	S	A	G	D	S	F	S	Q
		TCTP	F	S	D	I	Y	K	I	R	E	I	A	D	G	L	C	L
		ATR	S	I	L	W	S	A	L	K	Q	K	A	E	S	L	Q	I
		*BECN1	E	N	L	S	R	R	L	K	V	T	G	D	L	F	D	I

Fig. 6.4 Primary sequence alignment of BH3 motifs in BH3-like proteins. All sequences were retrieved from the uniprot ID present in BCL2DB [66] for the corresponding proteins. Low (blue) to high (red) sequence entropy for similar residues are shown.

with h hydrophobic residue in the canonical BH3 sequence. Notably, less identity variation is observed at h2 position, with a leucine residue for 95 % of the canonical BH3 motifs in BH3-only proteins. By comparison, no amino-acid identity above 50 % can be found at any of h1, h3 or h4 positions. However, BH3-like proteins were reported to have BH3-like

sequences that could not be described reliably using this description but are still active at Bcl-2 family proteins. This is not surprising considering that the definition of a canonical BH3 motif was first established regarding the pool of BH3-only proteins and evolutionary unrelated Bcl-2 family proteins known at this time, which represents less than a third of known BH3-containing proteins (Bcl-2 family, BH3-only and BH3-like proteins). Most importantly, the problem in giving a consensus sequence that only corresponds to a limited ensemble of BH3 motifs is that we can not properly apply algorithms to search and detected new BH3-containing proteins in databases. In consequence, it is of interest to unify all natural canonical and BH3-like motifs under the same description to permit the identification of more regulators of Bcl-2 family proteins and beyond.

Thus, the BH3 motif consensus was re-established to include only 3 more conserved residues embedded in a 6-residues stretch L-X<sub>2-4</sub>-G-D, with X any amino-acid between position 2-4 [93]. In the set of sequences we report, strict residue conservation is above 50 % at all three L (95 %), G (65 %) and D (87 %) positions whereas residues G/D were not included in the before-mentioned h1-h4 consensus, even though they are largely more conserved than any residue in h1, h3 or h4 positions. The BH3-like sequence in TCTP protein is unique in that it has not leucine residue (5 % of sequences) and no conservation of glycine (35 % of sequences) compared to L-X<sub>2-4</sub>-G-D consensus sequence. D16 residue is found in position h1 where we normally expect a hydrophobic residue considering the former h1-h4 consensus sequence. Strengthening TCTP sequence-function relationship, the BH3-like sequence of TCTP inhibits apoptosis (8 % of sequences/proteins) rather than promoting it for the vast majority of other BH3-only and BH3-like proteins.

Whereas Apolipoprotein L2 (ApoL2) has a BH3-like motif with unclear function in cells regarding apoptosis regulation [295], only two BH3-containing proteins were found to be antiapoptotic along with TCTP, namely the BH3-like proteins Cell death regulator Aven (AVEN) and Ataxia Telangiectasia and Rad3 related (ATR). The sequence of the BH3 motif in AVEN is canonical and includes all four hydrophobic residues h1-h4. It also respects the extended L-X<sub>2-4</sub>-G-D consensus and the protein stabilizes Bcl-xL upon interaction [296]. As for TCTP protein, AVEN also exhibits cell cycle regulatory function and is involved in DNA repair. Despite being evolutionary and structurally unrelated to Bcl-2 family proteins, the ATR protein contains a BH3-like sequence that enables association with Bid protein following DNA damage, preventing from Bid-mediated activation of Bax and thus pore formation and cytochrome c release [297]. So far it was not reported that TCTP either interacts or not with Bid proteins, but the implication of TCTP in DNA repair was described in several studies. Among the three TCTP, AVEN and ATR primary sequences in the BH3 segment, we observe

variability at a degree not allowing to propose consensus for antiapoptotic BH3 sequences. Comparing the BH3-like sequence from TCTP to all other reported from BH3-containing protein did also fail to identify unambiguous discriminant apart from those already discussed.

As a supplementary difficulty to predict the BH3 motifs and their function at regulating Bcl-2 family proteins, the L-X<sub>2-4</sub>-G-D consensus sequence still degenerates for a significant part of the BH3 sequences, yielding the L-X<sub>2-4</sub>-[G/A]-D which finally suggest no significant primary sequence conservation within the BH3 motifs and makes difficult to reliably detect the motif in databases of genes of proteins since it is too permissive and promotes false positive at great extent [93]. It can also promote false negative, since TCTP is the only BH3-containing protein with Bcl-w that has no leucine in first position of L-X<sub>2-4</sub>-[G/A]-D with an isoleucine and methionine, respectively. Consequently, the current nomenclature seems to be meaningless regarding the shortness of the consensus and the high divergence between experimentally established BH3-containing proteins.

Interestingly, it was proposed that the BH3 motif could be a Short Linear Motif (SLIM) [298]. They are generally stretches of 10-12 residues with three to five hot-spots that have a critical role to bind their target. Other SLIM include the ER-retention sequence K-D-E-L, the L-X<sub>2-3</sub>-L-L motifs that binds to transcription regulators, and others having similar sequence degeneration and organization compared to BH3 motifs. Moreover, same SLIM sequences can be found in very heterogeneous proteins in terms of size, cellular localization and main documented function. The BH3 motifs also correspond to these features since they can be found at the mitochondrial membrane and cytosol (Bcl-2 family proteins, BH3-only proteins) but also in the cell membrane as for the BH3-like ERBB2 protein. BH3-containing proteins can be as little as Noxa (54 amino-acids) and as big as Mule (4374 amino-acids). To add diversity in the topology of BH3-containing proteins, some were ported to have more than one BH3 motif in their primary sequence (Noxa/Bid). However, despite this very high variability in all features that could define a protein in the context of the cell, all these BH3-containing proteins bind to the same targets family, namely the Bcl-2 family proteins. Which is also a characteristic of SLIM which have in general common targets despite displaying strong variations in sequences that compose a given SLIM [93]. However the BH3 motif would still be an unusual SLIM since it is found in both unstructured and structured proteins whereas SLIM are generally included in loops and exposed to solvent to readily interact with partners.

The trick in redefining the BH3 motif [93] as a SLIM is that we do not need primary sequence elements to define it. The definition lies on functional and thermodynamic definition elements such as structure, binding affinity, activity at the Bcl-2 family proteins etc. Having a set of rules that represents well the diversity of BH3 motifs can still be used to screen and

to filter candidate sequences for new BH3-containing protein. The TCTP protein and its BH3-like motif is very well described using this definition, as well as the vast majority of other documented BH3-containing sequences and corresponding proteins. This without the need of any specific sequence description. Since this semantic chaos originating from a non-reasonable classification 30 years ago is still running up to day, with evident consequences at slowing down BH3-related research, we can wonder why sticking to this "classical" definition that should definitely be overridden to accept the evidence: functional motifs in proteins do not need a consensus sequence to be described and the BH3 SLIM motif is a good example.

# References

- [1] W. R. Hanahan D, “The hallmarks of cancer,” *Cell*, vol. 100, no. 1, pp. 57–70, 2000.
- [2] P. Collas, “Dedifferentiation : A new approach in stem cell research,” *Cytotherapy*, vol. 9, no. 3, pp. 236–244, 2007.
- [3] K. A. Schafer, “The cell cycle: A review,” *Veterinary Pathology*, vol. 35, no. 6, pp. 471–478, 1998.
- [4] T. Hunt, K. Nasmyth, and B. Novàk, “The cell cycle,” *Philosophical Transactions of the Royal Society B*, vol. 366, no. 1584, pp. 3494–3497, 2011.
- [5] B. Alberts, A. Johnson, L. Julian, M. Raff, K. Roberts, and P. Walter, “An overview of the cell cycle, overview of the cell cycle and its control,” *Molecular Biology of the Cell. 4th edition*, 1999.
- [6] K. Vermeulen, D. R. V. Bockstaele, and Z. N. Berneman, “The cell cycle : a review of regulation , deregulation and therapeutic targets in cancer,” *Cell Proliferation*, vol. 36, no. 3, pp. 131–149, 2003.
- [7] K. J. Barnum and M. J. O’Connell, “Cell cycle regulation by checkpoints,” *Methods in Molecular Biology*, vol. 1170, pp. 29–40, 2014.
- [8] J. Chen, “The cell-cycle arrest and apoptotic functions of p53 in tumor initiation and progression,” *Cold Spring Harbor Perspectives in Medicine*, vol. 6, no. 3, pp. 1–15, 2016.
- [9] C. L. C. Kastan, MB Canman, “P53, cell cycle control and apoptosis: implications for cancer,” *Cancer and Metastasis Reviews*, vol. 14, no. 1, pp. 3–15, 1995.
- [10] J. A. Choi, J. Y. Kim, J. Y. Lee, C. M. Kang, H. J. Kwon, Y. D. Yoo, T. W. Kim, Y. S. Lee, and S. J. Lee, “Induction of cell cycle arrest and apoptosis in human breast cancer cells by quercetin.” *International Journal of Oncology*, vol. 19, no. 4, pp. 837–44, 2001.
- [11] T. Ozaki and A. Nakagawara, “Role of p53 in cell death and human cancers.” *Cancers*, vol. 3, no. 1, pp. 994–1013, 2011.
- [12] G. Evan, L. Brown, M. Whyte, and E. Harrington, “Apoptosis and the cell cycle,” *Progress in Cell Cycle Research*, vol. 7, no. 6, pp. 825–834, 1995.
- [13] W. Meikrantz and R. Schlegel, “Apoptosis and the cell cycle,” *Journal of Cellular Biochemistry*, vol. 58, no. 2, pp. 160–174, 1995.

- [14] K. L. King, J. A. Cidlowski, and N. Carolina, "Cell cycle and apoptosis : Common pathways to life and death," *Journal of Cellular Biochemistry*, vol. 58, no. 2, pp. 175–180, 1995.
- [15] F. Alenzi, "Links between apoptosis, proliferation and the cell cycle.," *British Journal of Biomedical Science*, vol. 61, no. 2, pp. 99–102, 2004.
- [16] R. Fotedar, L. Diederich, and A. Fotedar, "Apoptosis and the cell cycle," *Progress in Cell Cycle Research*, vol. 2, pp. 147–163, 1996.
- [17] J. King, KL Cidlowski, "Cell cycle regulation and apoptosis," *Annual Review of Physiology*, vol. 60, pp. 601–617, 1998.
- [18] B. Pucci, M. Kasten, and A. Giordano, "Cell cycle and apoptosis 1," *Neoplasia*, vol. 2, no. 4, pp. 291–299, 2000.
- [19] G. I. Evan and K. H. Vousden, "Proliferation, cell cycle and apoptosis in cancer," *Nature*, vol. 411, no. 6835, pp. 342–8, 2001.
- [20] K. Vermeulen, Z. N. Berneman, and D. R. V. Bockstaele, "Cell cycle and apoptosis," *Cell Proliferation*, vol. 36, no. 3, pp. 165–175, 2003.
- [21] A. M. Senderowicz, "Targeting cell cycle and apoptosis for the treatment of human malignancies," *Current Opinion in Cell Biology*, vol. 16, no. 6, pp. 670–678, 2004.
- [22] F. Alenzi, "Links between apoptosis, proliferation and the cell cycle.," *British Journal of Biomedical Science*, vol. 61, no. 2, pp. 99–102, 2004.
- [23] J. R. Mcintosh, "Mitosis," *Cold Spring Harbor Perspectives in Biology*, vol. 8, no. 9, pp. 1–16, 2016.
- [24] H. Ohkura, "Meiosis : An overview of key differences from mitosis," *Cold Spring Harbor Perspectives in Biology*, vol. 7, no. 5, pp. 1–14, 2015.
- [25] R. Bravo, "Genes induced during the g0/g1 transition in mouse fibroblasts.," *Seminars in cancer biology*, vol. 1, no. 1, pp. 37–46, 1990.
- [26] G. Cooper, "The eukaryotic cell cycle.," *The Cell: A Molecular Approach. 2nd edition.*, 2000.
- [27] P. Ghule, D. Seward, A. Fritz, J. Boyd, A. van, Wijnen, J. Lian, J. Stein, and G. Stein, "Higher order genomic organization and regulatory compartmentalization for cell cycle control at the g1/s-phase transition.," *Journal of cellular physiology*, vol. 233, no. 10, pp. 6406–6413, 2018.
- [28] T. Kapoor, "Metaphase spindle assembly.," *Biology*, vol. 6, no. 1, 2017.
- [29] S. Reber and A. Hyman, "Emergent properties of the metaphase spindle.," *Cold Spring Harbor perspectives in biology*, vol. 7, no. 7, p. a015784, 2015.
- [30] D. Oriola, D. Needleman, and J. Brugués, "The physics of the metaphase spindle.," *Annual review of biophysics*, vol. 47, pp. 655–673, 2018.

- [31] M. Koziol and J. Gurdon, "Tctp in development and cancer," *Biochemistry Research International*, 2012.
- [32] H. Jeon, S. Yeop, Y. Seok, J. Wook, J. Kim, and J. Su, "Tctp regulates spindle microtubule dynamics by stabilizing polar microtubules during mouse oocyte meiosis," *BBA - Molecular Cell Research*, vol. 1863, no. 4, pp. 630–637, 2016.
- [33] F. R. Yarm, "Plk phosphorylation regulates the microtubule-stabilizing protein tctp," vol. 22, no. 17, pp. 6209–6221, 2002.
- [34] D. Guertin, S. Trautmann, and D. McCollum, "Cytokinesis in eukaryotes.," *Microbiology and molecular biology reviews : MMBR*, vol. 66, no. 2, pp. 155–78, 2002.
- [35] W. Wide and I. N. T. Kinetics, "Apoptosis : A basic biological phenomenon with wide-," *British Journal of Cancer*, vol. 26, no. 4, pp. 239–57, 1972.
- [36] P. Syntichaki and N. Tavernarakis, "Death by necrosis. uncontrollable catastrophe, or is there order behind the chaos?," *EMBO reports*, vol. 3, no. 7, pp. 604–9, 2002.
- [37] D. Glick, S. Barth, and K. Macleod, "Autophagy: cellular and molecular mechanisms.," *The Journal of pathology*, vol. 221, no. 1, pp. 3–12, 2010.
- [38] S. Elmore, "Apoptosis: A review of programmed cell death," *Toxicologic Pathology*, vol. 35, no. 4, pp. 495–516, 2007.
- [39] S. Kannan, K Jain, "Apoptosis : A basic biological phenomenon with wide-," *Pathophysiology*, vol. 7, no. 3, pp. 253–63, 2000.
- [40] D. R. Schultz and W. J. Harrington, "Apoptosis : Programmed cell death at a molecular level," *Seminars in Arthritis and Rheumatism*, vol. 32, no. 6, pp. 345–369, 2003.
- [41] R. Medh and E. Thompson, "Hormonal regulation of physiological cell turnover and apoptosis," *Cell and Tissue Research*, vol. 301, no. 1, pp. 101–124, 2000.
- [42] P. Meier, A. Finch, and G. Evan, "Apoptosis in development," *Nature*, vol. 407, pp. 796–801, 2000.
- [43] C. Feig and M. Peter, "How apoptosis got the immune system in shape," *European Journal of Immunology*, vol. 37, pp. 61–70, 2007.
- [44] J. Yuan and B. Yankner, "Apoptosis in the nervous system," *Nature*, vol. 407, no. 6805, 2000.
- [45] S. Lowe and A. W. Lin, "Apoptosis in cancer.," *Carcinogenesis*, vol. 21, no. 3, pp. 485–495, 2000.
- [46] M. Sciences, "Apoptosis: A target for anticancer therapy," *International Journal of Molecular Sciences*, vol. 19, no. 2, p. 448, 2018.
- [47] D. Green and G. Evan, "A matter of life and death," *Cancer Cell*, vol. 8, no. 4, pp. 30–36, 2002.

- [48] V. Jendrossek, "The intrinsic apoptosis pathways as a target in anticancer therapy.," *Current Pharmaceutical Biotechnology*, vol. 13, no. 8, pp. 1426–38, 2012.
- [49] P. Nair, M. Lu, S. Petersen, and A. Ashkenazi, *Apoptosis Initiation Through the Cell-Extrinsic Pathway*, vol. 544. 1 ed., 2014.
- [50] R. M. Locksley, N. Killeen, M. J. Lenardo, S. Francisco, and S. Francisco, "The tnfr and tnfr receptor superfamilies : Integrating mammalian biology," *Cell*, vol. 104, pp. 487–501, 2001.
- [51] H. Hsu, J. Xiong, and D. Goeddel, "The tnfr receptor i-associated protein tradd signals cell death and nf-kb activation," *Cell*, vol. 81, no. 4, pp. 495–504, 1995.
- [52] S. Grimm, B. Z. Stanger, and P. Leder, "Rip and fadd: Two "death domain"-containing proteins can induce apoptosis by convergent, but dissociable, pathways," *Proceedings of the National Academy of Sciences*, vol. 93, no. 20, pp. 10923–10927, 1996.
- [53] H. Wajant, "The fas signaling pathway: more than a paradigm," *Science*, vol. 296, no. 5573, pp. 1635–6, 2002.
- [54] F. Kischkel, S. Hellbardt, I. Behrmann, M. Germer, M. Pawlita, P. Krammer, and M. Peter, "Cytotoxicity-dependent apo-1 ( fas/cd95 ) - associated proteins form a death-inducing signaling complex (disc) with the receptor," *The EMBO Journal*, vol. 14, no. 22, pp. 5579–5588, 1995.
- [55] J. Corys, S Adams, "The bcl2 family: regulators of the cellular life-or-death switch," *Nature Reviews Cancer*, vol. 9, no. 2, pp. 647–656, 2002.
- [56] X. Saelens, N. Festjens, L. Vande Walle, M. van Gurp, G. van Loo, and P. Vandennebeele, "Toxic proteins released from mitochondria in cell death," *Oncogene*, vol. 23, no. 16, pp. 2861–2874, 2004.
- [57] M. Morales-cruz, C. M. Figueroa, T. González-robles, Y. Delgado, A. Molina, J. Mèndez, M. Morales, and K. Griebenow, "Activation of caspase-dependent apoptosis by intracellular delivery of cytochrome c-based nanoparticles," *Journal of Nanobiotechnology*, vol. 12, no. 33, pp. 1–11, 2014.
- [58] A. Chinnaiyan, "The apoptosome : Heart and soul of the cell death machine," *Neoplasia*, vol. 1, no. 1, pp. 5–15, 1999.
- [59] M. Hill, C. Adrain, P. Duriez, E. Creagh, and S. Martin, "Analysis of the composition , assembly kinetics and activity of native apaf-1 apoptosomes," *The EMBO Journal*, vol. 23, no. 10, pp. 2134–2145, 2004.
- [60] J. Garland and C. Rudin, "Cytochrome c induces caspase-dependent apoptosis in intact hematopoietic cells and overrides apoptosis suppression mediated by bcl-2, growth factor signaling, map-kinase-kinase, and malignant change," *Blood*, vol. 92, no. 4, pp. 1235–1247, 1998.
- [61] E. Slee, C. Adrain, and S. Martin, "Executioner caspase-3, -6, and -7 perform distinct, non-redundant roles during the demolition phase of apoptosis," *The Journal of Biological Chemistry*, vol. 276, no. 10, pp. 7320–7326, 2001.

- [62] H. Sakahira and M. Enari, "Cleavage of cad inhibitor in cad activation and dna degradation during apoptosis," *Nature*, vol. 391, pp. 1–4, 1998.
- [63] A. Aouacheria, F. Brunet, and M. Gouy, "Phylogenomics of life-or-death switches in multicellular animals: Bcl-2 , bh3-only , and bnip families of apoptotic regulators," *Molecular Biology and Evolution*, vol. 22, no. 12, pp. 2395–516, 2005.
- [64] R. Singh, A. Letai, and K. Sarosiek, "Regulation of apoptosis in health and disease: the balancing act of bcl-2 family proteins," *Nature Reviews Molecular Cell Biology*, vol. 20, no. 3, pp. 175–193, 2019.
- [65] T. Knight, D. Luedtke, H. Edwards, J. W. Taub, and Y. Ge, "A delicate balance - the bcl-2 family and its role in apoptosis, oncogenesis, and cancer therapeutics," *Biochemical Pharmacology*, vol. 162, pp. 250–261, 2019.
- [66] V. Rech de Laval, G. Deléage, A. Aouacheria, and C. Combet, "Bcl2db: database of bcl-2 family members and bh3-only proteins.," *Database : the journal of biological databases and curation*, 2014.
- [67] J. Kale, E. J. Osterlund, and D. W. Andrews, "Bcl-2 family proteins : changing partners in the dance towards death," *Cell Death Differentiation*, vol. 25, no. 1, pp. 65–80, 2017.
- [68] L. Mah and K. Ryan, "Autophagy and cancer," *Cold Spring Harbor Perspectives in Biology*, vol. 4, no. 1, pp. 1–14, 2012.
- [69] Y. Rong, G. Bultynck, A. Aromolaran, F. Zhong, J. Parys, H. Smedt, G. Mignery, H. Roderick, M. Bootman, and C. Distelhorst, "The bh4 domain of bcl-2 inhibits er calcium release and apoptosis by binding the regulatory and coupling domain of the ip3 receptor," *Proceedings of the National Academy of Sciences*, vol. 106, no. 34, pp. 14397–14402, 2009.
- [70] J. Hardwick and L. Soane, "Multiple functions of bcl-2 family proteins," *Cold Spring Harbor Perspectives in Biology*, vol. 5, no. 2, pp. 1–22, 2013.
- [71] J. M. Adams and S. Cory, "The bcl-2 arbiters of apoptosis and their growing role as cancer targets," *Cell Death and Differentiation*, vol. 25, no. 1, pp. 27–36, 2017.
- [72] C. Yang, "Mcl-1 inhibition in cancer treatment," *OncoTargets and Therapy*, vol. 11, pp. 7301–7314, 2018.
- [73] A. Bakhshi, J. R. Jensen, P. Goldman, J. J. Wright, O. W. McBride, A. L. Epstein, and S. J. Korsmeyer, "Cloning the chromosomal breakpoint of t ( 14 ; 18 ) human lymphomas : Clustering around jr on chromosome 14 and near a transcriptional unit on 18," *Cell*, vol. 41, no. 3, pp. 899–906, 1985.
- [74] T. McDonnell, N. Deane, F. Platt, N. Ulrich, J. Mckearn, and S. Korsmeyer, "Transgenic mice demonstrate extended b cell survival and follicular lymphoproliferation," *Cell*, vol. 57, no. 1, pp. 79–88, 1989.

- [75] L. H. Boise, M. Gonzalez-garcia, C. E. Postema, L. Ding, T. Lindsten, L. A. Turka, X. Mao, G. Nunez, and C. Thompson, "Bcl-x, a bcl-2-related gene that functions as a dominant regulator of apoptotic cell death," *Cell*, vol. 74, no. 4, pp. 597–606, 1993.
- [76] K. M. Kozopas, T. A. O. Yang, H. L. Buchan, P. Zhou, and R. W. Craig, "Mcl1, a gene expressed in programmed myeloid cell differentiation, has sequence similarity to bcl2," *Proceedings of the National Academy of Sciences*, vol. 90, no. 8, pp. 3516–3520, 1993.
- [77] Z. N. Oltvai, C. L. Milkman, and S. J. Korsmeyer, "Bcl-2 heterodimerizes in vivo with a conserved homolog, bax, that accelerates programmed cell death," *Cell*, vol. 74, no. 4, pp. 609–619, 1993.
- [78] T. Chittenden, E. Harrington, R. O'Connor, C. Flemington, R. Lutz, G. Evan, and B. Guild, "Induction of apoptosis by the bcl-2 homologue bak," *Nature*, vol. 374, no. 6524, pp. 733–6, 1995.
- [79] A. Petros, E. Olejniczak, and S. Fesik, "Structural biology of the bcl-2 family of proteins," *Biochimica et Biophysica Acta*, vol. 1644, no. 2-3, pp. 83–94, 2004.
- [80] Y. Hsu, K. Wolter, and R. Youle, "Cytosol-to-membrane redistribution of bax and bcl-x(l) during apoptosis," *Proceedings of the National Academy of Sciences of the United States of America*, vol. 94, no. 8, pp. 3668–72, 1997.
- [81] G. Hausmann, L. O'Reilly, R. van Driel, J. Beaumont, A. Strasser, J. Adams, and D. Huang, "Pro-apoptotic apoptosis protease-activating factor 1 (apaf-1) has a cytoplasmic localization distinct from bcl-2 or bcl-x(l)," *The Journal of cell biology*, vol. 149, no. 3, pp. 623–34, 2000.
- [82] S. Jeong, B. Gaume, Y. Lee, Y. Hsu, S. Ryu, S. Yoon, and R. Youle, "Bcl-xl sequesters its c-terminal membrane anchor in soluble, cytosolic homodimers," *The EMBO Journal*, vol. 23, no. 10, pp. 2146–2155, 2004.
- [83] V. Bhat, C. B. McDonald, D. C. Mikles, B. J. Deegan, K. L. Seldeen, M. L. Bates, and A. Farooq, "Ligand binding and membrane insertion compete with oligomerization of the bclxl apoptotic repressor," *Journal of Molecular Biology*, vol. 416, no. 1, pp. 57–77, 2012.
- [84] C. Chou and R. Lee, "Targeting of mcl-1 via a tom70-dependent pathway," *Molecular Biology of the Cell*, vol. 17, no. 9, pp. 3952–3963, 2006.
- [85] Q. Zhong, W. Gao, F. Du, and X. Wang, "Mule/arf-bp1, a bh3-only e3 ubiquitin ligase, catalyzes the polyubiquitination of mcl-1 and regulates apoptosis," *Cell*, vol. 121, no. 7, pp. 1085–1095, 2005.
- [86] M. Schwickart, X. Huang, J. Lill, J. Liu, R. Ferrando, D. French, H. Maecker, K. Rourke, F. Bazan, J. Eastham-anderson, P. Yue, D. Dornan, D. Huang, and V. Dixit, "Deubiquitinase usp9x stabilizes mcl1 and promotes tumour cell survival," *Nature*, vol. 463, no. 7277, pp. 103–7, 2010.

- [87] S. N. Willis, L. Chen, G. Dewson, A. Wei, E. Naik, J. I. Fletcher, J. M. Adams, and D. C. Huang, "Proapoptotic bak is sequestered by mcl-1 and bcl-xl, but not bcl-2, until displaced by bh3-only proteins.," *Genes & development*, vol. 19, no. 11, pp. 1294–305, 2005.
- [88] F. Llambi, T. Moldoveanu, S. W. Tait, L. Bouchier-Hayes, J. Temirov, L. L. McCormick, C. P. Dillon, and D. R. Green, "A unified model of mammalian bcl-2 protein family interactions at the mitochondria," *Molecular Cell*, vol. 44, no. 4, pp. 517–531, 2011.
- [89] Q. Liu, T. Moldoveanu, T. Sprules, E. Matta-Camacho, N. Mansur-Azzam, and K. Gehring, "Apoptotic regulation by mcl-1 through heterodimerization," *Journal of Biological Chemistry*, vol. 285, no. 25, pp. 19615–19624, 2010.
- [90] A. Tron, M. Belmonte, A. Adam, B. Aquila, L. Boise, E. Chiarparin, J. Cidado, K. Embrey, E. Gangl, F. Gibbons, G. Gregory, D. Hargreaves, J. Hendricks, J. Johannes, R. Johnstone, S. Kazmirski, J. Kettle, M. Lamb, S. Matulis, A. Nooka, M. Packer, B. Peng, P. Rawlins, D. Robbins, A. Schuller, N. Su, W. Yang, Q. Ye, X. Zheng, J. Secrist, E. Clark, D. Wilson, S. Fawell, and A. Hird, "Discovery of mcl-1-specific inhibitor azd5991 and preclinical activity in multiple myeloma and acute myeloid leukemia," *Nature Communications*, vol. 9, no. 1, p. 5341, 2018.
- [91] A. Shamas-din, H. Brahmabhatt, B. Leber, and D. Andrews, "Bh3-only proteins : Orchestrators of apoptosis," *BBA - Molecular Cell Research*, vol. 1813, no. 4, pp. 508–520, 2011.
- [92] L. Happo, A. Strasser, and S. Cory, "Bh3-only proteins in apoptosis at a glance," *Journal of Cell Science*, vol. 125, no. 5, pp. 1081–1087, 2012.
- [93] A. Aouacheria, C. Combet, P. Tompa, and J. Hardwick, "Redefining the bh3 death domain as a 'short linear motif'," *Trends in Biochemical Sciences*, vol. 40, no. 12, pp. 736–748, 2015.
- [94] M. Gouw, S. Michael, H. Sámano-Sánchez, M. Kumar, A. Zeke, B. Lang, B. Bely, L. Chemes, N. Davey, Z. Deng, F. Diella, C. Gürth, A. Huber, S. Kleinsorg, L. Schlegel, N. Palopoli, K. Roey, B. Altenberg, A. Reményi, H. Dinkel, and T. Gibson, "The eukaryotic linear motif resource - 2018 update.," *Nucleic acids research*, vol. 46, no. D1, pp. D428–D434, 2018.
- [95] E. Lee, G. Dewson, M. Evangelista, A. Pettikiriachchi, G. Gold, H. Zhu, P. Colman, and W. Fairlie, "The functional differences between pro-survival and pro-apoptotic b cell lymphoma 2 (bcl-2) proteins depend on structural differences in their bcl-2 homology 3 (bh3)," *The Journal of Biological Chemistry*, vol. 289, no. 52, pp. 36001–36017, 2014.
- [96] E. Lee, "The structural biology of bcl-xl," *International Journal of Molecular Sciences*, vol. 20, no. 9, pp. 1–18, 2019.
- [97] M. Hinds, C. Smits, J. Risk, M. Bailey, D. Huang, and C. Day, "Bim , bad and bmf : intrinsically unstructured bh3-only proteins that undergo a localized conformational change upon binding to prosurvival bcl-2 targets," *Cell Death Differentiation*, vol. 14, no. 1, pp. 128–136, 2007.

- [98] M. Kvaisakul and M. Hinds†, *The Structural Biology of BH3-Only Proteins*, vol. 544. 1 ed., 2014.
- [99] J. Lovell, L. Billen, S. Bindner, A. Shamas-din, C. Fradin, B. Leber, and D. Andrews, “Membrane binding by bid initiates an ordered series of events culminating in membrane permeabilization by bax,” *Cell*, vol. 135, no. 6, pp. 1074–1084, 2008.
- [100] T. Kuwana, M. Mackey, G. Perkins, M. Ellisman, M. Latterich, R. Schneider, D. Green, and D. Newmeyer, “Bid, bax, and lipids cooperate to form supramolecular openings in the outer mitochondrial membrane,” *Cell*, vol. 111, no. 3, pp. 331–342, 2002.
- [101] Y. Seo, J. Shin, K. Ko, J. Cha, J. Park, B. Lee, C. Yun, Y. Kim, D. Seol, D. Kim, X. Yin, and T. Kim, “The molecular mechanism of noxa-induced mitochondrial dysfunction in p53-mediated cell death,” *The Journal of Biological Chemistry*, vol. 278, no. 48, pp. 48292–48299, 2003.
- [102] M. Hekman, S. Albert, A. Galmiche, U. Rennefahrt, J. Fueller, A. Fischer, D. Puehringer, S. Wiese, and U. Rapp, “Reversible membrane interaction of bad requires two c-terminal lipid binding domains in conjunction with 14-3-3 protein binding,” *The Journal of Biological Chemistry*, vol. 281, no. 25, pp. 17321–17336, 2006.
- [103] M. Lutter, M. Fang, Luo, M. XNishijima, Xie, and X. XWang, “Cardiolipin provides specificity for targeting of bid to mitochondria,” *Nature Cell Biology*, vol. 2, no. 10, pp. 754–761, 2000.
- [104] Y. Zaltsman, L. Shachnai, N. Yivgi-Ohana, M. Schwarz, M. Maryanovich, R. Houtkooper, F. Vaz, F. De, Leonardis, G. Fiermonte, F. Palmieri, B. Gillissen, P. Daniel, E. Jimenez, S. Walsh, C. Koehler, S. Roy, L. Walter, G. Hajnóczky, and A. Gross, “Mtm2/mimp is a major facilitator of bid recruitment to mitochondria,” *Nature Cell Biology*, vol. 12, no. 6, pp. 553–562, 2010.
- [105] O. Kutuk and A. Letai, “Regulation of bcl-2 family proteins by posttranslational modifications,” *Current Molecular Medicine*, vol. 8, no. 2, pp. 102–118, 2008.
- [106] J. Chou, H. Li, G. Salvesen, J. Yuan, and G. Wagner, “Solution structure of bid, an intracellular amplifier of apoptotic signaling,” *Cell*, vol. 96, no. 5, pp. 615–624, 1999.
- [107] J. McDonnell, D. Fushman, C. Milliman, S. Korsmeyer, and D. Cowburn, “Solution structure of the proapoptotic molecule bid: A structural basis for apoptotic agonists and antagonists,” *Cell*, vol. 96, no. 5, pp. 625–634, 1999.
- [108] M. Kvaisakul, H. Yang, W. Fairlie, P. Czabotar, S. Fischer, M. Perugini, D. Huang, and P. Colman, “Vaccinia virus anti-apoptotic f1l is a novel bcl-2-like domain-swapped dimer that binds a highly selective subset of bh3-containing death ligands,” *Cell Death Differentiation*, vol. 15, no. 10, pp. 1564–1571, 2008.
- [109] L. Billen and D. Andrews, “Bid: a bax-like bh3 protein,” *Oncogene*, vol. 27, no. S1, pp. 93–104, 2009.

- [110] Y. Jin, L. You, H. Kim, and H. Lee, "Telomerase reverse transcriptase contains a bh3-like motif and interacts with bcl-2 family members.," *Molecules and cells*, vol. 41, no. 7, pp. 684–694, 2018.
- [111] S. Thebault, M. Agez, X. Chi, J. Stojko, V. Cura, S. B. Telerman, L. Maillet, F. Gautier, I. Billas-Massobrio, C. Birck, N. Troffer-Charlier, T. Karafin, J. Honore, A. Senff-Ribeiro, S. Montessuit, C. M. Johnson, P. Juin, S. Cianferani, J. C. Martinou, D. W. Andrews, R. Amson, A. Telerman, and J. Cavarelli, "Tctp contains a bh3-like domain, which instead of inhibiting, activates bcl-xl," *Scientific Reports*, vol. 6, p. 19725, 2016.
- [112] W. R. Hanahan D, "The hallmarks of cancer: the next generation," *Cell*, vol. 144, no. 5, pp. 646–74, 2011.
- [113] J. M. Bishop and R. A. Weinberg, "Molecular oncology," *Scientific American, Inc, New York*, 1996.
- [114] M. A. Lemmon and J. Schlessinger, "Cell signaling by receptor tyrosine kinases," *Cell*, vol. 141, no. 7, pp. 1117–1134, 2010.
- [115] E. Witsch, M. Sela, and Y. Yarden, "Roles for growth factors in cancer progression," *Physiology (Bethesda)*, vol. 25, no. 2, pp. 85–101, 2010.
- [116] A. R. M. R. Amin, P. Karpowicz, T. Carey, J. Arbiser, R. Nahta, Z. Chen, J. Dong, O. Kucuk, G. Khan, G. Huang, S. Mi, H. Lee, J. Reichrath, K. Honoki, A. Georgakilas, A. Amedei, A. Amin, B. Helferich, C. Boosani, M. Ciriolo, S. Chen, S. Mohammed, A. Azmi, W. Keith, D. Bhakta, D. Halicka, E. Niccolai, H. Fujii, K. Aquilano, S. Ashraf, S. Nowsheen, Yang, A. XBilsland, and D. Shin, "Evasion of anti-growth signaling: a key step in tumorigenesis and potential target for treatment and prophylaxis by natural compounds," *Seminars in Cancer Biology*, vol. 35, pp. 55–77, 2015.
- [117] F. Kaleigh and K. Manabu, "Evading apoptosis in cancer kaleigh," *Trends in Cell Biology*, vol. 23, no. 12, pp. 620–633, 2013.
- [118] S. J. Weroha and P. Haluska, "Igf system in cancer," *Endocrinology Metabolism Clinics of North America*, vol. 41, no. 2, pp. 1–15, 2012.
- [119] S. Vyas, E. Zaganjor, and M. C. Haigis, "Review mitochondria and cancer," *Cell*, vol. 166, no. 3, pp. 555–566, 2016.
- [120] S. Hwang and K. Shroyer, "Identifying molecular culprits of cervical cancer progression," *Journal of Oncology*, 2012.
- [121] A. Sidow and N. Spies, "Concepts in solid tumor evolution," *Trends in Genetics*, vol. 31, no. 4, pp. 208–214, 2015.
- [122] M. A. Jafri, S. A. Ansari, M. H. Alqahtani, and J. W. Shay, "Roles of telomeres and telomerase in cancer , and advances in telomerase- targeted therapies," *Genome Medicine*, vol. 8, p. 69, 2016.
- [123] G. Bergers, K. Javaherian, K. M. Lo, J. Folkman, and D. Hanahan, "Effects of angiogenesis inhibitors on multistage carcinogenesis in mice," *Science*, vol. 284, no. 5415, pp. 808–12, 1999.

- [124] S. Y. Kim, "Cancer energy metabolism : Shutting power off cancer factory," *Biomolecules Therapeutics*, vol. 26, no. 1, pp. 39–44, 2018.
- [125] S. M. Candèias and U. S. Gaipf, "The immune system in cancer prevention , development and therapy," *Anti-Cancer Agents in Medicinal Chemistry*, vol. 16, no. 1, pp. 101–107, 2016.
- [126] R. Amson, J. E. Karp, and A. Telerman, "Lessons from tumor reversion for cancer treatment," *Current Opinion in Oncology*, vol. 25, no. 1, pp. 59–65, 2013.
- [127] A. Telerman and R. Amson, "The molecular programme of tumour reversion: The steps beyond malignant transformation," *Nature Reviews Cancer*, vol. 9, no. 3, pp. 206–216, 2009.
- [128] M. Askanazy, "Die teratome nach ihrem bau, ihrem verlauf, ihrer genese und im vergleich zum experimentellen teratoid.," *Verhandlungen der Deutschen Gesellschaft für Pathologie*, vol. 11, pp. 39–82, 1907.
- [129] A. C. Braun, "Recovery of tumor cells from effects of the tumor-inducing principle in crown gall.," *Science*, vol. 113, pp. 651–653, 1951.
- [130] I. Macpherson, "Reversion in hamster cells transformed by rous sarcoma virus," *Science*, vol. 148, pp. 1731–3, 1965.
- [131] C. Shu-rong, L. Jia-xiang, and G. Long-jun, "Use of all-trans retinoic acid in the treatment of acute promyelocytic leukemia.," *Blood*, vol. 72, no. 2, pp. 567–572, 1988.
- [132] V. M. Weaver, O. W. Petersen, F. Wang, C. A. Larabell, P. Briand, C. Damsky, and M. J. Bissell, "Reversion of the malignant phenotype of human breast cells in three-dimensional culture and in vivo by integrin blocking antibodies," *The Journal of Cell Biology*, vol. 137, no. 1, pp. 231–245, 1997.
- [133] H. W. Toolan, "Lack of oncogenic effect of the h-viruses for hamsters.," vol. 214, no. 1036, pp. 1–12, 1967.
- [134] R. Amson, M. Nemani, J. Roperch, D. Israeli, L. Bougueleret, I. Le, Gall, M. Medhioub, G. Linares-Cruz, F. Lethrosne, P. Pasturaud, L. Piouffre, S. Prieur, L. Susini, V. Alvaro, P. Millasseau, C. Guidicelli, H. Bui, C. Massart, L. Cazes, F. Dufour, H. Bruzzoni-Giovanelli, H. Owadi, C. Hennion, G. Charpak, and A. Telerman, "Isolation of 10 differentially expressed cdnas in p53-induced apoptosis: activation of the vertebrate homologue of the drosophila seven in absentia gene.," *Proceedings of the National Academy of Sciences of the United States of America*, vol. 93, no. 9, pp. 3953–7, 1996.
- [135] D. Israeli, E. Tessler, Y. Haupt, A. Elkeles, S. Wilder, R. Amson, A. Telerman, and M. Oren, "A novel p53-inducible gene, pag608, encodes a nuclear zinc finger protein whose overexpression promotes apoptosis.," *The EMBO journal*, vol. 16, no. 14, pp. 4384–92, 1997.

- [136] J. Roperch, F. Lethrone, S. Prieur, L. Piouffre, D. Israeli, M. Tuynder, M. Nemani, P. Pasturaud, M. Gendron, J. Dausset, M. Oren, R. Amson, and A. Telerman, "Siah-1 promotes apoptosis and tumor suppression through a network involving the regulation of protein folding, unfolding, and trafficking: identification of common effectors with p53 and p21(waf1).," *Proceedings of the National Academy of Sciences of the United States of America*, vol. 96, no. 14, pp. 8070–3, 1999.
- [137] M. Tuynder, L. Susini, S. Prieur, S. Besse, G. Fiucci, R. Amson, and A. Telerman, "Biological models and genes of tumor reversion: cellular reprogramming through tpt1/tctp and siah-1.," *Proceedings of the National Academy of Sciences of the United States of America*, vol. 99, no. 23, pp. 14976–81, 2002.
- [138] R. S. Ohgami, D. R. Campagna, E. L. Greer, B. Antiochos, J. Chen, J. J. Sharp, Y. Fujiwara, J. E. Barker, and D. Mark, "Identification of a ferrireductase required for efficient transferrin- dependent iron uptake in erythroid cells," *Nature Genetics*, vol. 37, no. 11, pp. 1264–1269, 2005.
- [139] M. Tuynder, G. Fiucci, S. Prieur, A. Lespagnol, A. Gèant, S. Beaucourt, D. Duflaut, S. Besse, L. Susini, J. Cavarelli, D. Moras, R. Amson, and A. Telerman, "Translationally controlled tumor protein is a target of tumor reversion.," *Proceedings of the National Academy of Sciences of the United States of America*, vol. 101, no. 43, pp. 15364–9, 2004.
- [140] R. Amson, S. Pece, J. C. Marine, P. P. D. Fiore, and A. Telerman, "Tpt1/ tctp-regulated pathways in phenotypic reprogramming," *Trends in Cell Biology*, vol. 23, no. 1, pp. 37–46, 2013.
- [141] H. Thiele, M. Berger, C. Lenzner, H. Kühn, and B. Thiele, "Structure of the promoter and complete sequence of the gene coding for the rabbit translationally controlled tumor protein (tctp) p23," *European Journal of Biochemistry*, vol. 257, no. 1, pp. 62–8, 1998.
- [142] H. Andree, H. Thiele, M. Fähling, I. Schmidt, and B. Thiele, "Expression of the human tpt1 gene coding for translationally controlled tumor protein (tctp) is regulated by creb transcription factors," *Gene*, vol. 380, no. 2, pp. 95–103, 2006.
- [143] U. Bommer, A. Borovjagin, M. Greagg, I. Jeffrey, P. Russell, K. Laing, M. Lee, and M. Clemens, "The mrna of the translationally controlled tumor protein p23 / tctp is a highly structured rna , which activates the dsrna-dependent protein kinase pkr," *RNA*, vol. 8, no. 4, pp. 478–496, 2002.
- [144] C. A. Goodman, A. M. Coenen, J. W. Frey, J.-s. You, G. Robert, B. P. Frankish, R. M. Murphy, and T. A. Hornberger, "Insights into the role and regulation of tctp in skeletal muscle," *Oncotarget*, vol. 8, no. 12, pp. 18754–18772, 2017.
- [145] N. Assrir, F. Malard, and E. Lescop, *Structural Insights into TCTP and Its Interactions with Ligands and Proteins*, vol. 64. 2017.
- [146] P. Thaw, N. J. Baxter, a. M. Hounslow, C. Price, J. P. Waltho, and C. J. Craven, "Structure of tctp reveals unexpected relationship with guanine nucleotide-free chaperones.," *Nature structural biology*, vol. 8, no. 8, pp. 701–704, 2001.

- [147] X. Yao, Y.-j. Liu, Q. Cui, and Y. Feng, "Solution structure of a unicellular microalgae-derived translationally controlled tumor protein revealed both conserved features and structural diversity.," *Archives of Biochemistry and Biophysics*, vol. 655, pp. 23–29, 2019.
- [148] A. N. Lupas, H. Zhu, and M. Korycinski, "The thalidomide-binding domain of cereblon defines the cult domain family and is a new member of the b - tent fold," *PLOS Computational Biology*, vol. 11, no. 1, 2015.
- [149] L. Susini, S. Besse, D. Duflaut, a. Lespagnol, C. Beekman, G. Fiucci, a. R. Atkinson, D. Busso, P. Poussin, J.-C. Marine, J.-C. Martinou, J. Cavarelli, D. Moras, R. Amson, and a. Telerman, "Tctp protects from apoptotic cell death by antagonizing bax function.," *Cell death and differentiation*, vol. 15, no. 8, pp. 1211–1220, 2008.
- [150] G. Funston, W. Goh, S. Wei, Q. Tng, C. Brown, L. Jiah Tong, C. Verma, D. Lane, and F. Ghadessy, "Binding of translationally controlled tumour protein to the n-terminal domain of hdm2 is inhibited by nutlin-3," *PLoS ONE*, vol. 7, no. 8, pp. 1–8, 2012.
- [151] S. Li, M. Chen, Q. Xiong, J. Zhang, Z. Cui, and F. Ge, "Characterization of the translationally controlled tumor protein (tctp) interactome reveals novel binding partners in human cancer cells," *Journal of Proteome Research*, vol. 15, no. 10, pp. 3741–3751, 2016.
- [152] J.-i. Kashiwakura, Y. Kawakami, J.-i. Kashiwakura, T. Ando, K. Matsumoto, M. Kimura, J. Kitaura, R. P. Siraganian, D. H. Broide, Y. Kawakami, and T. Kawakami, "Histamine-releasing factor has a proinflammatory role in mouse models of asthma and allergy find the latest version : Histamine-releasing factor has a proinflammatory role in mouse models of asthma and allergy," *Journal of Clinical Investigation*, vol. 122, no. 1, pp. 218–28, 2012.
- [153] H. Wu, W. Gong, X. Yao, J. Wang, S. Perrett, and Y. Feng, "Evolutionarily conserved binding of translationally controlled tumor protein to eukaryotic elongation factor 1b.," *The Journal of biological chemistry*, vol. 290, no. 14, pp. 8694–710, 2015.
- [154] Y.-c. Hsu, J. J. Chern, Y. Cai, M. Liu, and K.-w. Choi, "Drosophila tctp is essential for growth and proliferation through regulation of drheb gtpase," *Nature*, vol. 445, pp. 785–8, 2007.
- [155] X. Zhang, "Etude de complexes protéine-protéine impliquant la chaperone de bas poids moléculaire hsp27: Implications dans le cancer de la prostate," *PhD thesis*, 2014.
- [156] M. Kim, H. J. Min, H. Y. Won, H. W. H. Park, J. C. Lee, H. W. H. Park, J. Chung, E. S. Hwang, and K. Lee, "Dimerization of translationally controlled tumor protein is essential for its cytokine-like activity," *PLoS ONE*, vol. 4, no. 7, pp. 1–14, 2009.
- [157] T. Eichhorn, D. Winter, B. Büchele, N. Dirdjaja, M. Frank, W. D. Lehmann, R. Mertens, R. L. Krauth-Siegel, T. Simmet, J. Granzin, and T. Efferth, "Molecular interaction of artemisinin with translationally controlled tumor protein (tctp) of plasmodium falciparum," *Biochemical Pharmacology*, vol. 85, no. 1, pp. 38–45, 2013.

- [158] T. Yoon, J. Jung, M. Kim, K. Lee, E. Choi, and K. Lee, "Identification of the self-interaction of rat tctp / ige- dependent histamine-releasing factor using yeast two-hybrid system," *Archives of Biochemistry and Biophysics*, vol. 384, no. 2, pp. 379–382, 2000.
- [159] A. Lucas, F. X. J. Liu, M. Brannon, J. Yang, D. Capelluto, and C. Finkielstein, "Ligand binding reveals a role for heme in translationally-controlled tumor protein dimerization," *PLoS ONE*, vol. 9, no. 11, pp. 1–17, 2014.
- [160] P. Maurya, A. Mishra, B. Yadav, S. Singh, P. Kumar, A. Chaudhary, S. Srivastava, S. Murugesan, and A. Mani, "Role of y box protein-1 in cancer : As potential biomarker and novel therapeutic target," *Journal of Cancer*, vol. 8, no. 17, pp. 1900–1907, 2017.
- [161] H. Dinkel, K. V. Roey, S. Michael, M. Kumar, B. Uyar, B. Altenberg, V. Milchevskaya, M. Schneider, K. Helen, A. Behrendt, S. L. Dahl, V. Damerell, S. Diebel, S. Kalman, S. Merrill, A. Staudt, S. Klein, A. C. Knudsen, M. Christina, V. Thiel, L. Welti, N. E. Davey, F. Diella, and T. J. Gibson, "Elm 2016 – data update and new functionality of the eukaryotic linear motif resource," *Nucleic Acids Research*, vol. 44, pp. 294–300, 2016.
- [162] U. Cucchi, L. M. Gianellini, A. De Ponti, F. Sola, R. Alzani, V. Patton, A. Pezzoni, S. Troiani, M. B. Saccardo, S. Rizzi, M. L. Giorgini, P. Cappella, I. Beria, and B. Valsasina, "Phosphorylation of tctp as a marker for polo-like kinase-1 activity in vivo," *Anticancer Research*, vol. 30, no. 12, pp. 4973–4986, 2010.
- [163] M. Lucibello, S. Adanti, E. Antelmi, D. Dezi, S. Ciafré, M. L. Carcangiu, M. Zonfrillo, G. Nicotera, L. Sica, F. D. Braud, and P. Pierimarchi, "Phospho-tctp as a therapeutic target of dihydroartemisinin for aggressive breast cancer cells," *Oncotarget*, vol. 6, no. 7, pp. 5275–91, 2015.
- [164] P. Ramani, R. Nash, E. Sowa-Avugrah, and C. Rogers, "High levels of polo-like kinase 1 and phosphorylated translationally controlled tumor protein indicate poor prognosis in neuroblastomas," *Journal of Neuro-Oncology*, vol. 125, no. 1, pp. 103–111, 2015.
- [165] N. Dephoure, C. Zhou, J. ZVillén, S. ZBeausoleil, C. ZBakalarski, S. ZElledge, and S. ZGygi, "A quantitative atlas of mitotic phosphorylation," *Proceedings of the National Academy of Sciences*, vol. 105, no. 31, 2008.
- [166] T. M. Johnson, R. Antrobus, and L. N. Johnson, "Plk1 activation by ste20-like kinase ( slk ) phosphorylation and polo-box phosphopeptide binding assayed with the substrate translationally controlled tumor protein ( tctp ) †," *Biochemistry*, vol. 47, pp. 3688–3696, 2008.
- [167] J. Maeng, M. Kim, H. Lee, and K. Lee, "Insulin induces phosphorylation of serine residues of translationally controlled tumor protein in 293t cells," *International Journal of Molecular Sciences*, vol. 16, no. 4, pp. 7565–7576, 2015.
- [168] S. Teshima, K. Rokutan, T. Nikawa, K. Kishi, and E. Alerts, "Macrophage colony-stimulating factor stimulates synthesis and secretion of a mouse homolog of a human ige-dependent histamine-releasing factor by macrophages in vitro and in vivo," *The Journal of Immunology*, vol. 161, no. 11, pp. 6356–66, 1998.

- [169] G. Munirathinam and K. Ramaswamy, "Sumoylation of human translationally controlled tumor protein is important for its nuclear transport," *Biochemistry Research International*, 2012.
- [170] S. Bae, J. Heon, M. Sun, H.-J. Byun, S. Kang, S.-S. Seo, J.-Y. Kim, and S.-Y. Park, "Anti-apoptotic protein tctp controls the stability of the tumor suppressor p53," *FEBS Letters*, vol. 585, no. 1, pp. 29–35, 2011.
- [171] Y. Yang, F. Yang, Z. Xiong, Y. Yan, X. Wang, M. Nishino, J. Nguyen, H. Wang, and X. Yang, "An n-terminal region of translationally controlled tumor protein is required for its antiapoptotic activity," *Oncogene*, vol. 24, no. 30, pp. 4778–4788, 2005.
- [172] H. Liu, H. Peng, Y. Cheng, H. Yuan, and H. Yang-Yen, "Stabilization and enhancement of the antiapoptotic activity of mcl-1 by tctp," *Molecular and Cellular Biology*, vol. 25, no. 8, pp. 3117–3126, 2005.
- [173] R. Amson, S. Pece, A. Lespagnol, R. Vyas, G. Mazzarol, D. Tosoni, I. Colaluca, G. Viale, S. Rodrigues-Ferreira, J. Wynendaele, O. Chaloin, J. Hoebeke, J. C. Marine, P. P. Di Fiore, and A. Telerman, "Reciprocal repression between p53 and tctp," *Nature Medicine*, vol. 18, no. 1, pp. 91–99, 2012.
- [174] S. B. Rho, J. H. Lee, M. S. Park, H.-J. Byun, S. Kang, S.-S. Seo, J.-Y. Kim, and S.-Y. Park, "Anti-apoptotic protein TCTP controls the stability of the tumor suppressor p53," *FEBS Letters*, vol. 585, pp. 29–35, 2011.
- [175] P. Graidist, M. Yazawa, M. Tonganunt, A. Nakatomi, C. C. Lin, J. Chang, A. Phongdara, and K. Fujise, "Fortilin binds ca<sup>2+</sup> and blocks ca<sup>2+</sup> dependent apoptosis," *Biochemical Journal*, vol. 408, no. 2, pp. 181–191, 2007.
- [176] Y. Feng, D. Liu, H. Yao, and J. Wang, "Solution structure and mapping of a very weak calcium-binding site of human translationally controlled tumor protein by nmr," *Archives of Biochemistry and Biophysics*, vol. 467, no. 1, pp. 48–57, 2007.
- [177] G. Greaves, M. Milani, M. Butterworth, R. J. Carter, D. P. Byrne, P. A. Eyers, X. Luo, G. M. Cohen, and S. Varadarajan, "Bh3-only proteins are dispensable for apoptosis induced by pharmacological inhibition of both mcl-1 and bcl-xl," *Cell death and differentiation*, vol. 26, no. 6, pp. 1037–1047, 2019.
- [178] B. Leber, J. Lin, and D. W. Andrews, "Embedded together: The life and death consequences of interaction of the bcl-2 family with membranes," *Apoptosis*, vol. 12, no. 5, pp. 897–911, 2007.
- [179] F. Edlich, S. Banerjee, M. Suzuki, M. M. Cleland, D. Arnoult, C. Wang, A. Neutzner, N. Tjandra, and R. J. Youle, "Bcl-xl retrotranslocates bax from the mitochondria into the cytosol," *Cell*, vol. 145, no. 1, pp. 104–116, 2011.
- [180] A. Aranovich, Q. Liu, T. Collins, F. Geng, S. Dixit, B. Leber, and D. W. Andrews, "Differences in the mechanisms of proapoptotic bh3 proteins binding to bcl-xl and bcl-2 quantified in live mcf-7 cells," *Molecular Cell*, vol. 45, no. 6, pp. 754–763, 2012.

- [181] D. Zhang, F. Li, D. Weidner, Z. H. Mnjoyan, and K. Fujise, "Physical and functional interaction between myeloid cell leukemia 1 protein (mcl1) and fortilin," *J. Biol. Chem.*, vol. 277, pp. 37430–37438, 2002.
- [182] P. Graidist, A. Phongdara, and K. Fujise, "Antiapoptotic protein partners fortilin and mcl1 independently protect cells from 5-fluorouracil-induced cytotoxicity," *The Journal of biological chemistry*, vol. 279, no. 39, pp. 40868–75, 2004.
- [183] J. Acunzo, V. Baylot, A. So, and P. Rocchi, "Tctp as therapeutic target in cancers," *Cancer Treatment Reviews*, vol. 40, no. 6, pp. 760–769, 2014.
- [184] E. Seo and T. Efferth, "Interaction of antihistaminic drugs with human translationally controlled tumor protein (tctp) as novel approach for differentiation therapy," *Oncotarget*, vol. 7, no. 13, pp. 16818–16839, 2016.
- [185] C. Zhang, P. Gong, P. Liu, N. Zhou, Y. Zhou, and Y. Wang, "Thioridazine elicits potent antitumor effects in colorectal cancer stem cells," *Oncology Reports*, vol. 37, no. 2, pp. 1168–1174, 2017.
- [186] R. Amson, C. Auclair, F. André, J. Karp, and A. Telerman, *Targeting TCTP with Sertraline and Thioridazine in Cancer Treatment*, vol. 64. 2017.
- [187] A. Zingone, D. Brown, E. Bowman, O. Vidal, and J. Sage, "Relationship between anti-depressant use and lung cancer survival," *Cancer Treatment and Research Communications*, vol. 10, pp. 33–39, 2017.
- [188] Cerep, "The clinical application of tumor reversion: a phase i study of sertraline. <https://www.lls.org/content/the-clinical-application-of-tumor-reversion-a-phase-i-study-of-sertraline-zoloft-in-combination-with-timed-sequential-cytosine-arabioside-ara-c-in>,"
- [189] Cerep, "Cerep. communiqué de presse, paris, france, 20 décembre 2005,"
- [190] A. Telerman and R. Ansom, *TCTP/TPT1 - Remodeling signaling from stem cell to disease*, vol. 64. 2017.
- [191] C. Dominguez, R. Boelens, and A. M. J. J. Bonvin, "Haddock : A protein - protein docking approach based on biochemical or biophysical information," *Journal of the American Chemical Society*, vol. 125, no. 7, pp. 1731–1737, 2003.
- [192] B. K. McIntosh, D. P. Renfro, G. S. Knapp, C. R. Lairikyengbam, N. M. Liles, L. Niu, A. M. Supak, A. Venkatraman, A. E. Zweifel, D. A. Siegele, and J. C. Hu, "Ecoliwiki : a wiki-based community resource for escherichia coli," *Nucleic Acids Research*, vol. 40, pp. 1270–1277, 2012.
- [193] "Crystallization-screens - crims, embl-gr." [https://htx.embl-hamburg.de/index.php?option=com\\_content&view=misc&id=32&Itemid=302](https://htx.embl-hamburg.de/index.php?option=com_content&view=misc&id=32&Itemid=302).
- [194] "pet-m11 (embl)." [https://www.embl.de/pepcore/pepcore\\_services/cloning/choice\\_vector/ecoli/embl/popup\\_emblvectors/](https://www.embl.de/pepcore/pepcore_services/cloning/choice_vector/ecoli/embl/popup_emblvectors/).

- [195] H. Liu and J. H. Naismith, “An efficient one-step site-directed deletion, insertion, single and multiple-site plasmid mutagenesis protocol,” *BMC biotechnology*, vol. 8, p. 91, 2008.
- [196] “Serial cloner (in silico molecular biology).”
- [197] “Quickchange material and methods (agilent).” <https://www.agilent.com/cs/library/usermanuals/public/200518.pdf>.
- [198] Y. Yao, A. A. Bobkov, L. A. Plesniak, and F. M. Marassi, “Mapping the interaction of pro-apoptotic bcl-2 with pro-survival bcl-xl,” *Biochemistry*, vol. 48, no. 36, pp. 8704–8711, 2009.
- [199] S. W. Muchmore, M. Sattler, H. Liang, R. P. Meadows, J. E. Harlan, H. S. Yoon, D. Nettleship, B. S. Chang, C. B. Thompson, S. L. Wong, S. C. Ng, and S. W. Fesik, “X-ray and nmr structure of human bcl-xl, an inhibitor of programmed cell death,” *Nature*, vol. 381, pp. 335–341, 1996.
- [200] “puc19 (wikipedia).” <https://fr.wikipedia.org/wiki/PUC19>.
- [201] J. Keeler, “Understanding nmr spectroscopy,” *Ed. Broché*, vol. Second edition, 2012.
- [202] M. P. Williamson, “Using chemical shift perturbation to characterise ligand binding,” *Progress in nuclear magnetic resonance spectroscopy*, vol. 73, pp. 1–16, 2013.
- [203] S. Mori, C. Abeygunawardana, M. O. Johnson, and P. C. Van Zijl, “Improved sensitivity of hsqc spectra of exchanging protons at short interscan delays using a new fast hsqc (fhsqc) detection scheme that avoids water saturation,” *Journal of Magnetic Resonance, Series B*, vol. 108, no. 1, pp. 94–98, 1995.
- [204] B. Brutscher and P. Schanda, “Sofast-hmqc experiments for recording two-dimensional heteronuclear correlation spectra of proteins within a few seconds,” *Journal of Biomolecular NMR*, vol. 33, no. 6, pp. 199–211, 2005.
- [205] C. Amero, P. Schanda, M. A. Durá, I. Ayala, D. Marion, B. Franzetti, B. Brutscher, and J. Boisbouvier, “Fast two-dimensional nmr spectroscopy of high molecular weight protein assemblies,” *Journal of the American Chemical Society*, vol. 131, no. 10, pp. 3448–9, 2009.
- [206] M. Tollinger, N. R. Skrynnikov, F. A. A. Mulder, J. D. Forman-kay, and L. E. Kay, “Slow dynamics in folded and unfolded states of an sh3 domain,” *Journal of the American Chemical Society*, vol. 123, no. 19, pp. 11341–11352, 2001.
- [207] P. Vallurupalli, G. Bouvignies, and L. E. Kay, “Studying “invisible” excited protein states in slow exchange with a major state conformation,” *Journal of the American Chemical Society*, vol. 134, no. 19, pp. 8148–8161, 2012.
- [208] A. Favier and B. Brutscher, “Nmrlib : user - friendly pulse sequence tools for bruker nmr spectrometers,” *Journal of Biomolecular NMR*, vol. 73, no. 5, pp. 199–211, 2019.
- [209] Z. Solyom, M. Schwarten, L. Geist, R. Konrat, D. Willbold, and B. Brutscher, “Best-trosy experiments for time-efficient sequential resonance assignment of large disordered proteins,” *Journal of Biomolecular NMR*, vol. 55, pp. 311–321, 2013.

- [210] G. Lipari and A. Szabo, "Cintx: A software tool for calculating the intrinsic exchange rates of labile protons in proteins," *Journal of Pharmaceutical Sciences and Research*, vol. 4, pp. 1852–1858, 1982.
- [211] K. Akasaka, "High pressure nmr spectroscopy," *Subcellular Biochemistry*, vol. 72, pp. 707–721, 2015.
- [212] T. Richa and T. Sivaraman, "Model-free approach to the interpretation of nuclear magnetic resonance relaxation in macromolecules. 1. theory and range of validity," *Journal of the American Chemical Society*, vol. 104, no. 6, pp. 4546–4559, 2012.
- [213] R. B. Best and M. Vendruscolo, "Structural interpretation of hydrogen exchange protection factors in proteins : Characterization of the native state fluctuations of ci2," *Structure*, vol. 14, no. 1, pp. 97–106, 2006.
- [214] S. P. Skinner, R. H. Fogh, W. Boucher, T. J. Ragan, L. G. Mureddu, and G. W. Vuister, "Ccpnmr analysisassign : a flexible platform for integrated nmr analysis," *Journal of Biomolecular NMR*, vol. 66, no. 2, pp. 111–124, 2016.
- [215] F. Delaglio, S. Grzesiek, G. W. Vuister, G. Zhu, J. Pfeifer, and A. Bax, "Nmrpipe: A multidimensional spectral processing system based on unix pipes," *Journal of Biomolecular NMR*, vol. 6, no. 3, pp. 277–293, 1995.
- [216] P. Dosset, J.-C. Hus, M. Blackledge, and D. Marion, "Efficient analysis of macromolecular rotational diffusion from heteronuclear relaxation data," *J. Biomol. NMR*, vol. 16, no. 1, pp. 23–28, 2000.
- [217] D. Franke, M. V. Petoukhov, P. V. Konarev, A. Panjkovich, A. Tuukkanen, H. D. T. Mertens, A. G. Kikhney, N. R. Hajizadeh, J. M. Franklin, C. M. Jeffries, and D. I. Svergun, "Atsas 2.8: a comprehensive data analysis suite for small-angle scattering from macromolecular solutions.," *Journal of applied crystallography*, vol. 50, no. Pt 4, pp. 1212–1225, 2017.
- [218] A. Micsonai, F. Wien, Bulyàki, J. Kun, Moussong, Y. H. Lee, Y. Goto, M. Rèfrègiers, and J. Kardos, "Bestsel: A web server for accurate protein secondary structure prediction and fold recognition from the circular dichroism spectra," *Nucleic Acids Research*, vol. 46, no. W1, pp. W315–W322, 2018.
- [219] G. Semisotnov, N. Rodionova, O. Razgulyaev, V. Uversky, A. Gripas, and R. Gilman-shin, "Study of the " molten globule " intermediate state in protein folding by a hydrophobic fluorescent probe," *Biopolymers*, vol. 31, no. 1, pp. 119–128, 1991.
- [220] N. Bai, H. Roder, A. Dickson, and J. Karanicolas, "Isothermal analysis of thermofluor data can readily provide quantitative binding affinities.," *Scientific reports*, vol. 9, no. 1, p. 2650, 2019.
- [221] K. Zillner, M. Jerabek-Willemsen, S. Duhr, D. Braun, G. Längst, and P. Baaske, "Microscale thermophoresis as a sensitive method to quantify protein: nucleic acid interactions in solution.," *Methods in molecular biology (Clifton, N.J.)*, vol. 815, pp. 241–52, 2012.

- [222] N. Technology, “User manual: Monolith ® nt.115,” pp. 1–24, 2017.
- [223] “Debian os (gnu/linux distribution).” <https://www.debian.org/>.
- [224] “Gnu software suite.” <https://www.gnu.org>.
- [225] “Bash (unix shell).” [https://en.wikipedia.org/wiki/Bash\\_\(Unix\\_shell\)](https://en.wikipedia.org/wiki/Bash_(Unix_shell)).
- [226] “Awk (programming language).” <https://en.wikipedia.org/wiki/AWK>.
- [227] “Python (programming language).” <https://www.python.org/>.
- [228] “Latex (typesetting system).” <https://www.latex-project.org/>.
- [229] “Grace (plotting tool).” <http://plasma-gate.weizmann.ac.il/Grace/>.
- [230] “Gnuplot (command-line graphing utility).” <http://www.gnuplot.info/>.
- [231] “Matplotlib (python 2d plotting library).” <https://matplotlib.org/>.
- [232] A. Rigsby, RE Parker, “Physical principles and physiological basis of magnetic relaxation,” *Biochemistry and Molecular Biology Education*, vol. 44, no. 5, 2016.
- [233] A. Saladin, S. Fiorucci, P. Poulain, C. Prèvest, and M. Zacharias, “Ptools : an opensource molecular docking library,” *BMC Structural Biology*, vol. 11, pp. 1–11, 2009.
- [234] F. Malard, N. Assrir, M. Alami, S. Messaoudi, E. Lescop, and T. Ha-Duong, “Conformational ensemble and biological role of the tctp intrinsically disordered region: Influence of calcium and phosphorylation,” *Journal of Molecular Biology*, vol. 430, no. 11, pp. 1621–1639, 2018.
- [235] S. Pronk, R. Apostolov, M. R. Shirts, J. C. Smith, P. M. Kasson, D. V. D. Spoel, B. Hess, and E. Lindahl, “Gromacs 4.5: a high-throughput and highly parallel open source molecular simulation toolkit,” *Bioinformatics*, vol. 29, no. 7, pp. 845–854, 2013.
- [236] E. Gasteiger, A. Gattiker, C. Hoogland, I. Ivanyi, R. D. Appel, A. Bairoch, and R. M. Servet, “Expasy : the proteomics server for in-depth protein knowledge and analysis,” vol. 31, no. 13, pp. 3784–3788, 2003.
- [237] J. GarcaTorre, M. L. Huertas, and B. Carrasco, “Hydronmr: Prediction of nmr relaxation of globular proteins from atomic-level structures and hydrodynamic calculations,” *Journal of Magnetic Resonance*, vol. 147, no. 1, pp. 138–146, 2000.
- [238] C. Combet, C. Blanchet, C. Geourjon, and G. Deléage, “Nps@: network protein sequence analysis.,” *Trends in biochemical sciences*, vol. 25, no. 3, pp. 147–50, 2000.
- [239] M. J. Betts, O. Wichmann, M. Utz, T. Andre, P. Minguez, L. Parca, F. P. Roth, A.-c. Gavin, P. Bork, and R. B. Russell, “Systematic identification of phosphorylation-mediated protein interaction switches,” pp. 1–20, 2017.

- [240] J. C. Kennan and R. P. Gore, "Physical principles and physiological basis of magnetic relaxation," *Magnetic Resonance Imaging*, vol. 1, no. ed. D. D. Stark and W. G. Bradley, Mosby, St. Louis, 3rd edn, 1999.
- [241] S. Rajagopal and S. Vishveshwara, "Short hydrogen bonds in proteins," *FEBS Journal*, vol. 272, no. 8, pp. 1819–1832, 2005.
- [242] N. Hunt, L. Gregoret, and F. Cohen, "The origins of protein secondary structure. effects of packing density and hydrogen bonding studied by a fast conformational search.," *Journal of Molecular Biology*, vol. 241, no. 2, pp. 214–225, 1994.
- [243] S. W. Englander, T. R. Sosnick, E. J. Englander, , and L. Mayne, "Mechanisms and uses of hydrogen exchange," *Current Opinion in Structural Biology*, vol. 6, no. 1, pp. 18–23, 1996.
- [244] M. P. Williamson and R. Kitahara, "Characterization of low-lying excited states of proteins by high-pressure nmr," *BBA - Proteins and Proteomics*, vol. 1867, no. 3, pp. 350–358, 2019.
- [245] L. M. Nguyen and J. Roche, "High-pressure nmr techniques for the study of protein dynamics , folding and aggregation," *Journal of Magnetic Resonance*, vol. 277, pp. 179–185, 2017.
- [246] K. Akasaka, H. U. A. Li, H. Yamada, R. Li, T. Thoresen, and C. K. Woodward, "Pressure response of protein backbone structure . pressure-induced amide 15 n chemical shifts in bpti," *Protein Science*, vol. 8, no. 10, pp. 1946–1953, 1999.
- [247] R. Frach, P. Kibies, S. Böttcher, T. Pongratz, S. Strohfeldt, S. Kurrmann, J. Koehler, M. Hofmann, W. Kremer, H. R. Kalbitzer, O. Reiser, D. Horinek, and S. M. Kast, "The chemical shift baseline for high-pressure nmr spectra of proteins," *Angewandte Chemie International Edition*, vol. 55, no. 30, pp. 8757–8760, 2016.
- [248] S. H. Oliveira, F. A. Ferraz, R. V. Honorato, J. Xavier-Neto, T. J. Sobreira, and P. S. de Oliveira, "Kvfinder: steered identification of protein cavities as a pymol plugin.," *BMC bioinformatics*, vol. 15, p. 197, 2014.
- [249] F. Rashid, S. Sharma, and B. Bano, "Comparison of guanidine hydrochloride ( gdnhcl ) and urea denaturation on inactivation and unfolding of human placental cystatin ( hpc )," *The Protein Journal*, vol. 24, no. 5, pp. 283–292, 2005.
- [250] C. Camilloni, A. Guerini Rocco, I. Eberini, E. Gianazza, R. Broglio, and G. Tiana, "Urea and guanidinium chloride denature protein l in different ways in molecular dynamics simulations," *Biophysical Journal*, vol. 94, no. 12, pp. 4654–4661, 2008.
- [251] M. Baptista and E. Gianazza, "Characterization of the protein unfolding processes induced by urea and temperature," *Biophysical Journal*, vol. 94, no. 6, pp. 2241–2251, 2008.
- [252] C. Camilloni, A. De Simone, W. F. Vranken, and M. Vendruscolo, "Determination of secondary structure populations in disordered states of proteins using nuclear magnetic resonance chemical shifts," *Biochemistry*, vol. 51, no. 11, pp. 2224–2231, 2012.

- [253] N. J. Greenfield, "Circular dichroism analysis for protein-protein interactions," *Methods for Molecular Biology*, vol. 261, pp. 55–77, 2004.
- [254] L. A. Munishkina and A. L. Fink, "Fluorescence as a method to reveal structures and membrane-interactions of amyloidogenic proteins.," *Biochimica et biophysica acta*, vol. 1768, no. 8, pp. 1862–85, 2007.
- [255] K. Arai, M Kuwajima, "Role of the molten-globule state in protein folding," *Advances in Protein Chemistry*, vol. 53, pp. 209–82, 2000.
- [256] D. Dolgikh, R. Gilmanishin, E. Brazhnikov, V. Bychkova, G. Semisotnov, S. Venyaminov, and O. Ptitsyn, "Alpha-lactalbumin: compact state with fluctuating tertiary structure?," *FEBS letters*, vol. 136, no. 2, pp. 311–5, 1981.
- [257] M. Ohgushi and A. Wada, "'molten-globule state': a compact form of globular proteins with mobile side-chains.," *FEBS letters*, vol. 164, no. 1, pp. 21–4, 1983.
- [258] N. H. Andersen, J. W. Neidigh, S. M. Harris, and G. M. Lee, "Extracting information from the temperature gradients of polypeptide nh chemical shifts . 1 . the importance of conformational averaging," *Journal of the American Chemical Society*, vol. 119, no. 36, pp. 8547–8561, 1997.
- [259] R. B. Tunnicliffe, J. L. Waby, R. J. Williams, M. P. Williamson, F. Court, and S. Sheffield, "An experimental investigation of conformational fluctuations in proteins g and l," *Structure*, vol. 13, no. 11, pp. 1677–1684, 2005.
- [260] T. Veltri, G. Oliveira, E. A. Bienkiewicz, and F. L. Palhano, "Amide hydrogens reveal a temperature-dependent structural transition that enhances site-ii ca 2 + -binding affinity in a c-domain mutant of cardiac troponin c," *Scientific Reports*, vol. 7, p. 691, 2017.
- [261] M. Zhu and Y.-M. Zhang, "Function of myeloid cell leukaemia-1 and its regulative relations with hepatocellular carcinoma," *Hepatoma Research*, vol. 3, no. 1, pp. 129–40, 2017.
- [262] J. A. Marsh, V. K. Singh, Z. Jia, and J. D. Forman-Kay, "Sensitivity of secondary structure propensities to sequence differences between alpha- and gamma-synuclein: implications for fibrillation.," *Protein science : a publication of the Protein Society*, vol. 15, no. 12, pp. 2795–804, 2006.
- [263] Y. Wang and O. Jardetzky, "Probability-based protein secondary structure identification using combined nmr chemical-shift data," pp. 852–861, 2002.
- [264] G. Liu, L. Poppe, K. Aoki, H. Yamane, J. Lewis, and T. Szyperski, "High-quality nmr structure of human anti-apoptotic protein domain mcl-1(171-327) for cancer drug design," *PLoS ONE*, vol. 9, no. 5, pp. 1–5, 2014.
- [265] A. V. Follis, F. Llambi, L. Ou, K. Baran, D. R. Green, and R. W. Kriwacki, "The dna-binding domain mediates both nuclear and cytosolic functions of p53.," *Nature structural & molecular biology*, vol. 21, no. 6, pp. 535–43, 2014.

- [266] S. Shangary and S. Wang, "Small-molecule inhibitors of the mdm2-p53 protein-protein interaction to reactivate p53 function: A novel approach for cancer therapy," *Annual Review of Pharmacology and Toxicology*, pp. 223–241, 2010.
- [267] A. Goncarenco, M. Li, F. Simonetti, B. Shoemaker, and A. Panchenko, "Exploring protein-protein interactions as drug targets for anticancer therapy with in silico workflows," *Methods in Molecular Biology*, vol. 1647, pp. 221–236, 2017.
- [268] M. Anson and A. Mirsky, "On some general properties of proteins.," *The Journal of general physiology*, vol. 9, no. 2, pp. 169–79, 1925.
- [269] A. Mirsky and L. Pauling, "On the structure of native, denatured, and coagulated proteins.," *Proceedings of the National Academy of Sciences of the United States of America*, vol. 22, no. 7, pp. 439–47, 1936.
- [270] C. Anfinsen, "Principles that govern the folding of protein chains.," *Science*, vol. 181, no. 4096, pp. 223–30, 1973.
- [271] M. R. Lella M, "Metamorphic proteins : Emergence of dual protein folds from one primary sequence," *Biochemistry*, vol. 56, no. 24, pp. 2971–2984, 2017.
- [272] M. K. Khan, H. Rahaman, and F. Ahmad, "Conformation and thermodynamic stability of pre-molten and molten globule states of mammalian cytochromes-cw," *Metallomics*, vol. 3, no. 4, pp. 327–338, 2011.
- [273] T. Banerjee and N. Kishore, "2,2,2-trifluoroethanol-induced molten globule state of concanavalin a and energetics of 8-anilino-naphthalene sulfonate binding: calorimetric and spectroscopic investigation.," *The journal of physical chemistry. B*, vol. 109, no. 47, pp. 22655–62, 2005.
- [274] J. Houwman, E. André, A. Westphal, W. van, Berkel, and C. van, Mierlo, "The ribosome restrains molten globule formation in stalled nascent flavodoxin.," *The Journal of Biological Chemistry*, vol. 291, no. 50, pp. 25911–25920, 2016.
- [275] K. Kuwajima, "The molten globule state as a clue for understanding the folding and cooperativity of globular-protein structure.," *Proteins*, vol. 6, no. 2, pp. 87–103, 1989.
- [276] D. Dolgikh, L. Abaturon, I. Bolotina, E. Brazhnikov, V. Bychkova, R. Gilmanshin, Y. Lebedev, G. Semisotnov, E. Tiktopulo, and O. Ptitsyn, "Compact state of a protein molecule with pronounced small-scale mobility: bovine alpha-lactalbumin.," *European biophysics journal : EBJ*, vol. 13, no. 2, pp. 109–21, 1985.
- [277] K. Kuwajima, "The molten state of a-lactalbumin," *The FASEB Journal*, vol. 10, no. 1, pp. 102–109, 1996.
- [278] N. Rodionova, G. Semisotnov, V. Kutysenko, V. Uverskiĭ, and I. Bolotina, "[staged equilibrium of carbonic anhydrase unfolding in strong denaturants].," *Molekuliarnaia biologiya*, vol. 23, no. 3, pp. 683–92, 1989.
- [279] J. Baum, C. Dobson, P. Evans, and C. Hanley, "Characterization of a partly folded protein by nmr methods: studies on the molten globule state of guinea pig alpha-lactalbumin.," *Biochemistry*, vol. 28, no. 1, pp. 7–13, 1989.

- [280] S. Bhattacharyya and R. Varadarajan, "Packing in molten globules and native states," *Current Opinion in Structural Biology*, vol. 23, no. 1, pp. 11–21, 2013.
- [281] V. Bychkova, G. Semisotnov, V. Balobanov, and A. Finkelstein, "The molten globule concept: 45 years later," *Biochemistry (Moscow)*, vol. 83, 2018.
- [282] A. Merrill, F. Cohen, and W. Cramer, "On the nature of the structural change of the colicin e1 channel peptide necessary for its translocation-competent state.," *Biochemistry*, vol. 29, no. 24, pp. 5829–36, 1990.
- [283] G. Semisotnov, N. Rodionova, V. Kutysenko, B. Ebert, J. Blanck, and O. Ptitsyn, "Sequential mechanism of refolding of carbonic anhydrase b.," *FEBS letters*, vol. 224, no. 1, pp. 9–13, 1987.
- [284] V. Cabiaux, R. Brasseur, R. Wattiez, P. Falmagne, J. Ruyschaert, and E. Goormaghtigh, "Secondary structure of diphtheria toxin and its fragments interacting with acidic liposomes studied by polarized infrared spectroscopy.," *The Journal of Biological Chemistry*, vol. 264, no. 9, pp. 4928–38, 1989.
- [285] J. Kim and H. Kim, "Fusion of phospholipid vesicles induced by alpha-lactalbumin at acidic pH.," *Biochemistry*, vol. 25, no. 24, pp. 7867–74, 1986.
- [286] V. Bychkova, R. Pain, and O. Ptitsyn, "The 'molten globule' state is involved in the translocation of proteins across membranes?," *FEBS letters*, vol. 238, no. 2, pp. 231–4, 1988.
- [287] M. Pedrote, G. de Oliveira, A. Felix, M. Mota, M. Marques, I. Soares, A. Iqbal, D. Norberto, A. Gomes, E. Gratton, E. Cino, and J. Silva, "Aggregation-primed molten globule conformers of the p53 core domain provide potential tools for studying p53c aggregation in cancer.," *The Journal of Biological Chemistry*, vol. 293, no. 29, pp. 11374–11387, 2018.
- [288] E. Lee, P. Czabotar, H. Yang, B. Sleebs, G. Lessene, P. Colman, B. Smith, and W. Fairlie, "Conformational changes in bcl-2 pro-survival proteins determine their capacity to bind ligands," *The Journal of Biological Chemistry*, vol. 284, no. 44, pp. 30508–30517, 2009.
- [289] S. Wuillème-Toumi, V. Trichet, P. Gomez-Bougie, C. Gratas, R. Bataille, and M. Amiot, "Reciprocal protection of mcl-1 and bim from ubiquitin-proteasome degradation.," *Biochemical and biophysical research communications*, vol. 361, no. 4, pp. 865–9, 2007.
- [290] Y. Mei, W. Du, Y. Yang, and M. Wu, "Puma(\*)mcl-1 interaction is not sufficient to prevent rapid degradation of mcl-1.," *Oncogene*, vol. 24, no. 48, pp. 7224–37, 2005.
- [291] P. E. Czabotar, E. F. Lee, M. F. van Delft, C. L. Day, B. J. Smith, D. C. S. Huang, W. D. Fairlie, M. G. Hinds, and P. M. Colman, "Structural insights into the degradation of mcl-1 induced by bh3 domains," *Proceedings of the National Academy of Sciences*, vol. 104, no. 15, pp. 6217–6222, 2007.

- [292] P. Gomez-Bougie, E. Ménoret, P. Juin, C. Dousset, C. Pellat-Deceunynck, and M. Amiot, “Noxa controls mcl-1 ubiquitination through the regulation of the mcl-1/usp9x interaction.” *Biochemical and biophysical research communications*, vol. 413, no. 3, pp. 460–4, 2011.
- [293] M. R. Warr, S. Acoca, Z. Liu, M. Germain, M. Watson, M. Blanchette, S. S. Wing, and G. C. Shore, “Bh3-ligand regulates access of mcl-1 to its e3 ligase.” *FEBS letters*, vol. 579, no. 25, pp. 5603–8, 2005.
- [294] E. Lomonosova and G. CHinnadurai, “Bh3-only proteins in apoptosis and beyond: an overview,” *Oncogene*, vol. 27, no. S1, pp. S2–S19, 2008.
- [295] J. Galindo-Moreno, R. Iurlaro, N. El Mjiyad, J. Díez-Pérez, T. Gabaldón, and C. Muñoz-Pinedo, “Apolipoprotein l2 contains a bh3-like domain but it does not behave as a bh3-only protein.” *Cell death & disease*, vol. 5, p. e1275, 2014.
- [296] R. G. Hawley, Y. Chen, I. Riz, and C. Zeng, “An integrated bioinformatics and computational biology approach identifies new bh3-only protein candidates.” *The open biology journal*, vol. 5, pp. 6–16, 2012.
- [297] B. A. Hilton, Z. Li, P. R. Musich, H. Wang, B. M. Cartwright, M. Serrano, X. Z. Zhou, K. P. Lu, and Y. Zou, “Atr plays a direct antiapoptotic role at mitochondria, which is regulated by prolyl isomerase pin1.” *Molecular cell*, vol. 60, no. 1, pp. 35–46, 2015.
- [298] R. Linding, R. B. Russell, V. Neduva, and T. J. Gibson, “Globplot: Exploring protein sequences for globularity and disorder.” *Nucleic acids research*, vol. 31, no. 13, pp. 3701–8, 2003.



# List of Figures

1.1	Cell cycle and mitosis . . . . .	2
1.2	Overview of apoptosis pathway . . . . .	4
1.3	Bcl-2 family and BH3-only proteins: structure, topology and sequences . . . . .	6
1.4	Bcl-2 family proteins at the MOM . . . . .	7
1.5	Bcl-xL IDR and electrostatic surface map of Bcl-xL and Mcl-1 . . . . .	9
1.6	The hallmarks of cancer . . . . .	11
1.7	The tumor reversion at a glance . . . . .	14
1.8	Structure of TCTP and particular elements . . . . .	16
1.9	Interactome and functions of TCTP protein . . . . .	17
1.10	Structural model of TCTP/YB-1 and TCTP/MDM2 complexes . . . . .	18
1.11	Intrinsic pathway activation via BH3-only proteins . . . . .	23
1.12	Structures of free Bcl-xL and Mcl-1 and complex with BH3 peptides . . . . .	24
1.13	State of the art in TCTP complex with Bcl-xL and Mcl-1 . . . . .	25
1.14	Ligands targeting TCTP available for studies . . . . .	27
1.15	TCTP interactome in apoptosis and beyond: PhD objectives . . . . .	68
2.1	TCTP constructs (Wetlab) . . . . .	80
2.2	Bcl-xL constructs (Wetlab) . . . . .	82
2.3	Other proteins constructs (Wetlab) . . . . .	83
2.4	Protein purification workflow: TCTP (Wetlab) . . . . .	86
2.5	Basic theory of NMR: energy levels and vector model . . . . .	90
2.6	Methods to study motions at different timescales in biomolecular systems . . . . .	93
3.1	SOFAST HMQC and backbone assignment of native TCTP (NMR) . . . . .	106
3.2	Secondary structures and dynamics in TCTP protein (NMR) . . . . .	107
3.3	The concentration-dependent monomer-dimer equilibrium in TCTP (NMR) . . . . .	110
3.4	Model of TCTP dimerization interface . . . . .	111
3.5	Importance of TCTP IDR for dimer formation (NMR) . . . . .	111

3.6	Overview of TCTP phosphorylation by Plk-1 (NMR) . . . . .	113
3.7	Characterization of phosphorylated TCTP by (NMR, MS) . . . . .	114
3.8	Impact of phosphorylation on TCTP backbone dynamics (NMR) . . . . .	117
3.9	Oligomeric state of native and phosphorylated TCTP (SEC-SAXS) . . . . .	118
3.10	Evaluation of TCTP thermal stability toward buffer conditions (TSA) . . . . .	140
3.11	Mapping of labile amide hydrogen in TCTP backbone (NMR) . . . . .	142
3.12	Typical CPMG and CEST profiles in TCTP (NMR) . . . . .	143
3.13	Impact of high-pressure on TCTP structure (NMR) . . . . .	145
3.14	Comparison of TCTP and TCTP* upon pressure induction (NMR) . . . . .	146
3.15	Comparison of TCTP and TCTP* upon urea induction (NMR) . . . . .	147
3.16	SOFAST HMQC spectra from TCTP* upon pressure or urea induction (NMR)	148
3.17	NMR characterization of TCTP* and secondary structure prediction (NMR)	152
3.18	Tertiary structure content in TCTP* (Fluorescence) (NMR) (CD) . . . . .	154
3.19	Oligomeric state of TCTP* and molecular envelope (NMR) (SEC) (SAXS)	156
3.20	Impact of temperature on TCTP structure (NMR) . . . . .	160
3.21	The diversity of TCTP structure: current model . . . . .	162
4.1	Integrity and size of TCTP/Mcl-1 complex (SDS-PAGE) (MS) (DLS) . . . . .	167
4.2	Heterogeneity of TCTP/Bcl-xL and TCTP/Mcl-1 complexes (SEC) . . . . .	169
4.3	Molecular size and stoichiometry of TCTP/Mcl-1 complex (SEC-SAXS) . . . . .	170
4.4	TCTP upon complex formation with Bcl-xL (NMR) . . . . .	172
4.5	Binding of TCTP $\Delta$ IDR to Mcl-1 (NMR) . . . . .	173
4.6	Assignment and structure in TCTP FL complex with Mcl-1 (NMR) . . . . .	174
4.7	TCTP in complex with Mcl-1: temperature (NMR) . . . . .	175
4.8	TCTP in complex with Mcl-1: solid state NMR (NMR) . . . . .	176
4.9	Secondary structures in TCTP and complexes with Bcl-xL or Mcl-1 (CD) . . . . .	179
4.10	Limited proteolysis of Mcl-1/TCTP complex (SDS-PAGE) . . . . .	180
4.11	Comparison of free TCTP* and in the complex with Mcl-1 (NMR) . . . . .	183
4.12	NMR fingerprint of Mcl-1 and overview of backbone assignment (NMR) . . . . .	186
4.13	Impact of transition from acidic to alkaline condition on Mcl-1 (NMR) . . . . .	187
4.14	Characterization of Mcl-1 structure and dynamics (NMR) . . . . .	188
4.15	Structural envelope of Mcl-1 (SEC-SAXS) . . . . .	189
4.16	Comparison of free Mcl-1 complex with TCTP <sub>BH3</sub> (NMR) . . . . .	191
4.17	NMR mapping of TCTP <sub>BH3</sub> binding site in Mcl-1 (NMR) . . . . .	192
4.18	Impact of temperature on Mcl-1/TCTP <sub>BH3</sub> complex (NMR) . . . . .	193
4.19	Comparison of free Mcl-1 complex with TCTP <sub>BH3</sub> at pH 8 (NMR) . . . . .	194
4.20	Mcl-1 and Bcl-xL in complex with TCTP (NMR) . . . . .	196

4.21	Determination of TCTP/Mcl-1 dissociation constant ( $K_d$ ) (MST) . . . . .	196
4.22	Comparison of free Mcl-1 and in complex with TCTP or TCTP <sub>BH3</sub> (NMR) . . . . .	199
4.23	Comparison of Mcl-1 complexes with TCTP FL or TCTP <sub>BH3</sub> (NMR) . . . . .	200
4.24	Mapping of TCTP FL binding site on Mcl-1 (NMR) . . . . .	201
4.25	Molecular envelopes of Mcl-1 and complex Mcl-1/TCTP (SAXS) . . . . .	204
4.26	NMR characterization of Bcl-xL in the transient complex with TCTP (NMR) . . . . .	205
4.27	NMR characterization of Mcl-1/TCTP transient complex (NMR) . . . . .	207
4.28	NMR characterization of Mcl-1/TCTP <sub>BH3</sub> transient complex (NMR) . . . . .	208
4.29	Structural characteristics of BH3-derived peptides (CD) . . . . .	210
4.30	Comparison of free Mcl-1 and in the complex with TCTP <sub>BH3D16I</sub> (NMR) . . . . .	211
4.31	NMR mapping of TCTP <sub>BH3D16I</sub> binding site in Mcl-1 (NMR) . . . . .	212
4.32	Comparison of free Mcl-1 and in complex with Mule <sub>BH3</sub> (NMR) . . . . .	214
4.33	Comparison Mcl-1 complex with TCTP <sub>BH3</sub> and D16I or Mule <sub>BH3</sub> (NMR) . . . . .	215
4.34	Binding interface of BH3-derived peptides at Mcl-1 protein (NMR) . . . . .	216
4.35	Comparison between Mcl-1 complex with TCTP <sub>BH3D16I</sub> or Mule <sub>BH3</sub> (NMR) . . . . .	217
4.36	Models of Mcl-1 complex with TCTP <sub>BH3</sub> and D16I variant (Docking) . . . . .	219
4.37	Relative affinity of TCTP <sub>BH3,BH3D16I</sub> and Mule <sub>BH3</sub> for Mcl-1 (NMR) . . . . .	221
4.38	Dissociation of transient Mcl-1/TCTP <sub>BH3</sub> by Mule <sub>BH3</sub> (NMR) . . . . .	223
4.39	Impact of pre-formed TCTP/Mcl-1 complex on TCTP <sub>BH3</sub> binding (NMR) . . . . .	224
4.40	Impact of pre-formed TCTP <sub>BH3</sub> /Mcl-1 complex on TCTP binding (NMR) . . . . .	225
4.41	Model for TCTP interactions with Bcl-2 family proteins Bcl-xL and Mcl-1 . . . . .	227
5.1	TCTP upon partial complex formation with MDM2 (NMR) . . . . .	230
5.2	Interaction of TCTP with RNAs from yeast (NMR) (MST) . . . . .	232
5.3	Comparison of free TCTP and in complex with YB-1 (NMR) . . . . .	234
5.4	Description of TCTP upon slow complex formation with YB-1 (NMR) . . . . .	235
5.5	TCTP upon fast complex formation with YB-1/RNAs (NMR) . . . . .	237
5.6	Description of TCTP in the fast forming complex with YB-1/RNAs (NMR) . . . . .	238
5.7	Impact of RNA on TCTP and YB-1 (1-180) complex (NMR) . . . . .	239
5.8	TCTP upon partial complex formation with YB-1 (1-180) (NMR) . . . . .	240
5.9	Description of TCTP upon complex formation with YB-1 (1-180) (NMR) . . . . .	241
5.10	Evaluation of ligands ability to target TCTP (NMR) . . . . .	242
5.11	Effect of sertraline at high concentration on TCTP (NMR) . . . . .	243
5.12	Thioridazine and toluidine blue induce covalent TCTP oligomers (PAGE) . . . . .	244
5.13	NMR titration of pTCTP by sertraline ligand (NMR) . . . . .	247
5.14	Evaluation of TCTP thermal stability toward ligands (TSA) . . . . .	248
5.15	Solubility of Mcl-1 selective ligands (NMR) . . . . .	249

---

5.16	FD-24-3 binds to human Mcl-1 with strong affinity (NMR) . . . . .	250
5.17	Relative affinity of FD-24-3 for Mcl-1 and Bcl-xL (NMR) . . . . .	252
5.18	Na-1-115-7 binds to human Mcl-1 with medium affinity (NMR) . . . . .	253
5.19	Mapping of Na-1-115-7 binding site on Mcl-1 (NMR) . . . . .	254
5.20	Na-1-115-7 binds to human Mcl-1 with low affinity (NMR) . . . . .	255
5.21	Mapping of Na-1-115-7 binding site on Bcl-xL (NMR) . . . . .	255
5.22	Comparison of free mMcl-1 and bound to Na-1-115-7 (NMR) . . . . .	257
6.1	Energetic model for the molten-globule state . . . . .	262
6.2	Impact of the BH3-like TCTP on MOMP via Bcl-xL and Mcl-1 . . . . .	264
6.3	Primary sequence alignment of BH3 motifs from BH3-only proteins . . . . .	266
6.4	Primary sequence alignment of BH3 motifs in BH3-like proteins . . . . .	267
5	Examples of pulse-programs used in NMR experiments (NMR) . . . . .	304
6	NMR structure of TCTP and electrostatic potential map . . . . .	305
7	The pH-dependent monomer-dimer equilibrium in TCTP (NMR) . . . . .	306
8	Impact of temperature transition on TCTP backbone residues (NMR) . . . . .	307
9	Evaluation of conformational changes under temperature gradient (NMR) . . . . .	308
10	Impact of prolonged exposition of TCTP to high temperature (NMR) . . . . .	309
11	Impact of low (1 M) concentration of urea on TCTP structure (NMR) . . . . .	310
12	Heterogeneity of TCTP/Bcl-xL complex (SEC) . . . . .	311
13	Heterogeneity of TCTP/Mcl-1 complex (SEC) . . . . .	312
14	Comparison Mcl-1 and complex with TCTP <sub>BH3</sub> or TCTP <sub>BH3D16I</sub> (NMR) . . . . .	313
15	Comparison Mcl-1 and complex with TCTP <sub>BH3</sub> or Mule <sub>BH3</sub> (NMR) . . . . .	314
16	Comparison Mcl-1 and complex with TCTP <sub>BH3D16I</sub> or Mule <sub>BH3</sub> (NMR) . . . . .	315

# List of Tables

2.1	Setup for PAGE-based experiments (Wetlab) . . . . .	78
2.2	Protein-specific information for the purification procedure (Wetlab) . . . . .	85
2.3	Routine NMR experiments (NMR) . . . . .	94
1	Inventory of glycerol stocks for DNA storage strains. . . . .	303
2	Inventory of glycerol stocks for protein expression strains. . . . .	303



# Listings

1	DNA sequence of template plasmids and genes from TCTP, Bcl-xL and Mcl-1317	
2	List of primers sequence, concentration and annealing properties for cloning.	319
3	Primary sequence of proteins presented for interaction studies in the current work . . . . .	320
4	Script <i>fid.com</i> to convert data from Bruker to NMRpipe format (adapted from sample generated with nmrDraw) [215]. . . . .	322
5	Script <i>nmrproc.com</i> to process raw FID in NMRpipe format. (adapted from sample generated with nmrDraw) [215]. . . . .	322
6	Script <i>ftab.sh</i> to clean up test_assign.tab generated with <i>ipap.tcl</i> module prior to extraction of peaks intensity. . . . .	322
7	Script <i>fitModPlot.csh</i> which sum up the procedure for extracting and fitting intensities from a given peaklist with NMRpipe [215]. . . . .	323
8	Script <i>getR2eff.sh</i> to extract CPMG parameter $R_{2\text{eff}}$ from a single <i>nlin.tab</i> output from the <i>autofit.tcl</i> procedure. . . . .	324
9	Script <i>calcHetNoe.sh</i> to compute intensity ratios between two <i>nlin.tab</i> files output of <i>autofit.tcl</i> procedure. . . . .	325
10	Script <i>fitPlotListXYdYinPDF.py</i> to plot XYdY *txt data files and to fit the requested equation to each file. Ultimately generate a PDF containing all plots and fits. . . . .	326
11	96-well plates organization and tested buffer conditions for TSA experiments assessing the stability of TCTP regarding pH and salt concentration (0-500 $\mu\text{M}$ ) or type (NaCl, KCl) . . . . .	327
12	Script <i>XYnFT.py</i> to format any text data matrix with automatic size detection for further processing based on comparison between lists of same nature. . .	329
13	Script <i>calc.sh</i> to compare peaklists and to compute chemical shift perturbations and intensity ratios. . . . .	330
14	Script <i>plotXY.sh</i> to quickly plot XY data file using bash and gnuplot. . . . .	330
15	Gnuplot configuration file <i>plotXY.conf</i> for <i>plotXY.sh</i> script. . . . .	331

- 
- 16 Script *grpXY.sh* to group residues in function of cutoffs and to generate corresponding pymol command for residues selection using Bash. . . . . 331
  - 17 Script *analyze.sh* which sum up the procedure for quick list comparison and results visualization. . . . . 333
  - 18 Script *2Pmed.py* to retrieve papers metadata and to manage bibliography from PMID list input. Generate word text citation and .bib bibliography files with associated PDF. The use of download module is deactivated by default. 333
  - 19 Script *2Gpat.py* to retrieve patents metadata from ID list input. Generate word text citation and .bib data. . . . . 336

Number	Construct	Strain	Plasmid	AntibioR	Tag	Cleavage	Origin
1	Mcl-1 $\Delta$ PEST $\Delta$ TM	DH5 $\alpha$	pET15b	Amp	His-MBP	PreScission	L. Carlier (UPMC)
2	T7 RNAP P226L	DH5 $\alpha$	Unknown	Amp	His	Unknown	S. Campagne (ETHZ)
3	TCTP BH3	DH5 $\alpha$	pRSET-A	Amp	His-GST	Enterokinase-Prescission	F. Malard (ICSN)
4	pGEX-6P1 DNA	DH5 $\alpha$	pGEX-6P1	Amp	-	-	C. Sizun (ICSN)
5	TCTP C27W	DH5 $\alpha$	pETM-11	Kan	His	TEV	F. Malard (ICSN)
6	TCTP C27R	DH5 $\alpha$	pETM-11	Kan	His	TEV	F. Malard (ICSN)
7	TCTP $\Delta$ I-10	DH5 $\alpha$	pETM-11	Kan	His	TEV	N. Assrir (ICSN)
8	TCTP FL	DH5 $\alpha$	pETM-11	Kan	His	TEV	N. Assrir (ICSN)
9	Bcl-xL $\Delta$ 45-84 $\Delta$ TM	DH5 $\alpha$	pETM-11	Kan	His	TEV	F. Malard (ICSN)
10	Bcl-xL $\Delta$ 27-82 $\Delta$ TM	DH5 $\alpha$	pETM-11	Kan	His	TEV	F. Malard (ICSN)

**Table 1 Inventory of glycerol stocks from DNA storing strains.** Antibiotics are diluted from a 1000 X stock at use.

Number	Construct	Strain	Plasmid	AntibioR	Tag	Cleavage	Origin	Expressed	Purified	Comment
1	TCTP <sub>BH3</sub>	BL21 STAR	pRSET-A	Amp	His <sub>6</sub> -GST	Enterokinase-Prescission	F. Malard (ICSN)	YES	YES	His <sub>6</sub> -GST-TCTP <sub>BH3</sub>
2	TCTP C27W	BL21 STAR	pETM-11	Kan	His	TEV	F. Malard (ICSN)	NO	NO	
3	TCTP C27R	BL21 STAR	pETM-11	Kan	His	TEV	F. Malard (ICSN)	NO	NO	
4	TCTP	BL21 STAR	pETM-11	Kan	His	TEV	N. Assrir (ICSN)	YES	YES	N <sub>ter</sub> G
5	TCTP $\Delta$ loop	BL21 STAR	pETM-11	Kan	His	TEV	N. Assrir (ICSN)	YES	YES	N <sub>ter</sub> G
6	Bcl-xL	BL21 STAR	pETM-11	Kan	His	TEV	N. Assrir (ICSN)	YES	NO	N <sub>ter</sub> G
7	Bcl-xL $\Delta$ TM	BL21 STAR	pETM-11	Kan	His	TEV	N. Assrir (ICSN)	YES	YES	N <sub>ter</sub> G
8	TCTP $\Delta$ N10	BL21 STAR	pETM-11	Kan	His	TEV	N. Assrir (ICSN)	NO	NO	
9	TCTP $\Delta$ TCTP1	BL21 STAR	pETM-11	Kan	His	TEV	N. Assrir (ICSN)	YES	YES	N <sub>ter</sub> G
10	Bcl-xL $\Delta$ 45-84 $\Delta$ TM	BL21 STAR	pETM-11	Kan	His	TEV	F. Malard (ICSN)	YES	YES	N <sub>ter</sub> G
11	Bcl-xL $\Delta$ 27-82 $\Delta$ TM	BL21 STAR	pETM-11	Kan	His	TEV	F. Malard (ICSN)	YES	YES	N <sub>ter</sub> G
12	Mcl-1 $\Delta$ PEST $\Delta$ TM	BL21 Rosetta	pET15b	Amp + Chlo	His-MBP	PreScission	L. Carlier (UPMC)	YES	YES	N <sub>ter</sub> GP
13	MDM2 1-125	BL21 STAR	pET28a	Kan	His	Thrombine	E. Jacquet (ICSN)	YES	YES	N <sub>ter</sub> GSHMAS
14	TEV	BL21 Rosetta	Unknown	Amp + Chlo	His	Unknown	N. Assrir (ICSN)	YES	YES	
15	PreScission	SE1	Unknown	Amp	His	Unknown	L. Carlier (UPMC)	YES	YES	

**Table 2 Inventory of glycerol stocks from protein expression strains.** Antibiotics are diluted from a 1000 X stock at use.

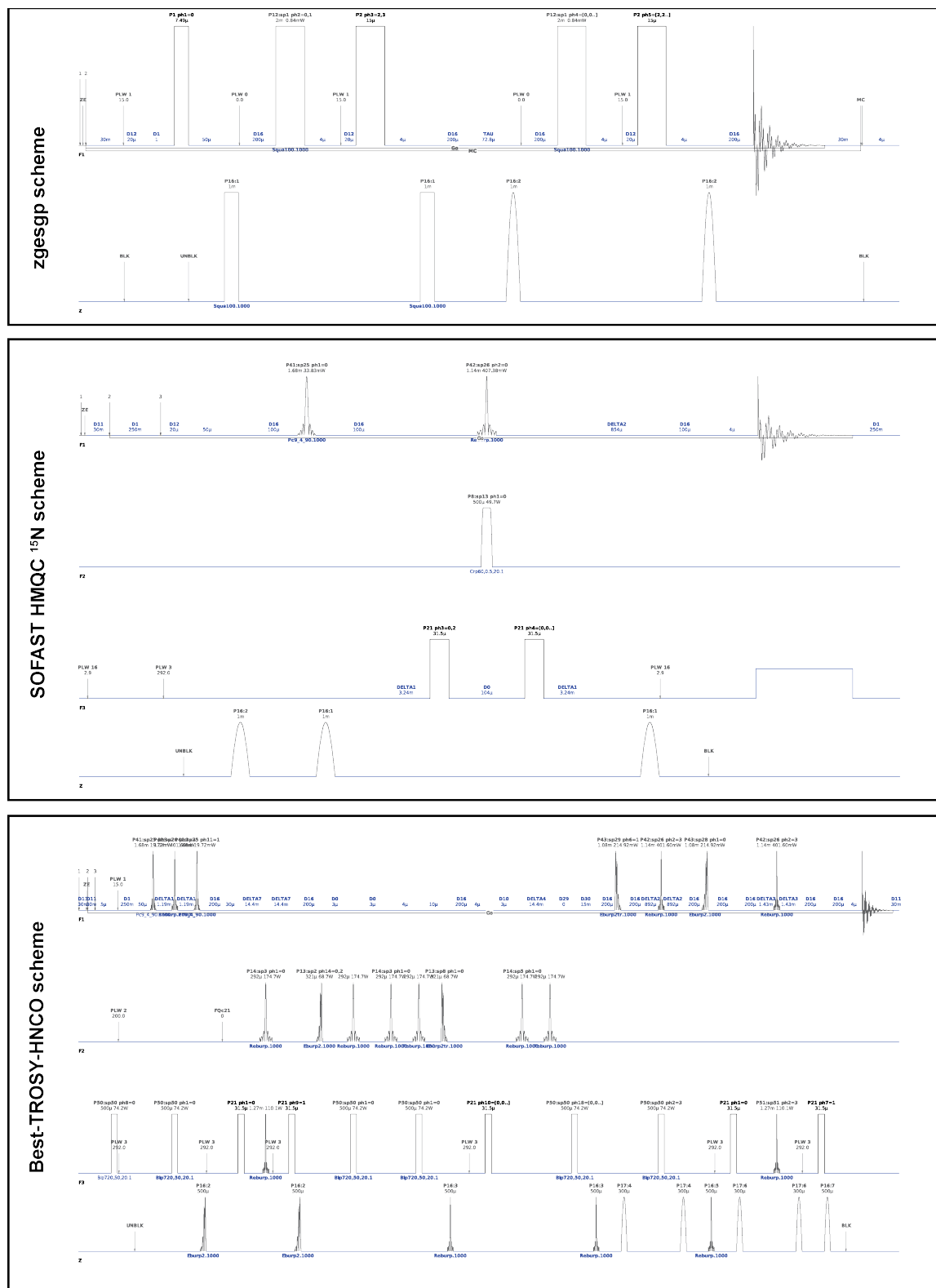
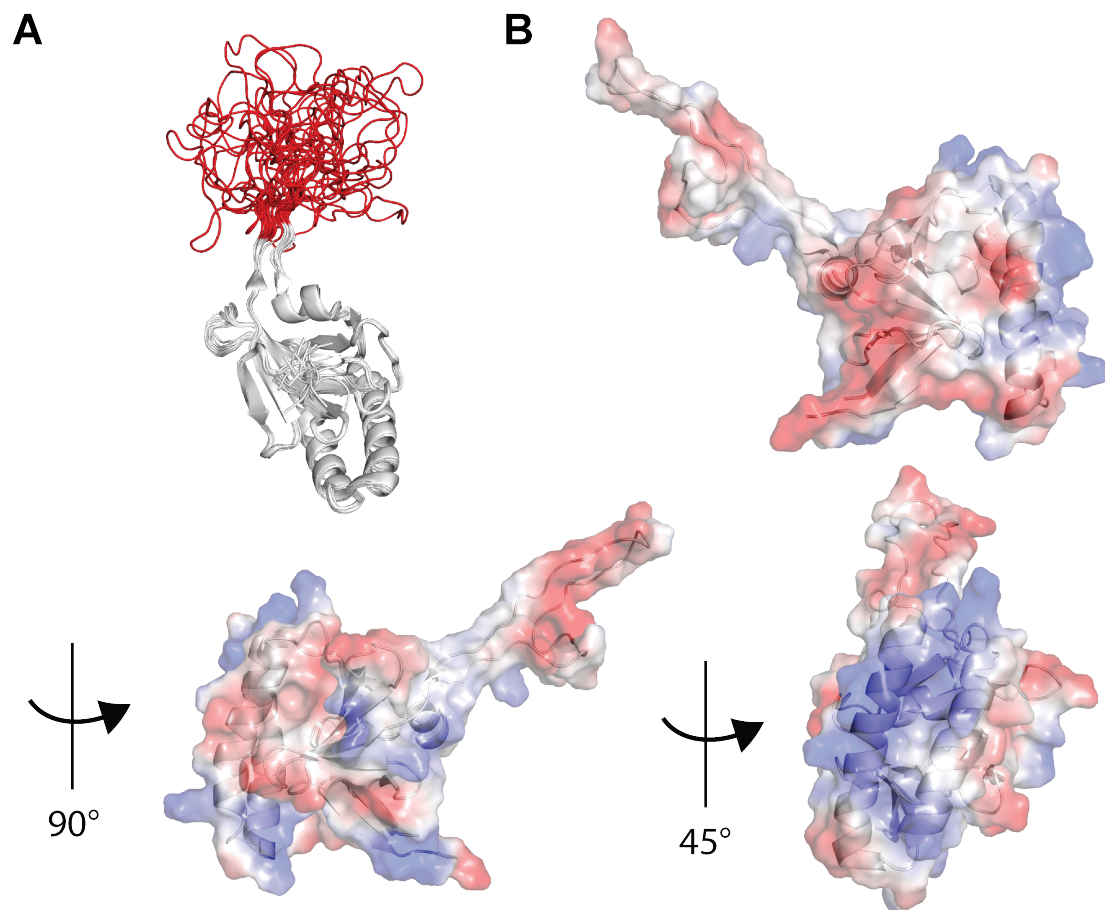


Fig. 5 Examples of pulse-programs used in NMR experiments The *zgesgp* (top), <sup>15</sup>N SOFAST HMQC (middle) and BEST-TROSY HNCO (bottom) are presented. Pulse-sequences are annotated in the Bruker notation system.



**Fig. 6 NMR structure of TCTP and electrostatic potential map.** (A) Structural alignment of the 20 NMR structures of TCTP protein [176] (pdb code: 2HR9). The protein segment containing the loop region (38-66) is highlighted (red). (B) Positively (blue) and negatively (red) charged residues on the surface of TCTP protein are highlighted.

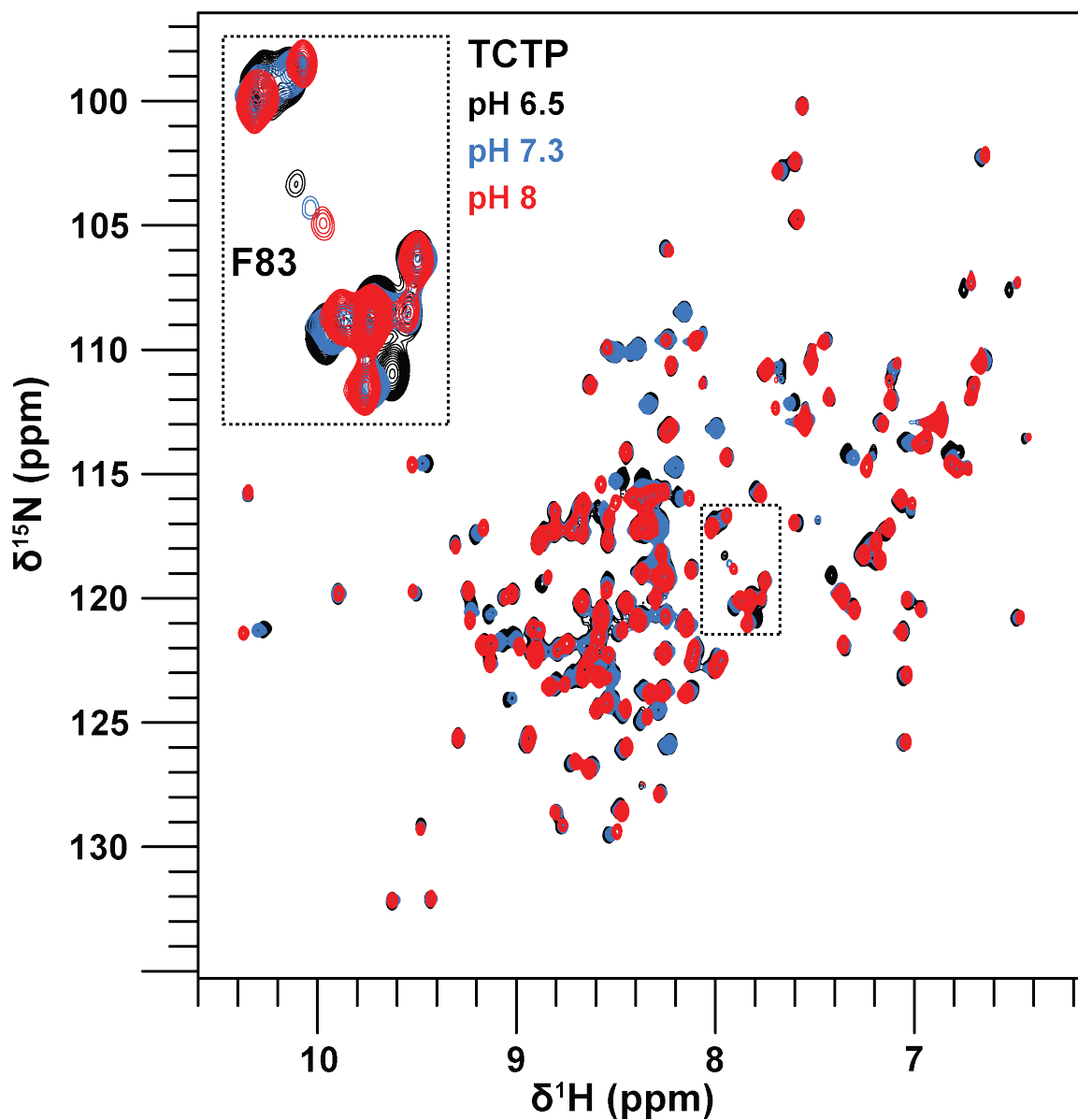


Fig. 7 **The pH-dependent monomer-dimer equilibrium in TCTP.** (A) Overlay of  $^1\text{H}$ - $^{15}\text{N}$  SOFAST HMQC spectra from TCTP upon acidification from alkaline (pH 8) (black) to lower pH (pH 6.5) (orange). Spectra were scaled arbitrary. Residue F83 (top-left) shows the largest perturbation upon dilution. Experiments were carried out at 950 MHz and 298 K in the following buffer: 50 mM HEPES and variable pH, 150 mM NaCl, 2 mM TCEP in 95 %  $\text{H}_2\text{O}$  / 5 %  $\text{D}_2\text{O}$ .

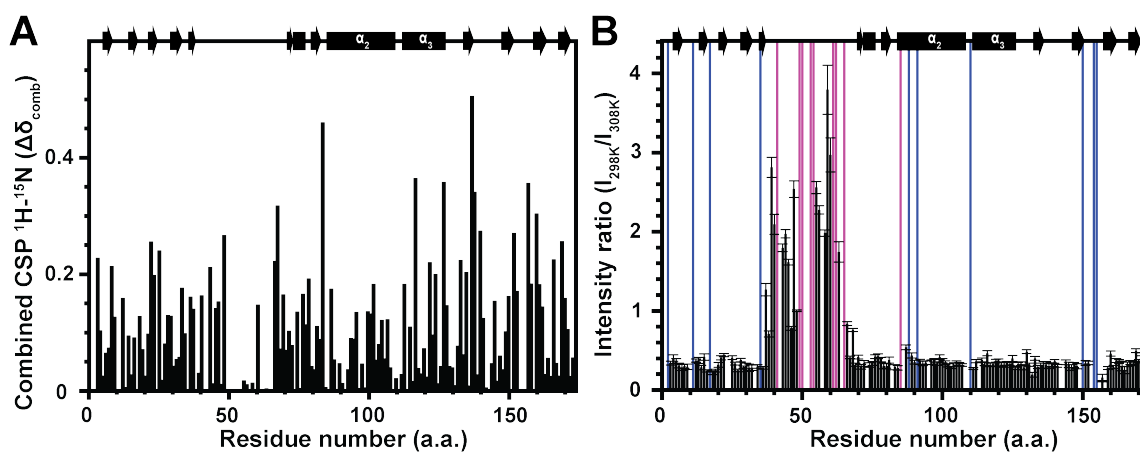
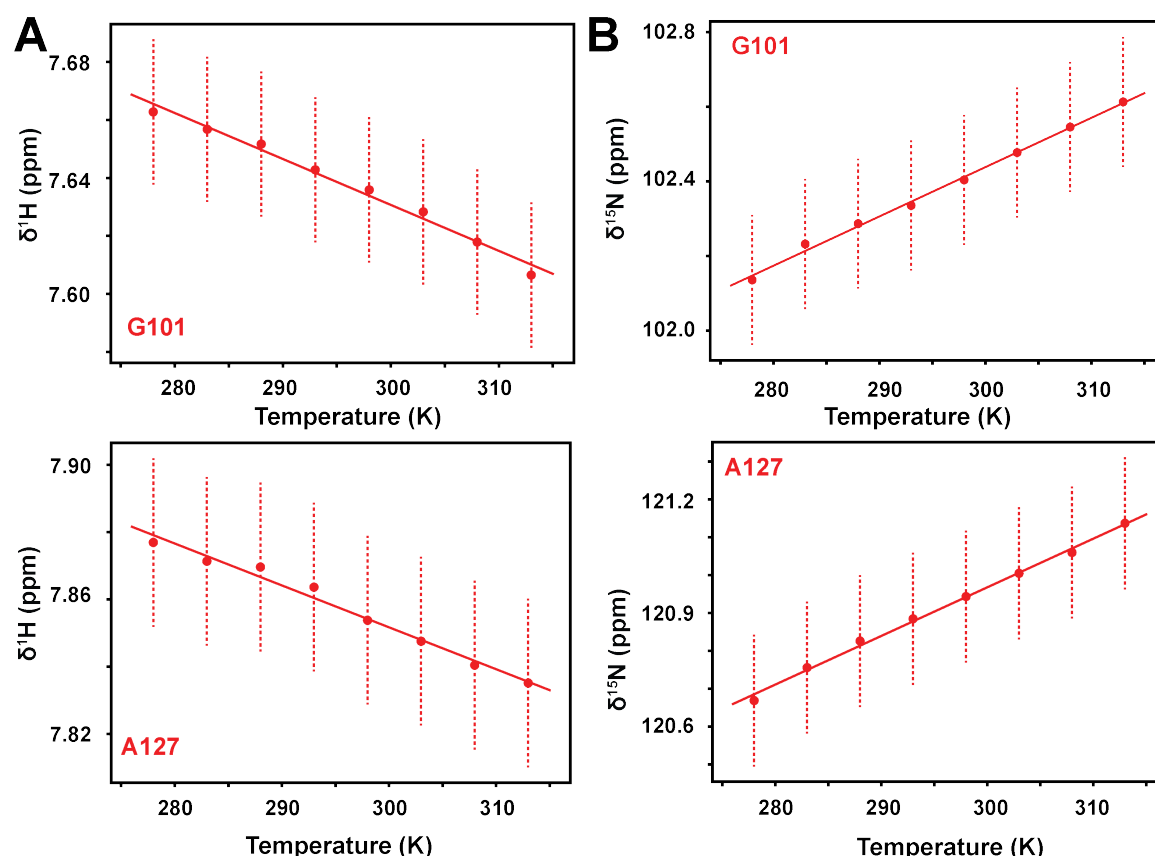


Fig. 8 **Impact of temperature transition on TCTP backbone residues.** (A) Combined  $^1\text{H}$ - $^{15}\text{N}$  chemical shift perturbations and (B) Intensity ratios computed between  $^1\text{H}$ - $^{15}\text{N}$  planes from TCTP (1 mM) at 308 K and 293 K. Disappearing (blue bar) or appearing (magenta bar) residues are shown.



**Fig. 9 Evaluation of conformational changes under temperature gradient.** Dependence of  $^1\text{H}$ - $^{15}\text{N}$  chemical shifts from TCTP residues toward temperature from 278 K to 313 K. (A)  $^1\text{H}$  chemical shift of residues G101 (top) and A127 (bottom) in function of the temperature. (B)  $^{15}\text{N}$  chemical shift of residues G101 (top) and A127 (bottom) in function of the temperature. Error on  $^1\text{H}$  and  $^{15}\text{N}$  chemical shift are highlighted (red dash). Experiments were recorded at 800 MHz in the following buffer: 50 mM EPPS pH 8, 50 mM NaCl, 1 mM TCEP in 95 %  $\text{H}_2\text{O}$  / 5 %  $\text{D}_2\text{O}$ .

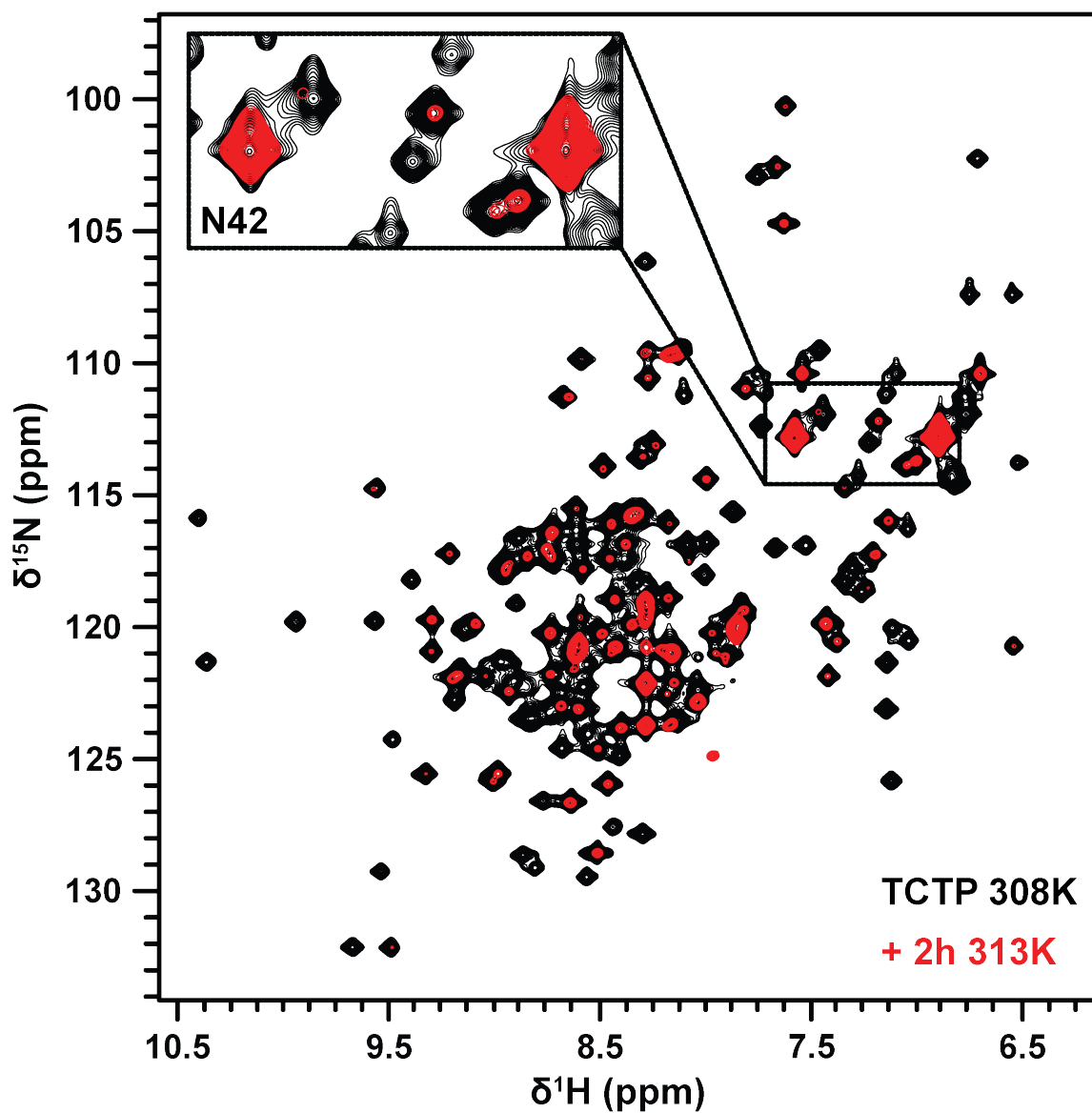


Fig. 10 **Impact of prolonged exposition of TCTP to high temperature.** Overlay of  $^1\text{H}$ - $^{15}\text{N}$  SOFAST HMQC spectra from TCTP (1 mM) before (black) and after (red) incubation during 2 hours at 313 K. A close-up view of the amide side-chain of residue N42 is shown. Experiments were recorded at 800 MHz at 308 K in the following buffer: 50 mM EPPS pH 8, 50 mM NaCl, 1 mM TCEP in 95 %  $\text{H}_2\text{O}$  / 5 %  $\text{D}_2\text{O}$ .

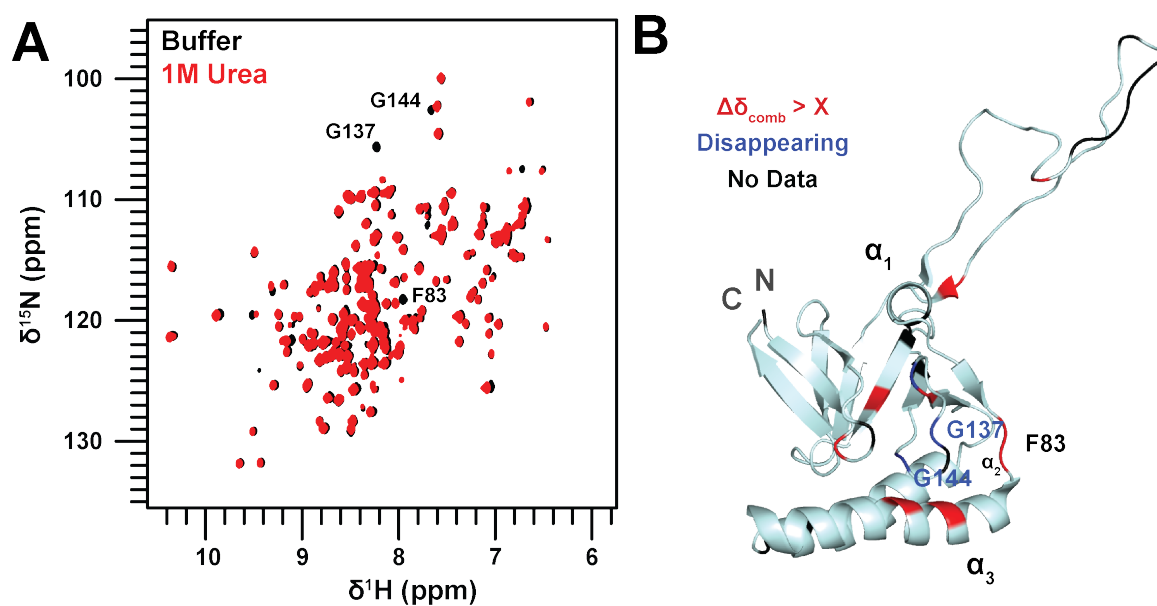
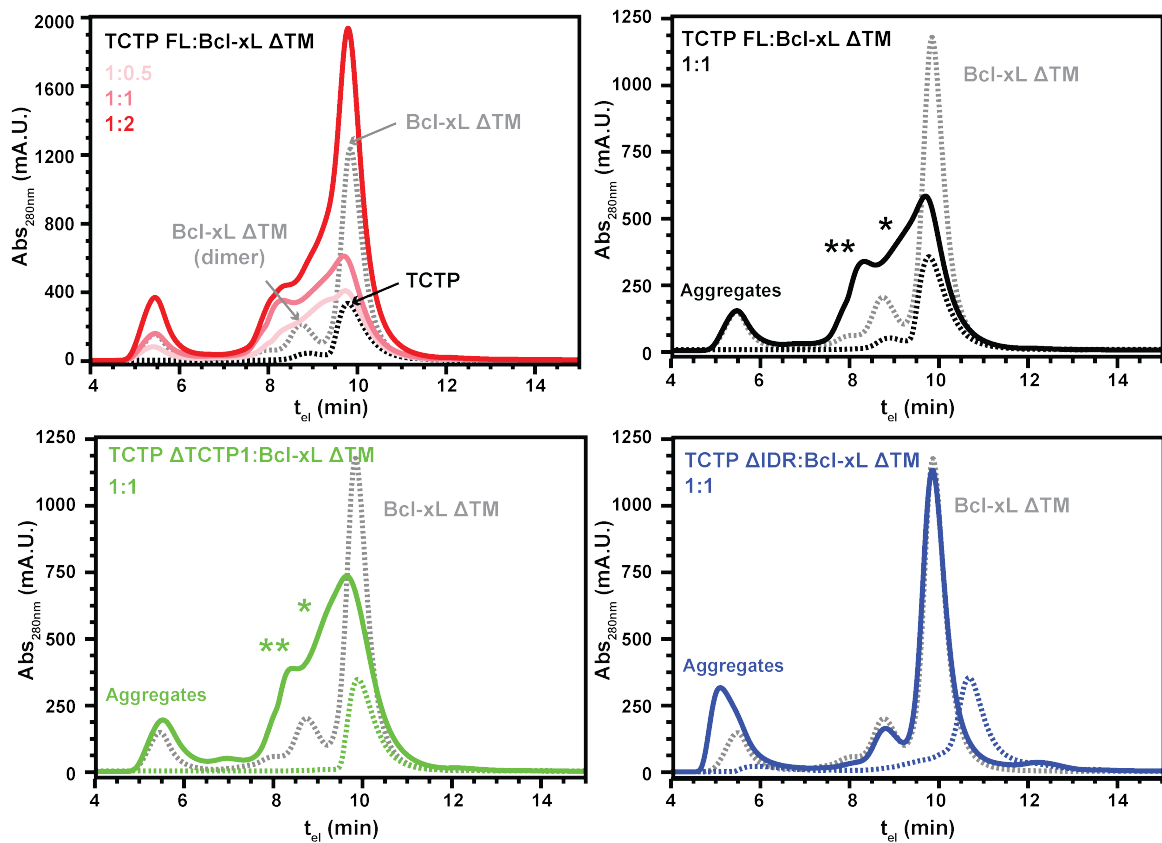
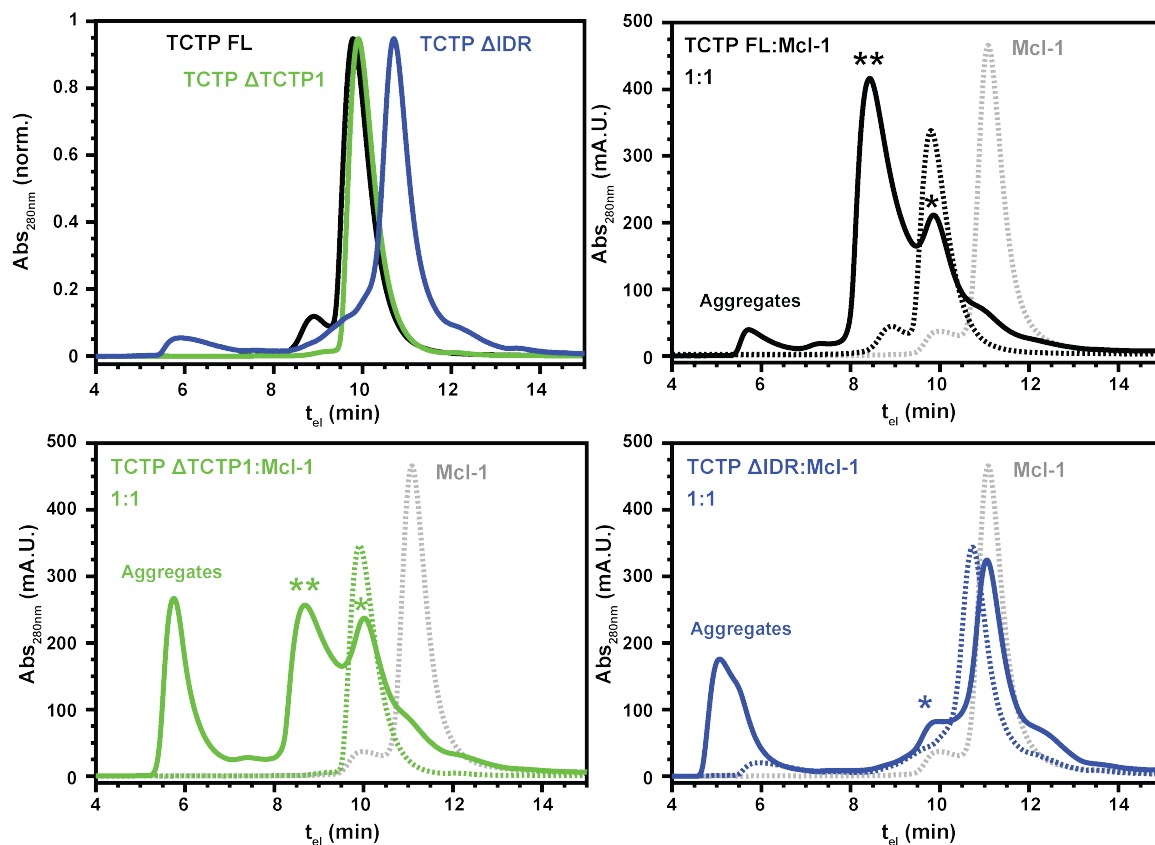


Fig. 11 **Impact of low (1 M) concentration of urea on TCTP structure.** (A) Overlay of  $^1\text{H}$ - $^{15}\text{N}$  SOFAST HMQC spectra from TCTP in buffer (black) and supplemented with urea (1 M) (red). (B) Mapping of disappearing residues (red) upon urea addition. Excluded residues are highlighted (black). Experiments were recorded at 950 MHz and 298 K in the following buffer: 50 mM EPPS, 50 mM NaCl, 2 mM TCEP in 95 %  $\text{H}_2\text{O}$  / 5 %  $\text{D}_2\text{O}$  and urea (0-1 M).



**Fig. 12 Heterogeneity of TCTP/Bcl-xL complex by SEC with TCTP variants.** Normalized SEC elution profiles from isolated (500  $\mu$ M) TCTP FL (black),  $\Delta$ TCTP1 (green) and  $\Delta$ IDR (blue). In (B), (C) and (D) SEC elution profiles from TCTP constructs (500  $\mu$ M) with an equimolar amount of Bcl-xL  $\Delta$ TM. Samples were prepared in 50 mM EPPS pH 8, 50 mM NaCl, 2 mM TCEP and all incubated 2 hrs at 37°C prior to SEC injection.



**Fig. 13 Heterogeneity of TCTP/Mcl-1 complex by SEC with TCTP variants.** Normalized SEC elution profiles from isolated (500  $\mu$ M) TCTP FL (black),  $\Delta$ TCTP1 (green) and  $\Delta$ IDR (blue). In (B), (C) and (D) SEC elution profiles from TCTP constructs (500  $\mu$ M) with an equimolar amount of Mcl-1. Samples were prepared in 50 mM EPPS pH 8, 50 mM NaCl, 2 mM TCEP and all incubated 2 hrs at 37°C prior to SEC injection.

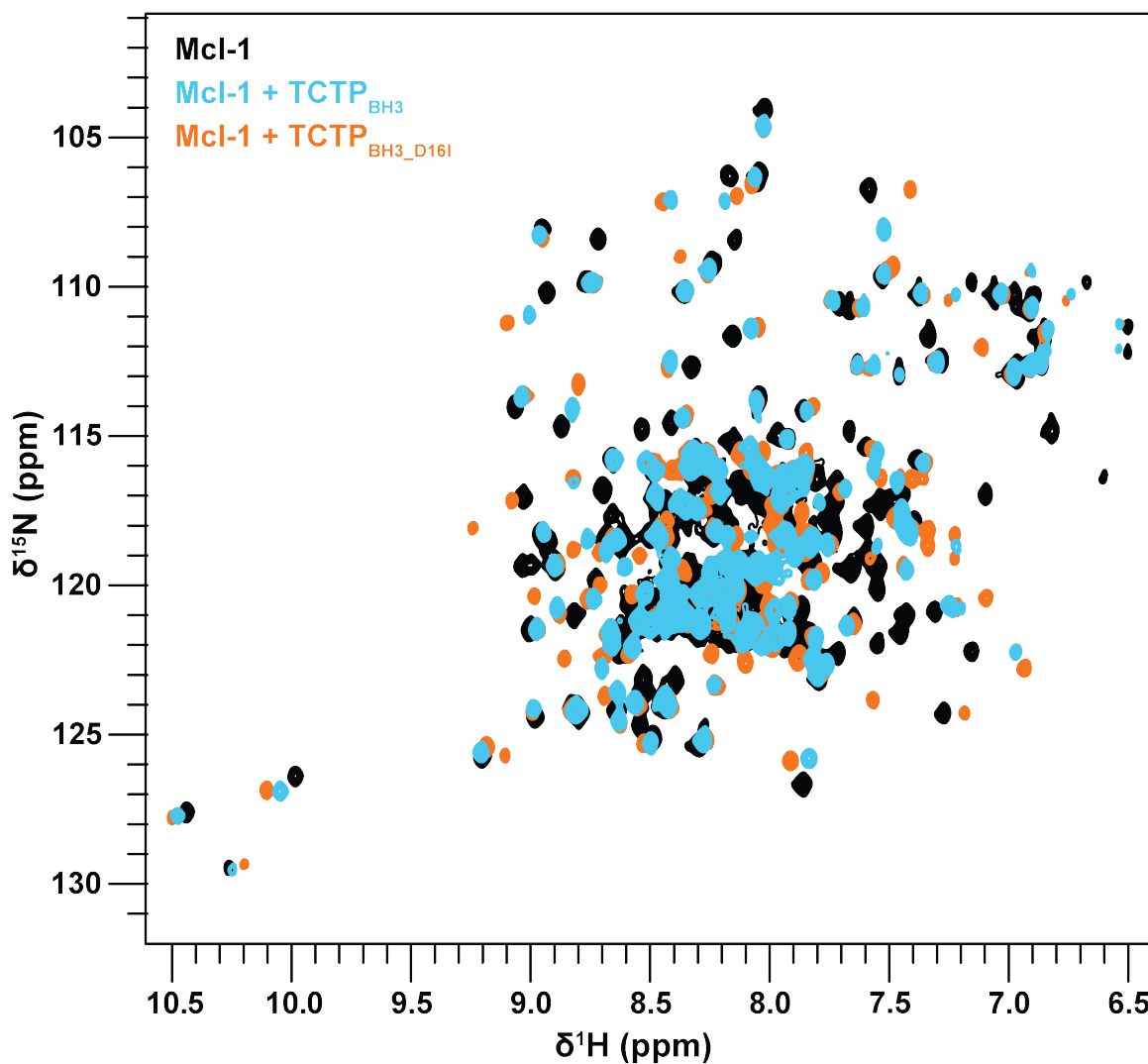


Fig. 14 Comparison of free Mcl-1 and in complex with TCTP<sub>BH3</sub> or TCTP<sub>BH3D16I</sub>. Overlay of  $^1\text{H}$ - $^{15}\text{N}$  SOFAST HMQC from isolated Mcl-1 (100  $\mu\text{M}$ ) (black) and in complex with TCTP<sub>BH3</sub> (blue) or with TCTP<sub>BH3D16I</sub> (yellow). Experiments were recorded at 950 MHz and 308 K in the following buffer: 50 mM MES pH 6.5, 50 mM EPPS, 50 mM NaCl, 1 mM TCEP in 95 %  $\text{H}_2\text{O}$  / 5 %  $\text{D}_2\text{O}$ .

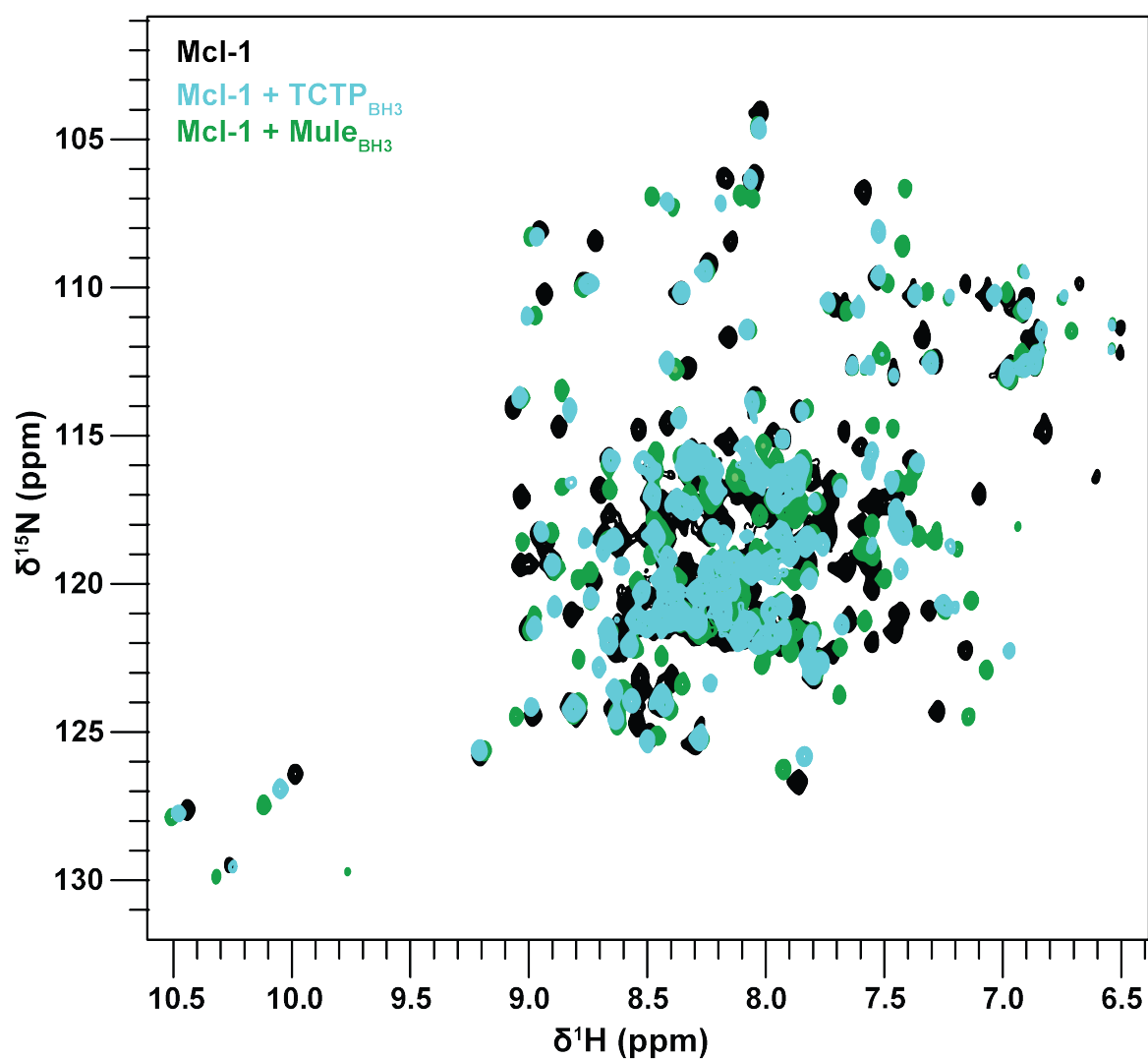


Fig. 15 Comparison between free Mcl-1 and in complex with TCTP<sub>BH3</sub> or Mule<sub>BH3</sub>. Overlay of  $^1\text{H}$ - $^{15}\text{N}$  SOFAST HMQC spectra from isolated Mcl-1 (100  $\mu\text{M}$ ) (black) and in complex with TCTP<sub>BH3</sub> (blue) or with Mule<sub>BH3</sub> (green). Experiments were recorded at 950 MHz and 308 K in the following buffer: 50 mM MES pH 6.5, 50 mM EPPS, 50 mM NaCl, 1 mM TCEP in 95 %  $\text{H}_2\text{O}$  / 5 %  $\text{D}_2\text{O}$ .

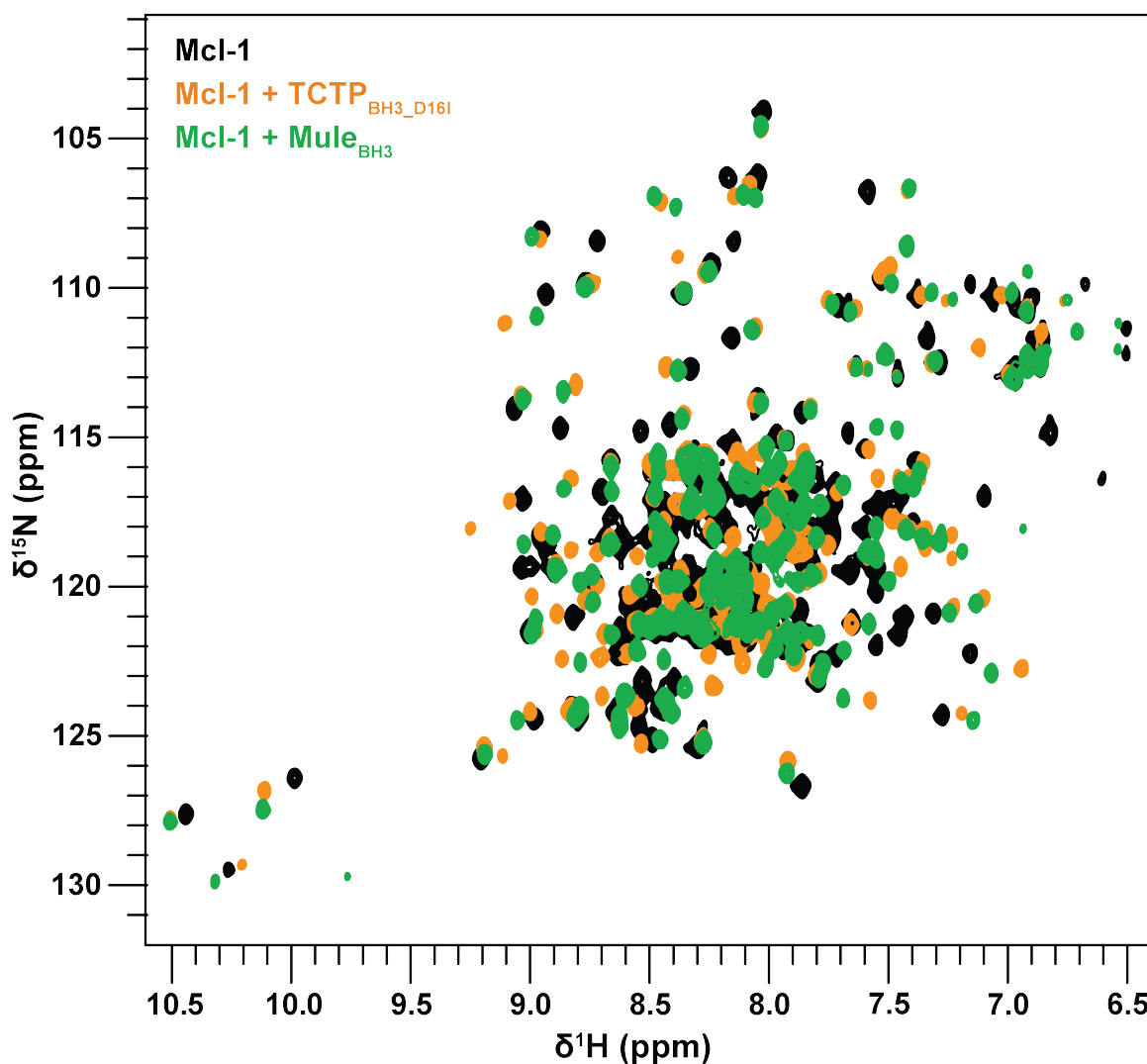


Fig. 16 Comparison between free Mcl-1 and in complex with TCTP<sub>BH3D16I</sub> or Mule<sub>BH3</sub>. Overlay of  $^1\text{H}$ - $^{15}\text{N}$  SOFAST HMQC spectra from isolated Mcl-1 (100  $\mu\text{M}$ ) (black) and in complex with TCTP<sub>BH3D16I</sub> (yellow) or with Mule<sub>BH3</sub> (green). Experiments were recorded at 950 MHz and 308 K in the following buffer: 50 mM MES pH 6.5, 50 mM EPPS, 50 mM NaCl, 1 mM TCEP in 95 %  $\text{H}_2\text{O}$  / 5 %  $\text{D}_2\text{O}$ .



1  
2 pET-M11 TCTP FL in fusion with His6 tag  
3  
4 1 8  
5 GATATACC  
6 9  
7 ATGAAACATCACCATCACCATACCCCATGAGCGATTACGACATCCCACACTGAGAATCTTTATTTTCAG  
8 GGCATGATTATCTACCGGACCTCATAGCCACGATGAGATGTTCTCCGACATCTACAAGATCCGGGAGATCGCGGACGG  
9 GTTGTGCTGGAGGTGGAGGGGAAGATGGTCAGTAGGACAGAAGTAACTATGATGACTCGCTCAITGGTGGAAATGCC  
10 CCGTGAAGGCCCGAGGGCCGAAGGTACCGAAAGCACAGTAATCACTGGTGTGATATTGTCATGAACCATCACCTGCAG  
11 GAAACAAAGTTTCAAAAAGAGCCTCAAGAAGTACATCAAAAGATTACATGAAATCAATCAAAAGGAAACTTGAAGAACA  
12 GAGACCAGAAAGAGTAAAACCTTTTATGACAGGGGCTGCAGAACAAATCAAGCACATCTTGTAAATTTCAAAAATACC  
13 AGTTCTTTATTTGGTGAACCATGAATCCAGATGGCATGGTTGCTCTATTGGACTACCCGTGAGGATGGTGTGACCCCATAT  
14 597  
15 ATGATTTTCTTTAAGGATGGTTTGAAGATGGAAAAAT  
16 598  
17 GTTAAGACCCAGCTTTCTTGTACAAAAGTGGTGTACCTCGA  
18 GCACCACCACCACCACCTGAGATCCGGCTGCTAACAAAGCCGAAAGGAAGCTGAGTTGGCTGCGCACCCGCTGAGC  
19 AATAACTAGCATAACCCCTTGGGGCTCTAAACGGGTCTTGGGGGTTTTTGTGAAAGGAGGAACATATCCGGATTG  
20 GCGAATGGGACGCGCCCTGTAGCGGGCAITTAAGCCGCGGGGTGTGGTGGTTACCGCGACCGTGACCCGTACACTTGGC  
21 AGCGCCCTAGCGCCCGCTCCTTTCGCTTTCTCCCTTCTCTCGCCAGGTTCCGCGGCTTTCCCGCTCAAGCTCAAA  
22 TCGGGGGCTCCCTTTAGGGTTCGGATTAGTGTCTTACGGCACCTCGACCCAAAAAAGCTGATTAGGGTGTGGTTTAC  
23 GTAGTGGGCCATCGCCCTGATAGACGGTTTTTCGCCCTTTGACGTTGGAGTCCACGTTCTTAAATAGTGGACTCTTGTTC  
24 CAAACTGGAACAACACTCAACCCATATCTCGGTCTATTCTTTGATTATAAGGGATTTTCCGGATTTCCGGCTATTGGTT  
25 AAAAAATGAGCTGATTTAACAAAAATTTAACCGGAATTTAACAAAAATTTAACCGTTTACAATTTACAGTGGCATTTC  
26 GGGGAAATGTGCGCGGAACCCCTATTTGTTATTTTCTAAATACATTCAAATATGATCCGCTCATGAATTAATCTTA  
27 GAAAAACTCATCGAGCATCAATGAACTGCAATTTATTCATATCAGGATTATCAATACCATATTTTGGAAAAAGCCGTT  
28 TCTGTATGAAGGAGAAAACCTGACCCGAGGAGTCCATAGGATGGCAAGATCCTGGTATCGGCTCGCGATTCCGACTCGT  
29 CCAACATCAATCAACCTTATTAATTTCCCGTCAAAAAATAAGGTTATCAAGTGAAGAAATCACCATGAGTGAAGACTGA  
30 ATCCGGTGAAGATGGCAAAAGTTTATGCAATTTCTTTCCAGACTTGTTCACAGGCCAGCATTACGCTCGTCATCAAAAT  
31 CACTGCGCATCAACAAACCGTTATTCATTCGTGATTGCGGCTGAGCGGAGACGAAATACGGGATCGCTGTAAAAGGACAA  
32 TTACAACAGGAATCGAATGCAACCGCGCAGGAACACTGCCAGCGCATCAACAATATTTTACCTGAATCAGGATATTC  
33 TICTAATACCTGGAAATGCTGTTTTTCCCGGGATTCGAGTGGTGAATTAACATGCATCATCAGGAGTACGGATAAAATGCT  
34 TGATGTCGGAAGAGGCATAAATCCGTCAGCCAGTTAGTCTGACCATCTCATCTGTGAACATCATTTGGCAACGCTACCT  
35 TTGCCATGTTTCAGAAAACACTTCCGGCATCCGGCTCCCATACAAATCGATAGATTGTCGCACCTGATTGCCGACATT  
36 ATCCGGAGCCATTTATACCCATATAAATCAGCATCCATGTTGGAATTTAATCGCGCCCTAGAGCAAGACGTTTCCGTT  
37 GAATATGGCTCATAACACCCCTTGTATTTACTGTTTATGTAAGCAGACAGTTTATTTGTCATGACCAAAAATCCCTTAAAG  
38 TGAGTTTTCGCTTCCACTGAGCGGTGACAGCCCGTAGAAAAGATCAAAAGGATCTTCTGAGATCCTTTTTTCTCGCGTAA  
39 TCTGTGCTTGCAAAACAAAAAACCCAGCTACCAGCGGTGGTTTGTTTGCGGATCAAGAGCTACCAACTCTTTTTCCG  
40 AAGGTAAGTGGCTTACGAGAGCGCAGATACCAAAACTGTCTTCTAGTGTAGCCGTAAGTTAGGCCACCCTTCAAGAA  
41 CTCTGTAGCACCCGCTACATACCTCGCTTGTCTGTAATCTGTTACCAAGTGGCTGCTGCGAGTGGCGATAAAGTGTCTTA  
42 CCGGTTTGGACTCAAGAGCATAGTTACCGGATAAGCGCGAGCGGTGCGGCTGAACGGGGGTTCTGTGCACAGCCAGC  
43 TTGGAGCGAAGACCTTACACCGAACTGAGATACTACAGCTGAGCTATGAGAAAAGCGCCACGCTTCCCGAAGGGAGAAA  
44 GCGGACAGGTATCCGTTAAGCGGCAGGTTGGAACAGGAGAGCGCACGAGGAGCTTCCAGGGGAAACGCTGTGTATC  
45 TTTATAGTCTGTCCGGTTTCCGCACTTCTGACTTGAAGCTCGATTTTGTGATGCTGTCAGGGGGGCGGAGCCTATGG  
46 AAAAAGCCAGCAACCGGGCTTTTACGGTTCCTGCGCTTTTGTGCGCTTTTGTCTACATGTTCTTCTGCGTTATC  
47 CCTGTATCTGTGGATAACCGTATTACCGCTTTGAGTGAAGTGTATACCCGCTCGCGCAGCGCAAGACCGGCGCAGCG  
48 AGTCAAGTGAAGGAGGAAAGCGGAGGCGCTGATGCGGATTTTCTCTTACGCATCTGTGCGGATTTTACACCCGATA  
49 TATGGTGCACCTCTCAGTACAATCTGCTCTGATGCCGATAGTTAAGCCAGTATACACTCCGCTATCGCTACGTGACTGGG  
50 TCATGGCTGCGCCCGACACCCGCCAACACCCGCTGACGCGCCCTGACGGGCTTGTCTGCTCCCGCATCCGCTTACAGA  
51 CAAGCTGTGACCGCTTCCGGAGCTGCATGTGTGACAGGTTTTTACCGTCACTACCGAAAACGCGGAGGCGAGCTGCGGTA  
52 AAGCTCATCAGCTGTGCTGTAAGCGGATTCACAGATGCTGCTGCTATCCGCTGTCAGCTGTTGAGTTTCTCCAGAA  
53 GCGTTAATGCTGGCTTCTGATAAAGCGGGCATGTTAAGGGCGGTTTTTCTGTTTGGTCACTGATGCTCCGTTGATA  
54 GGGGATTTCTGTTCATGGGGTAAATGATACCGATGAAACGAGAGAGGATGCTCAGGATACGGGTTACTGATGATGAACA  
55 TGCCCGTTACTGGAACGTTGTGAGGGTAAACAACCTGGCGGTATGGATGCGCGGAGCAGAGAAAAATCACTCAGGGT  
56 AATGCCAGCGCTTGTAAATACAGATGTAGGTGTTCCACAGGGTACCCAGCAGCATCTGCGATGACAGATCCGGAACATA  
57 ATGGTGCAGGCGCTGACTTCCGCTTCCAGACTTACGAAACAGGAAACCGAAGACCATTTATGTTGTGCTCAGGT  
58 CGCAGACGTTTTTGCAGCAGCAGTCCGTTACGTTCCGCTGCGGATGCGGTGATTCAATCTGCTAACAGTAAGGCAACCC  
59 CCGAGCTAGCCGGTCTCAAGCAGCAGGAGCAGCATATGCCACCCGTTGGGGCCGCTATGCCGCGATAATGGCTGC  
60 TTTCCGCGAAACGTTTGGTGGCGGACAGTGCAGAAAGGCTTGAAGCGGGGCTGCAAGATTCCGAATACCGCAAGCGA  
61 CAGCCGATCATGCTCGCGCTCCAGCGAAAGCGGTCTCGCCGAAAATGACCCAGAGCGCTGCCCGCACCTGCTCACGA  
62 GTTGCATGATAAAGACAGTCAATAGTGGCGGACGATAGTCAATGCCCGGCCACCCGAAGGAGCTGACTGGGTTG

63 AAGGCTCTCAAGGGCATCGGTCGAGATCCCGTGCCTAATGAGTGAAGTAACTACATTAATTGCGTTGGCCTACTGCC  
64 CGCTTTCCAGTCGGGAAACCTGTCTGCCAGTGCATTAATGAATCGGCCAACCGCGGGGAGAGCGGTTTGGTATTG  
65 GGCGCCAGGGTGGTTTTTCTTTTACCAGTGAAGACGGGCAACAGCTGATTCGCCCTTACCAGCTGGCCCTGAGAGAGTTG  
66 CAGCAAGCGGTCCACGCTGGTTTGGCCAGCAGGGGAAAATCTGTTTGTATGGTGGTTAACGGCGGGATATAACATGAGC  
67 TGTCTTGGTATCTGCTATCCACTACCGAGATATCCGCACCAACCGCGAGCCCGGACTCGGTAATGGCGGCATTGGC  
68 CCCAGCGCCATCTGATCGTTGGCAACACAGATCGCAGTGGGAACGATGCCCTCATTACGATTTGCATGGTTTGTGAAA  
69 ACCGGACATGGCACTCCAGTGCCTTCCGTTCCGCTATCCGCTGAATTTGATTGGCAGTGAAGATAATTTATGCCAGCCAG  
70 CCAGACCAGACGCGCCGAGACAAACTTAATGGGCCCGCTAACAGCCGATTTGCTGGTGAACCAATGGCAGCAGATGC  
71 TCCAGCCAGTCCGCTACCGTCTTACATGGGAGAAAATAACTGTTGATGGGTGCTGGTCCAGAGACATCAAGAAATAA  
72 CGCCGAAACATTTAGTGCAGGACGCTTCCACAGCAATGGCATCTGGTATCCAGCGGATAGTTAATGATCAGCCACTGA  
73 CGCGTTGGCGGAGAGATTGTGCACCGCCGCTTACAGGCTTCGACGCGCTTCTGTTTACCATCGACACACCCAGCTG  
74 GCACCCAGTTGATCGGCGGAGATTTAATCGCCGCGACAATTTGCGACGGCGGTCAGGGCCAGACTGGAGGTGGCAAC  
75 GCAATCAGCAACGACTGTTTGGCCCGCAGTGTGTGGCCAGCGGTTGGGAATGTAATTCAGCTCCGCCATCGCCGCTT  
76 CCACCTTTTCCCGGTTTTCGAGAAAACGGCTGGCTGGCTGGTTTCCACAGCGGGAACCGTCTGATAAGAGACACCGGCA  
77 TACTCTGCGACATCGTATAACGTTACTGGTTTACATTCACACCCCTGAATTGACTCTCTTCCGGGCGCTATCATGCCAT  
78 ACCGGAAAGGTTTTCGCCATTCGATGGTTCGCGGATCTCGACGCTTCCCTTATCGGACTCTCGATTAGGAAGCAG  
79 CCCAGTAGTGGTGGAGCCGTTGAGCACCCGCGGCAAGGAATGGTGCATGCAAGGAGATGGCGCCAAACAGTCCCCC  
80 GGCCACGGGGCTGCCACCATACCCACGCCGAAACAAGCGTCTATGAGCCGAAGTGGCGAGCCGATCTTCCCATCGG  
81 TGATGTCGCGATATAGGGCCAGCAACCCGACTTGTGGCGCGGATGATGCCGGCCAGATGCGTCCGGCTAGAGGATC  
82 GAGATCTCGATCCCGGAAATTAATACGACTACTATAGGGGAATTTGAGCGGGATAACAATTCCTCTAGAAAATAAT  
83 TTGATTTAACCTTAAGAAGGA  
84  
85  
86 pET-M11 Bcl-xL FL in fusion with His6 tag  
87  
88 TGGCGAATGGGACGCGCCCTGTAGCGCGCATTAAGCCGCGGGTGTGGTGGTTACCGCAGCGTGACCCCTACACTTG  
89 CCAGCGCCCTAGCGCCCGCTCTTTCGCTTTCCTTTCCTTTCCTGCGCACGTTCCCGGCTTTCGCCGTCAAGCTCTA  
90 AATCGGGGGTCCCTTATAGGTTTCGATTTAGTGTCTTACGGCACCTCGACCCCAAAAACTTGATTAGGGTATGGTTC  
91 ACGTAGTGGGCCATCGCCCTGATAGACGGTTTTTTCGCCCTTTCGACGTTGGAGTCCACGTTCTTAAATAGTGGACTCTTGT  
92 TCCAACTGGAAACAACACTCAACCTATCTCGGTCTATCTTTTGAATTTATAAGGGATTTTGGCGATTTCCGGCTATTGG  
93 TTAATAAATGAGCTGATTTAACAAAAATTTAACCGGAATTTTAAACAAAATTTAACGTTTACAAATTCAGTGGCCTTT  
94 TCGGGGAAATGTCCGGGAAACCCCTAATTTGTTATTTTCTAAATACATCAAATATGATCCGCTCATGAATTAATCT  
95 TAGAAAAACTCATCGAGCATCAAAATGAACTGCAATTTATTCATATCAGGATTAATCAATACCATATTTTGGAAAAAGCCG  
96 TTTCTGTAATGAAGGAAACTCACCGAGGCACTTCCATAGGATGGCAAGATCCTGGTATCGGTCGCGATTCCGACTC  
97 GTCCAACTCAATACAACCTATTAATTTCCCTCGTCAAAAATAAGTTTATCAAGTGAAGAAATCAACATGAGTACGACT  
98 GAATCCGGTGAAGATGGCAAAAGTTTATGCATTTCTTCCAGACTTGTCAACAGCCGACCCATTACGCTCGTCATCAA  
99 ATCACTCGCATCAACCAAAACCGTTATTCATTCGATTTCCGCTGAGCGAGACGAAATACCGGATCGCTGTTAAAAGGAC  
100 AATTACAACAGGAATCGAATGCAACCGGCGCAGGAACACTGCCAGCGCATCAACAATATTTTACCTGAATCAGGATAT  
101 TCTTCTAATACCTGGAATGCTGTTTTCCCGGGATCGCAGTGGTGAATAACCATGCAATCAGGAGTACGGATAAAAATG  
102 CTGTAGTTTTCGTTCCACTGAGCGTACAGCCCGTAGAAAAGATCAAAAGGATCTTCTTGAGATCTTTTTTTCGCGGT  
103 CTTTGCATGTTTCAGAAAACACTTGGCGCATCGGGTTCCTACATAATCGATAGATTGTCGACCTGATTGCCCGACA  
104 TTATCGGAGCCCTTTATACCATATAAATCAGCATCCATGTTGGAATTTAATCGCGGCTAGAGCAAGACGTTTCCCG  
105 TTGAATATGGCTATAACCCCTTGTATTACTGTTTATGTAAGCAGACAGTTTATTTGTTATGACCAAAAATCCCTTAA  
106 CGTAGTTTTCGTTCCACTGAGCGTACAGCCCGTAGAAAAGATCAAAAGGATCTTCTTGAGATCTTTTTTTCGCGGT  
107 AATCTGCTGTGCAAAAACAAACCCGCTACCGCGTGGTTTGTTCGCGGATCAAGAGCTACCAACTCTTTTTC  
108 CGAAGGTAACCTGGCTCAGCAGAGCGCATCAAAATACCTGCTTCTAGTGTAGCCGATGTTAGGCCACCCTTCAAG  
109 AACTCTGATGACCCGCTACATACCTCGCTTCTGCTAATCTGTTACCAGTGGCTGCTGCCAGTGGCGATAAGTGTGTCT  
110 TACCGGTTGGACTCAAGACGATAGTTACCGGATAAGGCGCAGCGTGGGCTGAACGGGGGTTGTCACACAGCCCA  
111 GCTTGGAGCGAACGACCTACACCGAAGTGAATCTACAGGCTGAGCTATGAGAAAGCCGACCGCTTCCCGAAGGGAGA  
112 AAGGGGACAGGATATCCGTTAAGCGGAGGGTCCGGAACAGGAGCGCAGGAGGAGCTTCCAGGGGAAACCGTCTGTA  
113 TCTTTATAGTCTGTGGGTTTCCGCACTCTGACTGAGCGTCTGATTTTGTGATGCTGTCAGGGGGGGGAGCCTAT  
114 GGAAAAAGCGCAGCAACGGGGCTTTTACCGTTCTGGCTTTTGTGGCTTTTGTCTCACATGTTCTTCTGCGTTA  
115 TCCCTGATTTCTGTGATAACCGTATACCGCTTTGAGTGTGCTGATACCGCTCGCCGACCGCAACGACCGAGCGCAG  
116 CGAGTCAAGTGGAGGAAAGCGGAGAGCGCTGATCGGATTTTCTCTTACGATCTGTGCGGATTTTACACCGCA  
117 TATATGTTGCACTCTCAGTACAATCTGCTGATGCCGATAGTTAAGCCAGTATACACTCCGCTATCGCTACGTGACTG  
118 GGTATGGCTGCGCCCGACACCCGCCAACACCCGCTGACCGGCCGTCAGGGGTTGTCGCTCCCGCATCCGCTTACA  
119 GACAAGCTGTGACCGTCTCCGGGAGTGCATGTGTGAGAGGTTTTCACCGTATCACCGAAACCGCGGAGGCACTGGCG  
120 TAAAGCTCATCAGCGTGGTGTGAAAGCAATTCAGATGTTCTGCTGTTATCCGCTCCAGCTCGTTGAGTTTCTCCAG  
121 AAGCGTTAATGTCTGGCTTCTGATAAAGCGGGCCATGTTAAGGCGGTTTTTCTGTTTGGTCACTGATGCCTCCGTTG  
122 AAGGGGATTTCTGTTTATGGGGTAAATGATACCGATGAAACGAGAGAGGATGCTACGATACGGGTTACTGATGATGAA  
123 CATGCCCGTTACTGGAACGTTGTGAGGGTAAACAACTGGCGTATGGATGGCGGGGACAGAGAAAAATCACTCAGGG  
124 TCAATGGCAGCGTTCGTTAATACAGATGTAGGTGTTCCACAGGGTAGCCAGCAGCATCTCGATGAGATCCGGAACA  
125 TAATGGTGCAGGGCGTACTTCCGCTTCCAGACTTACGAAACCGGAAACCGAAGACCATTTCAATGTTGTGCTCAG  
126 TGGCAGACGTTTTGACAGCAGCTGCTTACGTTCTGCTCGCTATCGGTGATTCATTCTGTAACCAAGTAAAGCAACC  
127 CCGCCAGCCTAGCCGGTCTCAACGACAGGAGCAGCATATGCGCACCCGTTGGGCGCCCATGCCGGGATAAATGGCCT  
128 GCTTTCGCGAAAACGTTTTGGTGGCGGGACAGTGAAGAGGCTTGGCGAGGGGCTGCAAGATTCGGAATACCGCAAGC  
129 GACAGCCGATCATCTGCGGCTCCAGCGAAAGCGGTTCTCGCCAAAATGACCCAGAGCGCTGCCGCACTGTTCTAC  
130 GAGTTGATGATAAAGAGACAGTCAATAGTGGCGGACGATAGTATGCCCCGCGCCACCGGAAGGAGCTGACTGGGT  
131 TGAAGGCTCTCAAGGGCATCGTTCGAGATCCCGGTGCCTAATGAGTGAAGTAACTTACATTAATTTGCGTTGGCTCACTG  
132 CCGCTTTCAGTCCGGAAACCTGTCTGCCAGTGCATTAATGAATCCGGCAACCGCGGGGAGAGCGGTTTTGCGTAT  
133 TGGGCGCAGGGTGGTTTTTCTTACCAGTGAAGCGGCAACAGCTGATTGCCCTTACCAGCTGGCCCTGGAGAGAT  
134 TGACGCAAGCGGTCCAGCTGTTTTCGCCAGCGGAAATTCCTGTTGATGTTGGTTAACGCGGGATATAACATGA  
135 GCTGTTTGGTATCTGCTATCCCACTCCGAGATATCCGCAACCGCGCAGCCGACTCGGTAATGGCGCGCAATTG  
136 CGCCAGCGCATCTGATCGTTGGCAACAGCATCGCAGTGGGAACGATGCCCTATTCAGCATTTGATGTTTGTGTA  
137 AAACCGGACATGGCACTCAGTGCCTTCCGTTCCGCTATCGGCTGAATTTGATTGCGAGTGAAGATTTATGCGACGG

```

138 AGCCAGACGCAGACGCCGAGACAGAACTTAATGGCCCGCTAACAGCGGATTGCTGGTGACCCAATGCGACCAGAT
139 GCTCCACGCCAGTCCGGTACCGTTCATCGGGAGAAAATAACTGTGTGGTGTCTGGTCAGAGACATCAAGAAAT
140 AACGCCGGAACTTAGTGCAGGCAGCTTCCACAGCAATGCCATCCGTCATCCAGCGGATAGTTAATGATCAGCCCACT
141 GACGCGTTGGCCGAGAAGATTGTGACCCGCCGCTTACAGGCTTCGACCGCGCTTCGTTCTACCATCGACACCACACGC
142 TGGCACCCAGTTGATCGCCGGAGATTAATCGCCCGACAATTTGCGACGGCGGTGCAGGGCCAGACTGGAGGTGGCA
143 ACGCCAATCAGCAACGACTGTTGCCCGCCAGTTGTGTGCCACGGGTTGGGAATGTAATTCAGTCCGCCATCGCCCG
144 TTCCACTTTTTCCCGCTTTTCGCGAAGAACGTTGGCTGGCTGGTTACACGCGGAAACGGTCTGTATAAGAGACACCGG
145 CATACTCTGGACATCGTATAACGTTACTGGTTTCACATTCACCACCTGAATTTGACTCTCTCCGGGCGCTATCATGCC
146 ATACCCGAAAAGGTTTTCGCCATTCGATGGTTCGGGATTCGACGCTCTCCCTTATGCGACTCTGCATTAGGAAGC
147 AGCCCACTAGTAGGTTGAGGCGGTTGAGCACCCGCCCGCAAGGAATGGTGCATGCAAGGAGATGGCGCCCAACAGTCCC
148 CCGGCCACGGGGCTGCCACCATACCACGCCGAAACAAGCGCTCATGAGCCGAAAGTGGCGAGCCGATCTTCCCCTC
149 GGTGATGTCGGGATATAGGCGCCAGCAACCGCACCTGTGGCCCGGTGATGCCGCCACGATGCGTCCGGGTAGAGGA
150 TCGAGATCTCGATCCCGGAAATTAATACGACTACTATAGGGGAATTTGAGCGGATAAACAATTCCTCTAGAAATAA
151 TTTTGATTTAACTTTAAGAAGGAGATATACCATGAAACATCACCATCACCATACCCCATGAGCGATTACGACATCCCA
152
153 5152
154 CTACTGAGAATCTTTATTTTCAGGGCGCCATG
155
156 5153
157 TCTCAGAGCAACCGGGAGCTGGTGGTTGACTTTCTCTCTACAAGCTT
158
159 TCCAGAAAAGGATACAGCTGGAGTACAGTTTAGTGTATGGAAGAGAACAGGACTGAGGCCCCAGAAAGGACTGAATCGGA
160 GATGGAGACCCCACTGATCAATGGCAACCCATCTGGCACCTGGCAGACAGCCCGGTTGAATGGAGCCACTGGCC
161 ACAGCAGCAGTTTGGATGCCCGGGAGGTGATCCCATGGCAGCAGTAAAGCAAGCGTGGAGGAGGAGCCGACGAGTGT
162 GAACCTGCGTACCGGGCGGATTCAGTACCTGACATCCAGCTCCACATCACCCAGGGACAGCATATCAGAGCTTTGA
163 ACAGGTAGTGAATGAACCTTCCCGGATGGGTAAACTGGGTGCGATTGTGGCTTTTTCTCTCCGGCGGGCACTGT
164 CCGTGGAAAGGTAGACAAGGAGATGCAGGTATTGGTGAAGTCCGATCGCAGCTTGGATGGCCACTTACCTGAATGACCAC
165 CTAGACCTTTGGATCCAGGAGAACCGCGCTGGGATACTTTTGTGAACTCTATGGGAACAATGCAGCAGCCGAGAGCCG
166 AAAGGCCAGGAACGCTTCAACCCGTGGTTCTGACGGCGATGACTGTGGCCGGCTGGTTCTGCTGGGCTCACTCTCA
167
168 5852
169 GTCGGAATGAC
170
171 5853
172 TCGACACCACCACCACCCTGAGATCCGGCTGCTAACAAAGCCGAAAGGAAGCTGAGTTGGCT
173
174 GCTGCCACCGCTGAGCAATAACTAGCATAACCCCTGGGGCTCTAAACGGGCTTTGAGGGTTTTTTGCTGAAAGGAGG
175
176 AACTATATCCGGAT
177
178 Coding sequence for human Mcl-1 in pET15b
179
180 CCATGGGATCGTCCATCATCATCACTCGGAAGAAGGTAAACTGGTCAATTTGGATCAACGGCGATAAAGGCTACA
181 ACGGCTCGCGGAAGTGGCAAAAATTCGAAAAGATACCGGTATCAAAGTGAACATCCGGACAAACTGGAAG
182 AAAAAATTTCCGAGGTTGCCGCAACCCGGTATGGTCCGGACATTAATCTTTTGGGCACACGATCGTTTGGCGTTATGCC
183 AGTCCGGTCTGCTGGCCGAAATCACCCGGATAAAGCCTTTCAAGACAAACTGTACCCGTTACAGTGGGATGCAGTCCGCT
184 ATAAATGGTAAACTGATTGCTTACCAGATCGCCGTGGAAGCACTGTCTGATTATAACAAGATCTGCTGCCGAATCCGC
185 CGAAAACCTGGGAAGAAATCCCGCGCTGGACAAGAAGTAAAGCGAAAGGCAAAAGTCCCTGATGTTAACCTGCAGG
186 AACCGTATTTACAGTGGCCGCTGATTGCACTGATGGCGGTTATGCCCTTCAAATACGAAAACGGCAAAATACGATATCAAAG
187 ACGTGGTGTGGATAACCGCGGCCCAAGCAGGTCTGACCTTTCTGGTGGACCTGATCAAAAACAACACATGAACCGCAG
188 ATACGGACTATTTCTATCGCTGAAGCGGCTTCAATAAAGCGAAACCGCGATGACGATTAACGGTCCGTGGCGCTGGTCTA
189 ATATGATACCAAGTAAAGTTAACTACGGCGTTACCCTCTGCCGACGTTAAAGGTCAGCCGAGCAAAACCGTTCGTGGCGG
190 TTCTGTGGCCCGTATTAACCGCAGTAGCCGAATAAAGAAGTGGCAAAAGAAATTTCTGGAATAATATCTGTGACCGGATG
191 AAGGCTGGAAGCGGTGAACAAGGACAAACCCGCTGGTGTGTGGCTGAAAAGCTATGAAGAAGAACTGGCGAAAGATC
192 CGGATATTCGGCCACGATGGAATAAGCCAGAAAGCGAAATTAAGCGAACATCCCGCAAATGTCCGCTTTTGGTATG
193 CGGTTGTAACGGCCGCTCAATCAATGAGCTAGCCGTGCCAGACCGTTGATGAAGCACTGAAAGACGCTCAAAACGAAACAGT
194 CTAGTCTGGAAGTCTGTTCAGGGCCGGATGAACCTGTATCGCCAATCCCTGGAAATTAATCTACGTTTACCTGCGGAAC
195 AGGCTACCGGTGCGAAAGATACGAAAACCGATGGGCCGTTCCGGTGCACACGCGTAAAGCTCTGGAACCGTCCGTCGCG
196 TGGCGGATGGTGTTCAGGTAATACGAAAACCGGTTTCAAGGCATGCTGCCCAAATGGACATTAATAAAGCAAGATGACG
197 TGAATAACCTGTACGTTGATGATCCATGTGTTCTCCGATGGCGTTACCAATTTGGGTGCGATTGTACCGCTGATCTCAT
198 TTGGTGCCTTCGTTGCAAAAACCTGAAAACCAATTAACCAAGAATCTTGATCGAACCCGTTGGCGGAAAGTATTACCGATG
199 TCCGTGGTGCATGAAACCGGACTGCTGTGTAACAGCGTGGTTGGGACGGCTTTGTGGAATTTTCATGTGGAGGAC
200 TGGAAAGCGGCTGACATATG

```

Listing 1 DNA sequence of template plasmids and genes from TCTP, Bcl-xL and Mcl-1

```

1
2 TCTP C27R
3
4 fw 5 -GGG TTG CGG CTG GAG GTG GAG GGG AAG ATG 3
5 rv 3 GCC CTC TAG CGC CTG CCC AAC GCC GAC CTC 5
6
7 TCTP C27W
8
9 fw 5 GGG TTG TGG CTG GAG GTG GAG GGG AAG ATG 3
10 rv 3 GCC CTC TAG CGC CTG CCC AAC ACC GAC CTC 5
11
12 Bcl-xL 45 -84 TM
13
14 fw 3' CTT CCC TGA CTT AGC CTC CGT CAT TTC 5'

```

```

15 rv 5 GAA TCG GAG GCA GTA AAG CAA GCG CTG 3
16
17 Bcl-xL 27 -82 TM
18
19 fw 3 CCT ATG TCG ACC TCA GTC TAC CGT CGT 5
20 rv 5 TGG AGT CAG ATG GCA GCA GTA AAG CAA 3

```

## Listing 2 List of primers sequence, concentration and annealing properties for cloning.

```

1
2 TCTP FL (E=11920)
3
4 -1 1
5 GP MIIYRDLISH DEMFSDIYKI REIADGLCLE VEGKMVSRTE GNIDDSLIGG NASAEGPEGE
6
7 GTTESTVITGV DIVMNHHLQE TSFTKEAYKK YIKDYMKSIK GKLEEQRPER VKPFMTGAAE
8 172
9 QIKHILANFK NYQFFIGENM NPDGMVALLD YREDGVIPYM IFFKDGLEME KC
10
11 TCTP TCTP1 (E=11920)
12
13 -1 1
14 GP MIIYRDLISH DEMFSDIYKI REIADGLCLE VEGKMVSRTE GNIDDSLIGP
15
16 EGEGETSTVI TGVDIVMNHHLQETSFTKEA YKDYMKSIK SIKGKLEEQR
17
18 PERVKPFMTG AAEQIKHILA NFKNYQFFIG ENMNPDMVA LLDYREDGVT
19 165
20 PYMIFFKDGL EMEKC
21
22 TCTP loop (E=11920)
23
24 -1 1
25 GP MIIYRDLISH DEMFSDIYKI REIADGLCLE VEGKMVSITG VDIVMNHHLQ
26
27 ETSFTKEAYK KYIKDYMKSIK IKGKLEEQRPE RVKPFMTGAA EQIKHILANF
28 143
29 KNYQFFIGEN MNPDMVAL LDYREDGVTPY MIFFKDGLEME EKC
30
31 TCTP BH3 recombinant (E=1490)
32
33 -1 11 31
34 GP DEMFSDIYKI REIADGLCLE V
35
36 Bcl-xL FL (E=47440)
37
38 -1 1
39 GA MSQSNRELVV DFLSYKLSQK GYSWSQFSDV EENRTEAPEG TESEMETPSA
40
41 INGSWHLAD SPAVNGATGH SSSLDAREVI PMAAVKQALR EAGDEFELRY
42
43 RRAFDLTSQ HITPGTAYQS FEQVVNELFR DGVNWGRIVA FFSFGGALCV
44
45 ESDKEMQVL VSRIAAMMAT YLNDHLEPWI QENGGWDTFV ELYGNNAAAE
46 233
47 SRKGQERFNR WFLTGMTVAG VVLLGSLFSR K
48
49 Bcl-xL TM (E=41940)
50
51 -1 1
52
53 GA MSQSNRELVV DFLSYKLSQK GYSWSQFSDV EENRTEAPEG TESEMETPSA
54
55 INGSWHLAD SPAVNGATGH SSSLDAREVI PMAAVKQALR EAGDEFELRY
56
57 RRAFDLTSQ HITPGTAYQS FEQVVNELFR DGVNWGRIVA FFSFGGALCV
58
59 ESDKEMQVL VSRIAAMMAT YLNDHLEPWI QENGGWDTFV ELYGNNAAAE
60 206
61 SRKGQE
62
63 Bcl-xL 45 -84 TM (E=36440)
64

```

65 -1 1  
66 GA MSQSNRELVV DFLSYKLSQK GYSWSQFSDV EENRTEAPEG TESEAVKQAL  
67  
68 REAGDEFELR YRRAFSDLTS QLHITPGTAY QSFQVNNEL FRDGVNWGRI  
69  
70 VAFFSFGGAL CVESVDKEMQ VLVSRIAAWM ATYLNDHLEP WIQENGGWDT  
71 168  
72 FVELYGNNAA AESRKGQE  
73  
74 Bc1-xL 27 -82 TM (E=36440)  
75  
76 -1 1  
77 GA MSQSNRELVV DFLSYKLSQK GYSWSQMAAV KQALREAGDE FELRYRRAFS  
78  
79 DLTSQLHITP GTAYQSFQV VNELFRDGVN WGRIVAFFSF GGALCVESVD  
80  
81 KEMQVLVSRI AAWMATYLD HLEPWQENG GWDTFVELYG NNAAESRKG  
82 152  
83 QE  
84  
85 Mc1-1 PESTTM (E=19480)  
86  
87 -1 1  
88 GP DELYRQSLEI ISRYLREQAT GAKDTKPMGR SGATSRKALE TLRRVGDGVQ  
89  
90 RNHETAFQGM LRKLDIKNED DVKLSLRVMI HVFSDGVTNW GRIVTLISFG  
91  
92 AFVAKHLKTI NQESCIEPLA ESITDVLVRT KRDWLKQRG WDGVEFFHV  
93 156  
94 EDLEGG  
95  
96 MDM2 N-terminal domain (E=10430)  
97  
98 -5 1  
99 GSHMAS MCNINMSVPT DGAVTTSQIP ASEQETLVRP KPLLLKLLKS VQAQKDIYTM  
100  
101 KEVLFYLGQY IMTKRLYDEK QQHIVYCSND LLGDLFGVPS FSVKEHRKIY  
102 125  
103 TMIYRNLVVV NQQESSDSGT SVSEN  
104  
105 YB-1 FL (E=29340)  
106  
107 1  
108 MSSEAETQQP PAAPPAAPAL SAADTKPGTT GSGAGSGGPG GLTSAAPAGG  
109  
110 DKKVIATKVL GIVKWFNVRN GYGFINRNDT KEDVVFHQTA IKKNNPRKYL  
111  
112 RSVGDGETVE FDVVEGEKGA EAANVTGPGG VPVQGSKYAA DRNHRYRYP  
113  
114 RRGPPRNYQQ NYQNSEGEK NEGSESAPEG QAQRRPYRR RRFPPYMR  
115  
116 PYGRRPQYSN PPVQGEVMG ADNQGAGEQG RPVRQNMVYRG YRPRFRGPP  
117  
118 RQRQPREDCN EEDKENQDE TQGQPPQRR YRRNFYRRR RPENPKPQDG  
119 324  
120 KETKAADPPA ENSSAPEAQ GGAE  
121  
122 YB-1 180 -324 (E=15930)  
123  
124 1  
125 MSSEAETQQP PAAPPAAPAL SAADTKPGTT GSGAGSGGPG GLTSAAPAGG  
126  
127 DKKVIATKVL GIVKWFNVRN GYGFINRNDT KEDVVFHQTA IKKNNPRKYL  
128  
129 RSVGDGETVE FDVVEGEKGA EAANVTGPGG VPVQGSKYAA DRNHRYRYP  
130 180  
131 RRGPPRNYQQ NYQNSEGEK NEGSESAPEG  
132  
133  
134 BH3-derived peptides peptides  
135  
136 TCTP BH3 commercial  
137  
138 DEMFSDIYKIREIADGLCLEVE  
139

```

140 TCTP BH3 D161 commercial
141
142 DEMFSIIYKIREIADGLCLEVE
143
144 Mule BH3 commercial
145
146 VMTQEVGQLQDMGDDVYQQYR

```

Listing 3 Primary sequence of proteins presented for interaction studies in the current work

```

1
2 #!/bin/csh
3
4 ### For T1 raw ser file conversion to NMRpipe fid format
5
6 bruk2pipe -in ./ser \
7   -bad 0.0 -ext -aswap -AMX -decim 1404 -dspfv 21 -grpdl 76 \
8   -xN      1792 -zN      50 -yN      10 \
9   -xT      806  -zT      25 -yT      10 \
10  -xMODE    DQD  -zMODE  Echo-AntiEcho -yMODE    Real \
11  -xSW      14245.014 -zSW    2790.917 -ySW      2790.179 \
12  -xOBS     949.655  -zOBS    96.227  -yOBS     96.239 \
13  -xCAR     4.701   -zCAR    116.500 -yCAR     116.484 \
14  -xLAB     HN     -zLAB    13C    -yLAB     TAU \
15  -ndim     3     -aq2D    Complex \
16  -out ./fid/test%03d.fid -verb -ov

```

Listing 4 Script *fid.com* to convert data from Bruker to NMRpipe format (adapted from sample generated with nmrDraw) [215].

```

1
2 #!/bin/csh
3
4 ### For T1 fid processing via NMRpipe
5
6 xyz2pipe -in fid/test%03d.fid -x -verb \
7   | nmrPipe -fn SOL \
8   | nmrPipe -fn SP -off 0.5 -end 0.98 -pow 2 -c 0.5 \
9   | nmrPipe -fn ZF -auto \
10  | nmrPipe -fn FT \
11  | nmrPipe -fn PS -p0 0 -p1 0.0 -di \
12  | nmrPipe -fn EXT -left -sw \
13  | pipe2xyz -out ft/test%03d.ft2 -x
14
15 xyz2pipe -in ft/test%03d.ft2 -z -verb \
16  | nmrPipe -fn SP -off 0.5 -end 0.98 -pow 2 -c 0.5 \
17  | nmrPipe -fn ZF -auto \
18  | nmrPipe -fn FT \
19  | nmrPipe -fn PS -p0 90.0 -p1 0.0 -di \
20  | pipe2xyz -out ft/test%03d.ft3 -y
21
22 xyz2pipe -in ft/test%03d.ft3 -x -verb \
23  | nmrPipe -fn POLY -auto \
24  | pipe2xyz -out ft/test%03d.ft4 -x

```

Listing 5 Script *nmrproc.com* to process raw FID in NMRpipe format. (adapted from sample generated with nmrDraw) [215].

```

1
2 #!/bin/bash
3
4 nbl=$(wc -l test_assign.tab | awk '{ print $1 }')
5 cutVal=$(echo $nbl-4 | bc)
6 file=$(echo test_assign.tab)
7 head -4 test_assign.tab > ft_${file}
8 tail -ScutVal test_assign.tab > tmp_test_assign.tab
9 file=$(echo tmp_test_assign.tab)
10 grep -v None ${file} > tmp

```

```

11 mv tmp ${file}
12 sed -i 's/.H//g' ${file}
13 sed -i 's/.N//g' ${file}
14 sed -i 's/\.*/1//g' ${file}
15 sed -i 's/1//g' ${file}
16 sort -n -k23 ${file} > tmp
17 mv tmp ${file}
18 awk '{S1=$23; print}' ${file} > tmp
19 sort -g -k1,3 tmp > tmp2 && mv tmp2 tmp
20 file=$(echo test_assign.tab)
21 echo " " >> ft_${file}
22 cat tmp >> ft_${file}
23 rm tmp*

```

Listing 6 Script *ftab.sh* to clean up *test\_assign.tab* generated with *ipap.tcl* module prior to extraction of peaks intensity.

```

1
2 ### In the NMR directory
3
4 tcsh
5
6 # Processing
7
8 ./fid.com
9 ./nmrproc.com
10
11 # Import ft/test001.ft4 in NMR analysis software and adjust peaklist
12 # Export peaklist in nmrDraw format as tab.tbl
13
14 cp ft/test001.ft4 ./test.ft2
15 sethdr test.ft2 -ndim 2
16
17 # Detect peaks in test.ft2 via nmrDraw. Add new peaks everywhere you know several resonances are close from each other.
18 # Save as test.tab file.
19 ipap.tcl -inName1 test.tab -specName1 test.ft2 -single -assName tab.tbl
20
21 # Save as test\_assign.tab after completion
22
23 # Peaklist was formatting and clustering
24
25 ./ftab.sh
26
27 clustTab.tcl -in ft_test_assign.tab -out clust_ft_test_assign.tab -x X_PPM Y_PPM -dist 0.075 0.75
28
29 # Time constant assignment to planes in ft/*ft4
30
31 awk '{print $1*10}' vclist > vdlist
32 set tim = `awk '{print $1}' vdlist`
33 set plane2D = `ls ft/*ft4`
34 @ j = 0
35 foreach i ($tim)
36 @ j+=1
37 sethdr $plane2D[$j] -tau $tim[$j]
38 end
39
40 # Fit and modeling
41
42 autoFit.tcl -specName ft/test%03d.ft4 -series -inTab clust_ft_test_assign.tab
43
44 modelExp.tcl nlin.tab nlin.spec.list 0.0
45
46 # Generation of PDF output and text files
47
48 cd txt/
49
50 # Import fitPlotListXYdYinPDF.py in the current directory
51
52 cp $PATH/fitPlotListXYdYinPDF.py ./
53

```

54 python fitPlotListXYdYinPDF.py

Listing 7 Script *fitModPlot.csh* which sum up the procedure for extracting and fitting intensities from a given peaklist with NMRpipe [215].

```

1
2 #!/bin/bash
3
4 rm *tmp*
5
6 nbL=$(wc -l nlin.tab | awk '{ print $1 }')
7
8 cutVal=$(echo $nbL-18 | bc)
9
10 file=$(echo nlin.tab)
11
12 #head -4 $file > ft_$file
13
14 tail -ScutVal $file | awk '{ print $1, $18, $19, $26*$18, $27*$18, $28*$18, $29*$18, $30*$18, $31*$18, $32*$18, $33*$1
15 8, $34*$18, $35*$18, $36*$18, $37*$18}' > tmp_intensities_$file
16
17 cp tmp_intensities_$file tmp_transpose.dat
18
19 ./transpose.sh > tr_tmp_intensities_$file
20
21 nbL=$(wc -l tr_tmp_intensities_$file | awk '{ print $1 }')
22
23 cutVal=$(echo $nbL-4 | bc)
24
25 head -1 tr_tmp_intensities_$file > tmp_resi
26
27 head -3 tr_tmp_intensities_$file | tail -2 > tmp_I0
28
29 cp tmp_I0 tmp_transpose.dat
30
31 ./transpose.sh > tr_tmp_I0
32
33 tail -ScutVal tr_tmp_intensities_$file > ft_tr_tmp_intensities_$file
34
35 resi=1
36
37 rm R2eff_out.dat
38 rm mean_err_tmp
39 rm int_err_tmp
40
41 touch R2eff_out.dat
42 touch mean_err_tmp
43 touch int_err_tmp
44
45
46 cat tr_tmp_I0 | while read -r line; do
47
48   int0=$(echo $line | awk '{print $1}')
49
50   err_int0=$(echo $line | awk '{print $2}')
51
52   awk -v var=$resi -v intIni=$int0 '{ ratio=$var/intIni; R2eff=(-1/(0.02*2))*log(ratio); print R2eff}' ft_tr_tmp
53   _intensities_$file > tmp
54   awk -v err=$err_int0 -v var=$resi -v intIni=$int0 '{ error=(Svar*err+intIni*err)/(intIni*intIni); ratio=$var/i
55   ntIni; sup_R2eff=(-1/(0.02*2))*log(ratio+error); inf_R2eff=(-1/(0.02*2))*log(ratio-error); print (sup_R2eff+inf_R2eff
56   /2)}' ft_tr_tmp_intensities_$file > tmp2
57   awk -v err=$err_int0 -v var=$resi -v intIni=$int0 '{ error=(Svar*err+intIni*err)/(intIni*intIni); ratio=$var/i
58   ntIni; sup_R2eff=(-1/(0.02*2))*log(ratio+error); inf_R2eff=(-1/(0.02*2))*log(ratio-error); intErr=(sup_R2eff-inf_R2eff
59   )/2; print (intErr>0)?intErr:-intErr}' ft_tr_tmp_intensities_$file > tmp3
60
61   paste R2eff_out.dat tmp > tmp4 && mv tmp4 R2eff_out.dat
62   paste mean_err_tmp tmp2 > tmp4 && mv tmp4 mean_err_tmp
63   paste int_err_tmp tmp3 > tmp4 && mv tmp4 int_err_tmp
64
65   let "resi = $resi + 1"
66
67 done
68

```

```

69
70 sed -i 's/\t/ /g' R2eff_out.dat
71 sed -i 's/\t/ /g' mean_err_tmp
72 sed -i 's/\t/ /g' int_err_tmp
73
74 cp R2eff_out.dat tmp
75 cat tmp_resi > R2eff_out.dat
76 cat tmp >> R2eff_out.dat
77
78 cp mean_err_tmp tmp
79 cat tmp_resi > R2eff_err.dat
80 cat tmp >> R2eff_err.dat
81
82 cp int_err_tmp tmp
83 cat tmp_resi > tmp_R2eff_err.dat
84 cat tmp >> tmp_R2eff_err.dat
85
86 echo Res > tmp_y_axis
87 sort -n vdlst | tail -11 >> tmp_y_axis
88
89 paste tmp_y_axis R2eff_out.dat > tmp && mv tmp R2eff_out.dat
90
91 paste R2eff_err.dat tmp_R2eff_err.dat > tmp && mv tmp R2eff_err.dat
92
93 paste R2eff_out.dat R2eff_err.dat > tmp && mv tmp R2eff_out.dat
94
95 column -t R2eff_out.dat > tmp && mv tmp R2eff_out.dat
96
97 rm *tmp*

```

Listing 8 Script *getR2eff.sh* to extract CPMG parameter  $R_{2\text{eff}}$  from a single *nlin.tab* output from the *autofit.tcl* procedure.

```

1 #!/bin/bash
2
3 #Calculate HetNoe as AcN,HetNoE,Error for two nlin.tab generated with autofit.tcl on separated ref/sat experiment
4
5 nAc=172
6 firstAc=1
7
8 read -p "nlin.tab from Reference experiment? " refexp
9 echo ""
10
11 read -p "nlin.tab from Saturated experiment? " satexp
12 echo ""
13
14 read -p "Output name ? " output_name
15 echo ""
16 echo ""
17 echo "Many thanks, gonna be processed soon!"
18
19 sleep 1
20
21 grep -v REMARK ${refexp} | grep -v FORMAT | grep -v VARS | grep -v '^$' | awk '{ print $1, $18, $19 }' > tmp_refexp
22 grep -v REMARK ${satexp} | grep -v FORMAT | grep -v VARS | grep -v '^$' | awk '{ print $1, $18, $19 }' > tmp_satexp
23
24 ##### fpl.sh like #####
25
26 for file in tmp_refexp tmp_satexp
27 do
28
29 count=${firstAc}
30
31 cat ./${file} | while read -r LINE; do
32
33 var_current=$(echo ${LINE} | awk '{ print $1 }')
34
35 if [ [ "$count" == "$var_current" ] ]
36 then
37 echo ${LINE} >> ${file}_formatted
38 let "count = $count +1"
39 fi
40

```

```

41 while [[ $count -lt $var_current ]]
42 do
43 echo ${count} NA NA >> ${file}_formatted
44 let "count = $count +1"
45 done
46
47 if [[ "$count" == "$var_current" ]]
48 then
49 echo ${LINE} >> ${file}_formatted
50 let "count = $count +1"
51 fi
52
53 echo ${count} > tmp_count
54
55 done
56
57 count=$(cat tmp_count | awk '{print $1}')
58
59 while [[ $count -le $nAc ]]
60 do
61 echo ${count} NA NA >> ${file}_formatted
62 let "count = $count +1"
63 done
64
65 awk -v var=${firstAc} 'BEGIN{NR=var-1};{ print NR " " $2 " " $3 " " $4 }' ${file}_formatted > temp
66 mv temp ${file}_formatted2
67 rm *formatted
68 rm *temp tmp_count
69 mv ${file}_formatted2 ${file}
70 done
71
72 ##### fpl.sh like #####
73
74 paste tmp_refexp tmp_satexp | sed 's/\t/ /g' | sed 's/ / /g' > tmp_refexp_satexp
75
76 cat tmp_refexp_satexp | awk '{ if($2!="NA" && $5!="NA"){ia_ib = $5 / $2 ; incertitude_int = ($5*$3+$2*$6)/($2*$2); pri
77 nt $1, ia_ib, incertitude_int}else if($2!="NA" && $5=="NA"){print $1, "DIS", "0"}else if($2=="NA" && $5!="NA"){print $
78 1, "APP", "0"}else if($2=="NA" && $6=="NA"){print $1, "NA", "NA"}}' > ${output_name}.dat
79
80 rm tmp*
81
82 echo "Done... "

```

Listing 9 Script *calcHetNoe.sh* to compute intensity ratios between two *nlin.tab* files output of *autofit.tcl* procedure.

```

1
2 #!/usr/bin/python
3
4 ### Sample for a three parameters non-linear regression with B as the constant of interest
5
6 import numpy as np
7 from scipy.optimize import curve_fit
8 import matplotlib.pyplot as plt
9 from io import StringIO
10 import glob, os
11 from fpdf import FPDF
12
13 def func(x,a,b,c):
14     return a*np.exp(-b*x)+c
15
16 os.chdir("./")
17
18 numberName = np.array([])
19
20 if os.path.isfile('./B.out'):
21     os.remove("B.out")
22
23 pdf = FPDF('L', 'mm')
24
25 for file in glob.glob("*.txt"):
26
27     fname = file.split(".")[0]

```

```

28 number = fname.split(".t")[1]
29
30 xydy = np.loadtxt(file)
31
32 numberName = np.append(numberName, number)
33
34 x = np.array ([])
35 y = np.array ([])
36 dy = np.array ([])
37
38 for line in xydy:
39     x = np.append(x, line[0])
40     y = np.append(y, line[1])
41     dy = np.append(dy, line[2])
42
43 while True:
44     try:
45         popt, pcov = curve_fit(func, x, y, sigma=dy, bounds=((0,0,-np.inf), (np.inf,np.inf,np.inf)))
46         break
47     except:
48         break
49
50 outFile = open(fname+".out", "w")
51 outFile.write("A = %f +/- %f\n" % (popt[0], pcov[0,0]**0.5))
52 outFile.write("B = %f +/- %f\n" % (popt[1], pcov[1,1]**0.5))
53 outFile.write("C = %f +/- %f\n" % (popt[2], pcov[1,1]**0.5))
54
55 outFile = open("B.out", "a")
56 outFile.write("%s %f %f\n" % (number, popt[1], pcov[1,1]**0.5))
57
58 fig, ax = plt.subplots()
59 ax.errorbar(x, y, yerr=dy, fmt="none")
60 xfine = np.linspace(0., 20., 100) # define values to plot the function for
61 ax.plot(xfine, func(xfine, popt[0], popt[1], popt[2]), 'r-')
62 ax.set_title('Residue number %s with B = %f +/- %f' % (number, popt[1], pcov[1,1]**0.5))
63
64 plt.savefig(number+".png")
65
66
67 numberName = map(int, numberName)
68 numberName.sort()
69
70 print numberName
71
72 for number in numberName:
73
74     pdf.add_page()
75     pdf.image(str(number)+".png", 1, 1, 280)
76
77 pdf.output("full_output.pdf", "F")

```

Listing 10 Script *fitPlotListXYdYinPDF.py* to plot XYdY \*txt data files and to fit the requested equation to each file. Ultimately generate a PDF containing all plots and fits.

```

1
2 Detector Reporter
3 SYPRO090324 SYPRO090324
4
5 Well Sample Name
6 1 Tris8.5
7 2 Tris8.5
8 3 Tris8.5+NaCl100
9 4 Tris8.5+NaCl100
10 5 Tris8.5+NaCl200
11 6 Tris8.5+NaCl200
12 7 Tris8.5+NaCl300
13 8 Tris8.5+NaCl300
14 9 Tris8.5+NaCl500
15 10 Tris8.5+NaCl500
16 11 Tris8.5+KCl300
17 12 Tris8.5+KCl300
18 13 Tris8.5+Gly10%
19 14 Tris8.5+Gly10%

```

20 15 Tris8.5+NaCl100+Gly10%  
21 16 Tris8.5+NaCl100+Gly10%  
22 17 Tris8.5+NaCl200+Gly10%  
23 18 Tris8.5+NaCl200+Gly10%  
24 19 Tris8.5+NaCl300+Gly10%  
25 20 Tris8.5+NaCl300+Gly10%  
26 21 Tris8.5+NaCl500+Gly10%  
27 22 Tris8.5+NaCl500+Gly10%  
28 23 Tris8.5+MgCl10  
29 24 Tris8.5+MgCl10  
30 25 NaKP7.5  
31 26 NaKP7.5  
32 27 NaKP7.5+NaCl100  
33 28 NaKP7.5+NaCl100  
34 29 NaKP7.5+NaCl200  
35 30 NaKP7.5+NaCl200  
36 31 NaKP7.5+NaCl300  
37 32 NaKP7.5+NaCl300  
38 33 NaKP7.5+NaCl500  
39 34 NaKP7.5+NaCl500  
40 35 NaKP7.5+KCl300  
41 36 NaKP7.5+KCl300  
42 37 NaKP7.5+Gly10%  
43 38 NaKP7.5+Gly10%  
44 39 NaKP7.5+NaCl100+Gly10%  
45 40 NaKP7.5+NaCl100+Gly10%  
46 41 NaKP7.5+NaCl200+Gly10%  
47 42 NaKP7.5+NaCl200+Gly10%  
48 43 NaKP7.5+NaCl300+Gly10%  
49 44 NaKP7.5+NaCl300+Gly10%  
50 45 NaKP7.5+NaCl500+Gly10%  
51 46 NaKP7.5+NaCl500+Gly10%  
52 47 Tp Prot ine  
53 48 Tp Prot ine  
54 49 Hepes7.0  
55 50 Hepes7.0  
56 51 Hepes7.0+NaCl100  
57 52 Hepes7.0+NaCl100  
58 53 Hepes7.0+NaCl200  
59 54 Hepes7.0+NaCl200  
60 55 Hepes7.0+NaCl300  
61 56 Hepes7.0+NaCl300  
62 57 Hepes7.0+NaCl500  
63 58 Hepes7.0+NaCl500  
64 59 Hepes7.0+KCl300  
65 60 Hepes7.0+KCl300  
66 61 Hepes7.0+Gly10%  
67 62 Hepes7.0+Gly10%  
68 63 Hepes7.0+NaCl100+Gly10%  
69 64 Hepes7.0+NaCl100+Gly10%  
70 65 Hepes7.0+NaCl200+Gly10%  
71 66 Hepes7.0+NaCl200+Gly10%  
72 67 Hepes7.0+NaCl300+Gly10%  
73 68 Hepes7.0+NaCl300+Gly10%  
74 69 Hepes7.0+NaCl500+Gly10%  
75 70 Hepes7.0+NaCl500+Gly10%  
76 71 Hepes7.0+MgCl10  
77 72 Hepes7.0+MgCl10  
78 73 Mes6.0  
79 74 Mes6.0  
80 75 Mes6.0+NaCl100  
81 76 Mes6.0+NaCl100  
82 77 Mes6.0+NaCl200  
83 78 Mes6.0+NaCl200  
84 79 Mes6.0+NaCl300  
85 80 Mes6.0+NaCl300  
86 81 Mes6.0+NaCl500  
87 82 Mes6.0+NaCl500  
88 83 Mes6.0+KCl300  
89 84 Mes6.0+KCl300  
90 85 Mes6.0+Gly10%  
91 86 Mes6.0+Gly10%  
92 87 Mes6.0+NaCl100+Gly10%  
93 88 Mes6.0+NaCl100+Gly10%  
94 89 Mes6.0+NaCl200+Gly10%

```

95 90 Mes6.0+NaCl200+Gly10%
96 91 Mes6.0+NaCl300+Gly10%
97 92 Mes6.0+NaCl300+Gly10%
98 93 Mes6.0+NaCl500+Gly10%
99 94 Mes6.0+NaCl500+Gly10%
100 95 Mes6.0+MgCl10
101 96 Mes6.0+MgCl10

```

Listing 11 96-well plates organization and tested buffer conditions for TSA experiments assessing the stability of TCTP regarding pH and salt concentration (0-500  $\mu$ M) or type (NaCl, KCl)

```

1
2 #For all *peaks (define in extension variable) in the current path output ft_*peaks file will be generated. Matrix size
  is automatically detected and headers are accepted. The script fills the blank entries from start to end parameters
  and add the blank character for Yn values.
3
4 #!/usr/bin/python
5
6 import sys
7 import csv
8 import glob
9
10 start=1
11 end=100
12
13 blank = "N"
14
15 extension = "*.peaks"
16
17 for dataXYn in glob.glob(extension):
18
19     with open(dataXYn, 'rw') as XYn:
20         header = XYn.readline()
21         nb_column = len(header.split())
22         XYn = csv.reader(XYn, delimiter=' ', skipinitialspace=True)
23         current = start
24
25         out_XYn = []
26         out_XYn.append(header.replace("\n", ""))
27
28         blank_line = []
29
30         for i in xrange(nb_column-1):
31             blank_line.append(blank)
32
33         blank_line = " ".join(blank_line)
34
35         for line in XYn:
36             while int(line[0]) > current:
37                 out_XYn.append(str(current)+" "+blank_line)
38                 current = current+1
39
40             if int(line[0]) == current:
41                 out_XYn.append(" ".join(line))
42                 current = current + 1
43
44         while current <= end:
45             out_XYn.append(str(current)+" "+blank_line)
46             current = current + 1
47
48         with open("ft_"+dataXYn, 'w') as out:
49             for line in out_XYn:
50                 out.write(line+"\n")
51             out.close()

```

Listing 12 Script *XYnFT.py* to format any text data matrix with automatic size detection for further processing based on comparison between lists of same nature.

```

1 #!/bin/bash
2
3 ### Calculate CCSP, dH, dN and intensity ratio for peaklists formatted with fpl.sh ###
4
5 read -p "Reference? " reference
6 echo " "
7 read -p "Treatment? " treatment
8 echo " "
9 read -p "Fichier noise ? " noise_file
10 echo " "
11
12
13 ref_title=$(echo ${reference} | cut -d "_" -f1 --complement | cut -d "." -f1)
14 treatment_title=$(echo ${treatment} | cut -d "_" -f1 --complement | cut -d "." -f1)
15
16 output=$(echo RESULT_${ref_title}_vs_${treatment_title})
17
18 echo ${output}.dat > output_name
19
20 if [ "$noise_file" == "" ]
21 then
22     noise_file=$(echo noise.noise)
23 fi
24
25 pr -m -t ${reference} ${treatment} > tmp
26
27 sed -i 's/\t/ /g' tmp
28
29 sd_noise=$(cat ${noise_file})
30
31 rm ${output}.dat
32
33 cat tmp | awk -v sdn=${sd_noise} '{ if ($2!="NA" && $6!="NA"){dh = $6 - $2 ; dn = $7 - $3 ; ccsp = sqrt(dh^2 + 0.144 * dn
    ^2) ; ia_ib = $8 / $4 ; incertitude_int = ($8*sdn+$4*sdn)/($4*$4); print $1, dn, dh, ccsp, ia_ib, incertitude_int}
    else if ($2!="NA" && $6=="NA"){print $1, "NA", "NA", "NA", "DIS", "0"}else if ($2=="NA" && $6!="NA"){print $1, "NA",
    "NA", "NA", "APP", "0"}else if ($2=="NA" && $6=="NA"){print $1, "NA", "NA", "NA", "NA", "0"}}' > ${output}.dat
34
35 rm tmp
36
37 rm ${output}_dh.dat
38 rm ${output}_dn.dat
39 rm ${output}_ccsp.dat
40 rm ${output}_intensity.dat
41
42 cat ./${output}.dat | while read -r LINE; do
43
44     var_current=$(echo ${LINE} | awk '{ print $1 }')
45
46     dh=$(echo ${LINE} | awk '{print $3}')
47     dn=$(echo ${LINE} | awk '{print $2}')
48     ccsp=$(echo ${LINE} | awk '{print $4}')
49     intensity=$(echo ${LINE} | awk '{print $5}')
50     incertitude_int=$(echo ${LINE} | awk '{print $6}')
51
52     echo ${var_current} ${dh} >> ${output}_dh.dat
53     echo ${var_current} ${dn} >> ${output}_dn.dat
54     echo ${var_current} ${ccsp} >> ${output}_ccsp.dat
55     echo ${var_current} ${intensity} ${incertitude_int} >> ${output}_intensity.dat
56 done

```

Listing 13 Script *calc.sh* to compare peaklists and to compute chemical shift perturbations and intensity ratios.

```

1 # Param tres
2 #set datafile missing 'NA'
3 #set style data boxes
4 set xlabel "Num. Res." font "Verdana,15"
5 set ylabel "Perturbations de d placements chimiques combin s IH-15N" font "Verdana,15"
6 binwidth=1
7 set boxwidth binwidth
8 set key outside bmargin left box
9 set style line 1 lt 2 lw 2
10 set xtics font "Verdana,20"

```

```

11 set ytics font "Verdana,20"
12 set autoscale x
13 set autoscale y
14
15 set style fill solid border -1
16
17 s(x)=0
18 f(x)=AAA
19 g(x)=BBB
20
21 # Dessin de la courbe
22 set term x11
23 plot 'XXX' using 1:(stringcolumn(2) eq "NA" ? 1/0 : column(2)) with boxes linecolor rgb "#0099FF" title 'XXX',\
24      "" using 1:(stringcolumn(2) eq "NA" ? 0 : 1/0) with points linecolor rgb "#ff0000" title 'Missing data',\
25      s(x) with lines linecolor rgb "#000000" notitle ,\
26      f(x) ls 1 linecolor rgb "#696969" notitle ,\
27      g(x) ls 1 linecolor rgb "#696969" title 'AV; AV+SD'
28
29 #with boxes linecolor rgb "#0099FF"
30
31 set term png size 1200,800
32 set output 'YYY.png'
33
34 replot
35
36 set term postscript
37 set output 'YYY.ps'
38
39 replot

```

Listing 14 Script *plotXY.sh* to quickly plot XY data file using bash and gnuplot.

```

1 #!/bin/bash
2
3 read -p "Fichier x y ? " topplot
4 echo ""
5
6 topplot_short=$(echo ${topplot} | cut -d "." -f1)
7
8 SD_data=$(grep -v 'NA' ${topplot} | awk '{sum+=$2; sumsq+=$2*$2}END{print sqrt(sumsq/NR - (sum/NR)**2)}')
9 AV_data=$(grep -v 'NA' ${topplot} | awk '{sum+=$2}END{av = sum/NR ; print av}')
10
11 cutoff1=$(echo ${AV_data})
12 cutoff2=$(echo ${SD_data} + ${AV_data} | bc -l)
13
14 sed -i "s/AAA/$cutoff1/g" gnuplot_ccsp.conf
15 sed -i "s/BBB/$cutoff2/g" gnuplot_ccsp.conf
16 sed -i "s/XXX/$topplot/g" gnuplot_ccsp.conf
17 sed -i "s/YYYY/$topplot_short/g" gnuplot_ccsp.conf
18
19 cat gnuplot_ccsp.conf | gnuplot
20
21 sed -i "s/$cutoff1/AAA/g" gnuplot_ccsp.conf
22 sed -i "s/$cutoff2/BBB/g" gnuplot_ccsp.conf
23 sed -i "s/$topplot/XXX/g" gnuplot_ccsp.conf
24 sed -i "s/$topplot_short/YYYY/g" gnuplot_ccsp.conf
25
26 display ${topplot_short}.png

```

Listing 15 Gnuplot configuration file *plotXY.conf* for *plotXY.sh* script.

```

1 #!/bin/bash
2
3 read -p "Cutoff most shifted? " cutoff1
4 echo ""
5
6 read -p "Second cutoff? (NA if not) " cutoff2
7 echo ""
8
9 read -p "Cutoff less shifted? (NA if not) " cutoff3
10 echo ""
11

```

```

12 read -p "File_name? " file_name
13 echo " "
14
15 file_name2=$(echo ${file_name} | cut -d "." -f1)
16
17 echo "Most shifted grp 1: x >" ${cutoff1}
18 echo "Most shifted grp 1: x >" ${cutoff1} > ${file_name2}.grp
19 awk -v var1=${cutoff1} '$2 >= var1 && $2!="NA"' ${file_name} | awk '{print $1}' > tmp_command
20 echo -n "sele resi "
21 cat tmp_command | while read -r line; do
22     echo -n ${line}+
23 done
24 echo " "
25
26 echo -n "sele resi " >> ${file_name2}.grp
27 cat tmp_command | while read -r line; do
28     echo -n ${line}+ >> ${file_name2}.grp
29 done
30 echo -n "DEL" >> ${file_name2}.grp
31 echo " " >> ${file_name2}.grp
32 awk -v var1=${cutoff1} '$2 >= var1 && $2!="NA"' ${file_name} >> ${file_name2}.grp
33
34
35
36 if [ $cutoff2 != "NA" ]
37 then
38     echo " "
39     echo " " >> ${file_name2}.grp
40     echo "Most shifted grp 2:" ${cutoff2} "< x <" ${cutoff1}
41     echo "Most shifted grp 2:" ${cutoff2} "< x <" ${cutoff3} >> ${file_name2}.grp
42     awk -v var2=${cutoff2} -v var1=${cutoff1} '$2 >= var2 && $2!="NA" && $2<=var1 && var2!="NA"' ${file_na
43 me} | awk '{print $1}' > tmp_command
44     echo -n "sele resi "
45     cat tmp_command | while read -r line; do
46         echo -n ${line}+
47     done
48     echo " "
49     echo -n "sele resi " >> ${file_name2}.grp
50     cat tmp_command | while read -r line; do
51         echo -n ${line}+ >> ${file_name2}.grp
52     done
53     echo -n "DEL" >> ${file_name2}.grp
54     echo " " >> ${file_name2}.grp
55     awk -v var2=${cutoff2} -v var1=${cutoff1} '$2 >= var2 && $2!="NA" && $2<=var1 && var2!="NA"' ${file_na
56 me} >> ${file_name2}.grp
57 fi
58
59
60
61 if [ $cutoff3 != "NA" ]
62 then
63     echo " "
64     echo " " >> ${file_name2}.grp
65     echo "Less shifted: x <" ${cutoff3}
66     echo "Less shifted: x <" ${cutoff3} >> ${file_name2}.grp
67     awk -v var3=${cutoff3} '$2 <= var3 && $2!="NA" && var3!="NA"' ${file_name} | awk '{ print $1}' > tmp_command
68     echo -n "sele resi "
69     cat tmp_command | while read -r line; do
70         echo -n ${line}+
71     done
72     echo " "
73
74     echo -n "sele resi " >> ${file_name2}.grp
75     cat tmp_command | while read -r line; do
76         echo -n ${line}+ >> ${file_name2}.grp
77     done
78     echo -n "DEL" >> ${file_name2}.grp
79     echo " " >> ${file_name2}.grp
80     awk -v var3=${cutoff3} '$2 <= var3 && $2!="NA" && var3!="NA"' ${file_name} >> ${file_name2}.grp
81 fi
82
83
84
85 echo " "
86 echo " " >> ${file_name2}.grp

```

```

87 echo "No Data"
88 echo "No Data" >> ${file_name2}.grp
89 awk '$2 == "NA" ' ${file_name} | awk '{ print $1 }' > tmp_command
90 echo -n "sele resi "
91 cat tmp_command | while read -r line; do
92     echo -n "${line}+
93 done
94 echo " "
95 #awk '$2 == "NA" ' ${file_name}
96 awk '$2 == "NA" ' ${file_name} | awk '{ print $1 }' > tmp_command
97
98     echo -n "sele resi " >> ${file_name2}.grp
99 cat tmp_command | while read -r line; do
100     echo -n "${line}+ >> ${file_name2}.grp
101 done
102 echo -n "DEL" >> ${file_name2}.grp
103 echo " " >> ${file_name2}.grp
104 awk '$2 == "NA" ' ${file_name} >> ${file_name2}.grp
105
106
107
108 rm tmp_command
109
110 sed -i 's/+DEL//g' ${file_name2}.grp
111 sed -i 's/DEL//g' ${file_name2}.grp

```

Listing 16 Script *grpXY.sh* to group residues in function of cutoffs and to generate corresponding pymol command for residues selection using Bash.

```

1
2 #!/bin/bash
3
4 ./fp1.sh # Format peaklist F1 F2 Ass Height in XY
5
6 ./calc.sh # Compare XY and calc CCSP dH dN Intensity ratio
7
8 ./plotXY.sh # Plot XY datafile
9
10 ./grpXY.sh # Make grp according to cutoffs and generate pymol commands

```

Listing 17 Script *analyze.sh* which sum up the procedure for quick list comparison and results visualization.

```

1
2 #!/usr/bin/env python3
3
4 #Requirements:
5 # pip3 install biopython
6
7 from Bio import Entrez
8 from scidownl.scihub import *
9 from scidownl.update_link import *
10 from subprocess import DEVNULL, STDOUT, check_call
11
12 import os
13 import time
14 import glob
15 import codecs
16 import re
17 import sys
18
19 path_bib = '/media/synthase/postDoc/biblio/'
20
21 create = True
22 scihub = False
23
24 nbtent = 5
25
26 update_link = False
27

```

```

28 if update_link == True:
29     update_link(mod='b')
30
31 Entrez.email = 'florian.malard@cncrs.fr'
32 Entrez.tool = '2Pmed.py'
33
34 def fetchdata(pmid):
35     handle = Entrez.esummary(db = 'pubmed', id = pmid)
36     result = Entrez.read(handle)
37     handle.close()
38     return result
39
40 with codecs.open('/media/synthase/apps/scripts/2Pmed.dat', 'r', encoding='utf8') as inputfile:
41
42     biblist=[]
43     titlecitelist=[]
44     citelist=[]
45
46     wordcite=[]
47
48     notfound=[]
49
50     filecount = 0
51
52     #total = sum(1 for line in inputfile)
53
54     for entry in inputfile:
55
56         print("\n\nFile no "+str(filecount+1)+"\n")
57
58         authors = []
59         pdf_title = []
60         wordauth = []
61
62         pmid = entry
63         metadata = fetchdata(pmid)
64
65         title = metadata[0]['Title'].replace("<i>", "").replace("</i>", "").replace("<sub>", "").replace("<-sub>", "")
66         jname = metadata[0]['FullJournalName'].replace("&", "\&")
67         number = metadata[0]['Issue']
68         vol = metadata[0]['Volume']
69         pages = metadata[0]['Pages']
70
71         if 'DOI' in metadata[0]:
72             DOI = metadata[0]['DOI']
73         elif 'DOI' not in metadata[0]:
74             print("No DOI..."+'\n')
75             notfound.append("No DOI: "+title)
76
77         if len(metadata[0]['EPubDate']) != 0:
78             years = metadata[0]['PubDate'].split(" ")[0]
79         if len(metadata[0]['PubDate']) != 0:
80             years = metadata[0]['PubDate'].split(" ")[0]
81
82         for item_authors in metadata[0]['AuthorList']:
83             tmplist = item_authors.split()
84             first = ". ".join(tmplist[-1])+"."
85             last = "_".join(tmplist[:-1])
86             ft_item_authors = last+" ", "+first
87             authors.append(ft_item_authors)
88
89         pages = pages.replace("-", "_")
90
91         first = authors[0].split(" ")[0]
92
93         ft_authors = '\n'.join(authors)
94         ft_authors = ft_authors.replace("\n", " and ")
95         ft_authors = ft_authors.replace(".", "")
96         ft_authors = ft_authors.replace("_", " ")
97
98         ft_title = title.replace(" ", "_")
99         ft_title = title.replace("/", "_").replace("/", "-")
100
101         cpt = 1
102

```

```

103 for authname in authors:
104     if cpt < len(authors):
105         wordauth.append(authname)
106         wordauth.append(", ")
107
108     if cpt == len(authors) and len(wordauth) != 0:
109         del wordauth[-1]
110         wordauth.append(" & "+authname)
111
112     cpt += 1
113
114 authors_list = ''.join(map(str, wordauth))
115
116 biblist.append('@article{%s%s, \n journal = {%s},\n year = {%s},\n volume = {%s},\n number = {%s},\n pages = {%s},\n
    title = {%s},\n author = {%s},\n pmid = {%s}}\n' % (first.replace(", ", " "), years, jname, years, vol, number, pages, title
    .replace("&", "\&"), ft_authors, pmid.replace("\n", "")))
117
118 titlecitelist.append('%s~\cite{%s%s}' % (title, first.replace(", ", " "), years))
119
120 citelist.append('~\cite{%s%s}' % (first.replace(", ", " "), years))
121
122 wordcite.append(authors_list.replace("_", " ")+" "+title+" "+jname+" "+vol+" "+pages.replace("—", "-")+ (" "+years+"
    ").\n")
123
124 full_path_bib = path_bib+first.replace(", ", " ") +years+"_"+pmid.replace("\n", " ")
125
126 if create == True:
127
128     print("Create processing ... "+ "\n")
129
130     if not os.path.isdir(full_path_bib):
131         os.mkdir(full_path_bib)
132         os.mkdir(full_path_bib+"/div")
133
134     print("New path created ... "+ "\n")
135
136     with codecs.open(full_path_bib+"/bib.bib", 'w', encoding='utf8') as bibfile:
137         bibfile.write('@article{%s%s, \n journal = {%s},\n year = {%s},\n volume = {%s},\n number = {%s},\n pages = {%s}
    },\n title = {%s},\n author = {%s},\n pmid = {%s}}\n' % (first.replace(", ", " "), years, jname, years, vol, number, pages,
    title.replace("&", "\&"), ft_authors, pmid.replace("\n", "")))
138         bibfile.close()
139
140     with codecs.open(full_path_bib+"/word.dat", 'w', encoding='utf8') as wordfile:
141         wordfile.write(authors_list.replace("_", " ")+" "+title+" "+jname.replace("\&", "&")+ " "+vol+" "+pages.replace(
    "—", "-")+ (" "+years+"").\n")
142         wordfile.close()
143
144     with codecs.open(full_path_bib+"/note.tex", 'w', encoding='utf8') as notefile:
145         notefile.write('\documentclass{article}\n\begin{document} \n\n\n')
146         notefile.write('%s~\cite{%s%s}\n\n' % (title, first.replace(", ", " ").replace("&", "\&"), years))
147         notefile.write('~\cite{%s%s}\n\n' % (first.replace(", ", " "), years))
148         notefile.write('\vspace{20mm}\n\n\bibliography{bib}\n\bibliographystyle{ieeetr}\n\end{document}')
149         notefile.close()
150
151     os.system("latexmk -quiet -output-directory="+full_path_bib+"/" + " -pdf -bibtex "+full_path_bib+"/note.tex > /dev/
    null")
152     os.rename(full_path_bib+"/note.aux", full_path_bib+"/div/note.aux")
153     os.rename(full_path_bib+"/note.bbl", full_path_bib+"/div/note.bbl")
154     os.rename(full_path_bib+"/note.blg", full_path_bib+"/div/note.blg")
155     os.rename(full_path_bib+"/note.fdb_latexmk", full_path_bib+"/div/note.fdb_latexmk")
156     os.rename(full_path_bib+"/note.log", full_path_bib+"/div/note.log")
157     os.rename(full_path_bib+"/note.flx", full_path_bib+"/div/note.flx")
158
159 if scihub == True and 'DOI' in metadata[0]:
160
161     dlFile = []
162     cpt = 0
163
164     print("Scihub processing ... "+ "\n")
165
166     while dlFile == [] and cpt < nbntent:
167         print("\nTry no "+str(cpt+1)+"/"+str(nbntent)+"\n\n")
168         sci = SciHub(DOI, full_path_bib+"/")
169         sci.download()
170         dlFile = [f for f in glob.glob(full_path_bib+"/"+"*.pdf") if full_path_bib+"/note.pdf" not in f]

```

```

171     cpt = cpt + 1
172
173     if cpt == nbntent:
174         notfound.append("Other: "+title)
175
176     for torename in dlFile:
177         newname = full_path_bib+"/"+ft_title.replace(".", "").replace("&","&")+ ".pdf"
178         os.rename(torename, newname)
179
180     filecount = filecount + 1
181
182     print('\n'.join(map(str, wordcite)))
183     print('\n'.join(map(str, biblist)))
184     print('\n'.join(map(str, citelist))+ "\n")
185     print('\n'.join(map(str, titlecitelist)))
186
187 if notfound != []:
188     print("\n\n\n!!!\!\!\ Titles below could not be downloaded on scihub !\!\!\!\!\")
189     print('\n'.join(map(str, notfound)))

```

Listing 18 Script *2Pmed.py* to retrieve papers metadata and to manage bibliography from PMID list input. Generate word text citation and .bib bibliography files with associated PDF. The use of download module is deactivated by default.

```

1
2 import requests
3 from bs4 import BeautifulSoup
4 import codecs
5 import re
6 import time
7
8 with codecs.open('2Gpat.dat', 'r', encoding='utf8') as inputfile:
9
10     biblist = []
11
12     for entry in inputfile:
13
14         inventors = []
15         ft_inventors = []
16         ft_ft_inventors = []
17
18         url = "https://patents.google.com/patent/"+entry.replace("\n","")
19
20         data = requests.get(url)
21         data_text = data.text
22         soup_data = BeautifulSoup(data_text, "lxml")
23
24         for inventor in soup_data.find_all("dd", itemprop="inventor"):
25             inventors.append(inventor.text)
26
27         for item_inventors in inventors:
28             tmplist = item_inventors.split()
29             first = tmplist[:-1]
30             first = [x[0] for x in first]
31             last = "".join(tmplist[-1])
32             ft_item_inventors = last+" "+ ".join(first)+". "
33             ft_inventors.append(ft_item_inventors)
34
35         title = soup_data.find("span", itemprop="title").text
36
37         for tag in soup_data.find_all("meta"):
38             if tag.get("name", None) == "citation_patent_number" or tag.get("name", None) == "
39                 citation_patent_publication_number":
40                 number = tag.get("content", None)
41             elif tag.get("name", None) == "DC.date":
42                 date = tag.get("content", None)
43             elif tag.get("name", None) == "DC.date" and tag.get("scheme", None) == "issue":
44                 date = tag.get("content", None)
45
46         year = date.split("-")[0]

```

```
47 first = ft_inventors[0].split(" ")[0]
48
49 ft_ft_inventors = '\n'.join(ft_inventors)
50 ft_ft_inventors = ft_ft_inventors.replace("\n", " and ")
51 ft_ft_inventors = ft_ft_inventors.replace(".", "")
52 ft_ft_inventors = ft_ft_inventors.replace("-", " ")
53
54 biblist.append('@misc{%s, \n author = {%s},\n year = {%s},\n number = {%s},\n title = {%s}}\n' % (first.replace(".", "",
55 " ")+year, ft_ft_inventors, date, number, title.replace("\n", "").replace(" ", "")))
56 print('\n'.join(map(str, biblist)))
```

Listing 19 Script *2Gpat.py* to retrieve patents metadata from ID list input. Generate word text citation and .bib data.





SUPPORTING INFORMATION FOR  
Conformational ensemble and biological role of the  
TCTP intrinsically disordered region: Influence of  
calcium and phosphorylation

Florian Malard<sup>a</sup>, Nadine Assrir<sup>a</sup>, Mouad Alami<sup>b</sup>, Samir Messaoudi<sup>b</sup>, Ewen  
Lescop<sup>a,\*</sup>, Tâp Ha-Duong<sup>b,\*</sup>

<sup>a</sup>*Institut de Chimie des Substances Naturelles, CNRS UPR 2301, Université  
Paris-Saclay, 1 avenue de la Terrasse, 91198 Gif-sur-Yvette, France*

<sup>b</sup>*BIOCIS, Université Paris-Sud, CNRS UMR 8076, Université Paris-Saclay, 5 rue  
Jean-Baptiste Clément, 92290 Châtenay-Malabry, France*

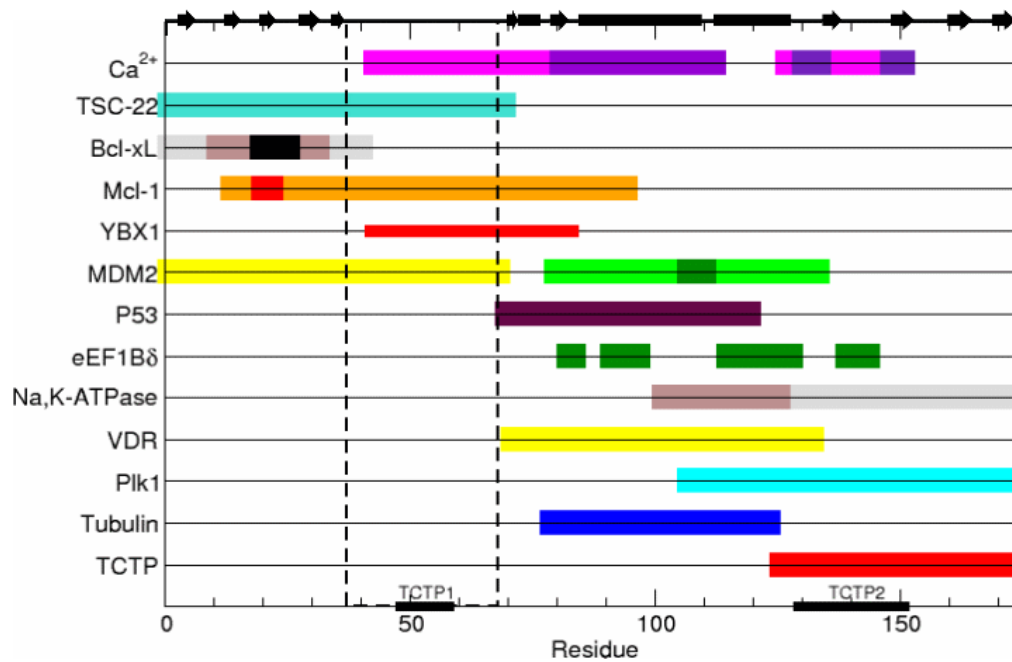
---

---

---

\*Corresponding authors: ewen.lescop@cnrs.fr and tap.ha-duong@u-psud.fr

## Supplemental Figures



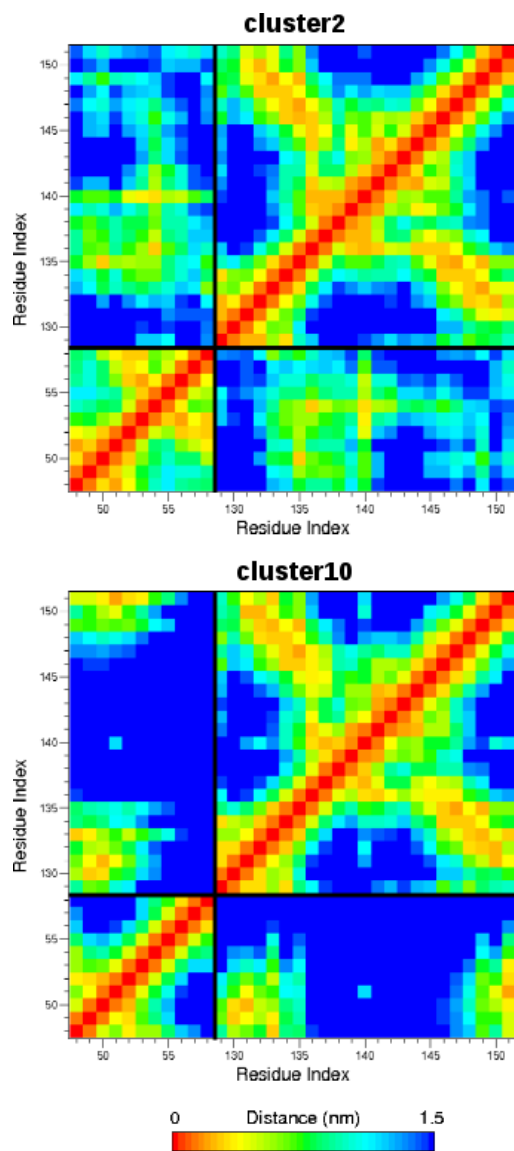


Figure S2: Contact maps between the residues 48-58 of the TCTP first signature and the residues 129-151 of TCTP2, for the clusters 2 and 10 of the noCa-noPhos simulations.

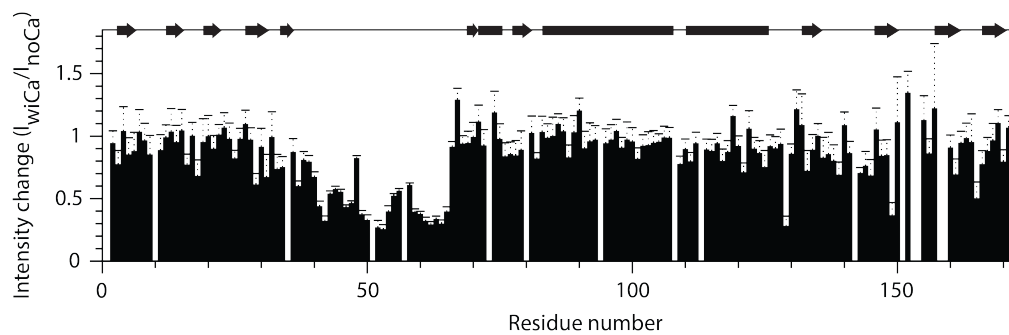


Figure S3: Changes in  $^1\text{H}$ - $^{15}\text{N}$  cross-peak intensity between TCTP  $500\ \mu\text{M}$  in absence and in presence of  $50\ \text{mM}\ \text{CaCl}_2$ .

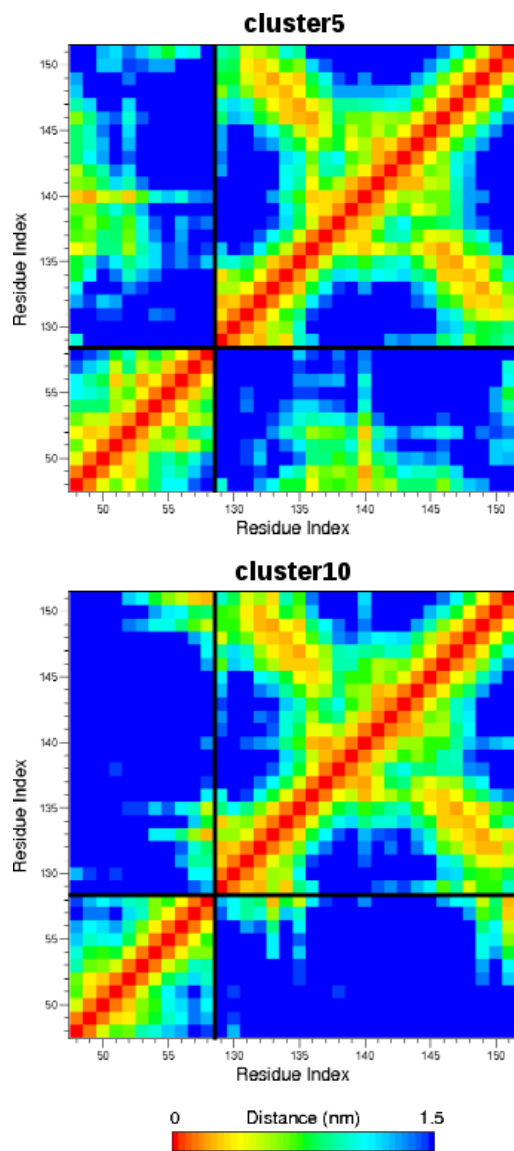


Figure S4: Same as Fig. S2 but for the clusters 1 and 5 of the wiCa-noPhos simulations.

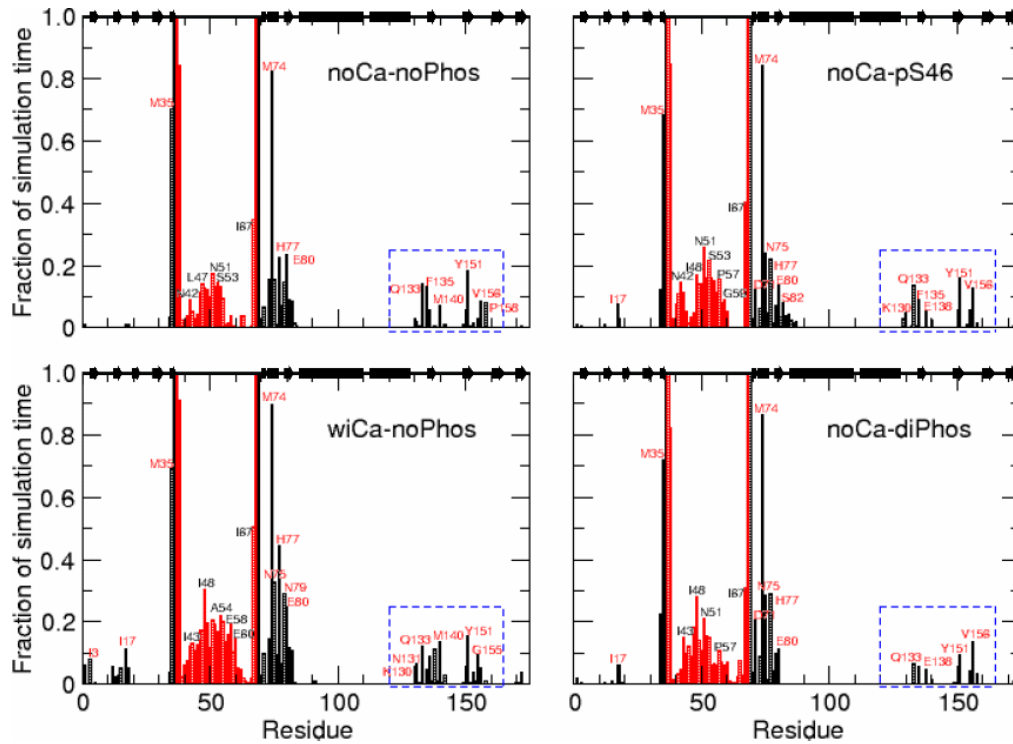


Figure S5: Fraction of the simulation times for which each residue of the TCTP core domain (black), or of the disordered loop (red), is contacted (distance  $< 3 \text{ \AA}$ ) by the long loop or the core domain, respectively. Dashed blue boxes indicate the TCTP regions which are the most affected by the binding of its intrinsically disordered loop.

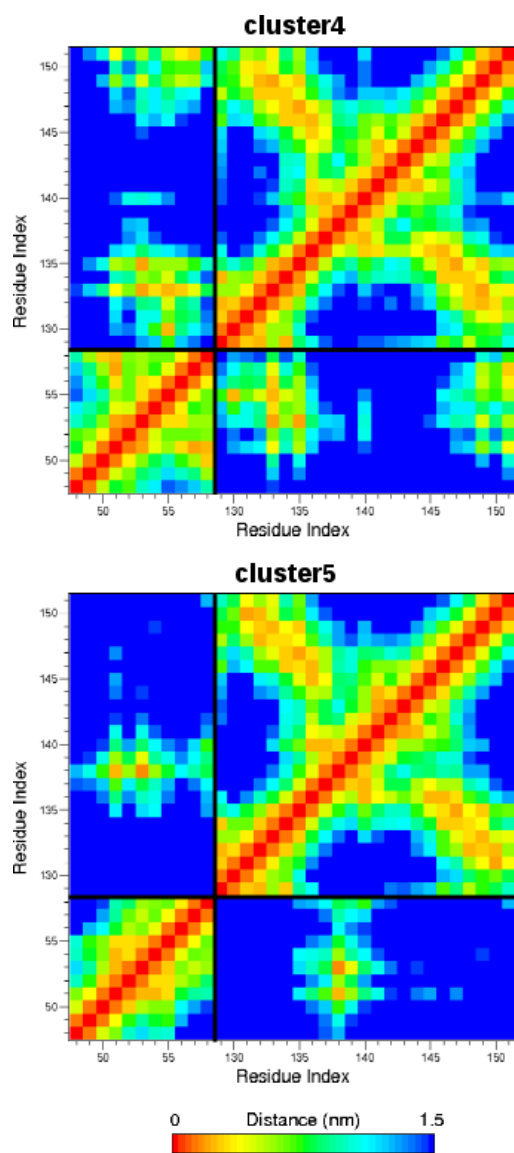


Figure S6: Same as Fig. S2 but for the clusters 4 and 5 of the noCa-pS46 simulations.

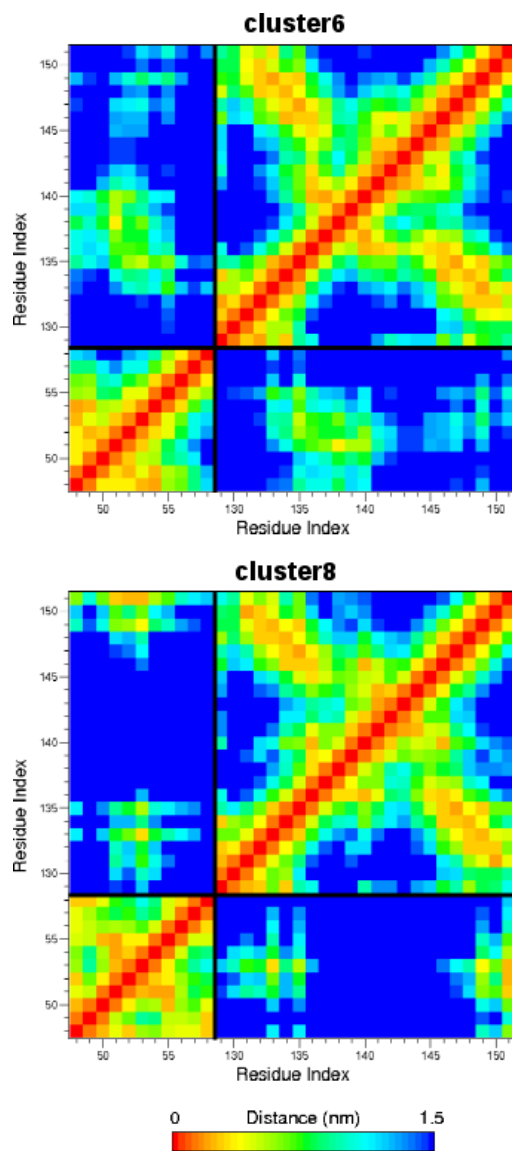


Figure S7: Same as Fig. S2 but for the clusters 6 and 8 of the noCa-diPhos simulations.

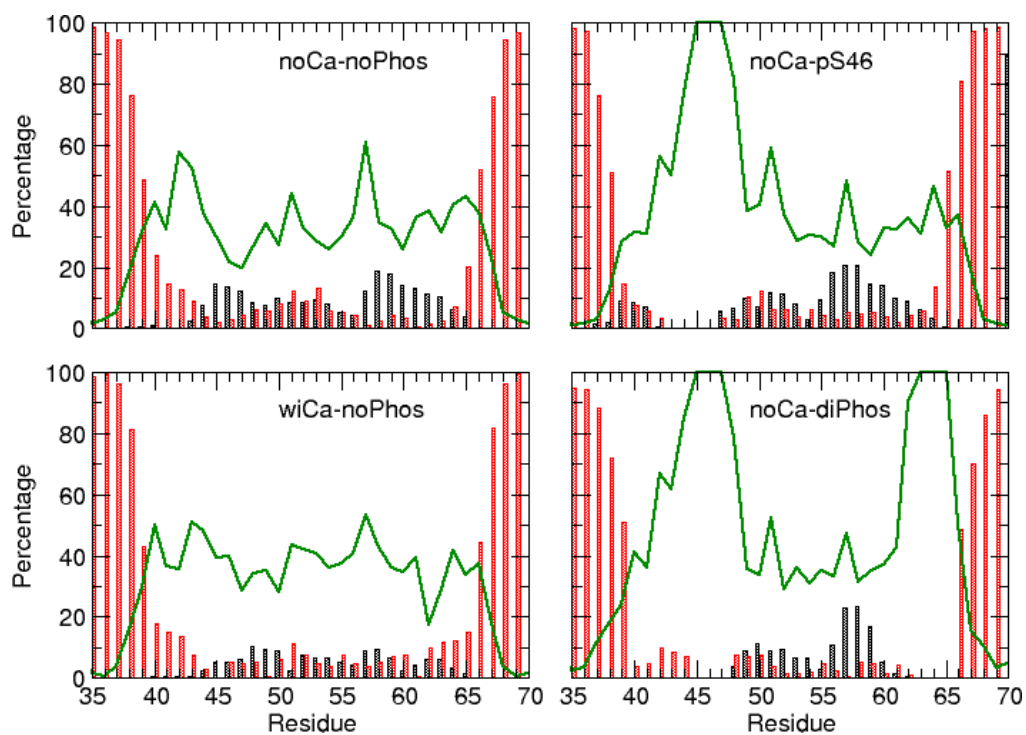


Figure S8: Percentages of the simulation times in which residues of region 35-70 are observed in  $\alpha$ -helix (black bars),  $\beta$ -strand (red bars), or random coil (green lines) conformations.

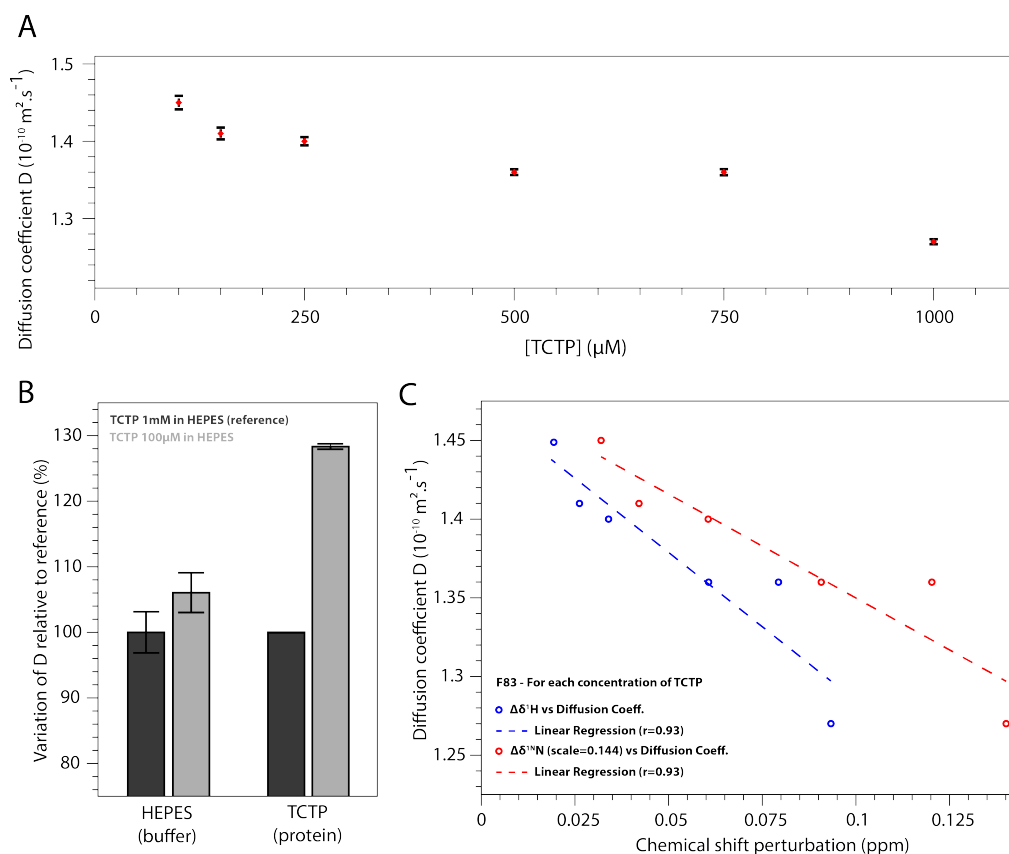


Figure S9: (A) Evolution of the diffusion coefficient of TCTP upon dilution from 1 mM to 100  $\mu\text{M}$ . Coefficient is shown (red dot) as well as the error (black) estimated by Monte-Carlo simulation. (B) Relative change in the diffusion coefficient of the HEPES buffer, used here as a probe of global solution viscosity, and of TCTP, when increasing TCTP concentration from 100  $\mu\text{M}$  to 1 mM. (C) The diffusion coefficient of TCTP is plotted versus  $^1\text{H}$  and  $^{15}\text{N}$  chemical shifts of F83. Under the assumption that both observed chemical shifts and diffusion coefficient are averaged over the relative fractions of monomer and dimer, a linear correlation should be observed between those two observables.

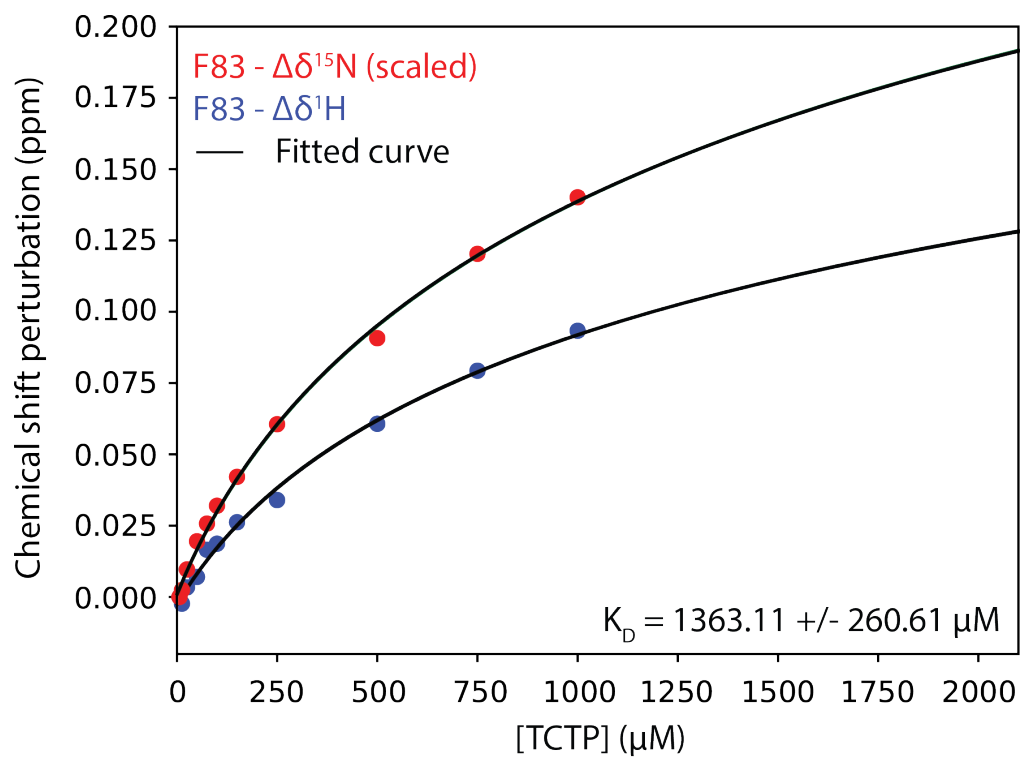


Figure S10: Estimation of the TCTP self-dissociation constant  $K_D$  using chemical shift perturbations observed over F83 cross-peak upon protein dilution from 1 mM to 6.25  $\mu\text{M}$ . Chemical shift perturbation  $\Delta\delta^{15}\text{N}$  was scaled by a -0.14 factor.

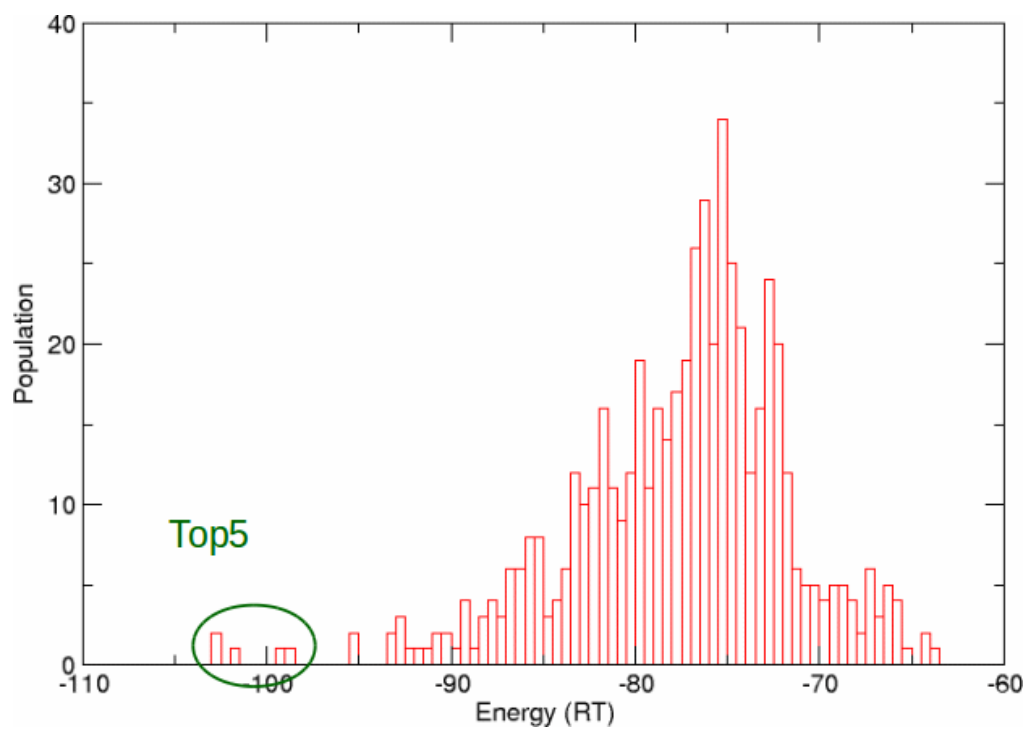


Figure S11: Energy distribution of the TCTP dimers generated by docking calculations.

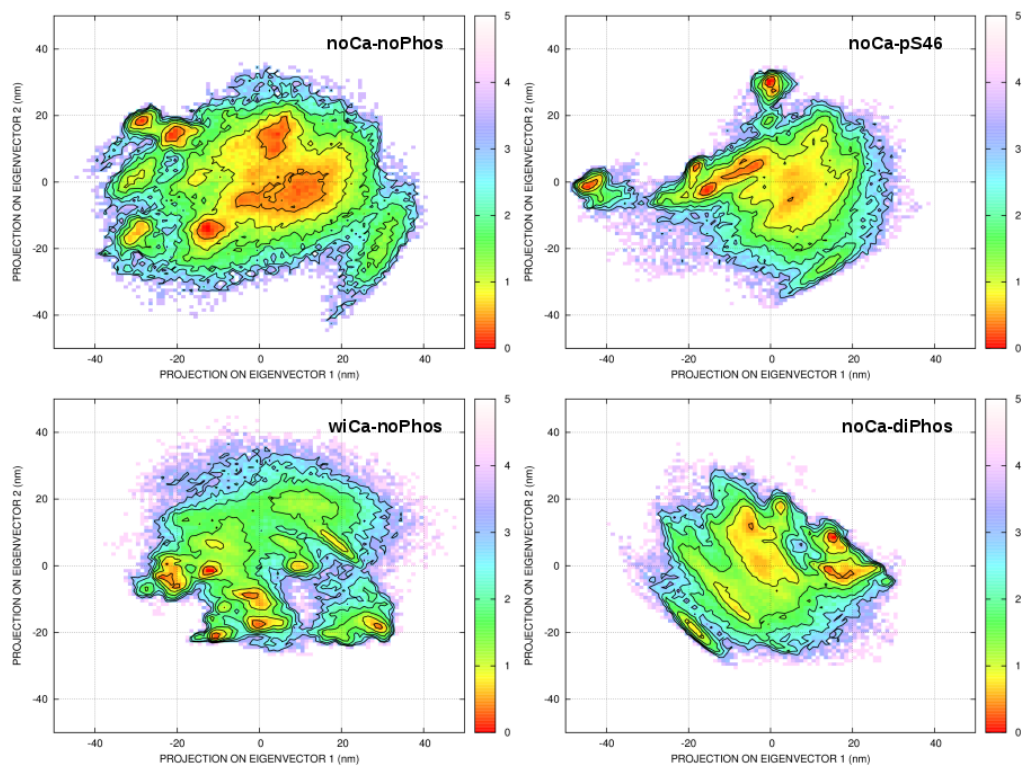


Figure S12: Free energy surfaces of the TCTP conformational ensembles projected onto the first two eigenvectors coming from principal component analyses of the protein trajectories.

## References

- [1] M. Kim, Y. Jung, K. Lee, C. Kim, Identification of the calcium binding sites in translationally controlled tumor protein, *Arch. Pharm. Res.* 23 (2000) 633–636.
- [2] Y. Feng, D. Liu, H. Yao, J. Wang, Solution structure and mapping of a very weak calcium-binding site of human translationally controlled tumor protein by NMR, *Archives of Biochemistry and Biophysics* 467 (2007) 48–57.
- [3] P. Graidist, M. Yazawa, M. Tonganunt, A. Nakatomi, C. C.-J. Lin, J.-Y. Chang, A. Phongdara, K. Fujise, Fortilin binds  $\text{Ca}^{2+}$  and blocks  $\text{Ca}^{2+}$ -dependent apoptosis in vivo, *Biochemical Journal* 408 (2007) 181–191.
- [4] J. H. Lee, S. B. Rho, S.-Y. Park, T. Chun, Interaction between fortilin and transforming growth factor-beta stimulated clone-22 (TSC-22) prevents apoptosis via the destabilization of TSC-22, *FEBS Letters* 582 (2008) 1210–1218.
- [5] Y. Yang, F. Yang, Z. Xiong, Y. Yan, X. Wang, M. Nishino, D. Mirkovic, J. Nguyen, H. Wang, X.-F. Yang, An N-terminal region of translationally controlled tumor protein is required for its antiapoptotic activity, *Oncogene* 24 (2005) 4778–4788.
- [6] S. Thébault, M. Agez, X. Chi, J. Stojko, V. Cura, S. B. Telerman, L. Maillet, F. Gautier, I. Billas-Massobrio, C. Birck, N. Troffer-Charlier, T. Karafin, J. Honoré, A. Senff-Ribeiro, S. Montessuit, C. M. Johnson, P. Juin, S. Cianférani, J.-C. Martinou, D. W. Andrews, R. Amson,

- A. Telerman, J. Cavarelli, TCTP contains a BH3-like domain, which instead of inhibiting, activates Bcl-xL, *Scientific Reports* 6 (2016) 19725.
- [7] D. Zhang, F. Li, D. Weidner, Z. H. Mnjoyan, K. Fujise, Physical and Functional Interaction between Myeloid Cell Leukemia 1 Protein (MCL1) and Fortilin, *J. Biol. Chem.* 277 (2002) 37430–37438.
- [8] H. Liu, H.-W. Peng, Y.-S. Cheng, H. S. Yuan, H.-F. Yang-Yen, Stabilization and Enhancement of the Antiapoptotic Activity of Mcl-1 by TCTP, *Mol. Cell. Biol.* 25 (2005) 3117–3126.
- [9] S. Li, M. Chen, Q. Xiong, J. Zhang, Z. Cui, F. Ge, Characterization of the Translationally Controlled Tumor Protein (TCTP) Interactome Reveals Novel Binding Partners in Human Cancer Cells, *J. Proteome Res.* 15 (2016) 3741–3751.
- [10] R. Amson, S. Pece, A. Lespagnol, R. Vyas, G. Mazzarol, D. Tosoni, I. Colaluca, G. Viale, S. Rodrigues-Ferreira, J. Wynendaele, O. Chaloin, J. Hoebeke, J.-C. Marine, P. P. Di Fiore, A. Telerman, Reciprocal repression between P53 and TCTP, *Nature Medicine* 18 (2011) 91–99.
- [11] G. Funston, W. Goh, S. J. Wei, Q. S. Tng, C. Brown, L. Jiah Tong, C. Verma, D. Lane, F. Ghadessy, Binding of Translationally Controlled Tumour Protein to the N-Terminal Domain of HDM2 Is Inhibited by Nutlin-3, *PLoS ONE* 7 (2012) e42642.
- [12] S. B. Rho, J. H. Lee, M. S. Park, H.-J. Byun, S. Kang, S.-S. Seo, J.-Y. Kim, S.-Y. Park, Anti-apoptotic protein TCTP controls the stability of the tumor suppressor p53, *FEBS Letters* 585 (2011) 29–35.

- 
- [13] H. Wu, W. Gong, X. Yao, J. Wang, S. Perrett, Y. Feng, Evolutionarily Conserved Binding of Translationally Controlled Tumor Protein to Eukaryotic Elongation Factor 1b, *J. Biol. Chem.* 290 (2015) 8694–8710.
- [14] J. Jung, M. Kim, M.-J. Kim, J. Kim, J. Moon, J.-S. Lim, M. Kim, K. Lee, Translationally Controlled Tumor Protein Interacts with the Third Cytoplasmic Domain of Na,K-ATPase Subunit and Inhibits the Pump Activity in HeLa Cells, *J. Biol. Chem.* 279 (2004) 49868–49875.
- [15] R. Rid, K. Onder, A. Trost, J. Bauer, H. Hintner, M. Ritter, M. Jakab, I. Costa, W. Reischl, K. Richter, S. MacDonald, M. Jendrach, J. Bereiter-Hahn, M. Breitenbach, H<sub>2</sub>O<sub>2</sub>-dependent translocation of TCTP into the nucleus enables its interaction with VDR in human keratinocytes: TCTP as a further module in calcitriol signalling, *Journal of Steroid Biochemistry and Molecular Biology* 118 (2010) 29–40.
- [16] F. Yarm, Plk Phosphorylation Regulates the Microtubule-Stabilizing Protein TCTP, *Molecular and Cellular Biology* 22 (2002) 6209–6221.
- [17] Y. Gachet, S. Tournier, M. Lee, A. Lazaris-Karatzas, T. Poulton, U. A. Bommer, The growth-related, translationally controlled protein P23 has properties of a tubulin binding protein and associates transiently with microtubules during the cell cycle, *Journal of Cell Science* 112 (1999) 1257–1271.
- [18] T. Yoon, J. Jung, M. Kim, K. M. Lee, E. C. Choi, K. Lee, Identification of the Self-Interaction of Rat TCTP/IgE-Dependent Histamine-

Releasing Factor Using Yeast Two-Hybrid System, *Archives of Biochemistry and Biophysics* 384 (2000) 379–382.

- [19] P. Thaw, N. J. Baxter, A. M. Hounslow, C. Price, J. P. Waltho, C. J. Craven, Structure of TCTP reveals unexpected relationship with guanine nucleotide-free chaperones, *Nat Struct Mol Biol* 8 (2001) 701–704.

## Résumé en français

TCTP est une petite protéine globulaire à des ligands en utilisant diverses méthodes biophysiques (20 kDa) qui interagit avec de nombreux partenaires et qui est impliquée dans diverses fonctions cellulaires et physiologiques. Elle a un rôle bien documenté dans la réversion tumorale qui est un phénomène rare et spontané où une cellule cancéreuse perd tout ou partie de son phénotype malin et retrouve des caractéristiques associées aux cellules bénignes telles que la sensibilité à l'apoptose. Le réseau d'interaction de TCTP dans l'apoptose est présenté Fig. 1. Dans les cellules cancéreuses, TCTP inhibe la dégradation de MDM2, diminuant ainsi les niveaux de p53 et favorisant le maintien et la progression du cancer. TCTP contient également un motif BH3-like connu pour réguler les membres de la famille Bcl-2 et elle interagit directement avec Bcl-xL et Mcl-1 pour renforcer leurs propriétés anti-apoptotiques. Dans la structure TCTP, le motif BH3-like n'est pas facilement accessible pour une interaction avec un partenaire. Conformément à son importance dans le maintien de la tumeur, TCTP est une cible pharmacologique validée dans le traitement du cancer et fait l'objet d'essais cliniques en cours avec une molécule d'abord connue comme anti-dépresseur, la sertraline. Cependant, on en sait peu sur la structure de TCTP en complexe avec ses partenaires, ce qui entrave le développement de médicaments et ne permet pas de comprendre comment TCTP peut s'adapter à une telle variété de partenaires. Ainsi, nous avons étudié le mécanisme moléculaire par lequel TCTP s'associe à des protéines, drogues et acides nucléïques en utilisant différentes méthodes (RMN, SAXS, CD, SEC, DSF...). Nous avons démontré que la protéine TCTP se lie à Bcl-xL et à Mcl-1 dans le sillon de liaison des motifs BH3. Dans les complexes, la région BH3-like est engagée dans l'interface intermoléculaire et la structure centrale de TCTP est déstabilisée dans un état de globule fondu (molten-globule). Nous avons en outre montré que seule une forme mineure pré-existante de TCTP, à savoir TCTP\*, est compétente pour les interactions avec les partenaires Bcl-xL et Mcl-1. Dans TCTP\*, la région BH3-like est détachée du domaine structuré et elle est accessible aux protéines Bcl-xL/Mcl-1 tandis qu'on retrouve un état globule fondu

dans la partie globulaire de TCTP\*. Un modèle pour l'interaction TCTP:Mcl-1 est présenté en Fig. 2. Nous avons également collecté des données d'interaction préliminaires entre TCTP et la sertraline, des ARN, la protéine YB-1 se liant à l'ARN et le domaine N-terminal de MDM2. Enfin, nous avons caractérisé TCTP phosphorylé (pTCTP) au résidu S46 en utilisant la Plk-1 car cette modification a un impact sur les interactions et est un marqueur de l'agressivité tumorale. En résumé, ces travaux ont établi la versatilité de TCTP en terme de structure (celles-ci sont récapitulées en Fig. 3) et ont montré que cette versatilité est indispensable pour exercer ses fonctions cellulaires. En conséquence, ceci devrait être pris en compte dans les stratégies de développement de nouvelles molécules thérapeutiques ciblant TCTP.

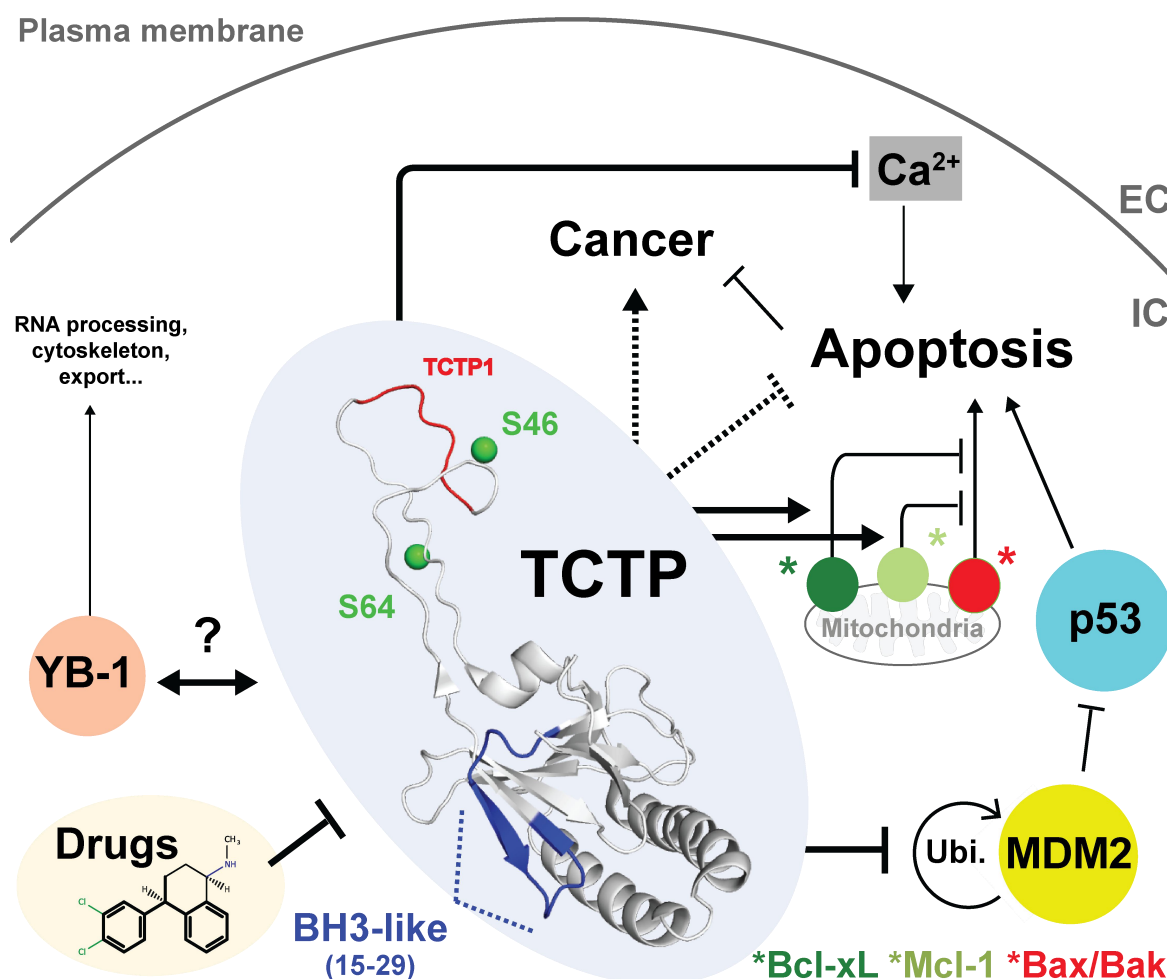


**Fig. 1: Interactome de TCTP dans l'apoptose et au-delà: objectifs de la thèse.** TCTP (blanc) inhibe l'apoptose en stimulant l'activité antiapoptotique de Bcl-xL (vert foncé) et Mcl-1 (vert clair). Indirectement, cela inhibe les protéines Bax et assimilées ce qui empêche le relargage de cytochrome c. TCTP inhibe aussi l'autoubiquitinylation de MDM2 et favorise

donc celle de p53, ce qui résulte aussi dans l'inhibition de l'apoptose. TCTP peut également séquestrer le calcium et protéger contre l'apoptose induite par la thapsigargine. Des molécules sont connues pour cibler TCTP et restaurent également les niveaux de p53. Ces molécules peuvent permettre de restaurer l'apoptose et diminuent les niveaux de TCTP dans les cellules cancéreuses. Au delà de l'apoptose, TCTP et YB-1 interagissent ensemble et il est possible TCTP ait un rôle dans le métabolisme des ARN qui dépend de YB-1. Le motif BH3-like, les signatures conservées TCTP1/2 et les sites de phosphorylation S64/S46 sur TCTP sont mis en évidence sur la structure de TCTP (pdb code: 2HR9).

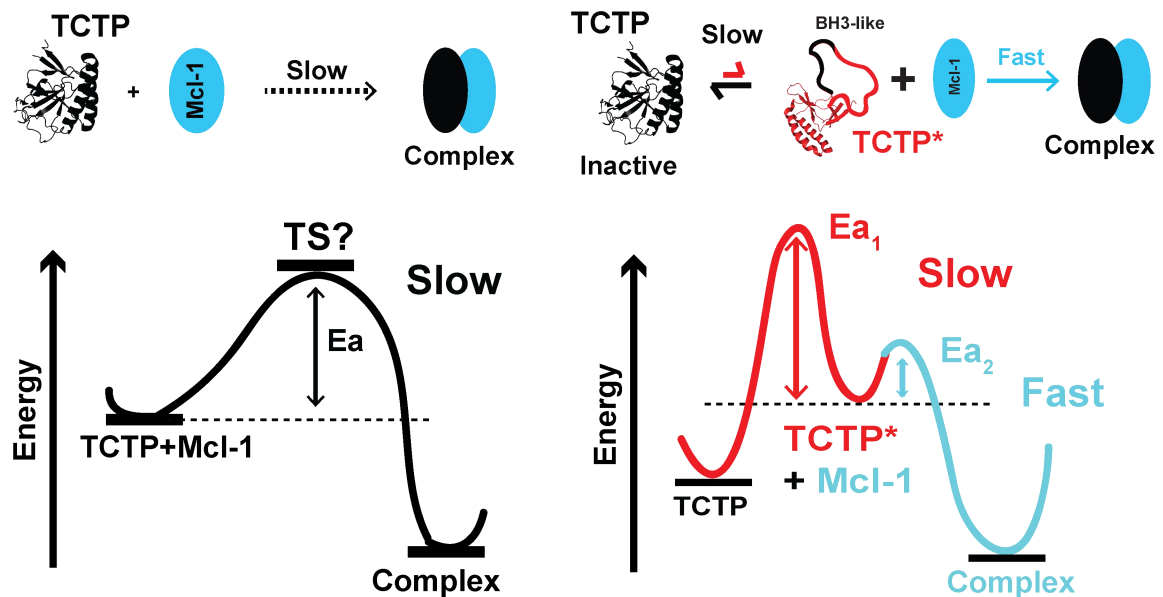


**Fig. 2: Modèle et diagramme d'énergie pour le complexe TCTP:Mcl-1.** La réaction d'association de TCTP et Mcl-1 est lente. Dans le modèle le plus simple, cela indique qu'une énergie d'activation importante est nécessaire pour former le complexe en passant par un état de transition de haute énergie (gauche). Nous avons montré que TCTP natif convertit avec un état minoritaire appelée TCTP\* et de manière lente. C'est cette étape qui est cinétiquement limitante lors de la formation du complexe avec Mcl-1 puisque TCTP\* est la forme active qui permet de lier Mcl-1 (droite).

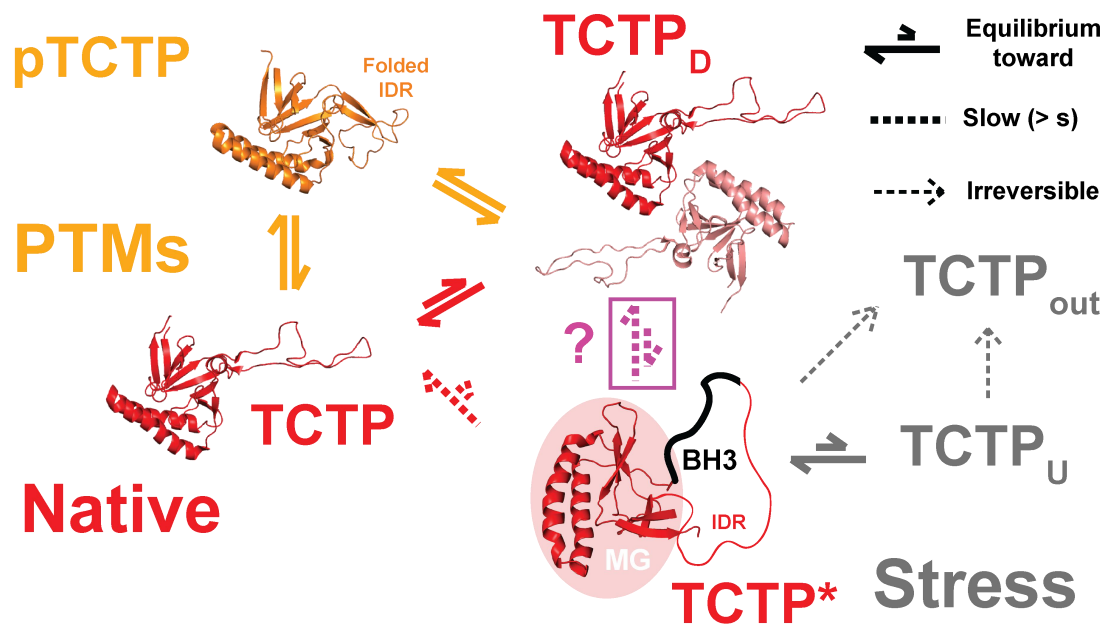


**Fig. 3: La diversité des structures de TCTP.** La protéine existe dans un état natif (TCTP), en tant que dimer (TCTPD) ou encore dans un état phosphorylé (pTCTP) biologiquement pertinent. pTCTP a probablement une forme plus compacte car la boucle a tendance à se replier plus fréquemment sur le domaine globulaire de la protéine après phosphorylation. Un état minoritaire existe également et TCTP\* se forme lentement à partir de TCTP natif. TCTP\* peut être peuplé en utilisant température, pression ou irrad. Dans TCTP\*, le BH3-like motif est décroché du domaine globulaire et exposé au solvant, s'associant facilement à Mcl-1. TCTP\* a une organisation de type globule fondu pour son domaine globulaire. TCTP can also unfold totally (TCTPU) et la protéine peut également s'aggréger dans certaines conditions de stress.

**Titre :** Etude structurale et dynamique de la protéine TCTP : vers la caractérisation d'un réseau d'interaction complexe dans la réversion tumorale

**Mots clés :** RMN, TCTP, sertraline, interactions protéine-protéine, BH3-like, reversion tumorale

**Résumé :** TCTP est une petite protéine globulaire (20 kDa) qui interagit avec de nombreux partenaires et qui est impliquée dans diverses fonctions cellulaires et physiologiques, avec un rôle bien documenté dans la réversion tumorale qui est un phénomène rare et spontané où une cellule cancéreuse perd tout ou partie de son phénotype malin et retrouve des caractéristiques associées aux cellules bénignes telles que la sensibilité à l'apoptose. Dans les cellules cancéreuses, TCTP inhibe la dégradation de MDM2, diminuant ainsi les niveaux de p53 et favorisant le maintien et la progression du cancer. TCTP contient également un motif BH3-like connu pour réguler les membres de la famille Bcl-2 et elle interagit directement avec Bcl-xL et Mcl-1 pour renforcer leurs propriétés anti-apoptotiques. Dans la structure TCTP, le motif BH3-like n'est pas facilement accessible pour une interaction avec un partenaire. Conformément à son importance dans le maintien de la tumeur, TCTP est une cible pharmacologique validée dans le traitement du cancer et fait l'objet d'essais cliniques en cours avec une molécule d'abord connue comme anti-dépresseur, la sertraline. Cependant, on en sait peu sur la structure de TCTP en complexe avec ses partenaires, ce qui entrave le développement de médicaments et ne permet pas de comprendre comment TCTP peut s'adapter à une telle variété de partenaires. Ainsi, nous avons étudié le mécanisme moléculaire par lequel TCTP s'associe à des protéines et

à des ligands en utilisant diverses méthodes biophysiques (RMN, SAXS, CD, SEC, DSF...). Nous avons démontré que la protéine TCTP se lie à Bcl-xL et à Mcl-1 dans le sillon de liaison des motifs BH3. Dans les complexes, la région BH3-like est engagée dans l'interface intermoléculaire et la structure centrale de TCTP est déstabilisée dans un état de globule fondu (molten-globule). Nous avons en outre montré que seule une forme mineure pré-existante de TCTP, à savoir TCTP\*, est compétente pour les interactions avec les partenaires Bcl-xL et Mcl-1. Dans TCTP\*, la région BH3-like est détachée du domaine structuré et elle est accessible aux protéines Bcl-xL/Mcl-1 tandis qu'on retrouve un état globule fondu dans la partie globulaire de TCTP\*. Nous avons également collecté des données d'interaction préliminaires entre TCTP et la sertraline, des ARN, la protéine YB-1 se liant à l'ARN et le domaine N-terminal de MDM2. Enfin, nous avons caractérisé TCTP phosphorylé (pTCTP) au résidu S46 en utilisant la Plk-1 car cette modification a un impact sur les interactions et est un marqueur de l'agressivité tumorale. En résumé, ces travaux ont établi la versatilité de TCTP en terme de structure et ont montré que cette versatilité est indispensable pour exercer ses fonctions cellulaires. En conséquence, ceci devrait être pris en compte dans les stratégies de développement de nouvelles molécules thérapeutiques ciblant TCTP.

**Title :** Structural and dynamic studies of TCTP protein: deciphering a complex interaction network involved in tumor reversion

**Keywords :** NMR, TCTP, sertraline, protein-protein interactions, BH3-like, tumor reversion

**Abstract :** TCTP is a small (20 kDa) globular protein that interacts with many partners with consequences in various cellular and physiological functions, with well-documented roles in tumoral reversion program. Cells that undergo such program spontaneously lose their malignant phenotype and recover characteristics associated with benign cells, such as apoptosis. In cancer cells, TCTP inhibits MDM2 degradation, thus decreasing p53 levels and favoring tumor maintenance and progression. TCTP also contains a BH3-like motif known to regulate Bcl-2 family members and TCTP directly interacts with Bcl-xL and Mcl-1 to reinforce their pro-survival properties. In TCTP structure, the BH3-like motif is not readily accessible for interaction. Consistently with its importance in tumor maintenance, TCTP is a validated pharmacological target in cancer treatment with ongoing clinical trials using the TCTP-targeting antidepressant drug sertraline. However, little is known about TCTP structure in complex with partners, thus impeding the development of drugs and the understanding of how TCTP could adapt to its myriad of partners. Thus, we investigated the molecular

mechanism by which TCTP associates with proteins and ligands using various biophysical methods (NMR, SAXS, CD, SEC, DSF...). We have demonstrated that full length TCTP binds to Bcl-xL and Mcl-1 in their BH3-binding groove. In the complexes, the TCTP BH3-like region is engaged in the intermolecular interface and the core TCTP structure is destabilized into a molten-globule (MG) state. We further showed that only a minor pre-existing form of TCTP, namely TCTP\*, is competent for interactions with the Bcl-2 protein partners. In TCTP\*, the BH3-like region is unpinned and accessible to Bcl-xL/Mcl-1 proteins and the core structure is also in MG state. We also collected preliminary interaction data between TCTP and sertraline, RNA, the RNA binding YB-1 protein and the MDM2 N-terminal domain. Finally, we characterized the Plk-1-mediated S46 phosphorylated TCTP (pTCTP), a marker of tumor aggressivity and its interaction properties. Overall, this work established the structural versatility of TCTP that is mandatory to exert its cellular functions and this versatility should be taken into account in drug-design strategies targeting TCTP.

